Author:
Zhu, Wuxue

Title:
Measurement and assessment of residual stresses for probabilistic fatigue life predictions.

MEASUREMENT AND ASSESSMENT OF RESIDUAL STRESSES FOR PROBABILISTIC FATIGUE LIFE PREDICTIONS

by

Wuxue ZHU

December 1996

A thesis submitted to the University of Bristol
in accordance with the requirements of
the degree of Doctor of Philosophy
in the Department of Mechanical Engineering
in the Faculty of Engineering

Engineering Materials and Structural Integrity Group,
University of Bristol, Department of Mechanical Engineering,
Bristol BS8 1TR, U.K.

To my family, wife and son

ABSTRACT

In the manufacture of large batches of forged components it is inevitable that there will be statistical variations in material properties, surface roughness and in the geometry of the component. To assess the fatigue life performance these variations may be accounted for by using probabilistic analysis. It is also recognised that various aspects of the manufacturing process will introduce residual stresses into the component. However, the influence of the component to component variability of the residual stresses is poorly understood.

This research has been mainly concerned with measuring residual stresses in forged components, establishing the relationship between residual stress relaxation and applied mechanical loading and providing a probabilistic approach to incorporating residual stresses into a fatigue life methodology.

The main objectives of the work were to measure the magnitude and distribution of residual stresses in hot forged steel samples using different techniques including X-ray and neutron diffraction and centre-hole drilling method, to establish the specimen to specimen variation of residual stresses, and also to relate the variation to particular manufacturing processes. The work also included an experimental programme that investigated the interaction between residual stresses and cyclic mechanical loading, and to determine lives in low (LCF) and high (HCF) cycle fatigue regimes. Finite element (FE) models were used to examine the interaction between residual and applied stresses. Finally the results of the modelling and experiments were used in a probabilistic model that was incorporated into a fatigue life methodology.

Several new cases of research were studied in detail: (i) measurement and interpretation techniques to obtain residual stresses using neutron diffraction and centre hole drilling methods were improved and developed, (ii) an analytical interpolation technique was developed to determine through-thickness residual stresses based on limited measurements, (iii) statistical distributions of surface residual stresses were found for different stages of the manufacturing process, (iv) compressive residual stresses relaxed during mechanical loading at strain ranges regarded as being in the elastic range, (v) fatigue life statistical distributions in the low cyclic and high cyclic fatigue regimes were found as a function of the various stages of the manufacturing process, (vi) a probabilistic analysis using the statistical variation of the relaxed residual stresses was developed and finally (vii) it was found that a joint distribution function taking account of residual stresses and other random variables was required in the HCF regime, although it was found that the statistical variation of the residual stresses was the dominant function.

DECLARATION

The accompanying dissertation entitled "MEASUREMENT AND ASSESSMENT OF RESIDUAL STRESSES FOR PROBABILISTIC FATIGUE LIFE PREDICTIONS" is submitted in support of an application for the degree of Doctor of Philosophy in Engineering at the University of Bristol. The dissertation is based on independent work by the candidate except where clearly referenced. This work has not been submitted for any other degree or diploma at this University or any other institution.

The view and opinions expressed in this thesis are solely those of the author and not the University of Bristol.

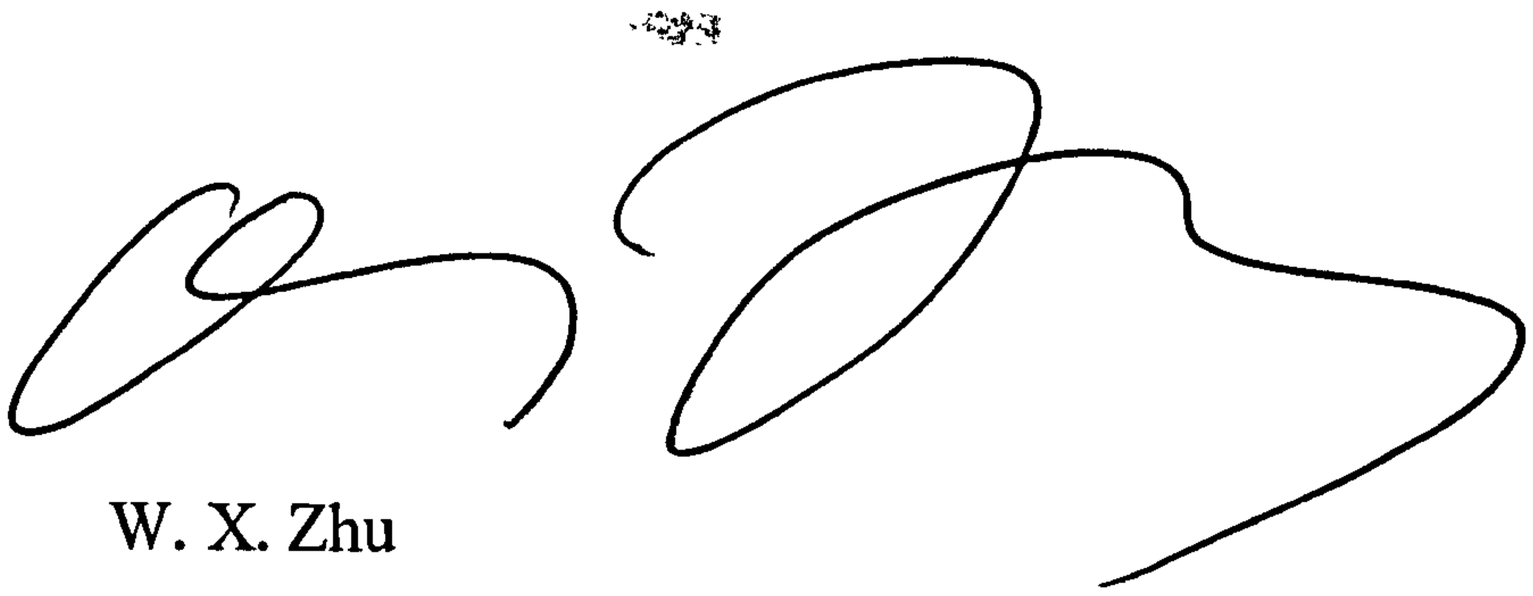

W. X. Zhu

December 1996

ACKNOWLEDGEMENTS

I wish to express my sincere thanks to my supervisor Prof. David Smith for his continuous support, encouragement and technical guidance throughout the course of this research. I am also grateful for the help and guidance given by Mr. Chris McMahon.

I also wish to extend my deep graduate to Dr. Martyn Pavier, Dr. Peter Mckeighan, Dr. Steve Kimmins, Dr. Giora Shatil and Mrs Maria Priest for their consistent help during my study. My thanks are also addressed to the members of Materials Lab and Mechanical Engineering Workshop, in particular to Mr. Troy Swankie and Mr. Des Neale for their patience and assistance in my experiments.

I would like to thank the members of the Engineering Materials and Structure Integrity Group for providing a very enjoyable and cosmopolitan working atmosphere. In particular, I wish to thank Dr. Christophe and Mr. Hamish Fowler for their help with my computing problems. My gratitude is expressed to Mr. Fraser McMaster for his time and effort to read this dissertation.

The financial sponsorship for this work, provided by EPSRC (EPSRC grant reference GR/H46800), is gratefully acknowledged. The assistance and advice of personnel from Rover Group and John Stoke and Sons Ltd have been invaluable: thanks especially to Dr J. Devlukia for his supervision of the project and Mr. Andrew Ciepalowicz for his surport of experiments throughout the research. My thanks are also extended to Dr. Torben Lorentzen for his help in my neutron diffraction measurements in Riso National Labs, Denmark.

Finally, I would like to thank all friends who contributed to a very enjoyable stay in Bristol. I can not thank enough the love and encouragement provided by my family who continuously believed in this expedition.

CONTENTS

LIST OF TABLES

Tables in Chapter 5:

Tables in Chapter 6:

Tables in Chapter 7:

Tables in Chapter 8:

LIST OF FIGURES

Figures in Chapter 5:

Figures in Chapter 6:

Figures in Chapter 7:

Figures in Chapter 8:

Chapter 1

INTRODUCTION

Under present commercial pressures, the automotive industry is trying to deliver cheaper, lightweight and durable vehicles which are environmentally friendly. Some research targets under development aim to allow higher working stresses in metallic components and to have increased confidence in their fatigue performance. Consequently there is a need to optimise fatigue strength-to-weight ratio in the early stage of design and thus facilitate weight reduction or the use of new/alternative materials (Devlukia, 1993). The majority of failures in machinery and structural components can be attributed to fatigue processes. Such failures generally take place under the influence of repeat loadings whose peak values are considerably smaller than the safe loadings estimated on the basis of static analyses. Fatigue is now one of the major considerations in design.

The fatigue life assessment of automotive structural parts has been traditionally carried out using the material Stress-Life (S-N curve) performance. Although residual stress has been known to exist widely in components, its influence on fatigue life has not been considered in design for its poor understanding of its variability from component to component

Hot forging is a common manufacturing process for the production of large quantities of engineering components. With their reputedly superior performance, forgings have been used for safety critical parts such as components operating under conditions of high dynamic stress or impact loading (Watkins, 1975). The largest material fraction of a typical car is made up of 25% forged steel (Devlukia, 1993). As a result of various aspects of the hot forging process, including subsequent cooling and shot blasting, internal and surface residual stresses are developed in forged components (Watkins, 1975; Myllymaki, 1987). Forging and thermal loading introduce long range residual stresses and surface treatment such as shot peening and shot blasting introduces short range or near surface residual stresses. Experience in

the automotive industry has shown that the presence of residual stresses represents a major source of uncertainty in determining multiaxial fatigue life. Therefore, a knowledge of residual stresses in forged components is necessary to be able to accurately assess the life of the components.

The residual stresses, which are produced during the manufacturing process, play an important role in the deformation and failure behaviour of the components. A compressive residual stress improves the fatigue behaviour of materials, while tensile residual stresses produce an opposite effect. Because of yielding behaviour and cyclic softening of material, the residual stresses in the specimen will be partly relaxed and redistributed under certain levels of cyclic mechanical loading or thermal energy. Heat treatment, such as annealing can also completely release the residual stresses. The relaxation behaviour under the cycle fatigue loading depends strongly on the material properties. The cyclic fatigue loading can release residual stresses significantly for some materials (James, et al, 1982). After many cycles, the residual stresses will no longer change and, therefore become stabilised. It is the stabilised residual stresses that contribute to the fatigue life. Thus, a knowledge of stability or relaxation behaviour of these residual stresses is of fundamental and practical interest (James, et al, 1981). Stable residual stresses are often desirable in design and are particularly important when compressive residual stresses are deliberately set up in the surface regions of structural components in order to improve their fatigue strength. If the residual stresses are taken into account in fatigue strength calculation, it is very important to consider the relaxation of residual stresses. However, in fatigue design applications, the relaxation phenomenon is often neglected.

It is difficult to model the generation of residual stress in the forging process and experimental approaches have been often employed to study residual stresses in forged components. The use of X-ray and neutron diffraction methods to measure residual stresses is well-established. The most important advantage of these methods is that they are non-destructive and capable of stress measurement without stress relaxation. X-ray is often used to measure near-surface values and neutron diffraction, which is of much greater penetrating power compared with X-ray, offers the possibility of stress measurement on the interior of the components. Bashun et al. (1986) and Appleton et al. (1987) have studied the residual stresses in forged components using the X-ray diffraction method and indicated that the forging process produces residual stresses in components.

Compared with X-ray diffraction, which only measures stresses on the surface, and the neutron diffraction method where it is difficult to measure stress near the surface of specimen, the hole-drilling method has been widely used to measure near surface residual stresses in engineering components (Schajer, 1988). The conventional method of hole-drilling assumes that the stress field does not vary with depth. However non-uniform residual stresses can be determined by using incremental technique. But so far the application of this technique is restricted to components with flat surfaces and no plastic reverse yielding around hole area has been taken into account.

Most components have a complicated geometry and are subjected to complex loadings which fluctuate in magnitude as well as direction. As a result of this, two or three principal stresses may be nonproportional or whose directions may change during the loading cycles. Fatigue under such stress states is known as multiaxial fatigue, and assessing multiaxial fatigue life is of considerable importance in design. Many proposals for different multiaxial fatigue criteria have been made but there is no single theory which is suitable for all materials and loading conditions.

Many experiments have indicated that there is considerable statistical scatter in fatigue test results. Thus, a quantitative estimation of the reliability of the predicted fatigue life is essential. Many studies have been done to examine methods to be used in analysing fatigue test data. The most commonly used and accepted procedures are smoothing techniques, which smooth out the observed fatigue data and hence tend to mask the inherent statistical scatter of the fatigue data. The major drawback in the application of these techniques is that the inherent statistical scatter is often ignored. Thus, a statistical analysis is necessary. There are many factors which contribute to the scatter, such as the material, loading conditions, surface roughness, misalignment, residual stresses and measurement techniques. The fatigue life and reliability are consequently a function of these variables. Therefore, probabilistic approaches are needed to both characterise, and interrelate, these variables for the design and maintenance of components.

The factors that influence fatigue life are random in nature and therefore the appropriate development of analysis and design methodology should be probabilistic. The relevant measure of structural performance is the probability of failure. Failure is defined, generally, as the inability of the structure to perform its intended functions. In other words, failure refers to attaining or exceeding some limit state, which may include damage necessitating repairs, rupture, and catastrophic

collapse. The advantage of the probabilistic approach to design lies in the logical framework for analysing design uncertainties and provides a quantitative basis for assessing structural integrity in the form of the risk or probability of unfavourable performance. To ensure adequate fatigue and fracture resistance, the design must employ design stresses that reflect uncertainties in fatigue and fracture behaviour and contain at least a tacit recognition of the probability that some amount of damage will be incurred. This permits the formalisation of an approach to the study of safety and performance of structures and, ultimately, would make it possible to achieve optimum designs within the constraints and cost limitations.

The main aim of the research reported in this thesis was to determine the statistical distribution of residual stresses, to explain how the residual stresses are influenced by cyclic loading and then to establish a probabilistic approach to incorporating the residual stresses into a fatigue life assessment. The residual stresses in forged components will be examined using different techniques to obtain residual stress profile in component and residual stress variation from sample to sample. The residual stress relaxation under mechanical loading will be studied. A probabilistic approach will be used to incorporate residual stress as an random variable into fatigue life analysis.

Chapter 2 reviews the experimental, analytical and numerical investigations of other workers on the residual stress measurement techniques, fatigue theories, residual stress influence of fatigue lives and its relaxation under fatigue loading, and probabilistic approaches for fatigue life and reliability analysis.

In Chapter 3, the overall experimental programme with the test procedures and test matrix is described.

The residual stress measurements on forged components using different techniques are presented in Chapter 4. Some new developments were made for both the experiments and analysis of results.

Chapter 5 presents the development of a theoretical approach for interpolating limited experimental residual stress results in round bar specimens. The theoretical analysis, together with a least squares method, has been developed to obtain the complete distribution of residual stresses in the round bar specimens. The interpolated results have been compared with results from using the centre hole

method and also using chemical etching combined with the X-ray diffraction method.

The experimental work and finite element (FE) analyses on the interaction between residual stresses and mechanical loading are presented in Chapter 6. Two hardening models were used in the FE analyses, linear kinematic hardening model and multilinear hardening model. The latter model has been developed for cyclic loading and written into a user subroutine UMAT for use in ABAQUS. Residual stress relaxation for different initial residual stresses and different cyclic strain ranges have been obtained.

Chapter 7 presents fatigue test data from four groups of specimens AF, HT, FS and HTS. The data were analysed using Weibull distributions. The influence factors of each stage of forging process on fatigue lives were studied and discussed. A more realistic fitting function with endurance limit was used for the S-N curve.

Chapter 8 summarises the statistical analysis of residual stress variation from specimen to specimen, its redistribution after interaction with cyclic loading and its influence on fatigue lives. A probabilistic approach has been developed to incorporate residual stresses into fatigue life prediction. The relationship among fatigue cyclic strain ranges, relaxed residual stress and the fatigue life has been derived. Some other random influence factors on fatigue life, excluding residual stresses, have been included. Simulations to determine fatigue lives have been made.

Chapter 9 summarises the main conclusions and suggests potential future work.

Chapter 2

LITERATURE REVIEW

Most of the literature reviewed in this chapter is directly related to the research work in this thesis. The review examines previous knowledge of residual stresses in forged components, residual stress measurement techniques and interpretation methods. Multi-axial fatigue theory and mean stress effects on fatigue life are reviewed. Then the effects of residual stress on fatigue life and residual stress relaxation due to fatigue cycles are reviewed. Probabilistic approaches to fatigue life and reliability analysis methods are also reviewed. Finally the limitations of current knowledge about residual stresses and their influence on fatigue life are discussed, and the work carried out to address the limitations are highlighted.

2.1 Residual Stress In Forged Components

Manufacturing processes, including forging, thermal loading and shot blasting, introduce significant residual stresses in components. In the operation of forging, tensile stresses may develop in the process of changing shape and failure can often be traced to the occurrence of these stresses (Watkins, 1975). The non-uniform plastic deformation, which is generated over the whole specimen by forging and thermal loading and on the surface by surface treatment, is a key factor in determining the distribution of the residual stresses. Forging and thermal loading introduce long range residual stresses and surface treatment, for instance shot peening and shot blasting, introduces short range residual stresses.

Compared with work on residual stresses in welded components, there is little work available on residual stress in forged components and complete methods for the non-

destructive monitoring of the level and distribution of residual stress do not exist (Bashun et al., 1986). The behaviour of workpieces can not be analysed easily using normal plasticity theory. Often finite element methods have been used previously to study the workpiece deformation using a rigid perfectly plastic model and in general do not provide residual stress distributions directly.

Experiments have been the best way to study residual stress in forged components. Bashun et al. (1986) studied the distribution of residual stresses in alloy AK4-1 drop forgings using an X-ray diffraction method. Their study indicated that the forging process introduces residual stresses in components. Also Appleton et al. (1987) studied the residual stress caused by the indentation phase of rotary forging by using an X-ray diffraction method.

Grit blasting of components as a preparation for surface cleaning is often the last process of hot forging before painting. Some concern has been expressed, however, that the grit blasting might impair the mechanical properties, particularly the fatigue strength. Myllymaki (1987) had carried out a series of tests to determine the effects of the grit blasting on aluminium alloys. Also X-ray diffraction was used to measure residual stresses on specimens with and without grit blasting. He concluded that the grit blasting did not have a significantly adverse effect on the fatigue strength of some materials and, indeed, had a beneficial effect with the very fine grit. The beneficial effect resulted from compressive residual stresses which were confirmed by X-ray measurements. Therefore the grit blasting may have a similar effect as shot peening which is commonly used process to induce compressive surface residual stresses and thereby improving the fatigue strength.

James (1982) obtained residual stress distribution using X-ray diffraction together with progressive etching of the surface for grit blasted Al 2219-T851 specimens. The profiles of the residual stresses showed maximum compressive residual stress (about -200 MPa) on the surface of the specimen and dropped rapidly to zero within 50 μm below the surface.

2.2 Residual Stress Measurements

Residual stresses exist in most of components and can be generated in almost every step of processing such as heat treatment (Beck & Ericsson, 1987; Mark, et al., 1987; Beck & Simon, 1987; Walker, 1981; Burnett, 1981), machining (Scholtes,

1987), welding (Wohlfahrt 1987; Kuznetsov, 1981), shot peening (Niku-Lari, 1982).

The residual stresses are classified as three different kinds of residual stresses, called residual stresses of the 1st, 2nd and 3rd kind (Macherauch, 1987). The 1st kind of residual stresses are macrostresses that are nearly homogeneous across large areas of a material and are in equilibrium over the bulk of the material. They extend over distances that are large relative to the grain size of the material and are of general interest in design and failure analysis. Macrostresses are tensor quantities, which magnitudes varying with direction at a single point in a body. When macrostresses are determined in three principal directions (or six stress components are obtained), the maximum and minimum residual stresses, the maximum shear stress and their orientation can be found. Macrostresses strain many crystals uniformly in the surface. This uniform distortion of the crystal lattice shifts the angular position of the diffraction peak selected for residual stress measurements

The 2nd kind of residual stresses are nearly homogeneous across microscopic areas and the 3rd kind residual stresses are inhomogeneous across submicroscopic areas. A combination of the 2nd and 3rd kinds of residual stresses are called microstresses and are resulted from imperfections in the crystal lattice. Microstresses are associated with strains within the crystal lattice that traverse distances on the order of or less than the dimensions of the crystals. Microstresses vary from point to point within the crystal lattice, altering the lattice spacing and broading the diffraction peak (Prevey, 1986).

Residual stress states in a material are always the combinations of macrostresses and microstresses. There is always influence of the 3rd kind residual stresses, even though the 1st kind residual stresses are removed by some method like annealing. Consequently, a residual stress free state can never be achieved.

There are various techniques that have been developed for measuring residual stresses. The X-ray diffraction and neutron diffraction have been widely used as non-destructive methods. The centre hole method is a semi-destructive method and has also been widely used. These three methods of measuring residual stresses have been employed to measure the residual stresses in hot forged components in this research. In the following a short review will be given on the three methods for determination of residual stresses concerning their principles, advantages and limitations.

2.2-1 X-ray diffraction technique

In real materials there are a number of atoms arranged in periodic planes called lattice planes. The planes can be denoted by Miller Indices (hkl). X-rays are invisible and travel in straight lines. Most of their properties are similar to visible light. In addition, X-rays penetrate materials opaque to visible light. When a X-ray beam, monochromated to a particular wavelength, λ, impinges on the atoms in the lattice planes, it is diffracted by crystalline materials whose lattice spacing is of the same order as the X-ray wavelength (Cullity, 1978). The British scientist W. L. Bragg in 1912 derived the relationship between diffraction angle and X-ray wavelength, which is called Bragg's law,

$$n\lambda = 2d\sin\theta \tag{2.1}$$

where n is an integer denoting the order of diffraction, λ is X-ray wavelength, d is the lattice spacing of crystal planes and θ is the diffraction angle as shown in Figure 2.1. Any change in the lattice spacing, d, results in a corresponding shift in the diffraction angle 2θ. In polycrystalline materials, the crystal planes are distributed in every direction as shown in Figure 2.2, where Q is a vector bisecting the incident beam and diffracted beam. For diffraction to occur Q must perpendicular to the lattice planes (diffracting planes). Therefore, the lattice spacing in any direction for the polycrystalline materials can be measured by the X-ray diffraction using Bragg's law. The lattice spacing in any direction may be denoted by $d_{\varphi\psi}$ where ϕ is the angle to which the surface stress σ_φ is related and ψ is a tilt angle measured from the normal direction of the surface. Then the strain in the direction defined by ϕ and ψ can be expressed in terms of changes in the linear dimensions of the crystal lattices

$$\varepsilon_{\varphi\psi} = \frac{d_{\varphi\psi} - d_0}{d_0} \tag{2.2}$$

where d_0 is the stress-free lattice spacing.

At the specimen surface, the stress state can be assumed to be biaxial. Based on elastic strain analysis, the strain $\varepsilon_{\varphi\psi}$ can be found as,

$$\varepsilon_{\varphi\psi} = \frac{1+\upsilon}{E}\sigma_\varphi \sin^2\psi - \frac{\upsilon}{E}(\sigma_1 + \sigma_2) \tag{2.3}$$

where E is Young's Modulus, ν is the Poisson's ratio, σ_1 and σ_2 are the two principal stresses on the surface plane and σ_φ is a normal stress within the surface plane with the angle being φ. Equation (2.3) is a form of the traditional X-ray residual stress equation and has been in use since 1925 (Noyan & Cohen, 1987). Combining Equations (2.2) and (2.3), then the lattice spacing for any orientation can be expressed as,

$$d_{\varphi\psi} = \left[\frac{1+\upsilon}{E}\sigma_\varphi d_0\right]\sin^2\psi - \frac{\upsilon}{E}(\sigma_1+\sigma_2)d_0 + d_0 \qquad (2.4)$$

Equation (2.4) describes the fundamental relationship between lattice spacing and the biaxial stresses in the surface of the specimen. From the Equation (2.4) it can be seen that the lattice spacing $d_{\varphi\psi}$ is a linear function of $\sin^2\psi$. If the lattice spacing is measured at two angles, the stress σ_φ can be determined from the slope of the line connected between the two points, in which the stress free lattice spacing d_0 is not sensitive and can be replaced by any lattice spacing $d_{\varphi\psi}$ that has been measured. This method is called the Two-Angle Technique and the two angles were normally taken as two extreme values, typically 0° and 45° (Hilley, 1971). When the lattice spacing is measured for multiple ψ tilts, a straight line can be fitted by least squares regression and the stress σ_φ is calculated from the slope of the best fit line. Again, the stress free lattice spacing d_0 is not sensitive and can be replaced by any lattice spacing $d_{\varphi\psi}$ measured. This technique is called "$\sin^2\psi$" technique (Hilley, 1971). There were also other similar techniques such as the Single Exposure Method in which the principle is the same (Hilley, 1971; Noyan & Cohen, 1987).

In highly texture materials, the anisotropic stress-strain Hook's law has to be considered. Therefore the relationship between strain $\varepsilon_{\varphi\psi}$ and stresses in surface plane would be different and more elastic constants related to the anisotropic behaviour should be involved. Marion and Cohen (1975) developed a technique in which an additional dependence of the lattice spacing on a texture distribution function $f(\psi)$ was introduced. This method requires simultaneous determination of the preferred orientation, or texture, in the specimen to determine the function $f(\psi)$. Along with the lattice spacing, all the parameters introduced are solved by multiple linear regression over the function $f(\psi)$ and $d_{\varphi\psi}$ as functions of $\sin^2\psi$.

There are restrictions and limitations associated with the X-ray measurements. Since X-ray wave lengths have only small depths of penetration into steel, the X-ray diffraction method is basically restricted to surface residual stress determination. The

irradiated area must be limited to an essentially flat region on the sample surface because the tilt angle ψ must be constant throughout the irradiated area. For a curved surface, such as round bar specimen, the tilt angle ψ is not constant and substantial error would be induced. Therefore a relatively small irradiated area is needed for the curve surface to reduce the error introduced by the curvature. Noyan and Cohen (1987) analysed the curvature influence. This curvature influence may prohibit X-ray diffraction from measuring residual stresses at notches and fillets where critical positions of specimen are located. The instrumental misalignment can also contribute to the measurement errors, such as sample displacement from the centre of the diffractometer, effect of ψ-axis not corresponding to the 2θ axis and missetting of true zero of the ψ-rotation. Noyan and Cohen (1987) have given a comprehensive discussion about these effects.

It is obvious that X-ray diffraction does not allow direct measurement at interior points of steel samples. Therefore a layer removal is necessary to let the X-ray reach the depth to take the measurements. Using mechanical methods, such as mechanical machining and polishing, to remove material will cause plastic deformation and introduce additional residual stresses. Therefore they were excluded (Prevey, 1986). Electropolishing and chemical etching processes have normally been used to remove surface layers. (Prevey, 1986; Noyan & Cohen, 1987; Ballard & Constantinescu, 1994). However, removal of material leads to stress relaxation which will result in inaccurate measurements of the interior residual stresses. Thus, the redistribution of residual stresses due to the removal of material has to be taken into account to modify the X-ray measurement results (Prevey, 1986; Noyan & Cohen, 1987; Ballard & Constantinescu, 1994). For the simple shapes such as flat plates or cylindrical bodies, closed-form solutions and calculation methods have been developed (Moore, et al., 1958; Sikarskie, 1967, Kang, et al., 1994; Ballard & Constantinescu, 1994). These corrections involve integration over the residual stresses measured in the layers removed from the exposed layer back to the original surface. The accuracy of these corrections depends on the depth of resolution over which the stress distribution is measured. Correction for layer removal can be combined with correction for sectioning to determine the total original state of the residual stresses.

2.2-2 Neutron diffraction technique

The methodology and analytical formalism for neutron diffraction is the same as X-ray diffraction. For the X-ray, the depth of penetration in most metals is limited to less than 100 μm (Stacey et al., 1985) and the diffraction takes place within a thin layer of about 20 μm (Noyan and Cohen, 1987) whereas the neutron can penetrate deeply into metals to about 30-40 mm (Allen, et al., 1985). Therefore X-ray diffraction can only be used non-destructively to measure residual stresses in near surface region and the neutron diffraction can be used to examine internal residual stresses within the bulk of materials.

The neutron diffraction measurement is over the volume of material sampled which is defined by intersection of the incident beam and diffracted beam. The size of volume can be controlled by using different neutron-absorbing cadmium masks. With Bragg's law used, the lattice spacing is measured in the direction that bisects the incoming beam and the diffracted beam. This measurement is an average value over the neutron volume (Allen, et al., 1985). The lattice spacing for the stress free d_0 must be known if the absolute strain is required. Inside the specimen, the stress state is generally in a 3D stress state and therefore unlike the X-ray diffraction method there is no simple way to obtain stress directly using the neutron diffraction. To obtain the full strain state requires at least six measurements in different directions. The stress components can be found by Hook's law, in which the macroscopic elastic constants can be used by using the effective diffraction elastic constants without the influence of texture (Allen, et al., 1985). If the material is isotropic the determination of the principal stresses from the principal strains can be obtained using (Smith, 1988)

$$\left.\begin{aligned}
\sigma_1 &= \frac{E}{(1+\nu)(1-2\nu)}[(1-\nu)\varepsilon_1 + \nu(\varepsilon_2+\varepsilon_3)] \\
\sigma_2 &= \frac{E}{(1+\nu)(1-2\nu)}[(1-\nu)\varepsilon_2 + \nu(\varepsilon_3+\varepsilon_1)] \\
\sigma_3 &= \frac{E}{(1+\nu)(1-2\nu)}[(1-\nu)\varepsilon_3 + \nu(\varepsilon_2+\varepsilon_1)]
\end{aligned}\right\}. \qquad (2.5)$$

where E and ν are the Young's Modulus and Poisson's ratio of the bulk material, respectively. If the sample is textured, the effects of crystalline anisotropy need to be considered (Sayers, 1984; Allen, et al., 1985).

To obtain the absolute lattice strain, a knowledge of either the lattice spacing d_0 or the scattering peak angle $2\theta_0$ of the unstressed materials is necessary. Actually, for the d_0 and $2\theta_0$, if one is known, the other can be found using Bragg's equation. However, Buttle and Hutchings (1992) pointed out that obtaining true values of d_0 or $2\theta_0$ may prove difficult in practice. They suggested that a small annealed sample with measurements made in several orientations and averaged, or at an extreme part of a component, may be taken to be in zero strain. A simple way to find d_0 is to measure on a small cube that is extracted from specimen (Smith, et. al, 1988 & 1992) where it is judged to be 'stress free'. Webster et al. (1995) presented an alternative method of determining d_0 in which an approximate value of d_0 is assumed and the strains and stresses are calculated using the lattice spacing measured. Then d_0 is adjusted by iteration until various line integrals of stress balance to zero. Prask et al. (1987) pointed out that a precise value for the unstressed lattice spacing d_0 was essential since the determination of residual stress depended on measurement of strain values. For a cylindrical geometry, the equilibrium conditions are fulfilled,

$$\left.\begin{aligned} \int \sigma_{zz} r dr d\theta = 0 \\ \int \sigma_{\theta\theta} dr dz = 0 \end{aligned}\right\} \tag{2.6}$$

by adjusting the d_0.

The X-ray diffraction measurement does not require accurate unstressed lattice spacing d_0 whereas it is important to neutron diffraction measurements. The unstressed lattice spacing d_0 can be affected by many factors, such as heat treatment (Noyan and Cohen, 1987), prior plastic strains (Smith & Webster, 1996) and compositional change (Webster et al., 1995). In many cases, the composition near the specimen surface can be different from that of the interior. Large changes in peak angle occur in steel for the (211) reflection have been observed.

In the neutron diffraction measurement, the neutron gauge volume is confined to within the sample and all measurements in the literature are well away from the sample surface (Smith et al., 1992; Rudkins, et al., 1994; Lorentzen and Ibsø, 1995). Lorentzen (1995) found that when the neutron gauge volume was moved out of the sample to obtain residual stress close to the sample surface, unrealistic values were obtained and the calculated residual stresses were much higher than the yield stress of the material. There is no literature found to discuss this particular problem.

2.2-3 Centre hole method

The centre hole method has been widely used as a semi-destructive technique for measuring residual stresses. This method consists of drilling a small hole in the material and measuring the resulting change in strain on the surface in the vicinity of the hole. The measurement of these strains due to stress relaxation gives the necessary data for calculating the original residual stresses at the hole area. Its popularity stems largely from its ease of use in many different applications and materials, its limited damage to the specimen, and its general reliability (Schajer, 1988).

In general the residual stresses in a sample are a function of location. Because the diameter of the hole drilled is very small compared with the dimension of the sample, the residual stresses have been treated as being uniform in the hole area but not through the depth.

For the conventional one step method, the residual stresses are assumed to be uniform with depth (Mathar, 1934; Rendler, et. al, 1966; ASTM Standard, 1985; Measurement Group, 1986). In this case the stress state is plane stress, which can be expressed by two principal stresses, σ_{max} and σ_{min}, and the direction of principal stress, α. After the hole is drilled, the hole surface traction related to the plane stress state is removed and radial strain change due to the removal can be expressed as (Rendler & Vigness, 1966),

$$\varepsilon_r = A(\sigma_{max} + \sigma_{min}) + B(\sigma_{max} - \sigma_{min})\cos 2\alpha \qquad (2.7)$$

where A and B are constants related to the material and geometry of strain gauge used. Equation (2.7) can be proved theoretically for a linear elastic isotropic material (Schajer, 1988). Normally, the specifically designed strain gauge rosette for the centre hole residual stress measurement has three strain gauges in three different directions, say 0°, 45° and 90° (Technical Note, Measurement Group, 1986). The measured data from the three strains are sufficient to calculate the stresses and direction using the Equation (2.7).

The coefficients A and B can be obtained by using experimental calibration (Bathgate, 1968; Bijak-Zochowski, 1978; ASTM Standard E837-85) which involves measuring the rosette strains under the same applied load or calibration stress both

before and after drilling the hole. This procedure eliminates the effect of the initial residual stress in the calibration specimen and is particularly attractive since it automatically accounts for the mechanical properties of the test material, strain gauge rosette geometry, hole depth and diameter, and the strain-averaging effect of the strain gauge grid. The drawback of it is that the coefficients obtained using this procedure are strictly applicable only for residual stress measurement conditions which exactly match the calibration conditions. The coefficients A and B can be also found by using finite element analysis as long as the material elastic constants, hole geometry and location of strain gauges are given (Rendler & Vigness, 1966; Schajer, 1981; Redner & Perry, 1982).

In order to make common use of finite element results, Schajer (1981) introduced two non-dimensionalised coefficients

$$\left.\begin{aligned} \bar{a} &= \frac{2E}{1+\nu}A \\ \bar{b} &= 2EB \end{aligned}\right\} \tag{2.8}$$

in which, based on the analytical results from through hole analysis, $\bar{a}$ was considered to be material-independent and $\bar{b}$ weakly dependent of Poisson's ratio. Schajer (1981) obtained partial-depth coefficients using finite element analyses and found $\bar{a}$ and $\bar{b}$ vary by less than 2% for the range of Poisson's ratio from 0.25 to 0.35. Nickola (1986) calculated these coefficients for different values of the dimension ratio, D/D_0, where D is strain rosette diameter and D_0 is the hole diameter.

One may think of the residual stresses obtained using the conventional one step method as representing weighted average values over a certain depth. In the case of the residual stresses varying with depth, the calculated residual stresses are always lower than the actual maximum.

To consider non-uniform residual stresses, Soete and Vancrombrugge (1950) and Kelsey (1956) developed an incremental strain method in which the strain relaxation after successive small increments of hole depth were measured and the stresses originally existing within each hole depth increment were calculated. In these methods it was assumed that the incremental strain relaxation was wholly due to the stresses existing within that depth increment. Equation (2.7) was used and the A and B were treated as functions of depth. These A and B values for different hole depth

were calibrated experimentally. Obviously, the assumption in this incremental strain method is not true because the stresses within the new depth increment are redistributed due to previous increments. The subsequent strain relaxation is not only by the stresses existing within that depth increment, but also by the stresses caused by previous drilling increments.

Nickola (1986) introduced a stress calculation method using the concept of equivalent uniform stress, called an average stress method. For any given depth z and $z + \Delta z$, the uniform stresses σ_z and $\sigma_{z+\Delta z}$ were calculated, respectively, using the conventional one step method but A and B varied with depth. Then the following balance was considered,

$$\sigma_{z+\Delta z}(z + \Delta z) = \sigma_z z + \sigma_{\Delta z} \Delta z \tag{2.9}$$

to obtain stress $\sigma_{\Delta z}$ at the region Δz. This method lacks theoretical basis and has a significant shortcoming (Schajer, 1988) and may be regarded as an approximate engineering method.

Schajer (1981) developed a power series method in which the strain relaxation was calculated using finite element method for different stress fields with power series variations with depth z, i.e., 1, z, z^2, etc. These strain responses were then used as basis functions in a least-squares analysis of the measured strain relaxation. In this way, the measured strains were decomposed into components corresponding to the power series stress fields. The actual stress field is then reconstructed by summing the stress fields corresponding to the individual strain relaxation components.

A more mathematically rigorous expression for the strain relaxation against residual stress and drilling depth was given by Bijak-Zochowski (1978),

$$\varepsilon(H) = \frac{1+\nu}{E} \int_0^H \hat{A}(z, H)\sigma(z)dz \qquad 0 \le z \le H \tag{2.10}$$

where $\hat{A}(z, H)$ is strain relax function. Theoretically, the residual stress distribution $\sigma(z)$ can be determined if the $\hat{A}(z, H)$ is known and strain relaxation $\varepsilon(H)$ is measured. But the strain function $\hat{A}(z, H)$ could not be determined either analytically or experimentally.

Niku-Lari and Flavenot (1985), Flaman and Manning (1985) and Schajer (1988) used a step-wise-constant distribution to replace actual residual stress distribution. Simultaneous equations were obtained

$$\sum_{j=1}^{j=i} \bar{a}_{ij}\sigma_j = \frac{E}{1+\upsilon}\varepsilon_i \qquad 1 \le j \le i \le n \tag{2.11}$$

where ε_i is the measured strain relaxation after the ith hole depth increment, σ_j is the equivalent uniform stress within the jth hole depth increment, $\bar{a}_{ij}$ is the strain relaxation due to a unit stress within increment j of a hole i increment deep and n is total number of hole depth increments. The coefficients $\bar{a}_{ij}$ are material and hole geometry dependent and had been determined numerically using finite element method.

After the hole is drilled to a certain depth z, say $z/D => 0.5$ where D is the average diameter of strain gauge rosette, stresses in the following increments have very little effect on strain relaxation. Therefore, for the best results from the incremental hole drilling, there should be a limitation in the hole depth which is reported to be about $z/D \approx 0.15 - 0.2$ (Kelsey, 1956, Schajer, 1988).

Because all stress results have been calculated from measured strain relaxation using elasticity, any plastic deformation during hole drilling may induce significant error in stress results. The drilling operation itself does cause plastic deformation around the hole surface. Many investigators have thoroughly studied the influence of different drilling techniques. The effects were generally small (Rendler & Vigness, 1966; Beaney & Procter, 1974; Beaney, 1978). For the ultra high-speed drilling using an air turbine, it had been shown that there was little influence on the residual stresses (Flaman, 1982, Niku-Lari & Flavenot, 1985).

Plastic deformation may also be induced after the hole is drilled if the magnitude of the redistributed stresses around the hole exceeds the yield strength of material. For the extreme case of uniaxial stress state, the stress concentration factor is 3. Therefore, if the residual stresses are larger than one third of yield strength, some plastic yielding will take place theoretically (Nawwar, et al, 1976; Lin & Chou, 1995). For equal biaxial stress state, the elastic limit is about half of the yield strength (Beghini, et al., 1995). Many investigators have studied the local yielding around the hole on residual stress results both experimentally and numerically. From the experimental results, the influence of plasticity is negligible when the residual

stress is less than 65-70% of the yield strength (Bynum, 1982; Nickola, 1984; Lin & Chou, 1995). For a through hole in a thin plate the potential error caused by the plastic deformation could reach 30% for residual stress near to 75% of yield strength (Nawwar, et al., 1976). Beghini et al. (1994) analysed through-hole with different biaxial stress state and linear hardening plastic material using finite element method. In the case of elastic-perfectly plastic material, Beghini's numerical results showed that the error could reach 140% for residual stress about 90% of the yield strength. For a blind hole, Lin & Chou (1995) tested specimens made from different materials and showed that the error was about 5-12% for the residual stress being 75% of the yield strength and 32-47% error for the residual stress about 95% of the yield strength. In fact, it is possible and quite reasonable that elastic behaviour of unyielded material, existing below blind-holes, can and would retard the plastic zone growth. This restraining plastic zone is non-existent for through-hole applications and the yield zone around the hole can experience a more rapid growth resulting in higher error caused by the plastic deformation (Nickola, 1984).

All theories and applications of the centre-hole method so far have been under the condition that the specimen surface is flat. Apparently, for specimens with curved surface, such as cylinder or bars, the effect of curvature has been ignored and any analyses for flat surfaces have been applied. No work has been found about the influence of curvature on residual stresses, especially for round bar specimens. A new method is needed however for applying the hole-drilling method to components with curved surfaces if there is significant curvature.

2.3 Theories of Multiaxial Fatigue

Fatigue damage in components may be classified into different stages, which include nucleation of micro defects, initiation of the crack, crack growth and fracture. These also can be roughly divided into two stages: crack initiation and crack growth. The total fatigue life is the sum of the number cycles to initiate a fatigue crack and the number of cycles to propagate it subcritically to some final crack size which will lead to failure. Since the crack initiation life constitutes a major component of fatigue life in smooth specimens (which may be up to 90% of the total fatigue life), the multiaxial fatigue theories represent, in many cases, design against fatigue crack initiation. For high cycle fatigue, which is normally in low stress situations, the deformation is primarily in the elastic regime. Stress-based criteria are consequently more suitable in predicting the high cycle fatigue failure (Krempl, 1974). For low

cycle fatigue, the stresses are generally high enough to cause appreciable plastic deformation prior to failure. Strain-based approaches are used in connection with the low cycle fatigue. To consider the interaction between the stress and strain in fatigue cycles, energy-based criteria have also been proposed (Sines & Ohgi, 1981; Lefebvre, et al., 1981; Garud, 1981; Ellyin, 1988).

2.3-1 Stress-Based Criteria

Stress-based criteria are normally used for high cycle fatigue, for which the fatigue life N is taken as being infinite. In reality, a fatigue life in excess of 10^7 or 10^8 is considered as an infinite life.

In the case of combined bending and torsion, two empirical relations had been developed (Gough, et al., 1951)

$$\left(\frac{\tau}{\tau_F}\right)^2+\left(\frac{\sigma}{\sigma_F}\right)^2=1 \tag{2.12}$$

for ductile materials and

$$\left.\begin{aligned}\left(\frac{\tau}{\tau_F}\right)^2+(t-1)\left(\frac{\sigma}{\sigma_F}\right)^2+(2-t)\left(\frac{\sigma}{\sigma_F}\right)=1\\ t=\sigma_F/\tau_F\end{aligned}\right\} \tag{2.13}$$

for brittle materials, where

σ = fatigue amplitude of normal stress of bending

τ = fatigue amplitude of shear stress of torsion

σ_F = fatigue endurance limit for normal stress

τ_F = fatigue endurance limit for shear stress

The above empirical formula can't be extended to general stress states.

The fatigue failure criteria are similar to strength theories and can be classified as maximum principal stress, equivalent stress (Von Mises) and maximum shear stress (Tresca) criteria. For brittle materials the maximum principal stress failure criterion is appropriate

$$\sigma_1/\sigma_F=1 \tag{2.14}$$

The equivalent stress criterion may be expressed as (Stanfield, 1935)

$$\beta\sqrt{(\sigma_1-\sigma_2)^2+(\sigma_2-\sigma_3)^2+(\sigma_3-\sigma_1)^2}=\sigma_F \qquad (2.15)$$

in which β is an experimental parameter which depends upon the particular material and a given cyclic life and

$\sigma_1,\sigma_2,\sigma_3$ = fatigue amplitude of principal stresses with $\sigma_1 \geq \sigma_2 \geq \sigma_3$

Maximum shear stress is regarded as the key factor in material failure and many theories have been based on this idea. The normal stress σ_n on the plane of maximum shear stress has also been considered as having an influence on material fatigue failure. Ellyin (1988) pointed out that many failure criteria proposed by several investigators (Stanfield, 1935; Findly, 1957; McDiarmid, 1974) can be expressed as general form

$$\tau_{max}+f(\sigma_n)=0 \qquad (2.16)$$

where

σ_n = amplitude of normal stress on maximum shear stress plane.

The classical approach to fatigue has focused on the S-N diagram which relates fatigue life (cycles to failure, N) to cyclic stress amplitude, S_a. The classical model is the Basquin equation (1910),

$$NS_a^m=C \qquad (2.17)$$

where C and m are empirical constants. For multiaxial stress cases the stress amplitude in the design can be used as maximum principal stress amplitude $\sigma_{1,a}$, or Von Mises stress amplitude $\sigma_{eq,a}$, or maximum shear stress amplitude $\tau_{max,a}$.

2.3-2 Strain-Based Criteria

Early investigators, who studied low cycle fatigue using strain-controlled test, were generally concerned with a uniaxial stress state. This leads to the development of different fatigue laws.

A strain range-cycles to failure model proposed by Langer (1962) for low cycle fatigue was,

$$\left.\begin{aligned} S_a &= BN^{-1/2} + S_e \\ S_a &= \frac{1}{2} E\Delta\varepsilon \end{aligned}\right\} \tag{2.18}$$

where B and S_e are empirical constants and $\Delta\varepsilon$ is the strain range. Only in the linear elastic range, S_a is the actual stress amplitude. Langer's law has been used to develop design curves in the American Society of Mechanical Engineering Boiler and Pressure Vessel Code.

The widely used Manson-Coffin relationship which includes low cyclic fatigue (Manson, 1962; Tavernelli & Coffin, 1962) is

$$\left.\begin{aligned} \frac{\Delta\varepsilon^e}{2} &= \frac{\sigma'_f}{E}(2N_f)^b \\ \frac{\Delta\varepsilon^p}{2} &= \varepsilon'_f(2N_f)^c \\ \frac{\varepsilon}{2} &= \frac{\Delta\varepsilon^e}{2} + \frac{\Delta\varepsilon^p}{2} = \frac{\sigma'_f}{E}(2N_f)^b + \varepsilon'_f(2N_f)^c \end{aligned}\right\} \tag{2.19}$$

in which the prefix Δ in front of a variable refers to its total range, superscript e and p refer to the elastic and plastic component, respectively, and

σ'_f = material strength coefficients
ε'_f = material ductility coefficients.

The exponents b and c are found from regression of the test data. The Manson-Coffin relationship was then extended to the multiaxial stress state by defining a suitable equivalent strain measure. This equivalent strain measure can be determined from several different parameters:

i) maximum normal strain (Libertiny, 1967),

$$\Delta\varepsilon_1 = kN_f^c \tag{2.20}$$

where k is a constant found from the best fit to the test data,

ii) maximum total strain (Zamrik & Fishmuth, 1973),

$$\left.\begin{aligned} \Delta\varepsilon'_{\max} &= kN_f^c \\ \varepsilon'_{\max} &= Max\sqrt{\varepsilon_1^2+\varepsilon_2^2+\varepsilon_3^2} \end{aligned}\right\} \qquad (2.21)$$

where

$\varepsilon_1, \varepsilon_2, \varepsilon_3$ = principal strains with $\varepsilon_1 \geq \varepsilon_2 \geq \varepsilon_3$

iii) Von Mises or octahedral equivalent strain (Sines & Ohgi, 1981; Pascoe & DeVilliers, 1967),

$$\left.\begin{aligned} \Delta\varepsilon_{eq} &= kN_f^c \\ \varepsilon_{eq} &= \beta\sqrt{(\varepsilon_1-\varepsilon_2)^2+(\varepsilon_2-\varepsilon_3)^2+(\varepsilon_3-\varepsilon_1)^2} \end{aligned}\right\} \qquad (2.22)$$

where β is related to the elastic-plastic Poisson's ratio.

iv) Von Mises's or octahedral equivalent plastic strain (Andrews & Ellison, 1973; Zamrik & Goto, 1968),

$$\left.\begin{aligned} \Delta\varepsilon^p_{eq} &= kN_f^c \\ \varepsilon^p_{eq} &= \frac{\sqrt{2}}{3}\sqrt{(\varepsilon_1^p)^2+(\varepsilon_2^p)^2+(\varepsilon_3^p)^2} \end{aligned}\right\} \qquad (2.23)$$

$$\left.\begin{aligned} \Delta\gamma^p_{oct} &= kN_f^c \\ \gamma^p_{oct} &= \frac{\sqrt{2}}{3}\sqrt{(\varepsilon_1^p)^2+(\varepsilon_2^p)^2+(\varepsilon_3^p)^2} \end{aligned}\right\} \qquad (2.24)$$

Many investigators suggested that fatigue failure resulted from slip during yielding along critically orientated planes. The slip process is primarily shear driven which implies that the maximum shear strain plays a key role. Failure criteria, based on the maximum shear strain or shear plastic strain, are in the form (Ellyin, 1988),

$$\left.\begin{aligned} \Delta\gamma_{\max} &= kN_f^c \\ \gamma_{\max} &= \varepsilon_1-\varepsilon_2 \end{aligned}\right\} \qquad (2.25)$$

$$\left.\begin{aligned} \Delta\gamma^{p}_{\max} &= kN_f^{c} \\ \gamma^{p}_{\max} &= \varepsilon_1^{p} - \varepsilon_3^{p} \end{aligned}\right\}. \tag{2.26}$$

Brown and Miller (1973) introduced a theory in which they suggested that the normal strain ε_n on the maximum shear strain plane was also a factor leading to fatigue failure. A function relating the two strains is given by,

$$\left.\begin{aligned} \gamma_{\max} &= f(\varepsilon_n) \\ \gamma_{\max} &= \varepsilon_1 - \varepsilon_3 \\ \varepsilon_n &= \frac{1}{2}(\varepsilon_1 + \varepsilon_3) \end{aligned}\right\} \tag{2.27}$$

in which function f can be made to vary with life. The Brown-Miller theory was modified by Lohr and Ellision (1980). It was argued that the biaxial fatigue failure was predominantly controlled by the shear strain acting in a through-thickness direction and not the maximum strain. In terms of the Brown-Miller function this was described as:

$$\left.\begin{aligned} \gamma^{*} &= f(\varepsilon_n^{*}) \\ \gamma^{*} &= \varepsilon_1 - \varepsilon_r \\ \varepsilon_n^{*} &= \frac{1}{2}(\varepsilon_1 + \varepsilon_r) \end{aligned}\right\} \tag{2.28}$$

in which γ^{*} is maximum shear strain on a plane-inclined 45° to the surface, ε_n^{*} is the normal strain on the γ^{*} plane and ε_r is normal strain on the surface. The Lohr-Ellison theory is subject to the condition that $\varepsilon_r \neq \varepsilon_1$ and the surface is under biaxial stress state. There are two cases for the Lohr-Ellison theory: case A is where $\varepsilon_r = \varepsilon_2$ which leads to $\gamma^{*} < \gamma_{\max}$; case B is where $\varepsilon_r = \varepsilon_3$ which leads to $\gamma^{*} = \gamma_{\max}$. For the case B the Lohr-Ellison theory is identical to the Brown-Miller criterion. There is substantial data to support the Lohr-Ellison theory (Socie & Waill, 1974; Shatil, 1990). Lefebvre (1985) thought that the tensile strain parameter $(\varepsilon_1 + \varepsilon_3)$ did not result in a good correlation of biaxial fatigue data for case A and suggested to use volumetric strain instead. This criterion is as follows,

$$\frac{\gamma_{\max}}{2} + b\varepsilon_s = c \tag{2.29}$$

where

$$\varepsilon_s = \begin{cases} \dfrac{\varepsilon_1 + \varepsilon_2}{2} & \textit{for case A} \\ \varepsilon_1 + \varepsilon_2 + \varepsilon_3 & \textit{for case B} \end{cases} \tag{2.30}$$

and b, c are constants related to material. Makinde (1989) proposed a general criterion based on the contours of constant fatigue life on a plot of maximum shear strain against the tensile strain acting normal to the plane of maximum shear strain.

2.3-3 Energy-Based Criteria

In the stress-based or strain-based criteria described above, either a stress range or strain range is chosen as a main parameter This implies that the interaction between stress and strain and strain history during fatigue process in terms of the stress-strain response of the material is not accounted for. For low cycle fatigue, the cyclic plastic deformation is generally believed to involve and depend on the loading path and strain history especially for nonproportional loading. An energy-based criteria may be used to overcome these shortcomings.

A total strain energy or plastic strain energy was proposed (Ellyin, 1974),

$$\Delta\sigma_{eq}\Delta\varepsilon_{eq} = kN_f^c \tag{2.31}$$

$$\Delta\sigma_{eq}\Delta\varepsilon_{eq}^p = k'N_f^c \tag{2.32}$$

in which the equivalent stress and strain are based on the Von Mises's criterion and k, k' are material constants. Garud (1981) proposed an approach which relates fatigue life to the plastic work per cycle W^p,

$$\Delta W^p = \int_{cycle} \sigma_{ij}\, d\varepsilon_{ij}^p = \sum_{cycle} \sigma_{ij}\, \Delta\varepsilon_{ij}^p \tag{2.33}$$

where σ_{ij} is the stress tensor and $d\varepsilon_{ij}^p$ is plastic strain increment tensor. The criterion was represented in the form of a power-law,

$$N_f = (\Delta W^p)^{\alpha} \tag{2.34}$$

where α is a material constant. Ellyin [Ellyin, 1988; Ellyin & Golos, 1988) derived a failure criterion,

$$\Delta W^t = kN_f^{\alpha} + c \tag{2.35}$$

which is based on the total strain energy density per cycle with a modification to consider the fact that superposed hydrostatic tension decreases the fatigue life and the compression increases it. Ellyin suggests,

$$\Delta W^t = [1 + H(\rho)]\Delta W^e + \Delta W^p \tag{2.36}$$

where

$$\Delta W^e = \int_{cycle} \sigma_{ij}\, d\varepsilon_{ij}^e \tag{2.37}$$

and

$$H(\rho) = \begin{cases} 1 & \rho \geq 0 \\ 0 & \rho < 0 \end{cases} \qquad \left(\rho = \frac{\varepsilon_2}{\varepsilon_1 - \varepsilon_3}\right). \tag{2.38}$$

A Ramberg-Osgood relationship was adopted for the specially designed stress-strain curve, called a master curve, to calculate the strain energy.

2.3-4 Effect of Mean Stress

Fully reversed fatigue stress cycles are not always representative of many engineering conditions. The stress state in the fatigue component often consists of a cycling stress and a superimposed mean stress. Figure 2.3 shows a fatigue cycle with a non zero mean stress in which the definitions are as follows:

$$\left.\begin{aligned} \textit{stress range:}\quad & \Delta\sigma = \sigma_{max} - \sigma_{min} \\ \textit{stress amplitude:}\quad & \sigma_a = (\sigma_{max} - \sigma_{min})/2 \\ \textit{mean stress:}\quad & \sigma_m = (\sigma_{max} + \sigma_{min})/2 \end{aligned}\right\} \tag{2.39}$$

The mean stress is also characterised in terms of the stress ratio

$$R = \frac{\sigma_{min}}{\sigma_{max}} \tag{2.40}$$

It is believed that the mean level of the imposed fatigue cycle plays an important role in influencing the fatigue behaviour of engineering materials. Experimental data shows that the mean stress is the second most important parameter after the stress range or strain range (Glinka, 1990). The residual stresses can be regarded as an example of superimposed mean stress.

Early work to consider the mean stress effect was mainly based on using empirical formulae, such as that for reversed torsion and static tension, given by (Dieter, 1988),

$$\left(\frac{\tau}{\tau_F}\right)^2 + \left(\frac{\sigma_m}{\sigma_u}\right)^2 = 1 \tag{2.41}$$

where σ_m is static tensile stress and σ_u the ultimate tensile stress and for reverse tension and static torsion by (Suresh, 1992),

$$\left(\frac{\sigma}{\sigma_F}\right)^2 + \left(\frac{\tau_m}{\tau_u}\right)^2 = 1 \tag{2.42}$$

where τ_m is static torsional stress and τ_u is the ultimate torsional stress. These two empirical formulae have no potential to be extended to other loading cases or stress states.

In the $\sigma_a - \sigma_m$ plane, there may exist constant fatigue life contours as shown in Figure 2.4. These may be expressed as

$$F(\sigma_m, \sigma_a, N_f) = 0 \tag{2.43}$$

satisfying the conditions

$$F(0, \sigma_f, N_f) = 0 \tag{2.44}$$

where σ_f is defined as the fatigue strength corresponding to fully reversed loading ($R = -1$) with a fixed fatigue life N_f and

$$F(\sigma_u, 0, N_f) = 0 \tag{2.45}$$

with the consideration that the ultimate tensile stress σ_u is the static failure strength ($R = 1$) or

$$F(\sigma_y, 0, N_f) = 0 \tag{2.46}$$

with the alternate consideration that the yielding stress σ_y is the static failure strength of the material. Many simplifications of the function F( ) have been made by many investigators. Among these, well known diagrams are those due to Goodman (1899), Gerber (1874) and Soderberg (1939) (Dieter, 1988):

i) Goodman's relation

$$\frac{\sigma_a}{\sigma_f} + \frac{\sigma_m}{\sigma_u} = 1 \tag{2.47}$$

ii) Gerber's relation

$$\frac{\sigma_a}{\sigma_f} + \left(\frac{\sigma_m}{\sigma_u}\right)^2 = 1 \tag{2.48}$$

iii) Soderberg's relation

$$\frac{\sigma_a}{\sigma_f} + \frac{\sigma_m}{\sigma_y} = 1. \tag{2.49}$$

The above diagrams are also shown in Figure 2.4. It was concluded that Soderberg's equation (2.49) provides a conservative estimate of fatigue life for most engineering alloys; Goodman's equation (2.47) matches experimental observations quite closely for brittle metals, but is very conservative for ductile alloys and Gerber's equation (2.48) is generally good for ductile alloys (Suresh, 1992). Because few test data exist for conditions where the mean stress is compressive and the fact that compressive residual stress (leading to compressive mean stress) increases the fatigue limit, it is dubious that the above diagrams could be used for the case of compressive mean stress. Some test results (Ransom, 1954) indicate that the allowable stress range increases with increasing compressive mean stress up to yielding stress in compression. Haigh diagrams (Flavenot, 1989), shown in Figure 2.5, may be better

than others for the case of compressive mean stress. The Haigh diagram is similar to the Goodman diagram and is a modification of it for high tension and compression mean stress ranges.

Unfortunately these fatigue charts only consider a simple uniaxial stress state. However, there also exist biaxial or triaxial stress states. A general criterion is needed for these cases. Earlier work on uniaxial stress state was extended to general cases by combining with multiaxial fatigue theories. Kiocecioglu (Kiocecioglu, 1975) suggested an extrapolation of Von Mises' criterion of plasticity to the fatigue limit under multiaxial stress state. The equivalent stress amplitude and mean stress are calculated in the usual fashion as,

$$\sigma_{eq,a} = \frac{1}{\sqrt{2}}\sqrt{(\sigma_{1a}-\sigma_{2a})^2+(\sigma_{2a}-\sigma_{3a})^2+(\sigma_{3a}-\sigma_{1a})^2} \tag{2.50}$$

$$\sigma_{eq,m} = \frac{1}{\sqrt{2}}\sqrt{(\sigma_{1m}-\sigma_{2m})^2+(\sigma_{2m}-\sigma_{3m})^2+(\sigma_{3m}-\sigma_{1m})^2}\,. \tag{2.51}$$

Sines (1981) suggested that the effect of the hydrostatic mean pressure P_m can be taken into account using

$$\left.\begin{aligned}\tau_{oct}+\alpha P_m &= \beta \\ P_m &= \frac{1}{3}(\sigma_{1m}+\sigma_{2m}+\sigma_{3m})\end{aligned}\right\} \tag{2.52}$$

where τ_{oct} is the amplitude of octahedral shear stress and α and β are the material constants. If the Von Mises equivalent stress is considered, Equation (2.52) can be changed to

$$\sigma_{eq}+\alpha' P_m = \beta'. \tag{2.53}$$

where α' and β' are material constants as well. Crossland (1956) considered maximum stress instead of mean stress in a criterion similar to Sines'

$$\tau_{oct}+\alpha\sigma_{oct,\max} = \beta. \tag{2.54}$$

If, as previously, the Von Mises equivalent stress and hydrostatic pressure, P_m, are used, the above criterion becomes

$$\left.\begin{aligned} \sigma_{eq} + \alpha' P_{\max} &= \beta' \\ P_{\max} &= \frac{1}{3}(\sigma_1 + \sigma_2 + \sigma_3)_{\max} \end{aligned}\right\}. \tag{2.55}$$

There are small differences between the Sines' and Crossland's criteria and they seemed to agree well with the results obtained by experiment (Flavenot & Skalli, 1989).

To consider shear stress on the plane of maximum shear as the main parameters, Findley (1959) and Matake (1980) proposed a criterion of the form

$$\tau + \alpha \sigma_{n,\max} = \beta \tag{2.56}$$

where $\sigma_{n,\max}$ is the maximum normal stress acting on the plane. Dang Van (1973) considered maximum hydrostatic pressure $P_{\max}$ instead of $\sigma_{n,\max}$ and suggested a criterion of the form,

$$\tau + \alpha P_{\max} = \beta \tag{2.57}$$

which is again similar to both Crossland's and Sines' criteria.

Morrow (1965) proposed that the fatigue life under mean stress effects can be estimated from the expression,

$$\sigma = (\sigma_f - \sigma_m)(2N_f)^b \tag{2.58}$$

The Manson-Coffin relationship (2.19) can then be changed to (Morrow, 1968),

$$\left.\begin{aligned} \frac{\Delta\varepsilon^e}{2} &= \frac{\sigma_f - \sigma_m}{E}(2N_f)^b \\ \frac{\Delta\varepsilon^p}{2} &= \varepsilon_f (2N_f)^c \\ \frac{\varepsilon}{2} &= \frac{\Delta\varepsilon^e}{2} + \frac{\Delta\varepsilon^p}{2} = \frac{\sigma_f - \sigma_m}{E}(2N_f)^b + \varepsilon_f (2N_f)^c \end{aligned}\right\} \tag{2.59}$$

Based on experimental data, Smith et al. (1970) proposed that, for a given life, $\sigma_a \varepsilon_a$ for a fully reversed cyclic fatigue test was equal to $\sigma_{\max} \varepsilon_a$ for a test having a mean stress. The general expression can be written as

$$\sigma_{max}\varepsilon_a = A_1 N_f^{a_1} + A_2 N_f^{a_2} \tag{2.60}$$

where A_1, A_2, a_1 and a_2 are material constants.

Lorenzo and Laird (1984) proposed an approach to predict fatigue life behaviour under the action of mean stress effect. The life data could be described adequately by the Coffin-Manson law. This approach was based on the observation of fatigue data under mean stress. The cyclic response under mean stress was closely correlated with that under zero mean stress.

It has been shown there are many fatigue failure criteria for multiaxial stress states. The existence of so many proposals in itself is an indication of the lack of agreement on an acceptable theory. Multiaxial stress tests are difficult to perform, and reliable data are very limited (Ellyin, 1988).

2.4 Residual Stress Effects on Fatigue Life

There is little doubt that residual stresses exist in engineering components. These may be induced from manufacturing processes or mechanical loading. They play an important role in integrity and reliability of components and their design optimisation (Macherauch, 1987). Compressive residual stresses induced by surface treatments such as shot peening and shot blasting appear to increase the fatigue strength of components. Conversely tensile residual stresses which often exist in welded and forged components decrease the fatigue strength of the components.

Residual stresses are most effective if they are of the opposite sign to the operating stresses, i.e. tensile residual and compressive operating stresses or compressive residual and tensile operating stresses (Glinka, 1990).

The beneficial effect of compressive residual stresses on fatigue life is often used for improving fatigue performance of components. The shot peening process, which produces surface compressive residual stress, has been used for prelongating fatigue life of components subjected to cyclic loading (Meguid & Chee, 1983). This technique is most effective in the long fatigue life range corresponding to low stress amplitudes. It is also known that this beneficial effect is most distinct under tension cyclic load.

If the residual stresses σ_R, combined with applied mechanical stresses, are in the elastic range, the residual stress field can be considered not to change during mechanical loading and the theory of superposition can be applied. Therefore, the normal way to consider the effect of the residual stresses in fatigue is by using the Haigh or Goodman charts shown in Figure 2.4 and Figure 2.5, in which σ_m, the mean stress in a fatigue cycle, is replaced by the combined mechanical and residual stress $\sigma_m + \sigma_R$ (Flavenot & Skalli, 1989; Glinka, 1990). Then criteria which consider mean stress effects in Equations (2.39-2.58) may be chosen. Numerous test results had been treated using the following relationship,

$$\sigma_a = \sigma_f - \alpha(\sigma_m + \sigma_R) \tag{2.61}$$

for constant fatigue life where α is a constant (Flavenot, 1989). Morrow's relationship (2.59) incorporating residual stress as a mean stress influence has been used widely by many investigators (Lawrence, et al., 1981; Glinka, 1990; Suresh, 1992; Kandarpa, et al., 1996). Lawrence et al. (1981) used the Morrow's relationship (2.59) to estimate crack initiation lives of 10^5 or greater, which corresponds to the high cyclic fatigue range.

2.5 Residual Stress Relaxation Due to Fatigue Loading

It is well accepted that the residual stress state may not be stable during fatigue. The influence of compressive residual stresses in increasing fatigue life is recognized to be highly dependent on stress stability, since relaxation may take place early in the fatigue (James, 1987). The effect of residual stresses decreases with increasing stress amplitude and number of cycles as a result of residual stress relaxation (Jhansale & Topper 1973; James & Morris, 1981; James, 1982).

In many cases, residual stresses relax and redistribute during cyclic loading especially in soft materials because of the Bauschinger effect and cycle softening (Sarkani & Lutes, 1988, Lu, et al., 1988; James, 1982; James & Morris, 1983; Vöhringer, 1987). X-ray diffraction methods has been used to study the relaxation of residual stress (James, 1982; James & Morris, 1983; Vöhringer, 1987; Zhang et al., 1991). A model using finite elements was introduced to predict the residual stress distribution during and after fatigue (Lu, et al., 1988). It was concluded that for a cyclic hardening material, residual stresses relax in the first series of cycles. For a

cyclic softening material, they relax with the increase of the number of cycles up to a stabilised state. In this case the residual stresses are more relaxed compared with hardening materials, which reduces the effect of residual stresses on fatigue strength.

When a large mean stress is applied, residual stresses can actually be induced at the surface due to ratcheting of microplastic surface strain (James & Morris, 1983). In this extreme case residual stress could be increased instead of relaxation.

In principle, residual stress relaxation occurs when the linear superposition of applied stress and residual stress reaches the yield point of material. The onset of stress relaxation is delayed by the presence of sufficient stable obstacles to dislocation movement (Vöhringer, 1987). Under the cyclic loading, the residual stress relaxation depends on the combined stress state of applied stress and residual stress. Therefore the mechanisms of relaxation can be separated into three regimes (James, 1987)

(i) The combined stress above the macroscopic yield strength.

(ii) The combined stress between the yield strength and endurance limit.

(iii) The combined stress below or near the endurance limit.

The relaxation of residual stress in a specimen is not always in one regime. For example, in the first regime, the residual stress can be relaxed rapidly due to plasticity and the combined stress could be changed below the yield strength in which the relaxation mechanism belongs to the second regime. For cyclic softening or hardening materials, the yielding strength can change with the cycles and therefore the relaxation could be between (i) and (ii).

2.5-1 Combined stress above yielding strength

The local residual stress distribution will change if the local yield strength is exceeded by the sum of the applied stress and the local residual stress. The sign of the change will be opposite to that of the applied loading direction that induces the change. For example, when the surface stress state is compressive, and the sample is fatigued in fully reversed loading, the surface yield strength may be exceeded in compression and the surface residual stress will decrease. Bulk yielding is not necessary; microplastic deformation such as at a surface or notch will relax the local

residual stress state. Relaxation is rapid at high stress amplitude and decreases exponentially with increasing cycles. James (1982) measured surface residual stress relaxation using X-ray diffraction after fatigue cycles. Results showed that the residual stress state did not fully relax to zero. In general, relatively soft materials that show reasonably homogeneous microplastic deformation characteristics will relax in this manner when cycled in fully reversed loading.

Boggs and Byrne (1973) investigated the relaxation of shot peened residual stresses in Ni-Co alloys, 60%Co alloy and 20%Co alloy (lower strength, higher stacking fault energy). Cycled at amplitudes just above the yielding strength in fully reversed cantilever bending, rapid relaxation took place in the first 100 cycles before equilibrating to a constant decay slope for the 20%Co alloy. And little such decay occurred in the higher strength, lower stacking fault energy 60%Co alloy. There was virtually no change of micro-hardness during cycling, from which the authors concluded that the residual stress relaxation in the 20%Co alloy was due to dynamic recovery in the same sense as the recovery produced in thermal stress relief prior to any recrystallization.

Many fatigue tests have shown that preloaded or overloaded specimens with tensile residual stress, such as in welded specimens, could significantly reduce the fatigue damage done by subsequent small amplitude cycles because the large tensile residual stresses were reduced or relaxed by the large plastic deformation resulted from the overload (Sarkani & Lutes, 1988; Nawwar & Shewchuk, 1983; Berge & Eide, 1981).

Berge and Eide (1982) did variable-amplitude loading tests on weldment specimens and found that short-range residual stresses were relaxed due to local yielding and the residual stresses were eliminated by peak stresses of yield magnitude for some specimens.

The residual stress effect was almost negligible in the low cycle fatigue range for $N < 10^5$ cycles (Glinka, 1990) because the residual stresses were totally eliminated by the plastic deformation.

2.5-2 Combined stress between yielding strength and endurance limit

Cycle-dependent relaxation of the residual stress is a counterpart of the cyclic creep mechanism (Suresh, 1992; Valluri, 1963). The process of creep results in a

progressive reduction in the mean stress (residual stress here is meant the same as a mean stress) with increasing strain cycling. The relaxation can occur not only in cyclically softening materials but also in cyclically hardening material (Sandor, 1972). It has generally been predicted that there is an exponential decrement of residual stress with the number of cycles. Jhansale and Topper (1973) used an empirical formula to estimate the residual stress (as mean stress) relaxation for high cyclic fatigue,

$$\sigma_m/\sigma_{ms} = (2N_I - 1)^k. \qquad (2.62)$$

where σ_{ms} is initial value of mean stress, $2N_I$ is elapsed reversals and k is relaxation exponent which is a function of strain amplitude.

After a certain number of cycles, the residual stress distributions appear to stabilize. The redistributed residual stresses can then be incorporated into fatigue life estimation as a mean stress effect. The criteria discussed previously therefore can be used.

2.5-3 Combined stress below or near endurance limit

Residual stresses may relax even though the maximum cyclic stress is well below and near to the endurance limit (Pattinson & Dugdale, 1982; Hayashi & Doi, 1971; Gould & Pittella, 1973). This kind of residual stress relaxation is probably by mechanisms different from those for large cyclic stress amplitudes. Many factors may contribute to the relaxation (James, 1987):

- *Stress concentrators, such as at grain junctions, dislocation pileups and phase boundary, provide the mechanism for the relaxation.*

- *Defects of microcracks generated during the latter phase of the cycling process may have initiated an elastic relaxation.*

- *Local temperature increases during fatigue at high rates of cyclic loading may induce the relaxation.*

- *For strain hardening materials microplastic deformation takes place below the fatigue limit until strain hardening occurs in deformed grains and relaxation is possible during this period.*

Generally speaking, residual stress relaxation at this level is quite small and can be negligible in most cases.

Vöhringer (1987) did not consider the relaxation in the third regime and summarised the relaxation behaviour during fatigue cycling as shown in Figure 2.6. In this figure $\overline{R}_e$ was defined as composite yield point that included both material yielding strength and residual stress and $\overline{R}_{e,cyc}$ was defined as cyclic composite yield point. Four curves represent different cyclic load conditions and material cyclic behaviour. For the curve 1, the cyclic load condition is $\sigma_a < \min(\overline{R}_e, \overline{R}_{e,cyc})$ and there is no relaxation. For the curve 2, the cyclic load condition is $\overline{R}_{e,cyc} < \sigma_a < \overline{R}_e$ that is for cyclic softening materials and the residual stress is relaxed gradually. For the curve 3, the cyclic load condition is $\overline{R}_e < \sigma_a < \overline{R}_{e,cyc}$ that is for cyclic hardening materials and the relaxation only occurs in first cycle. for the curve 4, the cyclic load condition is $\sigma_a > \max(\overline{R}_e, \overline{R}_{e,cyc})$ and most residual stress will be relaxed in this case. The relaxation described in Figure 2.6 by Vöhringer is schematic and it could be more complicated in actual cases.

2.6 Factors That Influence Scatter in Fatigue Test Data

There are many factors which influence the fatigue test and cause scatter in fatigue data. These factors vary randomly from specimen to specimen. Both quantitative estimation and statistical analysis are needed to characterize these variables and find the relationship between these variables and the scatter of fatigue results. These factors include (Jacoby & Nowack, 1972): type of material and its condition; type of loading; size and shape of a specimen and structure; and the environment. Some parameters used in the data analysis model, such as a cumulative damage analysis, probably also influence the resulting scatter.

Testing machine or installation may also be an important influence (Weibull, 1961; Heywood, 1962). The scatter caused by the testing machine can be attributed to many factors (Jacoby & Nowack, 1972), for instance, to misalignment of specimens due to careless clamping, to errors in the load-measuring system, to deviations in the control circuit, to faulty cycle counters, or simply to the various skills of different persons handling a machine. Accounting for all of these effects is inherently difficult. Kandil and Dyson (Kandil & Dyson, 1993a; Kandil & Dyson, 1993b) proposed a quantitative model which predicts the influence of bending caused by

load misalignment on the extent of life time scatter in low-cycle fatigue (LCF). They suggested that

i) The load-strain offset mechanism of bending leads to the largest data-scatter LCF test.

ii) The scatter in the data between laboratories is always greater than that observed in a single laboratory. Furthermore when a dual extensometer is used these differences disappear.

iii) The magnitude of the repeatability and reproducibility scatter bands are a function of the fatigue characteristics of the materials being assessed.

The relevant equations for the limits to reproducibility of lifetime $\hat{N}_{f1}$, the minimum number of cycle to failure, and $\hat{N}_{f2}$, the maximum number of cycle to failure, are

$$\left.\begin{aligned} \hat{N}_{f1} &= N_f^*\left[1+2\frac{\Delta\varepsilon_b}{\Delta\varepsilon_c}\right]^{-\frac{1}{\beta}} \\ \hat{N}_{f2} &= N_f^*\left[1-2\frac{\Delta\varepsilon_b}{\Delta\varepsilon_c}\right]^{-\frac{1}{\beta}} \end{aligned}\right\} \tag{2.63}$$

where N_f^* is the number of cycles to failure under zero bending, $\Delta\varepsilon_b$ is the bending strain range, $\Delta\varepsilon_c$ is the control total axial strain range and β is the slope of the tangent to the curve of $\log\Delta\varepsilon_c$ as a function of $\log N_f$.

The scatter in fatigue test data is also a function of mean stress and amplitude of cyclic loading (Schijve, 1961). Under the constant amplitude load in a fatigue life range below about 10^5 cycles, the scatter is about the same as that under program or random loading (Jacoby & Nowack, 1972; Schijve, 1961; Gassner & Schütz, 1961). For variable amplitude loading tests of any kind, the scatter is determined mainly by the highest loading level. Since residual stress can be viewed as a type of mean stress, some scatter can also be inferred to result from varying residual stress magnitudes.

Goto (Goto, 1992; Goto, Nisitani & Miyagawa, 1993) studied small crack growth and concluded that the scatter in fatigue life is due mainly to the growth behaviour of small cracks with dimensions on the order of the micro-structure. The influence of

micro-structure on microcrack propagation is especially large at lower stress ranges, i.e. near the fatigue limit.

Surface roughness influences crack initiation as well. Maiya and Busch (1985) concluded that decreases of the fatigue life owing to surface roughness resulted from the reduction in the number of cycles for the crack initiation. This is not surprising since the majority of a fatigue life is taken up initiating the crack. Ryu and Nam (1989) and Kim and Nam (1990) carried out low-cycle fatigue tests on Cr-Mo-V steel specimens with two different degrees of surface roughness at 550°C and found the fatigue life of specimens with a rough surface was approximately half of that of specimens with a smooth surface. Furthermore Wareing and Vaughan (1979) suggested that low-cycle fatigue was dominated by the crack propagation process and they insisted that the difference in fatigue life between machined and electropolished specimens of type 316 stainless steel resulted from the different initiated crack shapes. But for some materials, which cavitate at grain boundary during creep-fatigue cycling, the surface roughness has little effect on creep-fatigue life (Kim and Nam 1990). Devlukia and Parsons (1993) carried out tests dealing with the influence of surface roughness on fatigue behaviour of three steels. The results showed that in the low cyclic regime the fatigue life had a pronounced reduction and for high cycle fatigue the results demonstrated the conflicting effects of surface roughness and presence of residual compressive stresses. As it is evident from these results that there is still controversy over the influence of surface roughness. It clearly influences the life but the degree is dependent on several factors. For each specimen the surface roughness is not always the same and there is a statistical variation from specimen to specimen. Therefore surface roughness is another influence factor on the scatter of fatigue life data.

2.7 Probabilistic Approaches to Fatigue Life Analysis

Deterministic methods have been normally used to assess structural reliability or safety. The parameters in the methods, such as the fatigue strength of material, stress range, residual stresses, etc., have been typically based on average values. In some industries, the values used for strength and stress range are chosen as the worst case quantities. This then results in unrealistically conservative assessments of safety. In general, the statistical distributions of these parameters have been ignored in the deterministic models.

It has been generally recognized that most design parameters of engineering structure and system have statistical variations. The use of statistical methods in the planning and interpretation of fatigue experiments has become a necessity in modern technology. There are mainly two aspects in the statistical analysis of fatigue data: one assumes that the stress amplitude is constant with many influencing factors varying from specimen to specimen (or structure to structure). Many distribution functions have been proposed for the description of the statistical variations of fatigue (Weibull, 1961; Gertsbakh & Kordonskij, 1969; Freudenthal & Gumbel, 1956; Sobczyk, 1994). The other approach is that the loading is treated as a variable during fatigue. Consequently the variation of stress amplitude can be regarded as either a regular or random pattern.

If the scatter in fatigue failure is simply considered as being a function of stress amplitude σ and the number of load cycles N, the probability of fatigue failure P can be represented using a set of equiprobability curves in a P-σ-N diagram (Freudenthal, 1952),

$$P = F(\sigma, N) \tag{2.64}$$

in which the two quantities σ and N are assumed to be independent variables. This equation, (2.64), is actually the cumulative distribution function of the number of cycles to fatigue failure which is treated as a random variable. There are several distribution functions that have been applied to fatigue data analysis (Sobczyk, 1994; Sheikh et at., 1986). The most frequently used distributions are the logarithmic normal and Weibull distributions:

i) Logarithmic normal distribution

In this distribution, the logN is chosen as the random variable X. The probability density function is given by (Jacoby & Nowack, 1972; Engesvik & Moan, 1983),

$$\left.\begin{aligned} f(X) &= \frac{1}{\sqrt{2\pi}S}\exp\left[-\frac{(X-\bar{X})^2}{2S^2}\right] \\ X &= \log N \end{aligned}\right\} \tag{2.65}$$

and the cumulative distribution is given by

$$P = \int_{-\infty}^{X} \frac{1}{\sqrt{2\pi}S} \exp\left[-\frac{(X-\bar{X})^2}{2S^2}\right] dX \tag{2.66}$$

where $\bar{X}$ is the sample arithmetic mean and S is the sample standard deviation of the log-transformed life data. The estimation of $\bar{X}$ is,

$$\bar{X} = \frac{1}{n}\sum_{i=1}^{n} \log N_i, \tag{2.67}$$

and the unbiased estimation of S is

$$S = \sqrt{\frac{1}{n-1}\sum_{i=1}^{n} (\log N_i - \bar{X})^2} \tag{2.68}$$

in which n is the number of the constant fatigue tests, N_i is the fatigue life of the *i*th fatigue test. A minimum life parameter, N_0, can be incorporated into the logarithmic normal distribution (Jacoby & Nowack, 1972). In this case, the random variable is $\log(N - N_0)$.

ii) Weibull distribution

The general three-parameter Weibull distribution is expressed as (Weibull, 1961),

$$P = 1 - \exp\left[-\left(\frac{N-N_0}{N_a-N_0}\right)^{\beta}\right] \qquad N > N_0 \tag{2.69}$$

where N_a is a characteristic life and β is the Weibull slope. The probability density function for Weibull distribution can be obtained by differentiating equation (2.69)

$$\left.\begin{aligned} f(N) &= \frac{\beta}{N_a-N_0}\left(\frac{N-N_0}{N_a-N_0}\right)^{\beta-1} \exp\left[-\left(\frac{N-N_0}{N_a-N_0}\right)^{\beta}\right] \quad N > N_0 \\ f(N) &= 0 \qquad\qquad N \le N_0 \end{aligned}\right\}. \tag{2.70}$$

The form of equation (2.70) can be changed to

$$\log\left[\log\left(\frac{1}{1-P}\right)\right]=\beta\log(N-N_0)-\beta\log(N_a-N_0). \qquad (2.71)$$

From the above equation, we see that there is a linear relationship between $\log\left[\log\left(\frac{1}{1-P}\right)\right]$ and $\log(N-N_0)$ on which Weibull paper is based. Johnson (1964) gave a comprehensive introduction to the application of the Weibull distribution to fatigue experiments.

For high stress levels, using two parameters without N_0 the Weibull distribution fits experimental fatigue data quite well and the three-parameter Weibull distribution provides a better fit of the experimental fatigue data ((Sobczyk, 1994).

Both logarithmic normal and Weibull distributions were found to be applicable to a wide range of materials and testing conditions. Within certain limits (Gertsbakh & Kordonskij, 1969; Freudenthal & Gumbel, 1956) there is no real difference between these distribution functions. The Weibull distribution is often preferred because it leads to more realistic reliability analysis (Freudenthal, 1961). Parida (1991) used these two distributions to evaluate the reliability of a component, a connecting link, and found the difference to be only within 92 to 94%. The correlation coefficient from the linear regression analysis were 0.9255 and 0.9925 for these two distribution, respectively, which indicated that the life of the connecting link was more Weibull distributed than logarithmic normal distributed.

In these two distributions, the fatigue life is selected as the random variable and fatigue life distribution is assumed to be known. As discussed in section 2.6 in this Chapter, the scatter of fatigue life is caused by many stochastic influencing factors, say

$$X_1, X_2, \cdots, X_m \qquad (2.72)$$

These stochastic factors could be the randomness of material properties, random defects and imperfections of structural components and random loads.

In most cases, the random variables can be described by normal distribution (Frost, et al., 1974) with a density function described by

$$f(\sigma) = \frac{1}{\sqrt{2\pi}S} \exp\left(\frac{-(\sigma - \sigma_0)^2}{2S^2}\right) \tag{2.73}$$

where σ_0 and S are the arithmetic mean and standard deviation, respectively, of the normal distribution. In some cases of reliability analysis, normal variable can be approximated by an "equivalent normal". (Rackwitz & Fiessler, 1978; Ditlevson, 1984).

The relationship between fatigue life and these stochastic influence factors can be expressed in deterministic models (Ang, 1975; ASCE, 1982),

$$N = g(X_1, X_2, \cdots, X_m). \tag{2.74}$$

Considering these factors as random variables, The fatigue life N is also a random variable. Then the probability of failure, p_f, relative to a service life, n, can be estimated,

$$p_f = P[N < n] = \int_G \cdots \int f_x(x_1, x_2, \cdots, x_m) dx_1 \cdots dx_m \tag{2.75}$$

where $f_x(\,)$ is joint probability density function of $(X_1, X_2, \cdots, X_m)$, the integration is performed over the region G in which $G = \{g(X_1, X_2, \cdots, X_m) < n\}$. The cumulative distribution function (CDF) of N is expressed as (Wirsching, et al., 1991),

$$F_N(n) = P[N \le n]. \tag{2.76}$$

The measure of reliability is the probability of survival or successful performance which can be expressed as

$$R_N(n) = P[N > n] = 1 - \int_G \cdots \int f_x(x_1, x_2, \cdots, x_m) dx_1 \cdots dx_m \tag{2.77}$$

If the joint probability density function of $(X_1, X_2, \cdots, X_m)$ is known, the probability of failure p_f, the CDF and the reliability can be obtained through the integration. In many cases the random variables are assumed to be independent and the joint probability density function can be expressed by individual probability density functions for each random variable,

$$f_x(x_1, x_2, \cdots, x_m) = f_{x_1}(x_1) f_{x_2}(x_2) \cdots f_{x_m}(x_m) \tag{2.78}$$

which will make the integration much easier. Bargmann et al. (1994) used the Manson-Coffin relationship (2.19) as the deterministic model and Neuber's rule to obtain the notch strain ε_a from the nominal stress S_a and geometry dependent factor K_f. Therefore there were four random factors, σ'_f, ε'_f, K_f and S_a, that affected fatigue life distribution and reliability. For the given distribution densities of each random variable, Bargmann et al. then expressed the fatigue life in multiple-integral closed form. An algorithm termed the "complete-probability fast integration" (CPFI) was developed. Better results were obtained compared to those using the approximate methods.

In most structure reliability analyses there are two problems:

i) *When more random variables are included in the probabilistic model, the integration will get much more complicated and numerical methods to complete the integration need significant computer time.*

ii) *The full distribution density functions for the random variables are seldom known and only the first and the second moments of X_i may be available, such as mean and standard deviation estimated from sample data.*

These difficulties have led to the development of approximate reliability analysis methods such as the second-moment approach which relies on a knowledge of the first and second moments of random variables, means and standard deviation, rather than their probability distributions (Hasofer, 1974; Cornell, 1975). The function given by Equation (2.74) then is linearized using a Taylor's series expansion about the mean values. The reliability analyses based on the second-moment and the linearization had been named the first-order, second-moment (FOSM) methods (ASCE, 1982). The algorithm for FOSM has been improved by many investigators (Rackwitz & Fiessler, 1978; Chen & Lind; 1983). The point where Taylor's series expansion takes place had been recognized at design point on plane given by Equation (2.74) from which the distance to origin in "reduced variables" plane is minimum, where the reduced variable is conducted from $(X - X_0)/S$. The error of reliability calculation using FOSM depends on how well the straight line approximates the curve given by Equation (2.74) around the design point. The second-order reliability method (SOSM) had been proposed (Breitung, 1982; Fiessler, et al., 1979; Wu & Wirsching, 1987) to improve the accuracy of FOSM by

taking second order terms from Taylor's series expansion. However more complicated calculation procedures are required. The names FOSM and SOSM are sometimes called FORM (first-order reliability method) and SORM (second-order reliability method), respectively.

Kandarpa et al., (1996) adapted the same methods described by Bargmann et al. (1994) to obtain a deterministic model for the fatigue life calculation. The random variables were σ'_f, ε'_f, K_f and fatigue strength exponents and the mean stress was considered as an effect on strain life. The reliability methods FORM and SORM, which have been included into an analysis program PROBAN (PROBAN, 1989), were both used. The FORM gave over-predicted failure probability results. It was concluded that FORM and SORM provided the sensitivities of the reliability index with respect to any set of distribution or model parameters.

The recognition of the effects of the random loads on fatigue life has led to extensive studies of random processes and their application to the description of actual fatigue loads in the working environment. An example of this might be the loads produced by road-surface roughness for automobiles. Swanson (1968) has given an excellent review of random load testing. The effect of variable-amplitude loading on fatigue performance is normally accounted for with cumulative damage rules. Typically, these rules attempt to relate fatigue behaviour under a complex loading history to the known behaviour under constant amplitude loading. For the random cycle loading, a cumulative damage model, based on deterministic considerations, is normally needed in the analysis. Many theories of cumulative damage have been proposed to help the designer predict the fatigue life of components subjected to varying amplitude loading based on the presently available constant-amplitude fatigue response (Kujawski & Ellyin, 1988). If the load sequence effect is not important, a linear cumulative damage rule can then be used to calculate the fatigue life (Zapatero & Dominguez, 1990). The most frequently used cumulative damage model is Miner's linear cumulative rule (Miner, 1945)

$$\sum_i \frac{n_i}{N_i} = 1 \tag{2.79}$$

where N_i is the number of cycles to failure at stress amplitude σ_i and n_i is the number of cycles at stress amplitude σ_i. If the fatigue N_i is considered to be a random variable for the given σ_i, a median fatigue life $N_i(1/2)$ may be chosen to replace N_i (Nash, 1983).

Miner's linear cumulative rule has proven to be useful. It is simple to apply and predicts the number of cycles to crack initiation and failure. It was generally thought that the rule more accurately described fatigue damage of structure components whose life consisted mainly of crack initiation. Unfortunately this damage theory does not account for load sequence effects on fatigue life. In some cases the load sequence has little influence. Manson (1965) observed that Miner's rule was quite accurate for 2024-T4 aluminium and Ti-6Al-4V smooth axial specimens tested under a two level (i.e., high-low, low-high) strain sequence. Significant influences of the load sequence on fatigue life was also reported (Albrecht & Yamada, 1977; Abtahi, et al., 1976). Many other non-linear cumulative rules have been proposed (Collins, 1981; Morrow, 1986; Wu & Huang, 1991) but they are much more complicated than the Miner's rule. Saunders (1972) has shown that, under certain fairly general assumptions, Miner's rule yields the mean life of a fatigue components.

For the variable amplitude loading, Albrecht (1981) introduced the concept of an "equivalent" stress range to correlate data from variable amplitude cycle load tests with data from constant amplitude tests (this should not be confused with the range of the Von Mises stress). The idea is that for an equal number of cycles, the equivalent stress range will cause the same fatigue damage as the sequence of variable amplitude stress ranges it replaces. The computed stress range is expressed as

$$\sigma_e = \left[\sum \gamma_i \sigma_i^m\right]^{1/m} \tag{2.80}$$

where

σ_e = computed stress range
σ_i = ith stress range
γ_i = frequency of occurrence of ith stress range
m = slope of S-N curve.

In this analysis, the load spectra, in the form of histograms, was replaced by a lognormal distribution of equivalent stress ranges. The application was made to bridge stress histories. The fatigue properties of a structural detail was represented by a lognormal distribution about a straight line plotted in logarithmic coordinates of stress versus cycles to failure. The equivalent stress range distribution was

transformed to a lognormal distribution of design load cycles using the slope of the *S-N* curve. The fatigue reliability analysis was then determined by considering the difference between the two distributions.

The concept of random process has been applied to the fatigue damage process analysis under the random loads. The most common ones used are Gaussian process and Markoff process (Rychlik, 1994). The Markoff process discrete form is the Markoff chain (Bagdanoff, et al., 1978, 1982). Itagaki and Shinozuka (1972) used Monte Carlo techniques to simulate the fatigue failure under random loading in which the fatigue damage process was described by the sequence of stress peak point process. The statistical characteristics were found to be in excellent agreement with those from the experimental results.

In general, the basic idea underlying the probabilistic treatment is that a deterministic cumulative damage theory must first be developed for ideal nonvariable specimens. This can then be randomised to taken into account material, geometric and loading variability (Hashin, 1983).

2.8 Concluding Remarks

There is no doubt that residual stresses exist in hot forged components. But from literature there has be only a little work on determining the complete residual stress distribution in hot forged components (Bassinet al., 1986; Appleton, et al., 1987; James, 1982; Myllymaki, 1987). There is certainly no evidence available on the statistical distributions of the residual stresses from sample to sample for hot forged components.

Many methods have been developed to measure residual stresses. They can be classified as non-destructive, semi-destructive and destructive methods. The non-destructive methods are always preferred. It has the obvious benefit that specimens can be used for other tests after the measurements and the structures will be not interrupted from service. But every method has its own advantages and shortcomings.

The X-ray diffraction is a non-destructive method, and easy to use and is normally the first choice for measuring residual stress in steel components. The only limitations are that its measurements are only on surfaces of components and the

residual stresses measured are the combination of macrostresses and microstresses. To obtain residual stress inside the specimens, an etching technique needs to be introduced. The overall technique becomes a destructive method (Prevey, 1986).

Neutron diffraction can be used to measure residual stresses inside the specimens non-destructively. But because there are limited neutron sources and it is time-consuming, the method is not widely used in engineering applications. The stress free lattice spacing is required to determine the absolute strains (Prask, et al., 1987). Some methods have been proposed (Smith, et al., 1988 & 1992; Webster, et al., 1995). The neutron diffraction can not be used to measure residual stress near to the surface of a component (Lorentzen, 1995), and there is a need to investigate surface effects in neutron diffraction measurements.

The centre-hole method is a semi-destructive method which uses a small hole drilled into the specimen surface. It can be used to measure residual stresses near surface. Using the incremental technique, the residual stress distribution below the surface within the distance of hole radius can be obtained (Niku-Lari & Flavenot, 1985; Schajer, 1988). No work has been reported for hole drilling on curved surfaces. For round bar specimens the influence of the curvature may be significant and a method needs to be developed to calculate the stresses from strains measured from hole drilling. The plastic deformation during hole drilling has significant influence on residual stress outcome when residual stress is about 70% or more of the yielding strength of material (Nickola, 1984). In some special cases where the surface residual stresses result from surface plastic deformation, such as shot peening and shot blast treatment, the stress state on the surface is on the yielding surface because of the Bauchinger effect. The hole drilling operation will then cause further plastic yielding (Zhu & Smith, 1994). This kind of plastic deformation will have much more of an influence on the computed residual stresses than for normal yielding without Bauschinger effect. It is evident that there has been only limited work undertaken to consider how this influences the residual stress calculations.

The choice of which method to measure residual stresses depends on many factors, such as which residual stresses need to be measured, whether on specimen surfaces or in the bulk interior of the specimen. The availability of the method is also one of the major factors. Nevertheless, to use more methods is always better than one. Residual stress results from different methods can be verified with each other and whole residual stress profile can be built up using the different results. In Chapters 4 and 5, a comprehensive study of residual stresses in the hot forged components is

carried out. The residual stresses are measured using different measurement techniques. A theoretical analysis has been developed to interpolate residual stresses between surface and bulk interior measurements. The surface residual stress distributions from sample to sample for different specimen group are statistically analysed in Chapter 7.

There is no doubt that residual stresses have significant influence on fatigue life. In many earlier studies the residual stresses had been considered as a mean stress effect (Lawrence, et al. 1981; Flavenot & Skalli, 1989). Residual stresses will also relax during fatigue (James, 1987, Glinka, 1990). The relaxation of residual stresses during fatigue has been investigated experimentally (Weiss, et al., 1979 & 1980; Jhansale & Topper 1973; James & Morris, 1981; James, 1982). It has been generally recognized that residual stresses have no effect on low cyclic fatigue because the residual stresses are totally relaxed by the large plastic deformation (Glinka, 1990). There is no closed form relationship between fatigue strain range and relaxation of residual stress. There is also little consideration of the influence of residual relaxation during fatigue cycling on fatigue life.

The many influencing factors that contribute to the generation of residual stress are uncertain among specimens, and therefore the residual stresses vary from specimen to specimen. The residual stresses are therefore a random variable. To incorporate the residual stress as a random variable into reliability analysis, a deterministic model of fatigue life including residual stress is needed. Most investigators have used Morrow's relationship (Morrow, 1968), Equation (2.59), and have incorporated residual stress incorporating residual stress as a mean stress influence (Lawrence, et al., 1981; Glinka, 1990; Suresh, 1992; Kandarpa, et al., 1996). In a stochastic model by Kandarpa et al., (1996), the random variables were chosen σ'_f, ε'_f, K_f and fatigue strength exponents. The mean stress was included in their model as an effect on fatigue life but not as a random variable. No other studies have been found that incorporate residual stress as random variable into reliability analysis.

In Chapters 6 and 7, the residual stress relaxation for different cyclic strain ranges is studied. The redistribution of residual stresses for different samples under different cyclic strain range is obtained. A stochastic model is developed to incorporate residual stress into probability to failure or reliability analysis, and residual stress relaxation is considered as the relaxation being related to cyclic strain range.

Chapter 3

OVERALL EXPERIMENTAL PROGRAMME

This chapter presents the overall experimental programme for determining residual stresses in hot forged components and assessing the interaction with mechanical loading, and finally the influence on fatigue life. The material, specimens, test equipment, test procedure and test matrix are presented.

3.1 MATERIAL AND SPECIMENS

The material used in this work was medium alloy steel EN15R that is widely used in automotive components. The material was supplied by Rover Group and John Stokes and Sons, Ltd in the form of cylindrical bars. The composition of the alloy is given in Table 3.1. The forging processes, used in manufacturing the bars, simulated the manufacture of wheel suspension arms for automobiles that were hot die forged. The basic forging process consisted of initial induction heating of a steel billet to about 1200 to 1250 °C. The billet was then moulded in a hot forging press, followed by finish pressing. The excess material was clipped and the forged components were allowed to cool in air to room temperature. Then the components were heat treated (harden and tempered), followed by shot blasting to clean the surface of oxide scale. This cleaning was done so that components could then be painted. However the test bars were not painted. To understand how each stage of the forging process influenced the residual stresses and finally the fatigue life, some bars were extracted at each stage of the process. The forging process and each stage are shown in Figure 3.1. The results of tensile tests carried out by Rover (Devlukia, 1993b) for round bar specimens of this material are reported in Table 3.2.

Three forged suspension arms were also received for X-ray measurements to determine the residual stresses at the surface near fatigue critical locations. The suspension arm is shown in Figure 3.2.

Two rectangular bars, with cross section of 65×65 mm, were received. One bar was not subjected to shot blasting. Both X-ray diffraction and centre hole method were used to measure the residual stresses on these two bars. To verify the centre hole measurement a stress free sample was manufactured from one end of the non-shot blasted bar, machined to obtain parallel faces and then annealed at 600°C– 620°C. The stress free plate was 65×65×20 mm.

Twenty forged bars, identified as U-batch, were received. These specimens were subjected to the completed forging process. The geometry of the bars is shown in Figure 3.3. The specimens were used to determine residual stress distribution from sample to sample and also residual stress distribution across section of specimen.

To understand each stage of the forging process influenced residual stresses and fatigue lives, round bar specimens reflecting different stage of the process were produced. There were four groups of specimens:

(i) AF = as forged, without heat treatment and shot blast
(ii) HT = heat treated without shot blast treatment
(iii) FS = forged & shot blasted without heat treatment
(iv) HTS = subjected to the complete process

The residual stress distributions from sample to sample for each group of specimens were determined from X-ray measurements. For the U- and HTS batches, the profile of residual stress distribution was determined from measuring some specimens using various methods: X-ray diffraction, neutron diffraction and centre hole method.

Some of the round bars were subjected to the mechanical loadings to study the interaction between residual and applied stresses. To apply the loading, male screw threads were machined at both ends of the specimens to enable them to be fitted into a test machine.

3.2 EXPERIMENTAL EQUIPMENT AND MEASUREMENTS

3.2-1 Test equipment

X-ray diffractometer

The instrument used to carry out the X-ray diffraction measurements was a Philips horizontal diffractometer with a chromium X-ray source. The lattice plane examined was (211) and the corresponding diffraction angle (2θ) is approximately 156°. The $\sin^2\psi$ method was used to determine the residual stresses. Variables for the X-ray measurements are listed as follows:

Operating voltage	40 kV
Current	40 mA
Divergence slit	0.25°
Receiver slit	1.8 mm
Bragg angle	$2\theta \approx 156°$
Angle of scan	$155° \rightarrow 157°$
Step per peak	30–40
Dwell time each step	20–30 s

ψ values chosen with $\sin^2 \psi$ values:

0.0, 0.05, 0.1, 0.2, 0.3, 0.4, 0.5, 0.6	for suspension arms
0.0, 0.1, 0.2, 0.3, 0.4, 0.5	for round bars

A 'BBC B' microcomputer was used to control the scan with the program 'SET UP'. The post-processing of data to obtain residual stresses was carried out using this computer via the program 'ANALYSE1'.

Neutron diffractometer

Neutron diffraction measurements were carried out at the Risø National Laboratory, Denmark, using the TAS8 instrument in single detector mode. The reactor produced a continuous spectrum of thermal neutrons from which a monochromatic crystal selects the desired wavelength of about 3Å. The neutron diffractometer was controlled using a computer and allowed the detected counts to be recorded for a period time, or for a fixed number of counts detected in a low efficiency monitor counter placed in the incident beam. All measurements were obtained from the (110) reflection with the diffraction angle (2θ) close to 90 degree. The sample volume given by the diffractometer was defined by the intersection of the incident and scattered neutron beam, as shown in Figure 3.4. The centre of sample volume was located using a laser beam with an accuracy of ±0.5 mm at the exact point of intersection of incident beam and diffracted beam. The sample volumes used were $1 \times 1 \times 10\,mm$, $1 \times 1 \times 5\,mm$, $2 \times 2 \times 2\,mm$ for different measurements. The locations of these volumes are discussed.

Centre Hole Equipment

The RS-200 Milling Guide manufactured by the Measurements Group Inc. was used in hole drilling. The Milling Guide is a highly accurate instrument for analyzing residual stresses by the hole-drilling method. The holes were drilled in the centre of strain gauge rosettes with a precision carbide cutter using a high-speed air turbine to which a clean dry air of 40 psi capable of approximately 0.2 meter/min was supplied from a compressor. The drilling depth was controlled by the depth-setting micrometer for incremental drilling. The device is shown in Figure 3.5.

The model and types of strain gauge rosettes used were TEA-06-062RK-120 and WA-06-030WR-120 that were manufactured by the Measurements Group Inc. specially designed for the hole-drilling method. The geometry of the strain gauge rosette is shown in Figure 3.6. The parameters of the rosettes include

Type:	TEA-06-062RK-120	WA-06-030WR-120
Resistance:	120±0.4%	120±0.8%
Gauge factor:	2.06±1.0%	2.1±1.3%
Gauge length:	1.59 mm	0.8 mm
Mean diameter	5.13 mm	2.7 mm

For each of the rosettes, the diameter of the hole will be different. The larger one is mainly for use on flat surfaces and the smaller one was used for bars to reduce the influence of curvature.

Test machine for mechanical loading

The machine used to apply cyclic mechanical loading was a ball-screw driven DARTEC testing machine. The load capacity is ±100 kN. There are various forms of controls: load, extension, stroke and external input. The 9500 control cabinet is used to control the machine when setting up a specimen for testing. A series of finger touch controls and digital display meters are on the front of the cabinet. A personal computer was connected to the cabinet to set up the control programme, to monitor progress of the test and to record the test results. The load cell of the test machine was calibrated with the error within 0.1%. Alignment of the loading column was checked using a strain gauge specimen. The bending strain difference on opposite sides was within 2%. Two displacement transducers were used to measure displacements over the gauge length. The average of the displacements on both sides was used as the extension for control and output. The transducers were also calibrated.

Test machine for hardness measurements

The machine used to measure hardness was a Vickers hardness test machine made by Vickers-Armstrongs Ltd. The indenter is a diamond point in the shape of a pyramid with a square base. The depth of penetration, h, is one-seventh of the indentation size, d, measured on the diagonal. A wide range of standard force can be used between 1 and 120 Kg. The hardness number can be found from a given table by using the indentation size, d measured.

3.2-2 Strain Data Acquisition

Centre hole measurements

For the centre hole method, a strain rosette, shown in Figure 3.6, was bonded on each bar surface and a hole was drilled at the centre of the rosette. The strains were recorded after each drilling step. A strain measuring instrument, manufactured by Tinsley Strain Measurements, was used for the strain data acquisition. This instrument has ten channels with direct digital reading. The quarter bridge configuration was chosen for each strain gauge.

Mechanical loading tests

For the mechanical loading tests, strain gauge rosettes were bonded on both sides of the bars. The strains measured at each location were in three directions: axial, hoop and 45°. The strains, time, load and extension were recorded using an ADU MM700 unit. There are sixteen channels in this unit that can record 16 data channels plus time at the same time. This instrument is operated from a personal computer using the DIALOG software that reads data automatically at a given period. With use of this instrument, the strains, load and extensions against time can be recorded and saved to disk automatically.

3.3 TEST PROCEDURES AND TEST MATRIX

Tests carried out were mainly in three parts,

a) Determination of residual stresses in hot forged components and bars.

b) Interaction of residual stresses with applied mechanical loading.

c) Fatigue tests to determine the influence of residual stress on fatigue life

Table 3.3 lists all the specimens that were tested, and the various measurements taken.

3.3-1 X-ray diffraction

To understand the reliability of the X-ray diffraction method, measurements were first made on the stress free plate which was annealed at 600°C– 620°C. Repeatability of the X-ray measurements was tested on one specimen from the U-batch. For the suspension arms, the rectangular bars and round bars from the U-batch, residual stresses were measured on surface in three direction: axial, hoop and

45°. For the AF, HT, FS and HTS round bars the X-ray measurements were made on both sides of specimens and only in axial direction.

For one specimen from the HTS batch, the X-ray diffraction method combined with chemical etching method was used to obtain a residual stress distribution through the specimen. The X-ray measurements were made in axial and tangential directions after each etching. The original residual stresses then can be found by using an analysis described later.

3.3-2 Neutron diffraction

The neutron diffraction method was used to measure residual stresses inside the round bars. Six U-batch specimens were measured at the centre and 2mm either side of the centre of the specimens. All measurements were obtained from the (110) reflection with the diffraction (2θ) close to 90°. For radial and tangential strains the neutron gauge volume was $1\times1\times10$ mm for which the 10 mm length was orientated along the axial direction of the bars, and for axial strain measurements the volume was $2\times2\times2$ mm. The stress free lattice spacing was obtained from measuring specimen end where it was assumed that the stress state was approximately zero.

Detailed measurements were also made on specimens HTS19 and HTS22 specimens. To investigate possible surface effects of neutron diffraction method, measurements were first made on stress free samples that were obtained from the application of mechanical loading. The specimens were confirmed to be stress free by obtaining centre hole measurements. The methods of determining residual stress distributions from the neutron diffraction measurements were developed as described later in the thesis.

3.3-3 Centre hole measurements

Centre hole method was used to measure residual stresses near the surface of specimens. Prior to taking measurement on the forged bars, this method was first applied to a stress free plate to make sure that there were no additional stresses introduced by the hole drilling operation. For the two rectangular bars and the U-batch round bars, larger strain gauge rosettes were used. To avoid using the 3-D FE analysis for interpreting the strains (described later), smaller strain gauge rosettes were used for the round bars from HTS and FS batches. The strains were recorded after each drilling step. The drilling increment was about 0.08 mm for the larger strain gauge rosettes, and 0.0254 mm for the smaller strain gauge rosettes. The hole diameters were measured after drilling.

The strain gauges were bonded on the centre of one side of each specimen. For the round bar specimens, the strain gauge rosettes were carefully wrapped and bonded around the cylindrical part in the centre of the bar.

3.3-4 Mechanical loading

Residual stress relaxation was investigated by applying mechanical loading to round bars and then measuring residual stresses using X-ray diffraction. The specimen attachments are shown in Figure 3.7. The bars were loaded under total strain control. Two types of loading conditions were used, tensile loading and cyclic mechanical loading. A number of strain ranges were examined and applied step by step, up to 10000 με. The residual stresses were measured using X-ray diffraction after unloading after each step.

3.3-5 Fatigue tests

Fatigue tests were carried out at Rover on round bars. The test machine was an MTS testing, model 80010. A 10 mm extensometer was fixed to side of each specimen. The fatigue tests were carried out under total strain controlled. Fatigue life N was recorded after specimen failure.

To check the bending caused by the irregular shape of the forged round bar specimens, strain gauges were bounded on three specimens (on both sides) in each group. The strains were checked on both sides under tensile elastic loading before fatigue testing.

Sixty specimens were selected from the four batches of bars, AF, HT, FS and HTS. Fourteen in each group were fatigue tested. In each batch, two strain ranges were chosen for the fatigue tests, one ($\frac{\Delta\varepsilon}{2} = 2200\,\mu\varepsilon$) was for high cyclic fatigue tests and the other ($\frac{\Delta\varepsilon}{2} = 6000\,\mu\varepsilon$) was for low cyclic fatigue tests.

3.3-6 Hardness measurements

Hardness measurements were carried out on round bars from HTS, FS and U-batches. The measurement positions were near to the ends of each round bars. The measurements were carried on two sides, A and B, of each bar from HTS and FS batches and one measurement on each bar from U-batch. The force used was 30 kg. The hardness obtained was via the Vickers pyramid number that was converted from the measured indentation size d using a conversion table.

Chapter 4

RESIDUAL STRESS MEASUREMENT AND ANALYSIS

This Chapter presents the results of the measurements of residual stresses in hot forged components. The techniques used were X-ray diffraction, neutron diffraction and centre hole method. New developments were made in the experiments and subsequent analysis of the results. The residual stress results obtained by using different techniques are then compared.

4.1. Introduction

In this Chapter residual stresses in hot forged specimens are studied. Residual stress measurements were obtained from three different techniques, including X-ray diffraction, neutron diffraction and centre hole drilling. The X-ray diffraction method was mainly used to determine residual stresses on the surface of specimens. Together with chemical etching, the X-ray diffraction method was also used to determine residual stresses inside one sample. The neutron diffraction method was used to establish the residual stresses in the interior of specimens and the hole-drilling method used to measure near surface residual stresses, as illustrated in Figure 4.1. An analysis has also been developed for interpreting relaxed strain data from the incremental hole drilling method for components with curved surfaces.

4.2 X-ray Diffraction

4.2-1 Principles

Extending the analysis given in section 2.2-1, Equation 2.4 is reduced to

$$\frac{d_{\varphi\psi} - d_n}{d_0} = \frac{1+\nu}{E}\sigma_\phi \cdot \sin^2\psi \,. \tag{4.1}$$

where n denotes the normal direction and d_n is the spacing of the lattice planes parallel to the surface. The definition of local coordinate system for the X-ray measurements is shown in Figure 4.2 where z is the direction normal to the surface of specimen. Because elastic deformation is very small, that is $d_n/d_0 = 1+\varepsilon_n \approx 1$, d_0 can be replaced by d_n in Equation (4.1) without losing accuracy. Then Equation (4.1) becomes

$$\frac{d_\psi - d_n}{d_n} = \frac{1+\nu}{E}\sigma_\phi \sin^2\psi \,. \tag{4.2}$$

This equation (4.2) is a basic equation for X-ray diffraction analysis. It should be noted that in the above equation, the unstressed lattice spacing is no longer necessary and the equation is independent of the angle ϕ. From the Equation (4.2), we can see that two measurements are essential to determine the residual stress σ_ϕ, one of which is the tilt angle ψ being zero. In practice, there are always more than two measurements for different ψ together with the use of regression technique to reduce the experimental errors.

In the above analysis, the stress components near to the surface, σ_z, τ_{zx} and τ_{zy}, are ignored, where z is along the normal direction. The existence of these stress components near surface gives rise to errors in the measurement method. There are other aspects of the X-ray analysis that consider the influence of these stress components (Noyan, 1983; Hauk, 1983).

4.2-2 Analysis of Plane Stress

It has been assumed that near to the specimen surface, the state of stress is in plane stress and can be described by three parameters σ_x, σ_y and τ_{xy} as shown in Figure

4.3. In any direction, with the angle being ϕ measured from the x axis toward the y axis in a counterclockwise direction, the normal stress σ_ϕ can be expressed as

$$\sigma_\phi = \frac{\sigma_x + \sigma_y}{2} + \frac{\sigma_x - \sigma_y}{2}\cos 2\phi + \tau_{xy}\sin 2\phi\,. \tag{4.3}$$

By using the X-ray diffraction method, the stress σ_ϕ can be obtained directly. To determine the stress state σ_x, σ_y and τ_{xy}, measurements of stress σ_ϕ must be taken at a minimum of three directions. By using Equation (4.3)

$$\sigma_x = \sigma_\phi\big|_{\phi=0^\circ} \tag{4.4a}$$

$$\sigma_y = \sigma_\phi\big|_{\phi=90^\circ} \tag{4.4b}$$

$$\tau_{xy} = \sigma_\phi\big|_{\phi=45^\circ} - \frac{1}{2}(\sigma_x + \sigma_y) \tag{4.4c}$$

$$\tau_{xy} = -\sigma_\phi\big|_{\phi=-45^\circ} + \frac{1}{2}(\sigma_x + \sigma_y). \tag{4.4d}$$

The two principal stresses can be expressed as

$$\sigma_1 = \sigma_{max} = \frac{1}{2}(\sigma_x + \sigma_y) + \frac{1}{2}\sqrt{(\sigma_x - \sigma_y)^2 + 4\tau_{xy}^2} \tag{4.5a}$$

$$\sigma_2 = \sigma_{min} = \frac{1}{2}(\sigma_x + \sigma_y) - \frac{1}{2}\sqrt{(\sigma_x - \sigma_y)^2 + 4\tau_{xy}^2} \tag{4.5b}$$

4.2-3 Analysis for X-ray diffraction combined with surface layering using a chemical etching method

Surface material layer removal is required to measure residual stresses below the surface by using the X-ray diffraction method. Mechanical methods, such as mechanical machining and polishing, will however introduce additional residual stresses. Therefore they were not considered. Electropolishing and chemical etching method have been used to remove surface layer material. Significant relaxation of residual stress in the surface exposed by layer removal can occur. For solid circular cylinders, hollow cylinders and plates or bars with rectangular cross-sections, some

analyses have been derived to take account of the stress redistribution (Moore, et al., 1958; Sikarskie, 1967). In the following, a detailed description of the analysis for the redistribution of the residual stresses in a solid round bar subjected to layer removal is given.

Axial residual stress

Consider only the axisymmetrical case of a bar and assume the axial residual stress distribution is independent of z, then

$$\sigma_z = \sigma_z(r) \qquad 0 \le r \le 1 \tag{4.6}$$

where the radial co-ordinate r is non-dimensionalised by the radius of the bar.

According to equilibrium, the sum of total axial force should be zero,

$$\int_A \sigma_z(r)dA = 2\pi \int_0^1 r\sigma_z(r)dr = 0\,. \tag{4.7}$$

For a layer of material of thickness t removed, the force on the area removed is

$$F_t = \int_{A_t} \sigma_z(r)dA\,, \tag{4.8}$$

where A_t is the area removed. The area A_t is a ring shape which inner radius being *1-t* and out radius being *1*. Thus, integration Equation (4.8) becomes

$$F_t = 2\pi \int_{1-t}^1 r\sigma_z(r)dr\,. \tag{4.9}$$

The force on the remaining area before layer removal is

$$F_{1-t} = 2\pi \int_0^{1-t} r\sigma_z(r)dr\,. \tag{4.10}$$

From Equation (4.7), it can be shown that

$$F_{1-t} + F_t = 0. \tag{4.11}$$

After the layer removal, the force on the remaining area is changed from F_{1-t} to $F_{1-t} + F_u$ where F_u is to be determined. For the remaining area equilibrium dictates that the total axial force is still zero. Thus

$$F_{1-t} + F_u = 0. \tag{4.12}$$

Comparing Equations (4.11) and (4.12), the F_u is found that

$$F_u = F_t. \tag{4.13}$$

For the remaining bar the axial force increases by F_u which results in an axial stress increase. Assuming that the axial stress changing on the remaining bar, after the layer removal, is uniform, then the axial residual stress change is,

$$\Delta\sigma_{z,t} = \frac{F_u}{A_{1-t}} = \frac{2}{(1-t)^2}\int_{1-t}^{1} r\sigma_z(r)dr\,. \tag{4.14}$$

where $\Delta\sigma_{z,t}$ represents the axial residual stress increment after a layer of thickness t is removed. Therefore, the axial residual stress $\sigma'_{z,t}$ on the new surface after layer removal is

$$\sigma'_{z,t} = \sigma_z(r)\big|_{r=1-t} + \frac{2}{(1-t)^2}\int_{1-t}^{1} r\sigma_z(r)dr \tag{4.15}$$

where $\sigma'_{z,t}$ represents the axial residual stress on the exposed surface after layer removal. This residual stress $\sigma'_{z,t}$ can be directly measured by X-ray. Although Equation (4.15) is different from that given by Moore (1958) in formulation, they are equivalent as they can be derived from each other.

Tangential residual stress

There are also radial $\sigma_r(r)$ and tangential $\sigma_\theta(r)$ residual stresses in the sample and are assumed to be independent of z. According to equilibrium, the relationship between them is

$$\sigma_\theta = \frac{d}{dr}(r\sigma_r). \tag{4.16}$$

If a layer is removed, the radial distributed force which is equal to $\sigma_r(r)\big|_{r=1-t}$ on the new surface is removed. The tangential residual stress change, $\Delta\sigma'_{\theta,t}$, due to the radial distributed force removal is

$$\Delta\sigma'_{\theta,t} = -\sigma_r(r)\big|_{r=1-t}. \tag{4.17}$$

Therefore the tangential residual stress on the new surface, $\sigma'_{\theta,t}$, is changed due to the layer removal, so that

$$\sigma'_{\theta,t} = \sigma_\theta(r)\big|_{r=1-t} - \sigma_r(r)\big|_{r=1-t}. \tag{4.18}$$

which can also be measured directly by X-ray diffraction. Equation (4.18) is exactly the same as that given by Moore (1958).

4.2-4 Results on Specimen Surfaces

Measurements on stress free sample

To verify the reliability of the X-ray measurement on the material En15R, six measurements of residual stresses were made on a plate which was annealed to be stress free. The results are shown in Table 4.1. From the measurements, it can be seen that for the stress free plate the X-ray still measured some residual stresses which might result from the existence of 2nd and 3rd kind residual stresses (Macherauch, 1987). The residual stresses were found to be in compression with the largest value being -55 MPa, and the smallest -19 MPa.

Repeatability of the X-ray measurements

Many factors influence the accuracy of the results measured by X-ray diffraction. It was necessary to assess the repeatability of the measurements on one location using the X-ray diffraction. The work was carried out on specimen U1 at location M1, as shown in Figure 4.4. The results are listed in Table 4.2. It was evident that at the chosen location there was a compressive residual stress of about -300 MPa. The difference between the maximum and minimum values is about 27 MPa, within 10% error of the maximum compressive residual stress.

Suspension arms

Three suspension arms were examined. The measurement point for the residual stresses was near the critical location (and approximately 5 mm away). Figure 4.5 shows part of the suspension arm (see also Figure 3.2) and the reference frame. Residual stresses of the three suspension arms are listed in Table 4.3. It was evident that the maximum compressive principal residual stresses in the three components varied from -255 MPa to -316 MPa.

Rectangular bars

In the two rectangular bars, one was subjected to shot blasting and the other was not. The dimensions of the cross section is about 65×65 *mm*. Measurements were made on one side of each specimen. The results are also shown in Table 4.3. In the case of the bar not shot blast the surface residual stresses were in compression but at only about one half of those in the shot blast bar.

Round bar specimens, U-batch

For the U-batch round bars, the residual stresses were measured in the gauge length. Many measurements were made on several locations in one U-batch specimen U1. The reference frame is shown in Figure 4.4. The results for the specimen U1 are listed in Table 4.4. Excluding the measurements on flash line, the axial residual stresses varied from -285 MPa to -306 MPa and the tangential residual stresses varied from -277 MPa to -318 MPa.

For all other U-batch specimens, U2 to U20, the residual stresses were measured at location M1 on each specimen. The results are shown in Table 4.5. The results of residual stress variation from sample to sample are also shown in Figures 4.6-4.7. The axial residual stresses varied from -177 MPa to -346 MPa with average value about -286 MPa and the tangential residual stresses varied from -277 MPa to -318 MPa with an average value about -240 MPa. The principal direction varied from 0° to 23°.

Round bar specimens: AF, FS, HT and HTS groups

The four batches of specimens represented different stages of the hot forging processes. There were eighty specimens, twenty in each group measured by X-ray

diffraction. The residual stresses were measured only in axial direction on both sides of specimens which corresponding to locations M1 and M3, shown in Figure 4.4. Tables 4.6-4.9 show the measured axial residual stresses for each batch. The results of residual stress variations are also shown in Figures 4.8-4.11.

For AF batch, the axial residual stresses varied from 59 MPa to -69 MPa with average value about -16 MPa. For HTS batch, the axial residual stresses varied from –9 MPa to -69 MPa with average value about -25 MPa. Comparing the results from the HT batch with those from the AF batch, it can be seen that the heat treatment made the scatter of the residual stresses much less.

For FS batch, the axial residual stresses varied from -186 MPa to -369 MPa with average value about -272 MPa. For HTS batch, the axial residual stresses varied from –267 MPa to -469 MPa with average value about -373 MPa. Comparing the results from the HTS batch with those from the FS batch, it can be concluded that the heat treatment contributed to the much higher residual stresses in the HTS batch.

4.2-5 Residual Stresses by Chemical Etching Combined with X-Ray

To compare with other measurements for the distribution of residual stress in the round bars, the X-ray diffraction method together with the chemical etching method was used to obtain the subsurface residual stress distribution. Because it is a destructive method, this method was only applied to round bar specimens HTS05, HTS18 and HTS24 in which the HTS05 had been subjected to high cyclic fatigue and HTS18 had been subjected to cyclic mechanical loading with large plastic deformation.

The chemical etching process does not cause additional surface roughness and residual stresses if it is well controlled. As a trial, a mixture of strong acids, $HNO_3(78\%) + HCL(38\%)$, in the ratio 1:1 was used. Tables 4.10-4.11 present the diameter change for specimens HTS18 and HTS05 after each layer removal and residual stresses measured using X-ray diffraction. It is shown in Table 4.10 for HTS18 that after a layer removal of thickness 0.03 mm the axial residual stress dropped from -183 MPa to -30 MPa. Measurements on HTS05, shown in Table 4.11, has shown that the residual stresses decreased as each layer was removed. This meant that the actual residual stress distribution near surface decreased from the surface to the interior.

A full layering method was applied to specimen HTS24. For the metal removal process to be more controlled, a less acidic solution was used. The solution consisted of,

Nitric acid	+ Hydrogen peroxide	+ oxalic acid	+ water
HNO_3(15%)	+ H_2O_2	+ $C_2H_2O_4$	+ H_2O
150ml	50ml	20g	500ml

It took about one hour to remove a 0.05 mm layer. The sample was taken out every 5 minutes to clean the surface by using running water and soft paper.

Axial and tangential residual stresses were measured by the X-ray diffraction on the new surface after each chemical etching. The measured axial and tangential residual stress results are presented in Table 4.12.

The axial and tangential residual stresses measured after chemical etching were the stresses that had been redistributed. If it is assumed that the relaxation was elastic after the chemical etching, the original distribution of residual stresses can be derived from the measured results. Equations (4.15) and (4.18) give the relationships between the original distribution and the measured results after layer removal.

To determine the residual stress distribution in the round bar from the measured results, a method was developed which considers the conditions for equilibrium in the round bar, which are expressed as

$$\int_0^R r\sigma_z dr = 0 \tag{4.19}$$

for axial residual stress and

$$\int_0^R \sigma_\theta dr = 0 \tag{4.20}$$

for tangential residual stress, and the boundary condition

$$\sigma_r\big|_{r=R} = 0. \tag{4.21}$$

Let r be radial co-ordinate that is non-dimensionlised by radius of bar so that $0 \le r \le 1$ and the R is replaced by 1 in Equations (4.19-4.21). The distributions of axial and tangential residual stresses will be determined separately.

Axial residual stress distribution

Assume that the axial stress distribution is of the form

$$\sigma_z = \begin{cases} a & \xi \le 0 \\ a + b\xi^2 + c\xi^3 & \xi > 0 \\ where \;\; \xi = r - q \end{cases} \tag{4.22}$$

where a, b, c are constants to be determined and q represents the boundary between plastic region and elastic region. After the plastic zone is removed, the residual stress will be totally relaxed. And therefore q is estimated from the measurements of the axial residual stress on the new surface, $\sigma'_{z,l}$, with the condition that

$$\sigma'_{z,l}\Big|_{l=1-q} = 0. \tag{4.23}$$

Inserting Equation (4.22) into Equation (4.15) and integrating gives,

$$\sigma'_{z,l} = \sigma_z + \frac{2}{(\xi+q)^2}\left[\frac{a}{2}(1-(\xi+q)^2) + b(\frac{1}{4}t^4 + \frac{1}{3}qt^3 - \frac{1}{4}\xi^4 - \frac{1}{3}q\xi^3) + c(\frac{1}{5}t^5 + \frac{1}{4}qt^4 - \frac{1}{5}\xi^5 - \frac{1}{4}q\xi^4)\right] \tag{4.24}$$

for $\xi > 0$.

For equilibrium by inserting Equation (4.22) into Equation (4.19), the constants, a, b, c, must satisfy the following condition

$$\frac{a}{2} + b(\frac{1}{4}t^4 + \frac{1}{3}qt^3 - \frac{1}{4}\xi^4 - \frac{1}{3}q\xi^3) + c(\frac{1}{5}t^5 + \frac{1}{4}qt^4 - \frac{1}{5}\xi^5 - \frac{1}{4}q\xi^4) = 0 \tag{4.25}$$

Using Equation (4.24) and the condition (4.25) as the equations in curve fitting and the experimental data $\sigma'_{z,l}$ measured by X-ray diffraction, the constants a, b and c were obtained and are presented in the Table 4.13. The fitted distributions for both $\sigma'_{z,l}$ and σ_z are shown in Figure 4.12. From the Figure 4.12 it can be seen that there

is only a slight difference in the fitted results between side A and Side B. This may be due to the difference between measurements on both sides of the specimen or the specimen being not precisely axisymmetric.

Tangential residual stress distribution

Using same curve fitting technique, the radial stress distribution is assumed to take the form

$$\sigma_r = \begin{cases} a & \xi \le 0 \\ a + b\xi^2 + c\xi^3 & \xi > 0 \\ where \;\; \xi = r - q \end{cases} \tag{4.26}$$

where a, b, c are constants to be determined which satisfy the boundary condition (4.21),

$$a + bt^2 + ct^3 = 0 \tag{4.27}$$

and q is estimated from the measurements of the tangential residual stress on the new surface, $\sigma'_{\theta,t}$, with the condition that

$$\sigma'_{\theta,t}\Big|_{t=1-q} = 0. \tag{4.28}$$

The q value should be same as that estimated from axial residual stress measurements. Then the tangential residual stress distribution is found from using Equations (4.16) and (4.26) and differentiating, to give,

$$\sigma_\theta = \begin{cases} a & \xi \le 0 \\ a + b\xi^2 + c\xi^3 + (\xi + q)(2b\xi + 3c\xi^2) & \xi > 0. \\ where \;\; \xi = r - q \end{cases} \tag{4.29}$$

Inserting Equations (4.26) and (4.29) into Equation (4.18), it is found that

$$\sigma'_{\theta,t} = (\xi + q)(2b\xi + 3c\xi^3) \tag{4.30}$$

for $\xi > 0$.

Using Equation (4.30) as the equation in curve fitting and the experimental data $\sigma'_{\theta,l}$ measured by X-ray diffraction, the constants, b and c, were obtained. Then the constant, a, was found from using Equation (4.27). The fitted constants for both sides A and B are listed in Table 4.13. The fitted distributions for $\sigma'_{\theta,l}$, σ_r and σ_θ are shown in Figure 4.9. Because of the difference between measurements on both sides of specimen there was also a slight difference between the fitted results on sides A and B.

4.3 Neutron Diffraction

4.3-1 Principles

Bragg's law is also applicable to neutron diffraction. Any non zero stress state will introduce elastic deformation leading to a small lattice spacing change Δd. It will result in a corresponding peak angle shift $\Delta\theta$. Differentiating equation (2.1), when λ is constant, gives

$$\Delta\theta = -\tan\theta \cdot \frac{\Delta d}{d} \tag{4.31}$$

Thus the lattice strain ε^e, in the direction of the scattering vector Q which bisects the incoming beam and detected beam as shown in Figure 3.4, is obtained

$$\varepsilon^e = \frac{\Delta d}{d} = -\Delta\theta \cdot \cot\theta \cdot . \tag{4.32}$$

To obtain the absolute lattice strain, a knowledge of either lattice spacing d_0 or the scattering peak angle $2\theta_0$ of the unstressed materials is necessary. Actually, for the d_0 and $2\theta_0$, if one is known, the other can be found using Bragg's equation (2.1). As indicated earlier, a simple way to find d_0 is to measure on a small cube that is extracted from the specimen (Smith, et. al, 1988 & 1992) where it is judged to be 'stress free'.

In all estimates stress-induced strains are measured by using equation (4.32) and then stresses calculated. In the interior of the specimen, there are normally six independent components of stress, which requires at least six strain measurements in different directions. For some special cases, such as where the direction of the principal stresses are known, measurements in three orthogonal orientations are often sufficient for a full definition of the stress state. Also, if only three normal

stresses in three orthogonal orientations are concerned, three strain measurements in the three orthogonal directions are sufficient. Using Hooke's law, the stresses are given by

$$\left.\begin{aligned}
\sigma_x &= \frac{E}{(1+\nu)(1-2\nu)}[(1-\nu)\varepsilon_x^e + \nu(\varepsilon_y^e + \varepsilon_z^e)] \\
\sigma_y &= \frac{E}{(1+\nu)(1-2\nu)}[(1-\nu)\varepsilon_y^e + \nu(\varepsilon_z^e + \varepsilon_x^e)] \\
\sigma_z &= \frac{E}{(1+\nu)(1-2\nu)}[(1-\nu)\varepsilon_z^e + \nu(\varepsilon_x^e + \varepsilon_y^e)]
\end{aligned}\right\}. \qquad (4.33)$$

The measured strains and stresses can be regarded as average values over the sample volume. The volume sampled is illustrated in Figure 3.4. This method is sensitive to the volume of material sampled, absorption in the material and the angle resolution of the neutron diffractometer.

4.3-2 Results of Measurements on Six U-Batch Specimens

Interior residual strains were measured in only six bars, specimen U1, U9, U10, U13, U18 and U20, see Table 3.3. Prior to examination of the round bar specimens, peak angles were measured from one end of a specimen where it was judged to be "stress free". The diffraction peak angle 2θ measured for the lattice spacing [110] was approximately 95.3° which was taken as the reference peak angle $2\theta_0$. The cylindrical system was employed for the round bars, as shown in Figure 4.1. Strains in three directions, axial (z), radial (r) and tangential (θ), were measured. For radial and tangential strains the sample volume was $1\times1\times10\,mm$, and for axial strains the volume was taken $2\times2\times2\,mm$. The diameter of each round bar was about 8 mm. Strain measurements at the centre and 2 mm either side of the centre ensured that the sampling area (represented by a rhomboid of 2 mm equal sides for the axial strains) was entirely within the material. The stresses in the three directions, axial, radial and tangential, are given by

$$\left.\begin{aligned}
\sigma_r &= \frac{E}{(1+\nu)(1-2\nu)}[(1-\nu)\varepsilon_r^e + \nu(\varepsilon_\theta^e + \varepsilon_z^e)] \\
\sigma_\theta &= \frac{E}{(1+\nu)(1-2\nu)}[(1-\nu)\varepsilon_\theta^e + \nu(\varepsilon_r^e + \varepsilon_z^e)] \\
\sigma_z &= \frac{E}{(1+\nu)(1-2\nu)}[(1-\nu)\varepsilon_z^e + \nu(\varepsilon_\theta^e + \varepsilon_r^e)]
\end{aligned}\right\} \qquad (4.34)$$

in which ε_r^e, ε_θ^e and ε_z^e represent radial, tangential and axial strains measured by neutron diffraction and σ_r, σ_θ and σ_z represent radial, tangential and axial stresses, respectively.

Figures 4.14 to 4.16 show the residual strains measured in the six specimens. Figures 4.17 to 4.19 give the residual stresses calculated from the residual strains. In general the largest residual stresses were in the axial direction. However the variation from sample to sample was substantial.

4.3-3 Development of Analysis — Near Surface Effect of Neutron Diffraction

In the neutron diffraction method it has been normally required that the whole neutron gauge volume is in the sample (Rudkins, et. al, 1994; Lorentzen, et. al, 1995). When the neutron gauge volume moves out of the sample to obtain near surface strains or stresses, some unrealistic values were obtained. If the dimension of the gauge volume is chosen to be 1 mm, which is about the minimum that can be used in most cases, and the diagonal dimension is about 1.4 mm, the measurements of residual strains can not be made within 1.4 mm from surface.

However, residual stresses on and near the surface are quite important in evaluating the fatigue life of the components. In many cases, short range residual stresses exist in components, particularly when subjected to shot peening or shot blast treatments, and the residual stress gradient is quite large within short distances. The incremental centre-hole method is normally used to obtain residual stress profile within this region (Niku-Lari, et. al, 1987; Zhu & Smith, 1994). But there are some problems with using this method. One is that it is a semi-destructive method, and the second is the problem with the plastic deformation during hole-drilling resulting in overestimating residual stresses (Nickola, 1984, Zhu & Smith, 1994).

An investigation has been undertaken to examine the surface effect of neutron diffraction measurements and to determine a method of interpreting the near surface residual stress distributions.

Experimental results

To examine the surface effect without the presence of residual stresses, two forged bars were prepared for the neutron diffraction measurements, specimens U6 and HTS18. Cyclic mechanical loadings were applied to the two specimens and the half strain range was up to 10000-12000 με (details are given in Chapter 6). The centre hole method was used to measure the near surface residual stresses and it was found that there were no residual stresses left in these two specimens (details are given in Section 4.4).

Although the specimens were mounted fairly accurately for neutron diffraction measurements, there was always some misalignment. To locate the centre of the sample, the neutron diffraction peak intensity as a function of position were used. The neutron gauge volume was $1 \times 1 \times 5\,mm$. The neutron diffraction peak intensity depends mainly on the material absorption, the neutron gauge volume and the distance travelled by the neutron beam in the sample. Figure 4.20 shows the neutron peak intensity for specimen HTS18 for tangential strain measurements. It can be seen that the figure is not symmetrical about the centre. The centre was then shifted about 0.55 mm and the intensities for the left and right hand side were drawn as a function of the absolute distance from shifted centre. Figure 4.21 shows the results. All subsequent measurement locations were then adjusted based on the revised centre of the specimen.

Measurements were made in two directions, axial and tangential, across the section, and using overlapping neutron gauge volumes. The surface effect was found to be different for each side because different parts of the neutron gauge volume were involved as shown in Figure 4.22. To look at the surface effect on how the gauge volume was approached from different sides, specimen HTS18 was examined in detail for axial strain measurements. After the specimen was measured from the right hand side edge to the centre, the specimen was turned 180° and then continually measured from the centre to the left hand side edge. In this way, the axial peak angle profile scanned from the left to the right, shown in Figure 4.23, exhibited a purely surface effect from different approaches without the influence of differences in material, shape and stress state between the two sides. The peak angle was also measured on stress free sample U6 in the axial direction without turning the specimen around. The results are also shown in Figure 4.23. Figure 4.24 shows the results of measurements on specimen HTS18 in the tangential direction and show a similar trend to the measurements in the axial direction. It is shown from these

measurements on the stress free samples that the each side appears to have an opposite surface effect.

After completing the measurements on the stress free samples, two samples HTS19 and HTS22 were examined. The two specimens had been subjected to prior cyclic mechanical loading with that $\frac{\Delta\varepsilon}{2} = 1000\,\mu\varepsilon$ *and* $1800\,\mu\varepsilon$, respectively. Neutron diffraction strain measurements were obtained in the axial and tangential directions. The peak angle measured for HTS19 and HTS22 in axial and tangential direction are shown in Figures 4.25 and 4.26 and compared with those from the 'stress free' sample HTS18. It can be seen that the peak angle was moved upwards near to the edges of the specimens which means there were compressive residual stresses and strains near to the specimen surface.

Determination of measurement location from gauge volume centre

The neutron diffraction occurs over the whole neutron gauge volume. Thus, the result obtained is an average value over the gauge volume. It is practical to express the result of the measurement at a single point. Normally, the material volume weighted centre is used to determined the location of the material volume. The weighted centre can be found by

$$X_w = \frac{\int_{V_m} X dv}{\int_{V_m} dv} \tag{4.35}$$

where V_m is the material volume within neutron gauge volume V. If the neutron gauge volume is totally inside the sample, $V_m = V$ and material weighted centre is equal to neutron gauge volume centre. When the neutron gauge volume moves out of the specimen, $V_m < V$ and the material weighted centre is different from the neutron gauge volume centre.

In the case of a round bar sample, in which all components are assumed to be axisymmetrical, the weighted centre is not the best choice in expressing the location of measurement. For example, if a measurement is over an arc with $r = r_c$ & $-\theta_c \le \theta \le \theta_c$, the measured result will be the same as that at the location $r = r_c$ & $\theta = 0$. However, this location is not the weighted centre of the arc.

To express the location of the measurement for the axisymmetric case, a special parameter called the radial centre of material volume, r_c, is introduced

$$r_c = \frac{\int_{V_m} r dv}{\int_{V_m} dv} \tag{4.36}$$

which is similar to the Equation (4.35) for the material weighted centre. But there is significant difference between them, especially when measurement is within a short distance from the centre of the bar about the gauge volume dimension. When the neutron gauge volume is right at the centre of the bar the radial centre of material volume is not at the centre and is about half way between the bar centre and the edge of the gauge volume. A numerical integration method was used to obtain the radial centre from Equation (4.36). Figures 4.27 and 4.28 show axial strain and tangential strain profiles for specimen HTS19 when using both the neutron gauge volume centre and the radial centre.

Direct method of determining residual stresses using results from the stress free sample

After the peak angles 2θ were obtained from the neutron diffraction measurements across a section in a specimen in the axial and tangential directions, there were two parameters required for determining the strains. One was the peak angle $2\theta_0$ for the stress free state for the same material and conditions and the other was to take account of the surface effect. These two could be obtained from the measurements on the stress free samples. Two assumptions were made before making use of the measurement results from the stress free sample,

a) *The material and test conditions for both the stressed sample and stress free sample were the same and therefore the* $2\theta_0$ *'s in these two samples are equal.*

b) *The surface effect was independent of stress state and only influenced* $2\theta_0$. *The changes of* $2\theta_0$ *were the same in different samples as long as the geometrical shapes were same for these two samples.*

Therefore, based on these assumptions the strains were found by taking the difference between the measurements on the stressed and the stress free samples.

The measured peak angles for the stress free sample HTS18 and samples HTS19 and HTS22 in axial and tangential directions are presented in Figures 4.25 and 4.26 using the location of gauge volume centre. By taking the peak angle difference between samples, HTS19 and HTS22, and stress free sample HTS18, the axial and tangential strains, ε_z and ε_θ, were obtained for specimens HTS19 and HTS22. The results are shown in Figures 4.29 and 4.30 in which the locations are expressed in terms of the nondimensionlised radical centre, r_c/R. Linear interpolation was used to obtain values at a point which is located between measurement positions.

To obtain distributions of the stress components, σ_r and σ_θ, an assumption about distribution of radial strain or radial stress was required. The radial stress must satisfy the following conditions,

$$\sigma_r|_{r=0} = \sigma_\theta|_{r=0} \left(or\ \varepsilon_r|_{r=0} = \varepsilon_\theta|_{r=0}\right)\ and\ \ \sigma_r|_{r=R} = 0. \tag{4.37}$$

Using Hooke's law, the radial stress at the centre is given by

$$\sigma_r|_{r=0} = \frac{E}{(1+\upsilon)(1-2\upsilon)}\left(\varepsilon_\theta|_{r=0} + \upsilon\varepsilon_z|_{r=0}\right). \tag{4.38}$$

One assumption for the σ_r was that its maximum value is at the location $r = 0.5 \sim 0.6\,R$. Then a distribution of σ_r was taken the form,

$$\sigma_r = a + b\xi^2 + c\xi^3,\ \ \xi = r/R \tag{4.39}$$

where a, b and c are determined using the σ_r values at centre and surface and condition of its maximum value between $\xi = 0.5$ and $\xi = 0.6$. The distributions of σ_r are shown in Figures 4.31, 4.32, 4.33 and 4.34. The strain ε_r is then given by

$$\varepsilon_r = \frac{(1+\upsilon)(1-2\upsilon)}{(1-\upsilon)E}\sigma_r - \frac{\upsilon}{1-\upsilon}(\varepsilon_\theta + \varepsilon_z). \tag{4.40}$$

Finally, the axial and tangential stresses were obtained,

$$\left.\begin{aligned}\sigma_\theta &= \frac{E}{(1+\upsilon)(1-2\upsilon)}\left[(1-\upsilon)\varepsilon_\theta + \upsilon(\varepsilon_r + \varepsilon_z)\right] \\ \sigma_z &= \frac{E}{(1+\upsilon)(1-2\upsilon)}\left[(1-\upsilon)\varepsilon_z + \upsilon(\varepsilon_r + \varepsilon_\theta)\right]\end{aligned}\right\}. \tag{4.41}$$

The calculated residual stresses are shown in Figure 4.31 for HTS19 and Figure 4.32 for HTS22.

From the axial and tangential residual stresses shown in the Figures 4.31 and 4.32, it can be seen that they do not satisfy equilibrium, which has been expressed in Equations 4.19 and 4.20. This may be due to several reasons:

a) *There were measurement errors.*

b) *The stress free lattice spacing d_0 for different samples may not be guaranteed to be the same and it might vary within one sample, because the conditions of process and treatment may not be the same everywhere.*

c) *The stress free sample HTS18 had undergone large cyclic plastic deformation to relax the residual stresses which could result in changing the stress free lattice spacing d_0.*

Therefore it was possible that there were systematic differences in the stress free lattice spacing d_0 between the stress free sample HTS18 and samples HTS19 or HTS22. To correct it a constant strain was added to both axial strain ε_z and tangential ε_θ in Figures 4.29 and 4.30. The stresses and strains were recalculated using the procedure stated above. The modified stress results are shown in Figures 4.33 and 4.34 for specimens HTS19 and HTS22, respectively.

Average method of determining residual stresses without using the results of the stress free sample

From the neutron diffraction results obtained from the stress free samples HTS18 and U06, shown in Figures 4.23 and 4.24, it can be seen that the surface effects on right hand side and left hand side were approximately asymmetric. If the surface influence on peak angle measurements is assumed to be asymmetric about the centre, we have

$$\left.\begin{aligned}\theta(x) &= f_1(x) + f_2(x)\\ f_2(x) &= -f_2(-x)\end{aligned}\right\} \tag{4.42}$$

where $\theta(x)$ expresses the measured peak angle from the left hand side to the right hand side across the centre, $f_1(x)$ is the function that describes the contribution from elastic strain and $f_2(x)$ is the function that describes the contribution from the surface effect. In the following $f_1(x)$ is determined. In order to eliminate $f_2(x)$, the peak angles on the left side and the right side at the point of symmetry are summed, so that

$$\Theta(x) = \frac{\theta(x) + \theta(-x)}{2} = \frac{f_1(x) + f_1(-x)}{2} \qquad x \geq 0\,. \tag{4.43}$$

If the strains are symmetrical about the centre, Equation (4.43) becomes

$$\Theta(x) = f_1(x) \qquad x \geq 0 \tag{4.44}$$

which means that the function $\Theta(x)$ is purely related to the strain profile. If the strains are not symmetrical about the centre, the result from Equation (4.43) can be treated as an average value over both sides on the line of symmetry.

Therefore without using results from stress free sample and assuming that the geometrical influence by neutron diffraction on measured results were asymmetrical, the peak angles on the left and right sides were summed. Linear interpolation was also used because the measurements were not on the same location on both sides. For this technique, the stress free lattice spacing d_0 was first assumed, and then the axial and tangential strains distributions were obtained. The radial stress was assumed in the same way as previously. The resulting strains are shown in Figures 4.35 and 4.37. Then all stress components were calculated using Hooke's law. The parameter d_0 was finally adjusted by using the equilibrium shown in Equations 4.19 and 4.20. The resulting residual stress distributions are shown in Figures 4.36 and 4.38.

4.4 Centre Hole Method

4.4-1 Principles of Analyses for Flat Surfaces

Conventional One Step Method

The theory for the one step method is based on a through-thickness hole of a thin plate where the residual stresses are uniform (Mathar, 1934; Rendler, et. al, 1966). The residual stress state is assumed to be biaxial in a plane stress state. After a strain gauge rosette, which normally includes three strain gauges in three directions, is bonded to a sample surface, a hole is drilled in the centre of the rosette. Then the strain changes due to hole drilled are recorded. Usually a blind hole is enough because after the hole is deep enough (about the distance of hole diameter) there is no further measurable strain change. The plane strain state has three unknowns to be determined and there are three strain changes in three directions obtained. Therefore the surface stress state can be determined. Figure 3.6 shows a typical strain rosette arrangement and a description of the main dimensions. For either a through-hole or a blind-hole, elastic analysis gives the relationship between the measured surface radial strain ε_r and the relieved residual stresses after hole drilling (Schajer, 1988),

$$\varepsilon_r(\alpha) = A(\sigma_1+\sigma_2)+B(\sigma_1-\sigma_2)\cos 2\alpha \tag{4.45}$$

where A and B are constants related to the material, hole diameter, the geometry of the strain gauges and the depth of the hole, α is the relative location of the direction between strain gauge 1 and principal stress σ_1. After the hole is drilled and measurement of strains in three directions, 0°, 45° or 225° and 90°, obtained, then the relationship between the measured strains and the stress state, described by the two principle stresses σ_1 and σ_2 and the angle α, is found from the Equation (4.45),

$$\left.\begin{aligned}
\varepsilon_1 &= A(\sigma_1+\sigma_2)+B(\sigma_1-\sigma_2)\cos 2\alpha \\
\varepsilon_2 &= A(\sigma_1+\sigma_2)+B(\sigma_1-\sigma_2)\cos 2(\alpha+45°) \\
\varepsilon_3 &= A(\sigma_1+\sigma_2)+B(\sigma_1-\sigma_2)\cos 2(\alpha+90°)
\end{aligned}\right\}. \tag{4.46}$$

The σ_1, σ_2 and α can be solved from the Equations (4.46)

$$\left.\begin{aligned}\sigma_1 &= \frac{\varepsilon_1+\varepsilon_3}{4A}+\frac{\sqrt{2}}{4B}\sqrt{(\varepsilon_1-\varepsilon_2)^2+(\varepsilon_2-\varepsilon_3)^2}\\ \sigma_2 &= \frac{\varepsilon_1+\varepsilon_3}{4A}-\frac{\sqrt{2}}{4B}\sqrt{(\varepsilon_1-\varepsilon_2)^2+(\varepsilon_2-\varepsilon_3)^2}\\ \tan 2\alpha &= \frac{\varepsilon_1-2\varepsilon_2+\varepsilon_3}{\varepsilon_3-\varepsilon_1}\end{aligned}\right\}. \qquad (4.47)$$

In the Equations (4.47), the two constants, A and B need to be found. The method to obtain these constants has been reviewed in Section 2.2-3.

Incremental Hole-Drilling Method

Many methods have been developed to find non-uniform residual stress distribution by hole drilling (Schajer, 1988). Among these methods, the integral method (Bijak-Zochowski, 1978; Niku-Lari, 1985; Flaman, et. al, 1985) gave a good stepwise approximation to the actual stress variation with depth.

In order to determine the residual stress distribution from the integral method, some assumptions are required (Niku-Lari, 1985):

i) *The material is elastic. This means the stress released during drilling is less than the elastic limit and the plastic deformation caused by drilling is negligible.*

ii) *The stress components normal to the surface are very small compared to the other stress components.*

iii) *The stresses in each layer of material which is removed by drilling is uniform. An average value in each layer is therefore used.*

iv) *The material is isotropic and only two elastic constants are required, Young's Modulus, E, and Poisson's ratio,* υ. *If the material behaves anisotropically, more than two elastic constants are required.*

From the assumption 2, the stress state is plane stress and three independent parameters, principal stresses σ_1, σ_2 and angle α between strain gauge 1 and principal stress σ_1, need to be found to determine the stress state. Because the

residual stresses vary with depth, therefore the three parameters are the functions of depth

$$\sigma_1 = \sigma_1(h),\ \sigma_2 = \sigma_2(h)\ \textit{and}\ \alpha = \alpha(h) \tag{4.48}$$

where h is the normal distance from the surface. With this integral method, the actual stress distribution is to be replaced by a step-wise-constant distribution shown in Figure 4.39. For n total drilling steps the corresponding depth of the hole being h_n, the distribution is assumed as

$$\left.\begin{aligned} \sigma_1 &= \sigma_{1,i} \\ \sigma_2 &= \sigma_{2,i} \\ \alpha &= \alpha_i \end{aligned}\right\} \qquad \textit{for}\ \ h_{i-1} \le h \le h_i \qquad i = 1,\cdots,j,\cdots n\,. \tag{4.49}$$

Assuming only stresses in ith layer are removed after the hole is drilled with j steps, where $i \le j \le n$, Equation (4.45) is still valid and the strain changes at the surface can be expressed as

$$\left.\begin{aligned} \varepsilon_{1,i}^{(j)} &= A_{ji}(\sigma_{1,i} + \sigma_{2,i}) + B_{ji}(\sigma_{1,i} - \sigma_{2,i})\cos 2\alpha_i \\ \varepsilon_{2,i}^{(j)} &= A_{ji}(\sigma_{1,i} + \sigma_{2,i}) + B_{ji}(\sigma_{1,i} - \sigma_{2,i})\cos 2(\alpha_i + 45°) \\ \varepsilon_{3,i}^{(j)} &= A_{ji}(\sigma_{1,i} + \sigma_{2,i}) + B_{ji}(\sigma_{1,i} - \sigma_{2,i})\cos 2(\alpha_i + 90°) \end{aligned}\right\}. \tag{4.50}$$

The coefficients A_{ji} and B_{ji} are functions of the hole diameter, the geometry of the strain gauges, the position of the layer i and the depth of the hole. These coefficients can be calculated using finite element method (Niku-Lari, 1985; Schajer, 1988). Since all stresses are removed from the surface of the hole after hole drilling, the strain changes at three locations are,

$$\varepsilon_1^{(j)} = \sum_{i=1}^{j} \varepsilon_{1,i}^{(j)} \qquad j = 1,\cdots n \tag{4.51a}$$

$$\varepsilon_2^{(j)} = \sum_{i=1}^{j} \varepsilon_{2,i}^{(j)} \qquad j = 1,\cdots n \tag{4.51b}$$

$$\varepsilon_3^{(j)} = \sum_{i=1}^{j} \varepsilon_{3,i}^{(j)} \qquad j = 1,\cdots n \tag{4.51c}$$

which are the strains measured from the strain rosette after j steps. Equations (4.51) can be restated as

$$\varepsilon_{1,j}^{(j)} = \varepsilon_1^{(j)} - \sum_{i=1}^{j-1} \varepsilon_{1,i}^{(j)} \qquad j = 1,\cdots n \tag{4.52a}$$

$$\varepsilon_{2,j}^{(j)} = \varepsilon_2^{(j)} - \sum_{i=1}^{j-1} \varepsilon_{2,i}^{(j)} \qquad j = 1,\cdots n \tag{4.52b}$$

$$\varepsilon_{3,j}^{(j)} = \varepsilon_3^{(j)} - \sum_{i=1}^{j-1} \varepsilon_{3,i}^{(j)} \qquad j = 1,\cdots n \tag{4.52c}$$

Because stresses, $\sigma_{1,i}$, $\sigma_{2,i}$, and angles α_i, for *i* from *1* to *j-1* have been obtained from previous steps. Using Equations (4.50), the strains, $\varepsilon_{1,j}^{(j)}$, $\varepsilon_{2,j}^{(j)}$ and $\varepsilon_{3,j}^{(j)}$, for *i* from *1* to *j-1* can then be found. Then the strains, $\varepsilon_{1,j}^{(j)}$, $\varepsilon_{2,j}^{(j)}$ and $\varepsilon_{3,j}^{(j)}$, are obtained from Equations (4.58). Finally inserting the strains $\varepsilon_{1,j}^{(j)}$, $\varepsilon_{2,j}^{(j)}$ and $\varepsilon_{3,j}^{(j)}$, obtained into Equation (4.56), the stresses $\sigma_{1,i}$, $\sigma_{2,i}$ and principal direction angle α_i can be found.

4.4-2 Development of Analysis for Components With Curved Surfaces

All current theoretical and numerical analyses for the hole-drilling technique are based on the Equation (4.49). This formula only applies if axial symmetry about the hole is maintained before and after hole being drilled, and the specimen surface is flat. If a component has a curved surface, such as a round bar, the above formula is no longer valid. For an experiment using the solid round bar there was substantial surface curvature.

In order to determine the stress distribution from the incremental hole drilling method on a curved surface the same assumptions described in section 4.4-1 apply. In addition to these assumptions it is assumed that plane stress conditions exist in the area where a hole is drilled and that stresses only vary with depth (in the z-direction normal to the surface), so that the residual stresses can be expressed by using three independent parameters

$$\sigma_x = \sigma_x(h), \sigma_y = \sigma_y(h) \; and \; \tau_{xy} = \tau_{xy}(h) \tag{4.53}$$

where X-axis relates to the direction of gauge 1 direction, Y-axis gauge 3 direction and h is the normal distance from the surface. When a hole is being drilled to a depth *H*, the strain changes on the surface at three locations, say *a, b, c,* are measured

$$\varepsilon_a = \varepsilon_a(H), \; \varepsilon_b = \varepsilon_b(H), \; \varepsilon_c = \varepsilon_c(H) \tag{4.54}$$

Using matrix notation,

$$\vec{\sigma} = \vec{\sigma}(h) = \begin{Bmatrix} \sigma_x(h) \\ \sigma_y(h) \\ \tau_{xy}(h) \end{Bmatrix} \tag{4.55}$$

and

$$\vec{\varepsilon} = \vec{\varepsilon}(H) = \begin{Bmatrix} \varepsilon_a(H) \\ \varepsilon_b(H) \\ \varepsilon_c(H) \end{Bmatrix}. \tag{4.56}$$

Assuming that only stresses on the hole surface in the range $(h, h+dh)$, where $h \le H$, are being removed, then the strain change at the surface should be

$$d\vec{\varepsilon} = \hat{A}(h,H)\vec{\sigma}(h)dh \tag{4.57}$$

where the function $\hat{A}(h,H)$ is 3×3 matrix relating to material, the hole dimensions and the geometry of the strain gauges. Integrating Equation (4.57), we obtain the integral equation

$$\vec{\varepsilon}(H) = \int_0^H \hat{A}(h,H)\vec{\sigma}(h)dh \tag{4.58}$$

which is similar to that in the integral method described by Bijak-Zochowski (1978). If $\hat{A}(h,H)$ is known and $\vec{\varepsilon}(H)$ is measured as a function of H, then the unknown distributions of residual stresses $\vec{\sigma}(h)$ can be theoretically determined by solving the integral equation.

With the average strain method, the actual stress distribution is to be replaced by a step-wise-constant distribution as shown in Figure 4.39. For n drilling steps and h_n the corresponding depth of the hole, the distribution is assumed as

$$\vec{\sigma}(h)\big|_{h_{i-1} \le h \le h_i} = \vec{\sigma}_i = \begin{Bmatrix} \sigma_{x,i} \\ \sigma_{y,i} \\ \tau_{xy,i} \end{Bmatrix} \quad i = 1, \cdots n \text{ and } \begin{matrix} h_0 = 0 \\ h_n = H \end{matrix} \Big\}, \tag{4.59}$$

the integral equation (4.58) then becomes

$$\vec{\varepsilon}(h_j) = \sum_{i=1}^{j} \int_{h_{i-1}}^{h_i} \hat{A}(h,h_j)\vec{\sigma}(h)dh = \sum_{i=1}^{j} \tilde{A}_{ji}\vec{\sigma}_i \qquad i \le j \le n, \quad j = 1,\cdots,n \tag{4.60}$$

where

$$\tilde{A}_{ji} = \int_{h_{i-1}}^{h_i} \hat{A}(h,h_j)dh\,. \tag{4.61}$$

$\tilde{A}_{ji}$ is a 3×3 matrix and can be found by finite element analysis. If $\tilde{A}_{ji}$ is known and $\vec{\varepsilon}(h_j)$ is measured, then the unknown residual stresses $\vec{\sigma}_i$ can be determined by solving the linear algebra equations (4.61). However, $\tilde{A}_{ji}$ for all i and j have yet to be determined.

4.4-3 Finite Element Calculations to Determine Coefficients

Calculations of coefficients A_{ji} and B_{ji}

For the centre hole method used for components with flat surfaces, the geometry around the hole is axisymmetrical and those coefficients A_{ji} and B_{ji} used in Equation (4.50), have been calculated for many geometric cases, such as different hole diameters, using finite element (FE) analysis by Niku-Lari (1985) and Schajer (1988).

To determine the coefficients A_{ji} using FE, a unit pressure was applied on the surface of the ith layer. In this case both geometry and loading are axisymmetric. An axisymmetric FE model was therefore adopted. Two types of elements were used, 8 node isoparametric solid element and 6 node triangular solid element. A representative mesh is shown in Figure 4.40. From the FE analysis, the coefficient A_{ji} can be determined from the displacements by

$$A_{ji} = \frac{u_{r2} - u_{r1}}{2(r_2 - r_1)} \tag{4.62}$$

where r_1 and r_2 are radii of the strain rosette shown in Figure 3.6, u_{r1} and u_{r2} are the radial displacements at $r = r_1$ and $r = r_2$, respectively. Since nodes are at $r = r_1$ and $r = r_2$, then u_{r1} and u_{r2} are the node displacements.

To determine B_{ji}, three-dimensional FE analysis is normally required. Since the geometry is axisymmetric, by Fourier transformation, this problem can still be treated in two dimensions (Schajer, 1981) which is always preferred. Niku-Lari (1985) has suggested using a FE module EF2D of CASTOR 2D which performs elastic analyses of small strains and displacements of axisymmetric bodies, but under non-axisymmetric loadings. However this software was not available.

Schajer (1988) calculated A_{ji} and B_{ji} for many geometric cases but all applied to flat plates. The terms A_{ji} versus B_{ji} are plotted in Figure 4.41. Using linear regression, an approximate relationship between A_{ji} and B_{ji} is

$$B_{ji} = 1.4355 A_{ji} - 0.05271 \qquad (MPa^{-1}). \tag{4.63}$$

Also the coefficients A_{ji} and B_{ji} can be obtained by quadratic interpolation of the values of A_{ji} and B_{ji} presented by Schajer (1988) by using finite element method for different geometric cases.

Calculating coefficient matrixes $\tilde{A}_{ji}$ for a round bar

Since a round bar has a cylindrical surface, the geometry is no longer axisymmetric after a hole drilling and three-dimensional FE analyses are necessary. A particular mesh for the hot forged round bar is shown in Figure 4.42.

From Equation (4.60), we obtain the strain change caused by only removing $\bar{\sigma}_i$ from *i*th layer

$$\bar{\varepsilon}_{ji} = \tilde{A}_{ji}\bar{\sigma}_i. \tag{4.64}$$

Using a matrix format, Equation (4.64) becomes

$$\begin{Bmatrix} \varepsilon_a^{ji} \\ \varepsilon_b^{ji} \\ \varepsilon_c^{ji} \end{Bmatrix} = \begin{bmatrix} a_{11}^{ji} & a_{12}^{ji} & a_{13}^{ji} \\ a_{21}^{ji} & a_{22}^{ji} & a_{23}^{ji} \\ a_{31}^{ji} & a_{32}^{ji} & a_{33}^{ji} \end{bmatrix} \times \begin{Bmatrix} \sigma_x^i \\ \sigma_y^i \\ \tau_{xy}^i \end{Bmatrix}. \tag{4.65}$$

The procedure to obtain the coefficient matrix $\tilde{A}_{ji}$ using finite element (FE) analyses was as follows:

i) Generate FE mesh with the hole depth h_j.

ii) Let $\sigma_x^i = 1$, $\sigma_y^i = 0$ and $\tau_{xy}^1 = 0$, then calculate the surface traction of the hole in ith layer corresponding to this stress state.

iii) Convert the surface traction into node forces acting on the FE model.

iv) From FE calculations find the strain values at three locations at which the strain gauges are located.

v) Using Equation (4.65), we obtain the first column of the coefficient matrix $\tilde{A}_{ji}$

$$\begin{bmatrix} a_{11}^{ji} \\ a_{21}^{ji} \\ a_{31}^{ji} \end{bmatrix} = \begin{Bmatrix} \varepsilon_a^{ji} \\ \varepsilon_b^{ji} \\ \varepsilon_c^{ji} \end{Bmatrix}_{\sigma_x^i = 1} . \tag{4.66}$$

vi) Let $\sigma_y^i = 1$, $\sigma_x^i = 0$ *and* $\tau_{xy}^i = 0$, and using the same procedure as above to obtain

$$\begin{bmatrix} a_{12}^{ji} \\ a_{22}^{ji} \\ a_{32}^{ji} \end{bmatrix} = \begin{Bmatrix} \varepsilon_a^{ji} \\ \varepsilon_b^{ji} \\ \varepsilon_c^{ji} \end{Bmatrix}_{\sigma_y^i = 1} . \tag{4.67}$$

vii) Let $\tau_{xy}^i = 1$, $\sigma_x^i = \sigma_y^i = 0$. In this case, the loading condition is asymmetric and the constraint boundary condition should be different from the above cases. This yields the third column of the matrix $\tilde{A}_{ji}$

$$\begin{bmatrix} a_{13}^{ji} \\ a_{23}^{ji} \\ a_{33}^{ji} \end{bmatrix} = \begin{Bmatrix} \varepsilon_a^{ji} \\ \varepsilon_b^{ji} \\ \varepsilon_c^{ji} \end{Bmatrix}_{\tau_{xy}^i = 1} . \tag{4.68}$$

viii) In turn, let $j = 1, \cdots, n$ and $i = 1, \cdots, j$, then all the coefficient matrixes $\tilde{A}_{ji}$ are determined.

The FE element type chosen was a twenty-node isoparameteric element. A refined mesh surrounding the hole was used. Assuming the number of drilling steps is ten, then the number of loading cases was

$$N = 3 \times \sum_{j=1}^{10} j = 165. \tag{4.69}$$

Extensive finite element analyses were carried out. FORTRAN programs were written for procedures (iii) and (iv) to convert surface traction into node forces and node displacement results into strains. These results were then used to obtain the coefficient matrixes $\tilde{A}_{ji}$. Table 4.14 presents a example of coefficient matrix $\tilde{A}_{jl}$ for a round bar specimen with bar diameter 8 mm, with hole diameter 1.74 mm, drilling increment 0.08 mm, using the larger strain gauge type, gauge 1 along the hoop direction and gauge 3 along the axial direction.

4.4-4 Experiments

Procedure and specimens

The device and strain gauge rosettes for the hole drilling have been described in Chapter 3. The holes were drilled incrementally. The larger rosettes were mainly used for specimens with flat surfaces and only two round bar U-batch specimens, together with FE analysis for curved surfaces. The smaller rosettes were used for round bar specimens from the HTS and FS batches.

For the larger strain gauge rosette used, the hole diameter was 1.7-2.0 mm and the depth of most holes was about 1.6 mm. Within the first 60% of the total depth, the increment of the depth was equal to 10% of the total depth. For the remaining 40% of the depth, the increment are equal to 20% of the total depth. Therefore there were normally eight increments for one hole. In one case, specimen U5, two holes were drilled, one on each side. For one of the holes, drilling was done with ten drilling steps and a depth increment of about 0.08 mm.

The smaller strain gauge rosettes were mainly used for round bar specimens from U, HTS and FS batches. The motivation for using these smaller rosettes was to reduce the influence of the curvature of the round bar specimens on the strain results from hole drilling and therefore to use a simple analysis for flat surfaces. The hole

diameter was 0.9-1.0 mm. the holes were drilled incrementally with an incremental depth of 0.0254 mm. The strains were recorded at each step.

The specimens for the hole drilling using the larger strain gauge rosettes included two hot forged rectangular bars with dimensions 65×65×585 mm (one of which was subjected to shot blast treatment), a stress free plate and two hot forged round bar specimens U5 and U11.

Round bar specimens for the hole drilling with the use of smaller strain gauge rosettes included U15, HTS09, HTS17 HTS20 from HTS batch, FS16 and FS18 from FS batch.

4.4-5 Experimental Results

Effect of the drilling operation on residual stresses on En15R specimen

Niku-Lari (1985) had carried out a series of tests for different materials to analyse the hole-drilling condition, their effect on hole geometry and further the residual stresses. It was concluded that drilling methods had no effect on the micro-structure of the materials and residual stresses and using compressed-air turbine system had advantages over other drilling methods.

In order to determine any influence of the drilling operation on residual stresses for the En15R specimens, first drilling was carried out on the stress-free plate that had examined by X-ray. The strain changes measured by three gauges on the surface of the plate with respect to the depth of the hole were given in the Table 4.12. It can been seen that the strains were very small, and it can been assumed there were no residual stresses introduced by the hole drilling operation.

Two rectangular bars with flat surfaces

For the two rectangular bars, one of which had shot blast treatment, the surfaces were flat. The larger strain gauge rosettes were used. Two tests were made on each bar. The results of strain measurements with respect to the drilling depth are listed in Table 4.15 and shown in Figures 4.43 and 4.44. Comparing the strain results of the two rectangular bars, it can be seen that shot blast sample had more strain release compared to the non-shot blast sample, and therefore there were more residual stresses in shot blast specimen than in non-shot blast specimen.

By using the elastic analysis for flat surfaces, the residual stresses in the two rectangular bars are presented in Figures 4.45 to 4.48. From the results we can see that after 5 steps with drilling depth beyond 0.7 mm some of the interpolated stress results become unrealistic. The residual stresses at the surface for the shot blasted bar were quite high and the values from the second drilling were near to the yielding stress which was also unrealistic. This high prediction may be caused by plastic deformation during hole drilling. Detailed discussion of this behaviour will be given in Section 4.4-6.

Round bar specimens with larger strain gauge rosettes used

The larger strain gauge rosettes were bonded to round bar specimens U11 and U5, the latter specimen being drilled on both sides. The strain results were listed in Table 4.15 and also presented in Figures 4.49 and 4.50. From the strain results measured it can be seen that the strain relaxation from the three incremental centre hole measurements were quite similar. Therefore the residual stresses at these locations on the U-batch specimens would be expected to be similar. From Figure 4.49, it can be seen the strain release at the first step was quite small compared with other tests. This may be due to the effect of surface roughness of the specimen.

Because the strain gauge rosette used for round bar specimens was quite large compared with the dimensions of the round bar, there was a significant effect of curvature on the results of strains and 3-D FE analysis was necessary. Since FE work for each hole analysis was extensive, only the strain data from the second test on side B of specimen U5 were analysed.

The hole diameter for this analysis was 1.74 mm. The details of the procedure of the FE analysis have been described in previous sections 4.4-2 and 4.4-3. The residual stress results for the specimen U5 from using the 3-D FE analysis are given in Figure 4.51. The residual stresses of specimen U5 were much higher than those measured by X-ray diffraction method (shown in Table 4.5). We anticipate that if additional plastic deformation takes place then an elastic analysis would overestimate the magnitude of the residual stresses. This will be discussed in a later section, and the residual stresses will be modified by considering plastic yielding during the hole drilling process.

Round bar specimens using smaller strain gauge rosettes

To avoid extensive 3-D FE work, which was necessary when using a larger strain gauge rosette on the round bar specimen, smaller strain gauge rosettes, WA-06-030WR-120, were used for hole-drilling specimens U15 side B, HTS09 side A and B, HTS17 side A, HTS20 side B, FS16 side B and FS18 side B. The strain gauge rosettes were easier to wrap and bond around specimens than the previous larger ones. The holes were drilled incrementally using the high-speed air turbine. The hole diameter D_0 for each hole drilled was different and varied from hole to hole. The average value was about 0.9 mm.

The results of strain relaxation as a function of drilling depth are shown in Figures 4.52 to 4.58. Preliminary estimation of the residual stresses using these results indicated that the residual stresses were unrealistic high. Using the 2-D elastic analysis of incremental hole-drill described in section 4.4-2, most of the residual stress results estimated were up to -700 MPa. An extreme example was a result from specimen HTS09 where it was found that axial residual stress on the surface of side A reached -1300 MPa. These results were much higher than those measured by X-ray diffraction and some even higher than the yield stress of the material. This behaviour assumed to be a consequence of plastic deformation during hole drilling (Nickola, 1984) and more details will be in the next section. Therefore an introduction of a modification to consider the plastic deformation after hole drilling was inevitable. This work can be done by both theoretical and FE analyses.

4.4-6 Plastic Modification

Many investigators had noticed the effects of plasticity and local yielding around the drilled hole and the potential errors in determining the residual stresses were estimated (Nawwar, et al, 1977; Bynum, 1981; Procter, et al, 1982; Scaramangas et al, 1982; Nickola, 1984; Beghini, 1994; Lin, et al, 1995). But there are no effective methods to consider the influence of plastic yielding on the residual stress predictions.

To understand the effect of plastic yielding during hole drilling, two questions need to be answered.

1) *Is the stress state in a loading condition (the increment of Von Mises equivalent stress greater than zero, $d\sigma_{eq} \geq 0$) or in an unloading condition ($d\sigma_{eq} < 0$) during hole drilling?*

2) *Is the stress state on the yield surface before and after hole drilling?*

Examples can be given to answer the first question. Take a biaxial stress state for a plate, where

$$\sigma_x = \sigma_y = \sigma \quad or \quad \sigma_r = \sigma_\theta = \sigma \tag{4.70}$$

and the equivalent stress σ_{eq}. is σ. After a hole is drilled, the radial stress at the hole surface is released and the stress state at the hole surface is changed to,

$$\left.\begin{aligned} \sigma_r &= 0 \\ \sigma_\theta &= 2\sigma \end{aligned}\right\}. \tag{4.71}$$

The equivalent stress for this stress state is $\sigma_{eq} = 2\sigma$. Therefore the stress state during hole drilling is in a loading condition.

The second question is not easy to consider. It depends on many factors, such as stress state, material stress-strain behaviour and the strain history from which the residual stresses are introduced. For an elastic-perfectly plastic material, it is determined by the residual stress state. With a biaxial residual stress state, if the residual stress is greater than 50% of the yield stress, the stress state around the hole

area will be on the yielding surface. For the uniaxial residual stress state, measurements are inherently limited to stresses to within 1/3 of the yield stress to keep the stress state within the elastic region (Nawwar, et al, 1976).

So far, it appears that no one has considered the influence of strain history on strain relaxation during hole drilling. For residual stresses introduced by non-uniform plastic deformation, such as by the processes of shot peening or shot blasting, the residual stress state may already be on the yield surface before hole drilling, especially for the materials that exhibit a Bauschinger effect. To explain this, we just simply describe how the residual stresses are produced as a result of shot peening:

> *When a ball hits the sample surface (assume z is the normal direction of the surface), a pressure is applied. Let the stress state be* $\sigma_z < \sigma_y = \sigma_x < 0$ *and the deviatoric stresses* $S_z < 0$ *and* $S_y = S_x > 0$. *As there is large plastic deformation, the* σ_y *and* σ_x *will get close to* σ_z. *After impact, the pressure is relieved and the stress state becomes* $\sigma_z = 0$ *and* $\sigma_y = \sigma_x < 0$ *which are the residual stresses and the deviatoric stresses are* $S_z > 0$ *and* $S_y = S_x < 0$. *Thus the vector of deviatoric stresses is completely reversed after the pressure removed. If the material has a strong Bauschinger effect, there is no doubt that there is reverse yielding and therefore the residual stress state is on the yield surface.*

Because the stress state at every point on the specimen is on the yield surface, the deformation will be in the plastic region during the hole drilling operation. Large errors will be inevitable if an elastic analysis is simply used to interpret the measured strain.

For the round bars which had been subjected to shot blasting, we knew that there were high compressive residual stresses on the surface. These residual stresses mainly result from non-uniform plastic deformation during shot blasting. Therefore, the residual stress state is in reverse yielding and hole-drilling operation will cause further plastic flow. Thus the deformation by drilling a hole is partly elastic and plastic and depends on the residual stress state, hole geometry and stress-strain curve during reverse yielding. Tension-compression test have shown that En15R steel exhibits a significant Bauschinger effect (Shatil, 1990). Figure 6.5 shows cyclic stress-strain curve from a tensile-compressive test on specimen HTS18. From the stress-strain curve we can see that there is big difference between plastic

deformation from reverse yielding on the stress-strain curve and one which only considers elastic deformation.

For the shot blast specimens, since drilling a hole results in continued reverse yielding, the material response curve, shown in Figure 6.5, in the compression part was taken into account. The general solution for the strain release after hole-drilling is much more complicated but it may be possible to study this further by using FE analysis. Here a simple case is considered and an analytical solution is found.

For the analysis, we assume the following,

i) The residual stress is uniform in the surface layer and $\sigma_{max} = \sigma_{min}$.

ii) The material is uniform and isotropic and stress-strain curve satisfies $\sigma = A\varepsilon^n$.

The hole drilling operation can be idealised as being in two steps: first by drilling the hole but keeping the radial residual stress as a pressure on the hole surface and second by removing the pressure from the hole surface. In the first step, there is no strain change. The strain change is only caused by removing the radial residual stress as a pressure from the hole surface. The analytical solution for the strain release after a hole drilling was obtained based on Gao's work (1992)

$$\varepsilon_r = F(r, \sigma_{res}, A, n). \tag{4.72}$$

This solution (4.72) includes a set of equations which can be solved by using iterative procedures. The details of the analysis are given in Appendix 4A. A FORTRAN program to obtain a solution for Equation (4.72) is presented in Appendix 4B. Fig. 4.59 shows the results of strain release against residual stress for large rosette with hole diameter $D_0 = 1.89$ and small rosette with hole diameter $D_0 = 0.91$. Compared with elastic strain relaxation, the strain relaxation are much larger using the plastic analysis. In Figure 4.59, the plastic response curve may be represented as a function of strain relief, where

$$\sigma_R^p = f(\varepsilon). \tag{4.73}$$

where σ_R^p is the residual stress obtained from the plastic analysis and the elastic response curve is a straight line given by

$$\sigma_R^e = k\varepsilon \tag{4.74}$$

where σ_R^e is the residual stress obtained from the elastic analysis.

In the next step we may make use of the plastic result shown in Figure 4.59 to modify the residual stress results σ_R^e obtained from the elastic analysis. The procedure includes:

1) Obtain the residual stress value σ_R^e from elastic analysis
2) Find the strain value ε on the elastic straight line using the σ_R^e
3) Obtain stress value σ_R^p. from the plastic response curve

Consequently, the plastic modification can be expressed as

$$\sigma_R^p = f(\sigma_R^e/k). \tag{4.75}$$

In Figure 4.51, the elastic analysis results of specimen U5 were obtained using larger strain gauge rosette and 3-D FE analysis. Then plastic modification analysis was carried out on the elastic result and the residual stress result after the plastic modification is also shown in Figure 4.51.

For the specimens where smaller strain gauge rosettes were used, an elastic analysis for a flat surface with the average stress method was used, which was a good approximation to a stress distribution with a small gradient. Then the residual stress results were modified by using Equation (4.75). Figures 4.60 to 4.66 show the modified residual stress results for specimens from U-, FS and HTS batches. In general most of the results were in good agreement with those measured by X-ray diffraction method at the surface. Residual stresses in HTS specimens were higher than those in U and FS specimens. Specimen surface roughness appeared to have a large influence on hole drilling results. If the drilling location was just at the trough of the roughness, there would have been only small strain relief in the first few steps. Hole drilling results from specimen FS16 in Figures 4.57 and 4.65 show an extreme case.

4.5 Comparison of Residual Stress Results Obtained by Different Techniques

For the round bars, several techniques and methods have been used to measure and estimate the residual stresses. These techniques may be summarised as follows,

Technique 1: *X-ray diffraction used to measure residual stresses on the specimen surfaces. This is a non-destructive method.*

Technique 2: *X-ray diffraction combined with chemical etching used to obtain residual stress distributions across specimen sections. This is a totally destructive method.*

Technique 3: *Neutron diffraction used to measure residual stresses in the interior of the specimens. This is a non-destructive method.*

Technique 4: *Using detailed neutron diffraction measurements across specimen sections together with some techniques dealing with near surface effects to obtain residual stress distributions. This is a non-destructive method.*

Technique 5: *Centre hole method used to measure residual stresses near to the surface with in a depth of about 1 mm from specimen surface together with plastic modification analysis. This is a semi-destructive method.*

Techniques 1, 3 and 5 were used to measure the residual stresses in round bars from U-batch. Figures 4.67 and 4.68 show the results for axial and tangential residual stresses, respectively. From Figures 4.67 and 4.68, it can be seen that the residual stresses obtained by using technique 1 are in general in good agreement with those by technique 5 on the surface. The trend of residual stress distribution can be seen approximately.

Techniques 1, 2, 4 and 5 have been used to measure the residual stresses and residual stress distributions in specimens from the HTS batch. Figures 4.69 and 4.70 present the results for axial and tangential residual stresses, respectively. It can be seen that the results by these techniques broadly agree with each other.

4.6 Discussion

From Table 4.2, it can be seen that the scatter obtained from repeat measurements of residual stresses by using X-ray diffraction technique was in the range of about 20 MPa. So it may be considered that the experimental scatter of the X-ray measurements for the hot forged round bars was within ±20 MPa.

From the X-ray diffraction measurements on the 'stress-free' plate, listed in Table 4.1, the measured residual stresses were all in compression with a maximum value at 50 MPa. This gives same evidence of the presence of 2nd and 3rd kind residual stresses in the 'stress free' plate. But we are still not certain that the 2nd and 3rd kind residual stresses in the round bars are the same as in the 'stress-free' plate because of the influence of heat treatment. So a difference up to -55 MPa between residual stress measured by X-ray and macro-residual stress must be accepted. On the other hand, the residual stress measured using X-ray diffraction is an average value over a certain volume (Cullity, 1978) and the depth of penetration of the X-rays in steel is about 10 μm. It is also expected that the residual stress would be a minimum at the peak and a maximum in the trough of the surface profile as a result of surface roughness. Consequently the average value (as measured by X-ray) would be less than the value in the trough which is what we were attempting to measure. Removal of the surface roughness by low intensity polishing and subsequent X-ray residual stress measurement revealed that the compressive axial and tangential residual stresses increased by 100 MPa (Zhu, 1994). Table 4.22 presents the results of residual stress change before and after polishing for specimens HTS09, U15 and AF04 (without shot blast treatment). It can be seen that specimen AF04 without residual stress before polishing had about 200 MPa axial residual stress after polishing, which means that the process of material removal by polishing can itself introduce residual stresses. Consequently these higher compressive residual stress in HTS specimen as measured by X-ray must again be treated with caution. Therefore, the residual stresses measured by X-ray diffraction should be theoretically lower than those in the trough of the surface profile but errors caused by the presence of 2nd and 3rd kind residual stresses might compensate for this.

For round bars from U-batch, X-ray results in Table 4.5 show that in all cases the tangential and axial residual stresses were compressive, with axial residual stresses being lower than tangential stresses. This suggests that on the surface there was a compressive biaxial stress state. It is notable that the variation of residual stresses

from specimen to specimen was greater than the error associated with the X-ray experimental technique.

From the X-ray measurements on AF, HT, FS and HTS batches shown in Tables 4.6 to 4.9, we can see that there were much more compressive residual stresses in shot blasted bars than those with not shot blasted. This indicates that the surface residual stresses were mainly caused by shot blasting. The surface residual stresses in HTS bars were higher than those in FS bars while residual stresses in HT bars than in AF bars. The difference between HTS and FS and between HT and AF is associated with heat treatment, hardening and tempering. This means that heat treated bars had higher residual stresses introduced by shot blasting than those without heat treatment. The heat treatment made the material harder and consequently the yield stress was higher. For a harder material, residual stresses as a result of shot blasting will be larger. Hardness measurements were carried out for bars from HTS, FS and U-batches. The results are presented in Tables 4.16 to 4.18. The measured hardness as a function of surface residual stresses is shown in Figure 4.71. It can be seen that there is correlation between hardness of the steel and residual stresses produced by shot blasting. The HTS bars and U-batch bars were subjected same forging process including heat treatment, hardening and tempering which had been confirmed by microstructure examinations of bars from the two batches. (Zhu, 1995). But the measured residual stresses and hardness of U-batch bars were all lower than those of bars from HTS batches which may be explained as the difference of materials and treatment between different batches.

The shot blasting also introduced increased roughness on the bars. It can be seen clearly that shot blasted bars, such as those in the HTS and FS batches, surface roughness measurements were made on the bars from the AF, FS, HT and HTS batches. These measurements were carried out by Rover at Gaydon Test Centre using a Talysurf measuring device. Tables 4.19 to 4.20 present the measured roughness results. In the Tables 4.19 to 4.20, R_a is the arithmetic mean of the departures of the roughness profile from the mean line, R_t is the maximum peak to valley height of the profile and K_{sf} is a surface roughness related fatigue strength factor. Table 4.18 gives the mean values and standard deviation for normal distribution of R_t and K_{sf}. Figure 4.72 shows the surface roughness versus axial residual stress for shot blasted specimens from HTS and FS batches. It can be seen that rougher surfaces are associated with lower compressive residual stresses. This may be explained as follows,

> *Harder steel generally has a higher yield stress. Under the same conditions of shot blasting, the harder steel will exhibit less plastic deformation. This results in lower surface roughness, while the higher compressive residual stress is related to the higher yield stress.*

However, within one group of specimens, it is difficult to say that there is a correlation between surface roughness and residual stresses.

The technique of chemical etching combined with the X-ray technique to measure residual stress distribution in a specimen is a completely destructive method. Therefore this technique was only applied to a few specimens. Because of the influence of surface roughness, the measurements for the first few increments were uncertain. This can be seen in more detail in Tables 4.11 and 4.12.

Neutron diffraction results in Figure 4.14 show that the axial residual stresses in the interior of specimens were predominantly tensile. The other stress components, radial and tangential shown in Figures 4.18 and 4.19, exhibited some uncertainty in value, but the absolute values were less than those on the surface. Also the experiments show that the residual stresses vary from specimen to specimen and statistical analysis is necessary. In general the largest residual stresses were in the axial direction. However the variation from sample to sample was substantial.

Figures 4.15 and 4.16 show that the measured tangential residual stresses were not equal to radial residual stresses at the centre of the bars. This implies that the residual stress state in the specimens was not precisely axisymmetric. This was not surprising in view of the flash lines generated as a consequence of the non-axisymmetric forging technique.

When using neutron diffraction to measure residual strains across a sample section, the irregular geometry of the bars had a significant influence on the results. This can be seen from the profiles of the neutron peak intensity against measurement position shown in Figures 4.20 to 4.21. For the neutron diffraction measurements the neutron diffracted intensity must be kept to a certain level (Noyan, et al, 1987; Lorentzen, 1995). Because the diffracted neutron peak intensity dropped as the neutron gauge volume moved out of the sample, shown in Figure 4.20, the accuracy of the measurements near to the surface could be affected. To overcome this difficulty, longer scan time might be considered to improve the accuracy.

The surface effect of neutron diffraction was quite significant which can be seen from measurements on stress free samples shown in Figures 4.23 and 4.24. Without modification, the residual stress results could be unrealistically high. To explain this phenomena, we may consider a fact that the wave length of the neutron beam has a certain spread (Leffers, et al., 1987). Assume the wave length of the neutron beam varies from $\lambda_0 - \delta_\lambda$ to $\lambda_0 + \delta_\lambda$ where λ_0 is the wave length at the beam centre and δ_λ represents the spread. For simplicity it may be assumed that the variation of the wave length across the beam width is linear. Take the sample surface to be flat (without curvature). For neutron gauge volume being inside the sample, the weight centre of the gauge volume is same as the neutron beam centre and the average wave length equals to λ_0. Here we may assume the neutron gauge volume is a cube with the width being *W*. Let us move half of the gauge volume out of the sample, then the weight centre of the remaining gauge volume in the sample will shift $W/6$ where W is the beam width as well. Based on the linear variation of the neutron wave length, the average wavelength for the remaining gauge volume should be equal to $\lambda_0 - \frac{\delta_\lambda}{3}$ at the right hand side and $\lambda_0 + \frac{\delta_\lambda}{3}$ at left hand side as shown in Figure 4.73. Consequently, the average wave length changes due to the neutron gauge volume moving out the sample. Let us use the Bragg's law, Equation (2.1), and differentiate it, assuming λ is not constant

$$\Delta\theta = -\tan\theta \cdot \frac{\Delta d}{d} + \tan\theta \frac{\Delta\lambda}{\lambda} \tag{4.76}$$

where $\Delta\lambda$ represents the change of average wave length at the weight centre as the neutron beam moves out of the sample. Therefore the peak angle shift is not only contribution by lattice space changes but also by the wave length change at the weight centre. For stress free sample, the Δd is assumed to be zero and the peak angle shift is purely caused by the wave length change at the weight centre. This can be seen from the measurements on stress free samples U06 and HTS18 as shown in Figures 4.23 and 4.24. For further analysis, more details about the variation of wave length of the neutron along the beam width are required.

Centre hole measurements on stress free plate presented in Table 4.15 showed that drilling operation would not cause additional strain change and therefore it may be concluded that the drilling operation did not affect the results of residual stress measurements of the centre hole method.

For the hot forged rectangular bar without the shot-blasting, the residual stress results are shown in Figures 4.45 and 4.46. The first result has a large error when the depth reaches 0.8 mm which was close to the limit. The compressive residual stresses were only in a thin layer, 0.3 mm, which was close to the surface. The residual stress results from the rectangular bar subjected to shot-blasting, in Figures 4.47 and 4.48, show that the compressive stresses dominate the measurement region. Compared to the results of the bar without shot-blasting, it can be concluded that the shot-blasting increases the depth of compressive region from surface. This is intuitively what one might expect.

The analysis developed for interpreting the relaxed strain data obtained from centre hole measurements on round bars is general and would be suitable for any components with curved surfaces. However, there are limitations in using the incremental hole drilling method. From the FE analysis, the magnitude of the influence matrix $\tilde{A}_{ji}$ decreases with hole depth and decreases to less than 1% of $\tilde{A}_{11}$ (corresponding to the first increment) when the hole reaches a depth of about 1 mm. Therefore for the same error in strain measurement for any depth, the error for the calculated stress could be about one hundred times greater than in the first layer. This implies that there is a limitation to the depth to which the hole can be drilled. This depth for the round bar specimen is roughly the same as described by Schajer (1988) for plane surfaces. This depth is about 0.25 times the mean radius of the strain rosettes D and practically this limit is reduced to $0.15D-0.2D$. For $D=5.13mm$, the limit is about $0.8-1.0mm$.

The proposed plastic modification for the centre hole is an approximate method. In Gao's work (1992), his analysis was subjected to the condition that all the stress and strain components were uniform through the thickness of plate. But the residual stresses were not uniformly distributed along depth in our shot blasted specimens. However, This approach can be regarded as an average over depth. Nevertheless, further work is required using both theoretical and numerical methods to study the plastic influence on the residual stress measurements.

The calculated residual stresses $\bar{\sigma}_i$, shown in Equation (4.65), accumulates all the errors before this step i. This can be simply shown by taking $n=2$ in Equations (4.60),

$$\left.\begin{aligned}\vec{\varepsilon}(h_1) &= \tilde{A}_{11}\vec{\sigma}_1 \\ \vec{\varepsilon}(h_2) &= \tilde{A}_{21}\vec{\sigma}_1 + \tilde{A}_{22}\vec{\sigma}_2\end{aligned}\right\} \tag{4.77}$$

The solution for the above equations is

$$\left.\begin{aligned}\vec{\sigma}_1 &= \tilde{A}_{11}^{-1}\vec{\varepsilon}(h_1) \\ \vec{\sigma}_2 &= \tilde{A}_{22}^{-1}\vec{\varepsilon}(h_2) - \tilde{A}_{22}^{-1}\tilde{A}_{21}\tilde{A}_{11}^{-1}\vec{\varepsilon}(h_1)\end{aligned}\right\} \tag{4.78}$$

where $\tilde{A}_{11}^{-1}$ *and* $\tilde{A}_{22}^{-1}$ are the inverse matrixes of $\tilde{A}_{11}$ and $\tilde{A}_{22}$, respectively. Assuming that each matrix has an error from the FE analysis and measurement, we obtain the error for the stresses, given by

$$\left.\begin{aligned}\delta\vec{\sigma}_1 &= \delta\tilde{A}_{11}^{-1}\vec{\varepsilon}(h_1) + \tilde{A}_{11}^{-1}\delta\vec{\varepsilon}(h_1) \\ \delta\vec{\sigma}_2 &= \delta\tilde{A}_{22}^{-1}\vec{\varepsilon}(h_2) + \tilde{A}_{22}^{-1}\delta\vec{\varepsilon}(h_2) \\ &\quad - \delta\tilde{A}_{22}^{-1}\tilde{A}_{21}\tilde{A}_{11}^{-1}\vec{\varepsilon}(h_1) - \tilde{A}_{22}^{-1}\delta\tilde{A}_{21}\tilde{A}_{11}^{-1}\vec{\varepsilon}(h_1) \\ &\quad - \tilde{A}_{22}^{-1}\tilde{A}_{21}\delta\tilde{A}_{11}^{-1}\vec{\varepsilon}(h_1) - \tilde{A}_{22}^{-1}\tilde{A}_{21}\tilde{A}_{11}^{-1}\delta\vec{\varepsilon}(h_1)\end{aligned}\right\} \tag{4.79}$$

where δ expresses the error of each matrix. Obviously, the error $\delta\vec{\sigma}_2$ is much bigger than $\delta\vec{\sigma}_1$. Since the error accumulates, more increments do not imply improved results for the interpreted residual stresses. Therefore, the total number of increments and the depth of the hole need to be optimised.

In general, all of the elastic results show that the measurement error from the hole-drilling technique can be significant. It is partly due to the technique itself and partly due to the calculation method. So, great care must be taken in both the measurements and calculations. It is necessary to make sure that the strain gauge rosette is properly bonded, the hole is drilled exactly in the middle of the rosette and the depth increments and the hole diameter are determined as accurately as possible. Furthermore since the coefficients need to be determined very accurately, the finite element model must be built according to the measurements obtained on the geometry of the hole. The mesh must be fine enough in the area of the hole. The calculation method may need to be improved to obtain improved stress results. In the case of residual stress introduced by surface plastic deformation, such as shot blasting and shot peening, reverse yielding will take place whenever a hole is drilled particularly if the material exhibits the Bauschinger effect. The strains measured by the strain gauge rosettes will be much larger than the strains from elastic deformation alone. Therefore, plastic modification is required.

From the comparison of residual stress results by different techniques, shown in Figures 4.67 and 4.68 for U-batch specimens and Figures 4.69 and 4.70 for HTS specimens, we can see all the measurement techniques gave consistent results, compressive in the surface layer and tensile in the interior of the bar. In general the results from each measurement technique are in good agreement with each other within each region, although there was considerable scatter from both experimental error and the variation from specimen to specimen.

4.7 Conclusions

1) X-ray diffraction measurements have shown that there were large biaxial compressive residual stresses on the surface of the shot blasted bars.

2) In the complete hot forging process, X-ray diffraction measurements have shown that the residual stresses were mainly generated by shot blasting. The heat treatment (hardening and tempering) itself did not introduce residual stresses, but indirectly it led to an increase in the magnitude of the residual stresses, generated by shot blasting.

3) X-ray diffraction combined with a chemical etching method can be used to determine residual stress distributions in round bars, but it is a totally destructive technique.

4) The axial residual stresses in the interior of forged round bars, measured by the neutron diffraction method, were predominantly tensile, although there was considerable scatter from specimen to specimen.

5) The neutron diffraction method together with a technique to account of surface effects can be used to measure residual stresses near surface. The measurements have shown that the near surface residual stresses in the round bars were in compression. Also a new interpolation method have been developed to obtain residual stress distribution across section using a combination of the neutron diffraction results.

6) Centre hole measurements on a "stress-free" plate have shown that the drilling operation itself has no effect on the residual stress results.

7) The centre hole measurements have shown that the residual stresses near to the surface of shot blasted bars were in biaxial compression and that the maximum compressive residual stresses were on surface.

8) An incremental hole drilling technique has been developed for components with curved surfaces. Extensive 3-D FE calculations were carried out to obtain the coefficient matrices.

9) For the shot blasted bars, the plastic reverse yielding effect on the hole drilling results has been studied and a new method has been developed to modify the elastic results by taking into account of this effect.

10) Comparison has been made among the results by different techniques. All measurement techniques gave consistent results, compressive in the surface layer and tensile in the interior.

11) In general all results were found to broadly agree with each other, although there was considerable scatter from both experimental error and the variation from specimen to specimen.

Chapter 5

INTERPOLATION OF RESIDUAL STRESS DISTRIBUTIONS

This chapter presents the development of a theoretical approach for interpolating limited experimental residual stress results in round bar specimens. The theoretical analysis, together with a least squares method, has been developed to obtain the complete distribution of residual stresses in the round bar specimens. The interpolated results have been compared with results from using the centre hole method and also using chemical etching combined with the X-ray diffraction method. The results were found to be in good agreement.

5.1 Introduction

Residual stresses are the self-equilibrating internal stresses existing in a free body with no external loading being applied. Manufacturing processes, including forging, thermal loading and shot blast, introduce significant residual stresses in the components. The non-uniform plastic deformation field, which is generated in the interior of the specimen by forging and thermal loading and at the surface by surface treatment, is the key factor in determining the distribution of residual stresses. This plastic deformation field, related to the strain history during forging process and subsequent surface treatment, is difficult, even impossible, to completely determine. But there are a number of relationships between the residual stresses, elastic strains and plastic strains which can be used to estimate residual stresses from limited measurements.

Finite Element (FE) analysis has been used to investigate the interaction between residual stresses and fatigue cyclic loading. This is described in Chapter 6. To

incorporate residual stresses in the FE analysis requires an accurate distribution of the residual stresses in the component. Residual stresses have been measured using non-destructive methods, such as X-ray diffraction measuring residual stresses at specimen surface and neutron diffraction measuring residual stresses in the interior of specimens as described in Chapter 4. However, the detailed residual stress distribution across the complete section of a component is difficult to obtain. Numerical methods such as FE are now used to obtain approximate solutions.

Any stress and strain state in the components must satisfy the necessary equations and conditions. These include equilibrium equations, compatibility equations, constitutive equations, boundary conditions, plastic strain incompressibility and some constraint conditions. It is difficult and often impossible to find a solution satisfying all equations and conditions precisely. Using these equations and conditions a general solution, based on unknown plastic strains, is derived to determine the complete residual stresses distribution. An example of the technique is presented in this Chapter.

5.2 Basic Equations

5.2-1 Equations of Equilibrium

Take a cubic element at a point in a body with all components of stress acting on as shown in Figures 5.1 and 5.2 for rectangular or cylindrical co-ordinate system. There are six independent components of stress

$$\begin{aligned} &\sigma_x, \sigma_y, \sigma_z, \tau_{yz}, \tau_{zx}, \tau_{xy} && \textit{for rectangular system} \\ &\sigma_r, \sigma_\theta, \sigma_z, \tau_{\theta z}, \tau_{zr}, \tau_{r\theta} && \textit{for cylindrical system} \end{aligned} . \qquad (5.1)$$

For cylindrical co-ordinates (r,θ,z), which are often used for problems like stresses in circular rings, disks, cylinders and round bars, the element cut from the body with stresses acting on is shown in Figure 5.2. Also there are six independent components of stress. The stress transform from the rectangular co-ordinate system to the cylindrical co-ordinate system can be written as

$$\begin{bmatrix} \sigma_r & \tau_{r\theta} & \tau_{rz} \\ \tau_{\theta r} & \sigma_\theta & \tau_{\theta z} \\ \tau_{zr} & \tau_{z\theta} & \sigma_z \end{bmatrix} = \begin{bmatrix} \cos\theta & \sin\theta & 0 \\ -\sin\theta & \cos\theta & 0 \\ 0 & 0 & 1 \end{bmatrix} \begin{bmatrix} \sigma_x & \tau_{xy} & \tau_{xz} \\ \tau_{yx} & \sigma_y & \tau_{yz} \\ \tau_{zx} & \tau_{zy} & \sigma_z \end{bmatrix} \begin{bmatrix} \cos\theta & -\sin\theta & 0 \\ \sin\theta & \cos\theta & 0 \\ 0 & 0 & 1 \end{bmatrix}. \qquad (5.2)$$

Many problems in stress analysis which are of practical importance are concerned with a solid of revolution deformed symmetrically with respect to the axis of revolution, such as round bar by symmetrical loading. In this case, the equation of equilibrium becomes,

$$\left.\begin{aligned} &\frac{\partial \sigma_r}{\partial r}+\frac{\partial \tau_{rz}}{\partial z}+\frac{\sigma_r-\sigma_\theta}{r}=0 \\ &\frac{\partial \tau_{zr}}{\partial r}+\frac{\partial \sigma_z}{\partial z}+\frac{\tau_{rz}}{r}=0 \end{aligned}\right\}. \tag{5.3}$$

5.2-2 Components of Displacements and Strains

There are also three displacements and six independent strain components for each co-ordinate system. The displacement transform from the rectangular system to the cylindrical system is as follows,

$$\begin{Bmatrix} u_r \\ u_\theta \\ u_z \end{Bmatrix} = \begin{bmatrix} \cos\theta & \sin\theta & 0 \\ -\sin\theta & \cos\theta & 0 \\ 0 & 0 & 1 \end{bmatrix} \begin{Bmatrix} u_x \\ u_y \\ u_z \end{Bmatrix}. \tag{5.4}$$

And the strain transform from the rectangular co-ordinates system to the cylindrical co-ordinates system can be written as,

$$\begin{bmatrix} \varepsilon_r & \frac{\gamma_{r\theta}}{2} & \frac{\gamma_{rz}}{2} \\ \frac{\gamma_{\theta r}}{2} & \varepsilon_\theta & \frac{\gamma_{\theta z}}{2} \\ \frac{\gamma_{zr}}{2} & \frac{\gamma_{z\theta}}{2} & \varepsilon_z \end{bmatrix} = \begin{bmatrix} \cos\theta & \sin\theta & 0 \\ -\sin\theta & \cos\theta & 0 \\ 0 & 0 & 1 \end{bmatrix} \begin{bmatrix} \varepsilon_x & \frac{\gamma_{xy}}{2} & \frac{\gamma_{xz}}{2} \\ \frac{\gamma_{yx}}{2} & \varepsilon_y & \frac{\gamma_{yz}}{2} \\ \frac{\gamma_{zx}}{2} & \frac{\gamma_{zy}}{2} & \varepsilon_z \end{bmatrix} \begin{bmatrix} \cos\theta & -\sin\theta & 0 \\ \sin\theta & \cos\theta & 0 \\ 0 & 0 & 1 \end{bmatrix} \tag{5.5}$$

In the case of axially symmetrical deformation, $u_\theta = 0$, the relationship between strains and displacements is expressed as,

$$\left.\begin{aligned} &\varepsilon_r=\frac{\partial u_r}{\partial r}, \quad \varepsilon_\theta=\frac{u_r}{r}, \qquad \varepsilon_z=\frac{\partial u_z}{\partial z}, \\ &\gamma_{r\theta}=0, \quad \gamma_{rz}=\frac{\partial u_r}{\partial z}+\frac{\partial u_z}{\partial r}, \quad \gamma_{z\theta}=0 \end{aligned}\right\}. \tag{5.6}$$

5.2-3 Stress-Strain Relationship

Residual stresses in the specimens are produced during manufacturing processes, in which non-uniform plastic deformation are introduced. The plastic deformation is related to the strain history. Consequently it is difficult to find its magnitude and distributions. The deformation in the specimens will be partly elastic and partly plastic. It is generally assumed that strains in the specimens are divisible into elastic and plastic components, so that,

$$\varepsilon_{ij} = \varepsilon_{ij}^{e} + \varepsilon_{ij}^{p} \tag{5.7}$$

where ε_{ij}^{e} is elastic strain components and ε_{ij}^{p} is plastic strain components which satisfy the incompressibility condition,

$$\varepsilon_{ii}^{p} = 0. \tag{5.8}$$

The elastic strain components ε_{ij}^{e} is related to the residual stress components by Hooke's law. Thus, the relationship between stresses and strains for the cylindrical system is,

$$\varepsilon_r = \frac{1}{E}\left[\sigma_r - \nu(\sigma_\theta + \sigma_z)\right] + \varepsilon_r^p \tag{5.9a}$$

$$\varepsilon_\theta = \frac{1}{E}\left[\sigma_\theta - \nu(\sigma_r + \sigma_z)\right] + \varepsilon_\theta^p \tag{5.9b}$$

$$\varepsilon_z = \frac{1}{E}\left[\sigma_z - \nu(\sigma_r + \sigma_\theta)\right] + \varepsilon_z^p \tag{5.9c}$$

$$\gamma_{r\theta} = \frac{2(1+\nu)}{E}\tau_{r\theta} + \gamma_{r\theta}^p \tag{5.9d}$$

$$\gamma_{\theta z} = \frac{2(1+\nu)}{E}\tau_{\theta z} + \gamma_{\theta z}^p \tag{5.9e}$$

$$\gamma_{zr} = \frac{2(1+\nu)}{E}\tau_{zr} + \gamma_{zr}^p \tag{5.9f}$$

where E is Young's Modulus and ν is Poisson's ratio. The plastic strains, which are related to the strain history involved in the manufacturing processes, are quite difficult to find. Fortunately for residual stress measurements, the elastic strains ε_{ij}^{e} can be measured and then residual stresses σ_{ij} are calculated by Hooke's law.

5.2-4 Uniqueness and Non-Uniqueness of Solution

It can be proved that if the plastic strain distribution is known for a specimen, the distribution of residual stresses in the specimen can be determined uniquely. Conversely, with a given residual stress distribution, one cannot find a unique plastic strain distribution. For example, for zero residual stresses, the solution of plastic strain distribution for the rectangular system could be in the form,

$$\left.\begin{aligned} \varepsilon_x^p = a_1,\ \ \varepsilon_y^p = a_2,\ \ \varepsilon_z^p = -(a_1 + a_2), \\ \gamma_{xy}^p = a_3,\ \ \gamma_{xz}^p = a_4,\ \ \gamma_{zy}^p = a_5 \end{aligned}\right\} \tag{5.10}$$

where a_1, a_2, a_3, a_4 and a_5 are arbitrary constants. Therefore the solution for plastic strain distribution is not unique. From Equations (5.9), it can be seen that the plastic strains are equal to the total strains when there are no residual stresses. Therefore the plastic strains have to satisfy the compatibility equations just as is the case for the total strains.

The non-uniqueness of solution may be stated as: if the residual stress distribution in a component is given, the corresponding plastic strain distribution can be found to be not unique. The difference between any two solutions of the plastic strains corresponding to the same residual stress distribution is just same as one of the plastic strain distributions corresponding to the zero residual stress state and therefore satisfies the condition of the incompressibility and compatibility equations which all strain components should satisfy.

5.3 Solution for the Round Bar

The cylindrical co-ordinate system of round bar has been shown in Figure 4.1. Assuming that all components of stresses, strains and displacements are independent of z and θ, the round bar can be treated as a generalised plane strain problems and the equations of equilibrium (5.3) reduce to

$$\frac{\partial \sigma_r}{\partial r} + \frac{\sigma_r - \sigma_\theta}{r} = 0. \tag{5.11}$$

The strain components (5.6) are reduced to

$$\left.\begin{aligned} \varepsilon_r &= \frac{\partial u_r}{\partial r},\ \varepsilon_\theta = \frac{u_r}{r},\ \varepsilon_z = const \\ \gamma_{r\theta} &= 0,\quad \gamma_{\theta z} = 0,\quad \gamma_{zr} = 0, \end{aligned}\right\} \tag{5.12}$$

which lead to the compatibility equation,

$$r\frac{d\varepsilon_\theta}{dr} = \varepsilon_r - \varepsilon_\theta . \tag{5.13}$$

The relationship between stresses and strains in cylindrical co-ordinates is

$$\left.\begin{aligned} \varepsilon_r &= \frac{1}{E}\left[\sigma_r - \nu(\sigma_\theta + \sigma_z)\right] + \varepsilon_r^p \\ \varepsilon_\theta &= \frac{1}{E}\left[\sigma_\theta - \nu(\sigma_r + \sigma_z)\right] + \varepsilon_r^p \\ \varepsilon_z &= \frac{1}{E}\left[\sigma_z - \nu(\sigma_\theta + \sigma_r)\right] + \varepsilon_r^p \end{aligned}\right\} \tag{5.14}$$

where the plastic strains components satisfy incompressibility given by,

$$\varepsilon_\theta^p + \varepsilon_r^p + \varepsilon_z^p = 0. \tag{5.15}$$

The boundary conditions include free traction on the outer surface

$$\sigma_r|_{r=R} = 0 \tag{5.16}$$

where R is the radius of the round bar and the sum of all forces in the axial direction must be zero

$$\int_A \sigma_z\, dA = 0 \tag{5.17}$$

where A indicates that the summation must be carried out over the entire cross-sectional area of the bar.

By solving Equations (5.11 to 5.17), residual stresses can be determined as a function of the plastic strains

$$\left.\begin{aligned}\sigma_r = -\frac{E}{2(1-\nu^2)}\Big[\int_r^R \frac{\varepsilon_r^p - \varepsilon_\theta^p}{r'}dr' - (1-2\nu)\frac{1}{R^2}\int_0^R r'(\varepsilon_r^p + \varepsilon_\theta^p)dr' \\ + (1-2\nu)\frac{1}{r^2}\int_0^r r'(\varepsilon_r^p + \varepsilon_\theta^p)dr'\Big]\end{aligned}\right\} \tag{5.18}$$

$$\left.\begin{aligned}\sigma_\theta = -\frac{E}{2(1-\nu^2)}\Big[2(1-\nu)\varepsilon_\theta^p - 2\nu\varepsilon_r^p + \int_r^R \frac{\varepsilon_r^p - \varepsilon_\theta^p}{r'}dr' \\ - (1-2\nu)\frac{1}{R^2}\int_0^R r'(\varepsilon_r^p + \varepsilon_\theta^p)dr' + (1-2\nu)\frac{1}{r^2}\int_0^r r'(\varepsilon_r^p + \varepsilon_\theta^p)dr'\Big]\end{aligned}\right\} \tag{5.19}$$

$$\left.\begin{aligned}\sigma_z = -\frac{E}{2(1-\nu^2)}\Big[-2(1-\nu)\varepsilon_\theta^p - 2\varepsilon_r^p + 2\nu\int_r^R \frac{\varepsilon_r^p - \varepsilon_\theta^p}{r'}dr' \\ + 2(2-\nu)\frac{1}{R^2}\int_0^R r'(\varepsilon_r^p + \varepsilon_\theta^p)dr'\Big]\end{aligned}\right\}. \tag{5.20}$$

where r' is a integral variable.

The complete solution for the residual stress distribution requires information about the plastic strain distribution. In the following we consider an interpolation technique where limited information about the residual stresses are known together with an assumed plastic strain distribution.

5.4 Interpolation of residual stresses measured

In the round bar specimens the true plastic strains and their history are very difficult to obtain. Since for a given residual stress state the corresponding plastic strains are not unique we can use this non-uniqueness to choose an approximate plastic strain field. It is very important to chose a suitable plastic strain distribution to consider both short-range and long-range residual stresses. A linear plastic strain distribution gives rise to a linear residual stress distribution. We assume simple power law forms for the plastic strains ε_r^p and ε_θ^p, since we have an expectation of the form of the residual stress distribution.

$$\varepsilon_\theta^p = C_1 r^2 + C_2 r^3, \quad \varepsilon_r^p = C_3 r^2 + C_4 r^3, \tag{5.21}$$

where C_1, C_2, C_3, and C_4 are constants to be determined. After inserting Equation (5.21) into Equations (5.18 to 5.20), the residual stress distribution can be obtained as a function of a number of constants,

$$\left.\begin{aligned}\sigma_r &= C_1 f_{11}(r) + C_2 f_{12}(r) + C_3 f_{13}(r) + C_4 f_{14}(r)\\ \sigma_\theta &= C_1 f_{21}(r) + C_2 f_{22}(r) + C_3 f_{23}(r) + C_4 f_{24}(r)\\ \sigma_z &= C_1 f_{31}(r) + C_2 f_{32}(r) + C_3 f_{33}(r) + C_4 f_{34}(r)\end{aligned}\right\} \tag{5.22}$$

where $f_{ij}(r)$ are known functions obtained by integrating Equations (5.18 to 5.20) and shown in Appendix 5A. At several points where $r = r_m$, the stresses σ_r, σ_θ and σ_z are measured. These are denoted as σ_{km} where k=1, 2, 3 represents r, θ and z, respectively. The least squares method is used to determine the constants C_j (j=1,2,3 and 4). The total sum of squares of the errors is expressed as

$$ER(C_1, C_2, C_3, C_4) = \sum_{k=1}^{3}\sum_{m=1}^{n}\left(\sum_{j=1}^{4} C_j f_{kj}(r_m) - \sigma_{km}\right)^2 \tag{5.23}$$

where n is the number of data points. It can be shown that the minimum of the error is attained at unique of values C_1, C_2, C_3 and C_4 which are the solution of the simultaneous equations,

$$\frac{\partial ER(C_1, C_2, C_3, C_4)}{\partial C_j} = 0 \qquad j = 1, 2, 3, 4. \tag{5.24}$$

Then Equations (5.24) become simultaneous linear equations for C_1, C_2, C_3 and C_4,

$$\sum_{j=1}^{4} a_{ij} C_j = b_i \qquad i = 1, 2, 3, 4 \tag{5.25}$$

where,

$$\left.\begin{aligned}a_{ij} &= \sum_{k=1}^{3}\sum_{m=1}^{n} f_{ki}(r_m)\cdot f_{kj}(r_m)\\ b_i &= \sum_{k=1}^{3}\sum_{m=1}^{n} f_{ki}(r_m)\cdot \sigma_{km}\end{aligned}\right\} \tag{5.26}$$

After C_1, C_2, C_3 and C_4 are determined from the Equations (5.25), the residual stress distribution can be obtained from using the Equations (5.22).

5.5 Result of Interpolation

In the following the limited information obtained from X-ray and neutron diffraction measurements was used to determine the constants C_j. The average of the measured axial, tangential and radial residual stresses at 0, 0.5 and 1, from Figures 4.17 to 4.19 and Table 4.5 for the specimens U1, U9, U10, U13, U18 and U20 were used. The average values are listed in Table 5.1 and using the least square method outlined previously, the constants C_1 to C_4 were obtained by solving Equation (5.25) and presented in Table 5.2. Using these constants therefore provides a complete solution for the residual stress distribution. The results for the interpolated axial, tangential and radial residual stress distributions are shown in Figures 5.3 to 5.5. Figure 5.6 presents the comparison of the axial residual stress distribution with the centre hole results from U5 and U15. The axial residual stresses determined through chemical etching combined with X-ray diffraction of HTS24 are also presented in Figure 5.6.

5.6 Discussion

The limited neutron and X-ray diffraction measurements for U-batch specimens combined with a theoretical analysis and a least squares method, have provided an interpolated residual stresses distribution. The analysis is only considered for the axisymmetric case. However, it is possible to apply this method to more general cases. The general plane strain condition $\varepsilon_z = const$ can be modified to $\varepsilon_z = \varepsilon_z(r)$ which may be pertinent to different manufacturing process, such as the cold-drawing process. The assumption regarding the plastic strain distribution is also flexible since for a given residual stress distribution it is possible to have a number of plastic strain histories. Therefore the functional forms of the radial and hoop plastic strain distributions, Equation (5.21), are somewhat arbitrary but nevertheless chosen to provide sensible residual stress distributions. Another feature is that the analysis ensures that the errors are minimised. Clearly, if the residual stresses appear to be more localised, such that the short-range residual stresses dominate, the functional form of the plastic strains is no longer arbitrary since the plastic strains should be

considered to be localised. The equation (5.21) should therefore reflect the extent of the plastic strain distribution.

The forging process does not give rise to axisymmetric deformation since the bars were pressed between two dies. It would be expected that this would lead to long-range residual stress distributions in the centre of the gauge length of the bar that are not precisely axisymmetric. Figures 4.12 and 4.13 show that the measured tangential residual strains were not equal to radial residual strains at the centre of the bars, suggesting some degree of non-symmetry. Nevertheless, the shot blasting gives rise to short-range (near-surface) residual stress which would be expected to be axisymmetric. The interpolation method was based on axisymmetric deformation and consequently some errors would be inevitable due to the non-symmetry.

From the comparison of interpolated results and centre hole results for U-batch specimens, shown in Figure 5.6 for axial residual stress, we can see the both results agree broadly within a depth of 0.5 mm (0.5/R=1.25). Because the residual stresses near to the surface in the HTS specimens were higher than those in the U-batch specimens, there would be some differences expected near to the surface in the results for the two batches. It can be seen from the results obtained by different techniques that there was considerable variation in the residual stresses from bar to bar. The interpolated residual stress distributions, shown in Figures 5.3 to 5.5, may be considered as the average distributions of the residual stresses in the forged round bar specimens.

5.7 Conclusions

1) Residual stresses were introduced by non-uniform plastic deformation generated during manufacturing process.

2) Residual stresses can be found if the plastic strain field are given.

3) For a given residual stress field the corresponding plastic strain solution is not unique.

4) A theoretical solution for residual stresses has been found for the axisymmetric case with the plastic strains given.

5) Using limited experimental results from neutron and X-ray diffraction a theoretical analysis, together with a least squares method, has been developed to estimate the multiaxial residual stress distribution in the bars.

6) It has been shown that there was good agreement between interpolated results and measured centre hole results. Similar trends were also obtained from measurements obtained by the X-ray diffraction technique combined chemical etching.

Chapter 6

INTERACTION BETWEEN RESIDUAL STRESSES AND MECHANICAL LOADING

This chapter presents experimental work and FE analysis on the interaction between residual stresses and mechanical loading. Two hardening models were used in the FE analyses, linear kinematic hardening model and multilinear hardening model. The latter model has been developed for cyclic loading and written into a user subroutine UMAT for use in ABAQUS. Residual stress relaxation for different initial residual stresses and different cyclic strain ranges have been obtained. Comparisons have been made between results of experiments and FE analyses.

6.1 Introduction

An elastic-plastic finite element analysis can be used for the prediction of the residual stress redistribution during and after fatigue (Lu, et al, 1988). In the finite element model, the initial residual stress field, the plastic stress-strain state, the behaviour of cycle stress-strain curve of material and the condition of cycle loading have to be known. Also, the yield criterion influences the results of the calculation.

In Chapters 4 and 5, residual stresses were measured by different techniques. The complete distributions of the residual stresses were then determined by using an interpolation analysis for the hot forged round bars subjected to shot blasting. In this Chapter, surface residual stress changes due to the tension-tension loading and cyclic tension-compression loading were measured using the X-ray diffraction method. The surface strain history caused by the mechanical loading was also recorded using strain gauge rosettes.

Elastic-plastic finite element analyses were then carried out to predict the residual stress relaxation using different material models. A linear kinematic hardening model was used for tensile-tensile load case. The linear kinematic hardening model was also used for cyclic tensile-compressive load case. An improved material model, using multilinear kinematic hardening characteristics to simulate the cyclic stress strain behaviour, was developed. This model was written into a user subroutine UMAT in ABAQUS and used to simulate relaxation of residual stresses under cyclic mechanical loading.

6.2 Experiments

Forged bars, U06, U10, U14, U19, and HTS18 were tested. The tensile loadings were applied to specimens U10, U14 and U19. Axial loading was first applied to each specimen to produce a certain plastic deformation. Then the specimen was unloaded and removed to measure surface residual stresses using X-ray. The loading histories of specimens U14 and U19 are shown in Figures 6.1 and 6.2. For specimen U10, the strain gauge rosettes were put on both sides of the round bar specimens within the gauge length. The average axial stress versus surface strains on both sides is shown in Figure 6.3, from which it can be seen that the strains on each side were not equal. This means that there was bending effect which results from the specimen having an irregular shaped cross section. Tables 6.1 and 6.2 give the plastic deformation and residual stress changes due to tensile mechanical loadings for specimens U14, U19 and U10. The residual stress relaxation against tensile strain is also presented in Figure 6.8.

Cyclic loading was applied to specimens U06 and HTS18. In the first few cycles, the strain range was small. Then the strain range was increased to a given value and retained for several cycles. X-ray measurements were taken after several cycles. The stress-strain cyclic histories are shown in Figures 6.4 and 6.5 for specimens U06 and HTS18, respectively. The plastic strains obtained from strain gauges and the residual stresses measured by X-ray after cyclic loadings are given in Tables 6.3 and 6.4 for specimens U06 and HTS18, respectively.

Finally, specimens U06 and HTS18 were centre hole drilled to determine the residual stresses after the cyclic loadings. The equipment, small strain rosette and drilling steps are the same as those described in Chapter 4. The strain release due to hole drilling are shown in Figures 6.6 and 6.7 for specimens U06 and HTS18,

respectively. Also shown are the results for specimens U15 and HTS09 which had not subjected to mechanical loading. It can be seen that there were no residual stresses left in the specimens U06 and HTS18 after the cyclic mechanical loadings. The relaxation results due to cyclic loadings are shown in Figure 6.9. The difference between the results from X-ray diffraction method and centre hole method may indicate that the residual stress relaxation on specimen surface was different from that under the specimen surface because of the influence of surface roughness.

From the experimental results, it can be seen that both tensile loading and cyclic loading would relax residual stresses. For large tensile strain, the residual stresses would be relaxed completely. For cyclic loading, the residual stresses were relaxed under the surface and across the section, but the residual stresses may be generated and redistributed at the rough surface.

6.3 Material Modelling for Finite Element Analysis

Most structures under cyclic loading with plastic deformation have complex multiaxial stresses and strains which are strain-history dependent. Many incremental plasticity models have been developed to describe the stress-strain behaviour for general cases. Because of the complexity of the constitutive equations, few analytical solutions have been found and only approximate results can be obtained by using a numerical technique such as the finite element (FE) method.

Commercial packages of FE method have been widely distributed and available for both research and engineering design. Among these ABAQUS has a well known reputation for plasticity analysis.

In ABAQUS, only two material hardening models for metals can be directly used. One is isotropic hardening and the other is linear kinematic hardening. For many practical cases, these two models are not enough to describe material properties. Fortunately, ABAQUS allows users to develop their own material models, and provides an interface whereby any mechanical constitutive model can be added to the array. The constitutive model is then programmed in a user subroutine UMAT in FORTRAN code.

The user subroutine is called at each material calculation point at each iteration of every increment to define the mechanical constitutive behaviour of the material.

When the subroutine is called, it is provided with the material state at the start of any predefined field variables, such as increment stress, temperature and time; with the strain increments and time increments. The subroutine must perform two functions: it must update the stresses and solution dependent state variables to their values at the end of the increment, and it must provide the material Jacobian matrix, $\partial\Delta\sigma/\partial\Delta\varepsilon$, for the constitutive model. The accuracy with which the Jacobian matrix is defined will usually be a major determinant in the rate of convergence of the solution, and so have a strong influence on computational efficiency.

In order to model the complex material response using UMAT, a constitutive model and the method of determining Jacobian matrix for this model are required. In the following, a brief introduction of isotropic hardening and linear kinematic hardening is presented. Detailed multilinear kinematic hardening model and determination of Jacobian matrix are described.

6.3-1 Isotropic hardening model

In this isotropic hardening model, the hardening is governed by one scalar variable, such as accumulated plastic strain p in most cases

$$p = \int \sqrt{\frac{2}{3} d\varepsilon_{ij}^{p} d\varepsilon_{ij}^{p}}\,, \tag{6.1}$$

and the loading function is

$$f = f_Y(\sigma_{ij}) - k(p) = 0. \tag{6.2}$$

If f_Y is taken as the Von Mises yield function, Equation 6.2 becomes

$$f = \sqrt{\frac{3}{2} S_{ij} S_{ij}} - k(p) = 0 \tag{6.3}$$

where S_{ij} is a deviatoric stress tensor,

$$S_{ij} = \sigma_{ij} - \frac{1}{3}(\sigma_{11} + \sigma_{22} + \sigma_{33}). \tag{6.4}$$

The elastic strains are obtained by using Hooke's law and the plastic strain components are given by Prandtl-Reuss equation

$$d\varepsilon_{ij}^{p} = d\lambda \frac{\partial f}{\partial S_{ij}} \tag{6.5}$$

where $d\lambda$ is called plastic multiplier and can be determined by differentiating Equations 6.1-6.2 and making use of Equation 6.3

$$d\lambda = dp = \frac{d\sigma_{eq}}{k'(p)} \tag{6.6}$$

where σ_{eq} is Von Mises equivalent stress

$$\sigma_{eq} = \sqrt{\frac{3}{2} S_{ij} S_{ij}} \ . \tag{6.7}$$

For the simple case of uniaxial stress, the isotropic hardening becomes

$$\left.\begin{array}{ll} d\varepsilon_e = d\sigma / E & \\ d\varepsilon_p = d\sigma / k'(p) & if\ |\sigma + d\sigma| \geq k(p) \\ d\varepsilon_p = 0 & if\ |\sigma + d\sigma| < k(p) \\ p = \int |d\varepsilon_p| & \end{array}\right\} \tag{6.8}$$

where $k(p)$ is determined from uniaxial tensile test. If the stress-strain in uniaxial tension is expressed as

$$\left.\begin{array}{ll} \sigma = E\varepsilon & \sigma < \sigma_y \\ \sigma = \sigma_y + g(\varepsilon_p) & \sigma \geq \sigma_y \end{array}\right\}, \tag{6.9}$$

function $k(\,)$ then equals to function $g(\,)$. From Equation 6.3, it can be seen that Von Mises yielding surface expands isotropically as plastic strains are accumulated. This isotropic hardening behaviour is illustrated by considering a uniaxial case as shown in Figure 6.10.

6.3-2 Linear kinematic hardening model

For many materials, compressive yielding is often much lower after plastically deformed in tension. This is called Bauschinger effect. Obviously isotropic hardening cannot model this Bauschinger effect. The kinematic hardening then was

developed to deal with this kind of hardening behaviour. The idea is that the shape of loading surface is fixed while the centre of the loading surface can be moved. This kinematic hardening model can be expressed as,

$$f = f_Y(S_{ij} - X_{ij}) - \sigma_y = 0 \tag{6.10}$$

where the hardening variable X_{ij} is of a tensorial nature and indicates the present position of the loading surface. The linear relationship between X_{ij} and ε_{ij} is

$$X_{ij} = C_0 \varepsilon_{ij}^p \tag{6.11}$$

where C_0 is a constant which can be determined from uniaxial tension. The plastic strains can also be obtained using Prandtl-Reuss Equation 6.5. By adopting Equation 6.11 the kinematic hardening model (6.10) becomes a linear kinematic hardening model.

For the simple case of uniaxial stress, linear kinematic hardening becomes

$$\left.\begin{aligned} d\varepsilon_e &= d\sigma/E \\ d\varepsilon_p &= d\sigma \Big/ \left(\frac{3}{2}C_0\right) \qquad if\ \left|\sigma + d\sigma - C_0\varepsilon_p\right| \geq \sigma_y \\ d\varepsilon_p &= 0 \qquad\qquad\qquad if\ \left|\sigma + d\sigma - C_0\varepsilon_p\right| < \sigma_y \end{aligned}\right\} \tag{6.12}$$

where C_0 is determined from uniaxial tension stress-strain result

$$\left.\begin{aligned} \sigma &= E\varepsilon \qquad\qquad \sigma < \sigma_y \\ \sigma &= \sigma_y + H\varepsilon_p \qquad \sigma \geq \sigma_y \end{aligned}\right\}, \tag{6.13}$$

where H is linear hardening Modulus. By comparing Equation 6.12 with Equation 6.13, then

$$C_0 = \frac{2}{3}H. \tag{6.14}$$

The linear kinematic hardening model under the uniaxial stress case is also shown in Figure 6.10. The constants for the model are given in Table 6.5 for two batches, U and HTS of the forged En15R steel.

6.3-3 Comparison of the two hardening models with behaviour of En15R steel

Figures 6.4 and 6.5 show the stress-strain behaviour of En15R under cyclic loading for different batches. The stress shown in the figures is the axial average stress across the section and the strain is the axial surface strain. Because there were residual stresses in the specimens, the curve of average stress against surface strain was only an approximation of the real stress-strain behaviour of a residual stress free sample.

From the material curve shown in Figures 6.4 and 6.5, it can be seen that after tension beyond yielding followed by compression, the reverse yielding occurs much earlier than predicted by using the isotropic hardening, shown in Figure 6.10. Therefore, the isotropic hardening model does not correspond to the experimental observations of reverse yielding and was not suitable for the case of reverse loading.

Linear kinematic models are possibly better for modelling cyclic loading. Compared with the experimental cyclic stress-strain curves shown in Figures 6.4 and 6.5, the linear kinematic model has some deficiencies outlined below:

1. *The hardening Modulus is not constant for the real material, and it is plastic deformation and history dependant. The difference is quite large, and it is therefore a problem to chose the most suitable hardening Modulus when using the linear kinematic hardening model.*

2. *From the experimental stress-strain curves, the initial yielding stress is much higher and cannot be used as the radius of loading surface in the linear kinematic hardening model.*

3. *After initial yielding, the hardening Modulus in the experimental stress-strain curves is very small and the stress-strain curve is much closer to perfect-plasticity. Under unloading and compression there is a strong Bauschinger Effect. Both these aspects can not be included in the linear kinematic model.*

Therefore, the isotropic hardening model can only be used when there is no unloading. The linear kinematic model may be used for cyclic loading but is not truly representative for initial yielding and determining the appropriate hardening Modulus is a problem.

6.3-4 Multi-linear kinematic hardening model

For cyclic loading, a better model was required to consider initial yielding and reverse yielding (Bauschinger Effect). ABAQUS allows the user to develop their own material models. These can be included in the user subroutine UMAT as a FORTRAN program.

A theoretical multilinear kinematic model was proposed by Mroz (1967). This model consists of a certain number of surfaces in stress space, inserted one into another with linear kinematic hardening as shown in Figure 6.11. The key point is that there is kinematic movement of the surfaces. Let us assume we have *n* surfaces expressed by each function,

$$f_L = f_Y(S_{ij} - X_{ij,L}) - \kappa_L = 0 \qquad L = 1,2,\cdots,n \tag{6.15}$$

where f_Y takes Von Mises criterion function, $X_{ij,L}$ is the current centre of the surface L and κ_L is the radius of the surface L with

$$\kappa_1 < \kappa_2 < \cdots < \kappa_L < \kappa_{L+1} < \cdots < \kappa_n . \tag{6.16}$$

Surface L only is allowed to move around within surface $L+1$ and they can move together. When load point is on the L*th* surface, this loading point together with the surface will tend to move towards the point on the (L+1)*th* surface where its normal direction is the same as that as the point on the L*th* surface. The translation of L*th* surface is therefore,

$$dX_{ij,L} = d\mu(S_{ij,L+1} - S_{ij}) \tag{6.17}$$

where $S_{ij,L+1}$ is the stress point on (L+1)*th* surface such that the outward normal at this point is identical to the outward normal to the L*th* surface at the current point S_{ij} and $d\mu$ is a constant increment related to the stress increment.

$$d\mu = \frac{\dfrac{\partial f_L}{\partial S_{ij}} dS_{ij}}{\dfrac{\partial f_L}{\partial S_{ij}}(S_{ij,L+1} - S_{ij})} . \tag{6.18}$$

The plastic strain increments are given by Prandtl-Reuss equation,

$$d\varepsilon_{ij}^{p} = d\lambda \frac{\partial f_L}{\partial S_{ij}}. \tag{6.19}$$

The projection of the stress increment dS on the normal to the surface f_L is

$$dF = dS_{ij} * \frac{\partial f_L}{\partial S_{ij}} \Big/ \sqrt{\frac{\partial f_L}{\partial S_{ij}} * \frac{\partial f_L}{\partial S_{ij}}} \tag{6.20}$$

which contributes to the plastic deformation

$$dp = \sqrt{\frac{2}{3} d\varepsilon_{ij}^{p} d\varepsilon_{ij}^{p}}. \tag{6.21}$$

Assume the relationship between them is

$$dF = \sqrt{\frac{2}{3}} H_L dp \tag{6.22}$$

where the hardening Modulus H_L may depend on stress S but it is preferable to use a constant value, which may be determined from a uniaxial test. Under uniaxial stress Equations (6.20) and (6.21) become

$$dF = \sqrt{\frac{2}{3}} d\sigma \tag{6.23}$$

and

$$dp = d\varepsilon_p. \tag{6.24}$$

Inserting Equations (6.23) and (6.24) into Equation (6.22), we get

$$d\sigma = H_L d\varepsilon_p. \tag{6.25}$$

Thus the hardening Modulus H_L can be directly obtained from a uniaxial stress test.

Consequently, the multiplier $d\lambda$ can be derived from Equations (6.19 to 6.22)

$$d\lambda = \frac{dS_{ij} * \frac{\partial f_L}{\partial S_{ij}}}{H_L \frac{\partial f_L}{\partial S_{ij}} * \frac{\partial f_L}{\partial S_{ij}}}. \tag{6.26}$$

If the L*th* surface reaches the (L+1)*th* surface, the two surfaces will move together towards (L+2)*th* surface in the way same as the movement of L*th* surface towards (L+1)*th* surface. The n*th* surface is the initial yielding surface which follows the isotropic hardening rule.

For the four surfaces chosen, there are therefore four hardening Moduli H_1 to H_4 which are taken as functions of maximum equivalent plastic strain in the history,

$$H_1(\varepsilon_p^{eq,m}),\ H_2(\varepsilon_p^{eq,m}),\ H_3(\varepsilon_p^{eq,m}),\ H_4(\varepsilon_p^{eq,m}) \tag{6.27}$$

where

$$\varepsilon_p^{eq,m} = \max_{t>0}\left(\sqrt{\frac{2}{3}\varepsilon_{ij}^p(t)\varepsilon_{ij}^p(t)}\right). \tag{6.28}$$

The radii of surfaces 1, 2 and 3 are kept constant whilst the radius of the fourth surface, κ_4, equals the maximum equivalent stress in the history,

$$\kappa_1, \kappa_2, \kappa_3, \kappa_4 (= \sigma_{\max}^{eq}). \tag{6.29}$$

All these functional relationship and constants are determined from uniaxial cyclic stress-strain curves.

Figure 6.12 shows an example of how to determine the parameters of the multilinear kenematic hardening model using uniaxial stress-strain curve from HTS18. For the initial yielding which represents isotropic hardening of the fourth surface, the stress-strain curve is expressed as

$$\sigma = \begin{cases} \sigma_{y1} + HI_1 \varepsilon_p & \varepsilon_p \le 400\,\mu\varepsilon \\ \sigma_{y2} + HI_2 \varepsilon_p & 400 < \varepsilon_p \le 8000\,\mu\varepsilon \\ \sigma_{y3} + HI_3 \varepsilon_p & \varepsilon_p > 8000\,\mu\varepsilon \end{cases} \tag{6.30}$$

where HI_1, HI_2 and HI_3 are hardening modului for the fourth surface expansion and listed in Table 6.6. Therefore the fourth hardening modulus H_4 equals to HI_1 or HI_2 or HI_3. The maximum tensile plastic strain is,

$$\varepsilon_p^{eq,m} = \varepsilon_p^m = \varepsilon_{max} - \frac{\sigma_{max}}{E}. \tag{6.31}$$

Then the plastic strain from the point of maximum tensile stress to the next point of maximum compressive stress in one cycle equals to $2\varepsilon_p^m$. The diameters of each surface are measured from the point of tensile maximum stress as shown in Figure 6.12 and presented in Table 6.6. The hardening modului between surfaces are

$$\left.\begin{aligned} H_1 &= \frac{2\kappa_2 - 2\kappa_1}{0.1(2\varepsilon_p^{eq,m})} = \frac{\kappa_2 - \kappa_1}{0.1\,\varepsilon_p^{eq,m}} \\ H_2 &= \frac{\kappa_3 - \kappa_2}{0.2\,\varepsilon_p^{eq,m}} \\ H_3 &= \frac{\kappa_4 - \kappa_3}{0.7\,\varepsilon_p^{eq,m}} \end{aligned}\right\}. \tag{6.32}$$

The hardening modului are no longer constants and are plastic strain and history dependent.

The constants and parameters of multilinear kinematic hardening from U06 are also presented in Table 6.6.

This multilinear kinematic hardening model has been developed to consider both isotropic hardening and kinematic hardening behaviour. It also includes the perfect-elastic-plastic feature. Using a 3D-element, with uniaxial tension and compression, the strain range from 10,000με to -10,000με, Simulation trials has compared with experimental results. It was shown that satisfactory results were obtained regardless of the strain ranges. It can be seen that the multilinear kinematic model is an improved model.

6.3-5 Jacobian matrix

In the FE method, a constitutive rate equation must be transformed into an incremental equation with a suitable integration procedure. In ABAQUS STANDARD, a backward Euler integration has been used. It requires an

incremental expression for the internal state variables, such as stresses, strains, for the local iteration.

The relationship between stress increments and strain increments can be expressed as

$$\{\Delta\sigma\} = D\{\Delta\varepsilon\} \tag{6.33}$$

where D is the Jacobian matrix

$$D = \frac{\partial\Delta\sigma}{\partial\Delta\varepsilon}. \tag{6.34}$$

For isotropic hardening and linear kinematic hardening models, the Jacobian matrix can be obtained analytically. But for multilinear kinematic model, a numerical method was be developed to find the Jacobian matrix.

If there are six components in stress array $\{\sigma\}$ and strain array $\{\varepsilon\}$,

$$\{\sigma_1 \quad \sigma_2 \quad \sigma_3 \quad \sigma_4 \quad \sigma_5 \quad \sigma_6\} = \{\sigma_x \quad \sigma_y \quad \sigma_z \quad \tau_{zy} \quad \tau_{zx} \quad \tau_{xy}\} \tag{6.35}$$

$$\{\varepsilon_1 \quad \varepsilon_2 \quad \varepsilon_3 \quad \varepsilon_4 \quad \varepsilon_5 \quad \varepsilon_6\} = \{\varepsilon_x \quad \varepsilon_y \quad \varepsilon_z \quad \gamma_{zy} \quad \gamma_{zx} \quad \gamma_{xy}\} \tag{6.36}$$

the Jacobian matrix D is a 6×6 matrix

$$\begin{Bmatrix} \Delta\sigma_1 \\ \Delta\sigma_2 \\ \Delta\sigma_3 \\ \Delta\sigma_4 \\ \Delta\sigma_5 \\ \Delta\sigma_6 \end{Bmatrix} = \begin{bmatrix} d_{11} & \cdots & d_{16} \\ & \ddots & \\ & & \\ & & \\ & & \\ d_{61} & \cdots & d_{66} \end{bmatrix} \begin{Bmatrix} \Delta\varepsilon_1 \\ \Delta\varepsilon_2 \\ \Delta\varepsilon_3 \\ \Delta\varepsilon_4 \\ \Delta\varepsilon_5 \\ \Delta\varepsilon_6 \end{Bmatrix}. \tag{6.37}$$

The procedure to calculate the Jacobian matrix includes:

i) Let

$$\left.\begin{aligned} \Delta\varepsilon_{1'} &= 1 \\ \Delta\varepsilon_i &= 0, \quad i = 2,\cdots 6 \end{aligned}\right\}. \tag{6.38}$$

ii) Calculate the stress increment by using the constitutive equation.

iii) Using the Equation (6.37), we obtain the first column of the Jacobian matrix D

$$\begin{Bmatrix} d_{11} \\ d_{21} \\ d_{31} \\ d_{41} \\ d_{51} \\ d_{61} \end{Bmatrix} = \begin{Bmatrix} \Delta\sigma_1 \\ \Delta\sigma_2 \\ \Delta\sigma_3 \\ \Delta\sigma_4 \\ \Delta\sigma_5 \\ \Delta\sigma_6 \end{Bmatrix}_{\Delta\varepsilon_1=1} . \tag{6.39}$$

In turn, let $\Delta\varepsilon_j = 1$ for j= 2, 3..., and other strain components set to zero and using the same procedure as above, we get all the six columns of the Jacobian matrix D with

$$\begin{Bmatrix} d_{1i} \\ d_{2i} \\ d_{3i} \\ d_{4i} \\ d_{5i} \\ d_{6i} \end{Bmatrix} = \begin{Bmatrix} \Delta\sigma_1 \\ \Delta\sigma_2 \\ \Delta\sigma_3 \\ \Delta\sigma_4 \\ \Delta\sigma_5 \\ \Delta\sigma_6 \end{Bmatrix}_{\Delta\varepsilon_i=1} . \tag{6.40}$$

Because all stress increments are found by the numerical method, the Jacobian matrix obtained is therefore only an approximate solution. This procedure of determining Jacobian matrix is part of the UMAT routine.

For the forged and shot blast specimens, an axisymmetric analysis was carried out. An UMAT subroutine for this case is presented in appendix 6A.

6.4 Initial Residual Stress Input

In ABAQUS, residual stresses can be input as an initial condition. The residual stresses can be defined as either element by element or by its location. The residual stress calculation is programmed in a user subroutine SIGINI in FORTRAN code. This user subroutine is called for each material points. When this subroutine, SIGINI, is called, the location with coordinates is provided and the subroutine must provide the initial stress array (residual stresses). The number of stress components

depends on the element type for which this subroutine call is being made. The equilibrium of the residual stress input can be checked by ABAQUS. The SIGINI subroutines for two residual stress input cases are presented in Appendix 6B.

6.4-1 Residual stress distributions

In Chapter 5 residual stress distributions were determined from measurements in bars from U-batch. The functional form of the residual stresses was determined in section 5.4 and presented in Appendix 5A. It can be seen that the functions of residual stress distributions can be expressed in simplified form as,

$$\left.\begin{aligned}\sigma_r &= C_1(1-r^2)+C_2(1-r^3)\\ \sigma_\theta &= C_1(1-3r^2)+C_2(1-4r^3)\\ \sigma_z &= C_3(2-4r^2)+C_4(2-5r^3)\end{aligned}\right\} \tag{6.41}$$

where r is the nondimensionalised radius of the round bar, r/R, and C_1 to C_4 are constants determined in section 5.4.

Based on the measurements using the X-ray method together with chemical etching described in Chapter 4, the distributions of residual stresses in the HTS round bars, shown in Figure 6.14, take the form,

$$\sigma_r = \begin{cases} a & \xi \le 0 \\ a + b\xi^2 & \xi > 0 \end{cases} \tag{6.42}$$

$$\sigma_\theta = \frac{d}{dr}(r\sigma_r) \tag{6.43}$$

and

$$\sigma_z = \begin{cases} c & \xi \le 0 \\ c + d\xi & \xi > 0 \end{cases} \tag{6.44}$$

where $\xi = r - q$ and a, b, c, d are constants which can be determined by using equilibrium and boundary conditions. Assuming that the surface axial and tangential residual stresses are σ_{z1} and $\sigma_{\theta 1}$, the constants are

$$\begin{cases} a = -\dfrac{\sigma_{\theta 1}(1-q)}{2} \\ b = \dfrac{\sigma_{\theta 1}}{2(1-q)} \\ d = \dfrac{\sigma_{z1}}{1-q-t} \\ c = -d * t \end{cases} \tag{6.45}$$

where

$$t = \frac{(1-q)^2/2 + q(1-q)^3/3}{0.5 + q - q^2}. \tag{6.46}$$

q was taken as 0.84. In the FE simulation, the initial surface axial residual stresses, σ_{z1}, were taken as -450 MPa, -400 MPa, -350 MPa, -300 MPa and -250 MPa. The initial tangential residual stresses, $\sigma_{\theta 1}$, were about 50 MPa lower than σ_{z1}. The residual stress field was input by user subroutine SIGINI given in Appendix 6B

6.4-2 Initial state input for multilinear kinematic model

In many cases, the residual stresses are generated by nonuniform plastic deformation. The plastic strain state reflects the loading history and will influence the present stress-strain behaviour. Therefore an initial plastic strain state and the position of yield surfaces are required as an input when the interaction between applied load and residual stress is considered.

For isotropic hardening and kinematic hardening models, there is no option for including the initial plastic strain state in ABAQUS. However, for the multilinear kinematic hardening model developed, there is the possibility to input initial plastic strains and their related historic variables in the user subroutine UMAT when the routine is called at the first time.

If it is assumed that the maximum equivalent plastic strain $\varepsilon_p^{eq,m}$ from the previous strain history due to shot blasting is known, the corresponding maximum equivalent stress σ_{eq}^m can be obtained from the uniaxial tensile curve. The σ_{eq}^m is the radius of the 4th yield surface.

The initial state will be related to initial residual stress field. Only the residual stress distribution for the HTS batch, shown in Equations (6.42 to 6.46) is considered for determination of the initial state.

Determination of initial plastic strains

For the round bar, it is a generalised plane strain condition,

$$\varepsilon_z(r) = const \tag{6.47}$$

where z is along axial direction. It is assumed that the tangential strains also keep constant, that is

$$\varepsilon_\theta(r) = const\,. \tag{6.48}$$

When $r \le q$, there is no plastic deformation. Therefore,

$$\begin{cases} \varepsilon_z(r) = \varepsilon_z^e\big|_{r\le q} = \varepsilon_z^e(0) \\ \varepsilon_\theta(r) = \varepsilon_\theta^e\big|_{r\le q} = \varepsilon_\theta^e(0) \end{cases} \tag{6.49}$$

where $\varepsilon_z^e(0)$ and $\varepsilon_\theta^e(0)$ can be found using residual stresses at $r = 0$ together with Hooke's law,

$$\begin{cases} \varepsilon_z^e(0) = \dfrac{1}{E}[c - 2\nu a] \\ \varepsilon_\theta^e(0) = \dfrac{1}{E}[a - \nu(a + c)] \end{cases} \tag{6.50}$$

where the constants a and c are expressed in Equation (6.45). Consequently the plastic strains can be found,

$$\begin{cases} \varepsilon_z^p = \varepsilon_z^e(0) - \dfrac{1}{E}[\sigma_z - \nu(\sigma_\theta + \sigma_r)] \\ \varepsilon_\theta^p = \varepsilon_\theta^e(0) - \dfrac{1}{E}[\sigma_\theta - \nu(\sigma_z + \sigma_r)] \\ \varepsilon_z^p = -(\varepsilon_z^p + \varepsilon_\theta^p) \end{cases} \tag{6.51}$$

Determination of initial position of yield surfaces

The positions of first, second and third surface are determined based on the residual stress and loading condition of the shot blasting. The residual stress state is,

$$\sigma_1 = \sigma_r^R,\ \sigma_2 = \sigma_\theta^R,\ \sigma_3 = \sigma_z^R \tag{6.52}$$

where it has been shown for the forged bars that σ_2 and σ_3 are in compression and σ_1 is a small value. Then the deviatoric stresses are

$$\left.\begin{aligned} S_r^R &= \frac{2}{3}\sigma_r^R - \frac{1}{3}(\sigma_\theta^R + \sigma_z^R) \\ S_\theta^R &= \frac{2}{3}\sigma_\theta^R - \frac{1}{3}(\sigma_r^R + \sigma_z^R) \\ S_z^R &= \frac{2}{3}\sigma_z^R - \frac{1}{3}(\sigma_\theta^R + \sigma_r^R) \end{aligned}\right\}. \tag{6.53}$$

Considering that the surface loading type of shot blasting being along the radial direction, the maximum deviatoric stresses corresponding to the σ_{eq}^m can be expressed approximately

$$\left.\begin{aligned} S_r^m &= -\beta S_r^R \\ S_\theta^m &= -\beta S_\theta^R \\ S_z^m &= -\beta S_z^R \end{aligned}\right\} \tag{6.54}$$

where β is a constant value determined from follow condition

$$\begin{cases} \sqrt{\frac{3}{2}\left(S_r^m S_r^m + S_\theta^m S_\theta^m + S_z^m S_z^m\right)} = \sigma_{eq}^m \\ \sqrt{\frac{3}{2}\left(S_r^R S_r^R + S_\theta^R S_\theta^R + S_z^R S_z^R\right)} = \sigma_{eq}^R \end{cases}. \tag{6.55}$$

Then β is found by inserting Equation (6.54) into Equation (6.55) to give

$$\beta = \frac{\sigma_{eq}^m}{\sigma_{eq}^R}. \tag{6.56}$$

Figure 6.13 illustrates the loading points, surface movements for two surfaces in one dimension. When the stress state is on point A which corresponds to the maximum loading in the history, the location of 1st yield surface centre, shown in Figure 6.13, C_1' can be found,

$$\overline{OC_1'} = |OC_1'|\frac{\overline{OA}}{|OA|} = \frac{\sigma_{eq}^m - \kappa_1}{\sigma_{eq}^m}\overline{OA} \tag{6.57}$$

where OC_1' and OA are vectors,

$$\overline{OC_1'} = \begin{Bmatrix} X_{r,1} \\ X_{\theta,1} \\ X_{z,1} \end{Bmatrix}, \qquad \overline{OA} = \begin{Bmatrix} S_r^m \\ S_\theta^m \\ S_z^m \end{Bmatrix}. \tag{6.58}$$

Therefore the locations of centres for all surfaces for the maximum loading in history can be determined from

$$\begin{Bmatrix} X_{r,i} \\ X_{\theta,i} \\ X_{z,i} \end{Bmatrix} = \frac{\sigma_{eq}^m - \kappa_i}{\sigma_{eq}^m} \begin{Bmatrix} S_r^m \\ S_\theta^m \\ S_z^m \end{Bmatrix} \qquad i = 1,2,3. \tag{6.59}$$

For the present residual stress state being on the first yielding surface, point B in Figure 6.13, the centre for the first yield surface will move from C_1' to C_1, and

$$\overline{OC_1} = |OC_1|\frac{\overline{OB}}{|OB|} = \frac{\sigma_{eq}^R - \kappa_1}{\sigma_{eq}^R}\overline{OB} \tag{6.60}$$

which leads to

$$\begin{Bmatrix} X_{r,1} \\ X_{\theta,1} \\ X_{z,1} \end{Bmatrix} = \frac{\sigma_{eq}^R - \kappa_1}{\sigma_{eq}^R} \begin{Bmatrix} S_r^R \\ S_\theta^R \\ S_z^R \end{Bmatrix}. \tag{6.61}$$

The input of plastic strains and centres of yielding surfaces is included in the user subroutine UMAT which is shown in Appendix 6A.

6.5 Finite Element analysis for Residual Stress Relaxation

6.5-1 Tensile loading alone

For the round bar specimens, the axisymmetric shape and loading were assumed. Uniform displacement along the axial direction was applied to meet the generalised plane strain condition. The FE mesh and loading condition are shown in Figure 6.14. Because there was no reverse yielding during tensile loading and unloading, the initial state of plastic strain had little influence on residual stress relaxation results. Therefore, the multilinear hardening was not employed for this loading case. Results using linear kinematic hardening model for both U and HTS batches were obtained and compared with each other. The results of the analyses will be compared with experimental results from U-batch tests reported in Table 6.1 and 6.2.

Young's Modulus and Poisson's ratio were assumed to be the same for U and HTS batches. The yielding stress and hardening modului are different for the two batches and they were taken from uniaxial tension-compression curves Figure 6.4 for U-batch and Figure 6.5 for HTS batch. The constants for the linear kinematic hardening model are given in Table 6.5 for the two batches of forged En15R steel.

Based on X-ray measurements from U-batch bars, described earlier in section 4.2-4, the initial axial residual stresses at the surface were chosen 200 MPa as a representative low value and 297.5 MPa as the mean value of the distribution. The initial tangential residual stresses were chosen as 180 MPa and 234.5 MPa, respectively, based on the measured results shown in Figures 4.6 and 4.7.

For the residual stress relaxation simulation of the HTS specimen, the initial axial residual stresses at the surface were chosen 300 MPa as a representative low value and 400 MPa as the mean value of the distribution. The initial tangential residual stresses were chosen 280 MPa and 350 MPa, respectively.

The calculated residual stress relaxation as a function of total strain is shown in Figure 6.15. It can be seen that relaxation for different bars from different batches and different initial residual stresses has the same trend as the tensile strain increase. There is a elastic range of applied strain where there is no relaxation because the sum of residual stress and applied stress is less than yield stress. There also appears to be good agreement with experimental results.

6.5-2 Residual stress relaxation under cyclic loading

The FE mesh and loading conditions were the same as used for tensile loading case, shown in Figure 6.14. In the analysis two kinds of material models were used: linear kinematic hardening and multilinear kinematic hardening. The two linear kinematic hardening models were the same as used in the tensile loading case for U and HTS batches and their parameters are listed in Table 6.5.

Using linear kinematic hardening

For the parameters of linear kinematic model for the U-batch, the initial residual stress state at surface was taken with $\sigma_z^R = -297.5\ MPa$ and $\sigma_z^R = -234.5\ MPa$. The results for the residual stress relaxation as a function of number of cycles for different cyclic half strain ranges are shown in Figure 6.16.

For the linear kinematic model parameters for the HTS batch, the initial residual stress state at the surface was considered for two cases. Case 1 assumed that $\sigma_z^R = -300\ MPa$ and $\sigma_\theta^R = -280\ MPa$ and for case 2 it was assumed that $\sigma_z^R = -400\ MPa$ and $\sigma_\theta^R = -350\ MPa$. The residual stress relaxation as a function of number of cycles for different cyclic strain ranges is shown in Figure 6.17 for case 1 and in Figure 6.18 for case 2.

Using multilinear kinematic hardening

Table 6.6 lists the parameters of the multilinear kinematic model that were taken from the stress-strain curve of specimen HTS18, shown in Figure 6.12. The simulation for cyclic uniaxial loading using this model is shown in Figure 6.4. The FE mesh, loading and boundary conditions, and initial residual stress input are shown in Figure 6.14. Different initial surface axial residual stresses were chosen starting from $\sigma_z^R = -250\ MPa$ decreasing to $\sigma_z^R = -450\ MPa$ in steps of $-50\ MPa$.

For cyclic loading, the half total strain ranges were taken as 1000 με, 1400 με, 1800 με, 2200 με, 2600 με, 3000 με and 3200 με. As an example for an applied half total strain range $\frac{\Delta\varepsilon}{2} = 1000\ \mu\varepsilon$, first the axial load was applied to give a tensile strain $\varepsilon = 1000\ \mu\varepsilon$, then unloaded and compressed to give a compressive strain $\varepsilon = -1000\ \mu\varepsilon$ and finally unloaded to zero axial load. This is just for one cycle. For

more cycles, the load was just repeated as for the first cycle. In some cases the number of cycles was up to ten. Figures 6.19 to 6.23 show axial residual stress relaxation for different cyclic half strain ranges and initial surface axial residual stresses.

Figure 6.24 shows the redistribution of axial residual stress in specimens for different strain ranges after 1st cycle.

From Figures 6.19-6.23, it may be assumed that the surface residual stress relaxation on the surface eventually becomes stabilised. If it is assumed that the relaxation of the surface residual stresses conforms to the following function,

$$\sigma_{R,N} = \sigma_{R'} + b * e^{-cN} \tag{6.62}$$

where N is the number of cycles. $\sigma_{R,N}$, b and c are fitted constants. $\sigma_{R'}$ is the stabilised residual stress for $N = \infty$. Consequently the stabilised residual stresses for each cyclic loading range can be found without carrying out more calculations for many more cycles. The fitted curves using Equation (6.62) for different initial surface residual stresses and cyclic strain ranges are also shown in Figures 6.19 to 6.23.

The results for the stabilised residual stresses as a function of the initial residual stress for different cyclic strain ranges are shown in Figure 6.25. These relaxation results are also shown in 3-D in Figure 6.26 in which the relaxed residual stress $\sigma_{R'}$ was a function of both the initial residual stress σ_R and the applied cyclic half strain range $\Delta\varepsilon/2$. There are some boundary conditions for the relationship among the three variables $\sigma_{R'}$, σ_R and $\Delta\varepsilon/2$. When $\Delta\varepsilon = 0$ there is no relaxation, $\sigma_{R'} = \sigma_R$. If $\sigma_R = 0$, then $\sigma_{R'}$ should be zero for any $\Delta\varepsilon$. Assuming a functional form as an approximate relationship among the three variables,

$$\sigma_{R'} = \left[1 + A_1(\Delta\varepsilon/2) + A_2(\Delta\varepsilon/2)^2\right]\sigma_R \tag{6.63}$$

where A_1 and A_2 are two constants. Using curve fitting technique A_1 and A_2 were found to be

$$\left.\begin{aligned} A_1 &= -2.02\times10^{-5} \\ A_2 &= -8.43\times10^{-8} \end{aligned}\right\} \tag{6.64}$$

Figure 6.27 shows the fitted result expressed by Equation (6.63).

6.6 Discussion

It is obvious that residual stress can be released by mechanical loading. But how does relaxation take place? For the round bar steel, the yield stress was about 650-700 MPa from tensile results shown in Figures 6.1 to 6.3 for U-batch specimens. So the limit of elastic strain was about 3200-3400 με. On the surface, the axial residual stress was about -270 MP and the corresponding elastic strain, by Hooke's law, is about −1300 με. If we consider the yield stress on the surface is the same as about 650-700 MPa, then the range of surface elastic strain should be about 4500-4700 με. From the tensile tests on U-batch specimens, all surface strains under the mechanical loading are less than 5000 με. So the residual stress relaxation should be elastic which would mean that the curve of residual stress reduction versus surface plastic strain is linear. But the actual relaxation, shown in Tables 6.1 and 6.2 and Figure 6.15, indicated that relaxation of residual stresses was a non-linear function of the surface strain. To explain this, we should consider the Bauschinger effect for the material. This effect has been shown in Figures 6.4 and 6.5. The surface material had been subjected to various treatments with various complicated strain histories during the manufacturing process. The surface stress state was in biaxial compression which could be at yield surface. When tensile loading was applied, the yield stress would be much less than 650 MPa and the elastic range could be less than 3200 με which depends on the behaviour of the Bauschinger effect of the material. Figure 6.15 shows the nonlinear relaxation under the tensile loading by both experiments and FE analysis.

For cyclic mechanical loading, reverse yielding was the most likely case because of the presence of the compressive residual stresses. Consequently more relaxation of residual stress took place. From the FE analysis results, it can be seen that more residual stresses were relaxed under cyclic loading than under tensile-tensile loading. This can be explained by that residual stresses were in compression. The residual stress relaxation is mainly related to the yielding behaviour. The yielding point is much lower under compressive loading than under tensile loading because of the Bauschinger effect. Therefore under cyclic loading, there would be more plastic deformation resulting in more residual stress relaxation. The FE results have shown that residual stresses completely relax when the cyclic strain range is beyond the elastic limit.

Comparison of results from linear kinematic hardening and multi-linear kinematic hardening

The multi-linear kinematic hardening model is an improved model for the cyclic stress strain behaviour compared to the linear kinematic, especially for small plastic strains. If the plastic strains were large, there was not much difference between the hardening moduli of the two hardening models. Another advantage in using the multilinear kinematic hardening model was that the plastic deformation, generated by shot blasting, and consequently a history dependent variable could be input into the user subroutine UMAT.

The results using linear kinematic hardening model, shown in Figures 6.17 and 6.18, can be compared to those using multilinear kinematic hardening model, shown in Figures 6.20 and 6.22. The figures show the results for the HTS batches with the same conditions for the initial residual stress distribution. It can be seen that for a smaller cyclic strain range there was much more residual stress relaxation using multilinear kinematic hardening model than using linear kinematic hardening model. However for large cyclic strain range, there was not much difference between using these two hardening models and most of the residual stress was relaxed.

Comparison of results from hole drilling, X-ray and FE

From the FE analyses for cyclic loading, shown in Figures 6.16 to 6.23, it can be seen that as the cyclic strain range increased more relaxation of the residual stresses occurred. When the strain range reaches a certain value, residual stresses will be totally eliminated. Even for strain ranges that are regarded as within the elastic range a certain degree of relaxation will occur because the surface had already undergone plastic deformation due to shot blasting. This relaxation only takes place during the first cycle.

From hole drilling results, shown in Figures 6.6 and 6.7, it can be seen that the residual stresses in the U06 and HTS specimens, which had undergone large strain cyclic loading, had totally relaxed. This is in general agreement with the FE analysis.

However the X-ray measurements only indicated that about 40 to 60 % relaxation of the residual stresses, shown in Figure 6.9, had occurred. This may be due to the

surface roughness where the residual stresses in the peak of the surface profile do not relax in the same way as that under the surface. At a notch the residual stress could be built up instead of relaxed, but this would only influence a very thin layer which also depends on the surface roughness. The X-ray measurements would also include microstresses (Macherauch, 1987) which will not relax by mechanical loading.

6.7 Conclusions

1) Experiments have been carried out to study the residual stress relaxation in round bars subjected to tensile and fully reversed cyclic loading.

2) The Finite Element method has been used to simulate the residual stress relaxation under the mechanical loading.

3) The linear kinematic hardening model has been used in the finite element analysis of residual stress relaxation.

4) A multilinear kinematic model has been developed also to simulate cyclic stress-strain behaviour of EN15R steel. This material model has been written into user subroutine UMAT in ABAQUS.

5) Under the tensile loading, the residual stresses decrease as the tensile strain increase. Both experimental results and finite element prediction are shown to be in good agreement.

6) Under cyclic loading, most relaxation of the surface residual stresses occurs in the first cycle. The residual stress relaxation have been shown to stabilise after certain number of cycles.

7) Even for low cyclic strain ranges, regarded as in the elastic range, residual stress relaxation takes place because surface material had undergone prior plastic deformation due to shot blasting.

8) From the FE analysis, the residual stresses are shown to totally relax when the cyclic strain range is beyond a certain value.

9) Complete relaxation of residual stress under large cyclic strain ranges for specimens U06 and HTS18 was confirmed by centre hole drilling.

10) The relationship between the initial residual stress and relaxed residual stress for different cyclic strain ranges has been established.

Chapter 7

EXPERIMENTAL WORK ON STATISTICAL EFFECTS ON FATIGUE LIFE

This Chapter presents fatigue test data from four groups of specimens AF, HT, FS and HTS. Results were analysed using the Weibull distribution. The influence factors of each stage of forging process on fatigue lives were studied and discussed. A more realistic fitting function with endurance limit was used for the S-N curve.

7.1 Introduction

There were four stages in the complete forging process. At each stage the residual stresses generated are different. In Chapter 4, surface axial residual stresses have been measured for specimens from four batches representing the four stages. The results have been shown in Figures 4.8 to 4.11. It can be seen that the residual stresses were mainly due to shot blasting.

It is expected that residual stress has a strong effect on fatigue lives. However, other influencing factors were also generated for different stage of forging process, such as material property change and surface roughness, and there would also have a significant effect on fatigue lives as well.

In this chapter, fatigue test data from four batches, AF, HT, FS and HTS for half strain range being 2200 με and 6000 με are presented. The experimental data are analysed using the Weibull distribution. The influence of different forging process on fatigue lives in the high cycle (HCF) and low cycle (LCF) fatigue regimes are presented and discussed. A three-parameter function was suggested for the S-N curve fitting which included the endurance limit to take account of the HCF regime.

7.2 Analysis of Fatigue Data from AF, HT, FS and HTS Batches

The four batches of specimens, AF, HT, FS and HTS, represent the different stages of the forging process. It has been shown in Chapter 4 that the residual stresses and surface roughness for the bars from each batches were different. Therefore, the fatigue lives for each batch would be expected to be different. Sixty specimens selected from the four groups , fifteen in each group, were fatigue tested at Rover. Fourteen in each group were tested. In each group, two strain ranges were chosen for the fatigue tests, $\frac{\Delta\varepsilon_T}{2} = \varepsilon_c = 2200\,\mu\varepsilon$ for HCF lives and $\frac{\Delta\varepsilon_T}{2} = \varepsilon_c = 6000\,\mu\varepsilon$ was for LCF lives. Tables 7.2 to 7.6 list the test matrix and fatigue lives.

Assuming that the fatigue lives can be described by the Weibull distribution, where cumulative distribution function and distribution density have been given by Equations (2.69) and (2.70), respectively, the linear relationship between $\log\left[\ln\left(\frac{1}{1-P}\right)\right]$ and $\log(N-N_0)$ can be obtained from the Equation (2.71),

$$\log\left[\ln\left(\frac{1}{1-P_m}\right)\right] = \beta\log(N_m - N_0) - \beta\log(N_a - N_0) \tag{7.1}$$

where P_m is medium rank, N_m is the fatigue life from test, N_0 is the assumed minimum life, N_a is the characteristic life and β is the Weibull slope. Using regression analysis, N_0, N_a and β were obtained, and shown in Table 7.5, for each batch subjected to given fatigue strain ranges. Figure 7.1 shows the test results and the fitted curves using Equation (7.1). Figure 7.2 show the fatigue life Weibull distributions for the two strain ranges $2200\mu\varepsilon$ and $6000\,\mu\varepsilon$. Figure 7.3 present the probability of failure. The reliability can be obtained from the following expression

$$R(N) = 1 - P(N) = \exp\left[-\left(\frac{N-N_0}{N_a-N_0}\right)^{\beta}\right] \qquad N > N_0. \tag{7.2}$$

For high cycle fatigue with the half strain range being $2200\,\mu\varepsilon$, the effect of manufacturing process on fatigue lives can be seen from Figures 7.1 and 7.2. The HTS batch, which had been subjected to the complete manufacture process (forged plus hardening & tempering plus shot-blasting), had the best fatigue behaviour, whilst the AF batch, which had been subjected to only the forging process, had the shortest fatigue lives. Comparing the HT and AF batches, the heat treatment

enhanced the fatigue life and reduced the scatter. The shot blasting treatment improved the fatigue life significantly but also increased the scatter.

Under low cycle fatigue with the half strain range being 6000 με, the complete forging process had a complete opposite effect on fatigue lives, as shown in Figures 7.1 and 7.2. The AF batch had the longest fatigue lives whilst the HTS batch had shortest fatigue lives. But the scatter was small compared to that of the HCF specimens and the fatigue lives life for all the group was quite low.

For the influence of the residual stress on fatigue life, Figure 7.4 presents the correlation between residual stresses and fatigue lives for the HTS batch. It can be seen from this figure that for half cyclic strain range being 2200 με, which was in HCF regime, there was a limited correlation between residual stresses and fatigue lives and for larger compressive residual stress the fatigue life was longer. However, for half cyclic strain range being 6000 με, which was in LCF regime, it is shown from the figure that there was no correlation between residual stresses and fatigue lives. This may indicate that residual stresses has no effect on fatigue life in LCF regime.

Surface roughness is another influencing factor on fatigue lives. The surface roughness of round bar specimens has been measured and presented in Chapter 4. Figure 7.5 gives the correlation between surface roughness, R_t, and fatigue lives for the HTS batch. It can be seen from this figure that for the smaller half cyclic strain range of 2200 με there was a limited correlation between surface roughness and fatigue lives, so that the rougher the surface the shorter the fatigue life. For the half cyclic strain range of 6000 με, which involved large plastic deformation, there was almost no correlation between residual stresses and fatigue lives. This may indicate that large plastic deformation had reduced the influence of surface roughness on fatigue lives.

7.3. Fatigue Curve for En15R Steel

For the En15R steel, from another batch of hot forged shot blasted bars, many fatigue tests have been conducted at Rover (Devlukia, 1993) with different surface finishing conditions at Rover. The total fatigue strain ranges were from 2×1800 με to 2×10000 με. The S-N curve then was obtained by using curve fitting with Manson-Coffin relationship. The fatigue test data of the forged bars are shown in

Figure 7.6 and compared with fatigue data of HTS and HT. The Manson-Coffin relationship that includes elastic and plastic strain components has been normally used as a fitting function for low cycle fatigue (Tavernelli, et al, 1962; Manson, 1962). This approach was not adopted here. Considering that the residual stresses appear only to influence high cyclic fatigue and for En15R steel there was a lower limit to the fatigue strain corresponding to infinite fatigue life, the fitting function for the S-N curve is chosen as,

$$\frac{\Delta\varepsilon_T}{2} = c + a * N_f^b \tag{7.3}$$

where $\Delta\varepsilon_T$ is total strain range applied, N_f is fatigue life, a, b and c are fitting constants to be determined. The constant c is related to the endurance limit of materials on which residual stresses have significant influence (Desvignes, et al, 1987). For most steels and copper alloys the endurance limit is about 35% to 50% of the ultimate tensile strength (Suresh, 1992).

The fitting strategy was as follows

$$\textbf{Fit}\ \ Log(a) + b * \log(N_f) - Log(\frac{\Delta\varepsilon}{2} - c)\ \ \textbf{to}\ \ zero. \tag{7.4}$$

This procedure was similar to a linear regression and can be done by multi-step linear regression. With given c, a and b was obtained by linear regression from Equation (7.4) and the error was found to relate to c,

$$ER(c) = \sum_i \left[Log(a) + b * \log(N_{f,i}) - Log(\frac{\Delta\varepsilon_i}{2} - c) \right]^2 . \tag{7.5}$$

where *i* represents fatigue data point. Then c was taken as $ER(c)$ being the minimum. Using the fatigue data for the bars of Barstock batch 2, the fitted results of a, b and c are as follows,

$$\begin{cases} a = 2.1429 \times 10^5 \\ b = -0.4965 \\ c = 1477.6 \end{cases} \tag{7.6}$$

The fitted curve is also shown in Figure 7.6

For the purpose of predicting the influence of shot blasting on fatigue life, which can be seen by comparison of fatigue test results from HTS specimens with those from HT specimens, the fatigue test results of HT specimens (without shot blast treatment) were taken into account,

$\Delta\varepsilon/2$	Fatigue life N_f for HT specimens
2200	90750
6000	2700

which was the distribution centre based on analysis of Weibull distribution of the fatigue lives. A curve of Equation (7.3) can not be determined with only two data points. So assuming the endurance limit c equal to 1500, then the a and b were found using Equation (7.3),

$$\begin{cases} a = 3.0E+5 \\ b = -0.5315 \\ c = 1500 \end{cases} \tag{7.7}$$

which is slightly different from those in (7.6). These constants were used throughout the prediction of the fatigue life distribution of HTS samples (with shot blast treatment effect) in Chapter 8.

7.4 Discussion

The fatigue test results for bars from each batch, AF, HT, FS and HTS, are shown in Figure 7.1. The Weibull distribution densities for the batches are shown in Figure 7.2. From these two figures it can be seen that at HCF conditions the HTS batch exhibited the longest lives, whilst the AF batch had the shortest. Comparing the results of the HT batch during HCF with that of AF batch, the heat treatment reduced the scatter significantly without changing the mean life. Shot blasted forged samples (FS) improved the fatigue life, but not as significantly as for HTS batch. In contrast at a high strain range the difference between the various batches was not so pronounced. Nevertheless, it was evident that the complete forging process had a complete opposite effect with LCF conditions compared with HCF conditions. The HTS batch had the shortest fatigue lives, while the AF batch had the longest. However, under LCF conditions the heat treatment reduced the scatter as well.

To explain these experimental results, the following points are suggested:

1) *The hardening and tempering heat treatment made the material properties more uniform and removed residual stresses and subsequently reduced the scatter of fatigue lives as shown in Figure 7.2 for both HCF and LCF.*

2) *The heat treatment also increased the elastic limit which may enhance fatigue lives for HCF. However, the heat treatment reduced the ductility of the material which was detrimental for LCF because plastic deformation dominates during LCF.*

3) *Shot blasting has been shown to introduce compressive residual stresses and increase specimen surface roughness. Generally compressive residual stresses increase fatigue life and surface roughness has an opposite effect.*

4) *For HCF conditions, most of the residual stresses will not be relaxed during fatigue. The positive effect by compressive residual stresses on fatigue is much more than the negative effect caused by surface roughness. Thus, the fatigue life will increase for HCF. Consequently, the shot blasting increases the fatigue life under HCF conditions just as shown in Figures 7.1 and 7.2.*

5) *Large plastic deformation dominates under LCF and therefore residual stresses will be totally relaxed in a few fatigue cycles, which has been proved by both experiments and finite element analysis. Therefore, residual stresses introduced by shot blasting will have no effect on fatigue life. However, surface roughness caused by shot blasting decreases the fatigue life, as shown in Figures 7.1 and 7.2.*

6) *Through out the fatigue tests, other influence factors on fatigue lives still existed, such as bending effect. This may explain why some HTS specimens got higher lives than those for the HT specimens at the fatigue range of 6000* με *as shown in Figures 7.1 and 7.2.*

Therefore, to judge the influence of each stage of forging process would depend on what kind of fatigue load (cyclic strain range) the specimen would undertake. For high cyclic fatigue the complete forging process is the best. But for the specimens are mainly used under low cyclic fatigue, only a forging process without heat treatment and shot blasting may be suggested.

For fitting the S-N curve, generally, the more parameters the fitting function has, the better the fit will be. For Manson-Coffin relation (2.19), two parts are included; an elastic part for HCF and a plastic part for LCF. The Manson-Coffin relation has four parameters to fit the S-N curve and therefore it is quite good for LCF fatigue data and has been widely used. The only drawback is that it does not include a endurance limit (Suresh, 1992). The Fitting function Equation (7.3) used here has three parameters including the endurance limit. It is therefore a good equation for the HCF regime but not as good as the Manson-Coffin relation in the LCF regime as shown in Figure 7.6.

7.5 Conclusions

1) Fatigue test data from four batches, AF, HT, FS and HTS, were analysed using the Weibull distribution. The failure probability for two strain ranges, 2200με and 6000με, for each batch were obtained.

2) The shot blast treatment was shown for high cycle fatigue to improve fatigue lives significantly but increase scatter and for low cycle fatigue to reduce fatigue lives and also increase scatter.

3) The heat treatment enhanced fatigue lives slightly in HCF and reduce fatigue lives in LCF, and reduce scatter in both conditions dramatically.

4) It was found that compressive residual stresses had no benefit under LCF because the residual stresses were relaxed out due to large plastic deformation.

5) Fatigue S-N curve for En15R steel has been analysed using a non-linear curve fitting technique. A more realistic fitting function was adapted.

Chapter 8

PROBABILISTIC ANALYSIS FOR THE INFLUENCE OF RESIDUAL STRESS ON FATIGUE LIFE

This Chapter presents statistical analysis of residual stress variation from specimen to specimen, its redistribution after interaction with cyclic loading and its influence on fatigue life. A probabilistic approach is developed to incorporate residual stresses into fatigue life prediction. The relationship among fatigue cyclic strain range, relaxed residual stress and the fatigue life is derived. Some other random influence factors on fatigue life except the residual stress are included. Simulations to determine fatigue lives are then made.

8.1. Introduction

Because of the inherent randomness found in fatigue data it is doubtful that deterministic methods can be used adequately in constructing mathematical models of fatigue. Fatigue of real materials should be regarded as a random phenomenon and analysed by use of the probabilistic approaches.

In probability theory, the probability distribution are regarded as *a priori* given, whereas in the analysis of real phenomena the probability distribution are seldom known. Hence, in stochastic modelling, attention should be focused on determination of the probability distribution of random quantities entering the model. Often the probability distributions are introduced as hypotheses (such as Normal distribution and Weibull distribution); so, they should be subject to subsequent verification.

There are many uncontrolled factors that influence fatigue life and cause scatter of fatigue test data, and these were discussed in Chapter 2. The shot blast treatment has been shown to generate significant residual stresses in components. In the following therefore the residual stresses, in shot blast specimens, are considered as a main influencing factor on fatigue life and the residual stresses in specimens are treated as a random variable. The other influencing factors on fatigue life are introduced in a simple way. The residual stress distribution was assumed as normal distribution or Weibull distribution. The probability distribution density functions of fatigue life, for different simulation conditions, have been obtained and compared with fatigue test results.

8.2 Specimen to Specimen Variation of Residual Stresses

8.2-1 Histograms from X-ray Measurements

The residual stresses were introduced by forging process. Because in the manufacture of large batches of forged components there were statistical variations in the geometry of the components, material properties and surface roughness, the residual stresses in the forged components would be expected to have inevitable variability from component to component. The statistical method therefore was used to analyse the residual stress distribution from specimen to specimen.

The X-ray diffraction method was used to measure surface residual stresses on round bars from U, AF, HT, FS and HTS batches. The results were shown in Chapter 4. Figures 4.6 and 4.7 show the histograms of the distributions of surface axial and tangential residual stresses on the surface of a total of twenty hot forged round bars for the U-batch. Figures 4.8 to 4.11 show the histograms of the distribution of axial residual stresses for AF, HT, FS and HTS batches which represent different stages of the forging process. There were twenty specimens in each group and two measurements taken from each bar. From these figures, the differences between the variation in the residual stress distributions for each batch of specimens can be seen.

8.2-2 Statistical Analysis

There are two most frequently used distributions to express the random variables, normal and Weibull distributions. In Chapter 2, the Weibull distribution was described for fatigue date analysis. In the following normal and Weibull distributions have been fitted to the experimental results for the surface axial residual stresses.

Normal distribution

Assuming that the residual stresses satisfy the normal distribution, then the probability density function is given by

$$f(\sigma_R) = \frac{1}{\sqrt{2\pi}S}\exp\left[-\frac{(\sigma_R - \bar{\sigma}_R)^2}{2S^2}\right] \tag{8.1}$$

where $\bar{\sigma}_R$ is the sample arithmetic mean and S is the sample standard deviation. The estimation of $\bar{\sigma}_R$ is,

$$\bar{\sigma}_R = \frac{1}{n}\sum_{i=1}^{n}\sigma_{R,i}, \tag{8.2}$$

and the unbiased estimation of S is

$$S = \sqrt{\frac{1}{n-1}\sum_{i=1}^{n}(\sigma_{R,i} - \bar{\sigma}_R)^2} \tag{8.3}$$

in which n is the number of the measurements and $\sigma_{R,i}$ is the residual stress of the *i*th measurement. Table 8.1 gives the results of the means $\bar{\sigma}_R$ and standard deviation S of the normal distributions for each batch of specimens and Figure 8.1 presents the distribution density $f(\sigma_R)$ for each group.

The probability of residual stress σ_R at any stress point σ_u in an interval $\Delta\sigma$ can be given by integrating Equation (8.1)

$$P\{\sigma_u - 0.5\Delta\sigma < \sigma_R < \sigma_u + 0.5\Delta\sigma\} = \int_{\sigma_u-0.5\Delta\sigma}^{\sigma_u+0.5\Delta\sigma}\frac{1}{\sqrt{2\pi}S}\exp\left[-\frac{(\sigma_R-\bar{\sigma}_R)^2}{2S^2}\right]d\sigma_R \tag{8.4}$$

which gives the histogram of the normal distribution. The histograms from the normal distributions are compared with the histograms of experimental results for axial residual stresses of U, FS and HTS batches, shown in Figure 8.3.

Weibull distribution

It may be assumed also that the distribution of the surface axial residual stresses satisfy the Weibull distribution and its cumulative distribution function is given by

$$P(\sigma_R) = 1 - \exp\left[-\left(\frac{\sigma_R - \sigma_0}{\sigma_a - \sigma_0}\right)^{\beta}\right] \qquad \sigma_R > \sigma_0 \tag{8.5}$$

or

$$P(\sigma_R) = 1 - \exp\left[-\left(\frac{\sigma_0 - \sigma_R}{\sigma_0 - \sigma_a}\right)^{\beta}\right] \qquad \sigma_R < \sigma_0 . \tag{8.6}$$

where σ_0 is a minimum (or maximum) stress, σ_a is characteristic stress and β is the Weibull slope. The form of Equation (8.5) can be written as,

$$\log\left[\log\left(\frac{1}{1-P}\right)\right] = \beta\log(\sigma_R - \sigma_0) - \beta\log(\sigma_a - \sigma_0) . \tag{8.7}$$

Employing the least squares method, β and $\beta\log(\sigma_a - \sigma_0)$ can be found for a given value of σ_0. Table 8.2 gives the fitted results for σ_0, σ_a and β for each batch and Figure 8.2 presents the distribution density curves of $f(\sigma_R)$ for the Weibull distribution given by Equation (2.70).

The probability of residual stress σ_R at any stress point σ_u in an interval $\Delta\sigma$ can be obtained from using Equation (8.6)

$$\begin{aligned} &P\{\sigma_u - 0.5\Delta\sigma < \sigma_R < \sigma_u + 0.5\Delta\sigma\} \\ &= \exp\left[-\left(\frac{\sigma_u + 0.5\Delta\sigma - \sigma_0}{\sigma_a - \sigma_0}\right)^{\beta}\right] - \exp\left[-\left(\frac{\sigma_u - 0.5\Delta\sigma - \sigma_0}{\sigma_a - \sigma_0}\right)^{\beta}\right] \end{aligned} \tag{8.8}$$

which gives the histogram of the Weibull distribution. Figure 8.3 shows the histograms for both the Normal and Weibull distributions and compares them with

the histograms from the measured X-ray results. It can be seen that there are only negligible difference between these two distributions.

8.2-3 Analysis of Redistribution of Residual Stress after Interaction with Mechanical Loading

Residual stresses appear to have a significant influence on fatigue life, especially for high cycle fatigue (Flavenot, 1989, Glinka, 1990). During fatigue cycling, the residual stresses in a specimen interact with the external loading leading to additional plastic deformations occurring especially when the residual stresses have been created by non-uniform plastic deformation. The residual stresses will be redistributed and become stabilised after a certain cycles. This interaction between the residual stresses and fatigue loading has been studied in Chapter 6. It is the redistributed and stabilised residual stresses that play a key factor in determining influence on fatigue life. The residual stress distribution from sample to sample will also change. Let us assume that the surface axial residual stress distribution density function is $f_{\sigma_R}(\sigma_R)$, where σ_R represents the surface axial residual stress σ_z^R, and the probability of residual stress is given by

$$P_{\sigma_R}(\sigma_R) = \int_{\sigma_{R,\min}}^{\sigma_R} f_{\sigma_R}(\sigma_R)\, d\sigma_R \tag{8.9}$$

Under cyclic fatigue loading with the half strain range $\left(\frac{\Delta\varepsilon_T}{2}\right)$ given by ε_c, the residual stress σ_R relaxed to $\sigma_{R'}$,

$$\left.\begin{aligned} \sigma_{R'} &= g(\sigma_R, \varepsilon_c) \\ or \quad \sigma_R &= g^{-1}(\sigma_{R'}, \varepsilon_c) \end{aligned}\right\} \tag{8.10}$$

where function $g(\,)$ may be determined by both experimental and finite element methods. Differentiating Equation (8.10),

$$d\sigma_R = \frac{\partial g^{-1}(\sigma_{R'}, \varepsilon_c)}{\partial \sigma_{R'}} d\sigma_{R'}. \tag{8.11}$$

Inserting Equation (8.11) into Equation (8.9), we get

$$P_{\sigma_{R'}}(\sigma_{R'}) = \int_{\sigma_{R',min}}^{\sigma_{R'}} f_{\sigma_R}(g^{-1}(\sigma_{R'},\varepsilon_c))\frac{\partial g^{-1}(\sigma_{R'},\varepsilon_c)}{\partial \sigma_{R'}} d\sigma_{R'} . \qquad (8.12)$$

Therefore the density function, $f_\sigma(\sigma_{R'})$, for relaxed residual stress $\sigma_{R'}$ is obtained

$$f_{\sigma_{R'}}(\sigma_{R'}) = f_{\sigma_R}(g^{-1}(\sigma_{R'},\varepsilon_c))\frac{\partial g^{-1}(\sigma_{R'},\varepsilon_c)}{\partial \sigma_{R'}} . \qquad (8.13)$$

The functional relationship between $\sigma_{R'}$ and σ_R, Equation (8.10), have been obtained for the HTS specimens in Chapter 6, and are described by Equation 6.63 and also shown in Figure 6.27. By inserting Equation 6.63 in Equation (8.13), the distribution density of the relaxed residual stress becomes,

$$f_{\sigma_{R'}}(\sigma_{R'}) = f_{\sigma_R}\left(\frac{\sigma_{R'}}{1 + A_1\varepsilon_c + A_2\varepsilon_c^2}\right)\frac{1}{1 + A_1\varepsilon_c + A_2\varepsilon_c^2} . \qquad (8.14)$$

By using Equation (8.14), for the normal distribution of the surface axial residual stresses from specimen to specimen, the curves of redistribution density are obtained and shown in Figure 8.4 for different cyclic strain ranges. From the Figure 8.4, it can be seen that the residual stress distribution centre moves towards zero and the standard deviation becomes smaller as cyclic strain range increases. When the strain range is over 3400 με, the residual stresses will be relieved as the FE predicted and the influence of the residual stresses on fatigue life could be eliminated.

8.3 Probabilistic Model to Predict Fatigue Life for Hot Forged Shot-blast Bar Specimens

8.3-1 Residual stress influence on fatigue life as an applied mean stress

As indicated in Chapter 6 by FE analysis and in Chapter 7 by fatigue tests, the residual stresses take effect in the HCF regime and are completely relieved in the LCF regime. Therefore the analysis of the residual stress effect on fatigue life is mainly carried in HCF regime. Figure 2.5 shows the Haigh diagram of constant fatigue life which includes the effect of mean stress. The line of constant fatigue life can be expressed as

$$\frac{\sigma_a}{\sigma_f} + \frac{\sigma_m}{\sigma_u} = 1 \tag{8.15}$$

where σ_m is applied mean stress, σ_u is ultimate stress of the material and σ_a is applied cyclic loading which within the elastic regime can be expressed as

$$\sigma_a = \frac{\Delta\sigma}{2} = E\frac{\Delta\varepsilon}{2}. \tag{8.16}$$

The fatigue strength σ_f can be determined by letting $\sigma_m = 0$ in Equation (8.15) and making use of Equations (8.16) and (7.3),

$$\sigma_f = E*(c + a*N_f^b). \tag{8.17}$$

By considering the residual stress after relaxation, $\sigma_{R'}$, as being equivalent to a mean stress and using the yield stress σ_y to replace the ultimate stress σ_u for En15R steel, the fatigue S-N curve can be obtained,

$$\frac{\Delta\varepsilon}{2} = (1 - \frac{\sigma_{R'}}{\sigma_y})(c + a*N_f^b) \tag{8.18}$$

which has included the residual stress influence on fatigue life. The relaxed residual stress, $\sigma_{R'}$, is related to the initial residual stress, σ_R, and half the fatigue cyclic strain range, $\Delta\varepsilon/2$, given by Equation (8.10).

By comparing Equation (8.18) with that proposed by Morrow (1965), given by Equation (2.58), Equation (8.18) can be expressed as

$$\sigma_a = (\sigma'_f - \alpha\sigma_{R'})(c' + a' * N_f^b) \tag{8.19}$$

where

$$\alpha = \frac{\sigma'_f}{\sigma_y} \tag{8.20}$$

and $(c' + a' * N_f^b)$ is equivalent to $(2N_f)^b$ in Equation (2.58). In Morrow's model α equals one, and therefore Equation (2.58) would overestimate the mean stress effect (assuming that the relaxed residual stress $\sigma_{R'}$ is equivalent to a mean stress) on fatigue life.

8.3-2 Other factors that influence fatigue life

Apart from the effects from residual stresses, there are also other factors which influence the fatigue life and give rise to scatter in fatigue data, such as surface roughness introduced by shot blasting which has been shown in Chapter 4, the irregular shape of the forged bars, eccentric axial loading, etc. It is very difficult to consider all these influencing factors as individual random variables. For convenience here we introduce a general random variable D into Equation (8.18). The distribution density function for D is assumed $f_D(D)$ and satisfies the condition

$$\int f_D(D)dD = 1 . \tag{8.21}$$

If the fatigue life N is statistically distributed, whether the residual stresses exist or not, the random D can be put into Equation (8.18) as

$$\frac{\Delta\varepsilon}{2} = (1 - \frac{\sigma_{R'}}{\sigma_y})[c + a*(N_f/D)^b]. \tag{8.22}$$

If there are no residual stresses in the sample, the distribution of fatigue lives N is similar to the distribution of random variable D which reflects the influencing factors on fatigue lives except the residual stresses.

Alternately, the local strain range can be treated as a statistical distribution because of surface roughness caused by shot blasting results in different strain ranges at different locations even within the same sample. In this way, the random D may be put into Equation (8.18) as

$$D\frac{\Delta\varepsilon}{2} = (1-\frac{\sigma_{R'}}{\sigma_y})(c + a * N_f^b) \tag{8.23}$$

For both approaches, the distribution of D has to be determined to better fit the experimental results.

8.3-3 Distribution of fatigue life *N*

In both Equations (8.22) and (8.23), it can be seen that the residual stress $\sigma_{R'}$ is a random variable and D is introduced as a random variable to consider other influencing factors. Therefore, the fatigue life N_f is also a random variable. If the joint probability density of the two random variables $\sigma_{R'}$ (which is related to σ_R and $\Delta\varepsilon/2$), and D is known, the distribution of fatigue lives N_f and its distribution density can be found.

Equations (8.22) or (8.23) may be expressed in a general form

$$G(\sigma_{R'}, \Delta\varepsilon, D, N_f) = 0 \tag{8.24}$$

or alternatively in terms of the initial residual stresses as

$$G(\sigma_R, \Delta\varepsilon, D) = N_f \tag{8.25}$$

The probability of failure is given by,

$$F(N_f) = P(N \le N_f) = \iint_{G(\sigma_R, \Delta\varepsilon, D) \le N_f} f_{\sigma_R, D}(\sigma_R, D)\, d\sigma_R\, dD \tag{8.26}$$

where $f_{\sigma_R, D}(\sigma_R, D)$ is a joint probability density of the random variables, initial residual stress σ_R and random variable D.

It may be assumed that the random variables σ_R, and D are independent, and the density function $f_{\sigma_R,D}(\sigma_R, D)$ can be expressed by two independent density functions

$$f_{\sigma_R,D}(\sigma_R, D) = f_{\sigma_R}(\sigma_R) f_D(D). \tag{8.27}$$

Then Equation (8.26) becomes

$$F_N(N_f) = P(N \le N_f) = \iint_{G(\sigma_R, \Delta\varepsilon, D) \le N_f} f_{\sigma_R}(\sigma_R) f_D(D) d\sigma_R dD. \tag{8.28}$$

The density function $f_N(N_f)$ may be found by differentiating $F_N(N_f)$ provided that the $F_N(N_f)$ is differentiable,

$$f_N(N_f) = F_N'(N_f) = \frac{dF_N(N_f)}{dN_f} = \lim_{\Delta N_f \to 0} \frac{P(N \le N_f + \Delta N_f) - P(N \le N_f)}{\Delta N_f}$$

$$= \lim_{\Delta N_f \to 0} \frac{1}{\Delta N_f} \iint_{N_f < G(\sigma_R, \Delta\varepsilon, D) \le N_f + \Delta N_f} f_{\sigma_R}(\sigma_R) f_D(D) d\sigma_R dD \tag{8.29}$$

which can be derived into a single curve integration (see Appendix 8A)

$$\begin{cases} f_N(N_f) = \int_L \dfrac{f_{\sigma_R}(\sigma_R) f_D(D)}{\sqrt{G_{\sigma_R}'^2 + G_D'^2}} dL \\ L = \left\{ G(\sigma_R, \Delta\varepsilon, D) = N_f \right\} \end{cases} \tag{8.30}$$

where

$$\begin{cases} G_{\sigma_R}' = \dfrac{\partial G(\sigma_R, \Delta\varepsilon, D)}{\partial \sigma_R} \\ G_D' = \dfrac{\partial G(\sigma_R, \Delta\varepsilon, D)}{\partial D} \end{cases} \tag{8.31}$$

A parametric equation for the curve $L = \left\{ G(\sigma_R, \Delta\varepsilon, D) = N_f \right.$ may be expressed as

$$\begin{cases} D = D \\ \sigma_R = \sigma_R(D) \end{cases}. \tag{8.32}$$

Using an analysis given in Appendix 8B, Equation (8.30) becomes

$$f_N(N_f) = \int \frac{f_{\sigma_R}(\sigma_R) f_D(D)}{\left|G'_{\sigma_R}\right|} dD . \tag{8.33}$$

This integration can be done using a numerical method.

8.4 Simulations to Determine Fatigue Lives

To determine the fatigue life distribution using Equation (8.33), the distribution density functions of random variables residual stress σ_R and D need to be found. The distribution density function $f_{\sigma_R}(\sigma_R)$ is given by Equation (8.1) for Normal distribution derived from Equation (8.5) or (8.6) for Weibull distribution. The distribution function density $f_D(D)$. has not been determined.

Three approaches will be presented to simulate the fatigue lives:

(i) Assuming that there is only an influence from the residual stresses

(ii) Assuming that there is a combined influence of D and σ_R, where D is assumed to be independent of cyclic strain range and determined from results in the LCF regime.

(iii) Assuming that the local strain range is a random variable D because of surface roughness, irregular shape of specimens and eccentric load and using a perfect fit to D to produce the correct distribution of fatigue lives N_f.

8.4-1 Residual stress effect only

By considering the influence of residual stress as a random variable without any other effects, the relationship between the relaxed residual stress $\sigma_{R'}$ and the fatigue life, shown in Equation (8.18), was used to predict the fatigue life distribution of bars from the HTS batch. The relaxed residual stress can be expressed as a function of fatigue life

$$\sigma_{R'} = \sigma_y\left(1-\frac{\Delta\varepsilon}{2(c+a*N_f^b)}\right) \tag{8.34}$$

where $\Delta\varepsilon/2$ is taken as 2200 με. Then using an analysis given in Appendix 8C the distribution density of fatigue life N is given by,

$$f_N(N_f) = f_{\sigma_R}\left(\sigma_y\left(1-\frac{\Delta\varepsilon}{2(c+a*N_f^b)}\right)\right)\left|\frac{\partial\sigma_{R'}}{\partial N_f}\right| \tag{8.35}$$

This computed distribution is shown in Figure 8.5 and compared with Weibull distributions of HT and HTS lives derived from fatigue test results. The probability of failure is shown in Figure 8.8, and again compared with the HT and HTS test results. It appears that by considering the influence of residual stress alone the model overestimates the fatigue life.

8.4-2 Residual stress influence plus a random distribution on fatigue life

Here it is assumed that the fatigue life is statistically distributed, so that from Equation (8.22) where D_N replaces D to denote that the random variable is dependent on life

$$\frac{\Delta\varepsilon}{2} = (1-\frac{\sigma_{R'}}{\sigma_y})[c+a*(N_f/D_N)^b]. \tag{8.36}$$

The relaxed residual stress is also independent of the random variable D_N.

If we assume that the residual stresses were all relaxed when the half fatigue strain range was 6000 με, then from Equation (8.36) with $\sigma_{R'}=0$, the relationship between the random variables N_f and D is

$$N_f = \left(\frac{6000-c}{a}\right)^{-1/b} D_N \tag{8.37}$$

The distribution of fatigue life $f_{N,6000}(N_f)$ has been obtained for the strain range being 6000 με which was derived from fatigue test results. Then the distribution density of D_N using the analysis given in Appendix 8C is given by

$$f_D(D_N) = f_{N,6000}\left[\left(\frac{6000-c}{a}\right)^{-1/b} D_N\right]\left(\frac{6000-c}{a}\right)^{-1/b}. \tag{8.38}$$

This is shown in Figure 8.6. The distribution density of fatigue life simulated is also shown in Figure 8.5, and the probability of failure is shown in Figure 8.8. This estimate is better than the analysis for residual stress alone, where the mean is closer to the experimental mean and there is a degree of overlap, but again the model overestimates the effects.

8.4-3 Residual stress influence plus a random distribution of strain range

Here it is assumed that the strain range is randomly distributed so that from Equation (8.23) where D_ε replaces D to denote that the random variable is dependent on strain range

$$D_\varepsilon \frac{\Delta\varepsilon}{2} = (1-\frac{\sigma_{R'}}{\sigma_y})(c + a * N_f^b). \tag{8.39}$$

The relaxed residual stress $\sigma_{R'}$ now depends on the local strain range $D_\varepsilon \frac{\Delta\varepsilon}{2}$. Then Equation (8.10) can be expressed as

$$\sigma_{R'} = g(\sigma_R, D_\varepsilon \frac{\Delta\varepsilon}{2}). \tag{8.40}$$

where $\Delta\varepsilon$ is fixed. The Equation (8.39) then becomes

$$D_\varepsilon \frac{\Delta\varepsilon}{2} = \left(1-\frac{g(\sigma_R, D_\varepsilon \frac{\Delta\varepsilon}{2})}{\sigma_y}\right)(c + a * N_f^b) \tag{8.41}$$

where the function g has been shown in Equation (6.63) of Chapter 6. The distribution density of random variable D_ε may be chosen as

$$\begin{cases} f_D(D_\varepsilon) = 0 & D_\varepsilon < D_0 \\ f_D(D_\varepsilon) = \alpha e^{-\alpha(D-D_0)} & D_\varepsilon \geq D_0 \end{cases} \tag{8.42}$$

where D_0 and α are constants to be chosen to get best fit of fatigue life distribution. For D_0 = 0.9785 and α = 0.0445, the distribution density of the random variable D_ε, $f_D(D_\varepsilon)$, is shown in Figure 8.7. The predicted distribution of fatigue life for strain range being 2200 με is shown in Figure 8.5. The probability of failure is also shown in Figure 8.8.

8.5 Discussion

From the comparison of the histograms of Normal and Weibull distributions of residual stress with experimental data, shown in Figure 8.3, it can be seen that the both distributions fitted quite well. So both distributions can be applied to further analysis without much difference. The choice of distribution for further application depends on its convenience in the analysis. For example, if FOSM (see section 2.7) is used for reliability analysis, the Normal distributions for all random variables are required (ASCE, 1982).

For analysis of the redistribution of residual stress, Equation (6.63), representing a functional relationship between relaxed residual stress and initial residual stress and cyclic strain range, was used. Because we are limited to the selected functional form for fitting the FE results, it was not accurate to use Equation (6.63) to express the relaxed residual stress when it totally relaxed to zero. However, the influence of using this expression on fatigue life analysis may be small because the residual stress would be small. To express the relaxed residual more precisely, more functional terms are required in Equation (6.63) and some conditions must be applied. For example, if the calculated relaxed residual stress was less than zero, the zero relaxed residual stress should be imposed.

The analysis of the influence of residual stress on fatigue life was confined to the HCF regime, since it for it had been shown the residual stress relaxed in LCF regime at high applied strain ranges and had no influence on fatigue life. A more accurate expression Equation (7.3) for the S-N curve in the HCF regime was used. The Haigh

diagram was the simplest expression for the mean stress effect on fatigue lives. Its straight line may not fit the experimental data well and was very conservative for ductile alloys for tensile mean stress (Suresh, 1992). On the other hand, for compressive mean stress it could result in exaggerating the mean stress effect. The Gerber's relation (2.48) is not correct for compressive mean stress effects because it treats compressive mean stress the same as a tensile mean stress to reduce fatigue life. To improve the model to consider the compressive mean stress effect, a relation similar to Haigh's and Gerber's can be used

$$\left(\frac{\sigma_a}{\sigma_f}\right)^2 + \frac{\sigma_m}{\sigma_u} = 1. \tag{8.43}$$

Using Equation (8.43) and same procedure in Section 8.3-1, Equation (8.18) is changed to

$$\frac{\Delta\varepsilon}{2} = \sqrt{(1 - \frac{\sigma_{R'}}{\sigma_y})}(c + a * N_f^b). \tag{8.44}$$

Comparing Equation (8.44) with Equation (8.18), it can be seen that the compressive residual stress effect is reduced. For further application in using Equations (8.43) and (8.44), more work, which includes the following, needs to be done,

(i) *Experimental data to support the diagram expressed by Equation (8.43)*

(ii) *Simulations of fatigue lives under different conditions using Equation (8.44)*

By using Equations (8.13) and (8.18), the changes in the S-N curve for different residual stress (or mean stress) can be determined, respectively. These curves can then be compared with the experiments.

In the simulation with residual stress alone, the predicted mean value of the fatigue lives was about 66% larger than the experiment result. The exaggeration of mean stress effect from the Haigh relation Equation (8.15) could be one of the main reasons for the overestimation.

The random variable D_N was introduced to represent other influencing factors on fatigue lives apart from residual stress. The difficulties in determining the distribution density of D_N were:

(i) Separating the residual stress influence from other influencing factors in fatigue test data.

(ii) The random variable D_N could be dependent on half cyclic strain range, $\Delta\varepsilon/2$.

In the second simulation, the second point was ignored and the random variable D_N was assumed to be independent of cyclic strain range. The distribution density of D_N was determined from experimental fatigue data at the half cyclic strain range 6000 με at which there was no residual stress effect. The resultant estimate was better than the simulation for residual stress alone, where the mean was closer to the experimental mean and there was a degree of overlap. But again the model overestimated the effects with the predicted mean value of the fatigue lives about 43% larger than the experimental result. Except for the exaggeration of mean stress effect from the Haigh relation, another reason would be that the D_N was treated as being independent of the cyclic strain range $\Delta\varepsilon$ and was not sufficient to represent the other influencing effects at half cyclic strain range 2200 με.

In the third simulation, a random variable D_ε was introduced based on the fact that the main influencing factors, except the residual stress, were surface roughness, irregular shape of the bars and eccentric axial loading which would make the surface strain range different from applied axial strain range. The distribution density of D_ε could not be determined from experimental fatigue data on half cyclic strain range 6000 με since D_ε would be strongly dependent on the applied axial cyclic strain range. A distribution density function was proposed with some parameters to be determined. For each different applied cyclic strain range the parameters can be determined from best fit of experimental fatigue data.

8.6 Conclusions

1) The sample to sample variation of residual stresses for each batch were analysed using Normal and Weibull distributions. The histograms from the both distributions were compared with those from X-ray measurement results. It was found that there was little difference between the two distributions.

2) The redistribution of residual stresses due to cyclic loading and its sample to sample variation was analysed. The redistribution density functions for different cyclic strain ranges were obtained for the HTS batch.

3) The Haigh diagram was used to incorporate the influence of residual stress into fatigue life. The relationship among fatigue cyclic strain range, relaxed residual stress and the fatigue life was derived.

4) A general form of determining fatigue life density was derived based on the relationship between the fatigue life N_f and other two random variables.

5) Fatigue life distribution density with residual stress alone was obtained for the HTS batch.

6) To include the other statistical factors, general random variable D_N and D_ε were introduced into equation of fatigue life S-N curve.

7) The distribution density of D_N was determined based on the assumption that the distribution of D_N was similar to the distribution of fatigue lives and independent of cyclic strain range. Then fatigue life distribution density was obtained using the distribution densities of D_N and residual stress.

8) The random variable D_ε was based on the fact that the local surface strain range was a statistical distribution because of surface roughness and other factors. Its distribution density was proposed and the parameters were chosen to best fit the experimental fatigue test data.

Chapter 9

CONCLUDING COMMENTS AND RECOMMENDATIONS FOR POTENTIAL FUTURE WORK

In this thesis, detailed stress distributions in hot forged specimens were obtained through the application and development of various measurement techniques such as X-ray and neutron diffraction, together with centre-hole drilling. An analytical interpolation approach was developed to determine cross-section residual stress distribution based on limited measurements. The interaction of residual stress with mechanical loading was studied using both experiments and FE analyses for which a multilinear kinematic hardening model was formulated and written in user subroutine UMAT for use in ABAQUS. Fatigue tests were carried out on bars from different batch representing different stage of forging process. The fatigue data was analysed using Weibull distribution. A probabilistic approach using the statistical variation of the relaxed residual stress and other influencing factors was developed to predict fatigue lives.

9.1 Concluding Comments

Residual stresses in hot forged components have been measured using various measurement techniques such as X-ray and neutron diffraction, together with centre-hole drilling. Some of results and comparisons are shown in Figures 4.67 to 4.70. X-ray results showed compressive residual stresses on the specimen surface as a result of shot blasting. Neutron diffraction measurements gave the residual stress profile in

one specimen. Centre-hole drilling also indicated compressive residual stresses at the surface. Although no one technique provided definitive results, the combination of methods provided increased confidence in the results.

Measurements on specimens from AF, HT, FS and HTS batches extracted from different stages of hot forging process revealed that the residual stresses in the hot forged components were mainly due to shot blasting. The heat treatment prior to shot-blasting contributed to higher compressive residual stresses in HTS batch. The statistical distribution of surface residual stress within the batches of the samples have been obtained using both Normal and Weibull distributions.

To obtain additional residual stress distributions cross the section of the samples, surface chemical etching was used to create new surfaces and X-ray measurements were made on the new surfaces. Since material removal redistributed the residual stresses, an analysis was carried out to determine the original residual stress distribution. From these results, together with the measurements of centre-hole, the layer of compressive residual stress was found to be about 0.16 mm from surface.

To consider that cases when there are only limited interior (neutron) and surface (X-ray) measurements of residual stresses, a new analytical interpolation method, using equilibrium, compatibility, and elastic-plastic constitutive equations, was developed to estimate the complete cross-section residual stress distribution. The solution of the residual stresses was expressed as integration equation which included two independent plastic strain components. As an example, the two plastic strains were assumed to have simple power law forms and included constants which could be determined from the limited residual stress measurements using a fitting technique. From the results shown in Figures 5.3 to 5.5, it can be seen that the interpolated residual stress distributions are the average distribution of the measured residual stress in the hot forged bars.

To consider cyclic stress-strain behaviour, a multilinear kinematic hardening material model has been formulated. This model includes initial hardening and non-linear hardening under different cyclic strain ranges. To study the interaction of residual stresses with mechanical loading, FE analyses, using this multilinear kinematic hardening material model, have been carried out. Initial state inputs included initial residual stresses, initial plastic strains and initial positions of yielding surfaces. It has been found that the residual stress relaxation was mainly due to plastic deformation. It can be seen from Figures 6.19 to 6.23 that even if the

low cycle strain range is regarded as being in the elastic range, surface compressive residual stress can still relax because the material had undergone prior plastic deformation. Most relaxation occurs in the first cycle, and relaxation stabilises after a certain number of cycles. Complete relaxation will take place for cyclic strain ranges beyond the elastic limit. In general, it was found that the numerical results were not in agreement with the X-ray measurements of surface residual stress relaxation. However, near surface centre-hole measurements did confirm that the residual stress had relaxed for large cyclic strain ranges.

Uniaxial fatigue tests have been carried out for specimens from the AF, HT, FS and HTS batches of En15R steel in LCF and HCF regimes. The fatigue data has been analysed using a Weibull distribution. It was found that in the high cycle, low strain fatigue (HCF) regime, the HTS batch had the longest lives, which means that the presence of surface compressive residual stresses is a major contributing factor in improving fatigue life. In the low cycle, high strain fatigue (LCF) regime, the HTS batch had the shortest fatigue lives which means that the residual stresses had been relaxed completely and therefore had little influence on fatigue life while other influencing factors dominated, such as surface roughness and heat treatment.

There was no doubt that in the HCF regime, the longest fatigue lives were obtained when surface compressive residual stresses were present. Therefore in the probabilistic model for fatigue life analysis the variation of the residual stress together with the established relationship between initial and relaxed residual stresses for different cyclic strain ranges was taken into account. To include the other statistical factors, general random variables D_N and D_ε were introduced in the probabilistic model. For D_N the assumption was that the distribution of fatigue lives was similar to the distribution of D_N without the presence of residual stress. The distribution of D_N was assumed to be the same for whole cyclic strain range but in general it should be cyclic strain range dependent. For D_ε it was assumed that the local strain range is a statistical distribution because of the effects of surface roughness and geometric irregularities. These effects could only be assessed empirically. The distribution of D_ε was determined by assuming that the predicted fatigue life distribution best fitted the experimental fatigue life distribution.

The main feature of these studies has been to show that a probabilistic fatigue life analysis can take account of the statistical nature of the residual stresses. The experimental results have shown that the surface compressive residual stresses played a dominant role. However, the analysis has shown that the benefits were

slightly diluted by other deleterious effects such as surface roughness and geometric irregularities. Without further study these effects could only be assessed empirically in the current research.

Although the probabilistic model has been applied to results from uniaxial fatigue tests, the methodology is equally applicable to multiaxial fatigue. The functional relationship between the relaxed residual stresses, initial residual stresses and multiaxial strains under applied loading can be determined using the same model described in Chapter 6, with additional information required about the local geometry in the FE simulations. The fatigue life tests can be carried out on notched bars, and the fatigue lives can be expressed in terms of multiaxial strain parameters. The multiaxial fatigue life distribution density is then determined using the Equation (8.33). The results shown in this research, for uniaxial conditions, have demonstrated that there is considerable promise in the methodology proposed.

Overall, this research has shown that residual stresses increased high cycle fatigue strength significantly but the influence became smaller as the cyclic strain range increased and there were no effect of residual stresses on low cycle fatigue because of residual stress relaxation behaviour. This is in general agreement with those in literature review in sections 2.4 and 2.5. The variation of residual stresses from specimen to specimen also contributed to the scatter of fatigue life test data. The probabilistic model considered not only the original residual stress distribution but also the residual stress relaxation associated with cyclic strain range. Together with introduction of other influencing factors, this model gave better understanding about residual stresses in fatigue life assessment. In summary, the new developments and advances in the work include:

i) *Statistical distributions of surface residual stresses were found for different stages of the manufacturing process.*

ii) *Better understanding of residual stresses in forged components and their influence on fatigue life was obtained.*

iii) *Measurement and interpretation techniques for the neutron diffraction and centre hole residual stress measurement methods were developed.*

iv) An analytical interpolation technique to determine through thickness residual stress distributions using limited information from measurements was developed.

v) A multi-linear kinematic material hardening model was incorporated into an FE analysis, and introduced initial residual stresses and plastic deformation.

vi) It was found that residual stresses relaxed for cyclic strain ranges well below endurance because of the presence of prior plastic deformation arising from generation of residual stresses.

vii) Fatigue life statistical distributions in low cyclic and high cyclic fatigue regimes were found as a function of the various stages of the manufacturing process.

viii) A probabilistic model to incorporate relaxed residual stress as a random variable into fatigue life analysis was developed.

ix) It was found that a joint distribution function taking account of residual stresses and other random variables was required in the HCF regime, although it was found that the statistical variation of the residual stresses was the dominant function.

9.2 Recommendations for Future Work

1) It has been shown that the results of X-ray measurements include micro-stresses and the influence of surface roughness. Further investigations are required to separate the micro-stresses from macro-stresses and analyse quantitatively the influence of surface roughness for the hot forged En15R steel.

2) To determine near surface residual stresses (short range) using neutron diffraction, all influencing factors contributed to the surface effect need to be classified and analysed and more experimental work on differently prepared samples is necessary.

3) For the centre hole measurements on shot blasted specimens, it has been shown that plastic deformation during hole drilling had a significant influence on interpretation of measured strains using elastic analysis. The proposed plastic modification was based on Gao's work (1992) in which the stress and strain components were uniform along thickness. However, in the shot blasted specimens, the residual stresses had a near surface gradient and all stress and strain components and deformation in normal direction are not uniform. Therefore further investigations are required to study the surface strain changes during hole drilling considering both plastic stress-strain response and the stress gradient. This can be done using FE analysis for axisymmetrical conditions. For different location z, along the normal direction, the initial condition input and stress-strain response are different. The user subroutine UMAT may be required to carry out the input.

4) Under cyclic loading, residual stresses were equivalent to mean stress and there should be a ratchetting effect. The residual stress relaxation behaviour under cyclic loading with including ratchetting needs further investigation.

5) Further studies of residual stress relaxation under multiaxial loading are required. The relationship between the relaxed residual stresses, the initial residual stresses and the applied multiaxial loading needs to be determined.

6) The fatigue tests carried out were only on two cyclic strain ranges, 2200 με and 6000 με. More fatigue tests on different cyclic strain ranges are required to understand fully the influence of residual stress and its relaxation on fatigue in total cyclic ranges from LCF to HCF.

7) For modelling the influence of residual stresses on fatigue lives using probabilistic approach, the role of the compressive mean stress on fatigue life requires further investigation. More experimental data is required to examine the relations proposed by Haigh and Gerber and Equation (8.43).

8) The probabilistic model was developed for uniaxial loading. It is clear that more work is required to extend the model to multiaxial conditions.

REFERENCES

Abtahi, A., Albrecht, P and Irwin, G. R., 1976 Nov., Fatigue behaviour of a periodically overloaded transverse stiffener detail, *J of the Structural Division, ASCE*, Vol. 102, No., ST11, pp. 2103-2119.

Albrecht, P., 1981, S-N fatigue reliability analysis of highway bridge, in *Probabilistic Fracture Mechanics and Fatigue Methods: application for structure design and maintenance, Bloom, J. M. and Ekvall, J. C., Eds, ASTM, STP 798*, pp. 184-204.

Albrecht, P. and Yamada, K., 1977 Nov., Simulation of service fatigue loads for short span highway bridges, *Symposium on Service Fatigue, Loads Monitoring Simulation and Analysis, STP 671, American Society for Testing and Materials,* Atlanta, Ga.

Allen, A. J., Hutchings, M. T., Windsor, C. G. and Andreani, C., 1985, Neutron diffraction methods for the study of residual stress fields, *Advances in Physis*, Vol. 34, No. 4, pp. 445-473.

Andrews, J. M. and Ellison, E. G., 1973, A test rig for cycling at high biaxial strains, *J. Strain Anal.*, Vol. 8, pp. 168-175.

Ang, A. H-S., 1975, A comprehensive basis for reliability analysis and design, *Reliability Approach in Structural Engineering*, Edited by Freudenthal, et al., pp. 29-47.

Appleton, E, Day, C. M., Notter, I. M. and Moon, J. R., 1987, Residual stress caused by the indentation phase of rotary forging, *J. Mech. Working Tech.*, **15,** pp 375-384.

ASCE Committee, 1982, "Fatigue reliability: Introduction; Quality assurance and maintainability; Variable amplitude Loading; Development of criteria for design", *J. of the Structural Division-ASCE*, Vol. 108, No. 1, pp. 1-88.

ASTM Standard E837-85, "Determining residual stresses by the hole drilling strain gage method",.

Bagdanoff, J. L. and Kozin, F., 1982, On non-stationary cumulative damage models, *J. of Applied Mech.*, Vol. 49, pp. 37-42.

Bagdanoff, J. L., 1978, A new cumulative damage model, part 1, *ASME J. of Applied Mech.*, Vol. 45, pp. 246-250.

Bagdanoff, J. L. and Krieger, W., 1978, A new cumulative damage model, part 2, *ASME J. of Applied Mech.*, Vol. 45, pp. 251-257.

Bagdanoff, J. L., 1978, A new cumulative damage model, part 3, *ASME J. of Applied Mech.*, Vol. 45, pp. 733-739.

Bargmann, H., Rüstenberg, I. and Devlukia, J., 1994, Reliability of metal components in fatigue: A simple algorithm for the exact solution, *Fatigue Fracture Engineering Material Structure.* Vol. 17, No. 12, pp. 1445-1457.

Bashun, T. V., Vasileva, L. A., Urban, T. P. and Shterenzon, A. M., 1986, Distribution of residual stresses in alloy AK4-1 drop forgings, *Metal Science and Heat treatment,* 30, 1-2, pp 117-119.

Basquin, O. H., 1910, The exponential law of endurance tests. *Proceedings of the American Society for Testing and Materials*, Vol. 10, pp. 625-630.

Bathgate, R. G., 1968, Measurement of non-uniform bi-axial residual stresses by the hole drilling method, *Strain,* Vol. 4, No. 1-2, pp. 20-29.

Beaney, E. M., 1978, Accurate measuring of residual stresses on any steel using the centre-hole method, *Strain,* Vol. 12, No. 3, pp. 99-106.

Beaney, E. M. and Procter, E., 1974, A critical evaluation of the centre hole-drilling technology for the measurement of residual stresses, *Strain,* Vol. 1, pp. 6-14.

Beck, G. and Ericsson, T., 1987, Prediction of residual stresses due to heat treatment, *Residual Stresses in Science and Technology,* edited by E. Macherauch & V. Hauk, Vol. 1, pp. 27-40.

Beck, G. and Simon, A., 1987, Prediction of residual stresses, *Advances in surface treatments, edited by Niku-Lari A , Pergamon Press.* Vol 4., pp. 303-326.

Beghini, M, Bertini, L. and **Raffaelli, P.,** 1995, An account of plasticity in the hole-drilling method of residual stress measurement, *J. of Strain Analysis,* Vol. 30, No. 3, pp. 227-233.

Beghini, M, Bertini, L. and **Raffaelli, P.,** 1994, Numerical analysis of plasticity effects in the hole-drilling residual stress measurement, *J. of Testing and Evaluation,* Vol. 22, No. 6, pp. 522-529.

Berge, S. and Eide, O. I., 1982, Residual stresses and stress interaction in fatigue testing of welded joints, , *Residual Stress Effects in Fatigue, ASTM STP 776,* pp. 115-131.

Bijak-Zochowski, M., 1978, A semi-destructive method of measuring residual stresses, *VDI-Berichte,* Vol 313, pp. 469-476

Boggs, B. D. and Byrne, J. G., 1973, Fatigue stability of residual stress in shot peened alloys, *Metal. Trans,* Vol 4, No. 9, pp. 2153-2157

Bourke, M. A. M., Smith, D. J., Webster, G. A., and Webster, P. J., 1990, "Neutron diffraction measurements of residual stresses in plastically deformed cracked beams", *Proceedings of the 9th International Conference on Experimental Mechanics*, pp. 1196-1206.

Breitung, K., 1982, An asymptotic formula for the failure probability, DIALOG 6-28, Euromech 155, Danmarks Ingeniorakadem, Lyngby, Denmark.

Brown, M. W. and **Miller, K. J.,** 1973, A theory for fatigue failure under multiaxial stress-strain conditions, *Proc. Inst. Mech. Engrs.*, **187**, pp 745-755.

Burnett, J. A., 1981, Prediction of stresses generated during the heat treating of case carburized parts, *Residual Stress for Designers and Metallurgists, ASM,* edited by Larry J. Vande Walle, pp 51-69.

Buttle, D. J., Hutchings, M. T., 1992, Residual stress measurement at NNDTC, *British Journal of NDT*, Vol. 34, No. 4, pp 175-181.

Bynum, J. E., 1981, Modification to the hole-drilling technique of measuring residual stresses for improved accuracy and reproducibility, *Experimental Mechanics, J. of SESA,* Vol 21, No 1, pp. 21-33.

Chen. X. and Lind, N. C., 1983, Fast probability integration by three parameter normal tail approximation, *Structure Safty*, Vol. 1, pp. 269-276.y

Collins. J. A., 1981, Failure of materials in mechanical design, John Wiley & Sons, New York, pp. 243-268.

Cornell. C. A., 1975, Some comments on second-moment codes and on Bayesian methods, *Reliability Approach in Structural Engineering*, Edited by Freudenthal, et al., pp. 17-27.

Crossland, B., 1956, Effect of large hydrostatic pressures on the torsional fatigue strength of an alloy steel, *Pros. of Int. Conf. on the Fatigue of Metals,* Inst. of Mech. Engng., London, pp. 138-149

Cullity, B. D., 1978, *Elements of X-ray diffraction*, Addison-Wesley.

Dan Van, K.Y., 1973, Sur la résistance à la fatigue des métaux, *Sci. Techniques Armement,* 47, pp. 641-722.

Desvignes, M., Gentil, B and Castex, L., 1987, Fatigue progressing of shot peened steel, *Residual Stresses in Science and Technology,* edited by E. Macherauch & V. Hauk, Vol. 1, pp. 441-448.

Devlukia, J., 1993, Durability Design and enhanced material performance for metallic components, *A project proposal*, Gaydon test centre, Rover Group.

Devlukia, J., 1993, Compendium of test data on En15R (150M36)-Meadium carbon forged steel En15R- suspension arm, Durability Design and enhanced material performance for metallic components, *Draft report of ENDDURE*, Gaydon test centre, Rover Group.

Devlukia, J. and Parsons, P., 1993, Surface roughness effects on LCF behaviour of 3 steels, Presented at the EIS Workshop on "*Surfaces and Fatigue*" on 3rd November 1993 held at Peugeot Talbot Social Club, Coventry.

Dieter, G. E., 1988, *Mechanical metallurgy,* McGraw-Hill, 2nd edition, Ch. 12, pp 403-440.

Ditlevsen, O., 1981 Dec., Principle of normal tail approximation, *J. of Engineering Mechanics Division, ASCE,* Vol. 107, pp 1191-1208.

Ellyin, F. and Golos, K., 1988, Multiaxial fatigue damage criterion, *J. Engng. Mat. & Tech.*, 110, pp 63-68.

Ellyin, F., 1974, A criterion for fatigue under multiaxial state of stress, *Mech. Res. Communications,* 1, pp. 219-224.

Ellyin, F., 1988, Recent developments in predicting multiaxial fatigue failure, *RES Mechanica,* Vol 25, No 1, pp. 1-23.

Engesvik, K. M. and Moan, T., 1983, Probabilistic analysis of the uncertainty in the fatigue capacity of welded joints, Engng Fracture Mech., Vol. 18, No. 4, pp. 743-762.

Fiessler, B., Neumann, H. J. and Rackwitz, 1979, Quadratic limit states in structural reliability, *J. of the Engineering Mechanics Division*, ASCE, Vol. 105, Aug. 1979, pp. 661-676.

Findley, W. N., 1959, A theory of the effect of mean stress on fatigue of metals under combined torsion and axial load or bending, *J. Engng. Ind.*, Vol. 81, pp. 301-306.

Findley, W. N., 1957, Fatigue of metals under combinations of stress, *Trans. ASME,* 79, pp 1337-1348.

Flaman, M. T. & Manning, B. H., 1985, Determination of residual stress variation with depth by the hole-drilling method, *Experimental Mechanics*, Vol. 29, No. 9, pp. 205-207.

Flaman, M. T., 1982, Brief investigation of drilling induced stresses in the centre-hole method of residual stress measurement, *Experimental Mechanics*, Vol. 22, No. 1, pp. 26-30.

Flavenot, J. F. & Skalli, N., 1989, A comparison of multiaxial fatigue criteria, incorporating residual stress effects, EGF3, eds, Brown, M.W. and Miller, K.J., MEP Publ, pp. 437-457.

Freudenthal, A. M. and Gumbel, E. J., 1956, *Advances in Applied Mechanics, AAMCA,* Vol 4, pp. 117-158.

Freudenthal, A. M. and Shinozuka, M., 1961, Structure safety under conditions of ultimate load failure and fatigue, *Wadd Technical Report 61-177*, Aeronautical System Division.

Freudenthal, A. M., 1952, in *Statistical Aspects of Fatigue, ASTM STP 121*, pp. 3.

Frost, N. E., Marsh, K. J. and Pook, L. P., 1974, *Metal fatigue*, Clarendon Press, Oxford, pp. 322.

Garud, Y. S., 1981, A new approach to the evaluation of fatigue under multiaxial loading, *J. Engng. Mater. & Tech. Trans. ASME,* **103,** pp 119-125.

Garud, Y. S., 1981, Multiaxial fatigue: A survey of the state of art, *J. of Testing and Evaluation,* Vol 9, No 3, pp. 165-178.

Gassner, E. and Schütz, W., 1961, in *Full-scale fatigue testing of aircraft structures,* F. J. Plantema and J., Schijive, Eds., Pergamon Press, London, pp. 14-40.

Gao, X. L., 1992, An exact elasto-plastic solution for an open-ended thick-walled cylinder of a strain-hardening material, *Int. J. Pres. Ves. & Piping,* Vol. 52, pp. 129-144.

Gertsbakh, I and Kordonskij, K. B., 1969, in *Engineering Science library,* Spring-Verlag, Berlin.

Glinka, G., Residual stresses in fatigue, 1990, *113th Symp. of the Technical Research Centre of Finland: Fatigue Design 90,* Vol 113, No. 14, pp. 249-290.

Goto, M., Nisitani, H. and Miyagawa, H., 1993, Physical basis of scatter in fatigue life of carbon steels, *Fatigue 93*, Bailon, J. P. and Dickson, J. I., Eds., Vol 3, pp. 1459-1464.

Goto, M., 1992, Scatter characteristics of fatigue life and the behaviour of small cracks, *Fatigue & Fracture of Engineering Materials & Structures,* Vol 15, No. 10, pp. 953-963.

Gough, H. J., Pollard, H. V. and Clenshaw, W. J., 1951, Some experiments on the resistance of metals to fatigue under combined stress, *Memo 2522,* Aeronautial Research Council, His Majesty's Stationary Office, London.

Gould, R. W. and Pittella C. F., 1973, in *Advances in X-Ray Analysis,* Vol. 16, pp. 354-366.

Harris, W. J., 1976, The significance of fatigue, *Engineering Design Guides 14,* Oxford University Press.

Hashin, Z., 1983, Statistical cumulative damage theory for fatigue life prediction, *J. of Applied Mechanics,* Vol. 50, pp. 571-579.

Hasofer, A. M. and Lind, N. C., 1974, Exact and invariant second-moment code format, *J. of the Engineering Mechanics Division,* ASCE, Vol. 100, No. EM1, pp. 111-121.

Hauk, V., 1983, Advances in X-ray analysis, Vol 27, pp 27.

Hauk, V., Höller, P and Macherauch, E., 1987, Measuring techniques of residual stresses - present situation and future aims, *Residual Stresses in Science and Technology,* edited by E. Macherauch & V. Hauk, Vol. 1, pp. 231-242.

Hayashi, K. and Doi, S., 1971, *in X-Ray Study on Strength and Deformation of Metals,* Soc. of Metals. Sci., Japan, pp. 49-57.

Heywood, R. B., Chapman and Hall Ltd., London, 1962.

Hilley, M. E., 1971, Residual stress measurement by X-ray diffraction, SAE J784a, Society of Automotive Engineers, Warrendale, PA, pp 21-24

Itagaki, H. and Shinozuka, M., 1972, Application of the Monte Carlo Technique to fatigue-failure analysis under random loading, in *Probabilistic Aspects of Fatigue,* Heller, R. A. Eds., *STP 511,* pp. 168-184.

Jacoby, G. H. and Nowack, H., 1972, Comparison of scatter under program and random loading and influence factors, in *Probabilistic Aspects of Fatigue,* Heller, R. A. Eds., *STP 511,* pp. 61-74.

James, M. R., 1987, Relaxation of residual stresses—an overview, *Advances in surface treatments, edited by Niku-Lari A , Pergamon Press.* Vol 4., pp. 349-365.

James, M. R. and Morris, W. L., 1983, Fatigue induced changes in surface residual stress, *Scripta Metallurgica,* Vol. 17, pp. 1101-1104.

James, M. R. and Morris, W. L., 1981, The relaxation of machining stresses in aluminium alloys during fatigue, *Residual stress for designers and Metallurgists,* ASM, pp. 169-188

James, M. R., 1982, The relaxation of residual stresses during fatigue, *Residual stress and stress relaxation, Proceedings of 28th Army Materials Research conference,* E. Kula and V. Weiss Ed., pp. 297-314.

Jhansale, H. R. and Topper, T. H., 1973, Engineering analysis of the inelastic stress response of a structure metal under variable cyclic strains, in *Cyclic Stress-Strain Behavior - Analysis, Experimentation and Failure Prediction,* ASTM STP519, American Society for Testing and Materials, pp. 246-270.

John Stokes and Sons Ltd, 1992, Private communication to the University of Bristol, January.

Johnson, L. G., 1964, *The Statistical Treatment Of Fatigue Experiments,* Elsevier Publishing Company.

Kandarpa, S., Spencer, B. F. JR. and Kirkner, D. J., 1996, Reliability analysis of structural components utilizing the strain-life method, *Engineering Fracture Mechanics,* Vol 53, No. 5, pp. 761-774.

Kandil, F. A. and Dyson, B. F., 1993, The influence of load misalignment during uniaxial low-cycle fatigue testing .1. applications, *Fatigue & Fracture of Engineering Materials & Structures,* Vol 16, No. 5, pp. 509-527.

Kandil, F. A. and Dyson, B. F., 1993, The influence of load misalignment during uniaxial low-cycle fatigue testing .2. applications, *Fatigue & Fracture of Engineering Materials & Structures,* Vol 16, No. 5, pp. 529-537.

Kang, Z. Q., Li, J. B. and Wang, Z. G., May 1994, Stress correction for removal of material in X-ray stress determination, *J. of Testing and Evaluation, JTEVA,* Vol. 22, No. 3, pp. 217-221.

Kelsey, R. A., 1956, Measuring non-uniform residual stresses by the hole drilling method, *Proceedings SESA,* Vol. 14, No. 1, pp. 181-194.

Kim, J. J. and Nam, S. W., 1990, The sensitivity of surface crack initiation to surface roughness in low-cycle fatigue at high temperature, Materials Science and Engineering, Vol A130, pp. L7-L10.

Kiocecioglu, D. Stultz, J. D. and Nofl, C. F. Jr., 1975, Fatigue reliability with notch effects for AISI 4130 and 1038 steels, *Trans. J. Engng Ind.,* 97, pp 359-370.

Krempl, K., 1974, The influence of state of stress on low cycle-fatigue of structural materials: A literature survey and interpretative report, *STP 549, ASME.*

Kujawski, D. and Ellyin, F., 1988, On the concept of cumulative fatigue damage, *Int. J. Fracture,* Vol 37, No 4, pp. 263-278.

Kuznetsov, E. N., 1981, Residual stress in long weldments, *Residual Stress for Designers and Metallurgists, ASM,* edited by Larry J. Vande Walle, pp 997-1004.

Lange, B. F., 1962 Sept., Design of pressure vessels for low cyclic fatigue, *J. of Basic Engineering, American Society of Mechanical Engineering,* Vol. 84, No. 3, pp. 389-402.

Lawrence, F. V., Jr., Buck, J. D. and Yung, J. Y., 1982, Influence of residual stress on the predicted fatigue life of weldments, *Residual Stress Effects in Fatigue, ASTM STP 776,* pp. 33-43.

Leese, G. E., Halford, G. R., Kaisand, L. R. and Leis, B. N., 1988, *Engineering significance of recent multiaxial research, ASTM STP 942,* pp 861-873.

Lefebvre, D. F., 1985, Hydrostatic pressure effect on the life prediction in biaxial low-cycle fatigue, 2nd Int. Conf. on *Biaxial/Multiaxial fatigue* , Sheffield, UK.

Lefebvre, D., Neale, K. W. & Ellyin, F., 1981, A criterion for fatigue under biaxial states of stress, *J. Engng. Mater. & Tech. Trans. ASME,* **103**, pp 1-6.

Leffers, T., Loorentzen, T. Jensen, D. J. and Kjems, J., 1987, Measurement of internal stresses by neutron diffraction using a position-sensitive detector, *Residual Stresses in Science and Technology,* edited by E. Macherauch & V. Hauk, Vol. 1, pp. 143-150.

Libertiny, G. Z., 1967, Short-life fatigue under combined stress, *J. Strain Anal.,* **2**, pp 91-95.

Lin, Y. C., Chou, C. P., 1995, Error induced by local yielding around hole drilling method for measuring residual stress of materials, *Materials Science and Technology,* Vol. 11, pp 600-604.

Lohr, R. D., and Ellison, E. G., 1980, A simple theory for low cycle multiaxial fatigue, *Fatigue of Engng. Mat. & Struct.,* **3**, pp 1-17.

Lorentzen, T., 1994, Private discussion, Material Department, Risø, National Laboratory, Denmark.

Lorentzen, T. and Ibsø, J. B., 1995, Neutron-diffraction measurements of residual strains in offshore, *Materials Science & Engineering, A-structural materials properties*, Vol. 197, pp 209-214.

Lorenzo, F. and Laird, C., 1984, A new approach to predicting fatigue life behavior under the action of mean stresses, Neutron-diffraction measurements of

residual strains in offshore, *Materials Science and Engineering,* Vol. 62, pp. 205-210.

Lu, J., Flavenot, J. F., and Turbat, A, 1988, Prediction of residual stress relaxation during fatigue, *Mech. Relaxation of Residual stresses, ASTM STP 993,* pp 75-90.

Macherauch, E., 1987, Introduction to Residual Stress, *Advances in surface treatments, edited by Niku-Lari A , Pergamon Press.* Vol 4., pp. 1-36.

Maiya, P. S. and Busch, D. E., 1985, Effect of surface roughness on low-cycle fatigue behavior of type 304 stainless steel, *Metallographical Transaction,* Vol 6a. No 12, pp. 1761-1766.

Makinde, A and Neale, K. W., 1989, A general criterion for low-cycle multiaxial fatigue failure, *J. Engng. Mat. & Tech. Trans. ASME,* **111**, pp. 263-269.

Manson, S. S., 1962, *J. Basic Engng., Trans. ASME,* Vol. 84, pp. 537-541.

Manson, S. S., 1965, Fatigue: A complex subject—some simple approximations, *Experimental Mechanics,* Vol. 5, No. 7.

Marion, R. H. and Cohen, J. B., 1975, *Adv. X-ray Anal.,* Vol. 18, p 466.

Matake, T. and Imai, Y., 1980, Fatigue criterion for notched or unnotched specimens under combined stress state, *Z. AIRYO.*, **29**, pp. 993-997.

Mathar, J.,1934, Determination of initial stresses by measuring deformation around drilled hole, Trans ASME, Vol 56, No 4, 249-254.

McDiarmid, D. L., 1974, A new analysis of fatigue under combined bending and twisting, *Aero. J., Roy Aero. Soc.,* London, 78, pp. 325-329.

Measurement Group, Inc., 1986, Measurement of residual stress by hole-drilling strain-gauge method, Tech Note TN-503-3, Raleigh, NC.

Meguid, S. A. and Chee, E. B., 1983, The effect of peening and re-peening upon partially fatigued components, *J. of Mechanical Working Technology,* Vol. 8, No. 2, pp. 129-146.

Miner, M. A., 1945, Cumulative damage in fatigue, 1945, *J. of Applied Mechanics, Trans ASME,* Vol. 67, pp. A159.

Modlen, G. F., Webster, P. J., Wang, X. and Mills, G., 1992, An investigation of residual stresses in cold-extruded and in cold-drawn rods using neutron diffraction, in *Sheet Metal,* Shirvani, B. and Baggs, H., Eds., IOP Publishing Ltd, pp. 171-179.

Moore, M. G. and Evans, W. P., 1958, Mathematical correction for stress in removed layers in X-ray diffraction residual stress analysis, *SAE Transaction*, Vol. 66, pp. 340-345.

Mordfin, L., 19680, Measurement of residual stresses: problems and opportunities, *Residual Stress for Designers and Metallurgists, ASM,* edited by Larry J. Vande Walle, pp 189-210.

Morrow, J. D., 1965, in *Internal Friction, Damping and Cyclic Plasticity, ASTM Spec. Tech. Publ. 378,* pp. 45.

Morrow, J. D., 1968, in *Fatigue Design Handbook, Advances in Engineering, Society of Automotive Engineers, Warrendale, PA,* Vol. 4, pp. 21-29.

Morrow, J. D., 1986, The effect of selected subcycle sequences in fatigue loading histories. in *Random Fatigue Life Predictions, ASME Publication PVP*, Vol. 72, pp. 43-60.

Mroz, Z., 1967, On the Description of Anisotropic Work-Hardening, *J. Mech. Phys. Solids*, Vol 15, p 163.

Myllymaki, R., Alis, G. P., 1987, Fatigue testing and residual stress measurements of grit-blasted aluminium alloys, , *Residual Stress in Design, Process and Materials Selection*, edited by W. B. Young, pp 137-150.

Nash, C. D., 1983, A reliability based fatigue damage theory for safe design, *J. of Energy Resources Technology-Transactions of the ASME,* Vol 105, No. 2, pp. 212-216.

Nawwer, A. M. and Shewchuk, J., 1983, The effect of preload on fatigue-strength of residually stressed specimens, *Experimental Mechanics, J. of SESA,,* Vol 23, No. 4, pp. 409-413.

Nawwer, A. M., McLachlan, K. and Shewchuk, J., 1976, A modified hole-drilling Technique for determining residual stresses in thin plates, *Experimental Mechanics, J. of SESA,,* Vol 16, No 6, pp. 226-232.

Nickola, W. E., 1984, Post-yield effects on centre hole residual stress measurements, *Proc. of 5th Int. Con. on Experimental Mechanics,* Brookfield Centre, Connecticut: Society for Experiment Mechanics, pp. 126-136.

Nickola, W. E., 1986, Practical subsurface residual stress evaluation by the hole-drilling method., *Proceedings of 1986 SEM Spring Conference on Experimental Mechanics,* Brookfield Centre, Connecticut: Society for Experimental Mechanics.

Niku-Lari, A., Lu, J. and Flavenot, 1987, Measurement of residual stress distribution by the incremental hole-drilling method, *in Advances in Surface Treatment*, Niku-Lari, A., Eds., Vol 4, pp. 199-219.

Niku-Lari, A., Lu, J. and Flavenot, 1985, Measurement of residual stress distribution by the incremental hole-drilling method, *Experimental Mechanics*, Vol. 25, No. 6, pp. 175-185.

Niku-Lari, A., 1982, Shot peening, *Proceedings of 1st International Conference on Shot Peening, Paris*, Pergamon Press, Oxford, New York, p. 1.

Noyan, I. C, 1983, Met. Trans. A. 14A, pp. 1907.

Noyan, I. C. and Cohen, J. B., 1987, *Residual stress measurement by diffraction and interpretation*, Springer-Verlag.

Parida, N., 1991, Reliability and life estimation from component fatigue failures below the Go-No-Go fatigue life limit, *J. of Testing and Evaluation,*, Vol. 19, No. 6, pp. 450-453.

Pascoe, K. J. and DeVilliers, J. W. R., 1967, Low cycle fatigue of steels under biaxial straining, *J. Strain Anal.*, Vol. 2, pp. 117-126.

Pattinton, E. J. and Dugdale, D. S., 1982, *Metallurgia,* Vol. 66, pp. 259-263.

Prask, H. J. and Choi, C. S., 1987, Residual stress measurements in armament-system components by means of neutron diffraction, *Residual Stress in Design, Process and Materials Selection*, edited by W. B. Young, pp 21-26.

Prevey, P. S., 1986, X-ray diffraction residual stress technique, Materials Characterization, Metal Handbook, 9th edition, Vol. 10, pp. 380-392

Procter, E., Beaney, M., 1982, Recent developments in centre-hole technique for residual stress measurements, *Experimental Techniques,* Vol 6, No 6, pp. 10-15.

Rackwitz, R. and Fiessler, B., 1978, Structure reliability under combined random load sequences, J. of Computers and Structures, Vol. 9, pp. 489-494.y

Ransom, J. T., 1954, *Discussion in ASME Proc.*, Vol. 54, pp 847-848.

Redner, S. and Perry, C. C., 1982, Factors affecting the accuracy of residual stress measurements using the blind hole drilling method, *Proceedings of the 7th International Conference on Experimental Stress Analysis, mechanics,* Haifa, Isreal: Isreal Institute of Technology.

Rendler, N. J. and Vigness, I, 1966, Hole-drilling strain-gauge method of measuring residual stresses, *Experimental mechanics,* Vol 6, No 12, pp. 577-586.

Rudkins, N. T., Modlen, G. F. and Webster, P. J.,1994, Residual-stresses in cold-extrusion and cold drawing-a finite element and neutron-diffraction study, *J. of Materials processing technology*, Vol 45, pp 287-292.

Rychlik, I., 1994, Characterization of random fatigue loads, *Stochastic Approach to Fatigue: Experiments, Modelling and Reliability Estimation,* Spinger - Verlag, Wien - New York, pp 1-33.

Ryu, J. H. and Nam, S. W., 1989, Effect of surface roughness on low-cycle fatigue life of Cr-Mo-V steel at 500°C, *Int. J. of Fatigue,* Vol 11, No 6, pp. 433-436.

Sandor, B. I., 1972, *Fundamentals of Cyclic Stress and Strain*, Madison: University of Wisconsin Press.

Sarkani, S. and Lutes, L. D., 1988, Residual stress effects in fatigue of welded joints, *J. Struc. Engng., ASME,* Vol. 114, pp. 462-474

Sarkani, S. and Lutes, L. D., 1988, Residual stress effects in fatigue of welded joints, *J. Struc. Engng., ASME,* Vol. 114, pp. 462-474

Saunders, S., 1972, On the probabilistic determination of scatter factors using miner's rule in fatigue life studies, in *Probabilistic Aspects of Fatigue, STP 511,* Heller, R. A. Eds.

Scarmangas A. A., Porter, R. F. D. and **Leggatt, R H.,** 1982, On the correction of residual stress measurements obtained using the centre-hole method, *Strain, J. of BSSM,* Vol 18, No 3, pp. 88-97.

Schajer, G. S., 1981, Application of finite element calculations to residual stress measurements, *J. of Engineering Materials and Technology, Trans of ASME,* Vol 103, pp. 157-163.

Schajer, G. S., 1988, Measurement of non-uniform residual stresses using the hole-drilling method: Part I-stress calculation procedures, *J. of Engineering Materials and Technology, Trans of ASME,* Vol. 110, pp. 338-343.

Schajer, G. S., 1988, Measurement of non-uniform residual stresses using the hole-drilling method: Part II-Practical application of integral method, *J. of Engineering Materials and Technology, Trans of ASME,* Vol. 110, pp. 344-349.

Schijve, J., 1961, in *Full-scale fatigue testing of aircraft structures,* F. J. Plantema and J., Schijive, Eds., Pergamon Press, London, pp. 41-59.

Scholtes, B., 1987, Residual stresses introduced by machining, *Advances in Surface Treatments,* edited by A. Niku-Lari, Vol. 4, pp. 59-71.

Shatil, G., 1990, High strain multiaxial fatigue and life prediction of service component, Ph.D. Thesis, Dept. of Mech. Engng., University of Bristol.

Sheikh, A. K., Younas, M. and Ahmad, M., 1986, A comparative study of reliability models in fatigue life prediction, *Res Mechanica,* Vol. 19, No. 3, pp. 189-218.

Sines, G. & Ohgi, G., 1981, Fatigue criteria under combined stress or strains, *J. Engng. Mater. & Tech. Trans. ASME,* **103**, pp 82-90.

Smith, D. J., Leggatt, R. H., Webster, G. A., Macgillivray, H. J., Webster, P. J. and Mills, G., 1988, Neutron diffraction measurements of residual stress and plastic deformation in an aluminium alloy weld, *Journal of Strain Analysis,* **23,** 4, pp 201-211.

Smith, D. J., Bourke, M. A. M., Hodgson, A. P., Webster, G. A. and Webster, P. J., 1992, Interpretation of residual stress distributions in previously loaded cracked beams, *Journal of Strain Analysis,* Vol. 27, No. 2, pp 77-83.

Smith, D. J. and Webster, G. A. 1996, The measurement of prior plastic deformation in metallic alloys using the neutron diffraction technique, *To be submitted to Journal of Strain Analysis.*

Smith, K. N., Watson, P. and Topper, T. H., 1970, A stress-strain function for the fatigue of metals, *Journal of Materials,* Vol. 5, No. 4, pp 767-778.

Sobczyk, K., 1993, Stochastic modelling of fatigue: methodical background, *Stochastic Approach to Fatigue: Experiments, Modelling and Reliability Estimation.* Spinger - Verlag, Wien - New York, pp 1-33.

Socie, D. F., Waill, L. A., 1974, Biaxial fatigue of inconel 718 including mean stress effects, *Multiaxial Fatigue, STP 853, ASME,* pp 463-478.

Soete,W and Vancrombrugge, R., 1950, An industrial method for the determination of residual stresses, *Proceedings SESA,* Vol. 8, No. 1, pp. 17-28.

Stacey, A., Macgillivary, H. J., Webster, G. A., Webster, P. J. and Ziebeck, K. R. A., 1985, Measurement of residual stresses by neutron diffraction, *J. of Strain Analysis,* Vol 20, No 2, pp. 93-100.

Stanfield, G.,1935, *Proc. Inst. Mech. Engrs.,* **131**, pp 59.

Suresh, S., 1992, *Fatigue of Materials,* Cambridge University Press, Ch. 4, p. 128, p. 132 and p. 139.

Swanson, S. R., 1968, Evaluating component fatigue performance under programmed random and programmed constant amplitude loading, *Mat. Res. Stand.*, Vol 8, No 10.

Tavernelli, J. F. & Coffin, L. F. Jr., 1962, Experimental support for generalized equation predicting low cycle fatigue, J. Basic Engng., *Trans. ASME*, 84, pp 533-537.

Todaro, M. E., Doxbeck, M. A. & Capsimalis, G. P., 1987, Residual stress in quenched steel cylinders, , *Residual Stress in Design, Process and Materials Selection*, edited by W. B. Young, pp. 59-62.

Lorentzen, T., 1995, Private communication about neutron diffraction measurements.

Valluri, S. R., 1963, *Acta Metal*, Vol. 11, pp. 759-775.

Vöhringer, O., 1987, Relaxation of residual stresses by annealing or mechanical treatment, *Advances in Surface Treatments,* A. Niku-Lari Ed, 4, pp. 367-396.

Walker, E. W., 1981, Some aspects of residual stress in parts heat treated by the induction method, *Residual Stress for Designers and Metallurgists, ASM,* edited by Larry J. Vande Walle, pp 41-50.

Wareing, J. and Vaughan, H. G., 1979, Influence of surface finish on low-cycle fatigue characteristics of type 316 stainless steel at 400°C, *Metal Science,* Vol 13, No 1, pp. 1-8.

Watkins, M. T., 1975, *Metal Forming,* Oxford University Press.

Webster, P. J., Mills, G., Wang, X. D., Kang, W. P. and Holden, T. M., 1995 Neutron strain scanning of a small welded austenitic stainless-steel, *J. of strain analysis*, Vol 30, No 1, pp 35-43.

Weibull, W., 1961, Fatigue testing and analysis of results, Pergamon Press, London.

Weiss, V., Oshida, Y. and Wu, A., 1979, *Fatigue Engineering Materials and Structures*, Vol. 1, pp. 333-341.

Weiss, V., Oshida, Y. and Wu, A., 1980, *Nondestructive Evaluation,* Vol. 1, pp. 207-213.

Wirsching, P. H., Torng, T. Y. and Martin, W. S., 1991, Advanced fatigue reliability analysis, *Int. J. Fatigue*. Vol. 13, pp. 389-394.

Wu, Y. T. and Wirsching, P. H., 1987 Sep., New algorithm for structural reliability estimation, J. of Engineering Mechanics, ASCE, Vol. 113, No. 9, pp. 1319-1336.

Wu, W. F. and Huang, T. H., 1991, A statistical nonlinear cumulative damage rule and fatigue life prediction under random loading, *Int. J. Pres. Ves. & Piping.* Vol. 47, pp. 1-16.

Zamrik, S. K. and Fishmuth, R. E., 1973, The effect of out of phase biaxial strain cycling on low-cycle fatigue, *Exp. Mech. SESA,* **13**, pp 204-208.

Zamrik, S. Y., and Goto, T., 1968, The use of octahedral shear strain in biaxial low fatigue, *Materials technology on inter-American approach, ASME,* New York, pp 551-562.

Zapatero, J. and Dominguez, J., 1990, A statistical approach to fatigue life prediction under random loading, *Int. J. Fatigue*, Vol. 12, No. 2, pp. 107-114.

Zhang, D. Q., Xu, K. W. and He, J. W., 1991, Aspects of the residual stress field at a notch and its effect on fatigue, *Mater. Sci. & Engng.* **A136**, pp 79-83.

Zhu, W. X., 1994, Progress summary of the project: "PROBABILISTIC APPROACH TO RESIDUAL STRESS IN MULTIAXIAL FATIGUE LIFE PREDICATION", Department of Mechanical Engineering, University of Bristol.

Zhu, W. X. and McKeighan, P. C. and Smith, D. J, June 1994, Estimating residual stresses in hot forged steel components, *Engineering Systems Design and Analysis, Proceedings of the 1994 Engineering Systems design and Analysis Conference*, Vol. 8, Part A, pp. 27-34.

Zhu, W. X. and Smith, D. J, July 1994, Development of the incremental hole-drilling method for measuring residual stresses in components with curved surfaces, in *Advances Proceedings of 10th Int Conf on experimental mechanics, in Surface Treatment*, Niku-Lari, A., Eds., 4: 199-219

Zhu, W. X., Feb. 1995, Progress summary of the project: "PROBABILISTIC APPROACH TO RESIDUAL STRESS IN MULTIAXIAL FATIGUE LIFE PREDICATION", Department of Mechanical Engineering, University of Bristol, 9502.

Zhu, W. X., McMahon, C. A. and Smith, D. J, Mar 1996, Measurement and analysis of residual stresses in hot forged steel bars, Submitted for publication to Journal of Strain Analysis for Engineering Design.

Zhu, W. X. and Smith, D. J and Lorentzen, T., Oct. 1996, Measurement of near surface residual stresses using neutronand X-ray diffraction methods, in preparation for Journal of Strain Analysis for Engineering Design.

Appendix 4A

ANALYSIS OF STRAIN RELIEF AFTER A HOLE DRILLED IN A PLATE CONTAINING RESIDUAL STRESSES AND THE MATERIAL EXHIBITING EXPONENTIAL HARDENING.

This analysis is based on the Gao's work (1992) and most of the notations and definitions are same as those used in Gao's paper. As it has be proved that the stress state at every point on specimen surface is on the yield surface and the deformation will be in the plastic region during the hole drilling operation (see section 4.4-6), the material stress-strain curve is expressed as

$$\sigma_{eq} = A\varepsilon_{eq}^{n} \tag{4A-1}$$

where σ_{eq} and ε_{eq} are Von Mises equivalent stress and strain, respectively, and the σ_{eq} is expressed as,

$$\sigma_{eq} = \sqrt{\sigma_\theta^2 - \sigma_r\sigma_\theta + \sigma_r^2} \tag{4A-2}$$

A is a material constant and n is the strain hardening exponent. If the range of σ_{eq} or ε_{eq} during the plate loading ($d\sigma_{eq} \geq 0$) is known, the fitted value of A and n at that range can be used.

The equilibrium equation is,

$$\sigma_\theta - \sigma_r = r\frac{d\sigma_r}{dr}. \tag{4A-3}$$

The constitutive equations are,

$$\begin{cases} \varepsilon_\theta = \dfrac{\varepsilon_{eq}}{\sigma_{eq}}(\sigma_\theta - 0.5\sigma_r) \\ \varepsilon_r = \dfrac{\varepsilon_{eq}}{\sigma_{eq}}(\sigma_r - 0.5\sigma_\theta) \end{cases} \tag{4A-4}$$

The compatibility equation is,

$$r\frac{d\varepsilon_\theta}{dr}=\varepsilon_r-\varepsilon_\theta \tag{4A-5}$$

The boundary conditions are a little different from Gao's and there is no elastic-plastic boundary, $r_c=\infty$. Assuming the residual stress state is a biaxial compressive state,

$$\sigma_r=\sigma_\theta=\sigma_R,\ and\ \ \sigma_{eq0}=-\sigma_R. \tag{4A-6}$$

The initial residual stress state in the plate is

$$\sigma_r|_{r=a}=-\sigma_{eq0},\ \sigma_{eq}=\sigma_{eq0},\ \sigma_r|_{r=\infty}=-\sigma_{eq0}. \tag{4A-7}$$

where a is hole radius and the boundary conditions after pressure is removed from hole surface are expressed as,

$$\sigma_r|_{r=a}=0,\ \sigma_{eq}|_{r=a}>\sigma_{eq0},\ \sigma_r|_{r=\infty}=-\sigma_{eq0}. \tag{4A-8}$$

Using an auxiliary variable $\phi=\phi(r)$ and expressing stresses in the form,

$$\begin{cases}\sigma_\theta=\dfrac{2}{\sqrt{3}}\sigma_{eq}\sin(\phi-\dfrac{\pi}{6})\\ \sigma_r=-\dfrac{2}{\sqrt{3}}\sigma_{eq}\cos\phi\end{cases}, \tag{4A-9}$$

which satisfy the Equation (4A-2) automatically. From the boundary condition (4A-7), some auxiliary values of ϕ at $r=a$ and $r=\infty$ are found,

$$\begin{cases}\phi_a=\phi(r=a)=-\pi/2\\ \phi_\infty=\phi(r=\infty)=-\pi/6\end{cases}. \tag{4A-10}$$

Substituting Equation (4A-9) into Equation (4A-4), it is found that,

$$\begin{cases}\varepsilon_\theta=\varepsilon_{eq}\sin\phi\\ \varepsilon_r=-\varepsilon_{eq}\sin(\phi+\dfrac{\pi}{3})\end{cases}. \tag{4A-11}$$

Inserting Equations (4A-1), (4A-3), (4A-9) and (4A-11) into Equation (4A-5), we obtain,

$$\frac{d\sigma_{eq}}{\sigma_{eq}} = \frac{\cos\phi + \sqrt{3}\sin\phi}{\sqrt{3}\cos\phi - \frac{1}{n}\sin\phi} d\phi \,. \tag{4A-12}$$

Integrating the above equation for r from $r = \infty$ to r which corresponds to ϕ from ϕ_∞ to ϕ and σ_{eq} from σ_{eq0} to σ_{eq}, it is find

$$\sigma_{eq} = \sigma_{eq0} \left| \frac{\cos(\phi_\infty + \phi_n)}{\cos(\phi + \phi_n)} \right|^{\frac{3n^2+n}{3n^2+1}} \exp\left[\frac{\sqrt{3}n(n-1)}{3n^2+1} (\phi - \phi_\infty) \right]. \tag{4A-13}$$

where ϕ_n is defined as

$$\phi_n = \arccos \frac{\sqrt{3}n}{\sqrt{3n^2+1}}. \tag{4A-14}$$

Substituting Equations (4A-9) and (4A-13) into Equation (4A-3) and making some rearrangements, we obtain

$$\left.\begin{aligned} \frac{dr}{r} = {} & \frac{2\sin\phi\, d\phi}{\cos\phi + \sqrt{3}\sin\phi} + \frac{2\sqrt{3}n(1-n)}{3n^2+1} \frac{\cos\phi\, d\phi}{\cos\phi + \sqrt{3}\sin\phi} \\ & - \frac{3n^2+n}{3n^2+1} \frac{2\cos\phi\, tg(\phi+\phi_n) d\phi}{\cos\phi + \sqrt{3}\sin\phi} \end{aligned}\right\} \tag{4A-15}$$

Integrating this equation for r from a to r and ϕ from ϕ_a to ϕ, it is found that

$$r = a \sqrt{\frac{\sin(\phi_a + \frac{\pi}{6})}{\sin(\phi_a + \frac{\pi}{6})}} \left| \frac{\cos(\phi + \phi_n)}{\cos(\phi_a + \phi_n)} \right|^{\frac{2n}{3n^2+1}} \exp\left[\frac{\sqrt{3}}{2} \frac{1-n^2}{3n^2+1} (\phi - \phi_a) \right]. \tag{4A-16}$$

Assuming the strain gauge location is from $r = R_1$ to $r = R_2$. Using Equation (4A-16) together with iteration technique, auxiliary values, ϕ_1 and ϕ_2, are found

$$\phi_1 = \phi(R_1) \;\; and \;\; \phi_2 = \phi(R_2). \tag{4A-17}$$

Then divide $[\phi_1, \phi_2]$ into m steps with increment $\Delta\phi = (\phi_2 - \phi_1)/m$. For each ϕ_j,

$$\phi_j = \phi_1 + (j-1)\Delta\phi, \qquad j = 1, ..., m+1 \tag{4A-18}$$

the radius r_j corresponding to the ϕ_j is determined from the Equation (4A-16). $\sigma_{eq.j}$ at the location $r = r_j$ is calculated using Equation (4A-13),

$$\sigma_{eq,j} = \sigma_{eq0}\left|\frac{\cos(\phi_\infty + \phi_n)}{\cos(\phi_j + \phi_n)}\right|^{\frac{3n^2+n}{3n^2+1}} \exp\left[\frac{\sqrt{3}n(n-1)}{3n^2+1}(\phi_j - \phi_\infty)\right]. \qquad (4A\text{-}19)$$

Inserting $\sigma_{eq,j}$ into Equation (4A-1), $\varepsilon_{eq,j}$ is obtained. Then using Equation (4A-11), $\varepsilon_{r,j}$ is found.

Consequently, the average strain between $r = R_1$ and $r = R_2$ .for the strain gauge is obtained,

$$\bar{\varepsilon}_r = \frac{1}{R_2 - R_1}\int_{R_1}^{R_2}\varepsilon_r dr = \frac{1}{R_2 - R_1}\sum_{j=1}^{m}(\varepsilon_{r,j+1} + \varepsilon_{r,j})(r_{j+1} - r_j)/2\,. \qquad (4A\text{-}20)$$

The initial radial strain ε_{r0} can be found from using Equations (4A-1) and (4A-4)

$$\varepsilon_{r0} = -\frac{1}{2}\left(\frac{\sigma_{eq0}}{A}\right)^{1/n} \qquad (4A\text{-}21)$$

Consequently the strain change due to pressure being removed from hole surface is obtained,

$$\Delta\varepsilon_r = \bar{\varepsilon}_r - \varepsilon_{r0}\,. \qquad (4A\text{-}22)$$

The FORTRAN program of this analysis to obtain the strain $\Delta\varepsilon_r$ is presented in Appendix 4B.

Appendix 4B

FORTRAN PROGRAM OF DETERMINING STRAIN RELIEF AFTER A HOLE DRILLED IN A PLATE CONTAINING RESIDUAL STRESSES AND MATERIAL EXHIBITING EXPONENTIAL HARDENING.

```
      DIMENSION PAI(1001),RR(1001),STR(1001),STN(1001),STNR(1001)
       K=100
      PI=3.1415926
      A1=-PI/2.
      B1=(-PI/6.-PI/120.)
      RA=1.0                                  :hole radius
      R1=1.87                                 :strain gauge between R1 and R2
      R2=3.55
      DO 600 J=1,110                          :this loop is for different initial stress state
       SI0=5.*J
       S0=SI0
15      CALL MATERIAL(S0,EN,AA)               :AA--A, EN--n
      PAN=SQRT(1./(1.+1./(3.*EN*EN)))
      PAN=ACOS(PAN)                           :PAN--φn
     CALL PAICAL(R1,A1,B1,EN,PI,PAN,PA)       :get φ1
      PA1=PA
     CALL STRESS(SI0,EN,PAN,PA1,STR1)
      IF (ABS(STR1-S0).LT.0.1) THEN
        GOTO 25
                  ELSE
        S0=STR1
        GOTO 15                               :iteration here is to chose A and n at this point
       END IF
25      CALL STRESS(SI0,EN,PAN,A1,STRM)
     CALL PAICAL(R2,A1,B1,EN,PI,PAN,PA)
      PA2=PA                                  :get φ2
      CALL STRESS(SI0,EN,PAN,PA2,STR2
      H=(PA2-PA1)/K                           :Δφ
C      SI0=ABS(S0)
       DO 100 I=1,K+1
        PAI(I)=PA1+(i-1)*H                    :φj
      RR(I)=EXP(SQRT(3.)*(1-EN*EN)*(PAI(I)-A1)/(2.*(3.*EN*EN+1)))
      CC=ABS(COS(PAI(I)+PAN)/COS(A1+PAN))**(2.*EN/(3.*EN*EN+1))
      RR(I)=RA*RR(I)*CC*SQRT(SIN(A1+PI/6.)/SIN(PAI(I)+PI/6.))   :get rj
      STR(I)=EXP(SQRT(3.)*EN*(EN-1)*(PAI(I)+PI/6.)/(3.*EN*EN+1))
      CC=ABS(COS(PAN-PI/6.)/COS(PAI(I)+PAN))
      CC=CC**((3.*EN*EN+EN)/(3.*EN*EN+1))
      STR(I)=STR(I)*CC                        :get σeq,j
      STN(I)=(STR(I)/AA)**(1./EN)             :get εeq,j
      STNR(I)=-STN(I)*SIN(PAI(I)+PI/3.)       :get σr,j
```

```
100    CONTINUE
       SUM=0.0
         DO 120 I=1,K
           SUM=SUM+(RR(I+1)-RR(I))*(STNR(I+1)+STNR(I))/2.        :carry out integration
120        CONTINUE
       STRAIN1=SUM/(R2-R1)
       STRAIN=SUM/(R2-R1)+(1./AA)**(1./EN)/2.
       STRAIN1=STRAIN*(SI0**(1./EN))
C       WRITE(*,*)PAI(I),RR(I),STR(I)
       WRITE(*,550)SI0,STRAIN1,STRM,STR1,STR2
550      FORMAT(F5.0,4F8.2)
600    CONTINUE
        END
       SUBROUTINE PAICAL(R,A1,B1,EN,PI,PAN,PA)          :get ϕ from using Eq. (4A-16)
       PA1=A1
       PA3=B1
       PA2=A1/2.+B1/2.
200      R2=EXP(SQRT(3.)*(1-EN*EN)*(PA2-A1)/(2.*(3.*EN*EN+1)))
       CC=ABS(COS(PA2+PAN)/COS(A1+PAN))**(2.*EN/(3.*EN*EN+1))
       R2=R2*CC*SQRT(SIN(A1+PI/6.)/SIN(PA2+PI/6.))
         IF (ABS(R2-R).LT.0.00001) THEN
          GOTO 500
                        ELSE
         IF (R2.LT.R) THEN
         PA1=PA2
         PA2=PA1/2.+PA3/2.
         GOTO 200
                ELSE
         PA3=PA2
         PA2=PA1/2.+PA3/2.
          GOTO 200
           END IF
            END IF
500         PA=PA2
           RETURN
            END
     SUBROUTINE MATERIAL(SI,EN,AA)      :material parameters are function of stress state
        X=SI/100.
      EN=0.9607632+0.001668*X-0.00445*X*X
      AA=0.1980213+0.0101314*X-0.00383*X*X+0.0017485*X*X*X
       RETURN
       END
      SUBROUTINE STRESS(SI0,EN,PAN,PA1,STR1)                :get σ_eq using Eq. (4A-13)
        PI=3.1415926
       STR1=EXP(SQRT(3.)*EN*(EN-1)*(PA1+PI/6.)/(3.*EN*EN+1))
       CC=ABS(COS(PAN-PI/6.)/COS(PA1+PAN))
      CC=CC**((3.*EN*EN+EN)/(3.*EN*EN+1))
      STR1=STR1*SI0*CC
       RETURN
       END
```

Appendix 5A

FUNCTIONAL FORMS OF $f_{ij}(r)$ IN EQUATION (5.22)

The plastic strains were assumed as

$$\varepsilon_\theta^p = C_1 r^2 + C_2 r^3, \quad \varepsilon_r^p = C_3 r^2 + C_4 r^3, \tag{5A-1}$$

where C_1, C_2, C_3, and C_4 are constants to be determined. After inserting Equation (5A-1) into Equations 5.18 to 5.20, the residual stress distribution can be obtained as a function of a number of constants,

$$\left.\begin{aligned} \sigma_r &= C_1 f_{11}(r) + C_2 f_{12}(r) + C_3 f_{13}(r) + C_4 f_{14}(r) \\ \sigma_\theta &= C_1 f_{21}(r) + C_2 f_{22}(r) + C_3 f_{23}(r) + C_4 f_{24}(r) \\ \sigma_z &= C_1 f_{31}(r) + C_2 f_{32}(r) + C_3 f_{33}(r) + C_4 f_{34}(r) \end{aligned}\right\} \tag{5A-2}$$

$$f_{11}(r) = \frac{E}{2(1-\upsilon^2)} \frac{3-2\upsilon}{4}(1-r^2) \tag{5A-3}$$

$$f_{12}(r) = \frac{E}{2(1-\upsilon^2)} \frac{8-6\upsilon}{15}(1-r^3) \tag{5A-3}$$

$$f_{13}(r) = -\frac{E}{2(1-\upsilon^2)} \frac{1+2\upsilon}{4}(1-r^2) \tag{5A-4}$$

$$f_{14}(r) = -\frac{E}{2(1-\upsilon^2)} \frac{2+6\upsilon}{15}(1-r^3) \tag{5A-5}$$

$$f_{21}(r) = \frac{E}{2(1-\upsilon^2)} \frac{3-2\upsilon}{4}(1-3r^2) \tag{5A-6}$$

$$f_{22}(r) = \frac{E}{2(1-\upsilon^2)} \frac{8-6\upsilon}{15}(1-4r^3) \tag{5A-7}$$

$$f_{23}(r) = -\frac{E}{2(1-\upsilon^2)} \frac{1+2\upsilon}{4}(1-3r^2) \tag{5A-8}$$

$$f_{24}(r) = -\frac{E}{2(1-\upsilon^2)} \frac{2+6\upsilon}{15}(1-4r^3) \tag{5A-9}$$

$$f_{31}(r) = -\frac{E}{2(1-\upsilon^2)} \frac{2-3\upsilon}{2}(1-2r^2) \tag{5A-10}$$

$$f_{32}(r) = -\frac{E}{2(1-\upsilon^2)} \frac{6-8\upsilon}{15}(2-5r^3) \tag{5A-11}$$

$$f_{33}(r) = -\frac{E}{2(1-\upsilon^2)} \frac{2+\upsilon}{2}(1-2r^2) \tag{5A-12}$$

$$f_{34}(r) = -\frac{E}{2(1-\upsilon^2)} \frac{6+2\upsilon}{15}(2-5r^3) \tag{5A-13}$$

APPENDIX 6A

USER SUBROUTINE UMAT

```
      SUBROUTINE UMAT(STRESS,STATEV,DDSDDE,SSE,SPD,SCD,
1 RPL,DDSDDT,DRPLDE,DRPLDT,
2 STRAN,DSTRAN,TIME,DTIME,TEMP,DTEMP,PREDEF,DPRED,MATERL,
3 NDI,NSHR,NTENS,NSTATV,PROPS,NPROPS,COORDS,DROT,PNEWDT,
4 CELENT,DFGRDO,DFGRD1,NOEL,NPT,LAYER,KSPT,KSTEP,KINC)
       INCLUDE 'ABA_PARAM.INC'
        CHARACTER*8 MATERL
      DIMENSION STRESS(NTENS),STATEV(NSTATV),
1 DDSDDE(NTENS,NTENS),DDSDDT(NTENS),DRPLDE(NTENS),
2 STRAN(NTENS),DSTRAN(NTENS),TIME(2),PREDEF(1),DPRED(1),
3 PROPS(NPROPS),COORDS(3),DROT(3,3),DFGRDO(3,3),DFGRD1(3,3),
4 DES(6,6),DPS(6,6),SDS(6,6),DPSD(6,6),DSTRESS(6),DPSTRAN(6),
5 ALPH(4,6),HH(5),SYD(5),ALPHA1(6),ALPHA2(6),DALPHA(6)
      DIMENSION  EELAS(6),EPLAS(6),ALPHA(6),OLDS(6),OLDPL(6),
   1  DSTRANI(6),DSTRAN0(6),DPSTRANI(6),DDSDDEI(6,6),
   2  DDSDDE0(6,6),DSTRESSL(6),SS(6),SSS(6)
       PARAMETER(ZERO=0.D0,ONE=1.D0,TWO=2.D0,THREE=3.D0,SIX=6.D0,
   1       ENUMAX=.4999D0,NEWTON=10,TOLER=1.0D-10)
C
C  ************************************************************
C  ** THIS PROGRAM SUBDIVIDE STRAIN INCREMENT BASED ON STRAIN **
C  ************************************************************
C
       IF (NDI.NE.3)THEN
          WRITE(7,1)
1      FORMAT(//,30X,' ***ERROR - THIS UMAT IS ONLY FOR ',
   1       'ELEMENTS WITH 3 DIRECT COMPONENTS')
          CALL XIT
          END IF
       DEQPL=ZERO
       EMOD=PROPS(1)
       ENU=MIN(PROPS(2),ENUMAX)
       EBULK3=EMOD/(ONE-TWO*ENU)
       EG2=EMOD/(ONE+ENU)
       EG=EG2/TWO
       EG3=THREE*EG
       ELAM=(EBULK3-EG2)/THREE
       CALL ASET(DDSDDE0,ZERO,6*6)
       DO K1=1,NDI
         DO K2=1,NDI
              DDSDDE0(K2,K1)=ELAM
         END DO
```

```
          DDSDDE0(K1,K1)=EG2+ELAM
END DO
DO K1=NDI+1,NTENS
 DDSDDE0(K1,K1)=EG
END DO
CALL ROTSIG(STATEV(1),DROT,EELAS,2,NDI,NSHR)
CALL ROTSIG(STATEV(NTENS+1),DROT,EPLAS,2,NDI,NSHR)
CALL ROTSIG(STATEV(2*NTENS+1),DROT,ALPHA,1,NDI,NSHR)
    DO K1=1,NTENS
          ALPH(1,K1)=ALPHA(K1)
    END DO
CALL ROTSIG(STATEV(3*NTENS+1),DROT,ALPHA,1,NDI,NSHR)
    DO K1=1,NTENS
          ALPH(2,K1)=ALPHA(K1)
    END DO
CALL ROTSIG(STATEV(4*NTENS+1),DROT,ALPHA,1,NDI,NSHR)
    DO K1=1,NTENS
          ALPH(3,K1)=ALPHA(K1)
    END DO
C *** get elastic matrix
C
     CALL ASET(DES,ZERO,6*6)
          DO K1=1,NDI
           DO K2=1,NDI
            IF(NDI.EQ.2) THEN
                 DES(K1,K2)=-(ONE+ENU)/EMOD
                          ELSE
                 DES(K1,K2)=-ENU/EMOD
             END IF
           END DO
            IF(NDI.EQ.2) THEN
                 DES(K1,K1)=(ONE-ENU*ENU)/EMOD
                          ELSE
           DES(K1,K1)=ONE/EMOD
            END IF
          END DO
     DO K1=NDI+1,NTENS
          DES(K1,K1)=TWO*(ONE+ENU)/EMOD
     END DO
C
C *** Next is to input initial strain history state based only on the HTS residual stress state
C
        NIT=INT(STATEV(5*NTENS+9))
   IF(NIT.NE.11011959)THEN
        STATEV(5*NTENS+9)=11011959.1
             RP0=8.4D-1
IF(COORDS(1).GT.RP0)THEN
      e=EMOD
      v=ENU
     RR=COORDS(1)
      q=0.84
      X=RR-q
      st1=350.
      sz1=400.
       b=st1/(2*(1-q))
        a=-b*(1-q)**2
         cc=0.5+q-q**2
          dd=(1-q)**2/2+q*(1-q)**3/3
```

```
      t=dd/cc
            d=sz1/(1-q-t)
             c=-d*t
              sr0=a
              st0=a
              sz0=c
               sr1=STRESS(1)
               st1=STRESS(3)
               sz1=STRESS(2)
     er0=(sr0-v*(st0+sz0))/e
     et0=(st0-v*(sr0+sz0))/e
     ez0=(sz0-v*(sr0+st0))/e
C
          etp=et0-(st1-v*(sr1+sz1))/e
          ezp=ez0-(sz1-v*(st1+sr1))/e
          erp=-etp-ezp
           EPLAS(1)=erp
                EPLAS(2)=ezp
                 EPLAS(3)=etp
                  DO I=NDI+1,NTENS
                   EPLAS(I)=ZERO
                  END DO
        CALL GETDEQPL(EPLAS,DEQPL,NDI,NTENS,TWO,THREE)
          EQPL0=DEQPL
         DO II=1,NTENS
          ALPHA(II)=ZERO
         END DO
        CALL YIELDING(STRESS,ALPHA,ESTR0,NDI,NTENS,SIX,TWO,THREE)
C
C   find maximum stress in history
C
      DEQPL1=ZERO
           IF(ESTR0.GE.10.D0)THEN
          EQPL1=0.2*EQPL0
1212         DEQPL=EQPL0+DEQPL1
           IF(DEQPL.GE.PROPS(7))THEN
                    SMISES=PROPS(6)
                                        ELSE
                    IF(DEQPL.GE.PROPS(5))THEN
         HH(4)=(PROPS(6)-PROPS(4))/(PROPS(7)-PROPS(5))
         SMISES=PROPS(4)+HH(4)*(DEQPL-PROPS(5))
                                           ELSE
         HH(4)=(PROPS(4)-PROPS(3))/PROPS(5)
         SMISES=PROPS(3)+HH(4)*DEQPL
                    END IF
                   END IF
C
C  find H1 H2 H3
C
                DO K1=1,2
                 CC=PROPS(10+K1)*DEQPL
                 STATEV(5*NTENS+K1)=(PROPS(K1+8)-PROPS(K1+7))/CC
                END DO
                 H1=STATEV(5*NTENS+1)
                 H2=STATEV(5*NTENS+2)
                 CC=DEQPL*(ONE-PROPS(11)-PROPS(12))
                 H3=(SMISES-PROPS(10))/CC
                IF(ESTR0.LE.ABS(2.*PROPS(9)-SMISES))THEN
```

```
 DEQPL1=(ESTR0-ABS(2.*PROPS(8)-SMISES))/H1
                                        ELSE
IF(ESTR0.LE.ABS(2.*PROPS(10)-SMISES))THEN
 DEQPL1=(2.*PROPS(9)-2.*PROPS(8))/H1
 DEQPL1=DEQPL1+(ESTR0-ABS(2.*PROPS(9)-SMISES))/H2
                                        ELSE
 DEQPL1=(2.*PROPS(9)-2.*PROPS(8))/H1
 DEQPL1=DEQPL1+(2.*PROPS(10)-2.*PROPS(9))/H2
 DEQPL1=DEQPL1+(ESTR0-ABS(2.*PROPS(10)-SMISES))/H3
END IF
END IF
 CC=DEQPL-DEQPL1
 DD=ABS(CC-EQPL0)
    IF(DD.GE.0.1)THEN
       GOTO 1212
    END IF
   END IF
C
   STATEV(5*NTENS+7)=DEQPL
C
  SHYDRO=(STRESS(1)+STRESS(2)+STRESS(3))/THREE
  DO K1=1,NDI
   SS(K1)=STRESS(K1)-SHYDRO
  END DO
   DO K1=NDI+1,NTENS
     SS(K1)=STRESS(K1)
   END DO
    IF(SS(1).GT.10.D0)THEN
     STATEV(5*NTENS+6)=DEQPL
     STATEV(5*NTENS+7)=DEQPL1+EQPL0
      IF(DEQPL.GE.PROPS(7))THEN
       SMISES=PROPS(6)
        HH(4)=ZERO
                              ELSE
       IF(DEQPL.GE.PROPS(5))THEN
HH(4)=(PROPS(6)-PROPS(4))/(PROPS(7)-PROPS(5))
SMISES=PROPS(4)+HH(4)*(DEQPL-PROPS(5))
                                      ELSE
HH(4)=(PROPS(4)-PROPS(3))/PROPS(5)
SMISES=PROPS(3)+HH(4)*DEQPL
       END IF
      END IF
    STATEV(5*NTENS+5)=SMISES
    STATEV(5*NTENS+4)=HH(4)
   DO K1=1,2
    CC=PROPS(10+K1)*DEQPL
     STATEV(5*NTENS+K1)=(PROPS(K1+8)-PROPS(K1+7))/CC
    END DO
     CC=DEQPL*(ONE-PROPS(11)-PROPS(12))
     STATEV(5*NTENS+3)=(SMISES-PROPS(10))/CC
    DO K1=1,NTENS
     ALPHA(K1)=ZERO
     SSS(K1)=ZERO
    END DO
  CALL YIELDING(STRESS,ALPHA,BB,NDI,NTENS,SIX,TWO,THREE)
C
C    swape  z with t
C
```

```
      SSS(1)=SS(1)
      SSS(2)=SS(3)
      SSS(3)=SS(2)
 DO K1=1,NTENS
      CC=-SMISES*SSS(K1)/BB
      ALPH(1,K1)=(ONE-PROPS(8)/SMISES)*CC
      ALPH(2,K1)=(ONE-PROPS(9)/SMISES)*CC
      ALPH(3,K1)=(ONE-PROPS(10)/SMISES)*CC
      EELAS(K1)=ZERO
  DO K2=1,NTENS
       EELAS(K1)=EELAS(K1)+DES(K1,K2)*STRESS(K2)
  END DO
 END DO
C
C  PUT EQPL0 BACK
C
            DEQPL=EQPL0
            STATEV(5*NTENS+6)=DEQPL
            STATEV(5*NTENS+7)=DEQPL1+EQPL0
C
C  considering loading point located between f3 and f2
C
          DO K1=1,NTENS
           ALPHA(K1)=ALPH(2,K1)
          END DO
     CALL YIELDING(STRESS,ALPHA,DD2,NDI,NTENS,SIX,TWO,THREE)
            IF(DD2.GT.PROPS(9))THEN
                 BT2=ONE-PROPS(9)/DD2
                 DO K1=1,NTENS
                  ALPH(2,K1)=ALPH(2,K1)+BT2*(SS(K1)-ALPH(2,K1))
           ALPH(1,K1)=SS(K1)-(SS(K1)-ALPH(2,K1))*PROPS(8)/PROPS(9)
                 END DO
            END IF
C
C  considering loading point located between f2 and f1
C
          DO K1=1,NTENS
           ALPHA(K1)=ALPH(1,K1)
          END DO
     CALL YIELDING(STRESS,ALPHA,DD1,NDI,NTENS,SIX,TWO,THREE)
                IF(DD1.GT.PROPS(8))THEN
                 BT1=ONE-PROPS(8)/DD1
                 DO K1=1,NTENS
                  ALPH(1,K1)=ALPH(1,K1)+BT1*(SS(K1)-ALPH(1,K1))
                 END DO
                END IF
       END IF
 WRITE(7,*)
 WRITE(7,*)' STRESS='
  WRITE(7,*)(STRESS(I),I=1,3)
   WRITE(7,*)' ALPH(1,K1)='
  WRITE(7,*)(ALPH(1,K1),K1=1,3)
   WRITE(7,*)' ALPH(2,K1)='
  WRITE(7,*)(ALPH(2,K1),K1=1,3)
      WRITE(7,*)' ALPH(3,K1)='
  WRITE(7,*)(ALPH(3,K1),K1=1,3)
END IF
    END IF
```

```
C
C *** end of history input
C
                    DO K1=1,NTENS
                     ALPH(4,K1)=ZERO
                    END DO
               DO K1=1,NTENS
                  OLDS(K1)=STRESS(K1)
                  OLDPL(K1)=EPLAS(K1)
                  EELAS(K1)=EELAS(K1)+DSTRAN(K1)
                        DSTRESS(K1)=ZERO
                  DO K2=1,NTENS
                        DSTRESS(K1)=DSTRESS(K1)+DDSDDE0(K1,K2)*DSTRAN(K2)
                  END DO
                        STRESS(K1)=STRESS(K1)+DSTRESS(K1)
               END DO
                DO K1=1,NTENS
                 ALPHA(K1)=ALPH(1,K1)
                END DO
               CALL YIELDING(STRESS,ALPHA,SMISES,NDI,NTENS,SIX,TWO,THREE)
                 IF(STATEV(5*NTENS+5).GT.1.0D-6) THEN
                        SYIELD=PROPS(8)
                                              ELSE
                        SYIELD=PROPS(3)
                        HH(1)=1.0D8
                        HH(2)=1.0D8
                        HH(3)=1.0D8
                        HH(4)=(PROPS(4)-PROPS(3))/PROPS(5)
                   DO K3=1,4
                        STATEV(5*NTENS+K3)=HH(K3)
                   END DO
                  END IF
               IF(SMISES.GT.(ONE+TOLER)*SYIELD) THEN
                NED=1
                NFIX=1959
               IC=4
                        DO K3=1,NTENS
                         STRESS(K3)=OLDS(K3)
                        END DO
               DO K1=1,3
                SYD(K1)=PROPS(K1+7)
               END DO
                SYD(4)=STATEV(5*NTENS+5)
                 IF(SYD(4).LE.PROPS(3)) THEN
                        SYD(4)=PROPS(3)
                 END IF
                   IF(STATEV(5*NTENS+5).LT.PROPS(3))THEN
                        SYD1=PROPS(3)
                        H1=(PROPS(4)-PROPS(3))/PROPS(5)
                        STATEV(5*NTENS+4)=H1
                        SYD2=PROPS(4)
                        H2=(PROPS(6)-PROPS(4))/(PROPS(7)-PROPS(5))
     CALL ISOMAT(STRESS,DDSDDE0,DSTRAN,DPSTRAN,DQPL,NED,
1 SYD1,SYD2,H1,H2,NDI,NTENS,EG,EG3,EBULK3,ZERO,ONE,TWO,THREE,SIX)
                   JJ=4
                   GOTO 1050
                         END IF
    CALL FINDTT(ALPHA,STRESS,DSTRESS,SYIELD,NDI,NTENS,
```

```
1  THREE,TWO,ZERO,TT)
       IF(TT.LE.1.D-10)THEN
              TT=ZERO
             NST=1
       DO K3=1,NTENS
            DSTRANI(K3)=DSTRAN(K3)
       END DO
                                ELSE
                     NST=0
                     NFIX=NFIX+1
                  DO M1=1,NTENS
                       DSTRANI(M1)=(ONE-TT)*DSTRAN(M1)
                       STRESS(M1)=STRESS(M1)+TT*DSTRESS(M1)
                     END DO
                   END IF
         DO K3=1,4
          HH(K3)=STATEV(5*NTENS+K3)
         END DO
       DO M1=1,NTENS
        DPSTRAN(M1)=ZERO
       END DO
       DO 999 JJ=1,4
       IF(JJ.LT.4)THEN
CALL GETDEQPL(DSTRANI,DERO,NDI,NTENS,TWO,THREE)
        DERO=ABS(DERO)*1.D-9
        IF(DERO.LT.1.D-13)THEN
         DERO=1.D-13
        END IF
         DO K1=1,NTENS
           ALPHA(K1)=ALPH(JJ+1,K1)
  END DO
 CALL YIELDING(STRESS,ALPHA,SMISES,NDI,NTENS,SIX,TWO,THREE)
 IF(SMISES.GT.(ONE-TOLER)*SYD(JJ+1))THEN
         GOTO 998
 END IF
              IF(NFIX.EQ.1959)THEN
                   NST=JJ
                   NFIX=NFIX+1
              END IF
  DO K1=1,NTENS
         ALPHA1(K1)=ALPH(JJ,K1)
         ALPHA2(K1)=ALPH(JJ+1,K1)
         DSTRAN0(K1)=DSTRANI(K1)
  END DO
  H=HH(JJ)
CALL MATZHU(DES,STRESS,DSTRESS,ALPHA1,ALPHA2,DALPHA,
1 DSTRAN0,DPSTRANI,NDI,NTENS,SYD(JJ),SYD(JJ+1),H,DERO,NEG,
2 DSTRESSL,TL)
         DO M1=1,NTENS
              DPSTRAN(M1)=DPSTRAN(M1)+DPSTRANI(M1)
              STRESS(M1)=STRESS(M1)+DSTRESS(M1)
              DSTRANI(M1)=DSTRANI(M1)-DSTRAN0(M1)
          END DO
         IF(NEG.EQ.0)THEN
           NED=JJ
              GOTO 1000
         END IF
          GOTO 998
```

```
END IF
            IF(NFIX.EQ.1959)THEN
                NST=JJ
            END IF
             NED=JJ
 SYD1=STATEV(5*NTENS+5)
  H1=STATEV(5*NTENS+4)
          IF(SYD1.LT.PROPS(3))THEN
           SYD1=PROPS(3)
           H1=(PROPS(4)-PROPS(3))/PROPS(5)
           STATEV(5*NTENS+4)=H1
          END IF
         IF(SYD1.LT.PROPS(4))THEN
                SYD2=PROPS(4)
                 H2=(PROPS(6)-PROPS(4))/(PROPS(7)-PROPS(5))
                                ELSE
                SYD2=PROPS(6)
                 H2=ZERO
               END IF
                HH(5)=H2
                SYD(5)=SYD2
       DO M1=1,NTENS
            DO M2=1,NTENS
             DDSDDEI(M1,M2)=DDSDDE0(M1,M2)
            END DO
       END DO
     CALL ISOMAT(STRESS,DDSDDEI,DSTRANI,DPSTRANI,DQPL,NED,
1 SYD1,SYD2,H1,H2,NDI,NTENS,EG,EG3,EBULK3,ZERO,ONE,TWO,THREE,SIX)
        DO M1=1,NTENS
              DPSTRAN(M1)=DPSTRAN(M1)+DPSTRANI(M1)
          END DO
           GOTO 1000
998      I=I+1
999    CONTINUE
1000       IF(NST.NE.4)THEN
          DO K1=1,NTENS
           DSTRESS(K1)=STRESS(K1)-OLDS(K1)
          END DO
         CALL GETDDSDDE(DDSDDE0,DSTRAN,DES,OLDS,DSTRESS,ALPH,SYD,
   1 HH,NST,NED,NDI,NTENS,EG3,ZERO,ONE,TWO,THREE)
                            ELSE
           DO K1=1,NTENS
            DO K2=1,NTENS
                 DDSDDE0(K1,K2)=DDSDDEI(K1,K2)
            END DO
           END DO
          END IF
1050       IF(JJ.EQ.4)THEN
           DO K1=1,NTENS
                ALPHA(K1)=ZERO
           END DO
         CALL YIELDING(STRESS,ALPHA,SMISES,NDI,NTENS,SIX,TWO,THREE)
          STATEV(5*NTENS+5)=SMISES
         IF(SMISES.LT.PROPS(4))THEN
          STATEV(5*NTENS+4)=(PROPS(4)-PROPS(3))/PROPS(5)
                                ELSE
                IF(SMISES.LT.PROPS(6))THEN
          STATEV(5*NTENS+4)=(PROPS(6)-PROPS(4))/(PROPS(7)-PROPS(5))
```

```
                                    ELSE
   STATEV(5*NTENS+4)=ZERO
          END IF
  END IF
  SHYDRO=(STRESS(1)+STRESS(2)+STRESS(3))/THREE
DO MM=1,IC-1
DO K1=1,NDI
 ALPH(MM,K1)=(ONE-PROPS(7+MM)/SMISES)*(STRESS(K1)-SHYDRO)
END DO
 DO K1=NDI+1,NTENS
  ALPH(MM,K1)=(ONE-PROPS(7+MM)/SMISES)*STRESS(K1)
 END DO
END DO
      IF(SMISES.LE.PROPS(4))THEN
       EP=PROPS(5)*(SMISES-PROPS(3))/(PROPS(4)-PROPS(3))
                                    ELSE
        IF(SMISES.LE.PROPS(6))THEN
      EP=PROPS(5)+(PROPS(7)-PROPS(5))*(SMISES-PROPS(4))
1     /(PROPS(6)-PROPS(4))
                                    ELSE
        EP=PROPS(7)
      DO M1=1,NTENS
       DSTRAN0(M1)=EPLAS(M1)+DPSTRAN(M1)
      END DO
     CALL GETDEQPL(DSTRAN0,EQPL,NDI,NTENS,TWO,THREE)
      EP=MAX(EQPL,EP)
       END IF
      END IF
            DO K1=1,2
             CC=PROPS(10+K1)*EP
             STATEV(5*NTENS+K1)=(SYD(K1+1)-SYD(K1))/CC
            END DO
             CC=EP*(ONE-PROPS(11)-PROPS(12))
             STATEV(5*NTENS+3)=(SMISES-SYD(3))/CC
      GOTO 1100
     END IF
     SHYDRO=(STRESS(1)+STRESS(2)+STRESS(3))/THREE
     DO K3=1,NTENS
       ALPH(JJ,K3)=ALPH(JJ,K3)+DALPHA(K3)
     END DO
       IF(JJ.GT.1)THEN
     DO MM=1,JJ-1
     DO K1=1,NDI
      ALPH(MM,K1)=(ONE-SYD(MM)/SYD(JJ))*(STRESS(K1)-SHYDRO)
1  +ALPH(JJ,K1)*SYD(MM)/SYD(JJ)
     END DO
      DO K1=NDI+1,NTENS
       ALPH(MM,K1)=(ONE-SYD(MM)/SYD(JJ))*STRESS(K1)
1    +ALPH(JJ,K1)*SYD(MM)/SYD(JJ)
      END DO
     END DO
       END IF
1100  DO M1=1,NTENS
       EPLAS(M1)=EPLAS(M1)+DPSTRAN(M1)
       EELAS(M1)=EELAS(M1)-DPSTRAN(M1)
      END DO
       SPD=ZERO
      DO K1=1,NTENS
```

```
  SPD=SPD+(STRESS(K1)+OLDS(K1))*DPSTRAN(K1)/TWO
 END DO
CALL GETDEQPL(DPSTRAN,DEQPL,NDI,NTENS,TWO,THREE)
 STATEV(5*NTENS+7)=STATEV(5*NTENS+7)+DEQPL
CALL GETDEQPL(EPLAS,EQPL,NDI,NTENS,TWO,THREE)
  IF(EQPL.GT.STATEV(5*NTENS+6))THEN
        STATEV(5*NTENS+6)=EQPL
  END IF
        END IF
   BB=100.
  STATEV(5*NTENS+8)=STATEV(5*NTENS+8)+1.
  NMES=INT(STATEV(5*NTENS+8)/BB)
  IF(NMES.EQ.1)THEN
    STATEV(5*NTENS+8)=STATEV(5*NTENS+8)-BB
        END IF
1200    DO K1=1,NTENS
          STATEV(K1)=EELAS(K1)
          STATEV(K1+NTENS)=EPLAS(K1)
          STATEV(K1+2*NTENS)=ALPH(1,K1)
          STATEV(K1+3*NTENS)=ALPH(2,K1)
          STATEV(K1+4*NTENS)=ALPH(3,K1)
         END DO
         CALL ASET(DDSDDE,ZERO,NTENS*NTENS)
           DO K1=1,NDI
            DO K2=1,NDI
                DDSDDE(K1,K2)=DDSDDE0(K1,K2)
            END DO
           END DO
          DDSDDE(NTENS,NTENS)=EG
         RETURN
        END
C
C-------------------------------------------------------------
C
C       The next subroutine is to inverse a matrix
C
         SUBROUTINE INVERSEMT(A,ZERO,ONE,N,KEP)
        INCLUDE 'ABA_PARAM.INC'
         DIMENSION A(6,6),B(6)
          KEP=1
          DO 10 K=1,N
          KK=N-K+1
          W=A(1,1)
          IF(W.LE.ZERO) GOTO 30
          DO 20 I=2,N
          G=A(I,1)
          IF(I-KK) 2, 2, 3
3       B(I)=G/W
            GOTO 4
2       B(I)=-G/W
4       DO 20 J=2,I
20        A(I-1,J-1)=A(I,J)+G*B(J)
            A(N,N)=ONE/W
           DO 10 I=2,N
10        A(N,I-1)=B(I)
              DO K1=2,N
                  DO K2=1,K1-1
                   A(K2,K1)=A(K1,K2)
```

```
                END DO
              END DO
              RETURN
30          KEP=-KEP
              RETURN
              END
C
-----------------------------------------------------------------
C
C       The next subroutine is to find T for σ̄ + T* Δσ̄ just on the yield
C       surface
C
            SUBROUTINE FINDTT(ALPHA,STRESS,DSTRESS,SYIELD,NDI,
     1              NTENS,THREE,TWO,ZERO,TT)
          INCLUDE 'ABA_PARAM.INC'
          DIMENSION ALPHA(NTENS),STRESS(NTENS),DSTRESS(NTENS)
           SHYDRO=(STRESS(1)+STRESS(2)+STRESS(3))/THREE
           DSHYDRO=(DSTRESS(1)+DSTRESS(2)+DSTRESS(3))/THREE
            AS1=ZERO
            BS1=ZERO
            CS1=ZERO
             DO K1=1,NDI
              AS1=AS1+(DSTRESS(K1)-DSHYDRO)**2
              BS1=BS1+(DSTRESS(K1)-DSHYDRO)*(STRESS(K1)-SHYDRO-ALPHA(K1))
              CS1=CS1+(STRESS(K1)-SHYDRO-ALPHA(K1))**2
             END DO
            AS1=THREE*AS1/TWO
            BS1=THREE*BS1/TWO
            CS1=THREE*CS1/TWO
             DO K1=NDI+1,NTENS
              AS1=AS1+THREE*DSTRESS(K1)**2
              BS1=BS1+THREE*DSTRESS(K1)*(STRESS(K1)-ALPHA(K1))
              CS1=CS1+THREE*(STRESS(K1)-ALPHA(K1))**2
            END DO
                CS1=CS1-SYIELD*SYIELD
             TT=(SQRT(BS1**2-AS1*CS1)-BS1)/AS1
           RETURN
           END
C
-----------------------------------------------------------------
C
C       The next subroutine is to calculate Jacobian matrix, stress
C       increment and plastic strain increment
C
C

        SUBROUTINE MATZHU(DES,STRESS,DSTRESS,ALPHA1,ALPHA2,DALPHA,
     1 DSTRAN,DPSTRAN,NDI,NTENS,SYD1,SYD2,H,DERO,NEDGE,DSTRESSL,TL)
         INCLUDE 'ABA_PARAM.INC'
        DIMENSION DDSDDE(6,6),STRESS(NTENS),DSTRESS(NTENS),
     1 DSTRAN(NTENS),DPSTRAN(NTENS),ALPHA1(NTENS),ALPHA2(NTENS),
     2 DES(6,6),DPS(6,6),STRESSI(6),ALPHA(6),DALPHA(6),DSTRANI(6),
     3 ALPHA0(6),STRESS0(6),DSTRESSL(6)
       PARAMETER(ZERO=0.D0,ONE=1.D0,TWO=2.D0,THREE=3.D0,SIX=6.D0,
     1 TOLER=1.D-6)
          NEDGE=0
        DO K1=1,NTENS
          DPSTRAN(K1)=ZERO
           STRESS0(K1)=STRESS(K1)
```

```
          ALPHA0(K1)=ALPHA1(K1)
           STRESSI(K1)=STRESS(K1)
            ALPHA(K1)=ALPHA1(K1)
                DALPHA(K1)=ZERO
        END DO
         SYIELD=SYD1
CALL FINDDPS(DPS,STRESSI,ALPHA,SYIELD,H,NDI,NTENS,TWO,THREE)
         DO K1=1,NTENS
                DO K2=1,NTENS
                  DDSDDE(K1,K2)=DPS(K1,K2)+DES(K1,K2)
                END DO
         END DO
        CALL INVERSEMT(DDSDDE,ZERO,ONE,NTENS,KEP)
         IF(KEP.EQ.-1) THEN
           III=1
          GOTO 20
         END IF
         DO K1=1,NTENS
                DSTRESS(K1)=ZERO
          DO K2=1,NTENS
                DSTRESS(K1)=DSTRESS(K1)+DDSDDE(K1,K2)*DSTRAN(K2)
          END DO
         END DO
CALL YIELDING(DSTRESS,DALPHA,SMISES,NDI,NTENS,SIX,TWO,THREE)
      KK=INT(SMISES*5.D2/SYIELD)+2
      TL=ONE/DBLE(KK)
       DO K1=1,NTENS
        DSTRANI(K1)=TL*DSTRAN(K1)
        DSTRESS(K1)=TL*DSTRESS(K1)
       END DO
          MNK=1
           CALL DSHIFT(STRESS0,DSTRESS,ALPHA0,ALPHA2,DALPHA,SYD1,SYD2,
     1 MNK,NDI,NTENS,ZERO,ONE,TWO,THREE)
          DO K1=1,NTENS
           STRESSI(K1)=STRESS0(K1)+DSTRESS(K1)
           ALPHA(K1)=ALPHA0(K1)+DALPHA(K1)
          END DO
      DO 200 N1=1,KK
          MM=0
50     CALL FINDDPS(DPS,STRESSI,ALPHA,SYIELD,H,NDI,NTENS,TWO,THREE)
          MM=MM+1
          DO K1=1,NTENS
                DO K2=1,NTENS
                  DDSDDE(K1,K2)=DPS(K1,K2)+DES(K1,K2)
                END DO
          END DO
       CALL INVERSEMT(DDSDDE,ZERO,ONE,NTENS,KEP)
       IF(KEP.EQ.-1) THEN
         III=2
        GOTO 20
       END IF
       DO K1=1,NTENS
              DSTRESS(K1)=ZERO
        DO K2=1,NTENS
              DSTRESS(K1)=DSTRESS(K1)+DDSDDE(K1,K2)*DSTRANI(K2)
        END DO
       END DO
CALL DSHIFT(STRESS0,DSTRESS,ALPHA0,ALPHA2,DALPHA,SYD1,SYD2,
```

```
1 MNK,NDI,NTENS,ZERO,ONE,TWO,THREE)
      ERROR=ZERO
       DO K3=1,NTENS
        ERROR=ERROR+ABS(STRESSI(K3)-STRESS0(K3)-DSTRESS(K3))
       END DO
              IF(MM.GT.2)THEN
               IF(ERROR.GT.ERR1)THEN
                GOTO 92
               END IF
              END IF
       DO K3=1,NTENS
        STRESSI(K3)=STRESS0(K3)+DSTRESS(K3)
        ALPHA(K3)=ALPHA0(K3)+DALPHA(K3)
         END DO
       CALL YIELDING(STRESSI,ALPHA2,SMISES,NDI,NTENS,SIX,TWO,THREE)
                IF(SMISES.GT.SYD2)THEN
              CALL FINDTT(ALPHA2,STRESS0,DSTRESS,SYD2,NDI,NTENS,
   1  THREE,TWO,ZERO,TT0)
                CC=SYD1/SYD2
               MMM=0
55          DO K3=1,NTENS
                    TL=TL*TT0
                    DSTRANI(K3)=TT0*DSTRANI(K3)
                    DSTRESS(K3)=TT0*DSTRESS(K3)
          STRESSI(K3)=STRESS0(K3)+TT0*DSTRESS(K3)
         ALPHA(K3)=STRESSI(K3)-CC*(STRESSI(K3)-ALPHA2(K3))
            END DO
       CALL FINDDPS(DPS,STRESSI,ALPHA,SYIELD,H,NDI,NTENS,TWO,THREE)
        DO K1=1,NTENS
            DO K2=1,NTENS
             DDSDDE(K1,K2)=DPS(K1,K2)+DES(K1,K2)
           END DO
       END DO
       CALL INVERSEMT(DDSDDE,ZERO,ONE,NTENS,KEP)
       IF(KEP.EQ.-1) THEN
        III=3
        GOTO 20
       END IF
       DO K1=1,NTENS
            DSTRESS(K1)=ZERO
        DO K2=1,NTENS
             DSTRESS(K1)=DSTRESS(K1)+DDSDDE(K1,K2)*DSTRANI(K2)
        END DO
       END DO
            CALL FINDTT(ALPHA2,STRESS0,DSTRESS,SYD2,NDI,NTENS,
1  THREE,TWO,ZERO,TT0)
       MMM=MMM+1
        IF(MMM.GT.21)THEN
       WRITE(7,*)' TT0=',TT0,' SYD2=',SYD2
       WRITE(7,*)' NOT CONVERGE WHEN REACH THE NEXT YIELDING
1  SURFACE IN UMAT-MATZHU'
            GOTO 92
        END IF
            IF(MMM.GT.7)THEN
            END IF
         IF(ABS(TT0-ONE).GT.1.0D-11)THEN
      IF(MMM.EQ.7.OR.MMM.EQ.11.OR.MMM.EQ.15.OR.MMM.EQ.19)THEN
       WRITE(7,*)' MMM=',MMM,' TT0=',TT0
```

```
                TT0=(TT0+ONE)/TWO
               END IF
                GOTO 55
            END IF
56          TL=TL*TT0
            DO K1=1,NTENS
        DSTRAN(K1)=DSTRAN(K1)*DBLE(N1-1)/DBLE(KK)+TT0*DSTRANI(K1)
        DSTRESSL(K1)=TT0*DSTRESS(K1)
        STRESSI(K1)=STRESS0(K1)+DSTRESSL(K1)
        DSTRESS(K1)=STRESSI(K1)-STRESS(K1)
        DALPHA(K1)=STRESSI(K1)-ALPHA1(K1)-CC*(STRESSI(K1)-ALPHA2(K1))
            END DO
                NEDGE=1
                GOTO 300
                 END IF
         IF(ERROR.LT.DERO)THEN
          GOTO 100
         END IF
         IF(MM.GE.10)THEN
        CALL YIELDING(STRESSI,ALPHA1,SMISES,NDI,NTENS,SIX,TWO,THREE)
         WRITE(7,*)' ERROR=',ERROR,' SMISES1=',SMISES
        CALL YIELDING(STRESSI,ALPHA2,SMISES,NDI,NTENS,SIX,TWO,THREE)
         WRITE(7,*)' MM=',MM,'   SMISES2=',SMISES
        WRITE(7,*)' MNK=',MNK,' SYD1=',SYD1,'   SYD2=',SYD2
       WRITE(7,*)' STRESS0='
        WRITE(7,*)(STRESS0(I),I=1,6)
        WRITE(7,*)' STRESSI='
        WRITE(7,*)(STRESSI(I),I=1,6)
        WRITE(7,*)' DSTRESS='
         WRITE(7,*)(DSTRESS(I),I=1,6)
        WRITE(7,*)' DSTRANI='
         WRITE(7,*)(DSTRANI(I),I=1,6)
          WRITE(7,*)' ALPHA0='
         WRITE(7,32)(ALPHA0(I),I=1,6)
          WRITE(7,*)' ALPHA='
         WRITE(7,32)(ALPHA(I),I=1,6)
32      FORMAT(6E18.8)
          CALL XIT
         END IF
          IF(MM.GT.10)THEN
92       WRITE(7,94)
94      FORMAT(//,10X,' ***ERROR - NOT CONVERGE LOCATION 2 ',
     1 ' THERE IS SOMETHING WRONG FROM INPUT, TRY TO REDUCE INCREMENT')
       WRITE(7,*)' THE ABOVE ERROR MESSAGE IS FROM ZHUS UMAT DEVELOPED
     1 BY WUXUE ZHU IN DEPT OF MECH ENGNG  BRISTOL UNIVERSITY'
          CALL XIT
         END IF
          ERR1=ERROR
          GOTO 50
100     DO K1=1,NTENS
           STRESS0(K1)=STRESSI(K1)
           ALPHA0(K1)=ALPHA(K1)
           STRESSI(K1)=STRESS0(K1)+DSTRESS(K1)
           ALPHA(K1)=ALPHA0(K1)+DALPHA(K1)
            DO K2=1,NTENS
                 DPSTRAN(K1)=DPSTRAN(K1)+DPS(K1,K2)*DSTRESS(K2)
            END DO
           END DO
```

```
200     CONTINUE
          DO K1=1,NTENS
           DSTRESS(K1)=STRESS0(K1)-STRESS(K1)
           DALPHA(K1)=ALPHA0(K1)-ALPHA1(K1)
          END DO
          GOTO 300
20         WRITE(7,30)
30   FORMAT(//,30X,' **ERROR: THE COEFFICIENT MATRIX IS NOT POSITIVE',
    1 ' DETERMINANT, AND THERE IS AN ERROR IN THE DATA!  STOP!! ')
           WRITE(7,*)' III=',III,' KEP=',KEP,' ntens=',NTENS
           WRITE(*,*)' stress='
           write(7,*)(STRESS(I),I=1,6)
          write(7,*)' stran='
           write(7,*)(DSTRAN(I),I=1,6)
          write(7,*)' ALPHA1='
           write(7,*)(ALPHA1(I),I=1,6)
     CALL YIELDING(STRESS,ALPHA1,SMISES,NDI,NTENS,SIX,TWO,THREE)
          WRITE(7,*)' NDI=',NDI,' SMISES=',SMISES
           CALL XIT
300     RETURN
        END
C
C-------------------------------------------------------------------
C
C       The next subroutine is to find Von Mises stress
C
        SUBROUTINE YIELDING(STRESS,ALPHA,SMISES,NDI,NTENS,SIX,TWO,THREE)
         INCLUDE 'ABA_PARAM.INC'
        DIMENSION ALPHA(NTENS),STRESS(NTENS)
         SHYDRO=(STRESS(1)+STRESS(2)+STRESS(3))/THREE
        SMISES=(STRESS(1)-SHYDRO-ALPHA(1))**2
    1    +(STRESS(2)-SHYDRO-ALPHA(2))**2
    2    +(STRESS(3)-SHYDRO-ALPHA(3))**2
        SMISES=THREE*SMISES
        DO K1=NDI+1,NTENS
          SMISES=SMISES+SIX*(STRESS(K1)-ALPHA(K1))**2
        END DO
        SMISES=SQRT(SMISES/TWO)
         RETURN
         END
C****
C-------------------------------------------------------------------
C
C       The next subroutine is to find increment of yield surface centre
C
     SUBROUTINE DSHIFT(STRESS,DSTRESS,ALPHA1,ALPHA2,DALPHA,SYD1,SYD2,
    1 MM,NDI,NTENS,ZERO,ONE,TWO,THREE)
       INCLUDE 'ABA_PARAM.INC'
       DIMENSION STRESS(NTENS),DSTRESS(NTENS),ALPHA1(NTENS),
1 ALPHA2(NTENS),DALPHA(NTENS),STRESSI(6),ALPHA(6),DSTR(6),
2 DX(6),DY(6)
        DLT=ONE/DBLE(MM)
         TS=SYD2/SYD1-ONE
        DO K3=1,NTENS
              STRESSI(K3)=STRESS(K3)
              ALPHA(K3)=ALPHA1(K3)
              DSTR(K3)=DLT*DSTRESS(K3)
        END DO
      DSHYDRO=(DSTR(1)+DSTR(2)+DSTR(3))/THREE
```

```
 DO 100 M1=1,MM
SHYDRO=(STRESSI(1)+STRESSI(2)+STRESSI(3))/THREE
DO K1=1,NDI
  DY(K1)=STRESSI(K1)-SHYDRO+DSTR(K1)-DSHYDRO-ALPHA(K1)
   DX(K1)=ALPHA2(K1)-ALPHA(K1)+TS*DY(K1)
 END DO
 DO K1=NDI+1,NTENS
DY(K1)=STRESSI(K1)+DSTR(K1)-ALPHA(K1)
DX(K1)=ALPHA2(K1)-ALPHA(K1)+TS*DY(K1)
 END DO
 AS1=ZERO
 BS1=ZERO
 CS1=ZERO
  DO K1=1,NDI
   AS1=AS1+DX(K1)**2
   BS1=BS1+DX(K1)*DY(K1)
   CS1=CS1+DY(K1)**2
  END DO
 AS1=THREE*AS1/TWO
 BS1=THREE*BS1/TWO
 CS1=THREE*CS1/TWO
  DO K1=NDI+1,NTENS
   AS1=AS1+THREE*DX(K1)**2
   BS1=BS1+THREE*DX(K1)*DY(K1)
   CS1=CS1+THREE*DY(K1)**2
  END DO
        CS1=CS1-SYD1**2
   T=(BS1-SQRT(BS1**2-AS1*CS1))/AS1
DO K1=1,NTENS
  ALPHA(K1)=ALPHA(K1)+T*DX(K1)
    STRESSI(K1)=STRESSI(K1)+DSTR(K1)
  END DO
100  CONTINUE
      DO K3=1,NTENS
          DALPHA(K3)=ALPHA(K3)-ALPHA1(K3)
      END DO
     RETURN
     END
C
C-------------------------------------------------------------
C
C     The next subroutine is to find the matrix DPS with which
C     d(Δε⃗)_p = DPS * dΔσ⃗
C
      SUBROUTINE FINDDPS(DPS,STRESS,ALPHA,SYIELD,H,NDI,NTENS,TWO,THREE)
     INCLUDE 'ABA_PARAM.INC'
 DIMENSION DPS(6,6),STRESS(NTENS),ALPHA(NTENS),FLOW(6)
  SHYDRO=(STRESS(1)+STRESS(2)+STRESS(3))/THREE
DO K1=1,NDI
 FLOW(K1)=THREE*(STRESS(K1)-ALPHA(K1)-SHYDRO)/(TWO*SYIELD)
END DO
DO K1=NDI+1,NTENS
 FLOW(K1)=THREE*(STRESS(K1)-ALPHA(K1))/SYIELD
END DO
 DO K1=1,NTENS
  DO K2=K1,NTENS
       DPS(K1,K2)=FLOW(K1)*FLOW(K2)/H
```

```
          END DO
         END DO
         DO K1=2,NTENS
          DO K2=1,K1-1
                DPS(K1,K2)=DPS(K2,K1)
          END DO
         END DO
        RETURN
        END
C
C-----------------------------------------------------------------
C
C       The next subroutine is to get equivalent plastic strain increment
C
        SUBROUTINE GETDEQPL(DPSTRAN,DEQPL,NDI,NTENS,TWO,THREE)
        INCLUDE 'ABA_PARAM.INC'
        DIMENSION DPSTRAN(NTENS)
                DEQPL=0.D0
          DO K1=1,NDI
                DEQPL=DEQPL+DPSTRAN(K1)*DPSTRAN(K1)
          END DO
                DO K1=NDI+1,NTENS
                 DEQPL=DEQPL+DPSTRAN(K1)*DPSTRAN(K1)/TWO
                END DO
                 DEQPL=SQRT(TWO*DEQPL/THREE)
         RETURN
        END
C
C-----------------------------------------------------------------
C
C       The next subroutine is for the 4th yielding surface with
C       isotropic hardening to get plastic strain increment and
C       Jacobian matrix
C
C
     SUBROUTINE ISOMAT(STRESS,DDSDDE,DSTRAN,DPSTRAN,DEQPL,NED,
    1 SYD1,SYD2,H1,H2,NDI,NTENS,EG,EG3,EBULK3,ZERO,ONE,TWO,THREE,SIX)
          INCLUDE 'ABA_PARAM.INC'
           DIMENSION STRESS(NTENS),DDSDDE(6,6),DSTRAN(NTENS),
    1 DPSTRAN(NTENS),DSTRESS(6)
          DIMENSION FLOW(6),ALPHA(6),OLDS(6)
          DO K1=1,NTENS
            OLDS(K1)=STRESS(K1)
            DSTRESS(K1)=ZERO
             DO K2=1,NTENS
                   DSTRESS(K1)=DSTRESS(K1)+DDSDDE(K1,K2)*DSTRAN(K2)
             END DO
    STRESS(K1)=STRESS(K1)+DSTRESS(K1)
END DO
          DO K1=1,NTENS
            ALPHA(K1)=ZERO
            DPSTRAN(K1)=ZERO
          END DO
CALL YIELDING(STRESS,ALPHA,SMISES,NDI,NTENS,SIX,TWO,THREE)
 SYIELD=SYD1
 HARD=H1
  DEP1=1.D6
DEQPL=(SMISES-SYIELD)/(EG3+H1)
  IF(H1.LT.1.D-6)THEN
```

```
          GOTO 100
                        ELSE
          DEP1=(SYD2-SYD1)/H1
         END IF
        IF(DEQPL.GT.(ONE+1.D-6)*DEP1)THEN
         NED=5
         SYIELD=((H1-H2)*SYD2+H2*SYD1)/H1
         HARD=H2
         DEQPL=(SMISES-SYIELD)/(EG3+H2)
        END IF
100     SHYDRO=(STRESS(1)+STRESS(2)+STRESS(3))/THREE
        DO K1=1,NDI
         FLOW(K1)=(STRESS(K1)-SHYDRO)/SMISES
        END DO
        DO K1=NDI+1,NTENS
         FLOW(K1)=STRESS(K1)/SMISES
        END DO
        DO K1=1,NDI
         DPSTRAN(K1)=DPSTRAN(K1)+THREE/TWO*FLOW(K1)*DEQPL
         STRESS(K1)=FLOW(K1)*(SYIELD+HARD*DEQPL)+SHYDRO
        END DO
        DO K1=NDI+1,NTENS
         DPSTRAN(K1)=DPSTRAN(K1)+THREE/TWO*FLOW(K1)*DEP1
         STRESS(K1)=FLOW(K1)*(SYIELD+HARD*DEQPL)
        END DO
         DO K1=1,NTENS
           DSTRESS(K1)=STRESS(K1)-OLDS(K1)
         END DO
        EFFG=EG*(SYIELD+HARD*DEQPL)/SMISES
        EFFG2=TWO*EFFG
        EFFG3=THREE*EFFG
        EFFLAM=(EBULK3-EFFG2)/THREE
        EFFHRD=EG3*HARD/(EG3+HARD)-EFFG3
        DO K1=1,NDI
         DO K2=1,NDI
           DDSDDE(K2,K1)=EFFLAM
         END DO
           DDSDDE(K1,K1)=EFFG2+EFFLAM
        END DO
        DO K1=NDI+1,NTENS
           DDSDDE(K1,K1)=EFFG
        END DO
        DO K1=1,NTENS
         DO K2=1,NTENS
           DDSDDE(K2,K1)=DDSDDE(K2,K1)+EFFHRD*FLOW(K2)*FLOW(K1)
         END DO
        END DO
         RETURN
        END
C
C-----------------------------------------------------------------------
C       The next subroutine is to calculate Jacobian matrix using
C       the method decribed in Section 6.3-5
C
      SUBROUTINE GETDDSDDE(DDSDDE,DSTRAN,DES,STRESS,DSTRESS,ALPH,SYD,
     1 HH,NST,NED,NDI,NTENS,EG3,ZERO,ONE,TWO,THREE)
        INCLUDE 'ABA_PARAM.INC'
        DIMENSION DDSDDE(6,6),STRESS(NTENS),DSTRESS(NTENS),
```

```
1 DES(NTENS,NTENS),DSTRAN(NTENS),ALPH(4,NTENS),ALPHA1(6),ALPHA2(6),
2 DSTRESSI(6),DALPHA(6),DPSTRAN(6),DSTRANI(6),DDSDDI(2,6,6),DLT(2),
3 HH(5),SYD(5),DSTRAN0(6),FLOW(6),ALPHA(6),STRESSI(6),DSTRESSL(6)
      NSTN=NST
            DLT(1)=5.D-6
       CMAX=MAX(DSTRAN(1),DSTRAN(2),DSTRAN(3),DSTRAN(4),
1  DSTRAN(5),DSTRAN(6))
       CMIN=MIN(DSTRAN(1),DSTRAN(2),DSTRAN(3),DSTRAN(4),
1  DSTRAN(5),DSTRAN(6))
        IF(ABS(CMIN).GT.ABS(CMAX))THEN
            DLT(1)=-DLT(1)
        END IF
        DO K1=1,NTENS
            DSTRANI(K1)=DSTRAN(K1)
   END DO
DO 666 L1=1,1
DO 444 M1=1,NDI
   DO K1=1,NTENS
            STRESSI(K1)=STRESS(K1)
            DSTRANI(K1)=DSTRAN(K1)
   END DO
            DSTRANI(M1)=DSTRANI(M1)+DLT(L1)
 IF(NST.EQ.0)THEN
   NSTN=NST+1
  DO K1=1,NTENS
            DSTRESSI(K1)=ZERO
    DO K2=1,NTENS
DSTRESSI(K1)=DSTRESSI(K1)+DDSDDE(K1,K2)*DSTRANI(K2)
    END DO
  END DO
       DO K1=1,NTENS
        ALPHA(K1)=ALPH(1,K1)
       END DO
      CALL FINDTT(ALPHA,STRESS,DSTRESSI,SYD(1),NDI,NTENS,
1   THREE,TWO,ZERO,TT)
                DO K1=1,NTENS
              DSTRANI(K1)=(ONE-TT)*DSTRANI(K1)
              STRESSI(K1)=STRESS(K1)+TT*DSTRESSI(K1)
                END DO
      END IF
       IF(NED.GT.NSTN)THEN
       DO 400 JJ=NSTN,MIN(NED,4)-1
        DO K1=1,NTENS
            ALPHA1(K1)=ALPH(JJ,K1)
            ALPHA2(K1)=ALPH(JJ+1,K1)
            DSTRAN0(K1)=DSTRANI(K1)
        END DO
CALL GETDEQPL(DSTRANI,DERO,NDI,NTENS,TWO,THREE)
              DERO=ABS(DERO)*1.D-9
          IF(DERO.LT.1.D-13)THEN
           DERO=1.D-13
          END IF
C
        CALL MATZHU(DES,STRESSI,DSTRESSI,ALPHA1,ALPHA2,DALPHA,
   1 DSTRAN0,DPSTRAN,NDI,NTENS,SYD(JJ),SYD(JJ+1),HH(JJ),DERO,NEG,
   2 DSTRESSL,TL)
          DO K1=1,NTENS
            STRESSI(K1)=STRESSI(K1)+DSTRESSI(K1)
```

```
            END DO
             IF(NEG.EQ.0)THEN
                   GOTO 1000
             END IF
            DO K1=1,NTENS
                  DSTRANI(K1)=DSTRANI(K1)-DSTRAN0(K1)
            END DO
400     CONTINUE
     END IF
          IF(NED.LT.4)THEN
            DO K1=1,NTENS
                  ALPHA1(K1)=ALPH(NED,K1)
                  ALPHA2(K1)=ALPH(NED+1,K1)
                  DSTRAN0(K1)=DSTRANI(K1)
           END DO
 CALL GETDEQPL(DSTRANI,DER1,NDI,NTENS,TWO,THREE)
                  DERO=ABS(DER1)*1.D-9
         IF(DERO.LT.1.D-13)THEN
          DERO=1.D-13
         END IF
       CALL MATZHU(DES,STRESSI,DSTRESSI,ALPHA1,ALPHA2,DALPHA,
1 DSTRAN0,DPSTRAN,NDI,NTENS,SYD(NED),SYD(NED+1),HH(NED),DERO,NEG,
2 DSTRESSL,TL)
            IF(NEG.EQ.1)THEN
 CALL GETDEQPL(DSTRAN0,DER0,NDI,NTENS,TWO,THREE)
            CC=(DER1-DER0)/DER1
           DO K1=1,NTENS
                 DSTRESSI(K1)=DSTRESSI(K1)+CC*DSTRESSL(K1)/TL
           END DO
            END IF
   DO K1=1,NTENS
         STRESSI(K1)=STRESSI(K1)+DSTRESSI(K1)
   END DO
                        ELSE
 DO K1=1,NTENS
    DO K2=1,NTENS
          STRESSI(K1)=STRESSI(K1)+DDSDDE(K1,K2)*DSTRANI(K2)
    END DO
 END DO
          DO K1=1,NTENS
           ALPHA(K1)=ZERO
          END DO
CALL YIELDING(STRESSI,ALPHA,SMISES,NDI,NTENS,SIX,TWO,THREE)
 IF(NED.EQ.4)THEN
  SYIELD=SYD(4)
 HARD=HH(4)
          DEQPL=(SMISES-SYIELD)/(EG3+HARD)
                        ELSE
           SYIELD=((HH(4)-HH(5))*SYD(5)+HH(5)*SYD(4))/HH(4)
           HARD=HH(5)
           DEQPL=(SMISES-SYIELD)/(EG3+HARD)
          END IF
100       SHYDRO=(STRESSI(1)+STRESSI(2)+STRESSI(3))/THREE
          DO K1=1,NDI
           FLOW(K1)=(STRESSI(K1)-SHYDRO)/SMISES
          END DO
          DO K1=NDI+1,NTENS
           FLOW(K1)=STRESSI(K1)/SMISES
```

```
          END DO
          DO K1=1,NDI
           STRESSI(K1)=FLOW(K1)*(SYIELD+HARD*DEQPL)+SHYDRO
          END DO
          DO K1=NDI+1,NTENS
           STRESSI(K1)=FLOW(K1)*(SYIELD+HARD*DEQPL)
          END DO
           END IF
           DO K1=1,NTENS
            DSTRESSI(K1)=STRESSI(K1)-STRESS(K1)
           END DO
1000       DO M2=1,NTENS
                  DDSDDI(L1,M2,M1)=(DSTRESSI(M2)-DSTRESS(M2))/DLT(L1)
             END DO
444      CONTINUE
666    CONTINUE
            DO M1=1,NTENS
             DO M2=1,NTENS
            DDSDDE(M1,M2)=DDSDDI(1,M1,M2)
             END DO
            END DO
           RETURN
          END
```

Note:

1) XIT is an internal subroutine of ABAQUS to use before program stop.

2) ASET is an internal subroutine of ABAQUS to set matrix zero.

3) ROTSIG is an internal subroutine of ABAQUS to assign each components and adjust it with rotation caused by large deformation.

APPENDIX 6B

USER SUBROUTINE SIGINI FOR RESIDUAL STRESS INPUT

Subroutine for U-batch specimen residual stress input

```
      SUBROUTINE SIGINI(SIGMA,COORDS,NTENS,NCRDS,NOEL,NPT,LAYER)
C** --------IT IS A SUBROUTIN FOR INITIAL STRESS INPUT IN ABAQUS
c**-----the surface axial residual stress is -297.5 and tangential
c**-----residaul stress is -234.9
      INCLUDE 'ABA_PARAM.INC'
c---SIGMA(NTENS)--STRESS
C---COORDS--An array containing the initial coordinates of this point
c---Ntens--Number of stresses to be defined
C--Ncrds--Number of coordinates.
C--Noel--Element number
c--Npt--Material (constitutive) calculation point number in the element
c--Layer--Cross-section integration point number for beam or shell elements
C       IMPLICIT REAL*8(A-H,O-Z)
 DIMENSION SIGMA(NTENS),COORDS(NCRDS)
 DIMENSION CC(4),ST(3),FSCC(3,4)
 DATA CC/-280.347,265.199,-225.85,174.457/
  RR=COORDS(1)
  FSCC(1,1)=1.-RR**2
  FSCC(1,2)=1.-RR**3
  FSCC(1,3)=0.
  FSCC(1,4)=0.
 FSCC(2,1)=1.-3.*RR**2
 FSCC(2,2)=1.-4.*RR**3
 FSCC(2,3)=0.
 FSCC(2,4)=0.
  FSCC(3,1)=0.
  FSCC(3,2)=0.
  FSCC(3,3)=1.-2.*RR**2
  FSCC(3,4)=2.-5.*RR**3
DO 90 I=1,3
        ST(I)=0.
       DO 80 K=1,4
         ST(I)=ST(I)+CC(K)*FSCC(I,K)
80       CONTINUE
90     CONTINUE
       SIGMA(1)=ST(1)
       SIGMA(2)=ST(3)
       SIGMA(3)=ST(2)
       SIGMA(4)=0.
     RETURN
    END
```

Subroutine for HTS specimen residual stress input

```
      SUBROUTINE SIGINI(SIGMA,COORDS,NTENS,NCRDS,NOEL,NPT,LAYER)
C** --------IT IS A SUBROUTIN FOR INITIAL STRESS INPUT IN ABAQUS
c**----the differerence with sub-str1.f is for distribution of residual stress
c**----Sr=a+b*(r-q)^2, Sz=c+d*(r-q)
c**-----by changing cc(3), cc(4) with the factor 0.831932773=247.5/297.5
      INCLUDE 'ABA_PARAM.INC'
c---SIGMA(NTENS)--STRESS
C---COORDS--An array containing the initial coordinates of this point
c---Ntens--Number of stresses to be defined
C--Ncrds--Number of coordinates.
C--Noel--Element number
c--Npt--Material (constitutive) calculation point number in the element
c--Layer--Cross-section integration point number for beam or shell elements
c       IMPLICIT REAL*8(A-H,O-Z)
       DIMENSION SIGMA(NTENS),COORDS(NCRDS)
        RR=COORDS(1)
        q=0.84
        X=RR-q
        st1=350
        sz1=400
         b=st1/(2*(1-q))
          a=-b*(1-q)**2
           cc=0.5+q-q**2
            dd=(1-q)**2/2+q*(1-q)**3/3
          t=dd/cc
           d=sz1/(1-q-t)
            c=-d*t
           IF(RR.LE.q)THEN
             sr=a
             st=a
             sz=c
                   ELSE
            sr=a+b*X**2
            st=a+3*b*X**2+2*b*q*X
            sz=c+d*X
          END IF
       SIGMA(1)=sr
       SIGMA(2)=sz
       SIGMA(3)=st
       SIGMA(4)=0.
   RETURN
   END
```

Appendix 8A

DERIVATION OF DISTRIBUTION DENSITY FUNCTION—I

Assume that the probability of z can be expressed as

$$F(z) = \iint_{g(x,y)\le z} f(x,y)dxdy\,. \tag{A-1}$$

Then the differentiation of $F(z)$ is

$$f_z(z) = F'(z) = \lim_{\Delta z\to 0}\frac{F(z+\Delta z)-F(z)}{\Delta N} = \lim_{\Delta z\to 0}\frac{1}{\Delta z}\iint_{\Omega} f(x,y)dxdy\,. \tag{A-2}$$

where Ω is an area on X-Y plane

$$\Omega = \{z < g(x,y) \le z+\Delta z\} \tag{A-3}$$

From Figure A-1, it can be seen that the integration in Equation (A-2) can be transformed to

$$\iint_{\Omega} f(x,y)dxdy = \iint_{\Omega} f(x,y)dLdt\,. \tag{A-4}$$

The slope of the curve $g(x,y) = const$ at a point (x, y) is

$$k = -\frac{g'_x}{g'_y}. \tag{A-5}$$

Then the slope of normal of the curve $g(x,y) = const$ at the point (x, y) is

$$k' = -\frac{1}{k} = \frac{g'_y}{g'_x}. \tag{A-6}$$

On the other hand, the k' can be obtained in another way,

$$k' = \frac{\Delta y}{\Delta x} \tag{A-7}$$

Hence from Equations (A-6) and (A-7), it is found

$$\frac{\Delta y}{\Delta x} = \frac{g'_y}{g'_x} . \tag{A-8}$$

By differentiating the equation $g(x, y) = z$ of the curve, it is found

$$\Delta z = g'_x \Delta x + g'_y \Delta y . \tag{A-9}$$

Solving Equations (A-8) and (A-9), the following relationships among the increments Δx, Δy and Δz are obtained

$$\left.\begin{aligned} \Delta x &= \frac{g'_x}{g'^2_x + g'^2_y} \Delta z \\ \Delta y &= \frac{g'_y}{g'^2_x + g'^2_y} \Delta z \end{aligned}\right\} \tag{A-10}$$

It leads to

$$\Delta t = \sqrt{\Delta x^2 + \Delta y^2} = \frac{1}{\sqrt{g'^2_x + g'^2_y}} \Delta z . \tag{A-11}$$

Hence,

$$\begin{aligned} &\frac{1}{\Delta z} \iint_{\Omega} f(x, y) dx\, dy = \frac{1}{\Delta z} \iint_{\Omega} f(x, y) dL\, dt \approx \frac{1}{\Delta z} \int \left(\int dt \right) f(x, y) dL \\ &\approx \frac{1}{\Delta z} \int \Delta t\, f(x, y) dL \approx \int_L \frac{f(x, y)}{\sqrt{g'^2_x + g'^2_y}} dL \end{aligned} . \tag{A-12}$$

Then Equation (A-2) becomes

$$f_z(z) = \lim_{\Delta z \to 0} \frac{1}{\Delta z} \iint_{\Omega} f(x, y) dL dt = \int_L \frac{f(x, y)}{\sqrt{g'^2_x + g'^2_y}} dL . \tag{A-13}$$

where L is a curve,

$$L = \{ g(x, y) = z \quad . \tag{A-14}$$

Appendix 8B

DERIVATION OF DISTRIBUTION DENSITY FUNCTION—II

A parametric equation for $g(x, y) = z$ may be expressed as

$$\begin{cases} x = x \\ y = y(x) \end{cases}. \tag{B-1}$$

The curve integration Equation (A-13) becomes,

$$f_z(z) = \int_L \frac{f(x,y)}{\sqrt{g_x'^2 + g_y'^2}} dL = \int_L \frac{f(x,y)}{\sqrt{g_x'^2 + g_y'^2}} \sqrt{1 + y'^2}\, dx\,. \tag{B-2}$$

Differentiating equation $g(x, y) = z$, where z is treated as a constant, it is found that

$$g_x' + g_y' y' = 0\,. \tag{B-3}$$

It leads to

$$y' = -\frac{g_x'}{g_y'}. \tag{B-4}$$

Inserting Equation (B-4) into Equation (B-2), The curve integration finally becomes,

$$f_z(z) = \int_L \frac{f(x,y)}{|g_y'|} dx \tag{B-5}$$

Appendix 8C

DERIVATION OF DISTRIBUTION DENSITY FUNCTION—III

Assume x is a random variable defined in the range (x_a, x_b) which distribution density is $f_X(x)$. The probability of x is

$$F_X(x) = P(X \le x) = \int_{x_a}^{x} f_X(x)dx \,. \tag{C-1}$$

For a random variable y, its functional relationship with x is

$$\begin{aligned} &x = g(y) \quad g'(y) > 0 \ \text{or} \ g'(y) < 0 \quad y \in (y_a, y_b) \\ &x_a = g(y_a) \quad x_b = g(y_b) \\ &\textit{and its reverse function: } y = h(x) \end{aligned} \tag{C-2}$$

Then for $g'(y) > 0$, the probability of y is

$$\begin{aligned} F_Y(y) &= P(Y \le y) = P(h(X) \le y) = P(X \le g(y)) \\ &= \int_{x_a}^{g(y)} f_X(x)dx = \int_{y_a}^{y} f_X(g(y)g'(y)dy \end{aligned} \tag{C-3}$$

The probability density of y is obtained

$$f_Y(y) = f_X(g(y)g'(y)) \,. \tag{C-4}$$

With the same way, for $g'(y) < 0$, the probability of y is found

$$f_Y(y) = f_X(g(y)[-g'(y)] \,. \tag{C-5}$$

Consequently, combining equations (C-4) and (C-5), the probability density of y is

$$f_Y(y) = f_X(g(y)|g'(y)| \,. \tag{C-6}$$

Table 3.1. Material chemical composition for mild steel En15R, (%) by weight

C	Si	S	P	Mn	Ni	Cr	Mo
0.4	0.17	0.004	0.022	1.59	0.17	0.07	0.02

Note: The remainder is Fe.

Table 3.2. Mechanical test results of a bar sample of En15R for cyclic loading from ROVER (Devlukia, 1993b).

σ_U	$\sigma_{0.5}$	A^*/A_0	δ	E	E_t	n
831 MPa	583 MPa	21%	60%	195 GPa	1.25 GPa	0.14

Note: σ_U – ultimate stress; $\sigma_{0.5}$ – tensile stress plastic strain 0.5%;
A_0 – area of cross section; A^* – area of cross section after fracture;
δ – $(L - L_0)/L_0$, L_0 is gauge length and L is the gauge length after fracture;
E – Young's Modulus; E_t – linear hardening modulus;.
n – Hardening exponent

Table 3.3. Specimens and Tests.

Specimens	X-ray diffraction	Neutron diffraction	Centre hole	Mechanical loading	Hardness	Roughness	Fatigue test
U01	√	√					
U02	√				√		
U03	√				√		
U04	√						
U05	√		√				
U06	√	√		√			
U07	√				√		
U08	√						
U09	√	√			√		
U10	√	√		√			
U11	√		√				
U12	√				√		
U13	√	√			√		
U14	√			√			
U15	√		√		√		
U16	√						
U17	√				√		
U18	√	√			√		
U19	√			√			
U20	√	√			√		

Note: U8 had been cut to examine microstructure .

Table 3.3. Continued.

Specimens	X-ray diffraction	Neutron diffraction	Centre hole	Mechanical loading	Hardness	Roughness	Fatigue test
Suspension arm No 37	√						
Suspension arm No 38	√						
Suspension arm No 39	√						
Square bar 1	√		√				
Square bar 2	√		√				
AF01	√	√				√	√
AF02	√					√	√
AF03	√					√	√
AF04	√						
AF05	√					√	√
AF06	√					√	√
AF07	√					√	√
AF08	√					√	
AF09	√	√				√	√
AF10	√	√				√	√
AF11	√					√	√
AF12	√					√	√
AF13	√	√				√	√
AF14	√					√	√
AF15	√					√	√
AF16	√					√	√
AF17	√						
AF18	√	√					
AF19	√						
AF20	√	√					
HT01	√	√				√	√
HT02	√					√	√
HT03	√					√	√
HT04	√					√	√
HT05	√					√	√
HT06	√					√	√
HT07	√					√	√
HT08	√					√	
HT09	√	√				√	√
HT10	√	√				√	√

Table 3.3. Continued.

Specimens	X-ray diffraction	Neutron diffraction	Centre hole	Mechanical loading	Hardness	Roughness	Fatigue test
HT11	√					√	√
HT12	√					√	√
HT13	√	√				√	√
HT14	√					√	√
HT15	√					√	√
HT16	√						
HT17	√						
HT18	√	√					
HT19	√			√			
HT20	√	√					
FS01	√				√	√	√
FS02	√				√	√	√
FS03	√				√	√	√
FS04	√				√	√	√
FS05	√				√	√	
FS06	√				√	√	√
FS07	√				√	√	√
FS08	√				√	√	√
FS09	√				√	√	√
FS10	√				√	√	√
FS11	√				√	√	√
FS12	√				√	√	√
FS13	√				√	√	√
FS14	√				√	√	√
FS15	√				√	√	√
FS16	√		√		√		
FS17	√				√		
FS18	√		√		√		
FS19	√				√		
FS20	√				√		

Table 3.3. Continued.

Specimens	X-ray diffraction	Neutron diffraction	Centre hole	Mechanical loading	Hardness	Roughness	Fatigue test
HTS01	√				√	√	√
HTS02	√				√	√	√
HTS03	√				√	√	√
HTS04	√				√	√	√
HTS05	√				√	√	√
HTS06	√				√	√	√
HTS07	√				√	√	√
HTS08	√				√	√	√
HTS09	√		√		√		
HTS10	√				√	√	√
HTS11	√				√	√	√
HTS12	√				√	√	
HTS13	√				√	√	√
HTS14	√				√	√	√
HTS15	√				√	√	√
HTS16	√				√	√	√
HTS17	√		√		√		
HTS18	√	√		√	√		
HTS19	√	√			√		
HTS20	√		√		√		
HTS22	√	√					
HTS24	√						

Note: HTS24 and HTS05 had been layer removed using chemical etching.

Table 4.1. Measurements of residual stress on the stress free plate at a random location.

Measurement No.	σ , MPa	STD, MPa
1	-19	6
2	-31	11
3	-21	2
4	-40	8
5	-55	12
6	-50	6
7	-34	5

Note: STD is standard deviation when using regression method using equation (4.7) to obtain residual stresss σ_ϕ.

Table 4.2. Repeat measurements of axial residual stress on the round bar specimen U1 at the location M1.

Measurement No.	σ MPa	STD MPa	Time interval	Note
1	-304	6		After test, the bar was taken away
2	-312	11	17 days later	The bar was re-installed in X-ray rig.
3	-303	9	2 hours later	The bar wasn't moved.
4	-316	11	2 hours later	The bar wasn't moved.
5	-299	11	19 hours later	The bar wasn't moved.
6	-289	7	2 hours later	The bar wasn't moved.
7	-304	15	17 hours later	The bar wasn't moved.
8	-305	6	2 hours later	The bar wasn't moved.
9	-291	8	4 hours later	The bar was re-installed again in X-ray rig.

Note: STD is standard deviation when using regression method using equation (4.7) to obtain residual stresss σ_ϕ.

Table 4.3 Residual stresses in suspension arms and rectangular bars measured by X-ray diffraction.

No.	σ_{xx} MPa	σ_{45} MPa	σ_{yy} MPa		τ_{xy} MPa	σ_1 MPa	σ_2 MPa	Principal direction, θ
SA 37	-249	-261	-219		27	-204	-265	20°
SA 38	-255	-316	-263		56	-203	-316	10°
SA 39	-217	-243	-243		-22	-205	-255	20°
Bar 1	-154	-152	-165		8	-150	-169	20°
Bar 2	-280	-295	-274		-18	-259	-295	22°

Note: SA: Suspension arm
Bar 1: Hot forged rectangular bar, not shot blasted.
Bar 2: Hot forged rectangular bar, shot blasted.

Table .4.4 Residual stresses in round bar U1 measured by X-ray diffraction. (see Fig. 4.5)

Location	Hoop σ_{xx} MPa	σ_{45} MPa	Axial σ_{yy} MPa		τ_{xy} MPa	σ_1 MPa	σ_2 MPa	Principal direction θ
T1	-277	-242	-294		43	-241	-329	22°
B1	-279	-250	-285		32	-249	-314	22°
M1	-277	-182	-305		108	-181	-400	22°
M2	-261	-172	-182		50	-158	-285	19°
M3	-318	-304	-306		-7	-302	-321	19°
M4	-288	-181	-296		111	-181	-402	23°

Table 4.5. Residual stresses in MPa of U-batch round bar specimens measured by X-ray diffraction.

specimen No.	Hoop σ_{xx} MPa	σ_{45} MPa	Axial σ_{yy} MPa		τ_{xy} MPa	σ_1 MPa	σ_2 MPa	Principal direction 0
U1	-277	-182	-305		108	-181	-400	22°
U2	-240	-224	-302		47	-214	-327	20°
U3	-315	-244	-274		51	-240	-349	22°
U4	-291	-281	-329		29	-275	-345	20°
U5	-204	-225	-261		7	-203	-262	7°
U6	-150	-212	-276		1	-150	-276	0.5°
U7	-185	-208	-284		26	-179	-290	13°
U8	-205	-238	-255		-8	-204	-256	9°
U9	-246	-226	-286		40	-222	-311	21°
U10	-186	-151	-177		31	-151	-212	23°
U11	-270	-219	-303		67	-218	-356	22°
U12	-261	-245	-249		10	-243	-267	20°
U13	-222	-281	-328		-6	-221	-328	2°
U14	-224	-255	-270		-8	-223	-271	9°
U15	-195	-261	-339		6	-194	-340	2°
U16	-220	-182	-238		47	-181	-277	22°
U17	-242	-228	-321		53	-220	-343	20°
U18	-246	-319	-346		-23	-241	-351	11°
U19	-316	-279	-298		28	-277	-337	22°
U20	-302	-210	-292		87	-210	-384	22.5°

Table 4.6 Axial residual stresses of AF bars by X-ray diffraction.

Specimen No.	Side A, MPa	Side B, MPa
AF01	-17	24
AF02	26	19
AF03	-2	-43
AF04	4	-2
AF05	-32	-12
AF06	-28	-27
AF07	-25	-25
AF08	36	0
AF09	-11	-23
AF10	-15	-25
AF11	59	22
AF12	-35	-6
AF13	-2	26
AF14	-48	-32
AF15	-41	-59
AF16	-36	-49
AF17	-53	-69
AF18	-37	-21
AF19	45	-6
AF20	-45	-64

Note that side A and side B correspond to locations M1 M3 in Figure 4.4

Table 4.7 Axial residual stresses of FS bars by X-ray diffraction.

Specimen No.	Side A, MPa	Side B, MPa
FS01	-293	-369
FS02	-232	-214
FS03	-252	-307
FS04	-298	-321
FS05	-273	-232
FS06	-357	-285
FS07	-268	-279
FS08	-259	-272
FS09	-272	-314
FS10	-243	-186
FS11	-289	-328
FS12	-238	-271
FS13	-269	-299
FS14	-277	-261
FS15	-326	-286
FS16	-313	-337
FS17	-235	-260
FS18	-233	-200
FS19	-238	-229
FS20	-252	-215

Note that side A and side B correspond to locations M1 M3 in Figure 4.4

Table 4.8. Axial residual stresses of HT bars by X-ray diffraction.

Specimen No.	Side A, MPa	Side B, MPa
HT01	-59	-27
HT02	-21	-35
HT03	-23	-25
HT04	-14	-30
HT05	-11	-10
HT06	-33	-41
HT07	-17	-23
HT08	-32	-13
HT09	-24	-11
HT10	-23	-25
HT11	-15	-26
HT12	-44	-32
HT13	-25	-20
HT14	-9	-22
HT15	-14	-17
HT16	-47	-29
HT17	-23	-31
HT18	-11	-26
HT19	-18	-25
HT20	-24	-35

Note that side A and side B correspond to locations M1 M3 in Figure 4.4

Table 4.9. Axial residual stresses of HTS bars by X-ray diffraction.

Specimen No.	Side A, MPa	Side B, MPa
HTS01	-447	-347
HTS02	-335	-371
HTS03	-334	-410
HTS04	-291	-293
HTS05	-363	-318
HTS06	-383	-318
HTS07	-376	-391
HTS08	-347	-416
HTS09	-376	-355
HTS10	-404	-349
HTS11	-424	-377
HTS12	-383	-363
HTS13	-393	-276
HTS14	-469	-474
HTS15	-331	-328
HTS16	-397	-441
HTS17	-333	-405
HTS18	-375	-348
HTS19	-353	-358
HTS20	-404	-447

Note that side A and side B correspond to locations M1 M3 in Figure 4.4

Table 4.10 Axial residual stress measurements for HTS18 by X-ray with surface layer removal by chemical method.

Steps	Diameter mm	Residual stress MPa
original diameter	8.30	-348
after cyclic load (10000με)	8.30	-183
after 1st corrosion	8.24	-30
after 2nd corrosion	6.74	73
Note: HTS18 had been subjected to cyclic mechanical loading and shown to be stress free by hole-drilling method		

Table 4.11 Axial residual stress measurements for HTS05 by X-ray with surface layer removal by chemical etching method.

Steps	Diameter mm	Side A. MPa	Side B MPa
original diameter	8.56	-363	-319
after fatigue (2200με)	8.56	-316	-354
after 1st corrosion	8.46	-353	-309
after 2nd corrosion	8.38	-263	-226
after 3rd corrosion	8.30	-219	-217
after 4th corrosion	7.88	-118	-104
Note: HTS05 had been subjected to cyclic fatigue with strain range being $\frac{\Delta\varepsilon}{2} = 2200\mu\varepsilon$, $N_f = 518054$			

Table 4.12 Axial residual stress measurements for HTS24 by X-ray with surface layer removal using chemical etching method.

Diameter mm	$\sigma'_{z,f}$, Side A. MPa	$\sigma'_{z,f}$, Side B MPa	$\sigma'_{\theta,f}$, Side A. MPa	$\sigma'_{\theta,f}$, Side B MPa
8.44	-440	-375	-393	-337
8.25	-383	-317	-360	-280
8.13	-401	-343	-309	-262
7.90	-361	-310	-306	-327
7.64	-203	-192	-157	-177
7.40	-48	-58	-48	-63
7.20	-3	-14	-1	-9

Table 4.13 Fitted constants a, b and c in equations (4.22) and (4.26) for residual stress distribution in HTS24 by X-ray with surface layer removal using chemical etching method.

Constants	for axial Side A.	for axial Side B	for hoop Side A.	for hoop, Side B
a	83.785	68.378	37.421	34.327
b	-6.827E+4	-5.229E+4	-1.932E+3	-1.905E+3
c	3.001E+5	2.166E+5	2.938E+3	3.528E+3

Table 4.14 Coefficient matrix A_{ji} for a round bar specimen with bar diameter 8mm, hole diameter 1.74 mm, drilling increment 0.08mm, strain gauge type TEA-06-062RK-120, gauge 1 in hoop direction and gauge 3 in axial direction.

	i=1	i=2	i=3	i=4	i=5
j=1	-.0897 .0158 .0194 -.0353 -.0265 -.1323 .0193 -.0846 .0000				
j=2	-.1096 .0162 .0205 -.0442 -.0330 -.1600 .0226 -.1041 .0000	-.1022 .0185 .0278 -.0376 -.0282 -.1405 .0215 -.0857 .0000			
j=3	-.1287 .0174 .0224 -.0520 -.0384 -.1846 .0258 -.1186 .0000	-.1216 .0200 .0304 -.0461 -.0344 -.1676 .0253 -.1044 .0000	-.1142 .0211 .0357 -.0377 -.0277 -.1425 .0233 -.0831 .0000		
j=4	-.1521 .0194 .0295 -.0587 -.0428 -.2068 .0292 -.1308 .0000	-.1449 .0226 .0373 -.0528 -.0389 -.1904 .0292 -.1179 .0000	-.1410 .0241 .0438 -.0460 -.0337 -.1697 .0279 -.1018 .0000	-.1195 .0231 .0414 -.0362 -.0257 -.1399 .0249 -.0788 .0000	
j=5	-.1644 .0216 .0336 -.0641 -.0463 -.2256 .0324 -.1404 .0000	-.1581 .0249 .0413 -.0582 -.0424 -.2094 .0325 -.1282 .0000	-.1556 .0266 .0479 -.0516 -.0374 -.1895 .0315 -.1134 .0000	-.1389 .0258 .0464 -.0439 -.0312 -.1650 .0293 -.0957 .0000	-.1082 .0239 .0347 -.0337 -.0232 -.1335 .0254 -.0720 .0000
j=6	-.1767 .0239 .0370 -.0687 -.0490 -.2421 .0352 -.1483 .0000	-.1708 .0274 .0447 -.0628 -.0452 -.2258 .0354 -.1364 .0000	-.1690 .0293 .0513 -.0563 -.0404 -.2063 .0345 -.1224 .0000	-.1542 .0289 .0500 -.0491 -.0346 -.1832 .0328 -.1061 .0000	-.1288 .0276 .0392 -.0410 -.0284 -.1574 .0298 -.0878 .0000
j=7	-.1887 .0261 .0401 -.0726 -.0512 -.2561 .0376 -.1546 .0000	-.1829 .0299 .0477 -.0666 -.0473 -.2399 .0379 -.1430 .0000	-.1814 .0320 .0543 -.0601 -.0426 -.2205 .0372 -.1294 .0000	-.1673 .0318 .0532 -.0531 -.0371 -.1981 .0356 -.1139 .0000	-.1438 .0310 .0427 -.0456 -.0313 -.1736 .0331 -.0971 .0000
j=8	-.1992 .0280 .0430 -.0757 -.0529 -.2680 .0397 -.1598 .0000	-.1936 .0321 .0505 -.0697 -.0490 -.2517 .0401 -.1483 .0000	-.1921 .0344 .0572 -.0632 -.0443 -.2324 .0395 -.1349 .0000	-.1784 .0344 .0561 -.0563 -.0389 -.2102 .0380 -.1199 .0000	-.1557 .0338 .0458 -.0490 -.0333 -.1865 .0357 -.1039 .0000
j=9	-.2079 .0296 .0456 -.0783 -.0542 -.2780 .0415 -.1639 .0000	-.2023 .0339 .0531 -.0722 -.0502 -.2616 .0420 -.1525 .0000	-.2009 .0364 .0597 -.0657 -.0455 -.2423 .0414 -.1392 .0000	-.1873 .0365 .0587 -.0588 -.0402 -.2202 .0400 -.1245 .0000	-.1649 .0361 .0484 -.0517 -.0348 -.1968 .0379 -.1089 .0000
j=10	-.2145 .0308 .0479 -.0803 -.0551 -.2860 .0429 -.1670 .0000	-.2090 .0353 .0554 -.0742 -.0511 -.2696 .0435 -.1557 .0000	-.2077 .0379 .0620 -.0677 -.0464 -.2502 .0430 -.1425 .0000	-.1941 .0382 .0609 -.0608 -.0411 -.2282 .0417 -.1279 .0000	-.1719 .0379 .0507 -.0538 -.0357 -.2049 .0396 -.1126 .0000

Table 4.14 Continued

	i=6	i=7	i=8	i=9	i=10
j=6	-.1025 .0247 .0334 -.0307 -.0199 -.1254 .0256 -.0650 .0000				
j=7	-.1234 .0290 .0378 -.0374 -.0244 -.1472 .0299 -.0794 .0000	-.0935 .0248 .0323 -.0271 -.0163 -.1152 .0254 -.0575 .0000			
j=8	-.1372 .0323 .0411 -.0414 -.0269 -.1615 .0330 -.0875 .0000	-.1132 .0293 .0365 -.0332 -.0203 -.1349 .0296 -.0704 .0000	-.0813 .0241 .0306 -.0235 -.0128 -.1041 .0249 -.0500 .0000		
j=9	-.1473 .0348 .0438 -.0443 -.0285 -.1725 .0353 -.0933 .0000	-.1251 .0323 .0396 -.0366 -.0223 -.1474 .0324 -.0775 .0000	-.0988 .0283 .0345 -.0288 -.0162 -.1216 .0288 -.0614 .0000	-.0674 .0227 .0288 -.0198 -.0095 -.0926 .0241 -.0429 .0000	
j=10	-.1546 .0367 .0462 -.0465 -.0296 -.1810 .0372 -.0974 .0000	-.1332 .0344 .0421 -.0390 -.0236 -.1566 .0345 -.0823 .0000	-.1086 .0309 .0373 -.0317 -.0178 -.1321 .0313 -.0673 .0000	-.0821 .0266 .0324 -.0244 -.0123 -.1076 .0277 -.0525 .0000	-.0534 .0209 .0270 -.0162 -.0064 -.0806 .0230 -.0358 .0000

Table 4.15 Results of strain measurement by hole-drilling method, with using the larger strain gauge rosette TEA-06-062RK-120

Drilling depth (mm)		0.16	0.32	0.48	0.65	0.8	0.97	1.29	1.61
Stress free plate	ε_1	1	0	0	-1	-2	-2	-3	-4
	ε_2	1	1	0	0	0	-1	-2	-4
	ε_3	0	0	0	0	-1	-1	-2	-3
Non-shot blasted bar: 1st test	ε_1	45	66	78	84	87	88	94	98
	ε_2	46	73	87	87	82	76	70	69
	ε_3	55	83	95	85	71	57	42	38
Non-shot blasted bar: 2nd test	ε_1	55	115	145	158	109	106	122	129
	ε_2	49	88	107	110	61	55	58	57
	ε_3	48	87	103	103	50	41	39	33
Shot blasted bar: 1st test	ε_1	43	117	168	210	239	271	273	272
	ε_2	39	105	143	174	193	222	226	227
	ε_3	72	154	203	240	277	326	330	329
Shot blasted bar: 2nd test	ε_1	114	190	240	280	303	319	335	339
	ε_2	94	148	192	227	245	260	277	283
	ε_3	108	177	228	268	288	302	317	321
Round bar No. U11:	ε_1	-5	43	153	272	322	343	360	350
	ε_2	20	107	202	286	334	385	412	468
	ε_3	2	59	160	240	272	280	270	262
Round bar No. U5: 1st test	ε_1	67	160	239	310	348	375	400	399
	ε_2	87	172	237	290	319	339	349	346
	ε_3	206	297	346	372	384	390	392	388

Drilling depth (mm)		0.08	0.16	0.24	0.32	0.40	0.48	0.56	0.65	0.73	0.8
Round bar No. U5: 2nd test	ε_1	22	72	122	163	202	241	268	289	304	320
	ε_2	18	54	89	120	147	176	202	226	247	268
	ε_3	23	64	107	140	165	187	199	205	208	208

Table 4.16 Hardness measurement of round bar specimens from HTS batch. Vickers Pyramid Numerals

Specimen No.	Side A	Side B
HTS01	293	281
HTS02	281	298
HTS03	301	301
HTS04	293	285
HTS05	307	293
HTS06	299	285
HTS07	290	283
HTS08	277	292
HTS09	280	271
HTS10	285	301
HTS11	305	308
HTS12	305	285
HTS13	275	263
HTS14	298	298
HTS15	289	293
HTS16	290	298
HTS17	298	282
HTS18	301	295
HTS19	290	287
HTS20	317	323

Table 4.17 Hardness measurement of round bar specimens from FS batch. Vickers Pyramid Numerals

Specimen No.	Side A	Side B
FS01	249	263
FS02	246	254
FS03	261	274
FS04	283	280
FS05	266	255
FS06	263	263
FS07	275	251
FS08	253	256
FS09	268	252
FS10	266	253
FS11	293	272
FS12	258	249
FS13	247	265
FS14	261	264
FS15	263	251
FS16	266	269
FS17	278	241
FS18	269	262
FS19	240	255
FS20	245	263

Table 4.18 Hardness measurement of round bar specimens from U-batch. Vickers Pyramid Numerals

Specimen No.	Axial residual stress	Hardness
U02	-302	261
U03	-274	254
U07	-284	264
U09	-286	251
U12	-249	251
U13	-328	260
U15	-339	271
U17	-321	271
U18	-346	268
U20	-292	256

Table 4.19 Surface roughness K-factor of forged specimens AF and FS

Sample reference	Ra (μm)	Rt (μm)	Ksf	Sample reference	Ra (μm)	Rt (μm)	Ksf
AF01-A	6.22	42.9	0.768	FS01-A	7.83	46.4	0.762
AF01-B	5.44	43.5	0.769	FS01-B	7.10	55.4	0.745
AF02-A	6.25	48.5	0.757	FS02-A	7.73	56.5	0.743
AF02-B	6.42	41.8	0.771	FS02-B	8.52	71.0	0.722
AF03-A	5.24	34.0	0.791	FS03-A	7.30	60.3	0.737
AF03-B	3.11	22.2	0.830	FS03-B	7.68	48.0	0.758
AF05-A	6.69	49.4	0.756	FS04-A	7.07	46.9	0.761
AF05-B	3.83	25.4	0.818	FS04-B	6.73	46.1	0.762
AF06-A	4.75	36.4	0.784	FS05-A	8.26	60.3	0.737
AF06-B	2.84	20.7	0.837	FS05-B	7.48	56.8	0.743
AF07-A	7.27	61.6	0.736	FS05-A	6.78	46.9	0.761
AF07-B	3.82	32.2	0.796	FS06-B	10.68	72.3	0.720
AF08-A	4.83	47.5	0.759	FS07-A	6.89	54.8	0.746
AF08-B	3.29	28.6	0.807	FS07-B	5.31	39.1	0.778
AF09-A	3.07	22.1	0.831	FS08-A	7.09	65.2	0.730
AF09-B	2.90	21.5	0.833	FS08-B	8.4	55.8	0.744
AF10-A	4.32	29.6	0.803	FS09-A	8.06	47.8	0.759
AF10-B	4.62	35.1	0.788	FS09-B	9.24	55.1	0.746
AF11-A	3.91	26.3	0.814	FS10-A	7.64	44.7	0.765
AF11-B	5.00	36.7	0.783	FS10-B	7.04	50.6	0.753
AF12-A	2.60	19.7	0.841	FS11-A	9.54	80.8	0.710
AF12-B	5.06	37.0	0.783	FS11-B	8.19	53.7	0.749
AF13-A	5.54	60.4	0.737	FS12-A	7.14	48.3	0.758
AF13-B	3.62	20.6	0.837	FS12-B	6.33	39.1	0.778
AF14-A	3.02	22.2	0.830	FS13-A	8.51	51.9	0.751
AF14-B	3.87	44.8	0.765	FS13-B	7.79	66	0.729
AF15-A	3.66	25.8	0.816	FS14-A	7.04	39.5	0.777
AF15-B	3.70	23.3	0.826	FS14-B	8.54	58.7	0.741
AF16-A	3.54	30.5	0.801	FS15-A	6.78	61.9	0.735
AF16-B	3.83	24.6	0.821	FS15-B	7.31	47.3	0.762

Table 4.20 Surface roughness K-factor of forged specimens HT and HTS

Sample reference	Ra (μm)	Rt (μm)	Ksf	Sample reference	Ra (μm)	Rt (μm)	Ksf
HT01-A	5.87	41.1	0.773	HTS01-A	5.34	36.9	0.783
HT01-B	4.71	29.6	0.803	HTS01-B	5.85	41.5	0.772
HT02-A	4.47	28.1	0.808	HTS02-A	7.49	46.2	0.762
HT02-B	4.14	34.0	0.791	HTS02-B	9.01	45.4	0.764
HT03-A	3.76	27.2	0.811	HTS03-A	6.91	47.6	0.761
HT03-B	4.67	34.4	0.789	HTS03-B	7.23	36.9	0.783
HT04-A	4.08	27.1	0.812	HTS04-A	7.19	42.1	0.771
HT04-B	5.45	45.8	0.763	HTS04-B	7.45	50.2	0.754
HT05-A	4.28	27.7	0.809	HTS05-A	5.18	33.2	0.793
HT05-B	4.55	33.1	0.793	HTS05-B	5.52	39.7	0.776
HT06-A	3.06	20.3	0.839	HTS05-A	6.43	43.5	0.768
HT06-B	4.80	37.5	0.781	HTS06-B	8.22	48.6	0.757
HT07-A	4.28	24.7	0.820	HTS07-A	7.02	44.5	0.765
HT07-B	3.41	23.4	0.825	HTS07-B	6.32	42.7	0.769
HT08-A	3.68	33.8	0.791	HTS08-A	6.12	35.6	0.786
HT08-B	3.99	30.5	0.801	HTS08-B	6.44	48.5	0.757
HT09-A	4.48	28.9	0.806	HTS10-A	6.23	40.8	0.774
HT09-B	4.46	46.4	0.762	HTS10-B	7.61	39.6	0.776
HT10-A	4.68	29.1	0.805	HTS11-A	4.45	29.6	0.803
HT10-B	3.84	25.1	0.819	HTS11-B	5.70	48.4	0.758
HT11-A	4.47	37.8	0.781	HTS12-A	5.40	37.7	0.781
HT11-B	3.57	25.3	0.818	HTS12-B	5.12	52.5	0.751
HT12-A	3.83	34.4	0.789	HTS13-A	6.57	50.0	0.755
HT12-B	3.37	26.0	0.816	HTS13-B	7.83	45.1	0.764
HT13-A	3.49	36.7	0.783	HTS14-A	6.77	38.8	0.778
HT13-B	4.76	31.9	0.796	HTS14-B	5.60	40.1	0.775
HT14-A	3.94	30.5	0.801	HTS15-A	7.50	56.1	0.744
HT14-B	4.10	31.3	0.798	HTS15-B	8.52	51.8	0.751
HT15-A	4.66	33.4	0.792	HTS16-A	6.06	42.0	0.771
HT15-B	4.16	29.4	0.804	HTS16-B	5.69	39.3	0.777

Table 4.21 Parameters of normal distribution for Rt and Ksf

	Rt (μm)				Ksf			
	HT	HTS	AF	FS	HT	HTS	AF	FS
Mean	31.48	43.16	33.83	54.24	0.799	0.769	0.796	0.749
STD	6.13	6.10	11.84	10.04	0.0176	0.0133	0.0313	0.0169

Table 4.22 Axial residual stress change on the surface before and after polish measured by X-Ray. MPa

	HTS09		U15		AF04	
	Side A	Side B	Side A	Side B	Side A	Side B
Before polish	-376	-355	-279	-336	4	-2
1st polish 0.15-0.2 mm (in axial)	-456	-443	-394	-367	-190	-157
2nd polished 0.1 mm (in tangential)					-214	-198

Table 5.1 The average of the measured axial, tangential and radial stresses used in the fitting for the specimens U1, U9, U10, U13, U18 and U20.

Location, r/R	0	0.5	1.0
$\bar{\sigma}_r$, MPa	-25.2	18.77	0
$\bar{\sigma}_\theta$, MPa	-25.2	25.32	-241.5
$\bar{\sigma}_z$, MPa	119.39	156.34	-286.5

Table 5.2 The constants, in Equation (5.21), obtained from solving Equation (5.25).

C_1	C_2	C_3	C_4
-267.44	311.644	334.181	-577.537

Table 6.1 Plastic deformation and axial residual stress change due to tensile mechanical loading for specimens U14 and U19.

	U14				U19	
	Side A		Side B		Side A	
	ε, με	σ_R, MPa	ε, με	σ_R, MPa	ε, με	σ_R, MPa
Original	0	-235	0	-252	0	-298
1st plastic deformed	2200	-245	2746	-217	3955	-169
2nd plastic deformed	3517	-229	4203	-179		
3rd plastic deformed	3925	-143	5076	-115		

Note: ε -- surface axial tensile strain

σ_R -- surface axial residual stress

Table 6.2 Plastic deformation and residual stress change due to tensile mechanical loading for specimen U10.

	Side A				Side B			
Loading Steps	ε, axial με	σ_R, axial MPa	$\sigma_{R.}$, 45° MPa	σ_R, hoop MPa	ε, axial με	σ_R, axial MPa	$\sigma_{R.}$, 45° MPa	σ_R, hoop MPa
Original.	0	-255	-235	-248	0	-240	-235	-248
1st	4257	-110	-202	-257	6633	-69	-170	-234
2nd	4375	-166	-237	-224	7305	-133	-203	-238
3rd	4531	-104	-179	-260	7578	-102	-178	-263
4th	5195	-88	-185	-238	8383	-47	-156	-220
5th	5508	-71	-152	-228	9180	-15	-151	-242

Table 6.3 Plastic deformation and residual stress change due to cyclic mechanical loading for specimen U06.

	Side A		Side B	
Loading Steps	Plastic Strain Range, $\Delta\varepsilon_p$, με	Axial Stress, MPa	Plastic Strain Range $\Delta\varepsilon_p$, με	Axial Stress, MPa
Original	0	-296	0	-234
1	1330	-232	1280	-193
2	5100	-183	5330	-158
3	6700	-200	6700	-204
4	8400	-127	8300	-159
10	9000	-156	9000	-134

Table 6.4 Plastic deformation and residual stress change due to cyclic mechanical loading for specimen HTS18.

	Side A		Side B	
Loading Steps	Plastic Strain Range, $\Delta\varepsilon_p$, με	Axial Stress, MPa	Plastic Strain Range. $\Delta\varepsilon_p$, με	Axial Stress. MPa
Original	0	-375	0	-348
1	4100		4100	
2	12600	-169	12600	-207
4	13000-14000	-217	13000-14000	-206
9	12500-13000	-208	12500-13000	-180

Table 6.5 Constants of linear kinematic model for U-batch and HTS group

Batch	Young's Modulus	Poisson's ratio	Radius of yielding surface	Hardening Modulus, H
U	208 GPa	0.28	538 MPa	22.7 GPa
HTS	208 GPa	0.28	653 MPa	24.1 GPa

Table 6.6 Parameters of multilinear kinematic model for HTS and U batches.

	HTS	U
Young's Modulus	208 GPa	208 GPa
Poisson's ratio	0.28	0.28
Initial yielding stress σ_{y1} in initial tension	$\sigma_{y1} = 800\,MPa$	$\sigma_{y1} = 600\,MPa$
Second yielding stress σ_{y2} in initial tension and corresponding tensile plastic strain ε_{p1}, and hardening Modulus HI_1 between σ_{y1} and σ_{y2}	$\sigma_{y2} = 835\,MPa$ $\varepsilon_{p1} = 400\mu\varepsilon$ $HI_1 = 87.5\,GPa$	$\sigma_{y2} = 670\,MPa$ $\varepsilon_{p1} = 500\mu\varepsilon$ $HI_1 = 140\,GPa$
Third yielding stress σ_{y3} in initial tension and corresponding plastic tensile strain ε_{p2}, and hardening Modulus HI_2 between σ_{y2} and σ_{y3}	$\sigma_{y3} = 870\,MPa$ $\varepsilon_{p2} = 8000\mu\varepsilon$ $HI_2 = 4.6\,GPa$	$\sigma_{y3} = 700\,MPa$ $\varepsilon_{p2} = 7000\mu\varepsilon$ $HI_2 = 4.6\,GPa$
Hardening Modulus in initial tension HI_3 when $\sigma > \sigma_{y3}$,	$HI_3 = 0$	$HI_3 = 0$
Maximum equivalent plastic strain in the strain history	$\varepsilon_p^{eq,m}$	$\varepsilon_p^{eq,m}$
Radius of 1st surface, κ_1	470 MPa	420 MPa
Radius of 2nd surface, κ_2	630 MPa	540 MPa
Radius of 3rd surface, κ_3	750 MPa	600 MPa
Radius of 4th surface, κ_4	$\sigma_{eq,\max}$ corresponding to the $\varepsilon_p^{eq,m}$	$\sigma_{eq,\max}$ corresponding to the $\varepsilon_p^{eq,m}$
Hardening Modulus between surface 1 and surface 2	$\frac{(\kappa_2 - \kappa_1)}{10\%\,\varepsilon_p^{eq,m}}$	$\frac{(\kappa_2 - \kappa_1)}{10\%\,\varepsilon_p^{eq,m}}$
Hardening Modulus between surface 2 and surface 3	$\frac{(\kappa_3 - \kappa_2)}{20\%\,\varepsilon_p^{eq,m}}$	$\frac{(\kappa_3 - \kappa_2)}{20\%\,\varepsilon_p^{eq,m}}$
Hardening Modulus between surface 3 and surface 4	$\frac{(\kappa_4 - \kappa_3)}{70\%\,\varepsilon_p^{eq,m}}$	$\frac{(\kappa_4 - \kappa_3)}{70\%\,\varepsilon_p^{eq,m}}$

Table 7.1. Fatigue test matrix and results for FS specimens, * Strain gauged

Specimen No.	RS (MPa)	Rank	Rt (μm)	Rank	T.I.R. (mm)	Rank	Δε (half)	Life (N)
FS01 A	-293	6	46.4	11	0.06 B	6	2200	135830
FS02 B	-214	15	71	3	0.03 A	11	2200	117164
FS03 A	-252	13	60.3	6	0.09 B	3	2200	132596
FS04 B	-321	3	46.1	12	0.04 A	10	6000	3330
FS05 A	-273	9	60.3	7	0.01 B	14	spare	
* FS06 A	-357	1	72.3	2	0.02 B	13	6000	1992
FS07 A	-268	12	54.8	10	0.00	15	6000	3174
FS08 B	-272	10	55.8	8	0.03 A	12	6000	3684
FS09 B	-314	4	55.1	9	0.05 A	7	2200	89744
FS10 A	-243	14	44.7	13	0.07 B	5	6000	3168
FS11 A	-289	7	80.8	1	0.04 B	9	6000	3706
* FS12 B	-271	11	39.1	15	0.11 A	2	2200	125038
FS13 B	-299	5	66	4	0.04 A	8	6000	3104
* FS14 A	-277	8	39.5	14	0.20 A	1	2200	170614
FS15 A	-326	2	61.9	5	0.08 B	4	2200	135834

Note: T.I.R. is a short for Total Indicate Reading which indicate the offset of crosee section.

Table 7.2. Fatigue test matrix and results for HTS specimens, * Strain gauged

Specimen No.	RS (MPa)	Rank	Rt (μm)	Rank	T.I.R. (mm)	Rank	Δε (half)	Life (N)
HTS01 A	-447	2	36.9	14	0.09 B	4	2200	527502
HTS02 B	-371	10	45.4	5	0.07 A	5	6000	3430
HTS03 B	-410	4	36.9	15	0.02 A	15	2200	513896
* HTS04 B	-293	14	50.2	2	0.06 A	7	6000	2944
HTS05 B	-318	13	39.7	11	0.05 A	12	2200	518054
HTS06 A	-383	7	43.5	7	0.06 B	8	6000	2160
HTS07 B	-391	6	42.7	8	0.07 A	6	2200	714770
* HTS08 B	-416	3	48.5	3	0.15 A	2	6000	2032
HTS10 B	-349	11	39.6	12	0.10 A	3	2200	234984
HTS11 B	-377	9	48.4	4	0.06 A	9	2200	165464
HTS12 A	-383	8	37.7	13	0.05 B	10	spare	
HTS13 B	-276	15	45.1	6	0.05 A	11	2200	348658
* HTS14 B	-474	1	40.1	10	0.20 A	1	6000	3008
HTS15 B	-328	12	51.8	1	0.04 A	13	6000	1920
HTS16 A	-397	5	42	9	0.02 B	14	6000	1664

Table 7.3. Fatigue test matrix and results for AF specimens, * Strain gauged

Specimen No.	RS (MPa)	Rank	Rt (μm)	Rank	T.I.R. (mm)	Rank	Δε (half)	Life (N)
* AF01 B	24	12	43.5	4	0.04 A	10	2200	78208
AF02 A	26	13	48.5	2	0.05 B	7	2200	61498
* AF03 A	-2	10	34	8	0.18 B	1	2200	116942
* AF05 B	-12	8	25.4	11	0.08 A	3	2200	89280
AF06 A	-28	4	36.4	6	0.06 B	4	2200	84924
AF07 A	-25	5	61.6	1	0.01 B	14	6000	3640
AF08 B	0	11	28.6	9	0.05 A	8	spare	
AF09 B	-23	7	21.5	14	0.06 A	5	6000	4302
AF10 B	-25	6	35.1	7	0.04 A	9	6000	3562
AF11 A	59	15	26.3	10	0.03 B	11	6000	3530
AF12 B	-6	9	37	5	0.00	15	6000	2754
AF13 B	26	14	20.6	15	0.05 A	6	2200	65218
AF14 B	-32	3	44.8	3	0.03 A	12	6000	2846
AF15 B	-59	1	23.3	13	0.01 A	13	2200	80790
AF16 B	-49	2	24.6	12	0.09 A	2	6000	4234

Table 7.4. Fatigue test matrix and results for HT specimens, * Strain gauged

Specimen No.	RS (MPa)	Rank	Rt (μm)	Rank	T.I.R. (mm)	Rank	Δε (half)	Life (N)
* HT01 B	-27	5	29.6	9	0.10 A	2	2200	84016
HT02 B	-35	2	34	5	0.02 A	14	6000	2400
HT03 B	-25	8	34.4	4	0.04 A	13	2200	76868
HT04 B	-30	4	45.8	1	0.10 A	3	6000	2680
HT05 A	-11	14	27.7	12	0.06 B	9	6000	2878
* HT06 B	-41	1	37.5	2	0.11 A	1	2200	95580
HT07 A	-17	11	24.7	15	0.05 B	10	2200	80848
HT08 B	-13	13	30.5	8	0.05 A	11	spare	
HT09 A	-24	9	28.9	11	0.10 B	4	2200	84764
HT10 A	-23	10	29.1	10	0.10 B	5	6000	2966
HT11 B	-26	6	25.3	14	0.08 A	6	6000	2546
HT12 B	-32	3	26	13	0.06 A	8	2200	92508
HT13 A	-25	7	36.7	3	0.04 B	12	6000	2332
* HT14 A	-9	15	30.5	7	0.00	15	6000	2496
HT15 A	-14	12	33.4	6	0.08 B	7	2200	99044

Table 7.5. Fitted parameters of Weibull distribution for fatigue tests data of AF, FS, and HTS batches

	N_0	N_a	β
AF ($\Delta\varepsilon/2 = 2200\mu\varepsilon$)	0	89809	4.82
FS ($\Delta\varepsilon/2 = 2200\mu\varepsilon$)	0	140271	5.36
HT ($\Delta\varepsilon/2 = 2200\mu\varepsilon$)	0	91378	11.27
HTS ($\Delta\varepsilon/2 = 2200\mu\varepsilon$)	0	500453	2.04
AF ($\Delta\varepsilon/2 = 6000\mu\varepsilon$)	0	3820	5.97
FS ($\Delta\varepsilon/2 = 6000\mu\varepsilon$)	0	3470	4.69
HT ($\Delta\varepsilon/2 = 6000\mu\varepsilon$)	0	2724	11.44
HTS ($\Delta\varepsilon/2 = 6000\mu\varepsilon$)	0	2717	3.8

Table 8.1. Parameters of Normal distribution of axial residual stresses for 5 specimen groups. (MPa)

Specimen Group	Distribution Centre $\overline{\sigma}$	Standard Deviation S
HT	-24.7	10.7
HTS	-372.9	46.7
AF	-15.6	30.6
FS	-272.1	41.8
U	-286	39.7

Table 8.2 Parameters of Weibull distribution of axial residual stresses for 5 specimen groups. (MPa)

Specimen Group	Weibull slope β	Minimum stress σ_0	Characteristic stress σ_a
HT	1.60	-7.1	-27.1
HTS	5.12	-587.3	-353.
AF	2.27	-81.5	-6.9
FS	5.42	-474.4	-255.1
U	1.91	-361.1	-276.2

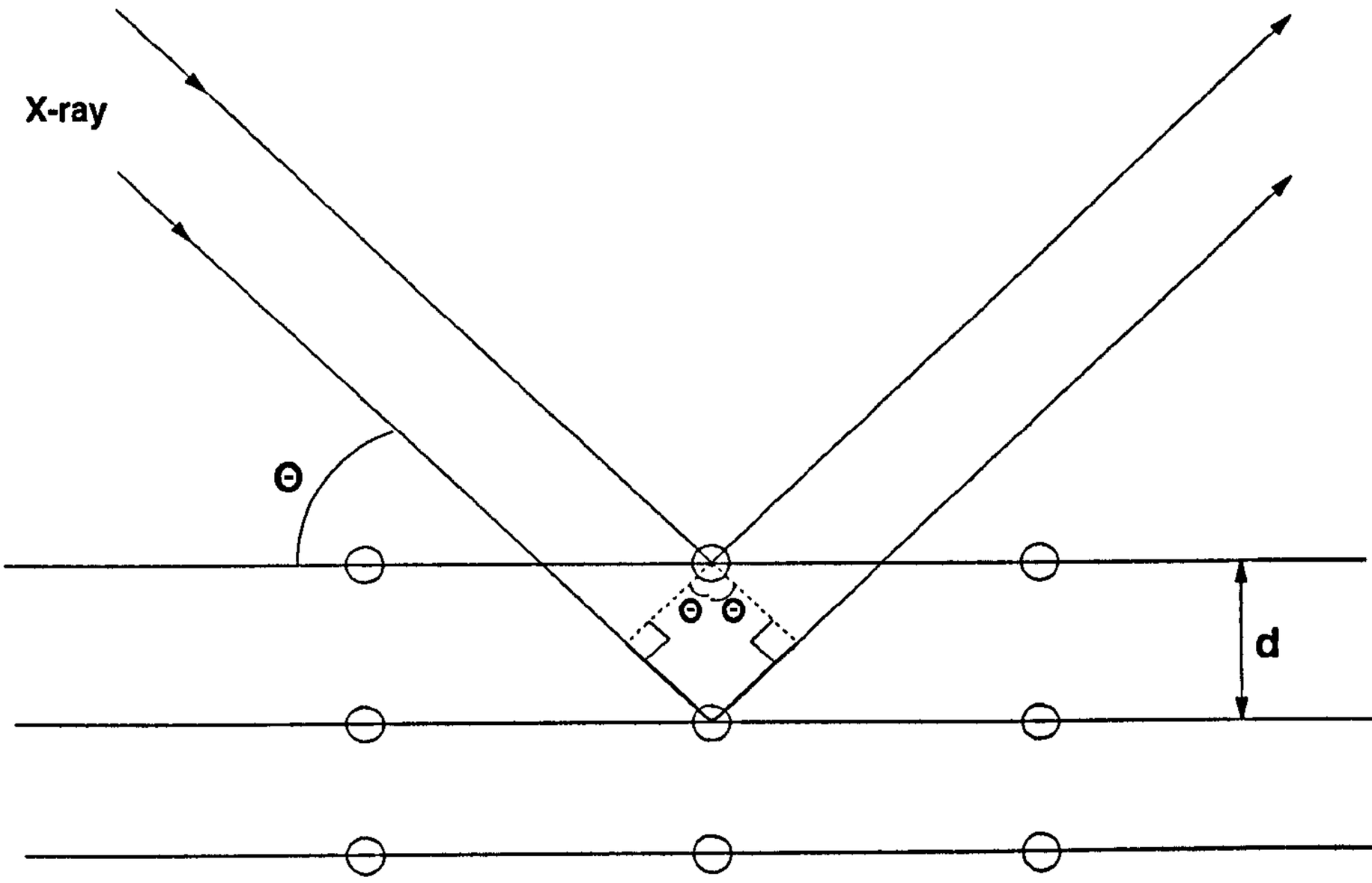

Fig. 2.1 Diffraction of X-ray by a crystal

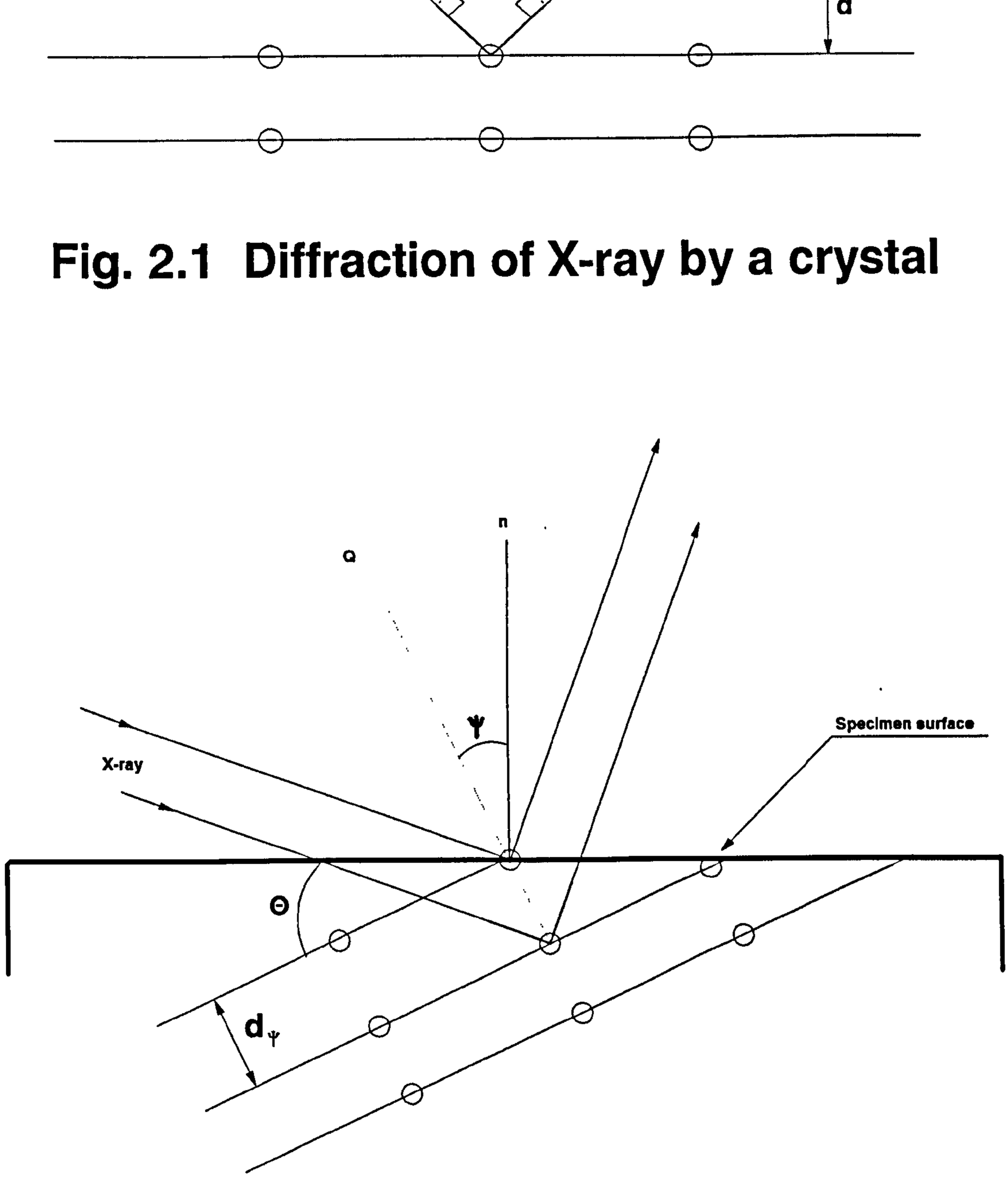

Fig. 2.2 X-ray diffraction with a tilt angle Ψ

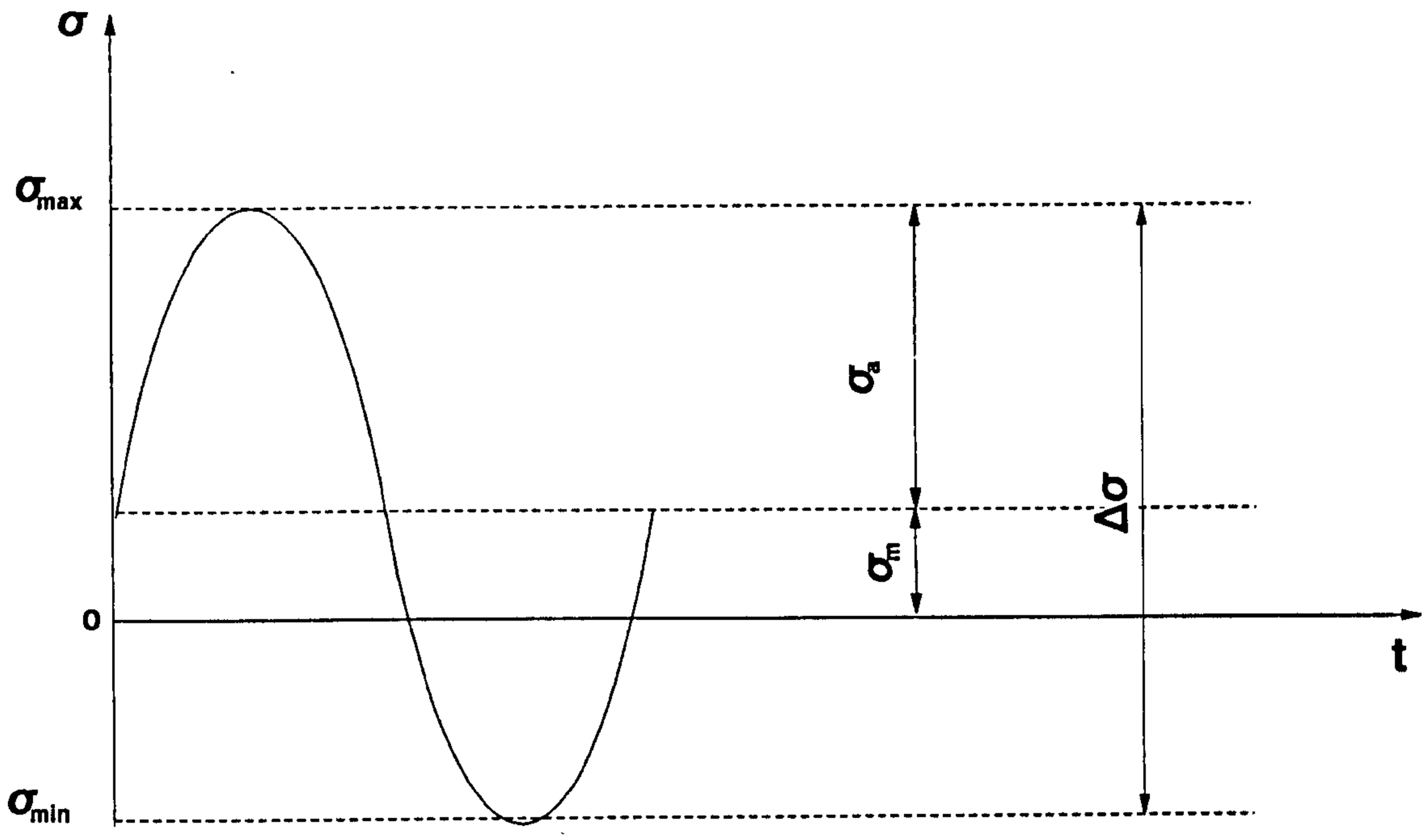

Fig 2.3 Non-symmetrical stress cycle

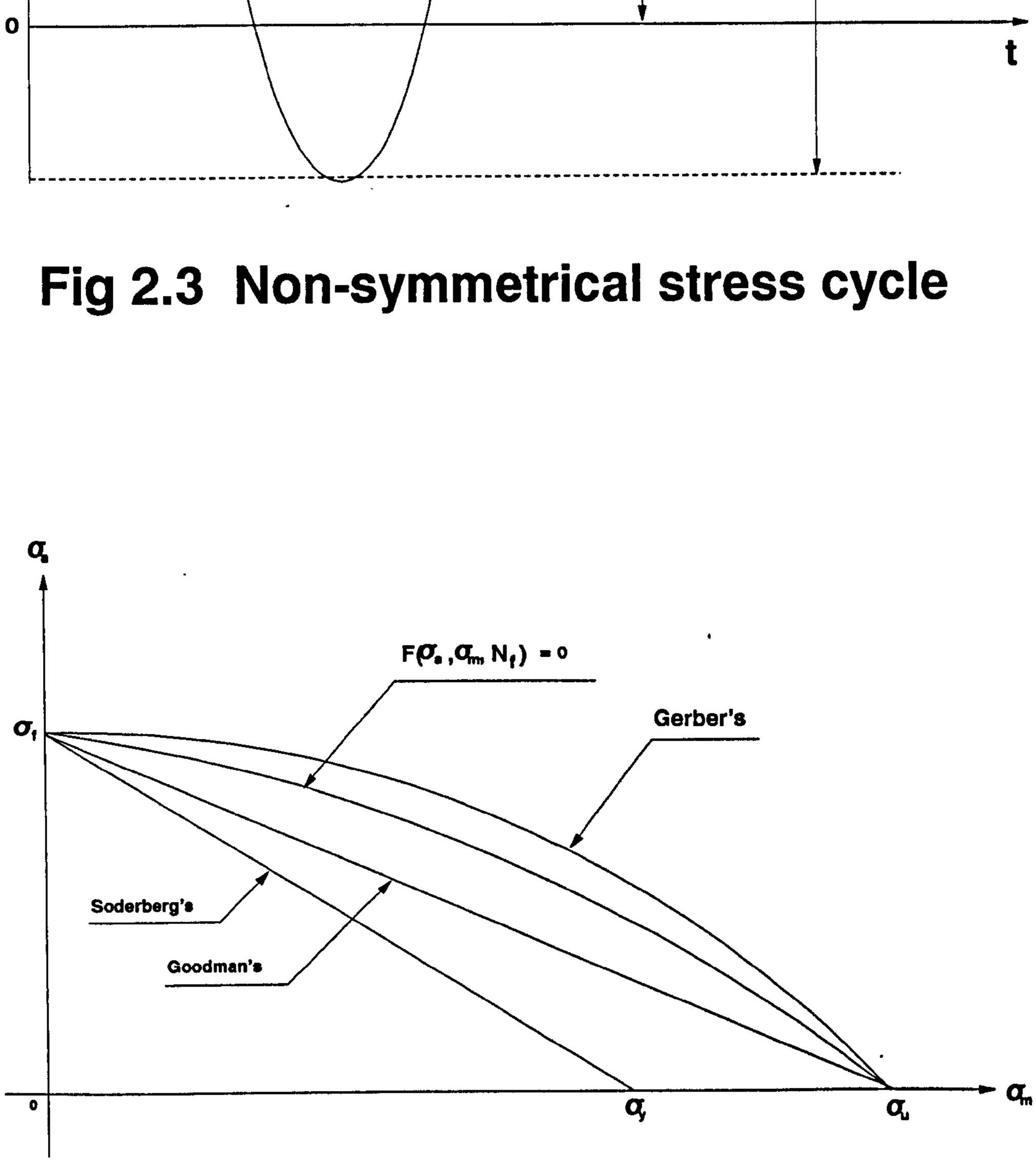

Fig 2.4 Diagrams of constant fatigue life with the mean stress effect.

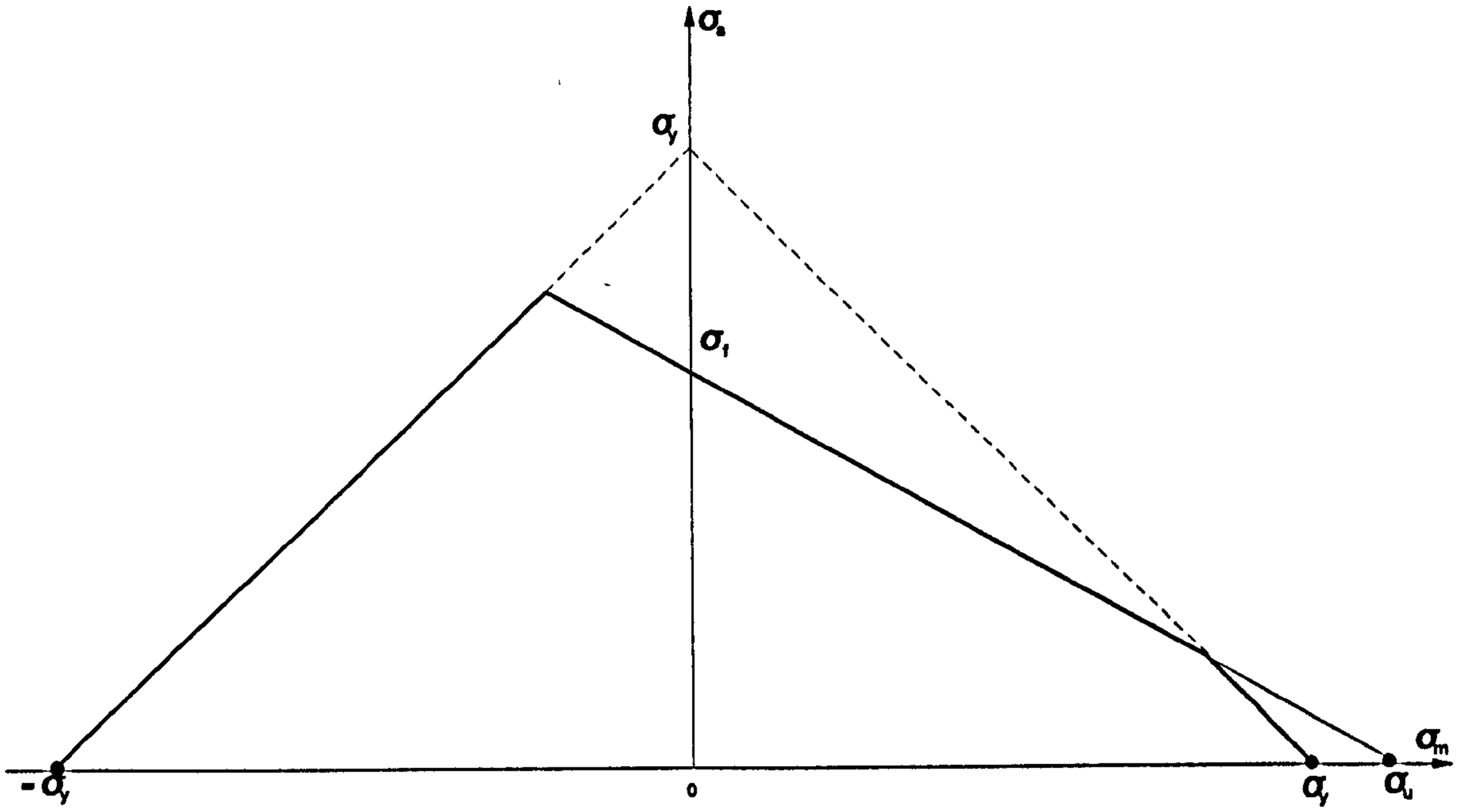

Fig 2.5 Haigh digram of constant fatigue life with the mean stress effect

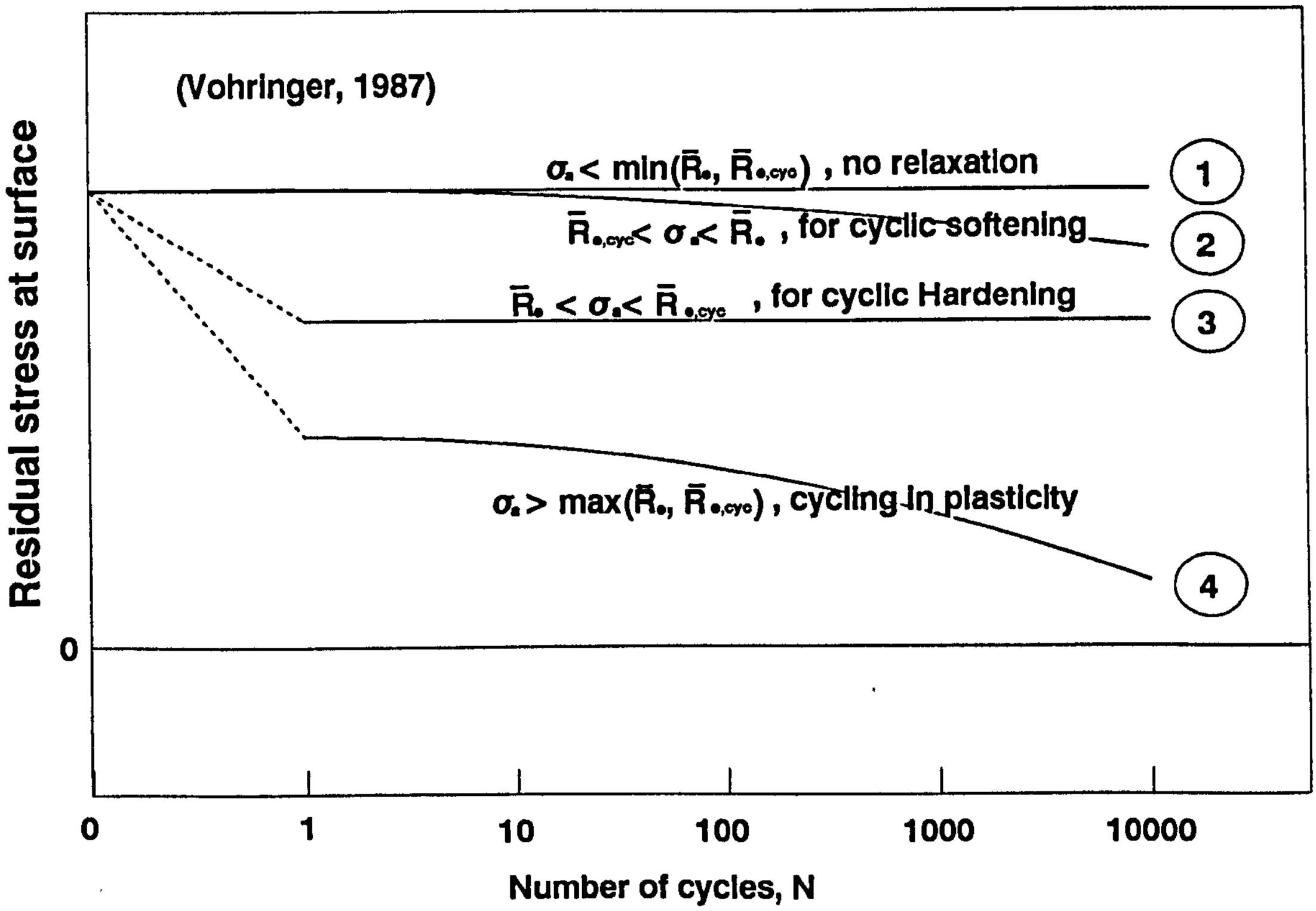

Fig 2.6 Schematic diagram of surface residual stress relaxation under cyclic loading

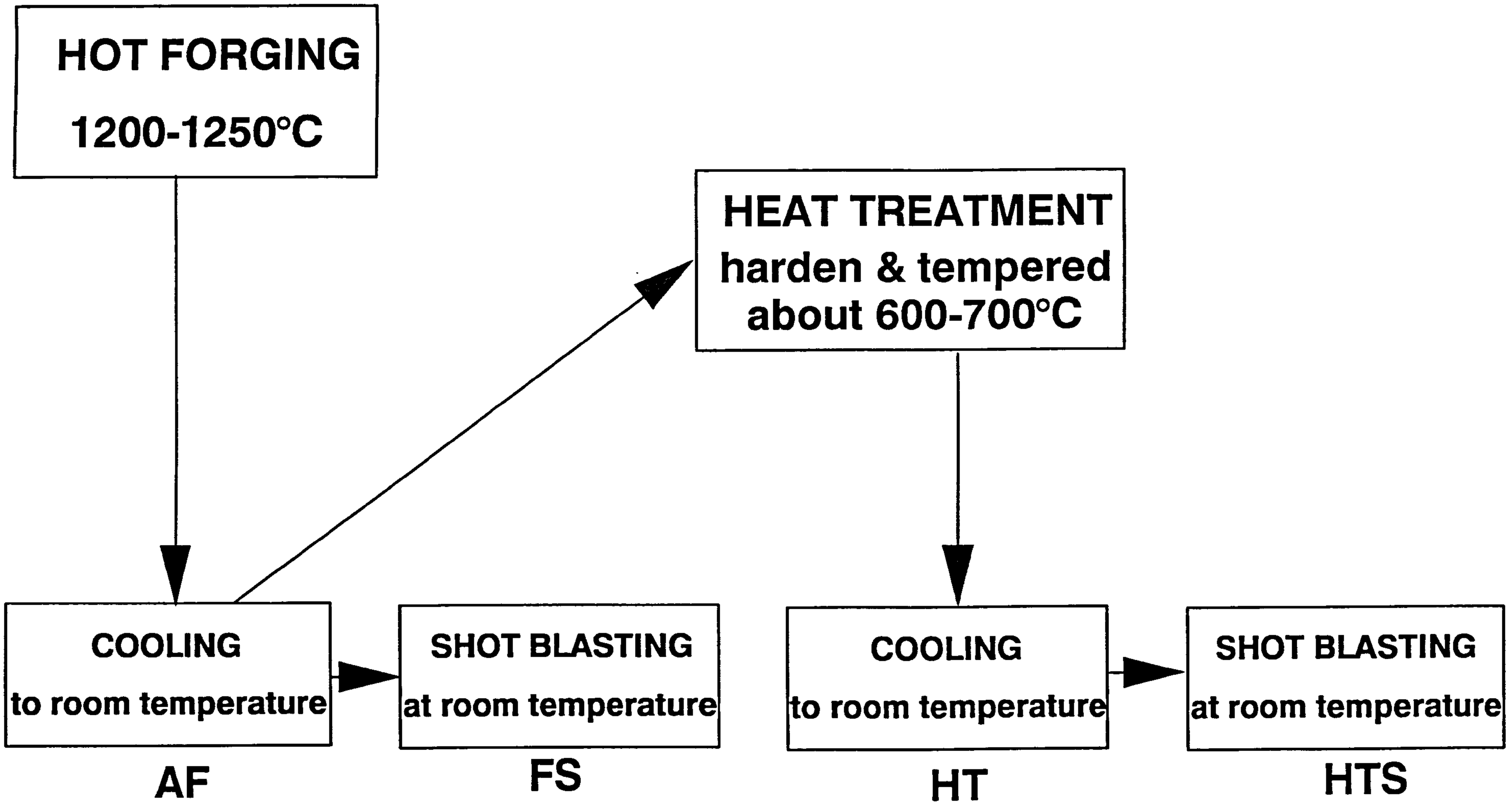

Fig. 3.1 Forging process

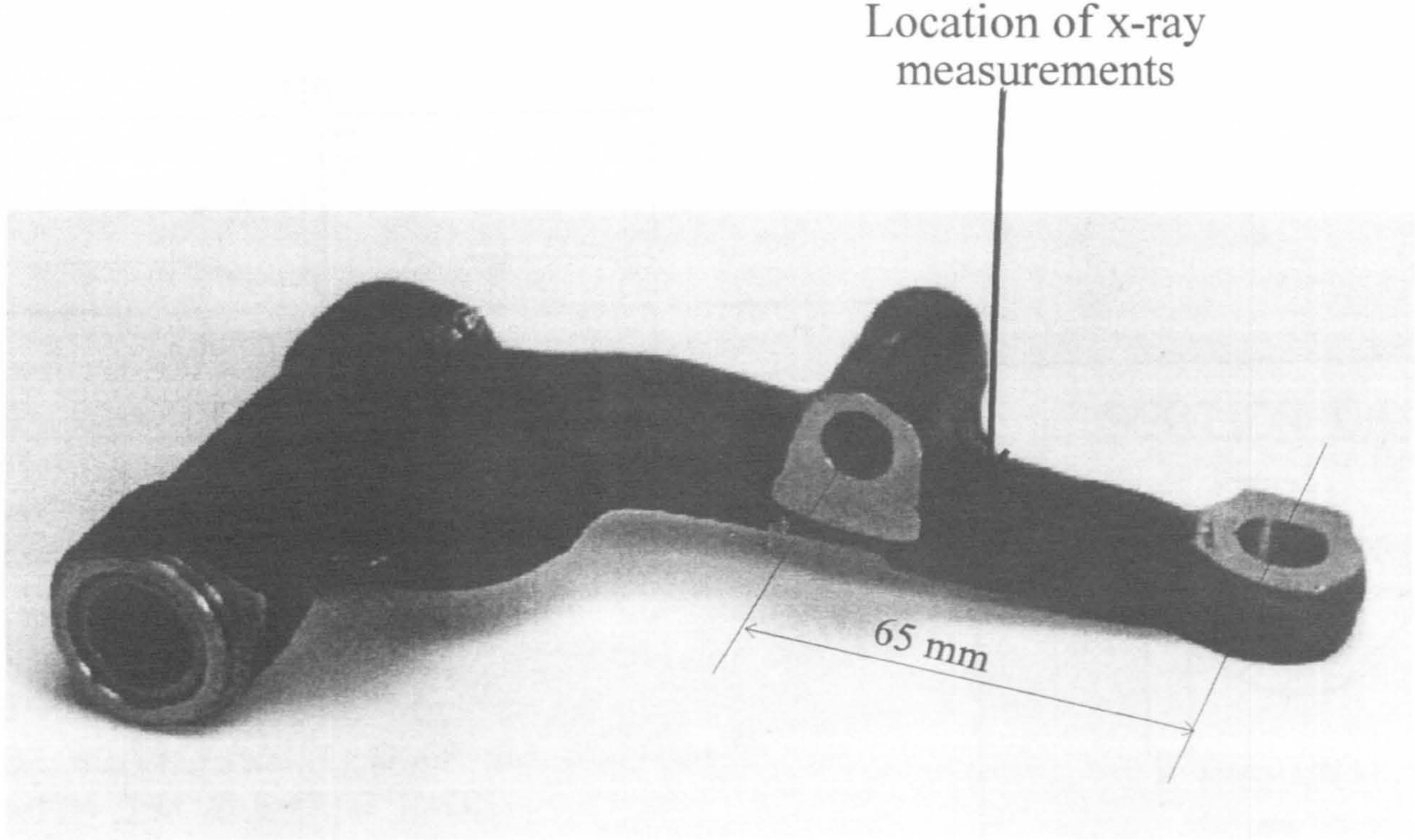

Fig. 3.2 Suspension arm

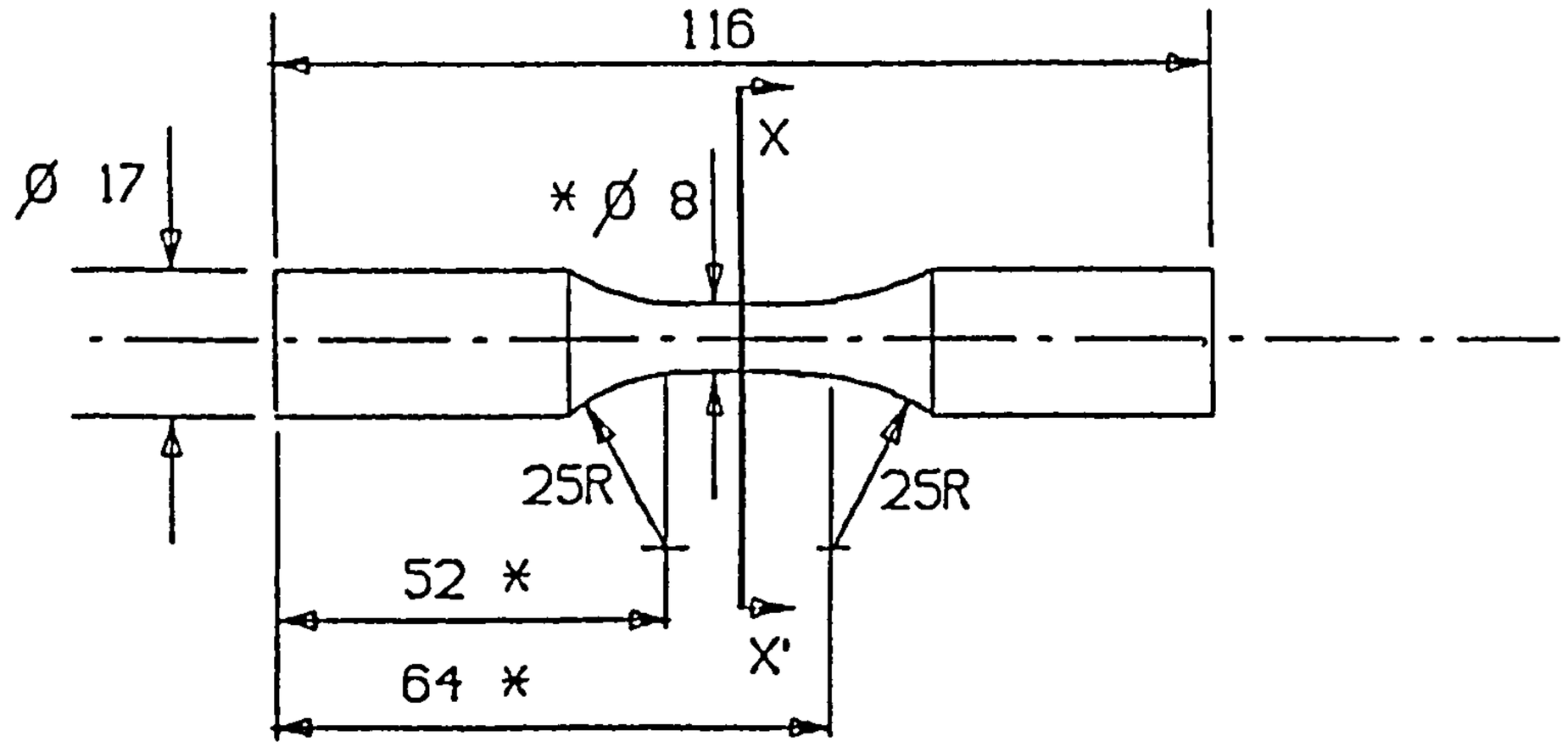

NOTES

* 1. ENDS MUST BE PARALLEL

* 2. THERE MUST BE NO UNDERCUTTING OF Ø8 SECTION AT TRANSITION WITH 25R BLENDING RADII

* 3. CENTRE SECTION MUST BE CONCENTRIC WITH ENDS

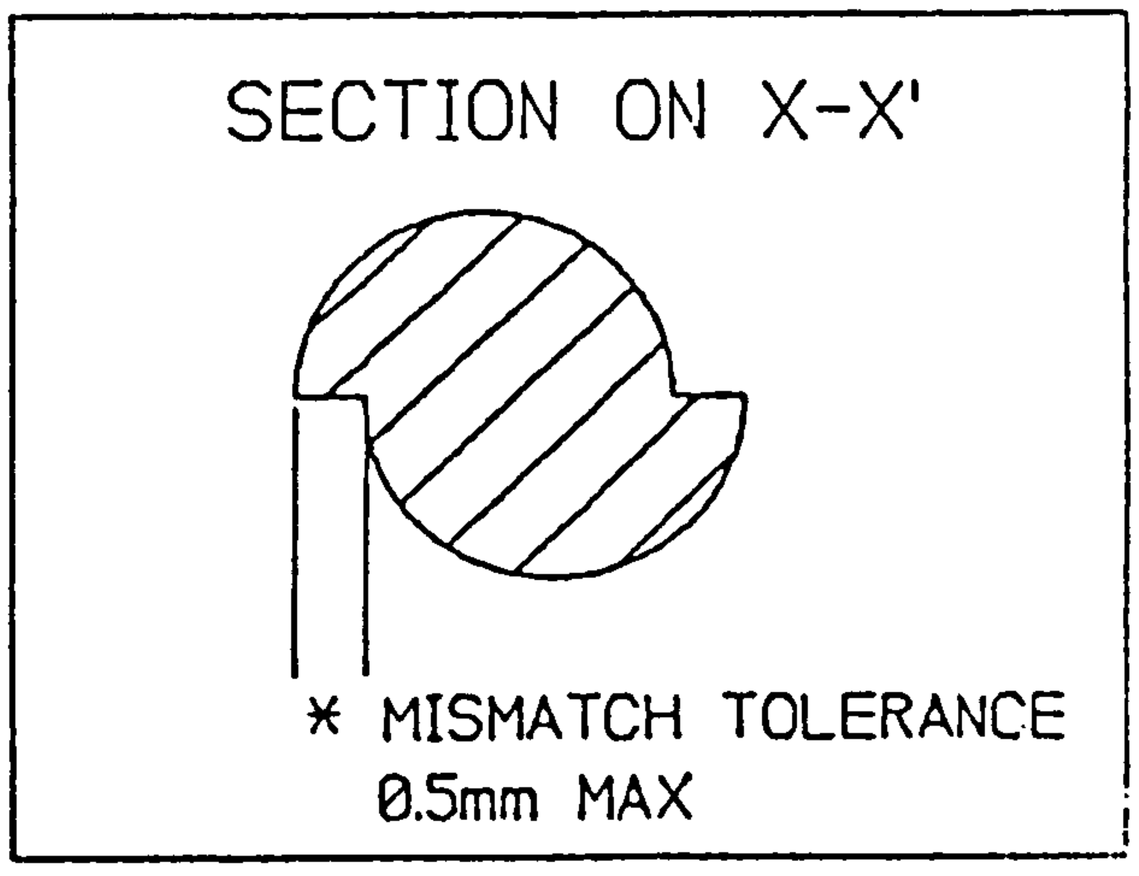

Fig. 3.3 Design of hot forged round bar specimen

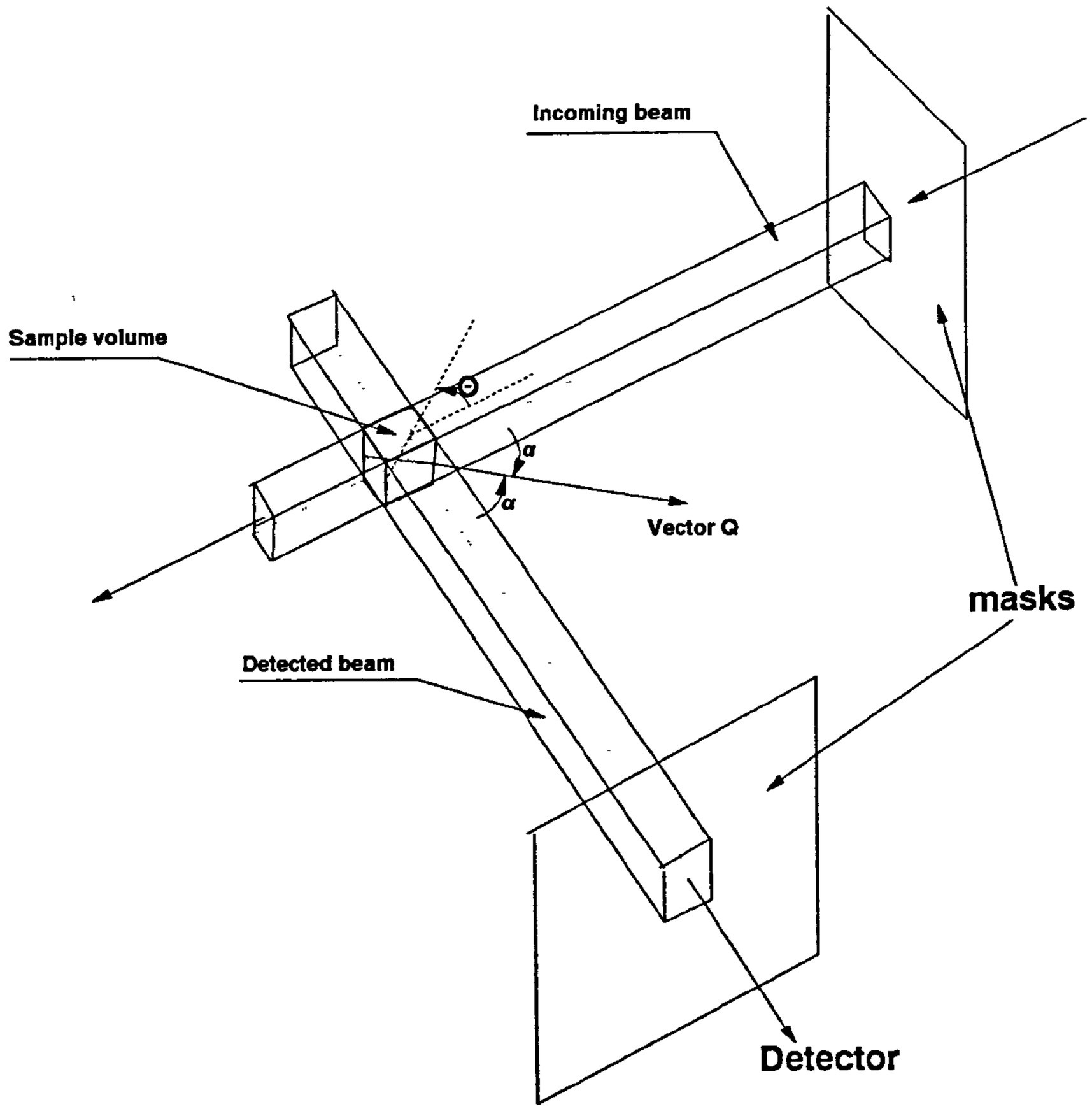

Fig. 3.4 Illustration of sample volume, scattering vector for neutron diffraction measurements

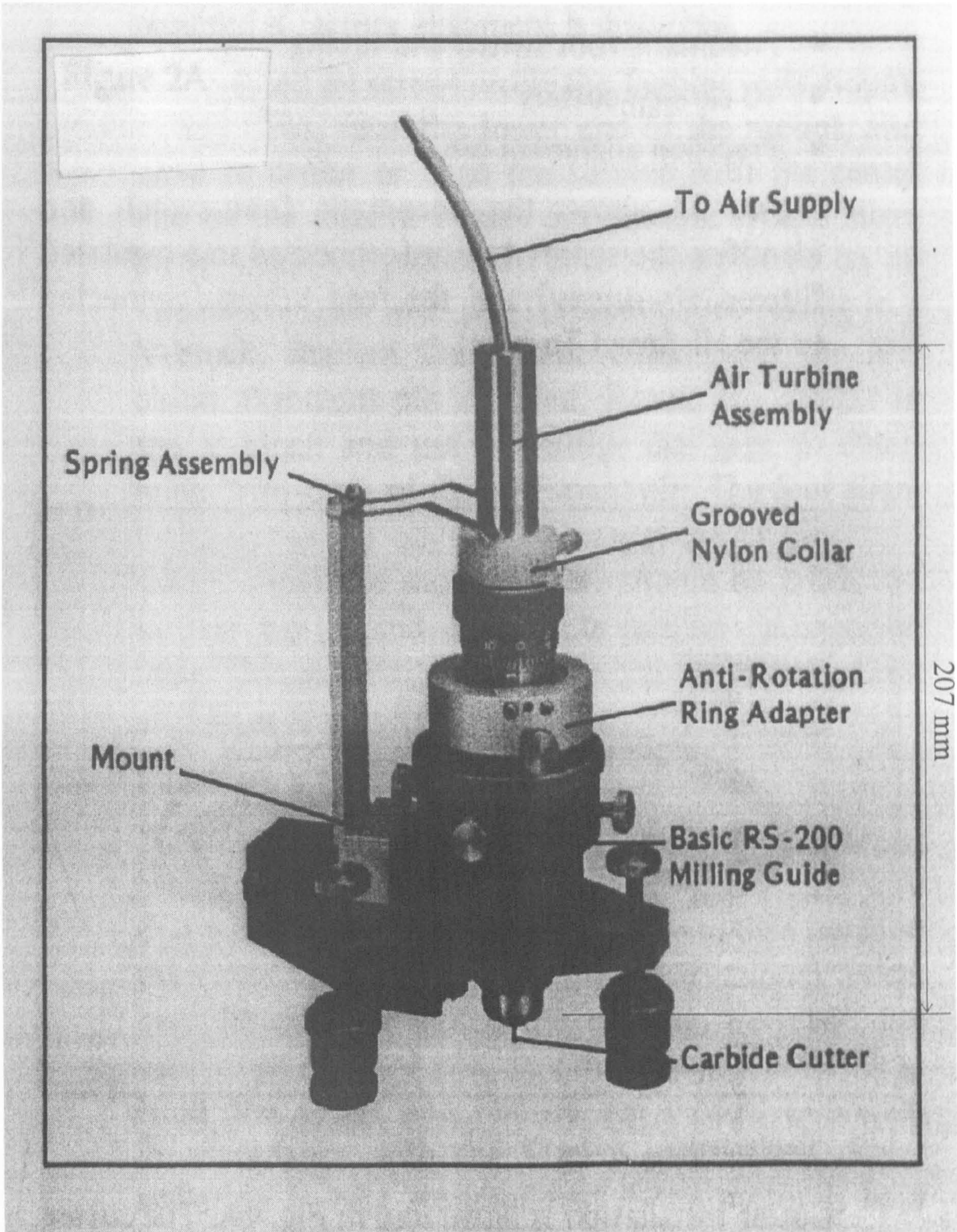

Fig. 3.5 Hole drilling device

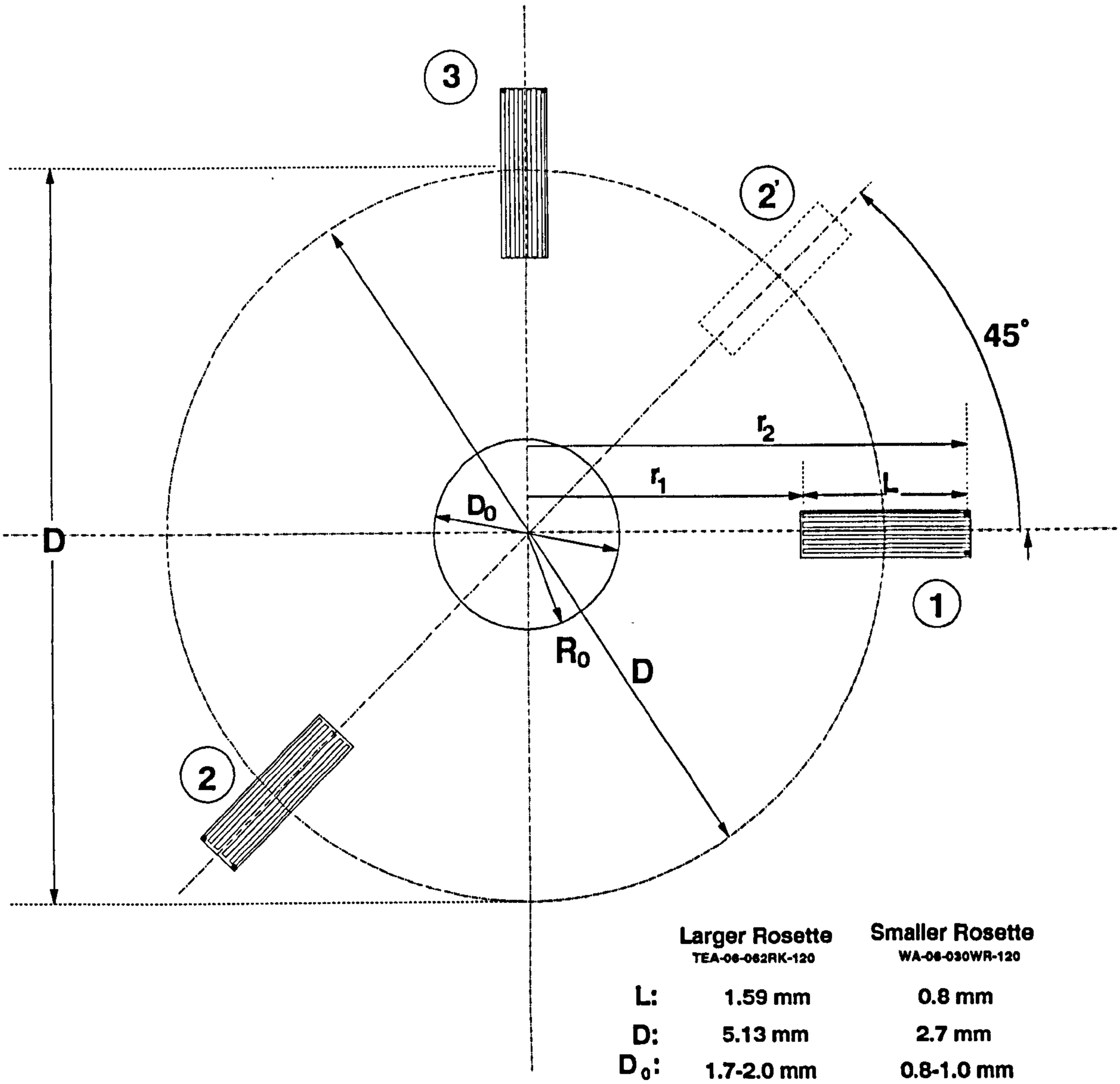

	Larger Rosette TEA-06-062RK-120	Smaller Rosette WA-06-030WR-120
L:	1.59 mm	0.8 mm
D:	5.13 mm	2.7 mm
D_0:	1.7-2.0 mm	0.8-1.0 mm

Fig. 3.6 Strain gauge rosette arrangement for determining residual stresses

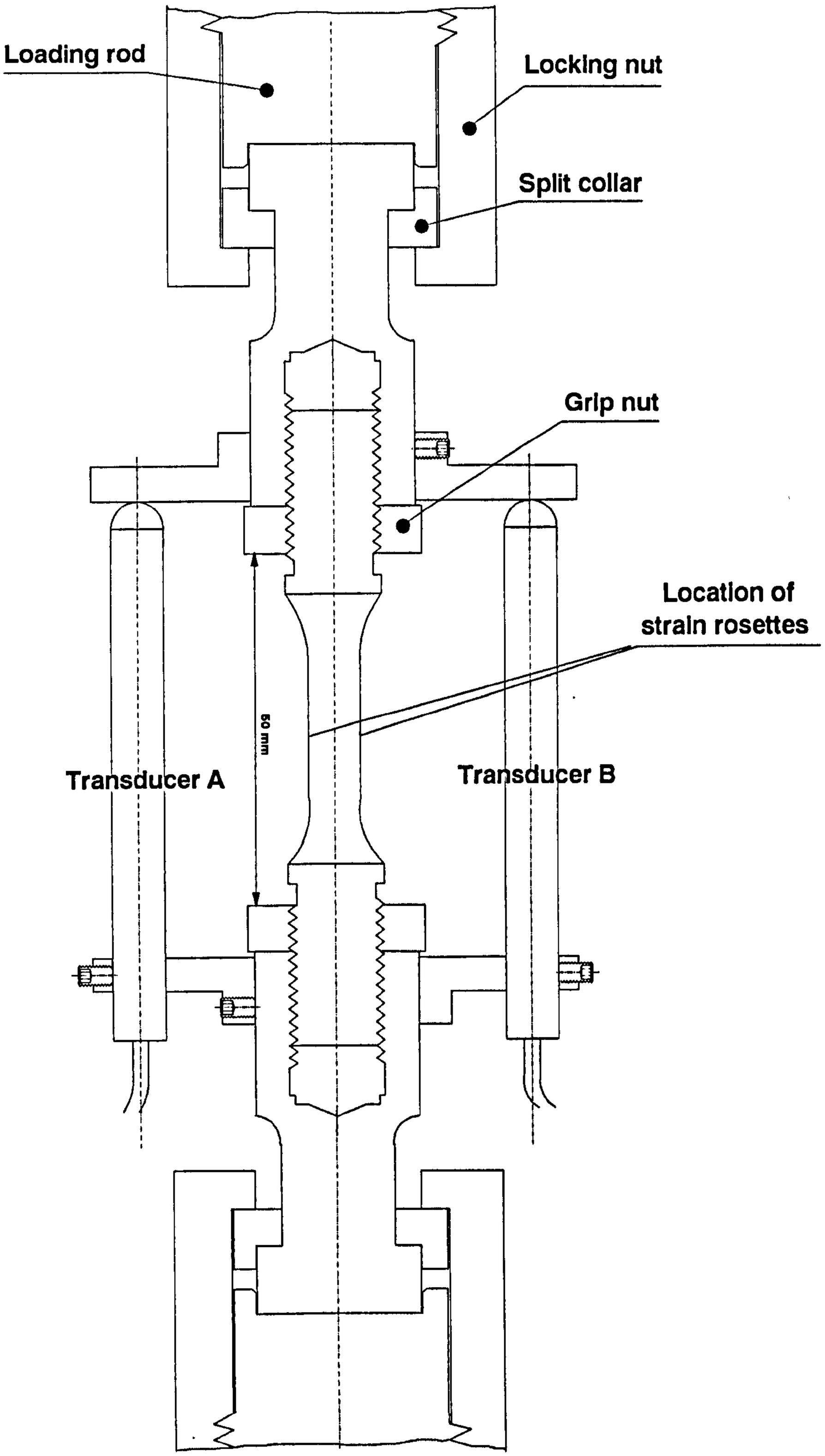

Fig. 3.7 Specimen attachments

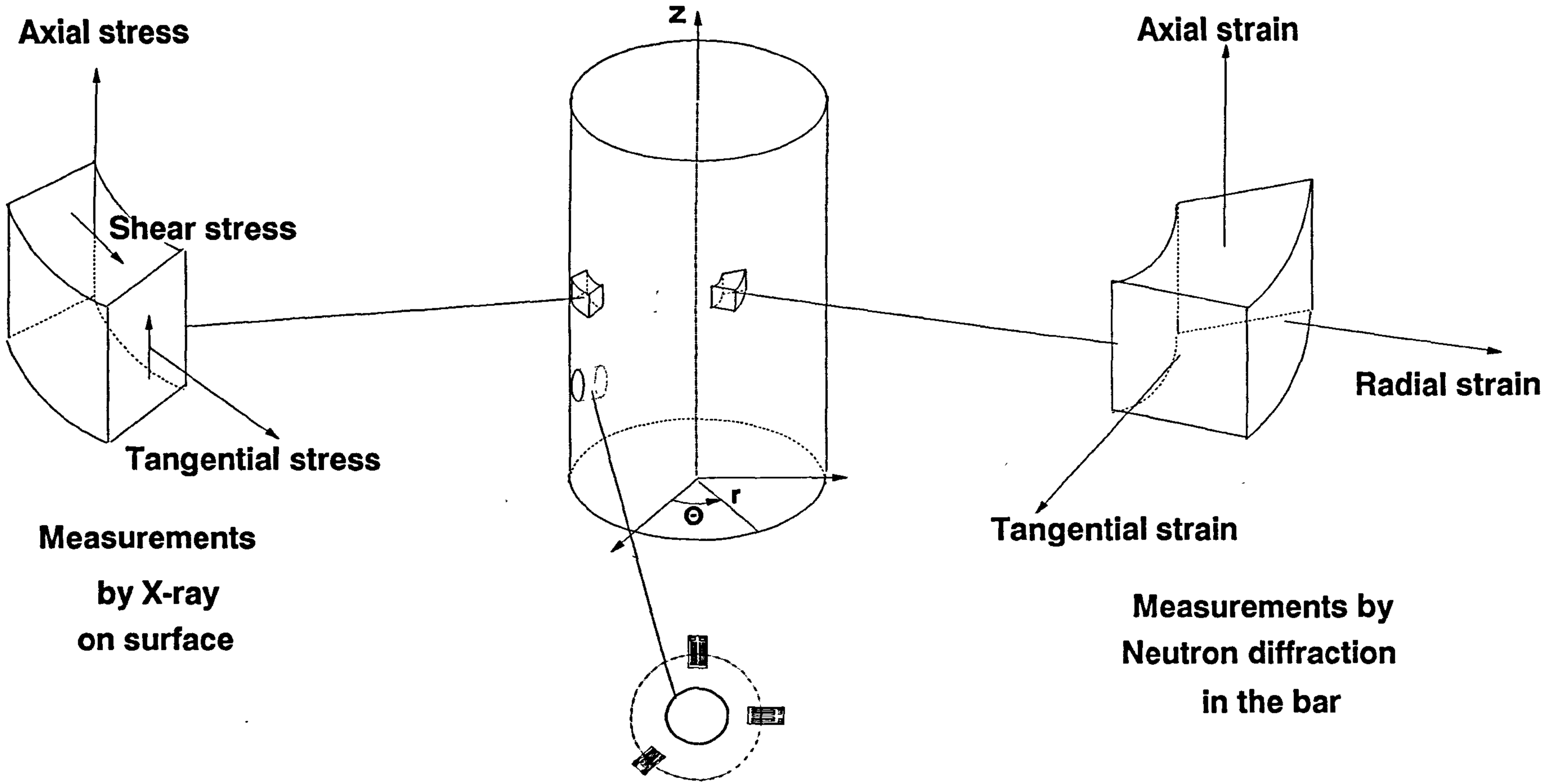

Fig. 4.1 RESIDUAL STRESS MEASUREMENTS IN FORGED ROUND BARS

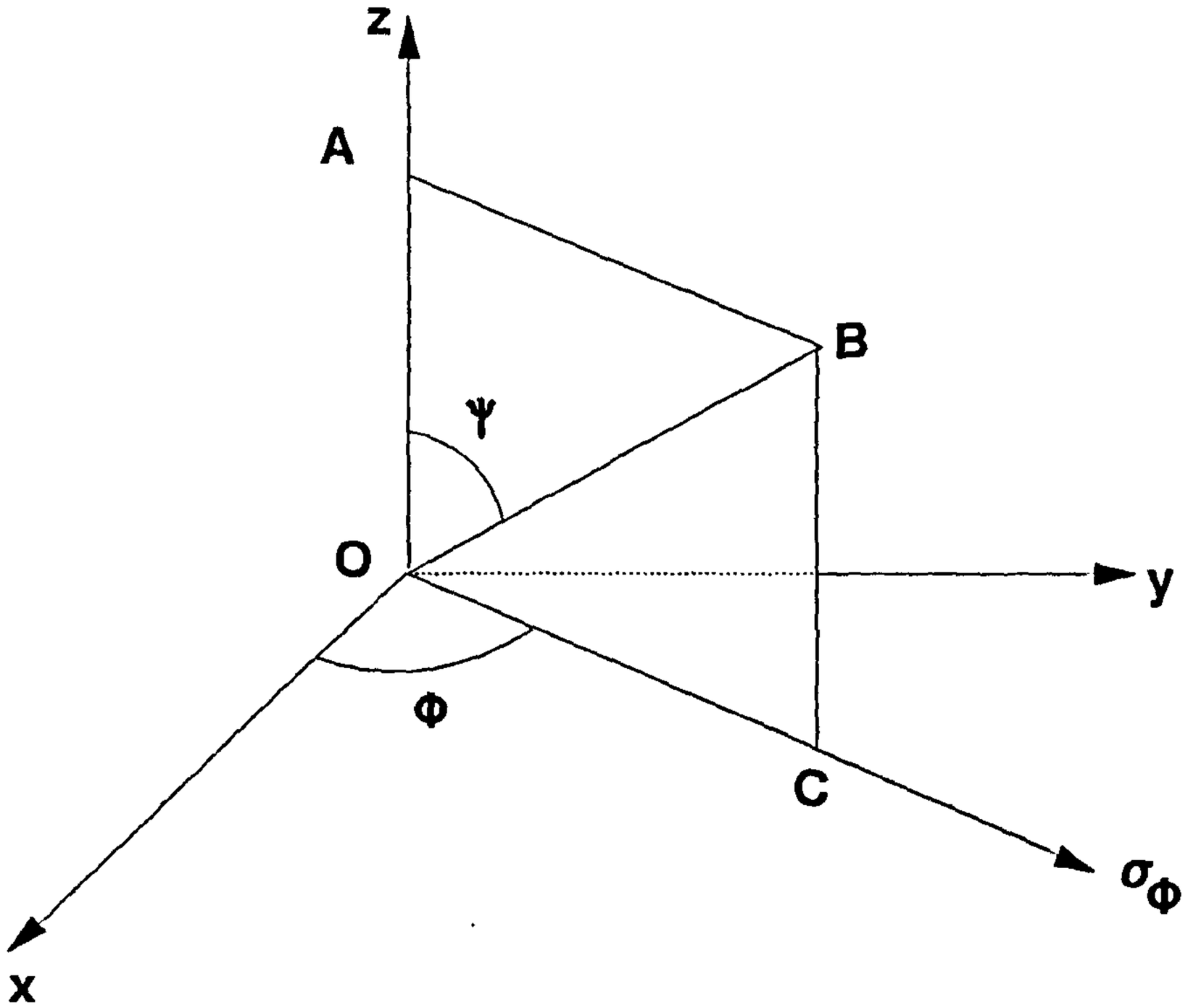

Fig 4.2 Definition of local coordinate system for X-ray measurement

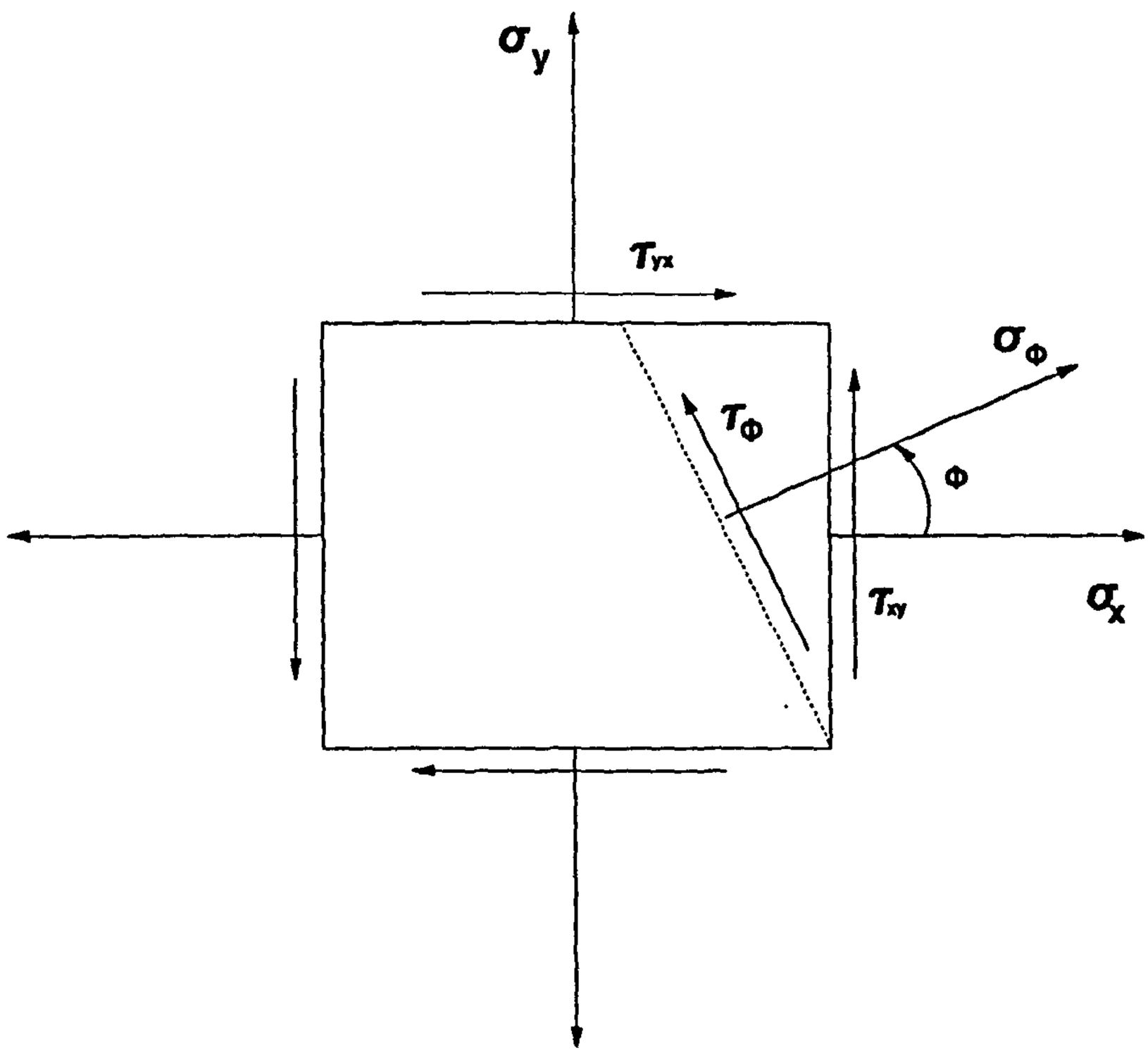

Fig 4.3 Plane stress analysis element

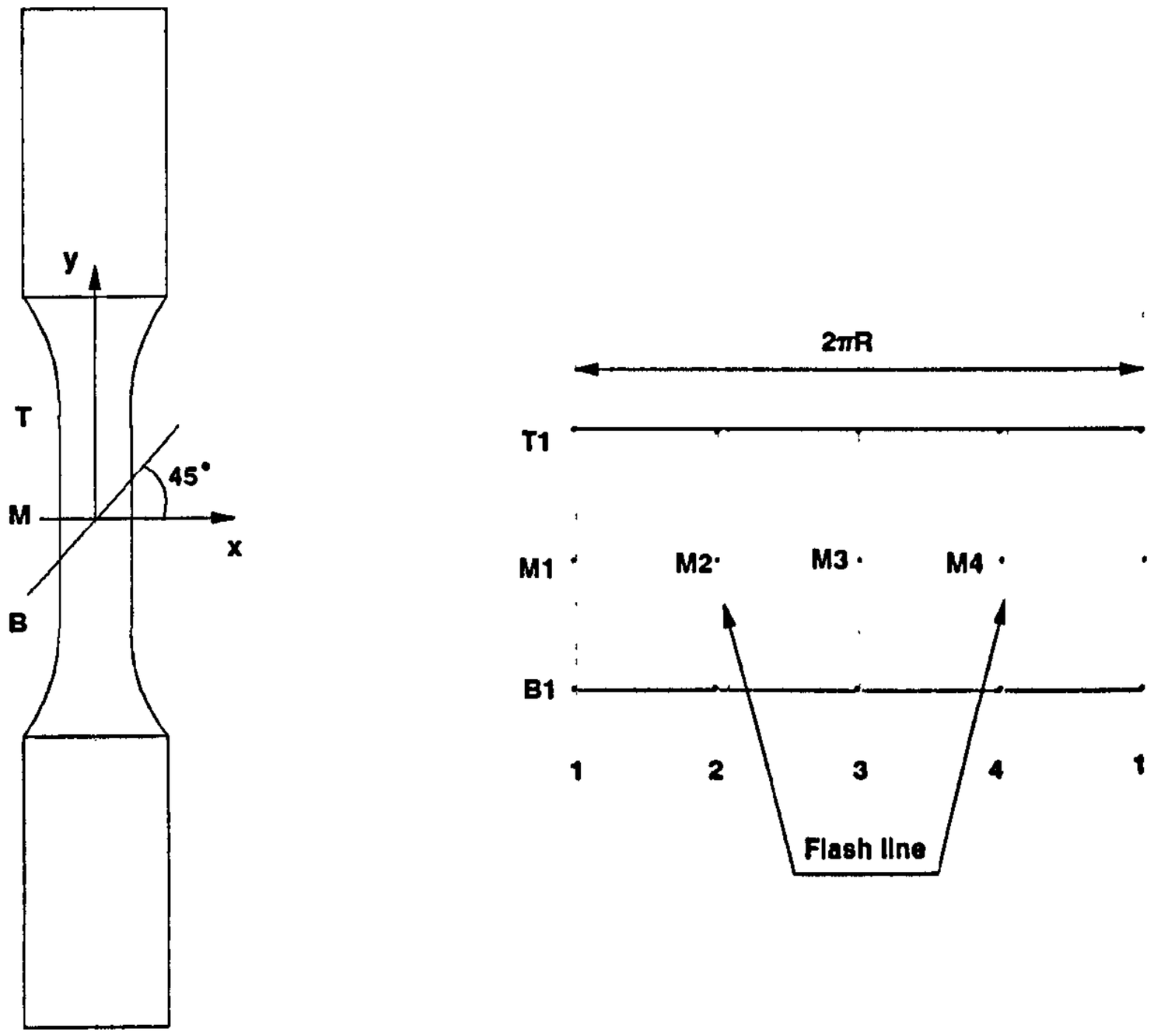

Fig 4.4 Round bar specimen and reference frame

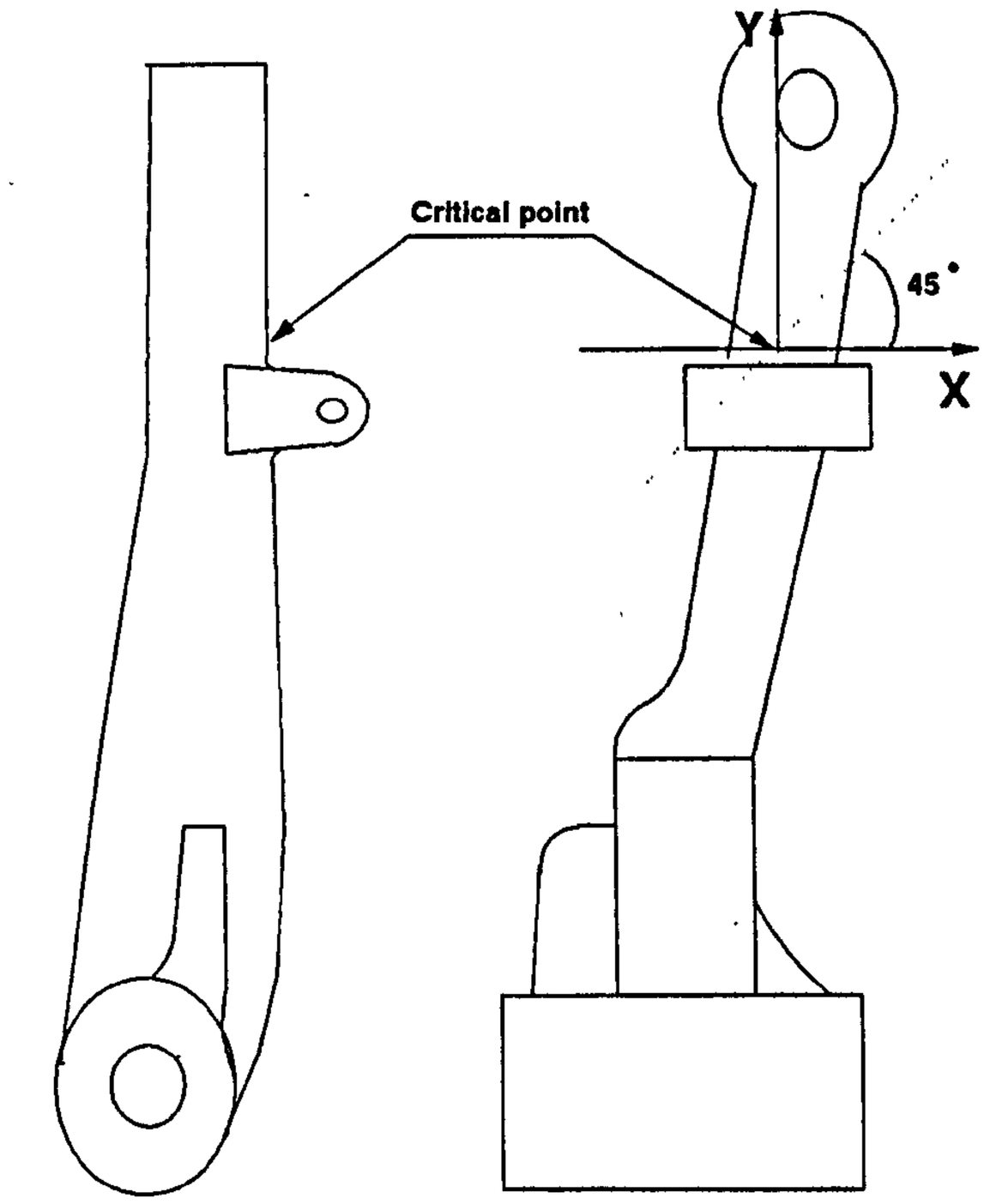

Fig 4.5 Illustration of suspension arm for the X-ray measurements

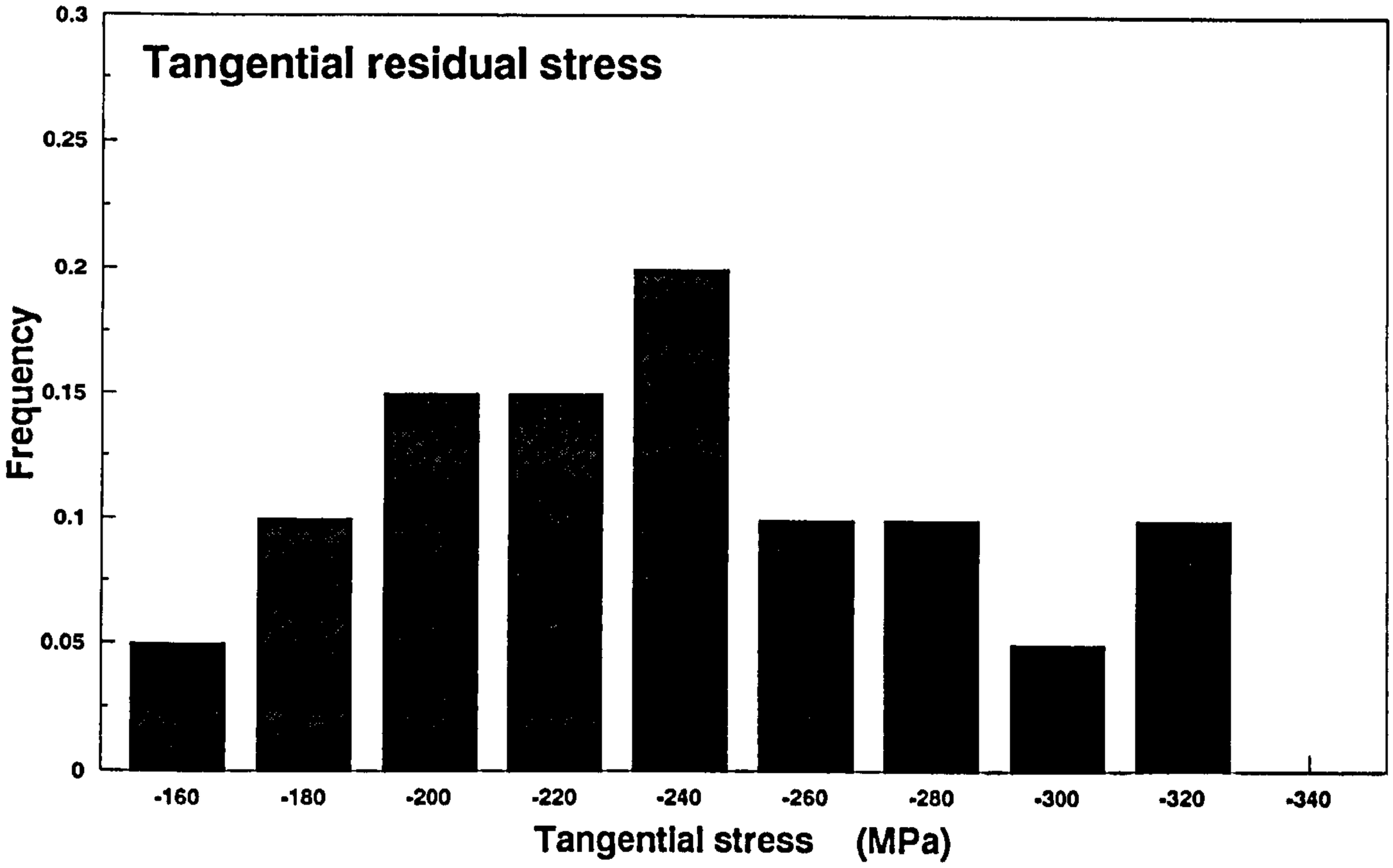

Fig 4.6 Tangential residual stress distribution of twenty U-batch specimens measured by X-ray

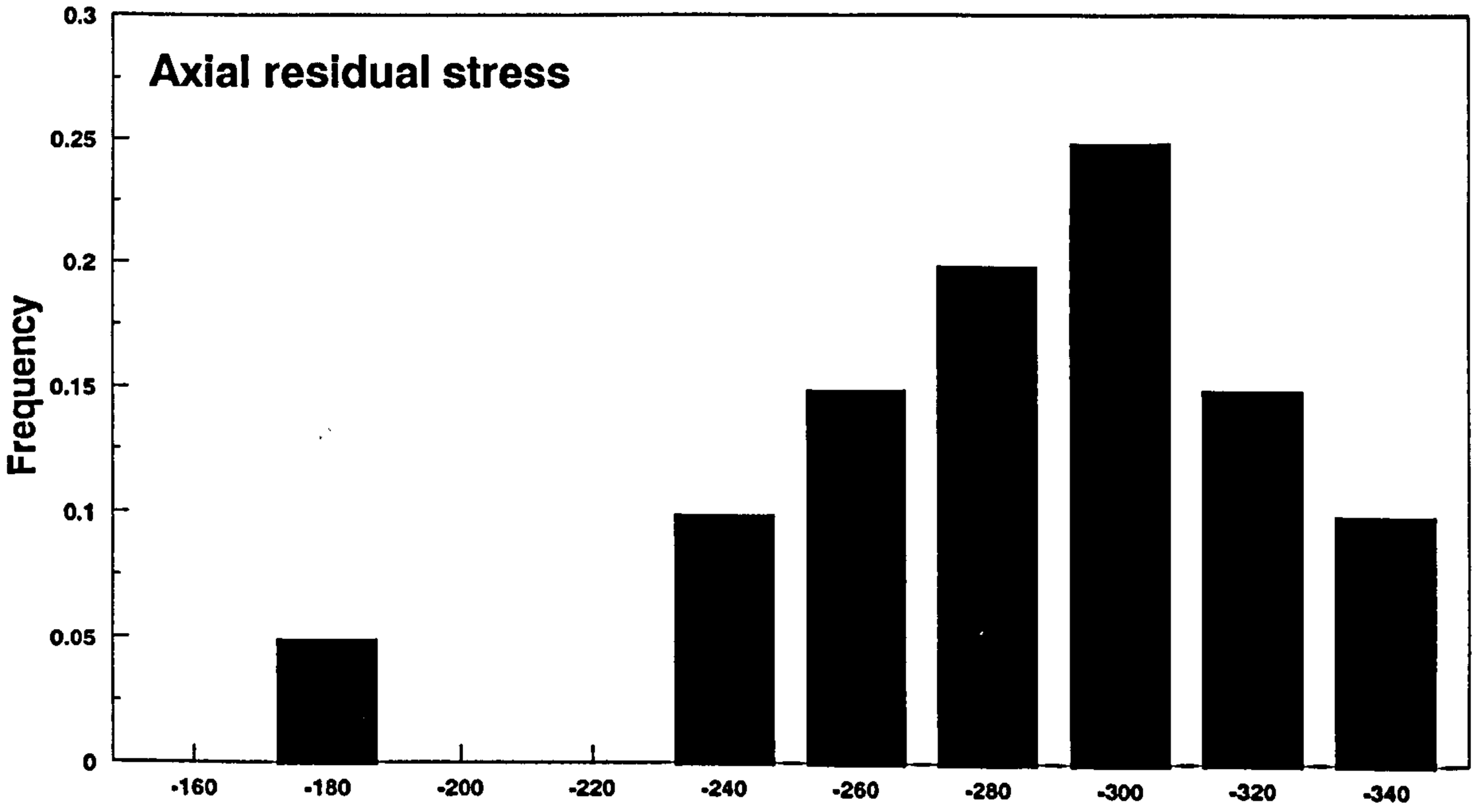

Fig 4.7 Axial residual stress distribution of twenty U-batch specimens measured by X-ray

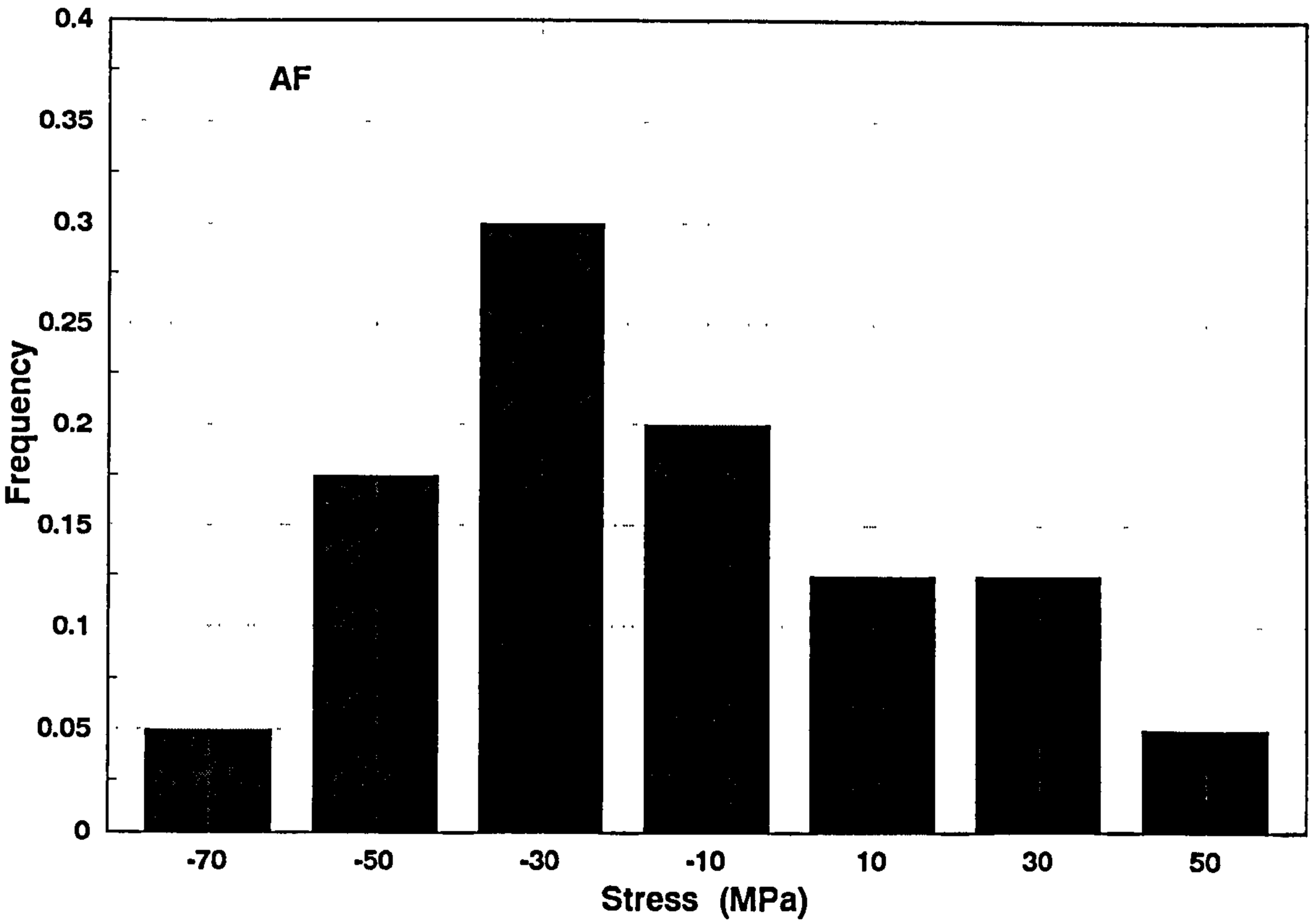

Fig 4.8 Axial residual stress distribution of 20 AF specimens

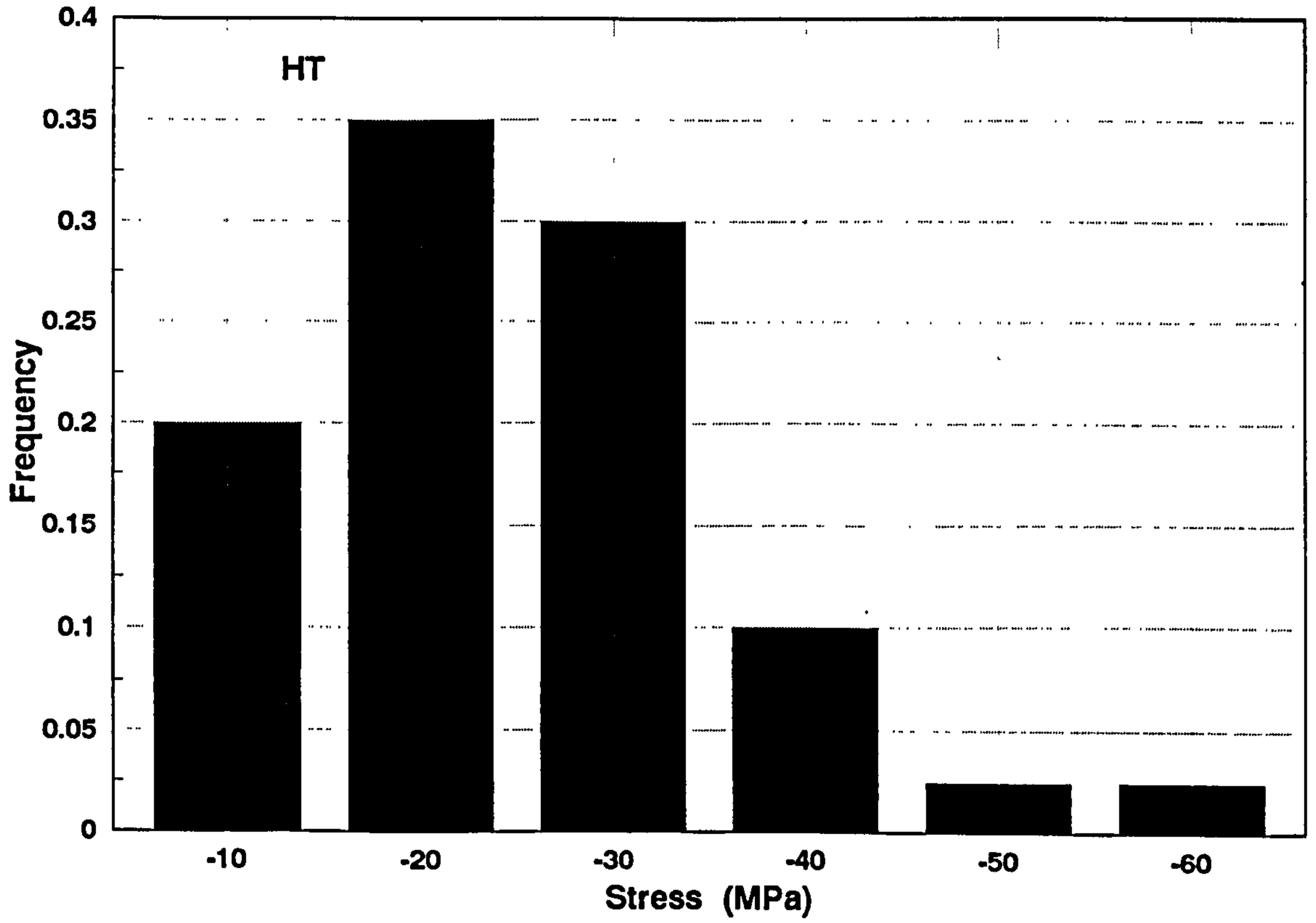

Fig 4.9 Axial residual stress distribution of 20 HT specimens

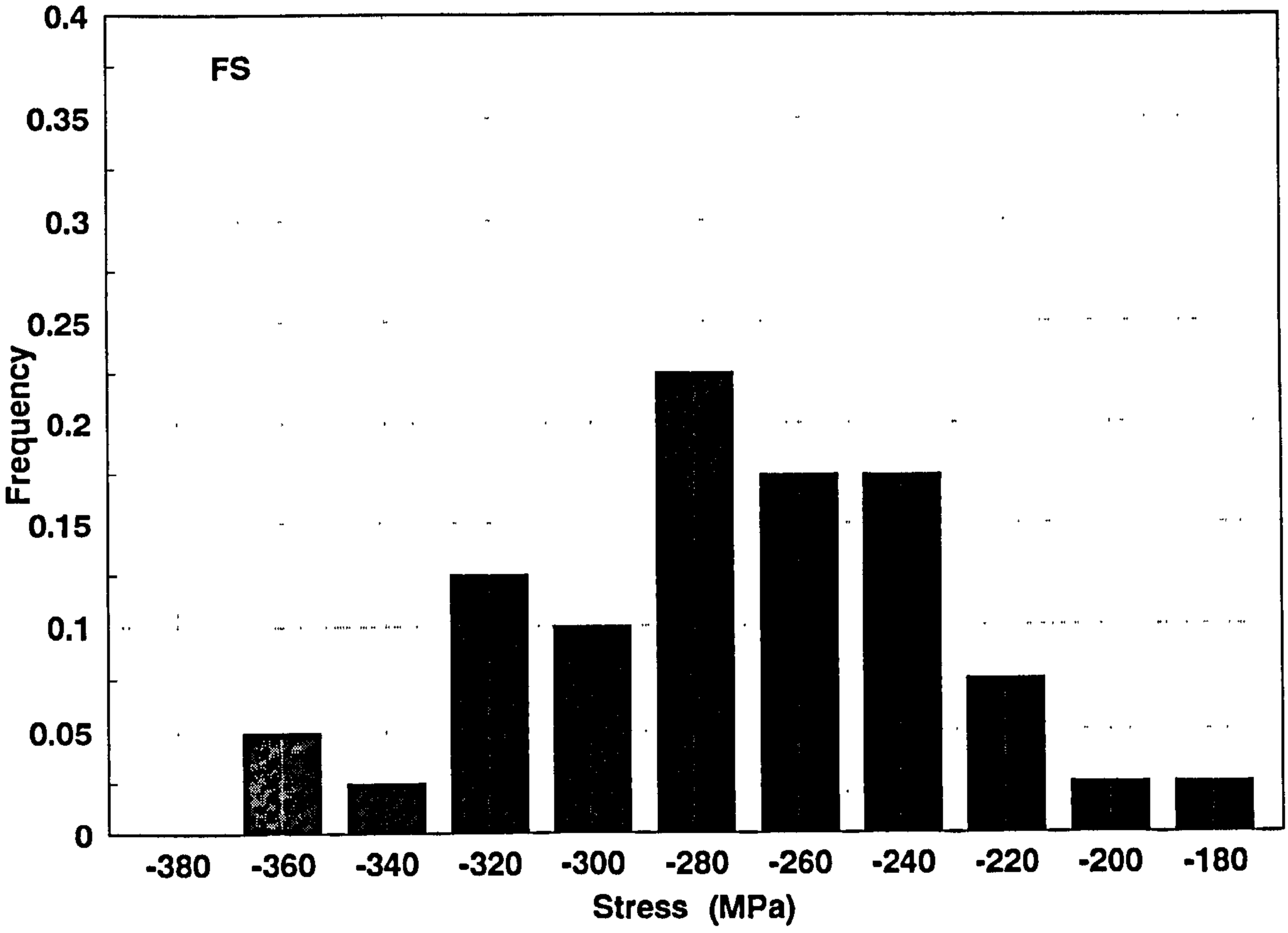

Fig 4.10 Axial residual stress distribution of 20 FS specimens

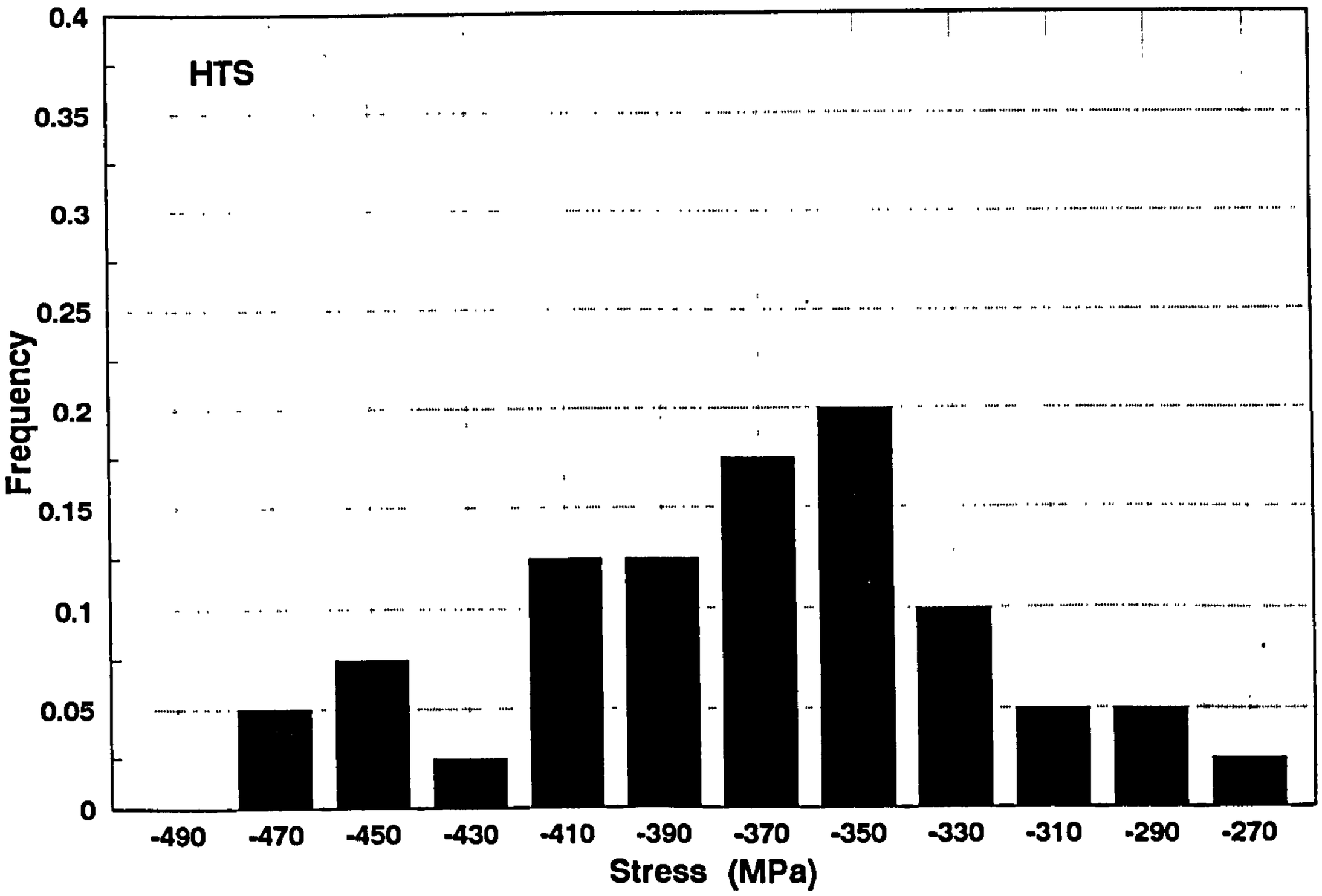

Fig 4.11 Axial residual stress distribution of 20 HTS specimens

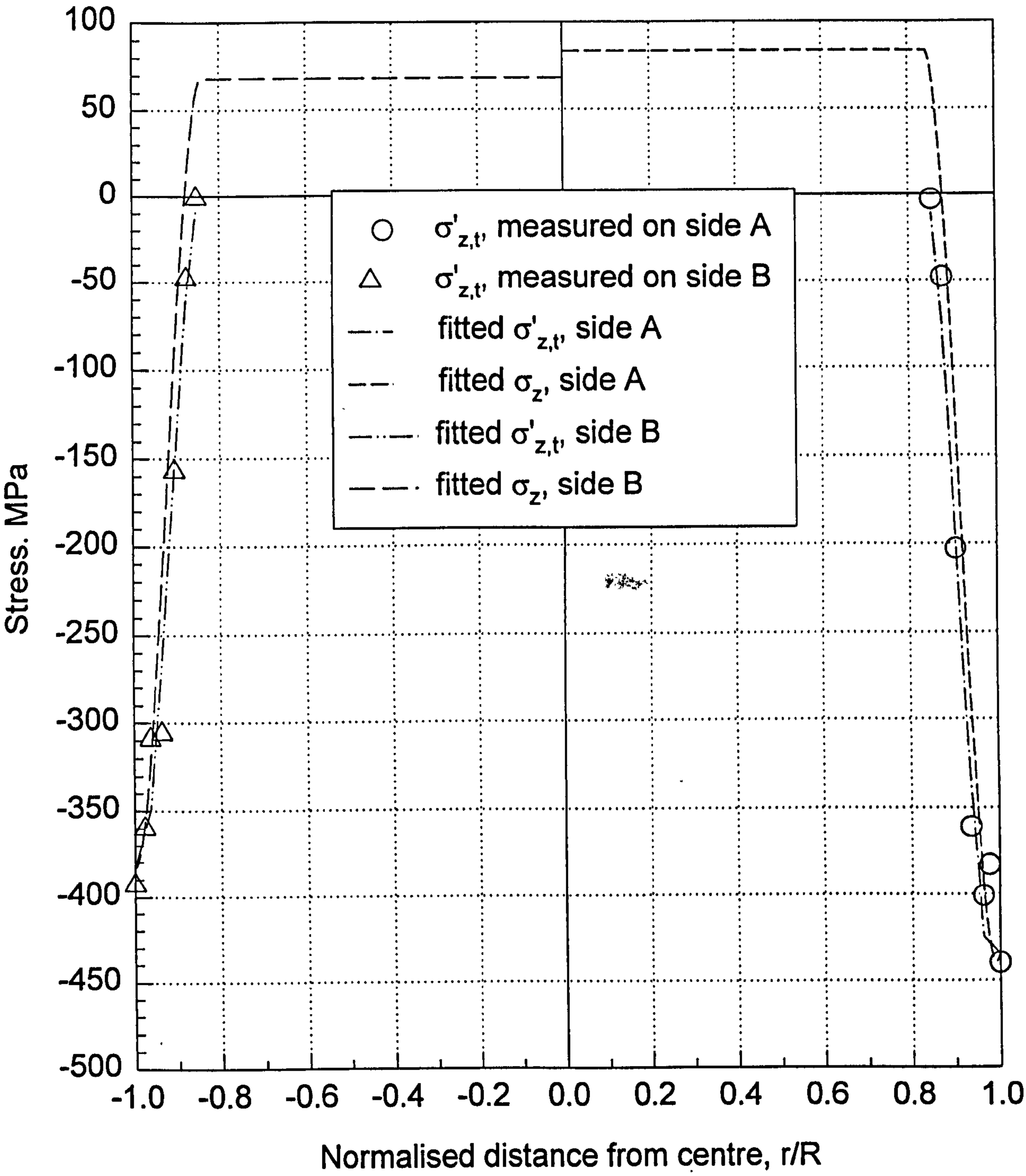

Fig 4.12 Axial residual stresses of HTS24 measured by X-ray after surface metal removal using chemical etching method.

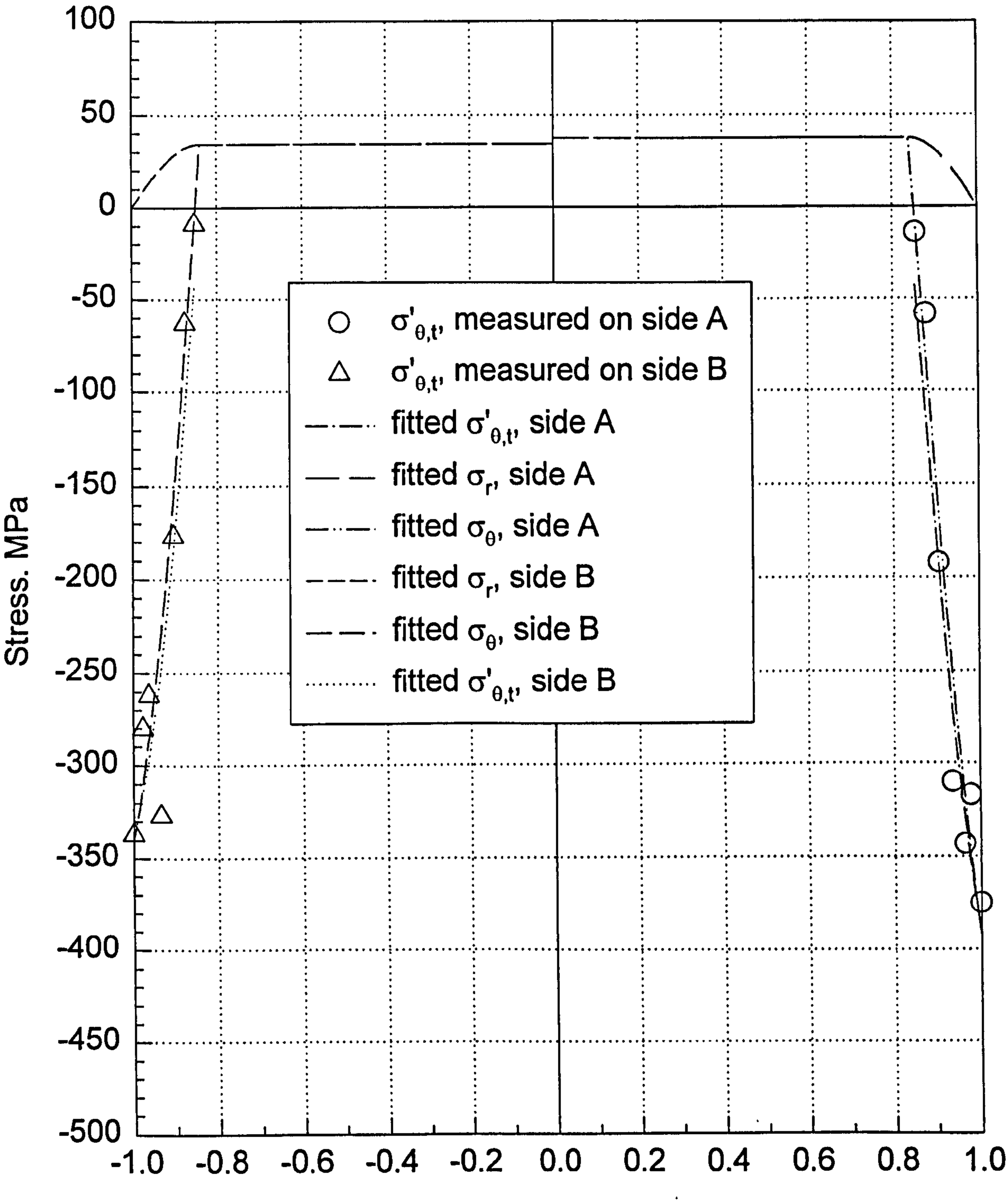

Fig 4.13 Tangential residual stresses of HTS24 measured by X-ray after surface metal removal using chemical etching method.

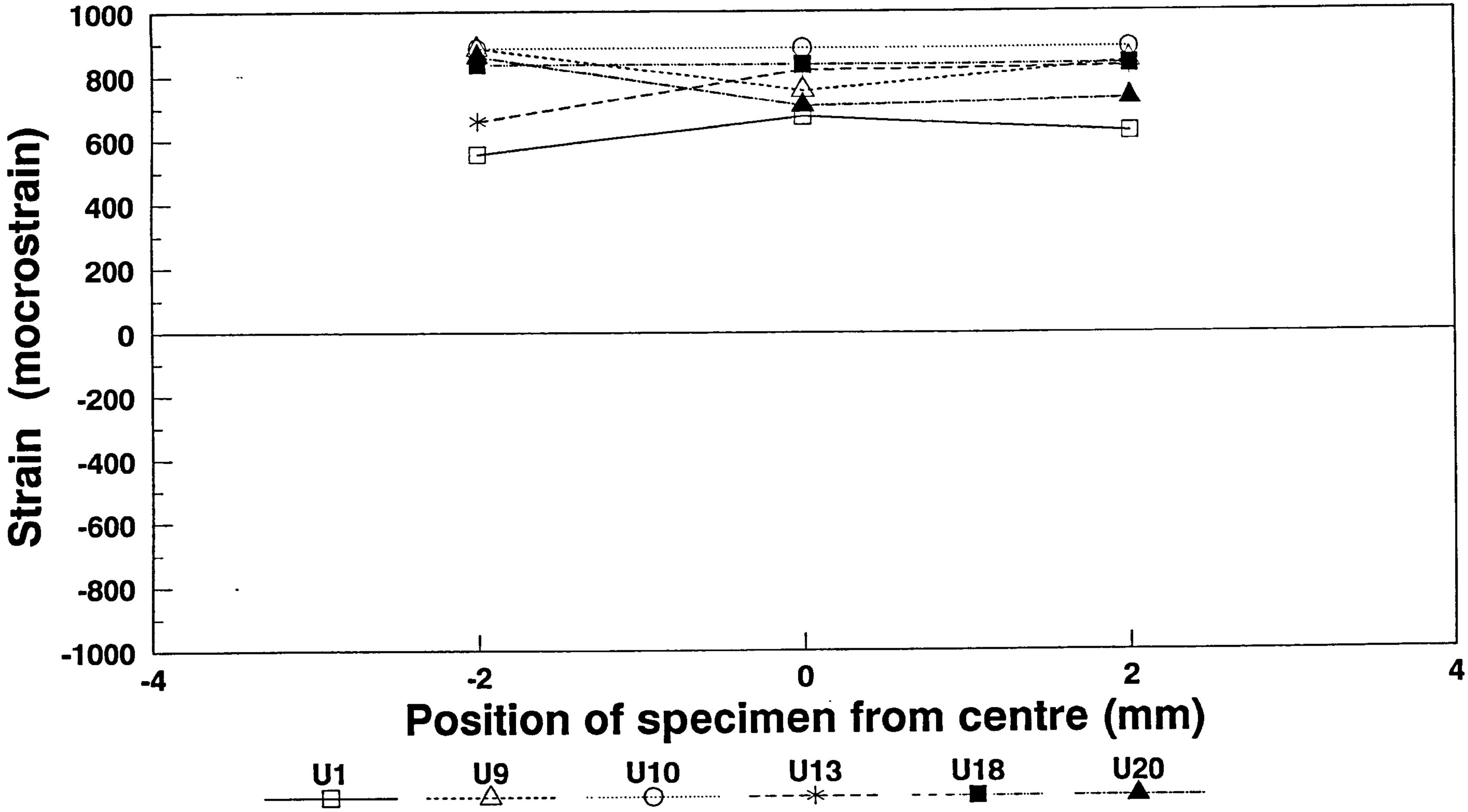

Fig 4.14 Axial strain in the interior of round bars measured with neutron diffraction

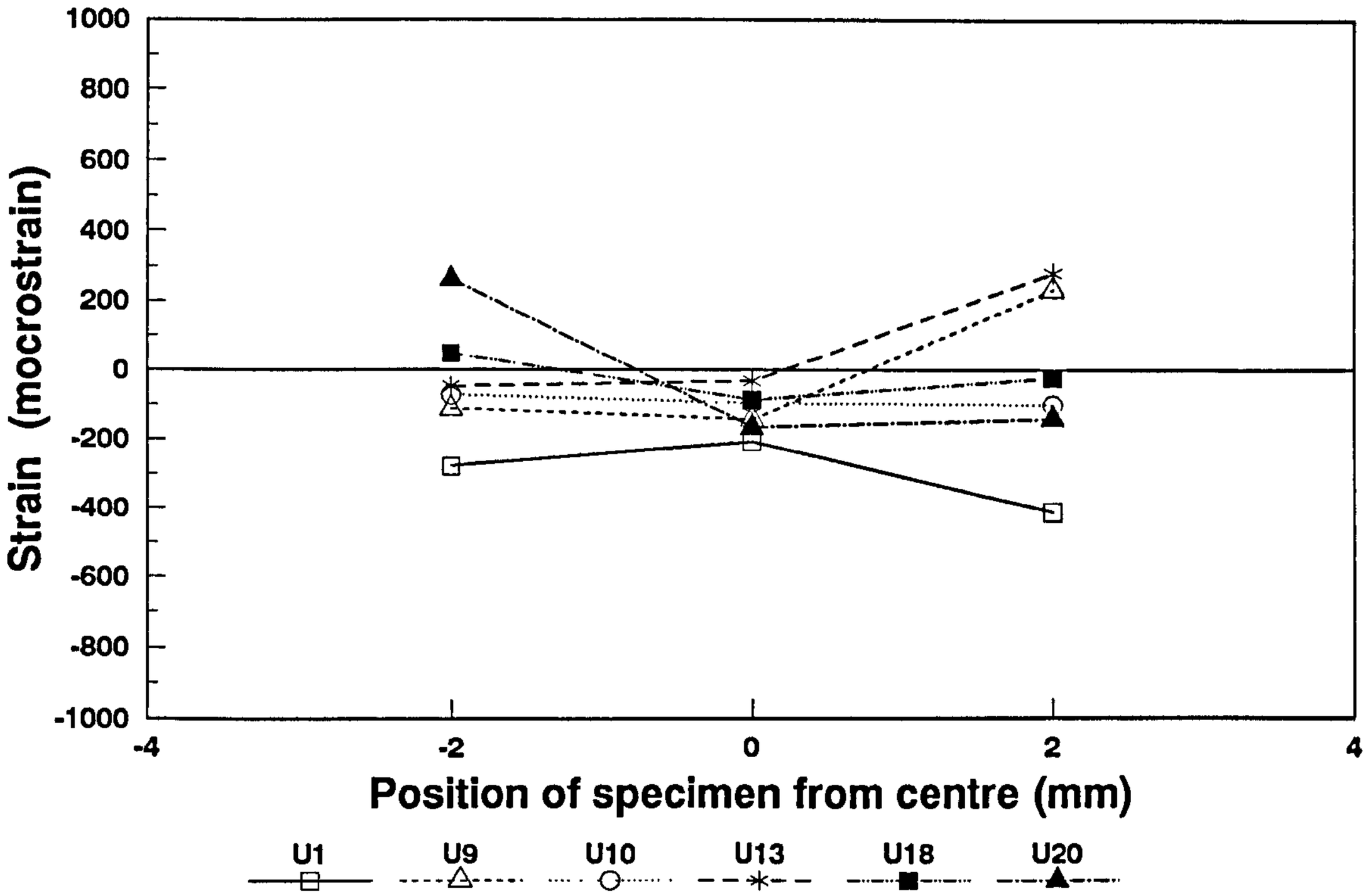

Fig. 4.15 Tangential strains in the interior of round bars measured with neutron diffraction

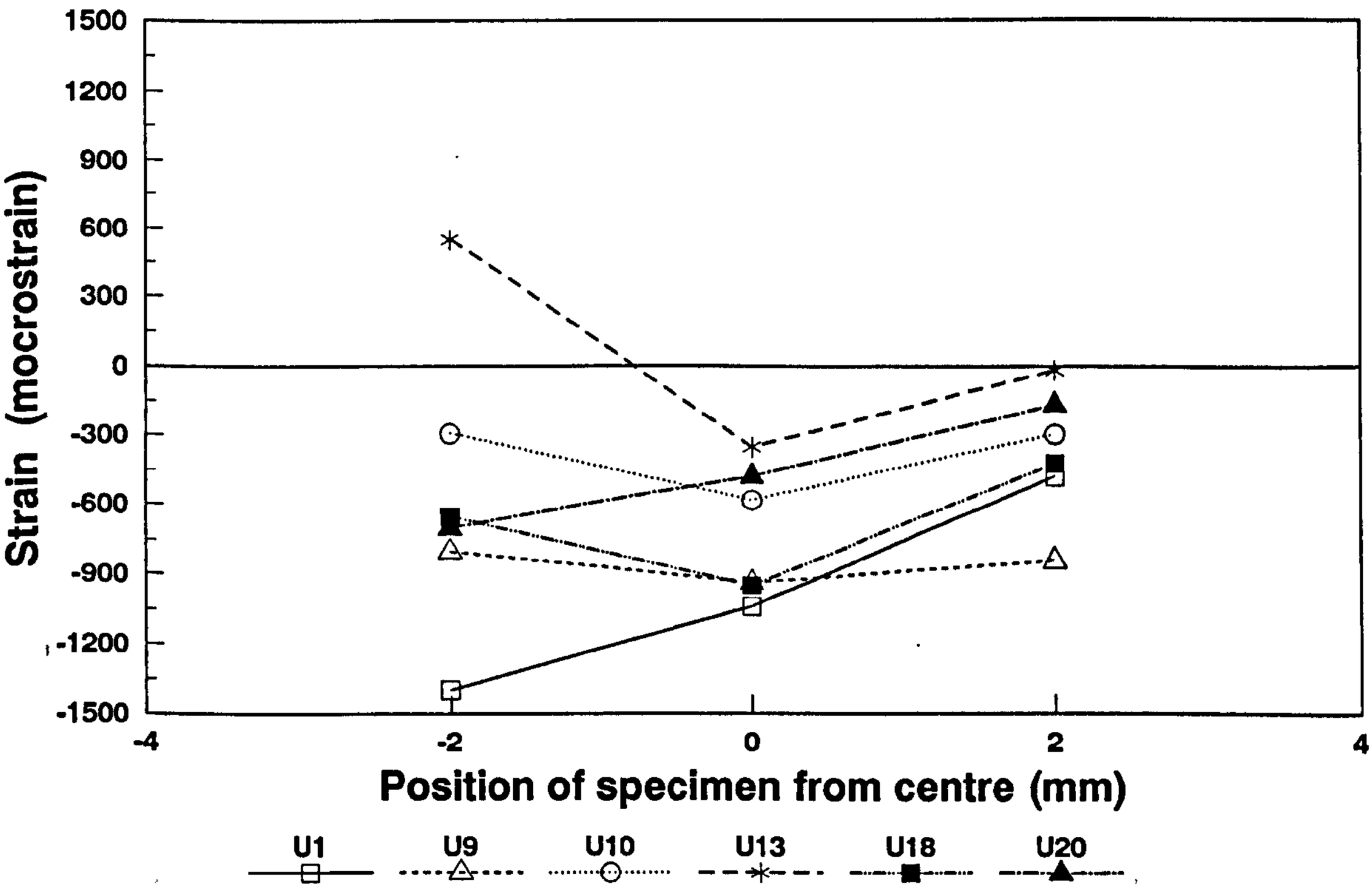

Fig. 4.16 Radial strains in the interior of round bars measured with neutron diffraction

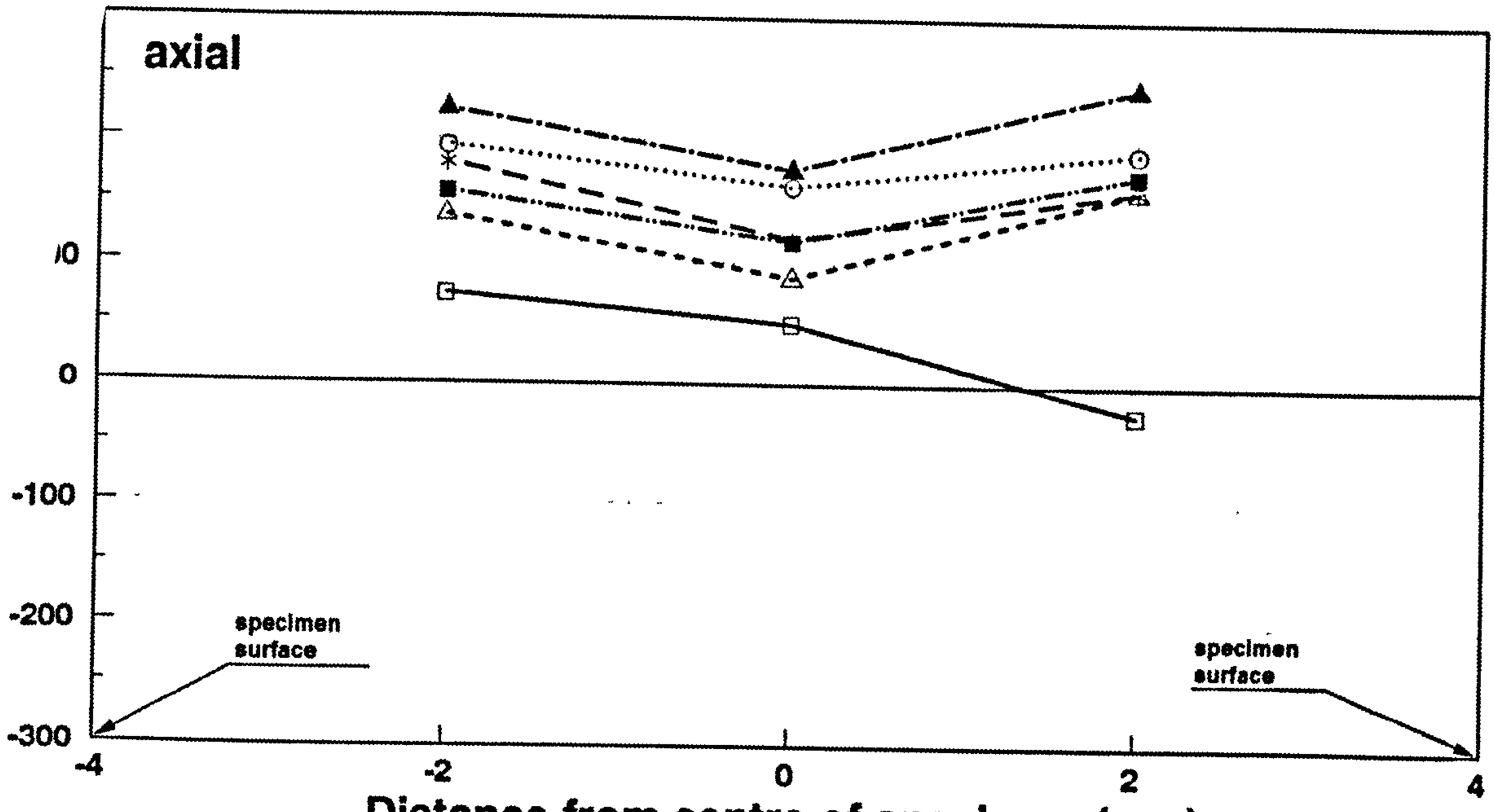

Fig. 4.17 Axial residual stress distribution for six specimens measured with neutron diffraction

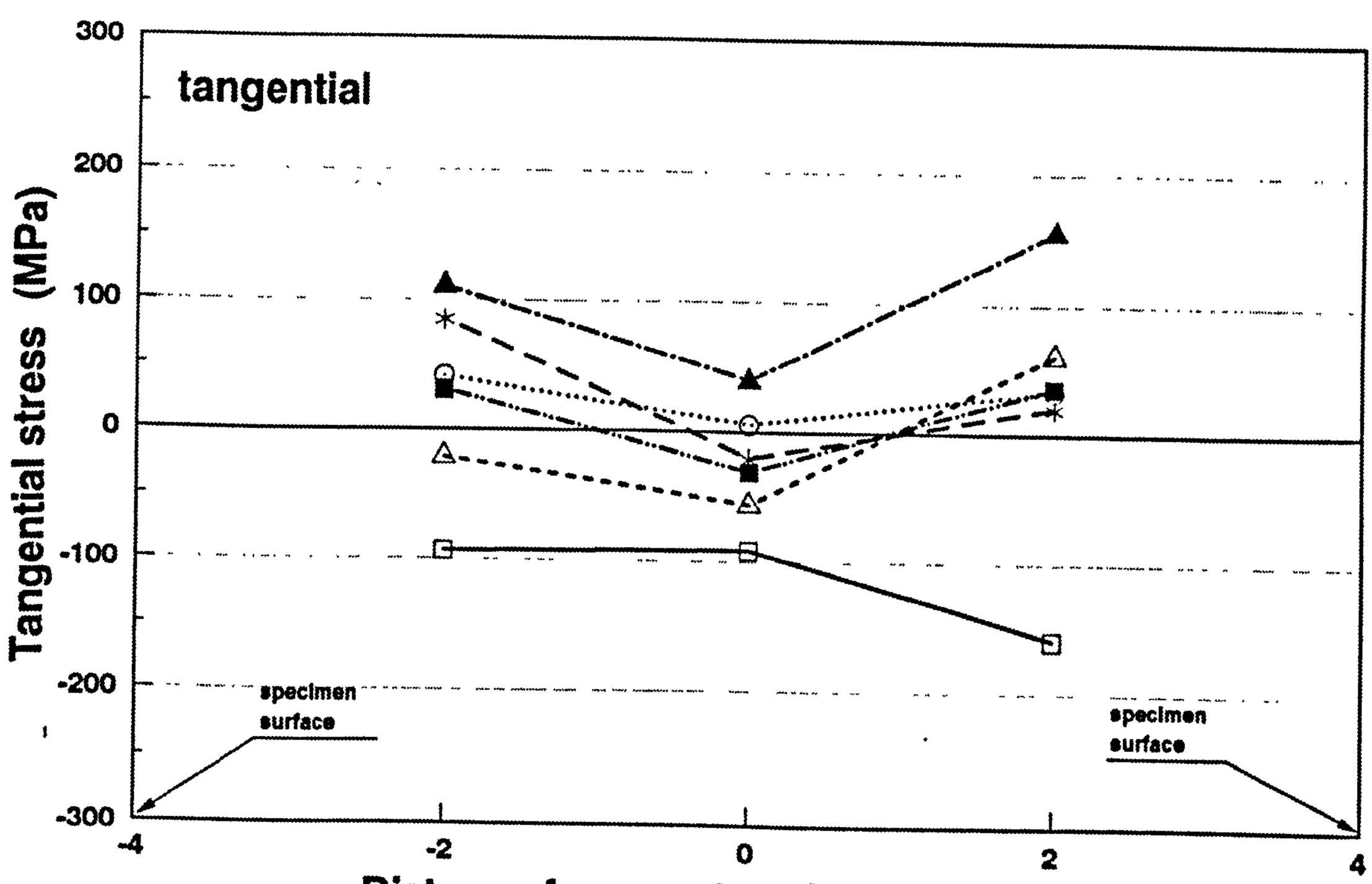

Fig. 4.18 Tangential residual stress distributio for six specimens measured with neutron diffraction

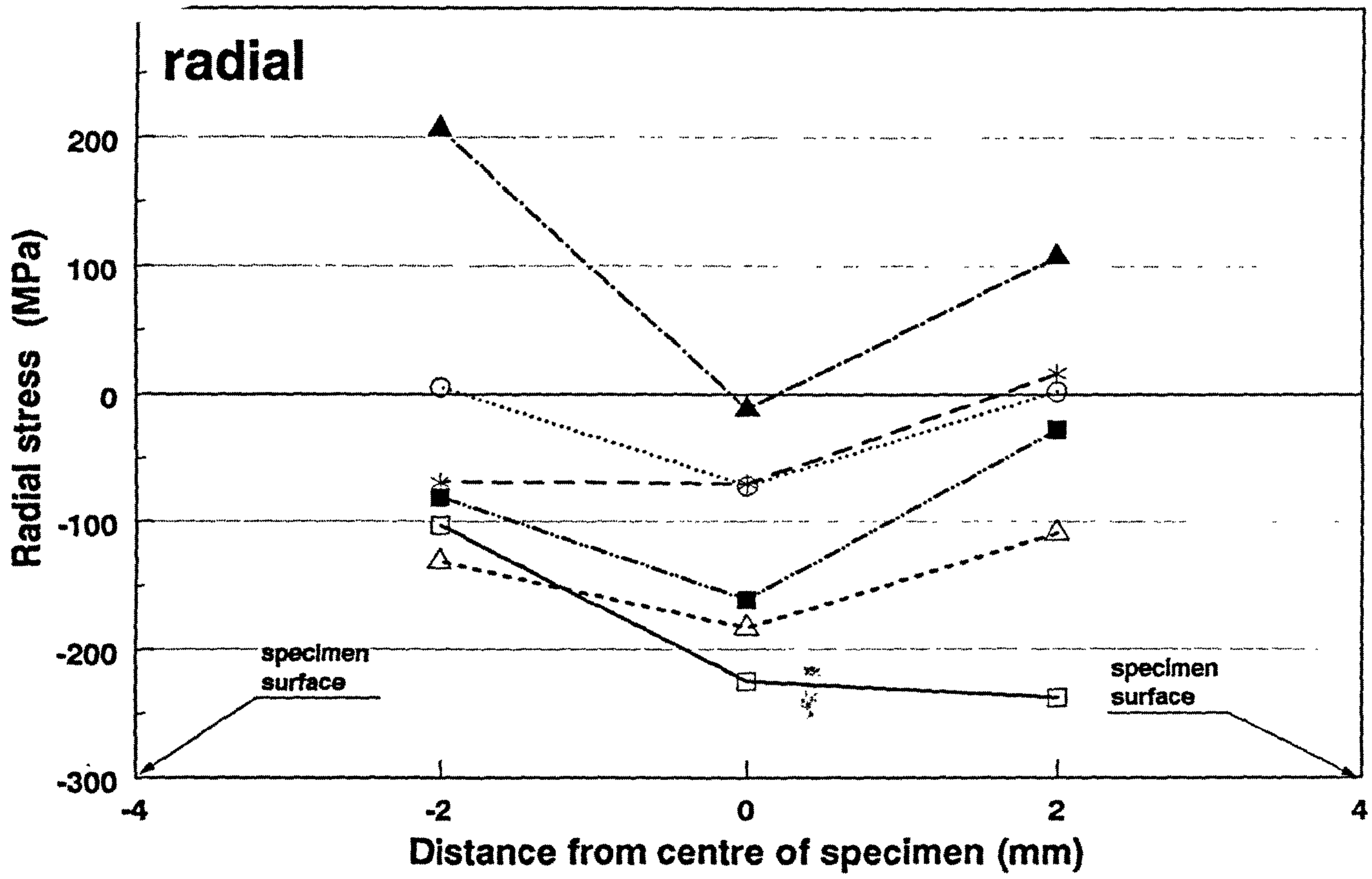

Fig. 4.19 Radial residual stress distribution for six specimens measured by neutron diffracti

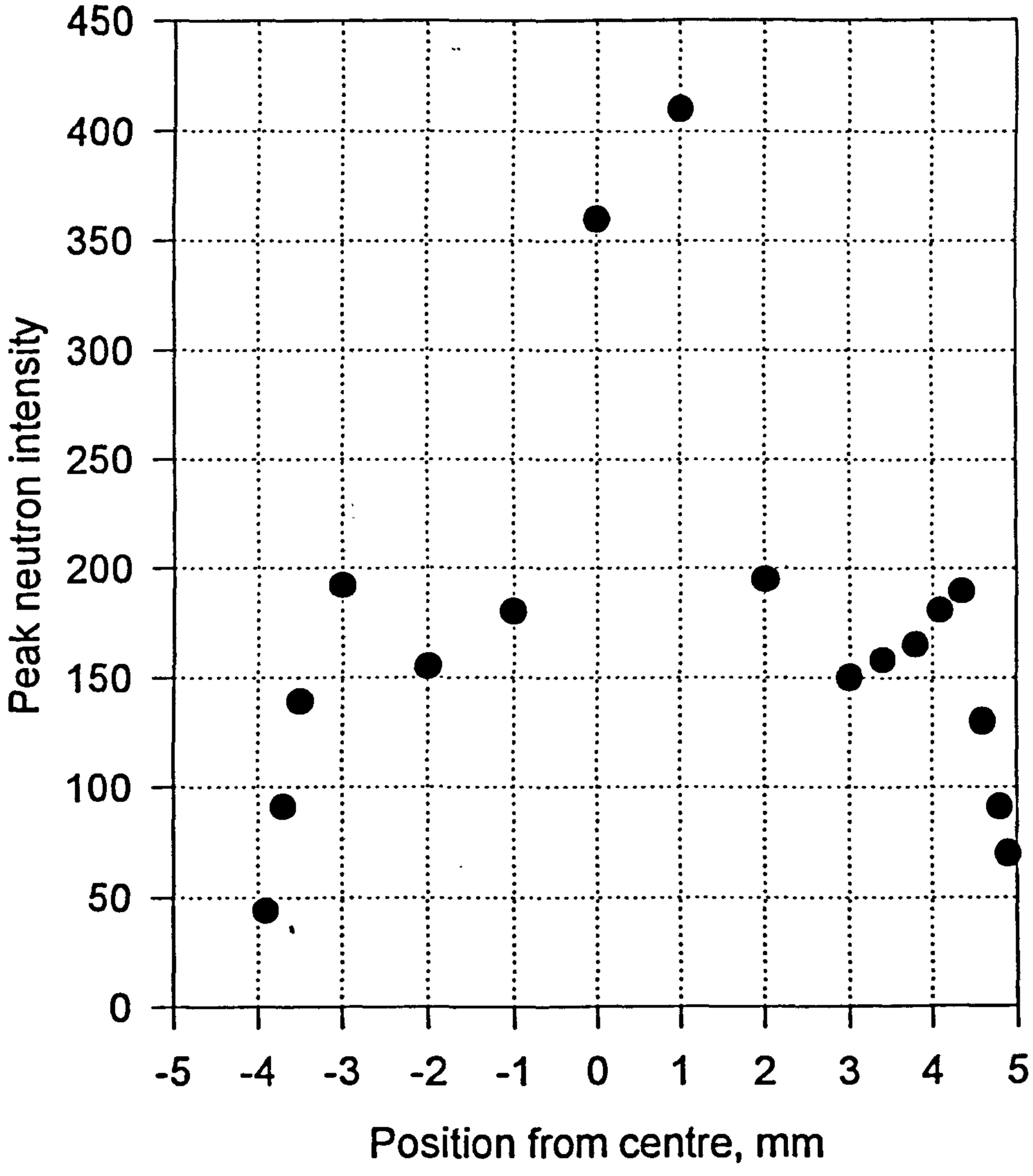

Fig 4.20 Neutron Peak Intensity of HTS18 stress free sample, tangential

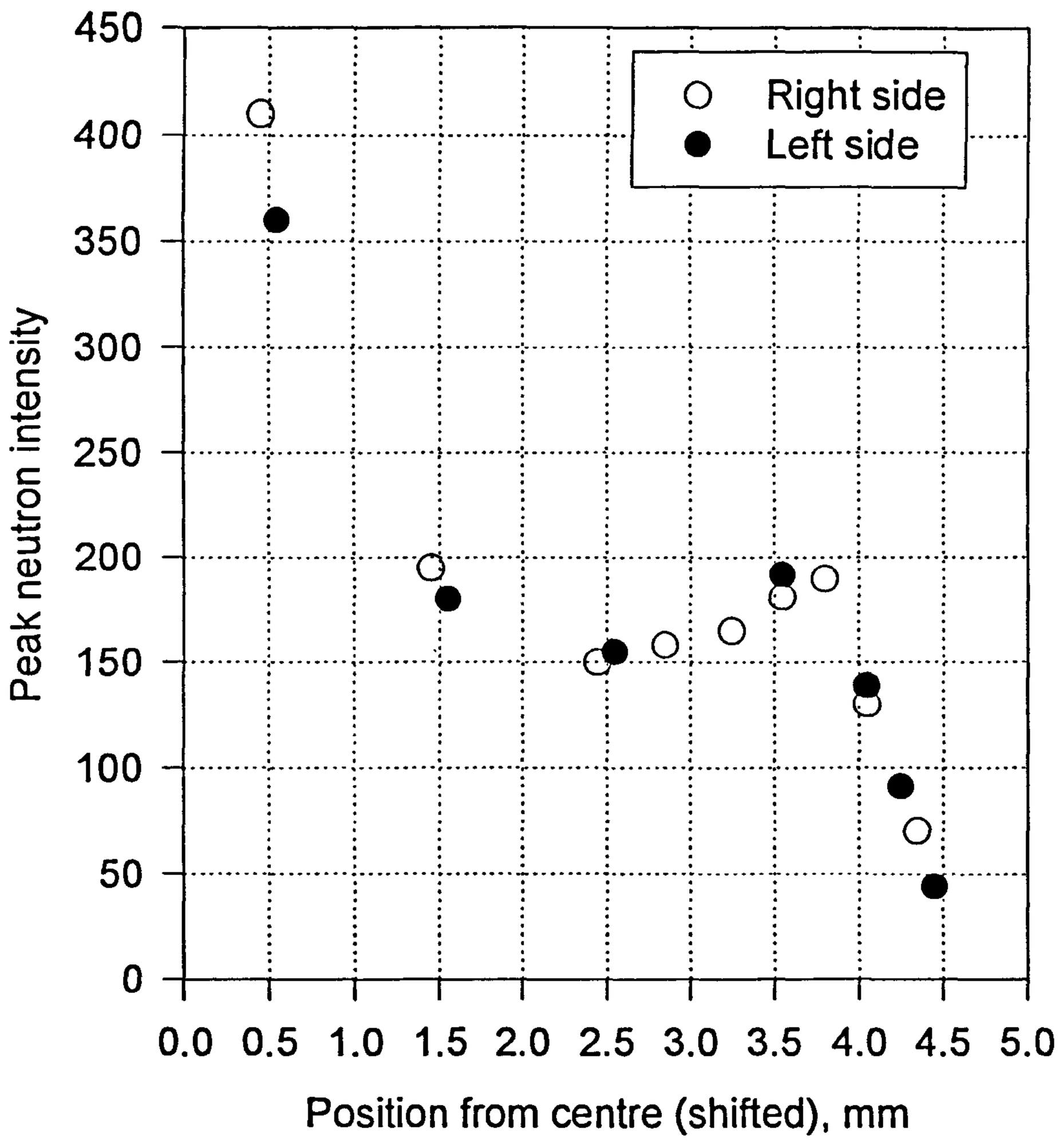

Fig 4.21 Neutron peak intensity of HTS18, comparison between left and right sides after centre shifted 0.55 mm

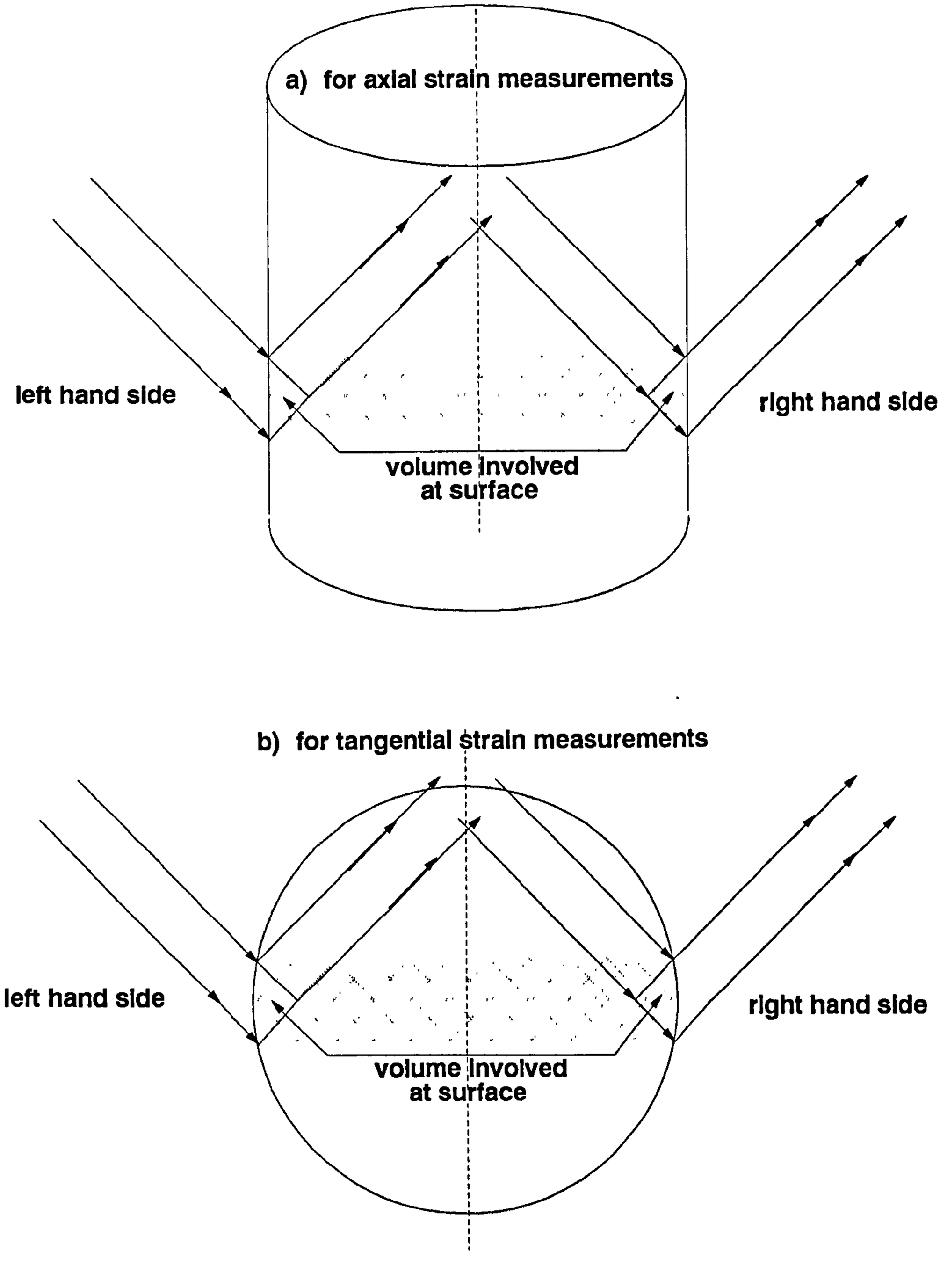

Fig 4.22 Neutron diffraction measurements across section for both axial and tangential strain measurements

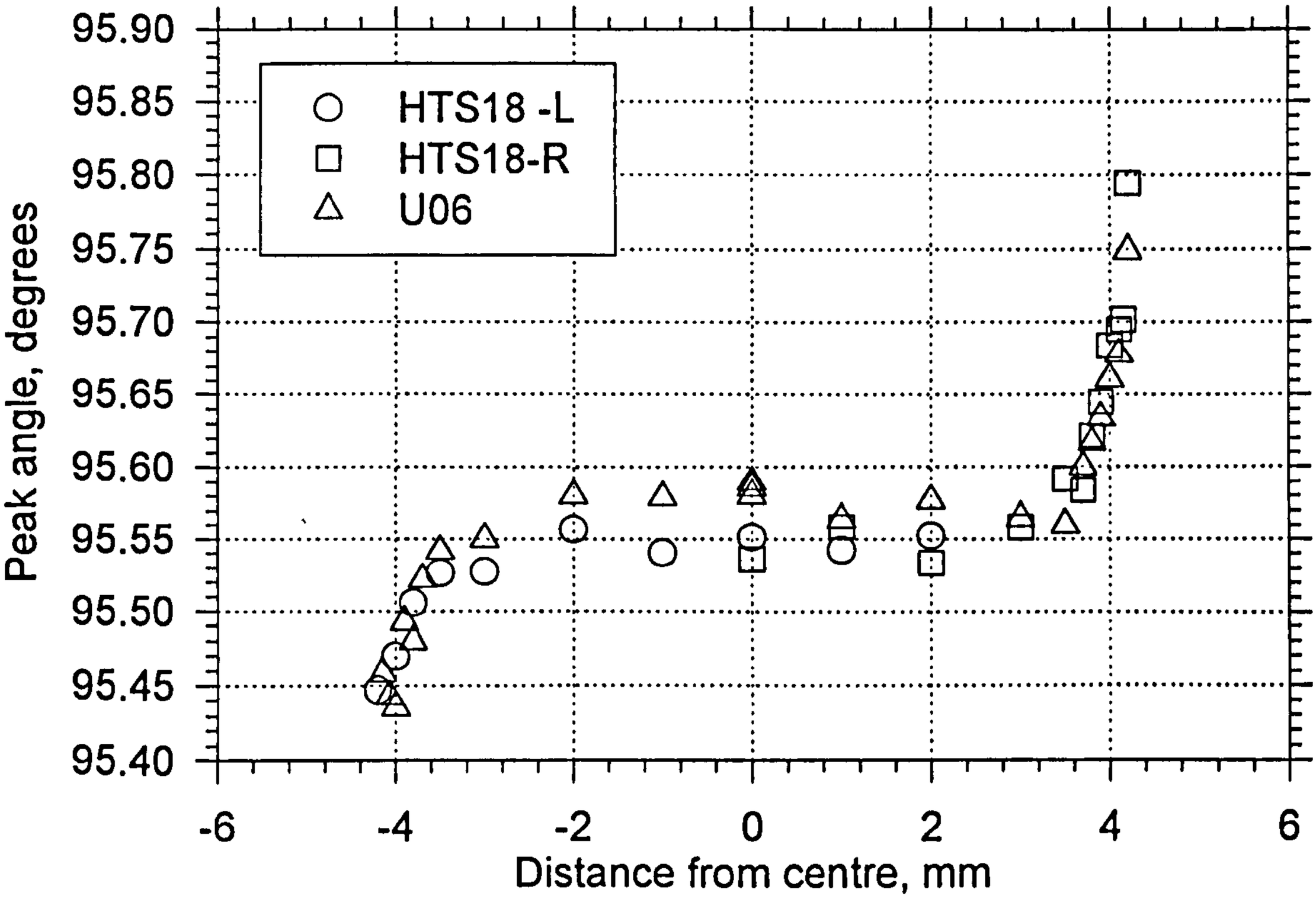

Fig 4.23 Peak angle in axial direction for stress free specimens HTS18 and U06

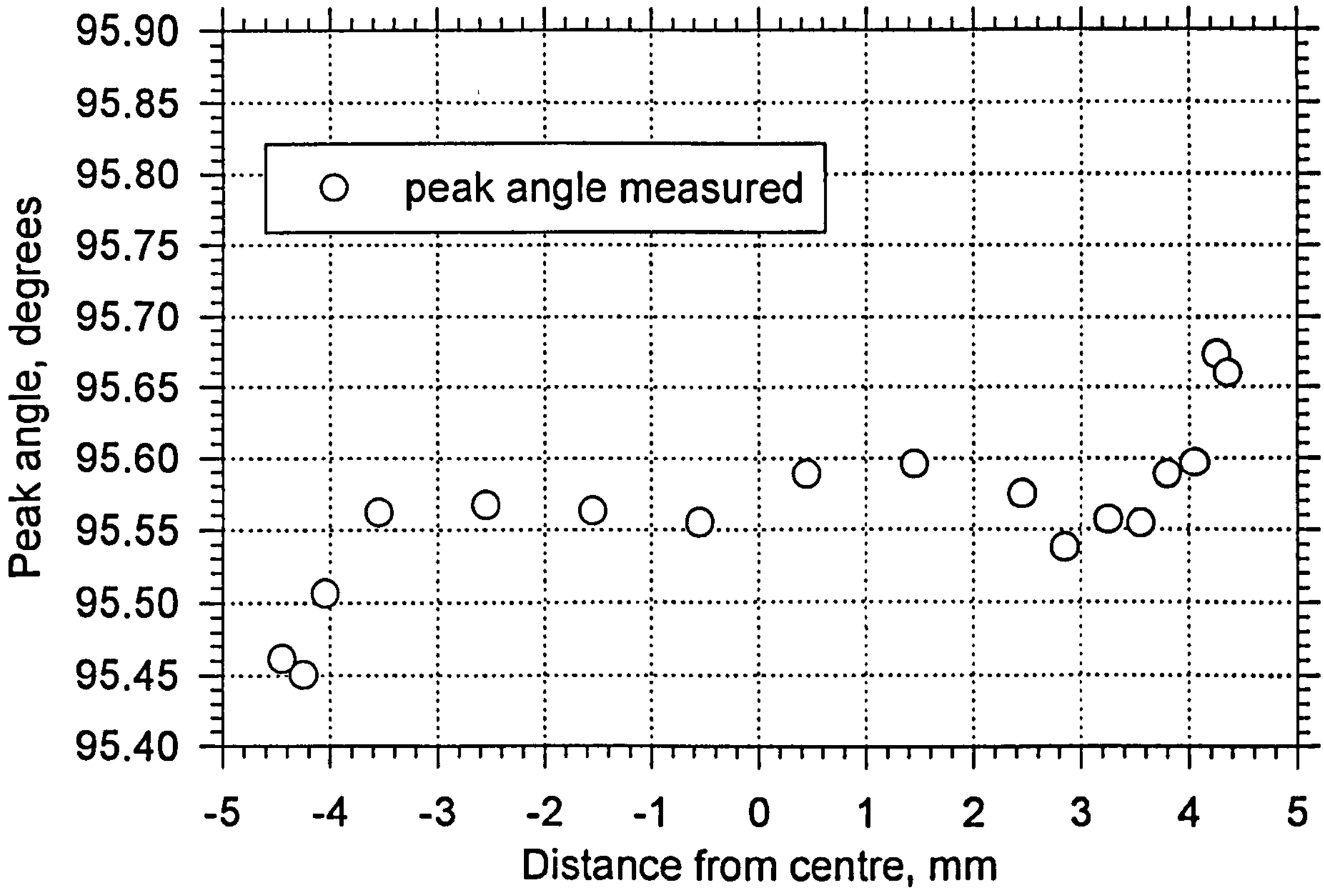

Fig 4.24 Peak angle in tangential direction for stress free specimens HTS18 and U06

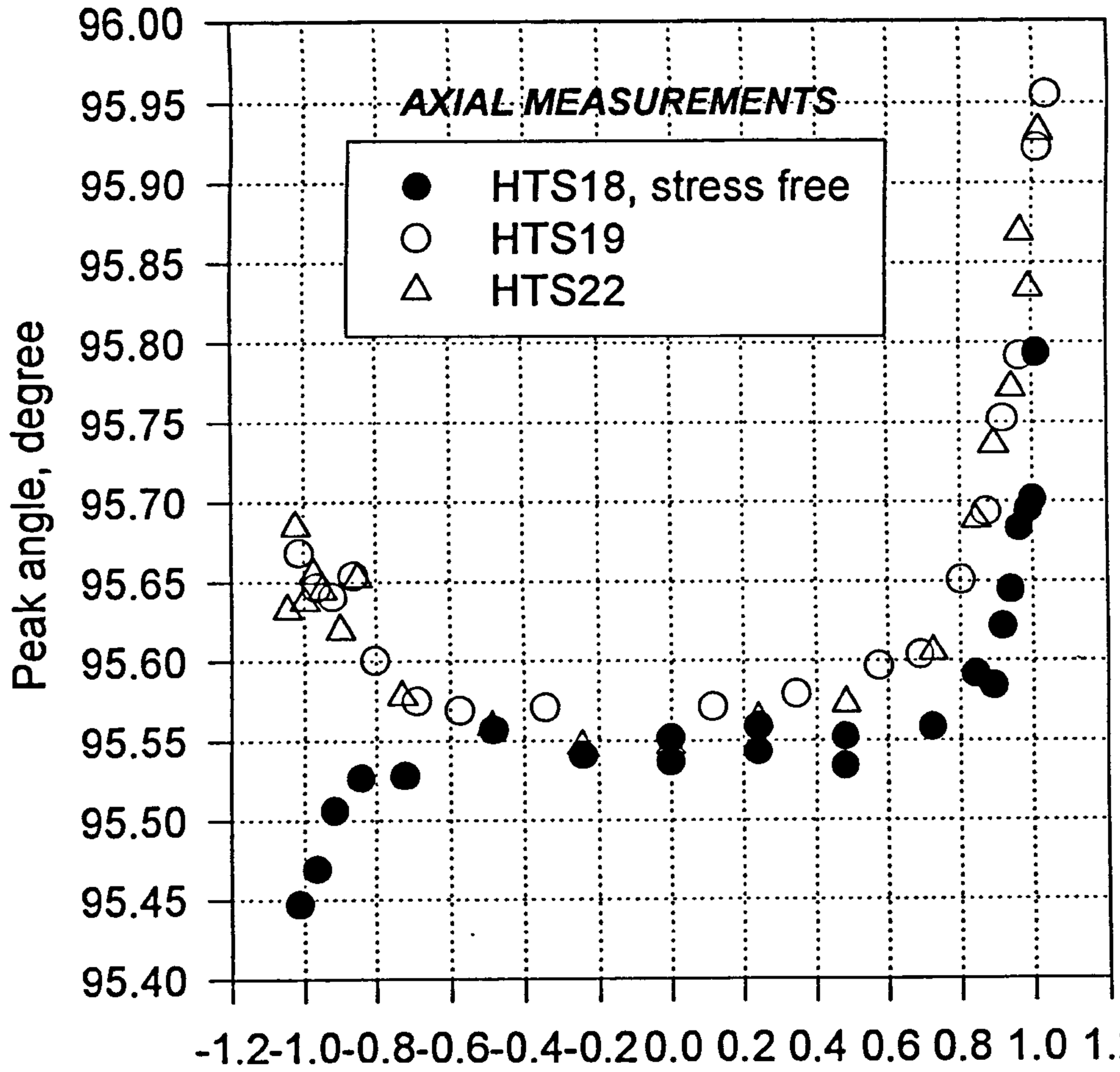

Fig 4.25 Peak angle measured for axial strain of HTS19 and HTS22, and comparison with that of HTS18

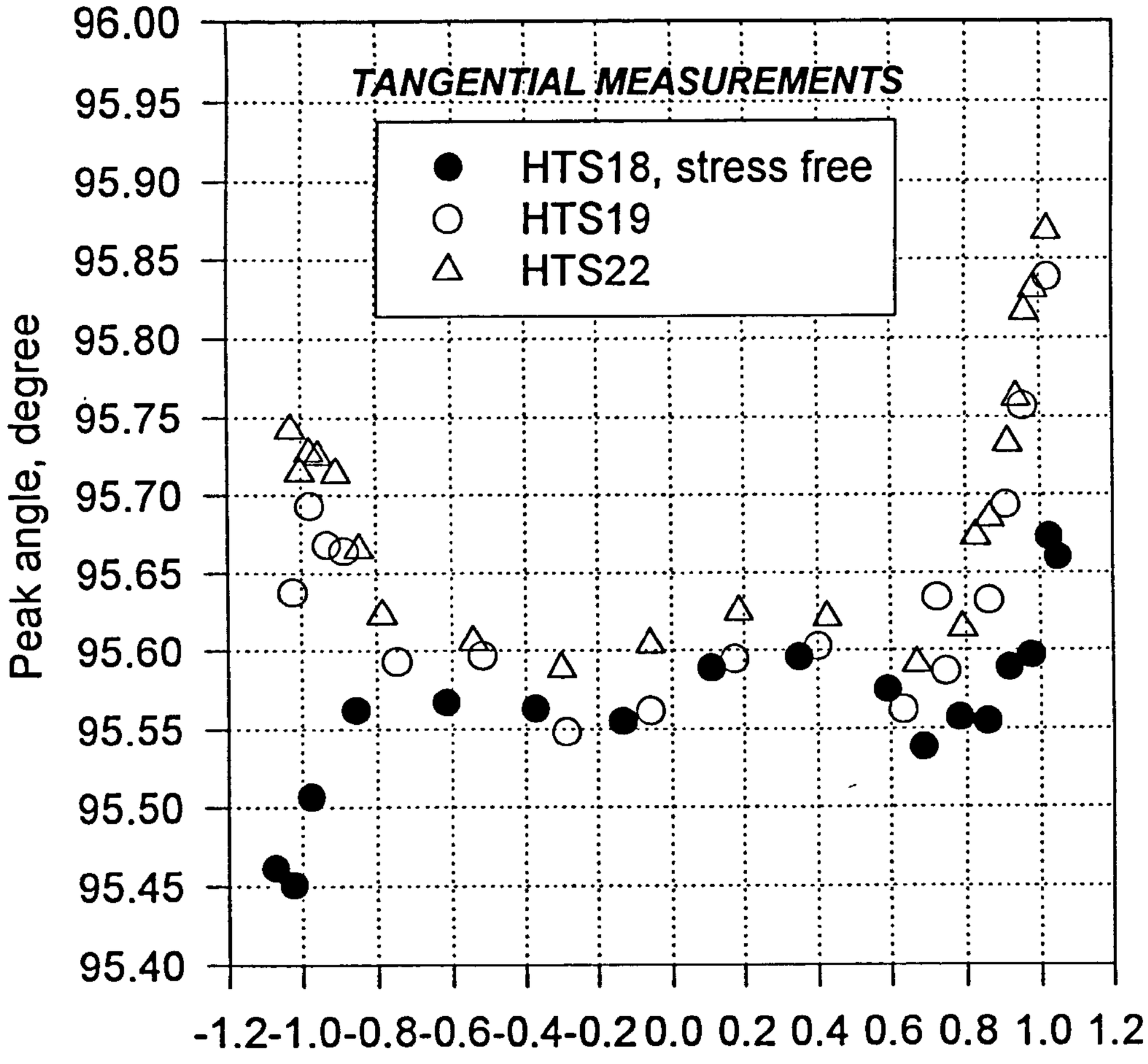

Fig 4.26 Peak angle measured for tangential strain of HTS19 and HTS22, and comparison with that of HTS18

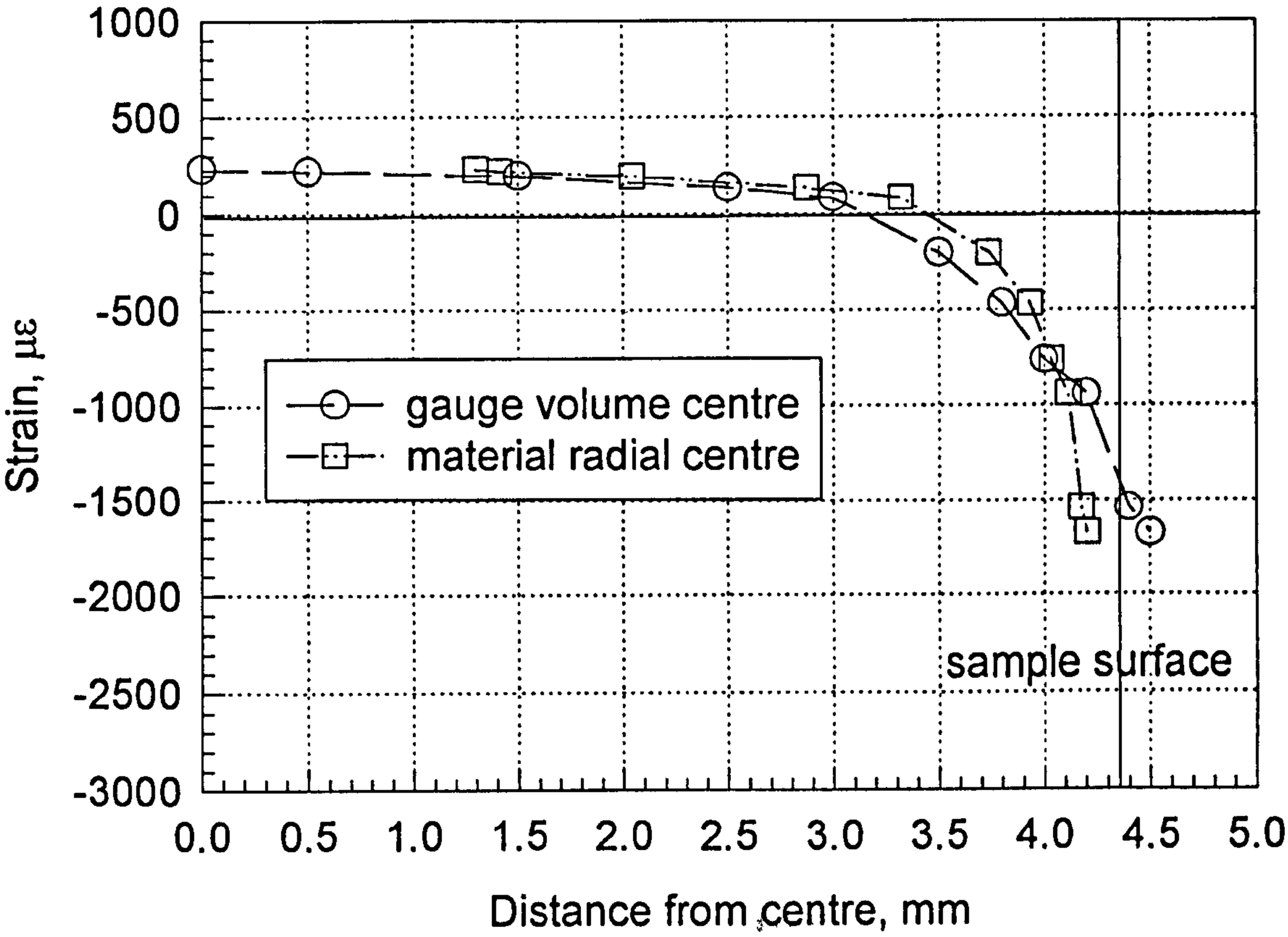

Fig 4.27 Axial strains of HTS19 by neutron diffraction

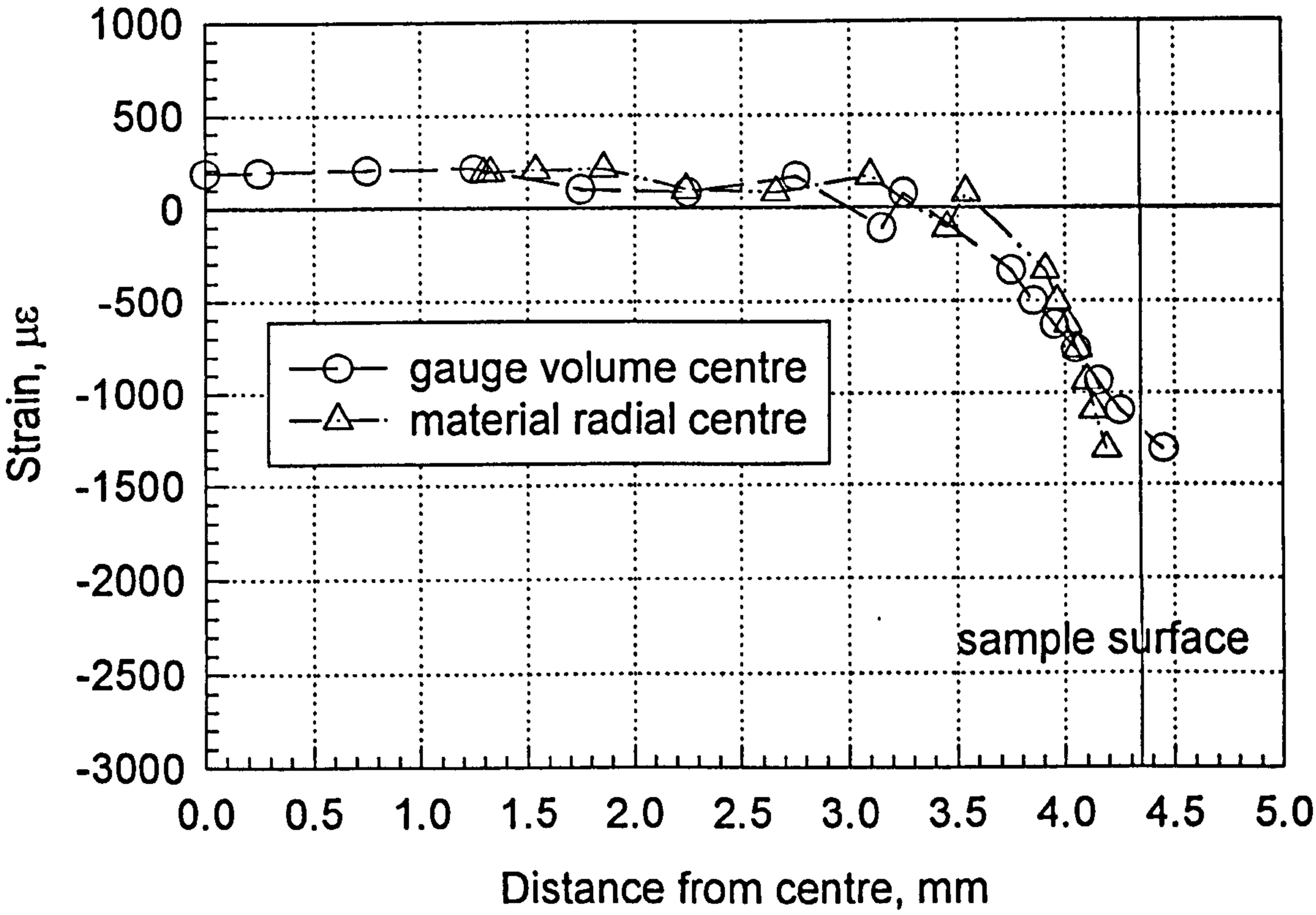

Fig 4.28 Tangential strains of HTS19 by neutron diffraction

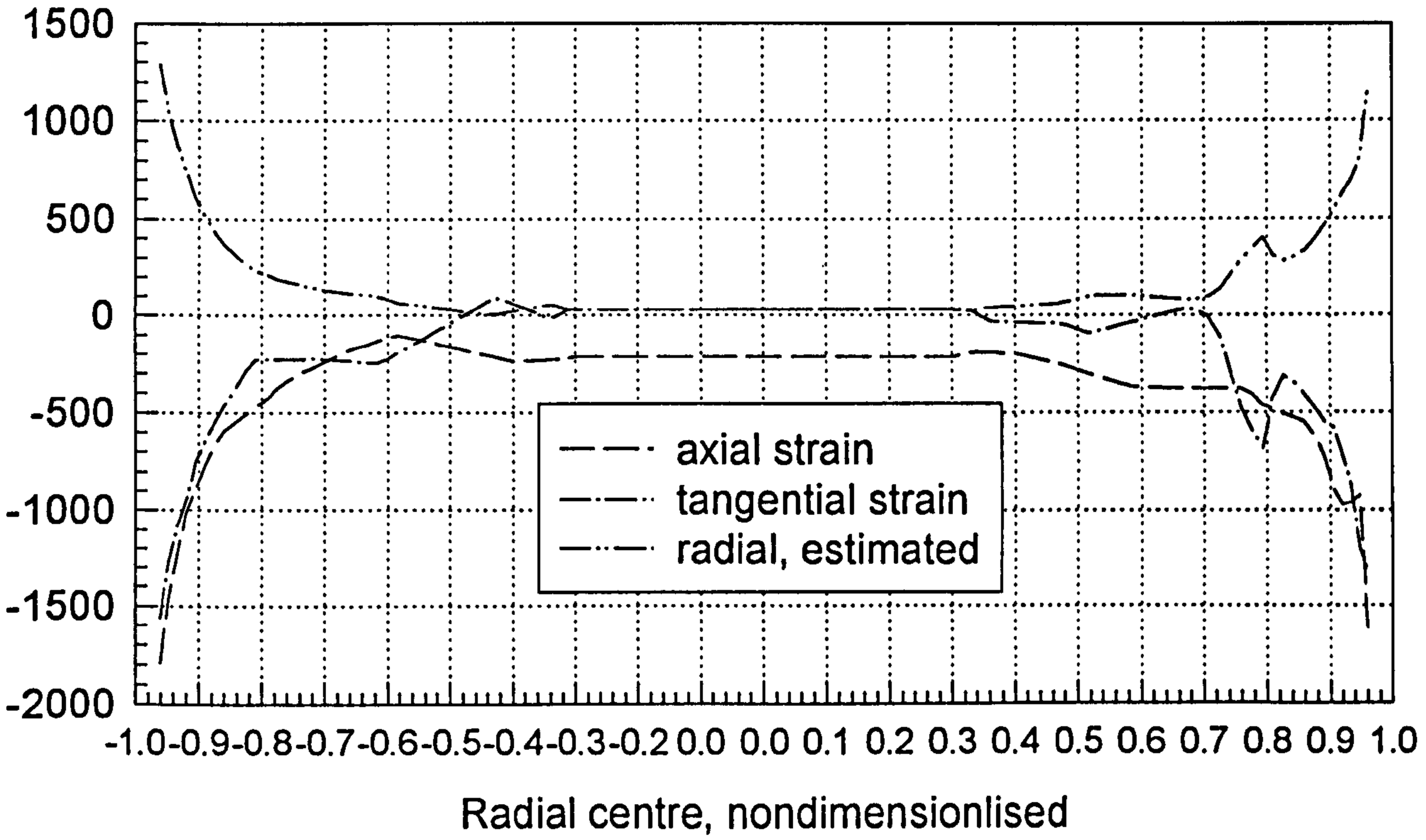

Fig 4.29 Strains in HTS19 by taking the difference of peak angle between HTS19 and stress free sample HTS18

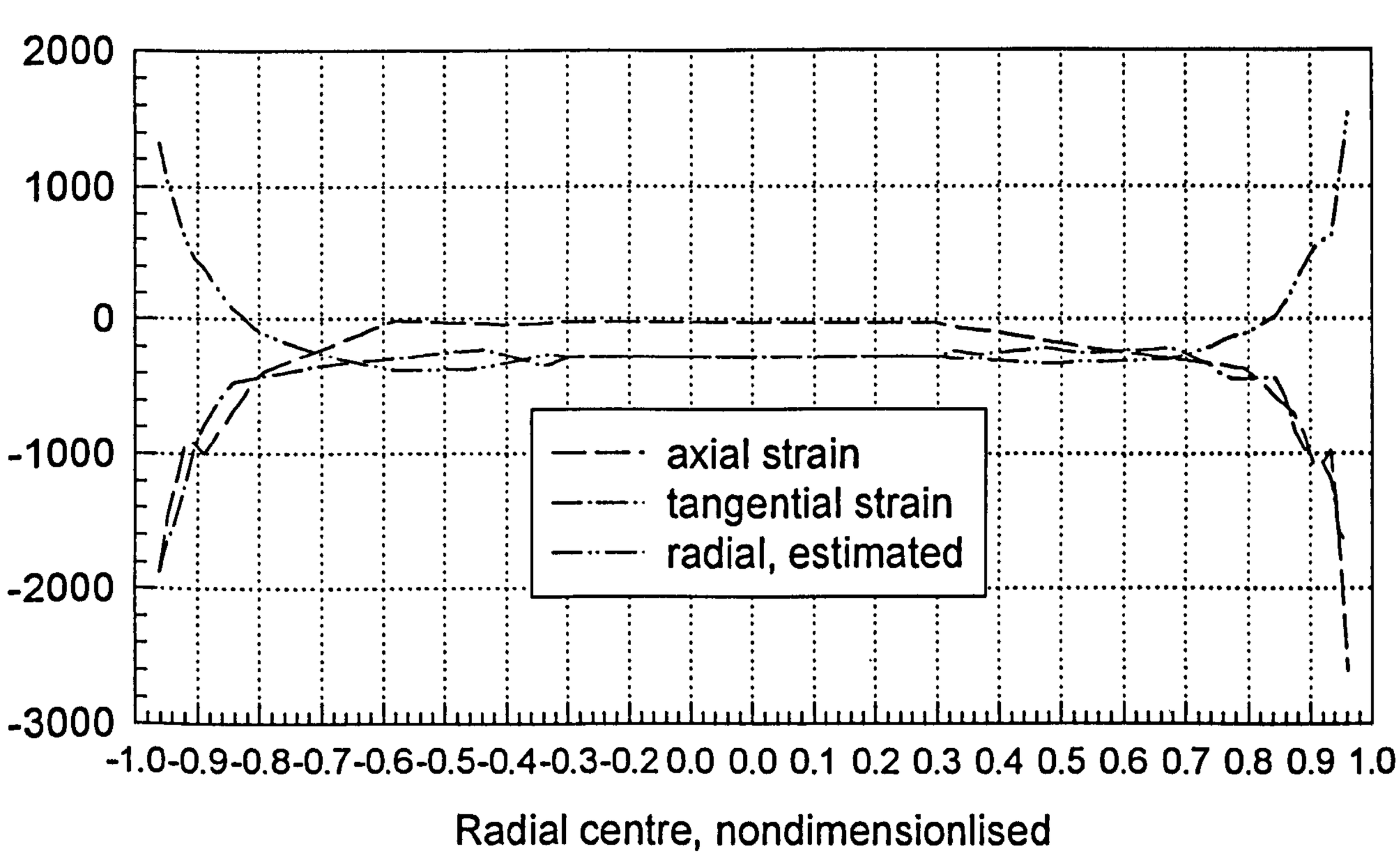

Fig 4.30 Strains in HTS22 by taking the difference of peak angle between HTS22 and stress free sample HTS18

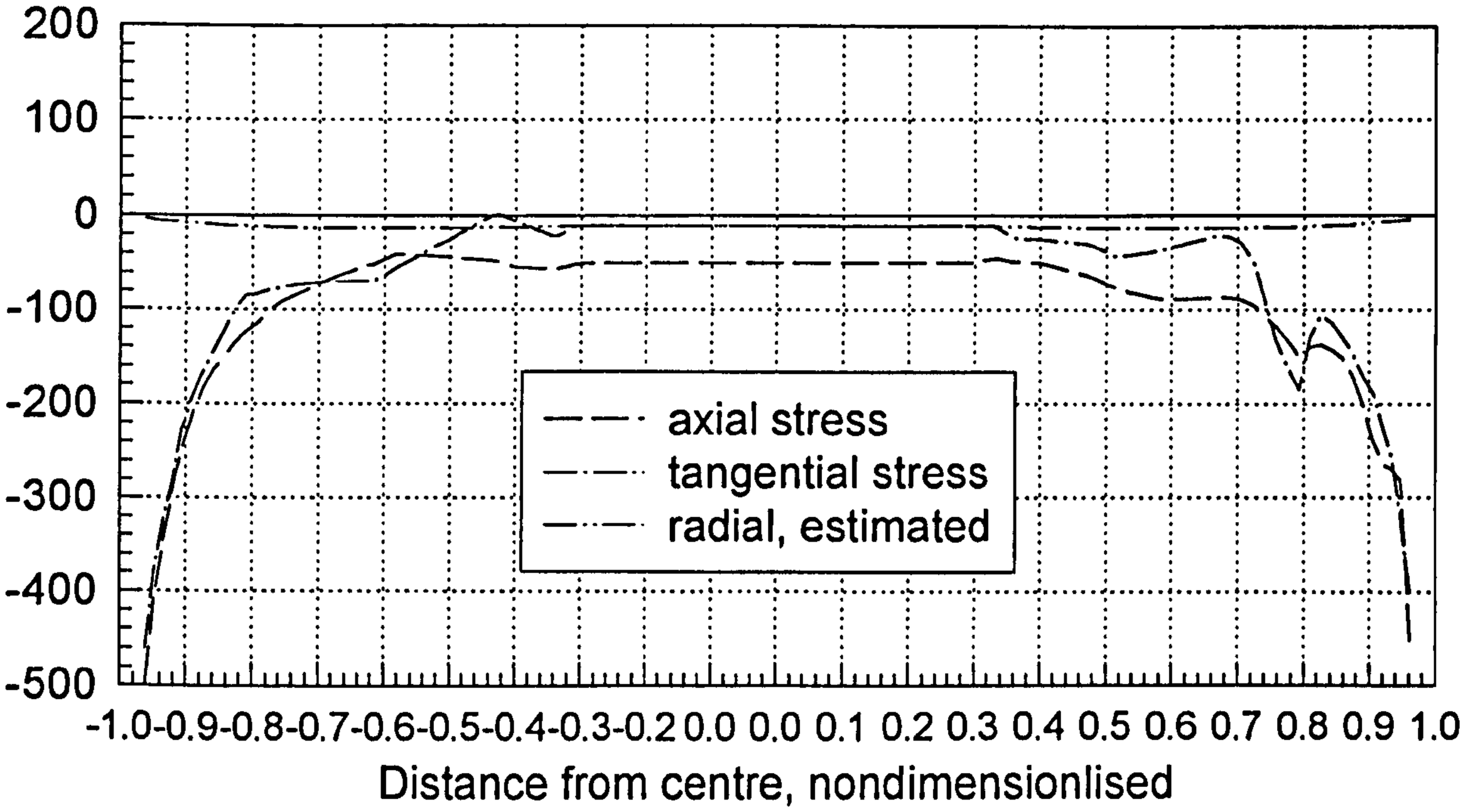

Fig 4.31 Residual stresses in HTS19 calculated from strains obtained by taking the difference of peak angle between HTS19 and stress free sample HTS 18

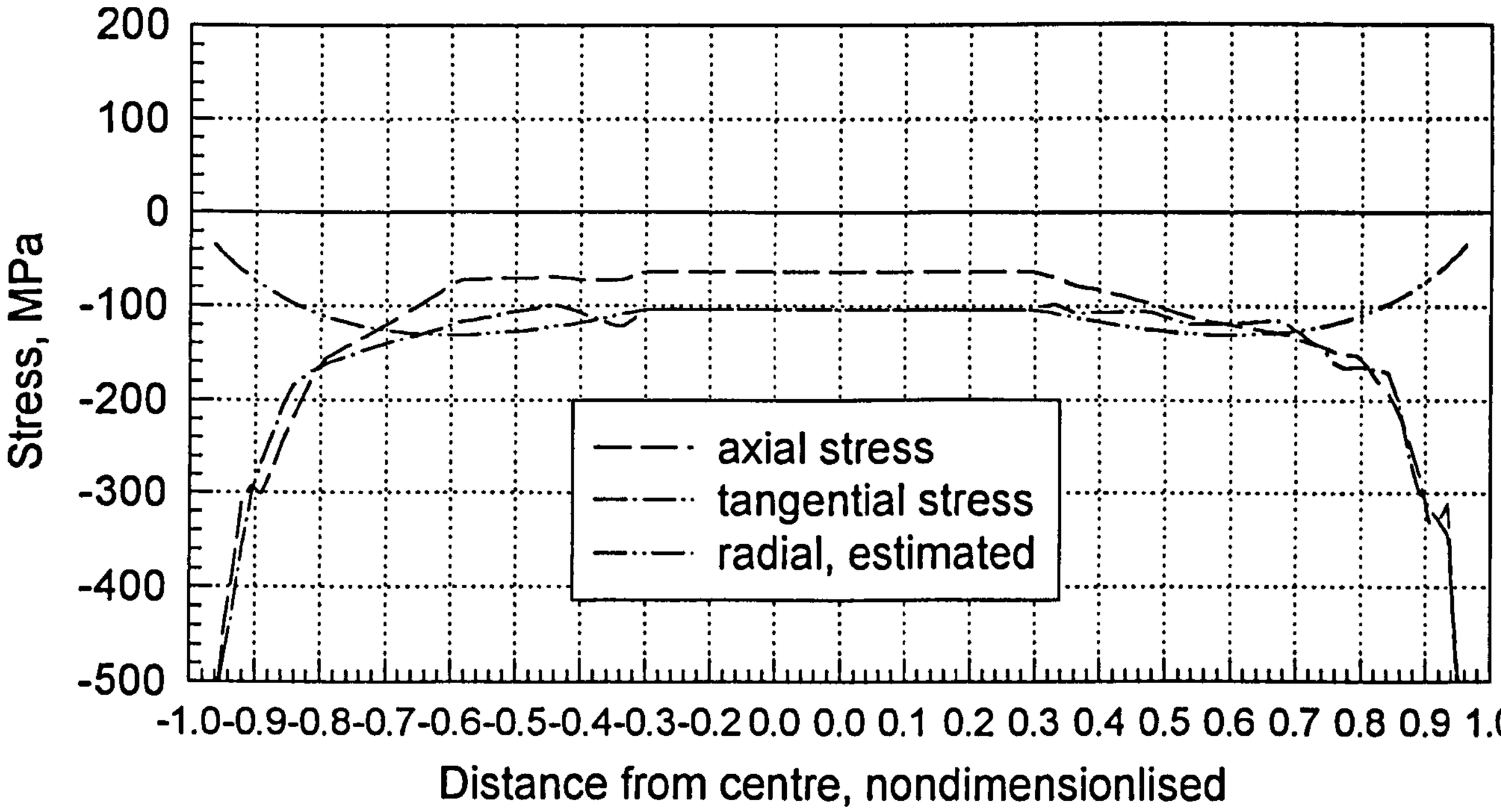

Fig 4.32 Residual stresses in HTS22 calculated from strains obtained by taking the difference of peak angle between HTS22 and stress free sample HTS 18

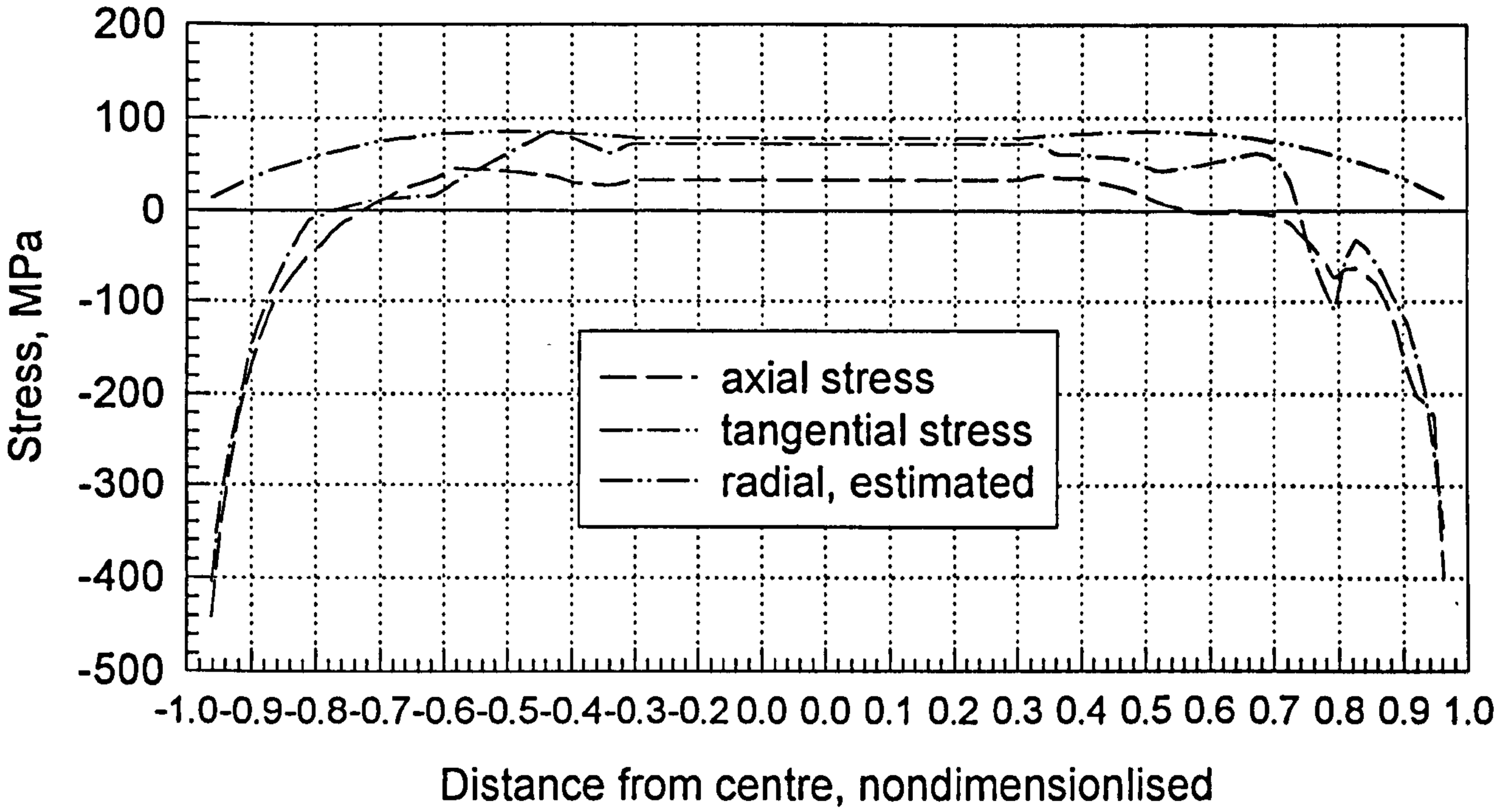

Fig 4.33 Residual stresses in HTS19 calculated from strains modified by adding a constant strain

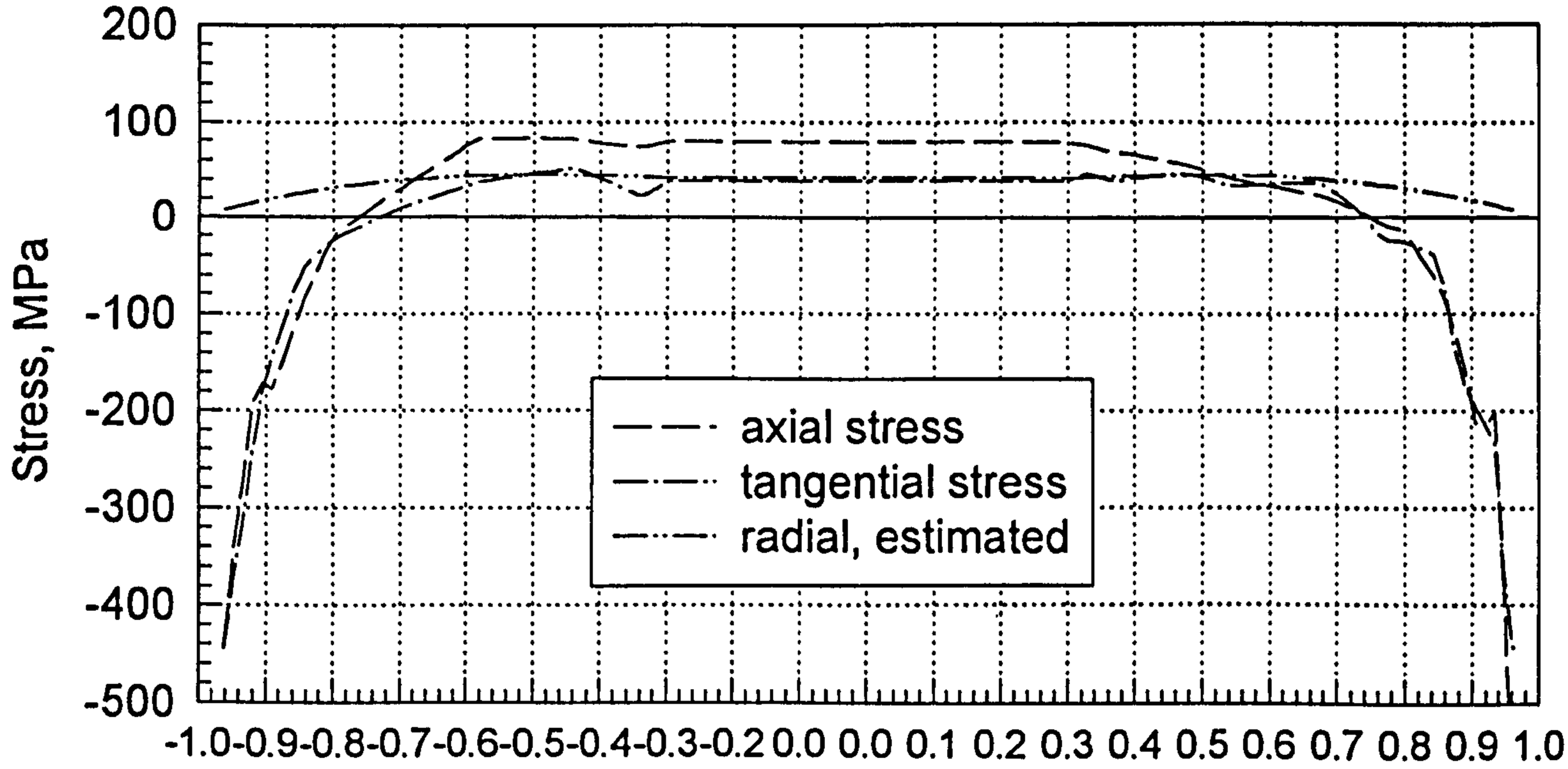

Fig 4.34 Residual stresses in HTS22 calculated from strains modified by adding a constant strain

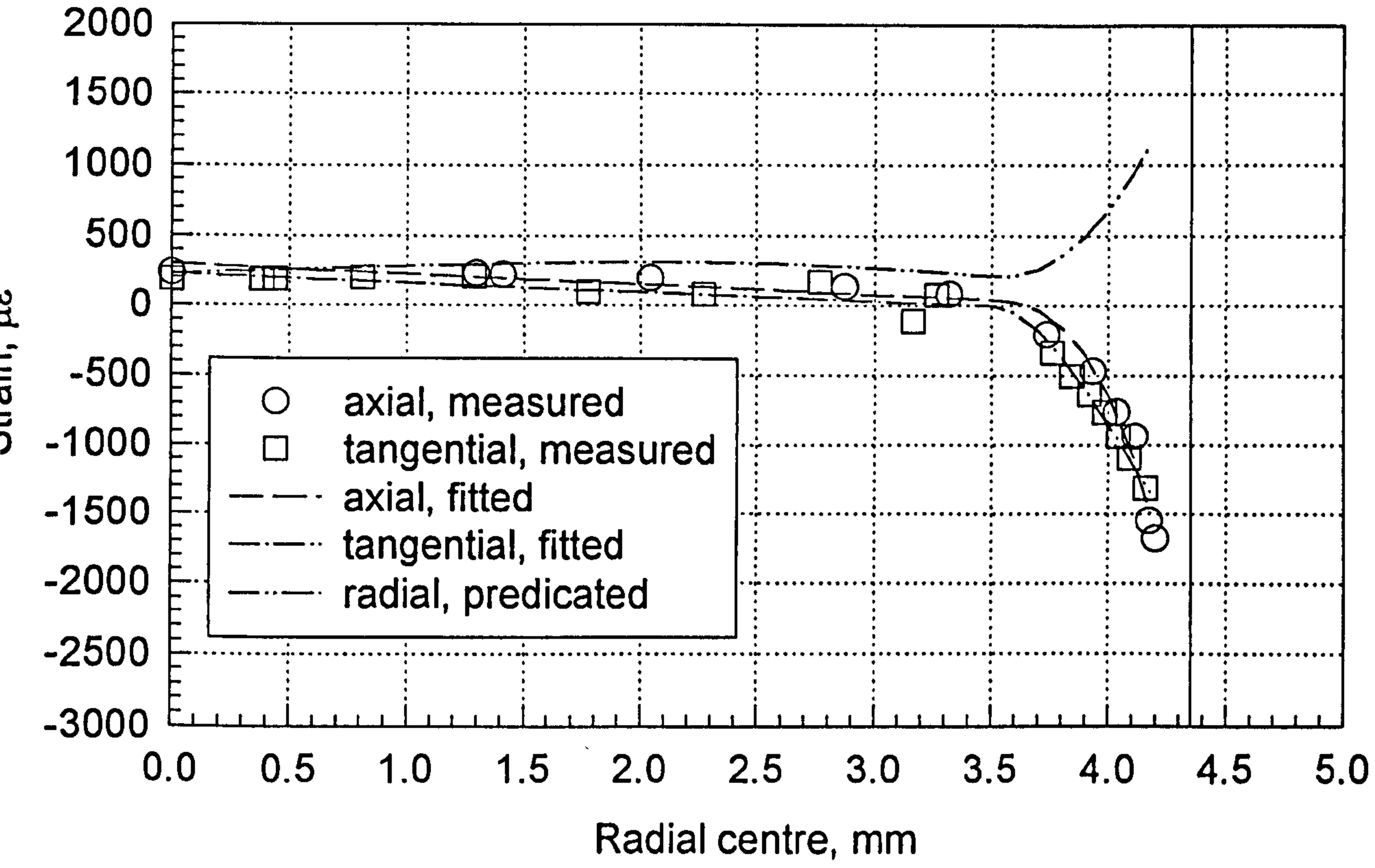

Fig 4.35 Strains in HTS19 from neutron measurements by average method

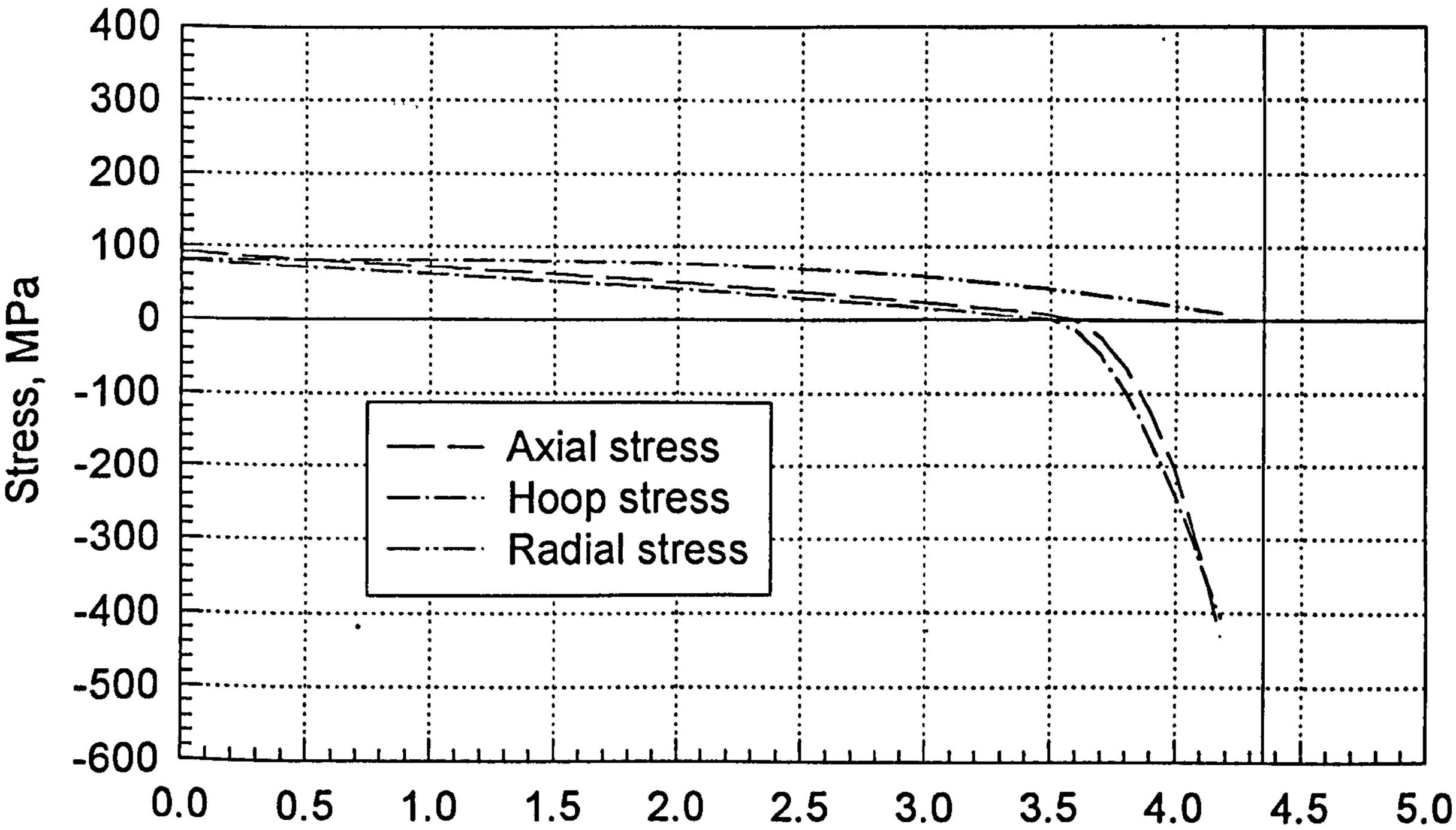

Fig 4.36 Stress distribution for specimen HTS19 by average method

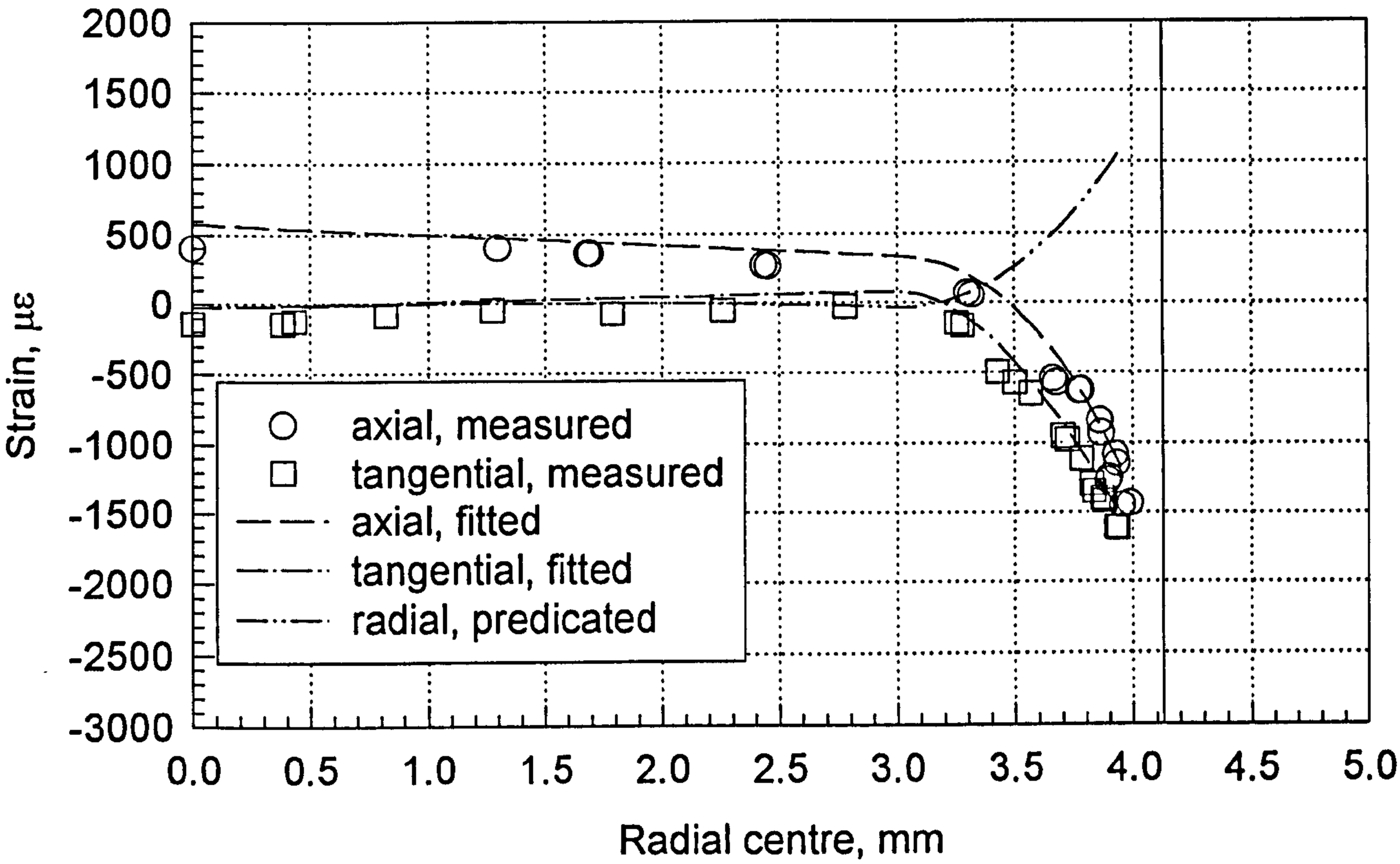

Fig 4.37 Strains in HTS22 from neutron measurements by average method

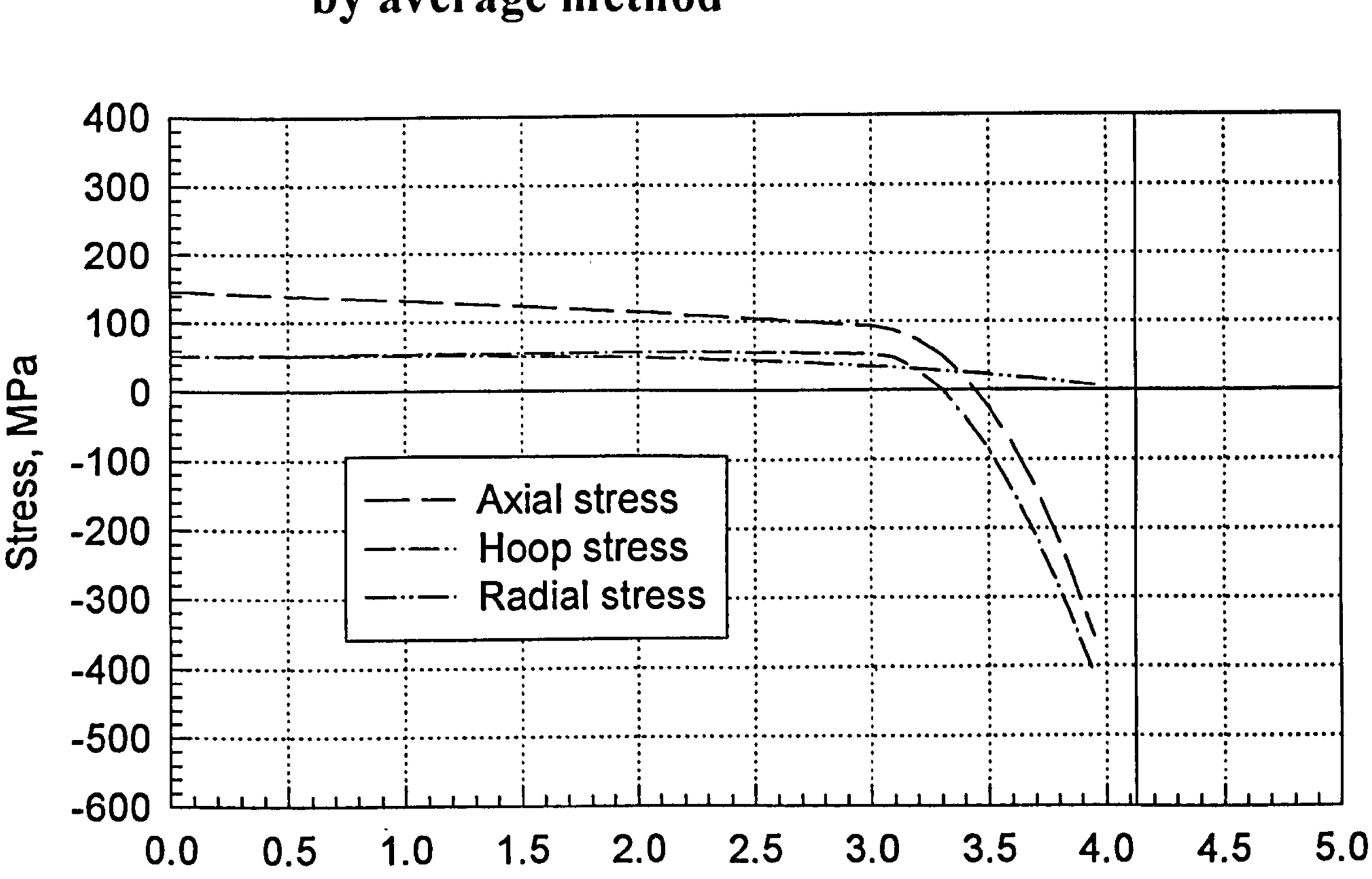

Fig 4.38 Stress distribution for specimen HTS22 by average method

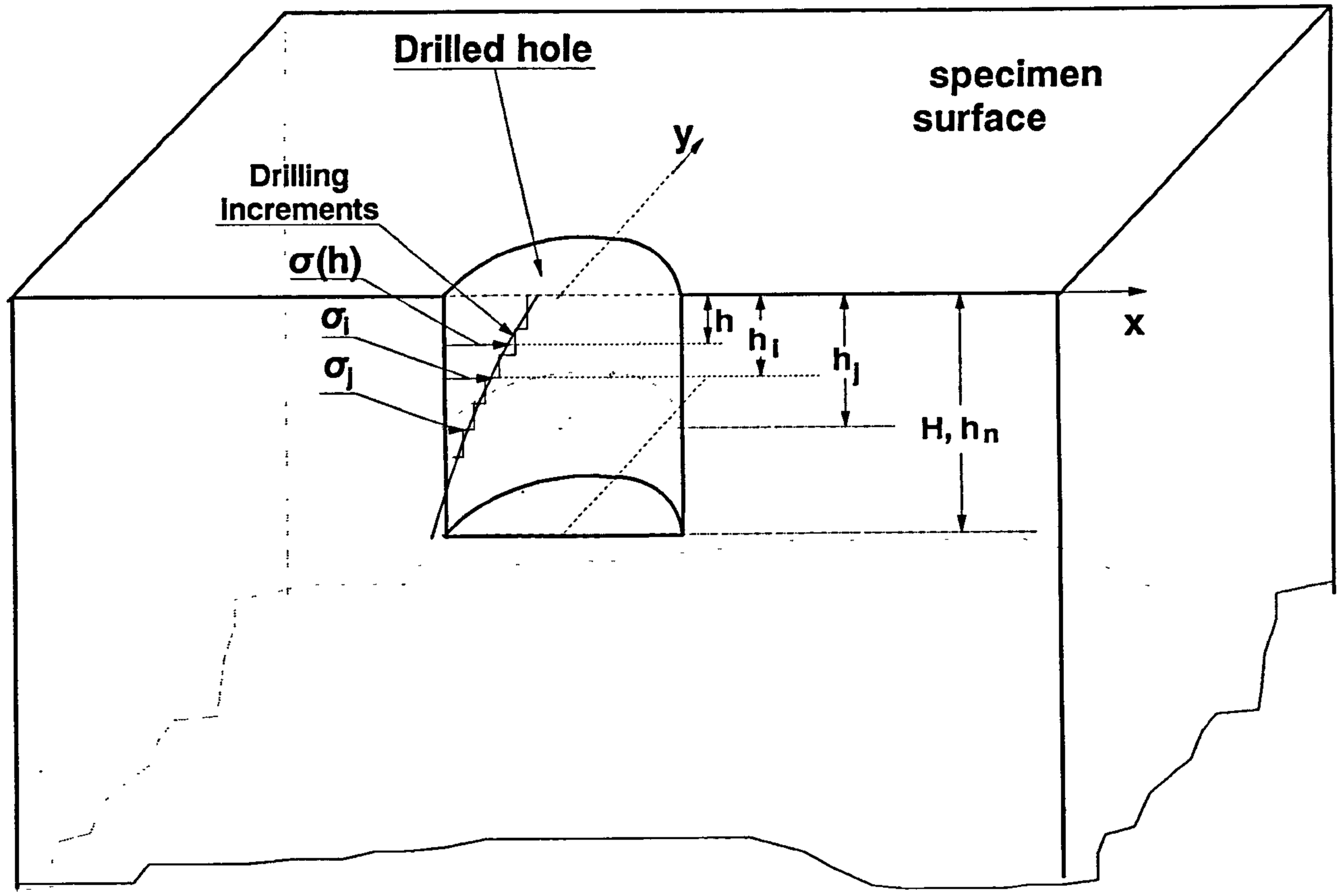

Fig 4.39 Incremental hole drilling and its parameters

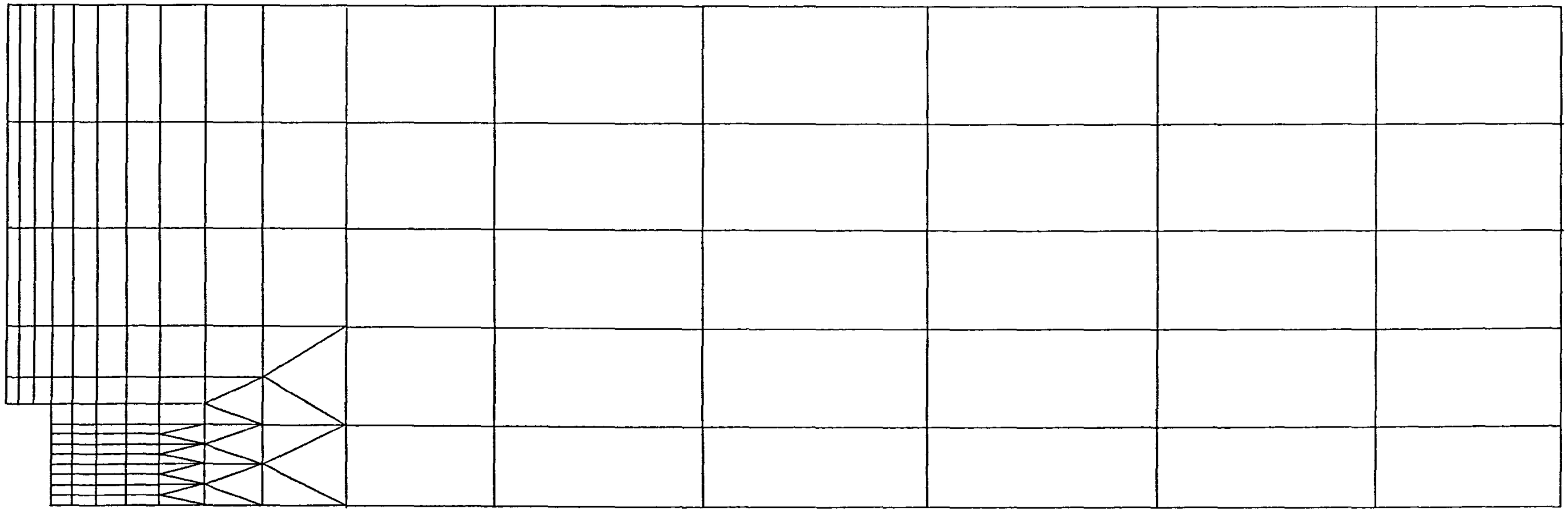

Fig 4.40 A FE mesh for the hole depth 1.6 mm, axisymmetric case

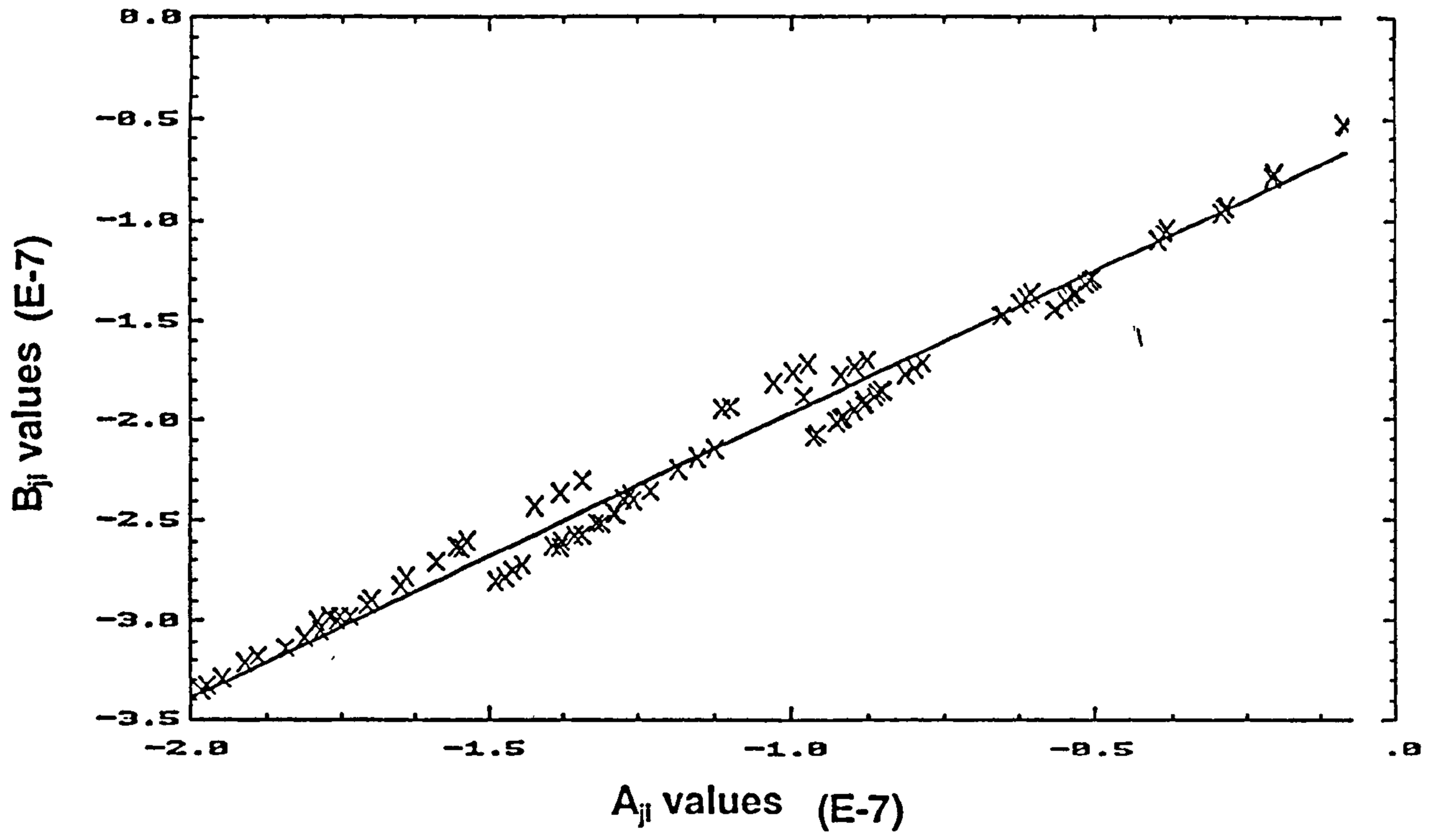

Fig 4.41 Plot of B_{ji} versus A_{ji} and regressio

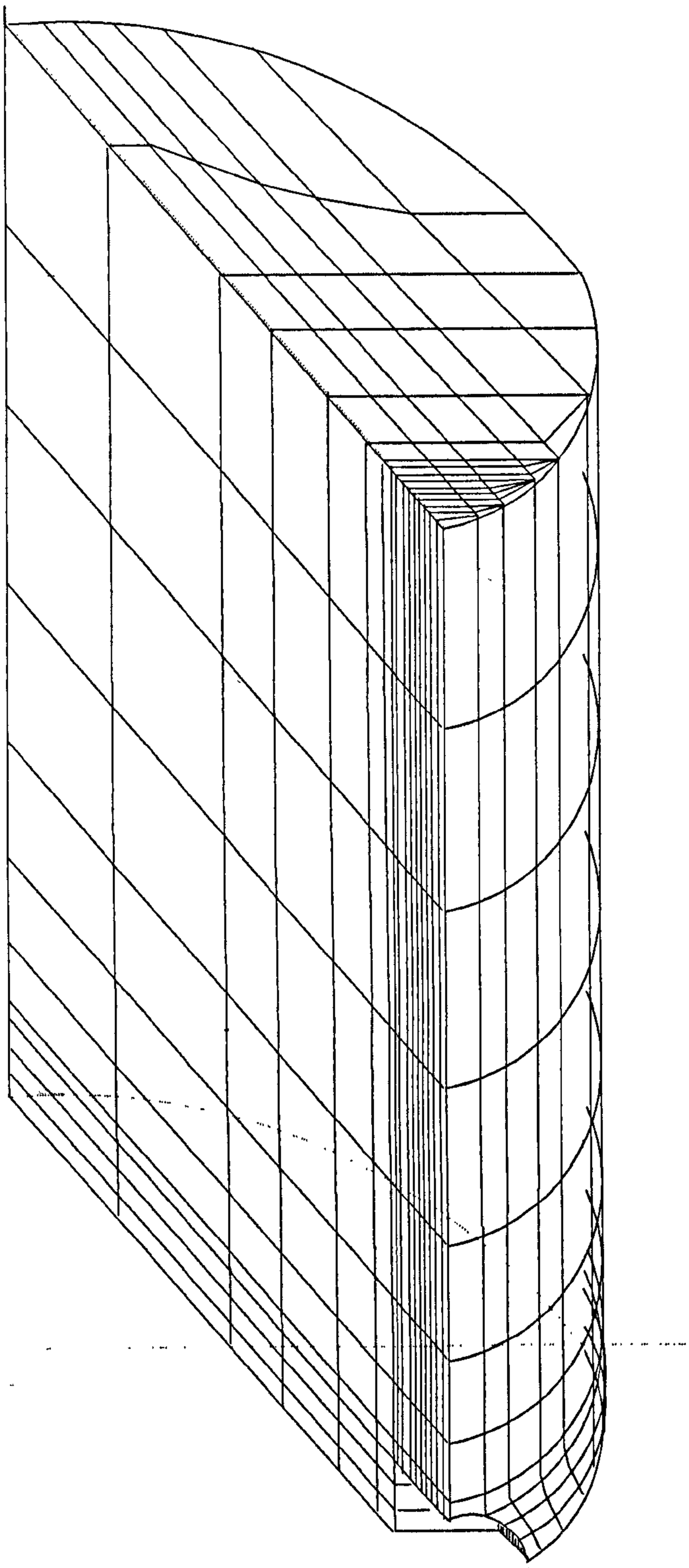

Fig 4.42 A FE mesh of round bar specimen for hole-drilling technique

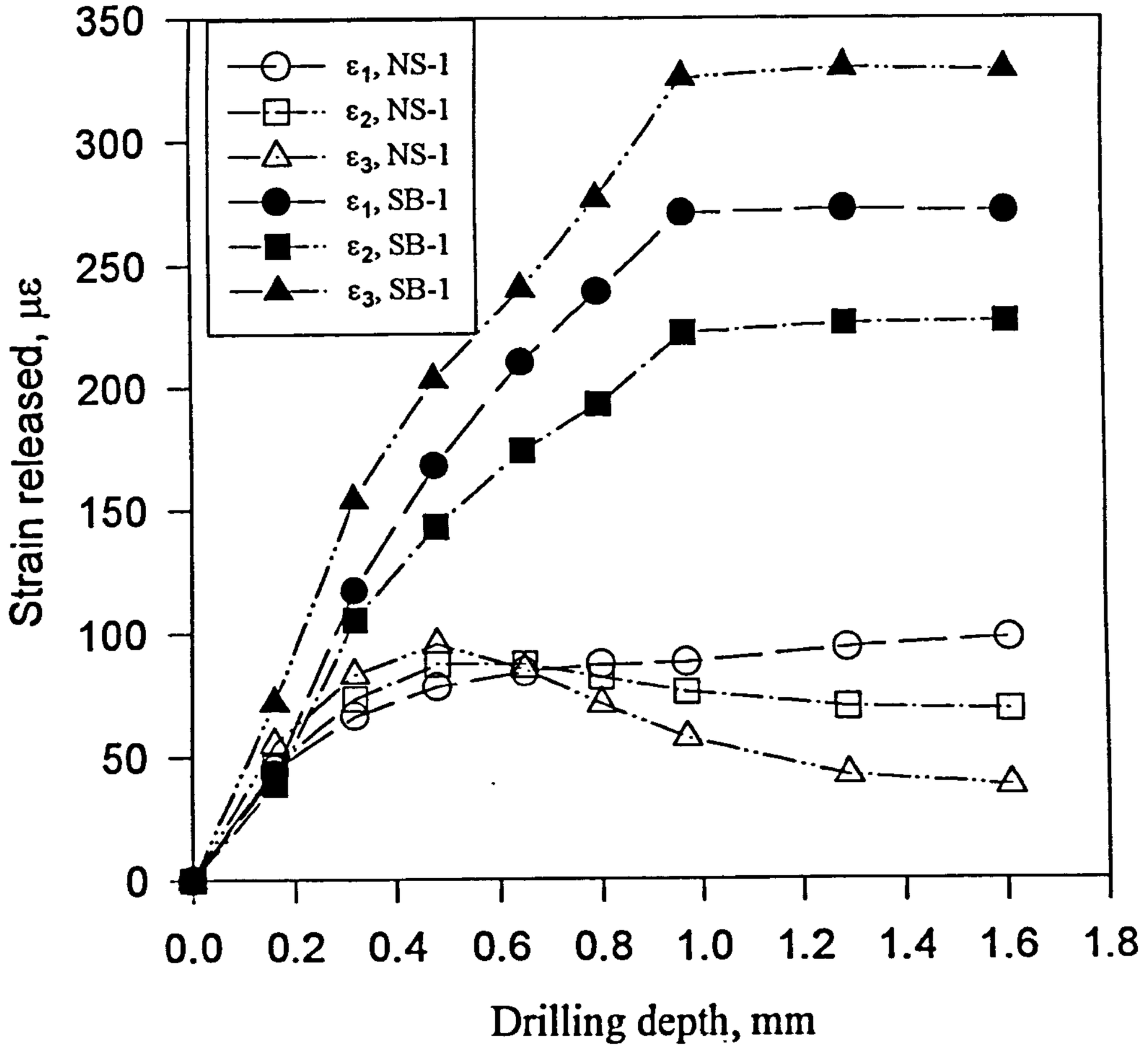

Fig 4.43 Strain release during hole drilling for non-shot blasted bar 1st test (NS-1) and shot blasted bar 1st test (SB-1)

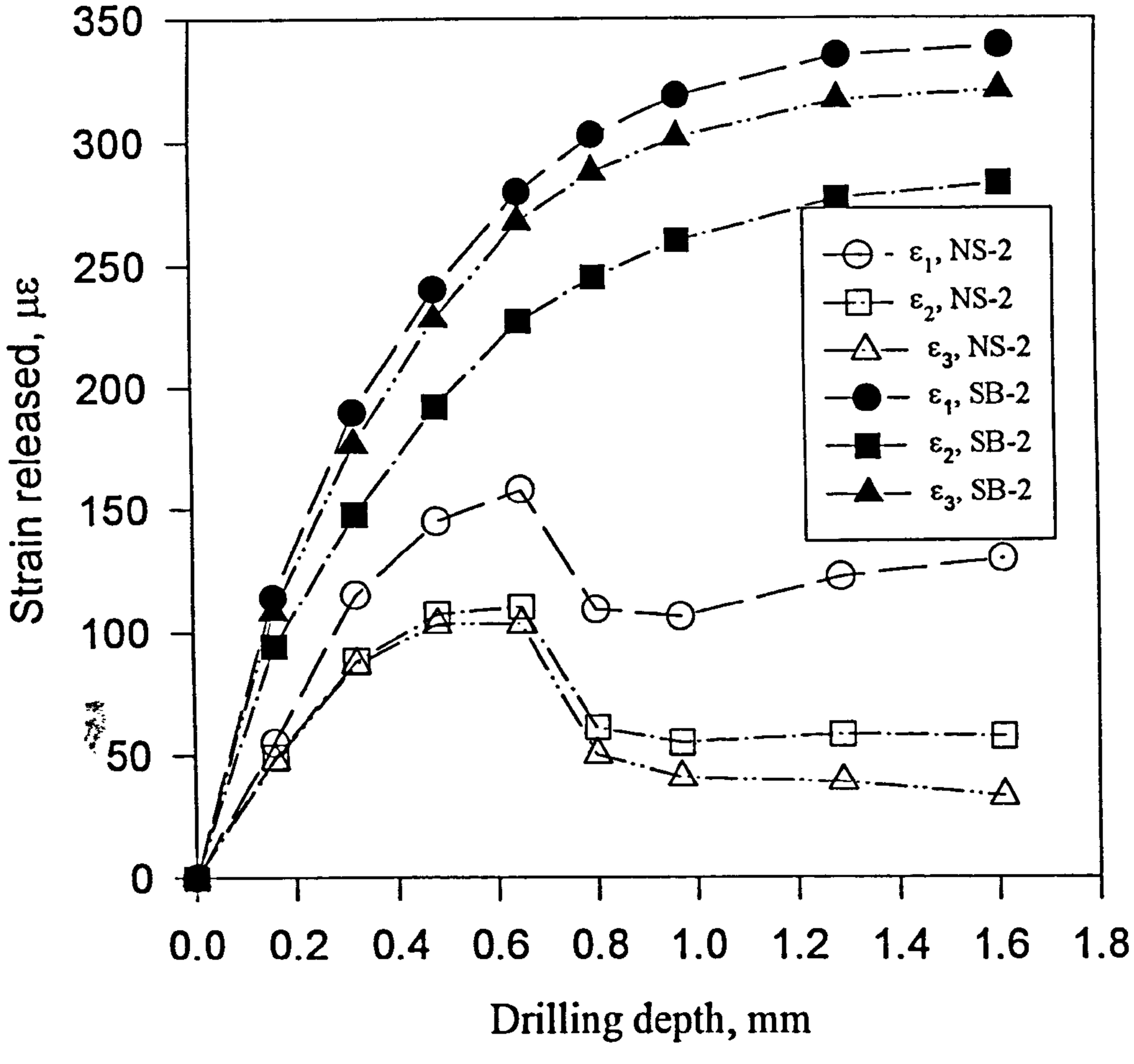

Fig 4.44 Strain release during hole drilling for non-shot blasted bar 2nd test (NS-2) and shot blasted bar 2nd test (SB-2)

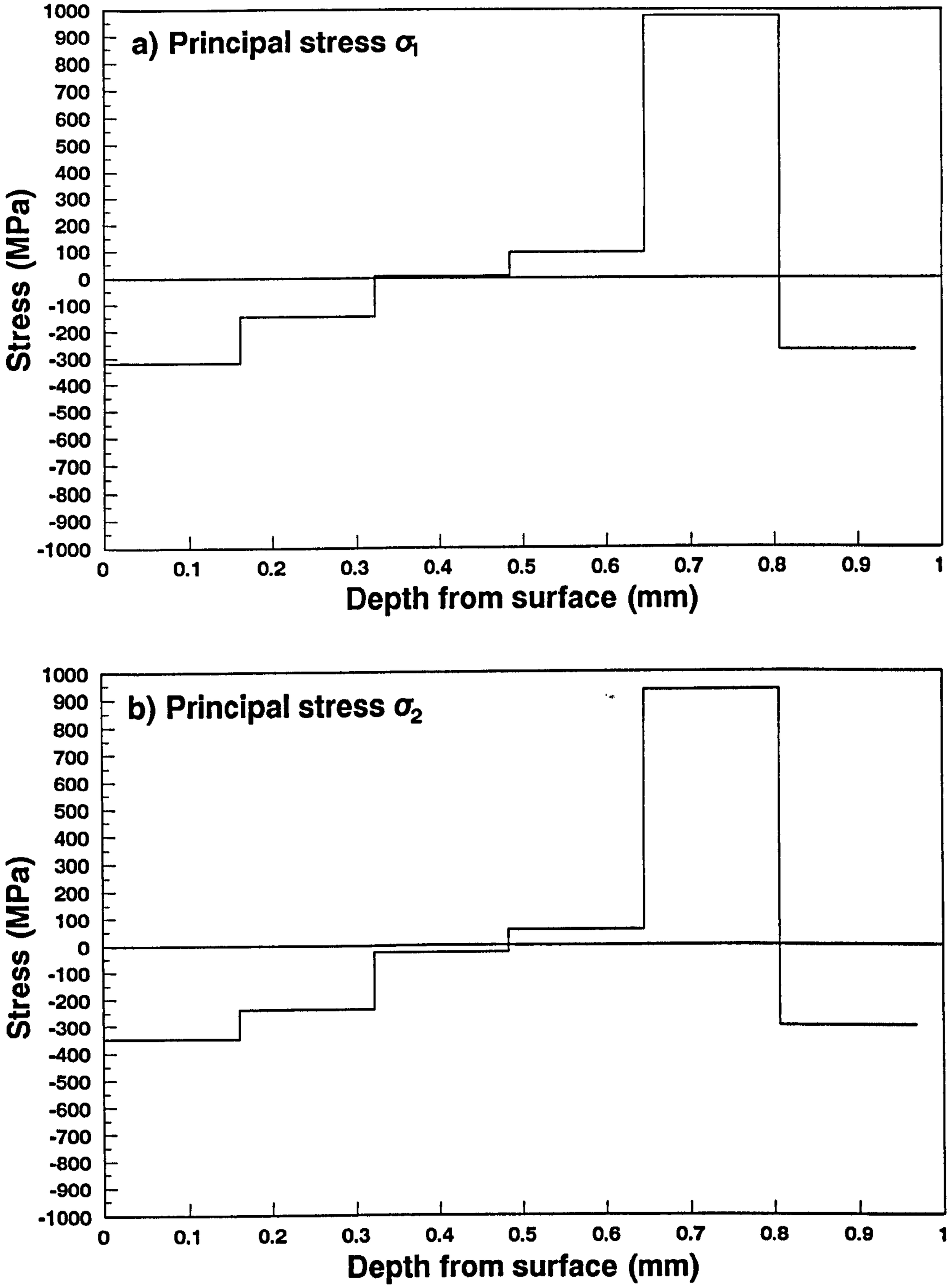

Fig 4.45 Residual stress distribution in non-shot blasted bar by hole-drilling method
i) first drilling

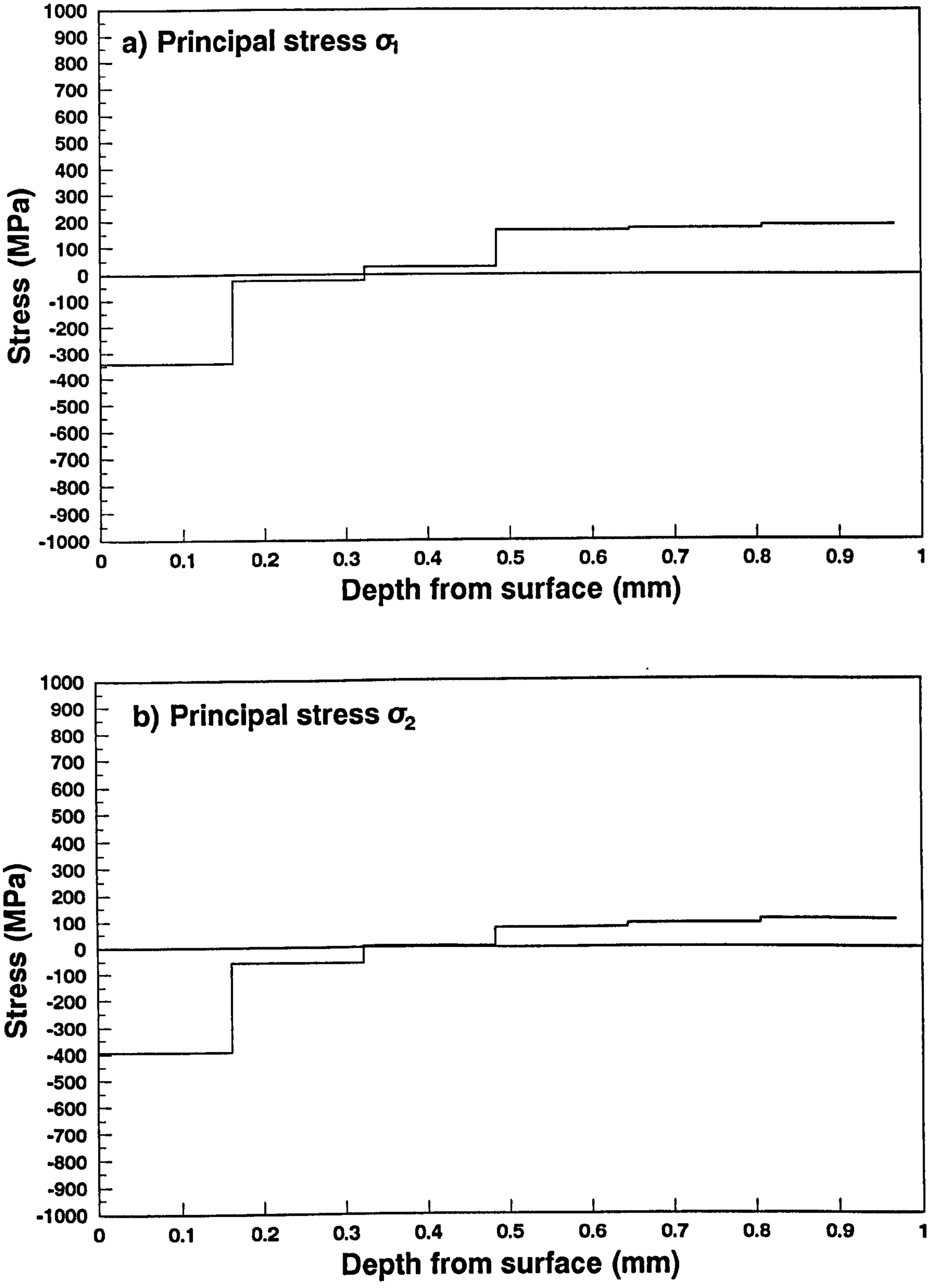

Fig 4.46 Residual stress distribution in non-shot blasted bar by hole-drilling method ii) second drilling

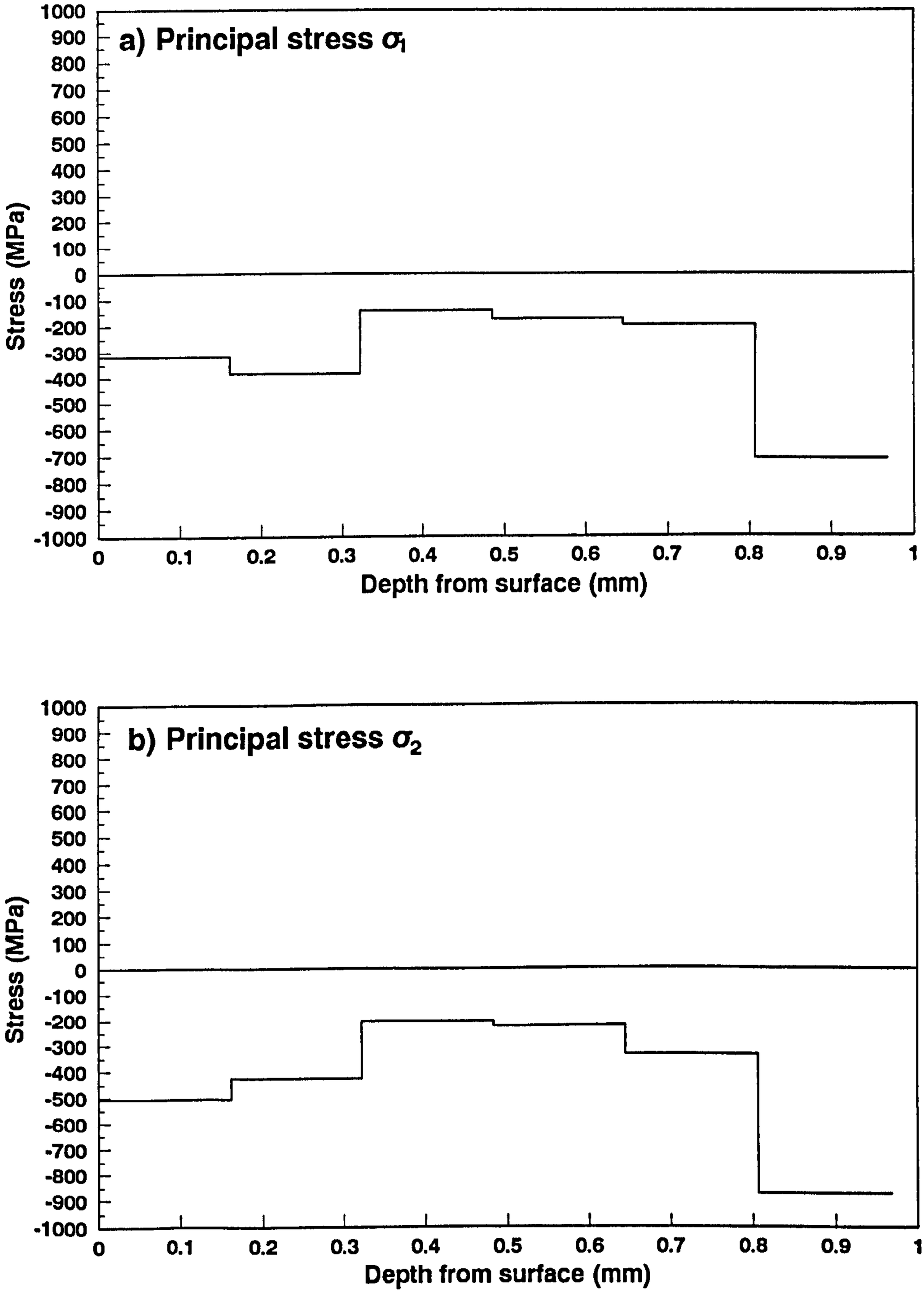

Fig 4.47 Residual stress distribution in the shot blasted bar by hole-drilling method
i) first drilling

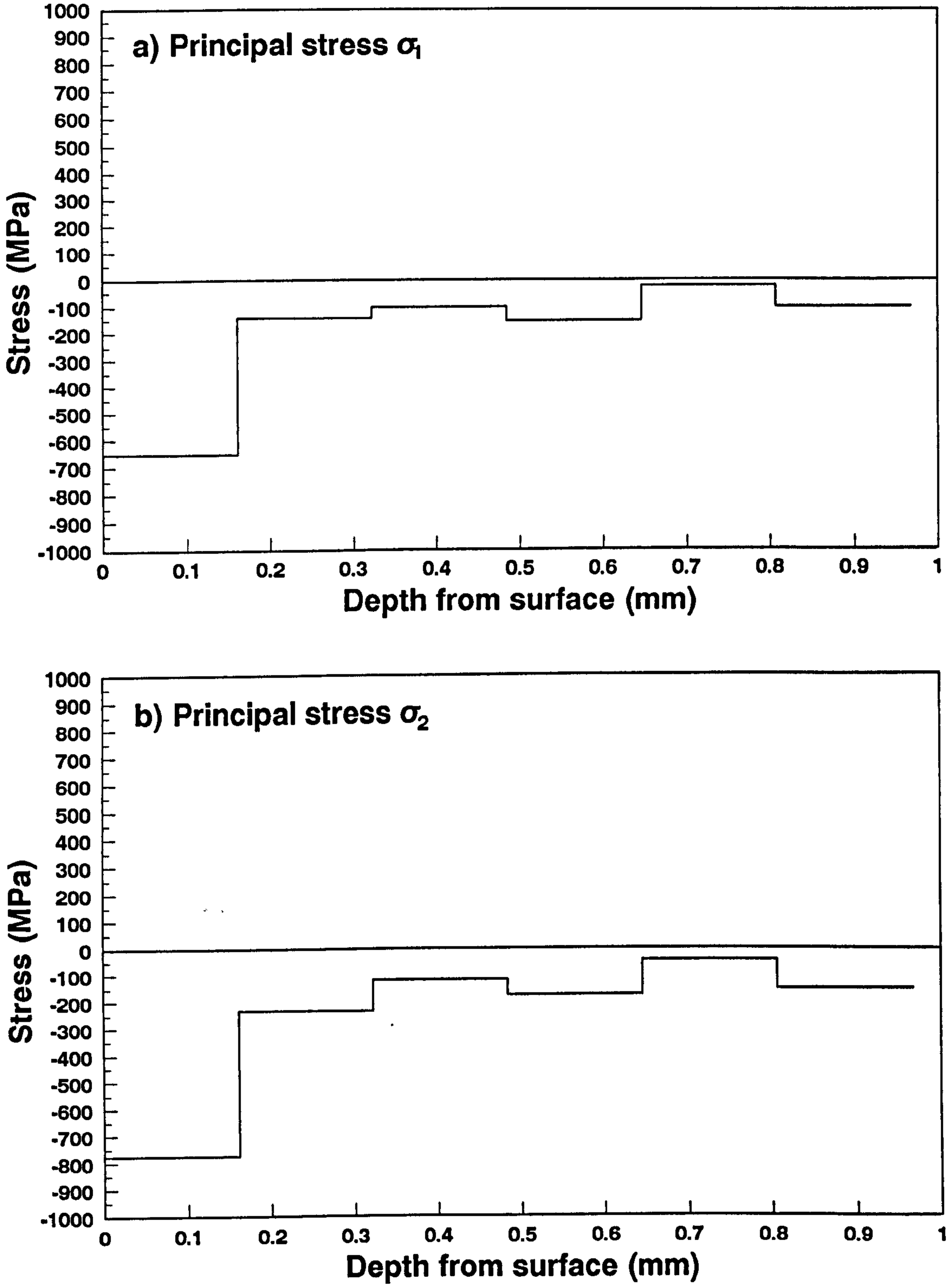

Fig 4.48 Residual stress distribution in the shot blasted bar by hole-drilling method ii) second drilling

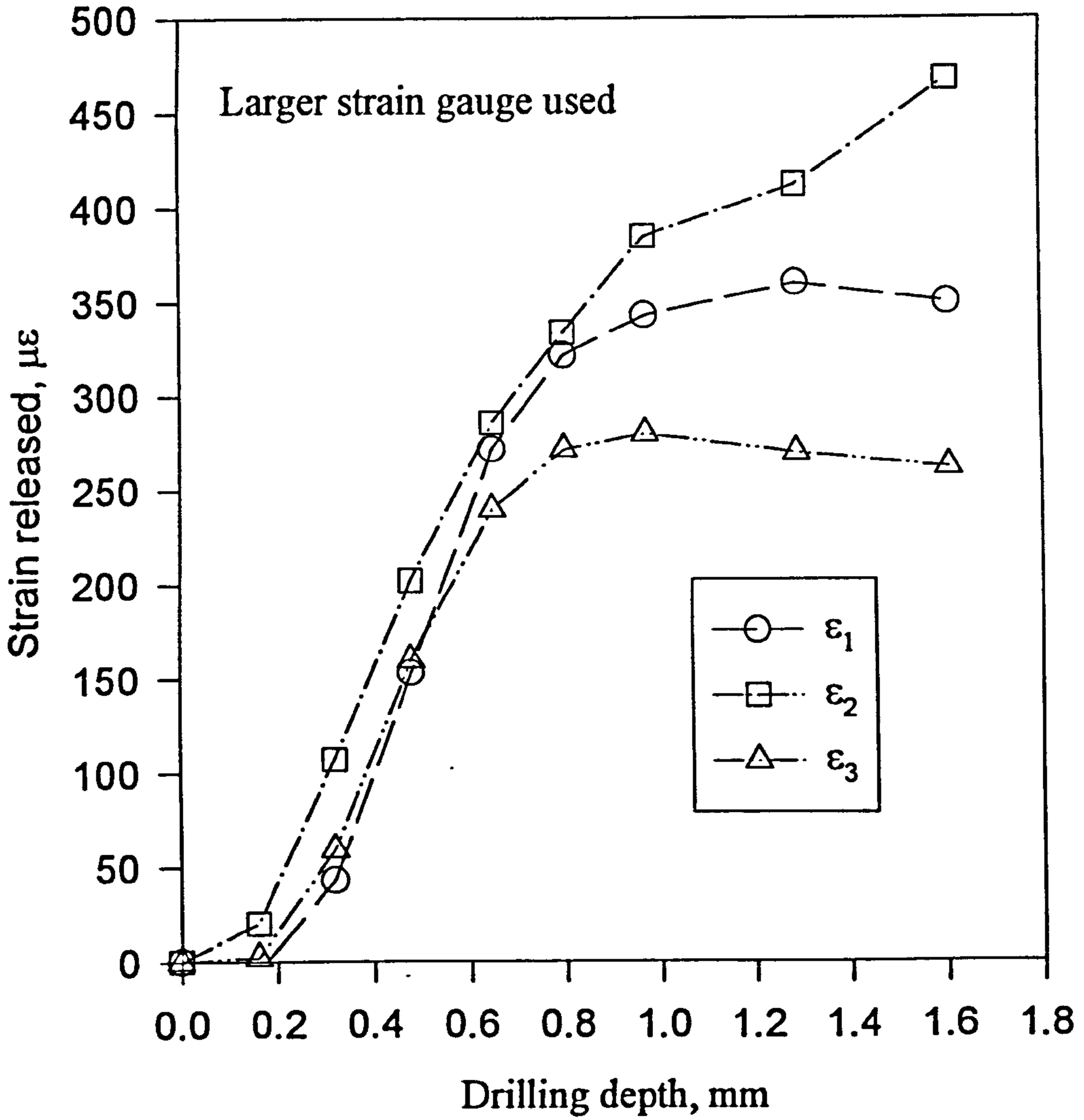

Fig 4.49 Strain release during hole drilling for specimen U11

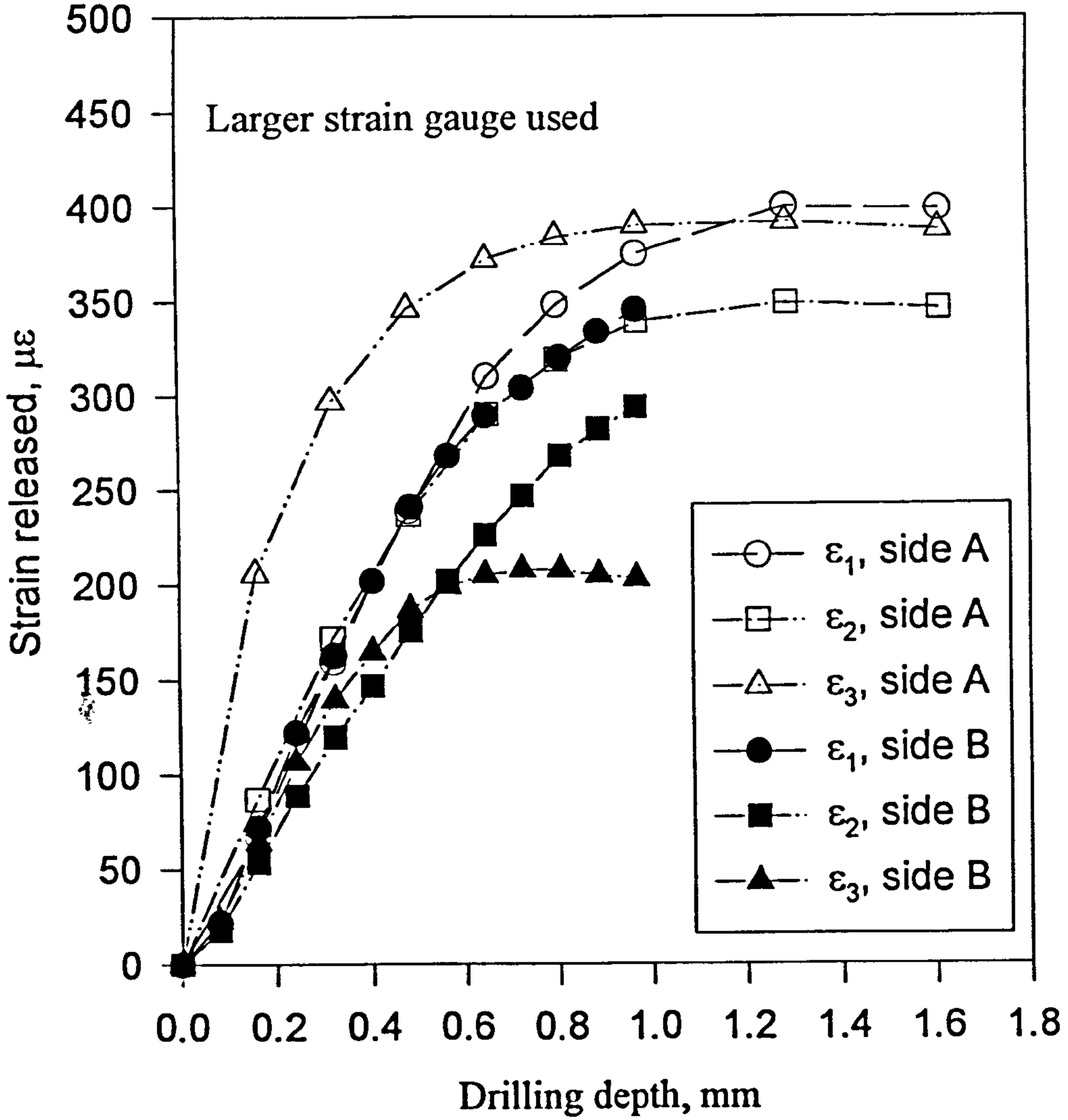

Fig 4.50 Strain release during hole drilling for specimen U5 on side A and side B

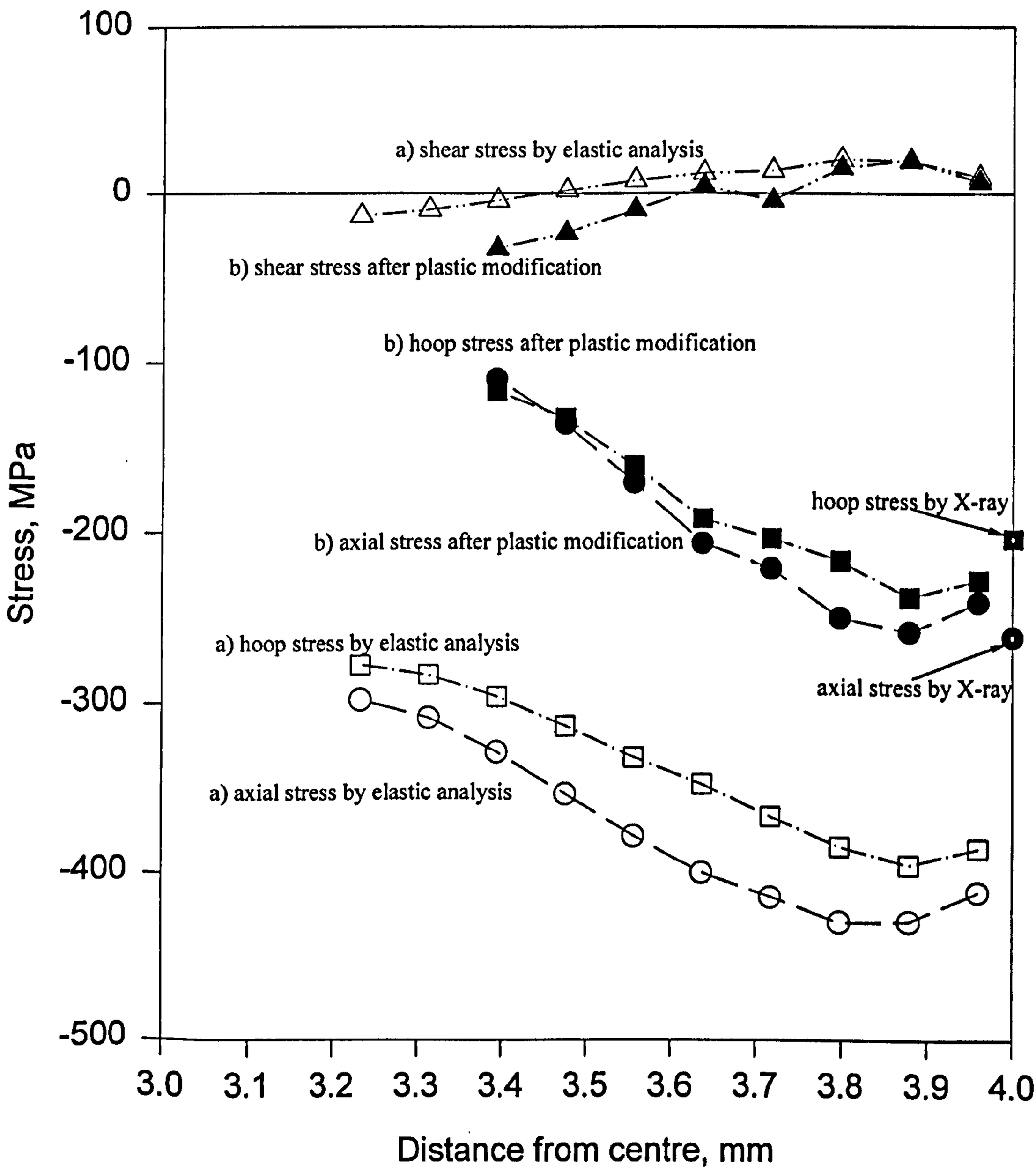

Fig 4.51 Residual stresses of U5 by centre hole method with 3-D FE analysis using
a) elastic analysis
b) after plastic modification

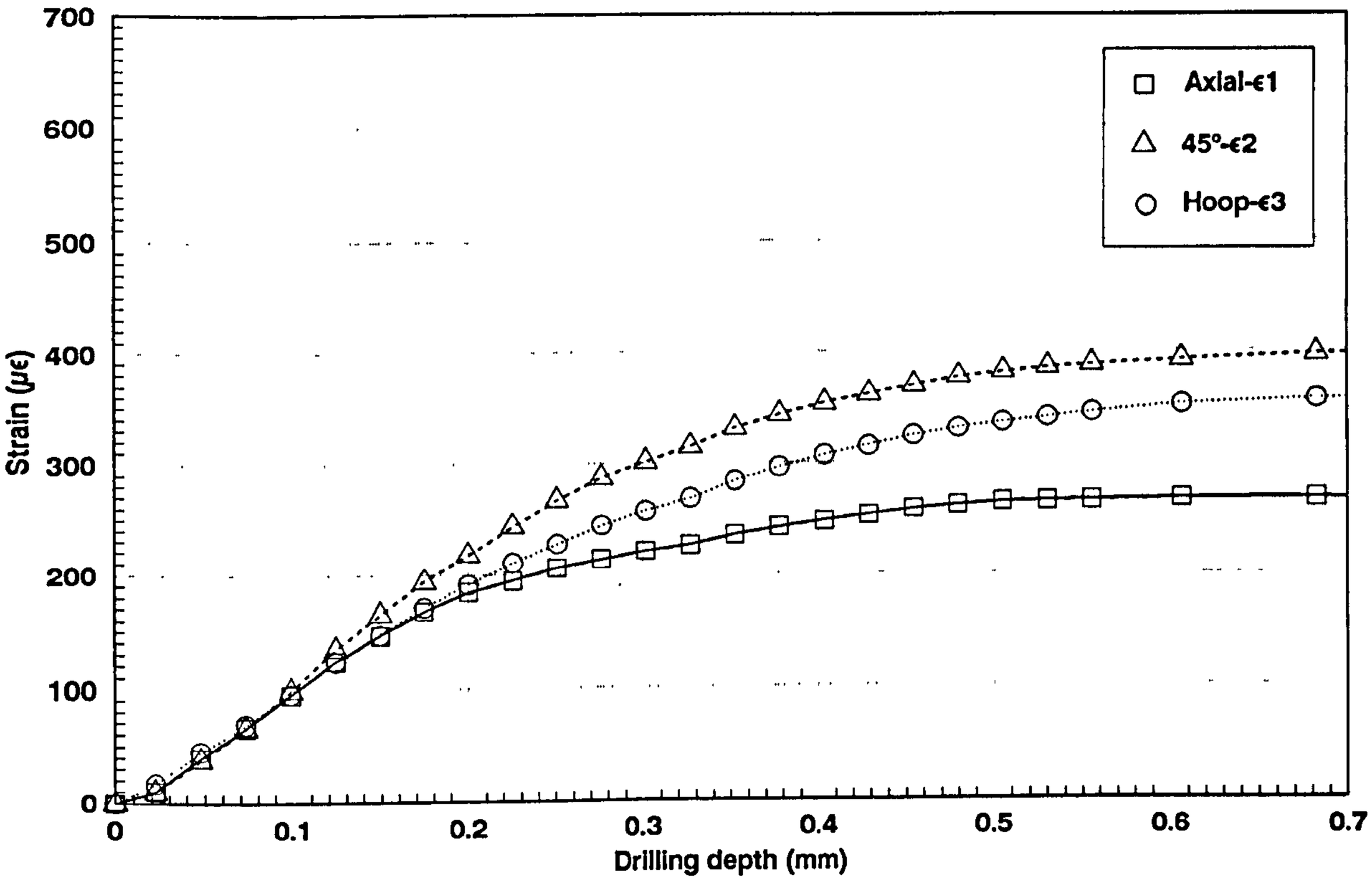

Fig 4.52 Strain release during hole drilling for U15 on side B

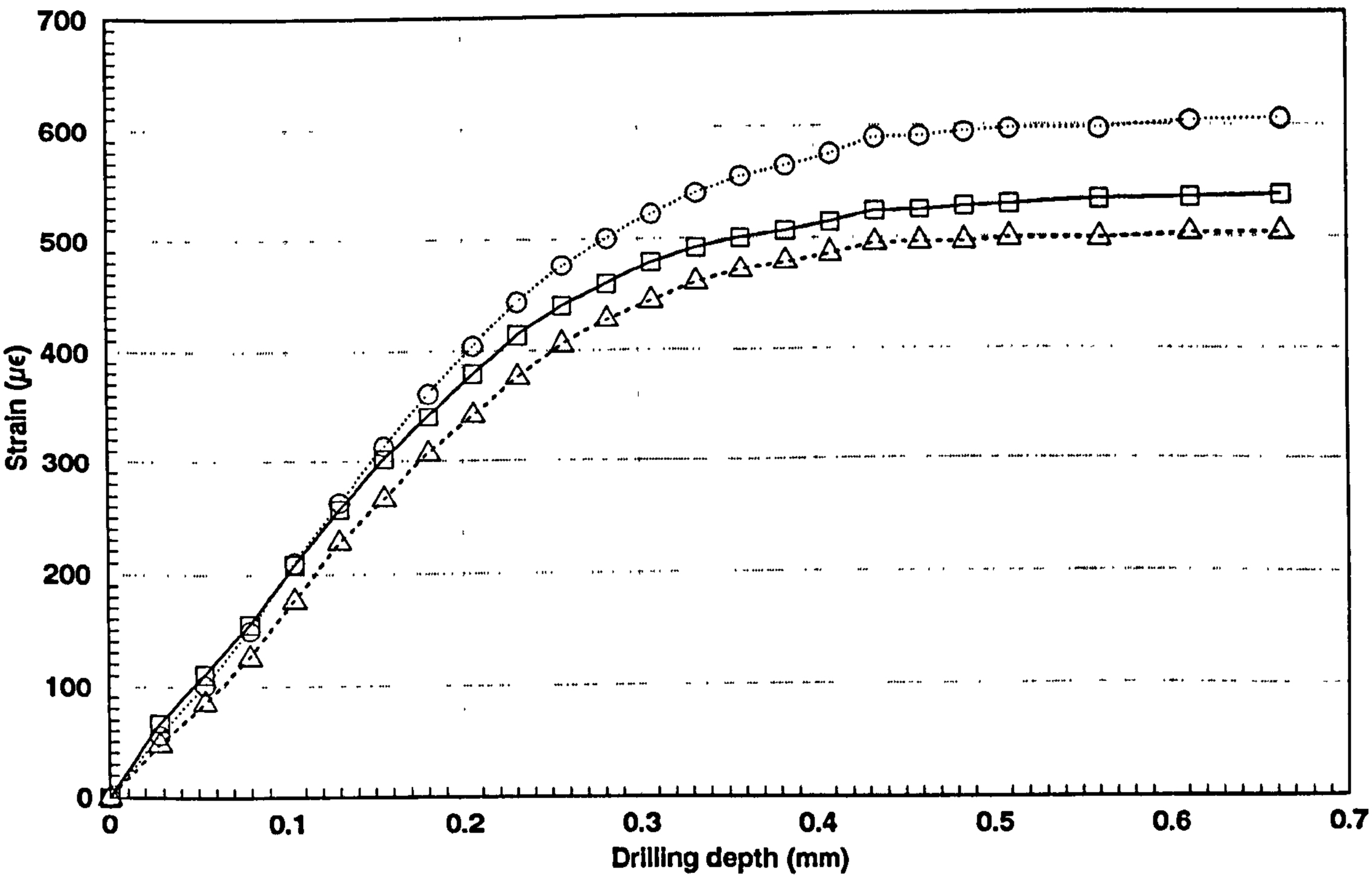

Fig 4.53 Strain release during hole drilling for HTS09 on side A

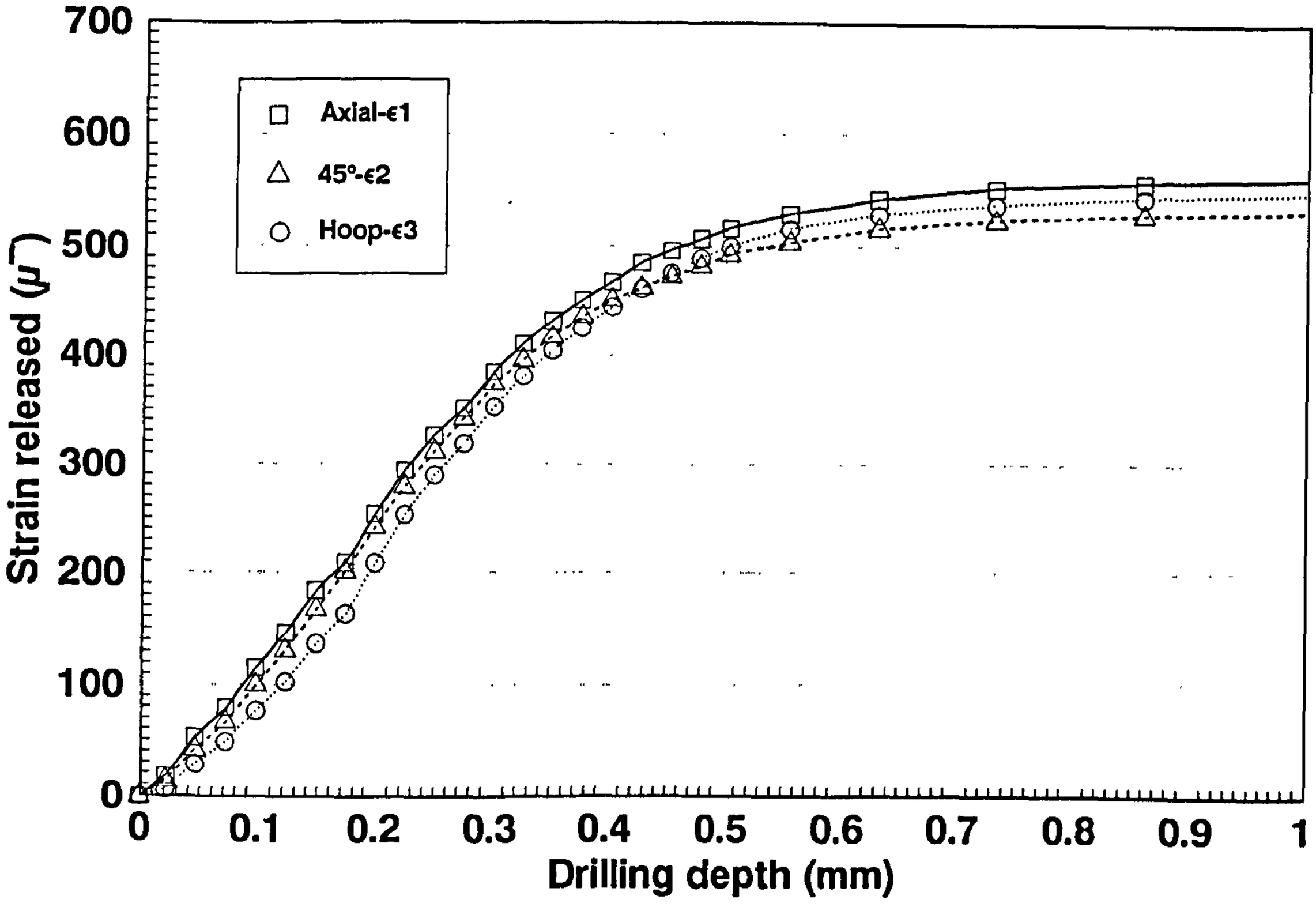

Fig 4.54 Strain release during hole drilling for HTS09 on side B

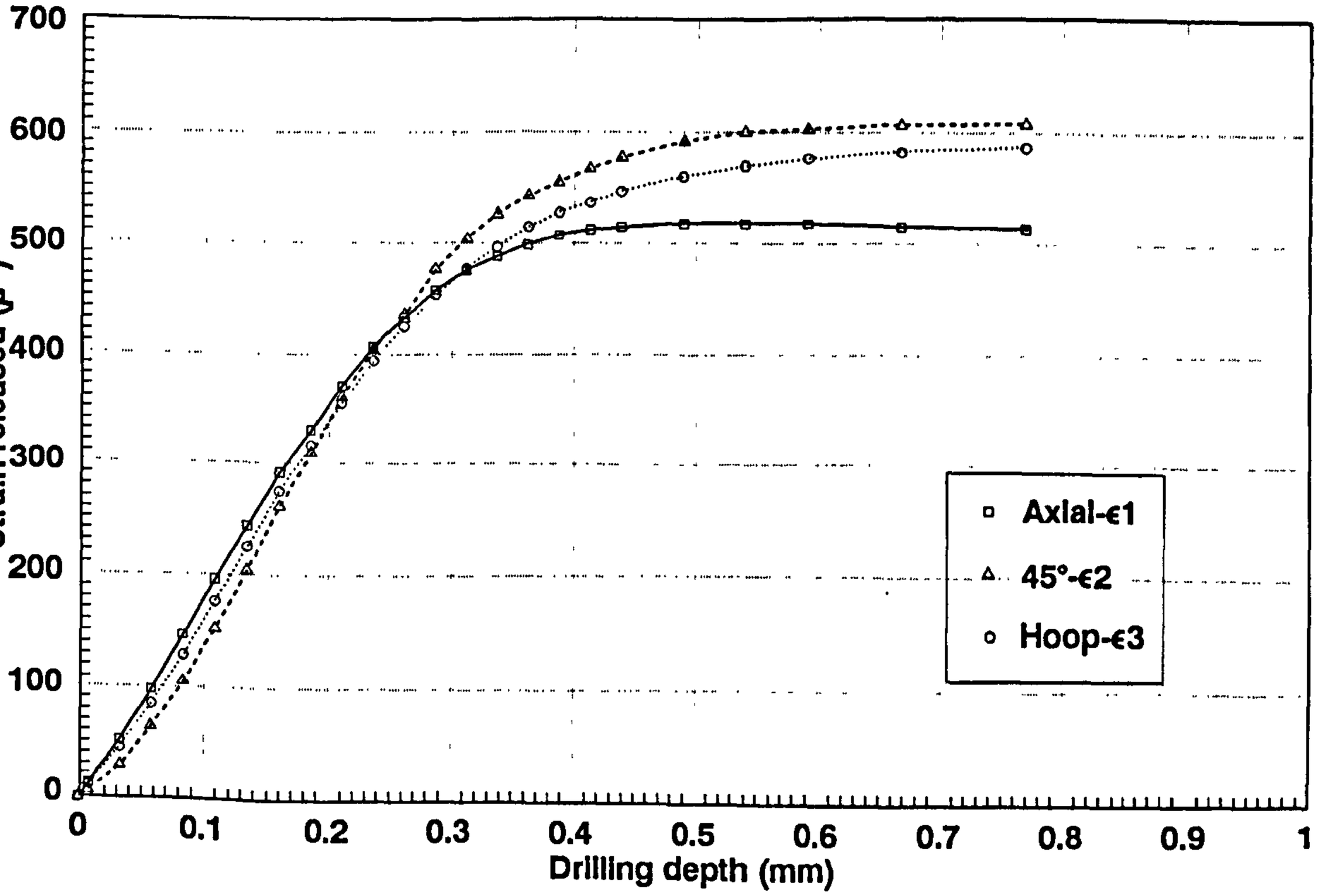

Fig 4.55 Strain release during hole drilling for HTS20 on side B

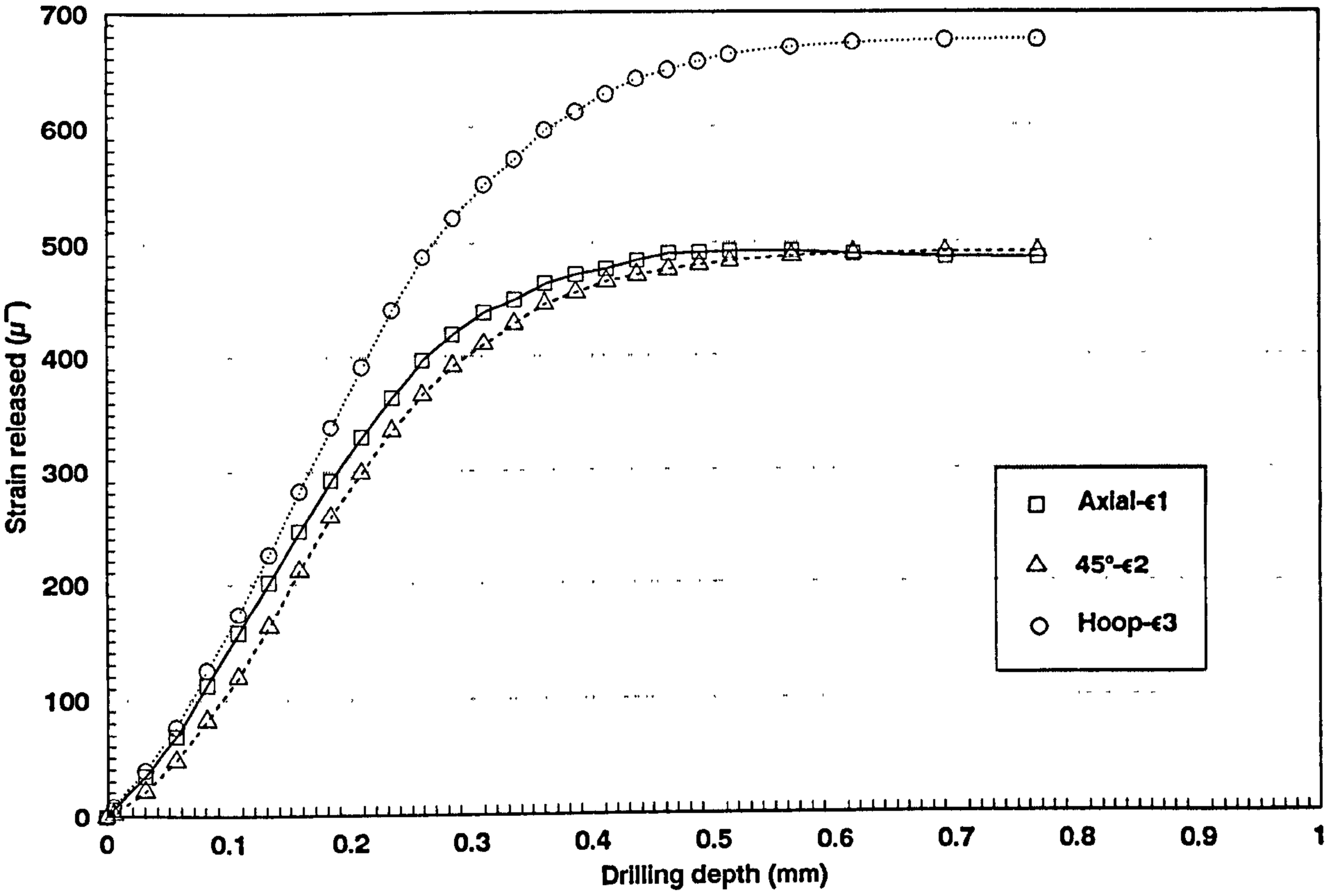

Fig 4.56 Strain release during hole drilling for HTS17 on side A

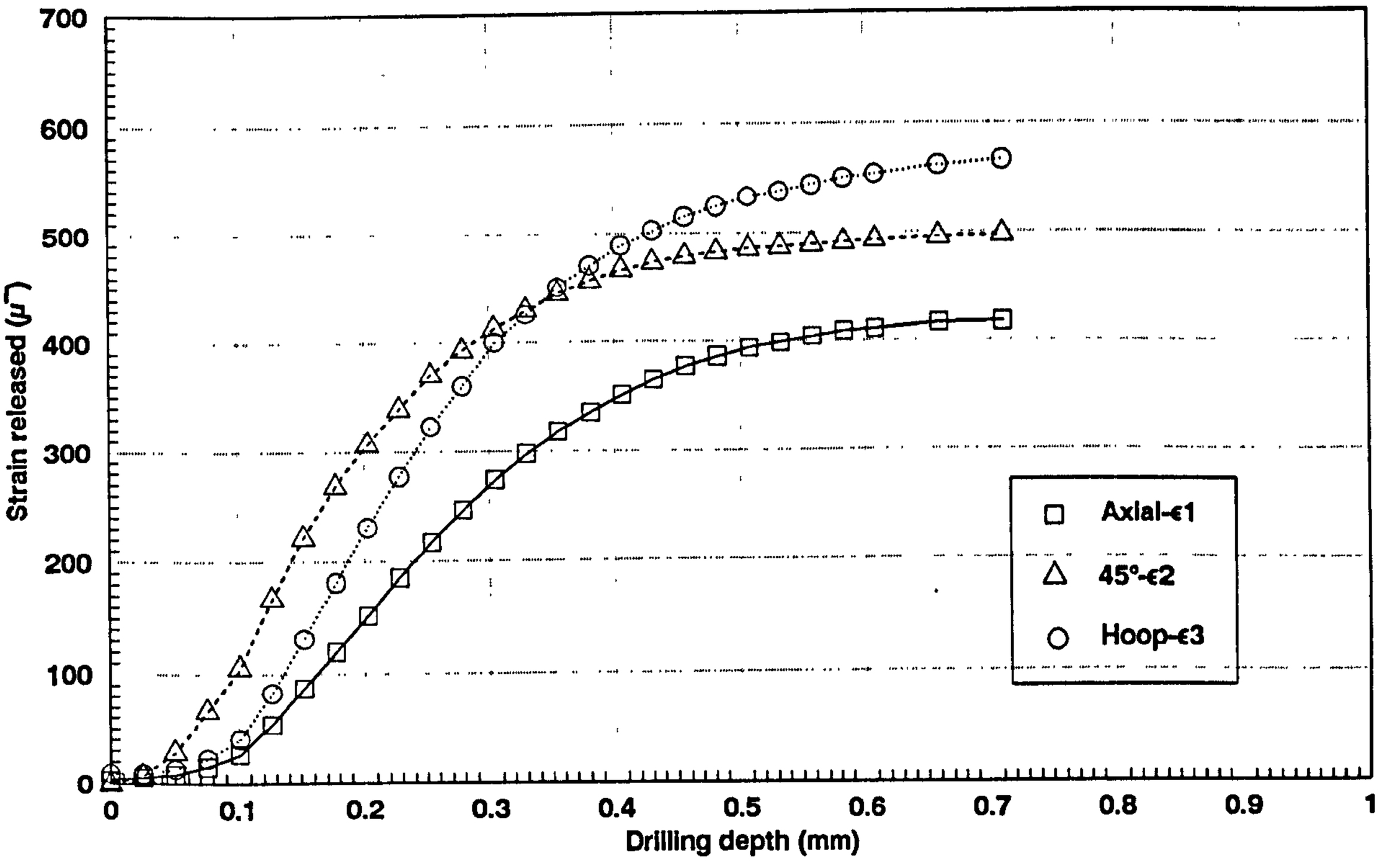

Fig 4.57 Strain release during hole drilling for FS16 on side B

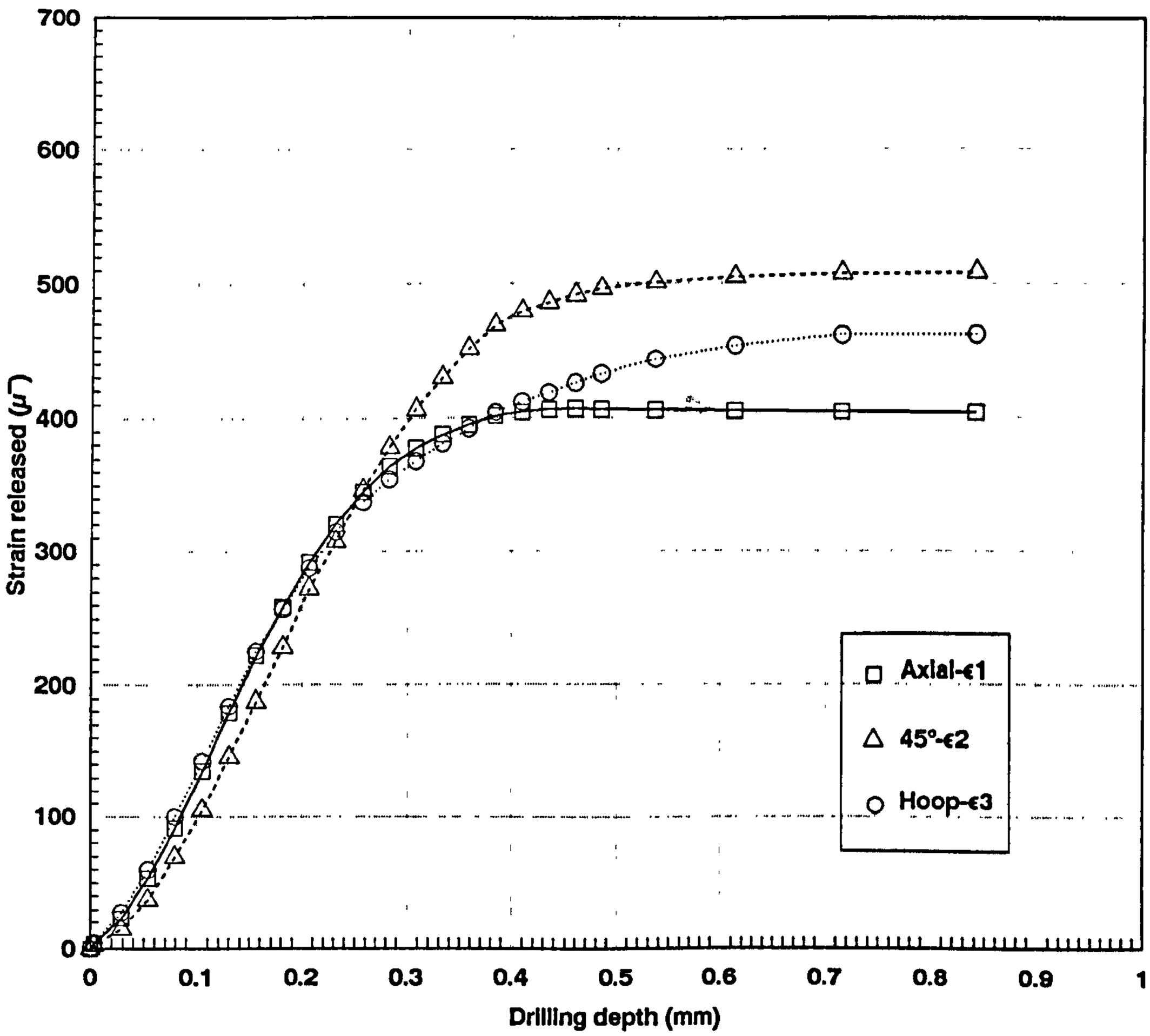

Fig 4.58 Strain release during hole drilling for FS18 on side B

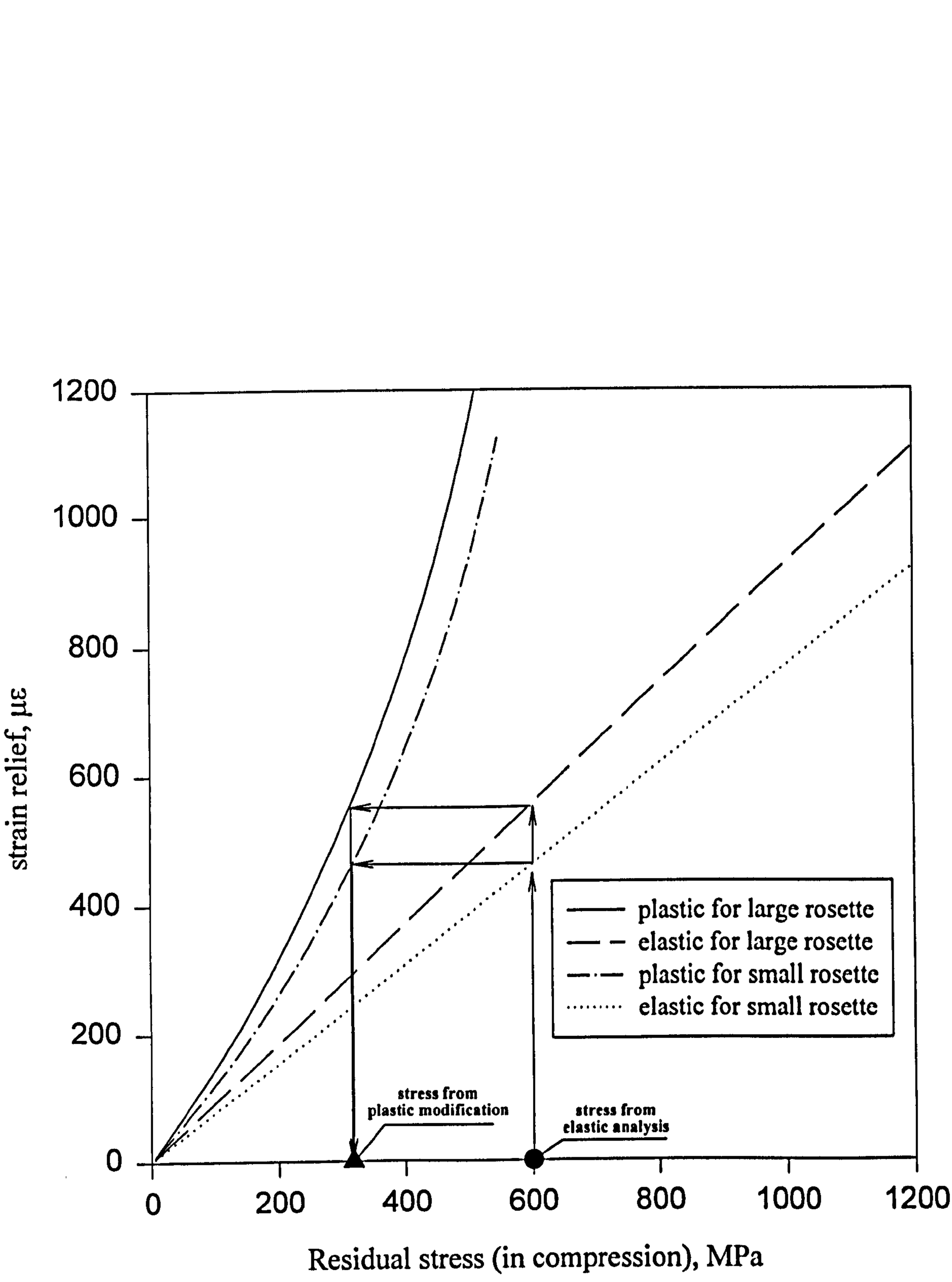

Fig 4.59 Strain relaxation versus residual stress and plastic modification

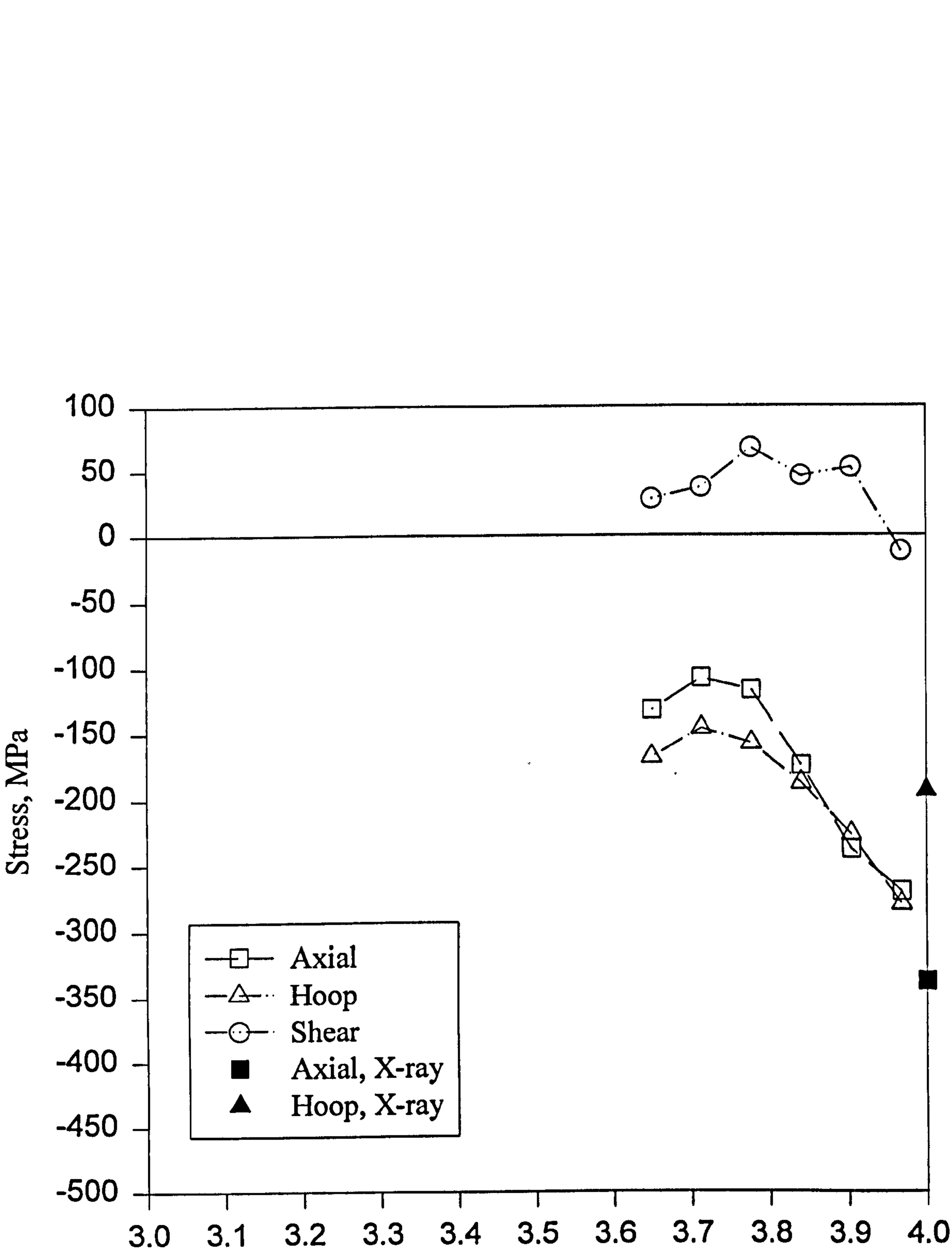

Fig 4.60 Residual stresses of U15 on side B by centre hole using average stress method and plastic modification

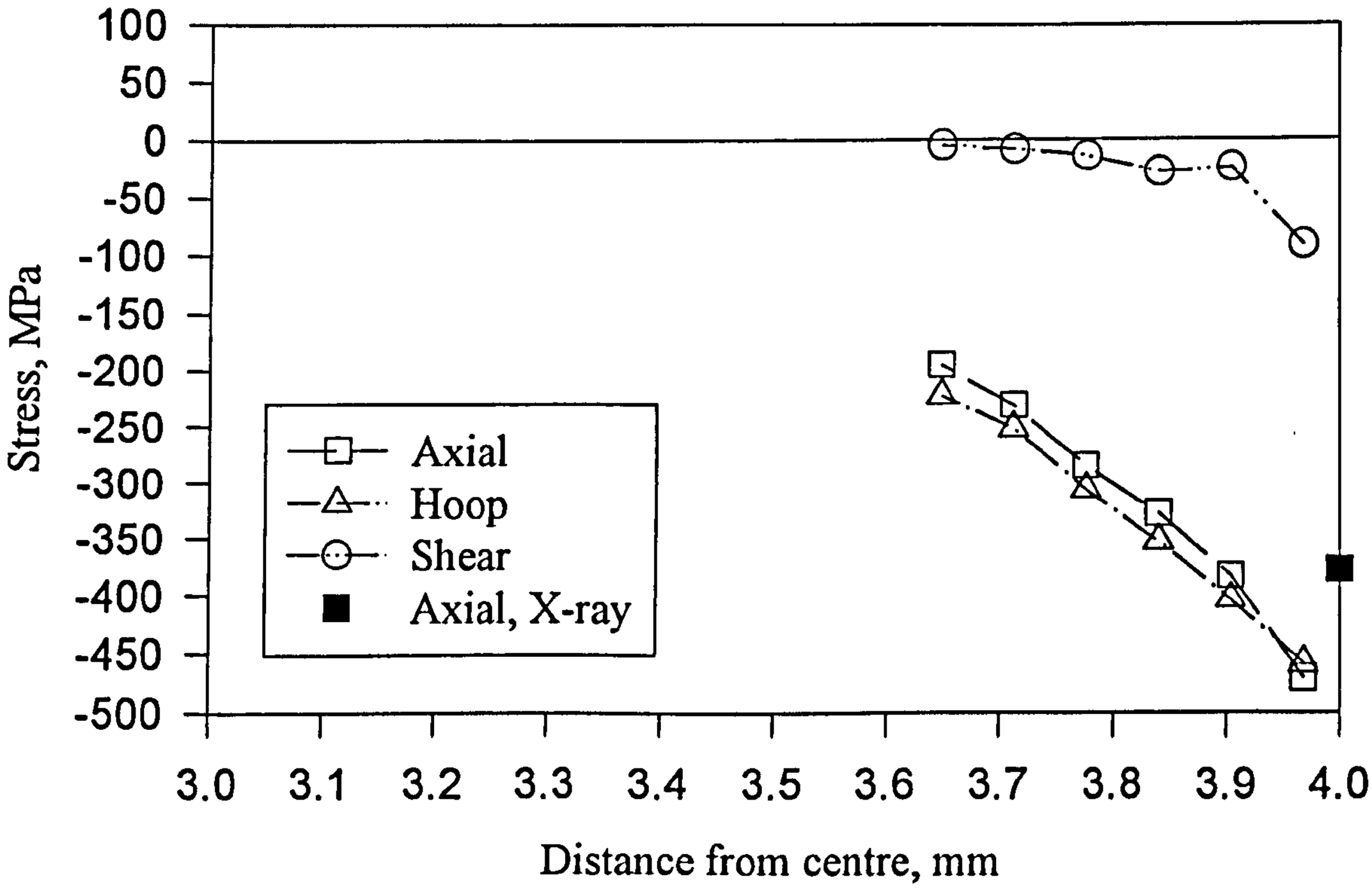

Fig 4.61 Residual stresses of HTS09 on side A by centre hole using average stress method and plastic modification

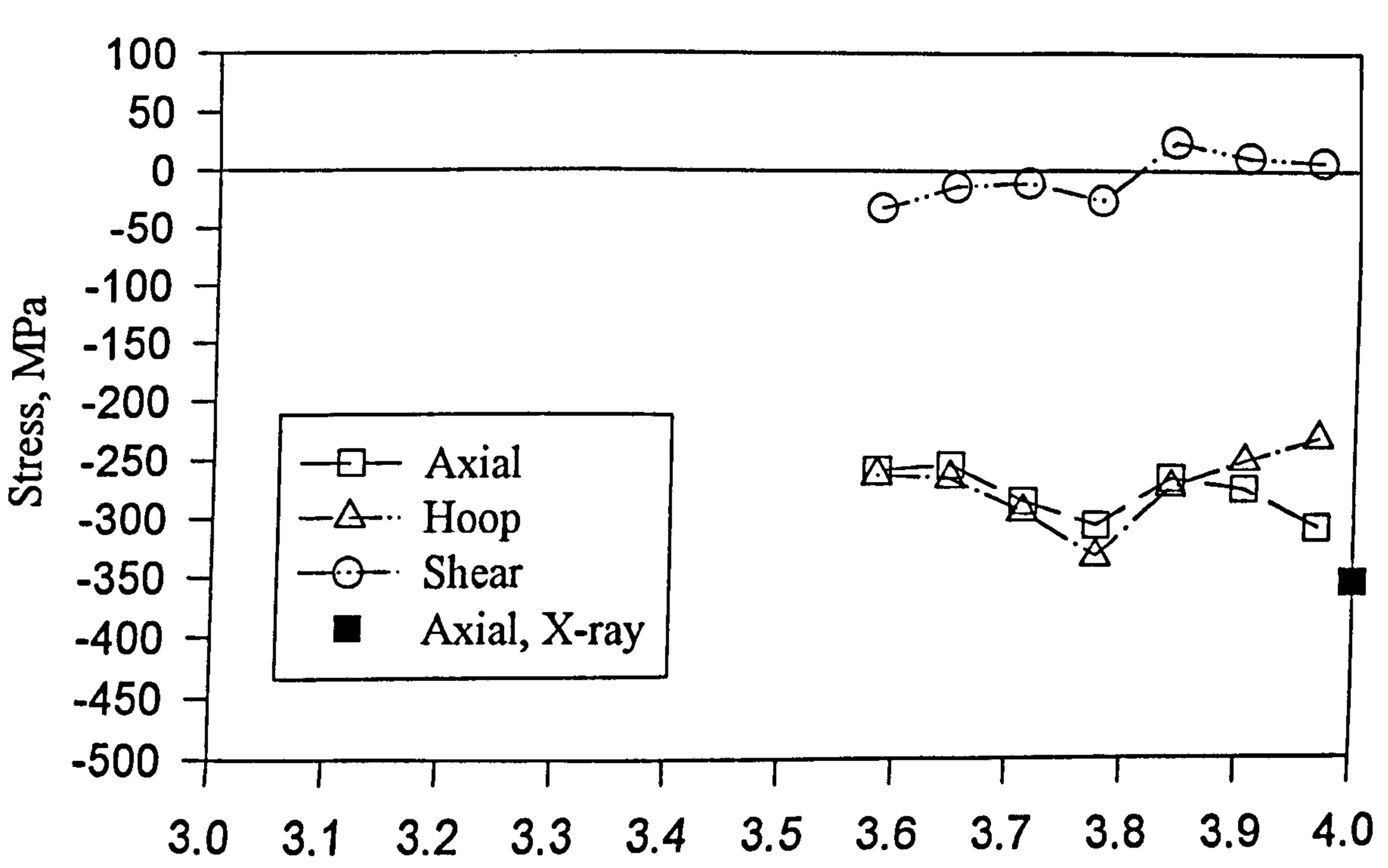

Fig 4.62 Residual stresses of HTS09 on side B by centre hole using average stress method and plastic modification

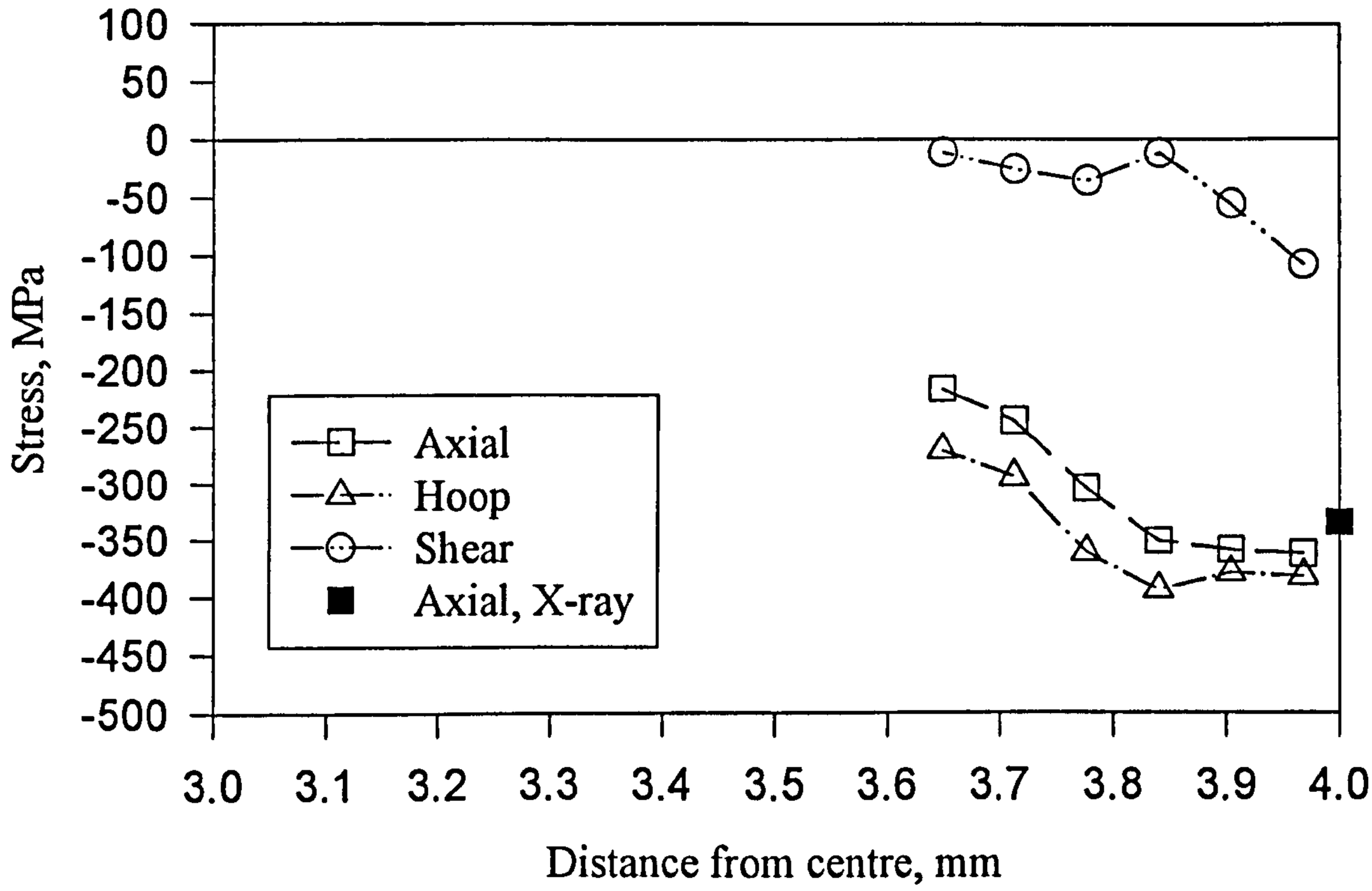

Fig 4.63 Residual stresses of HTS17 on side A by centre hole using average stress method and plastic modification

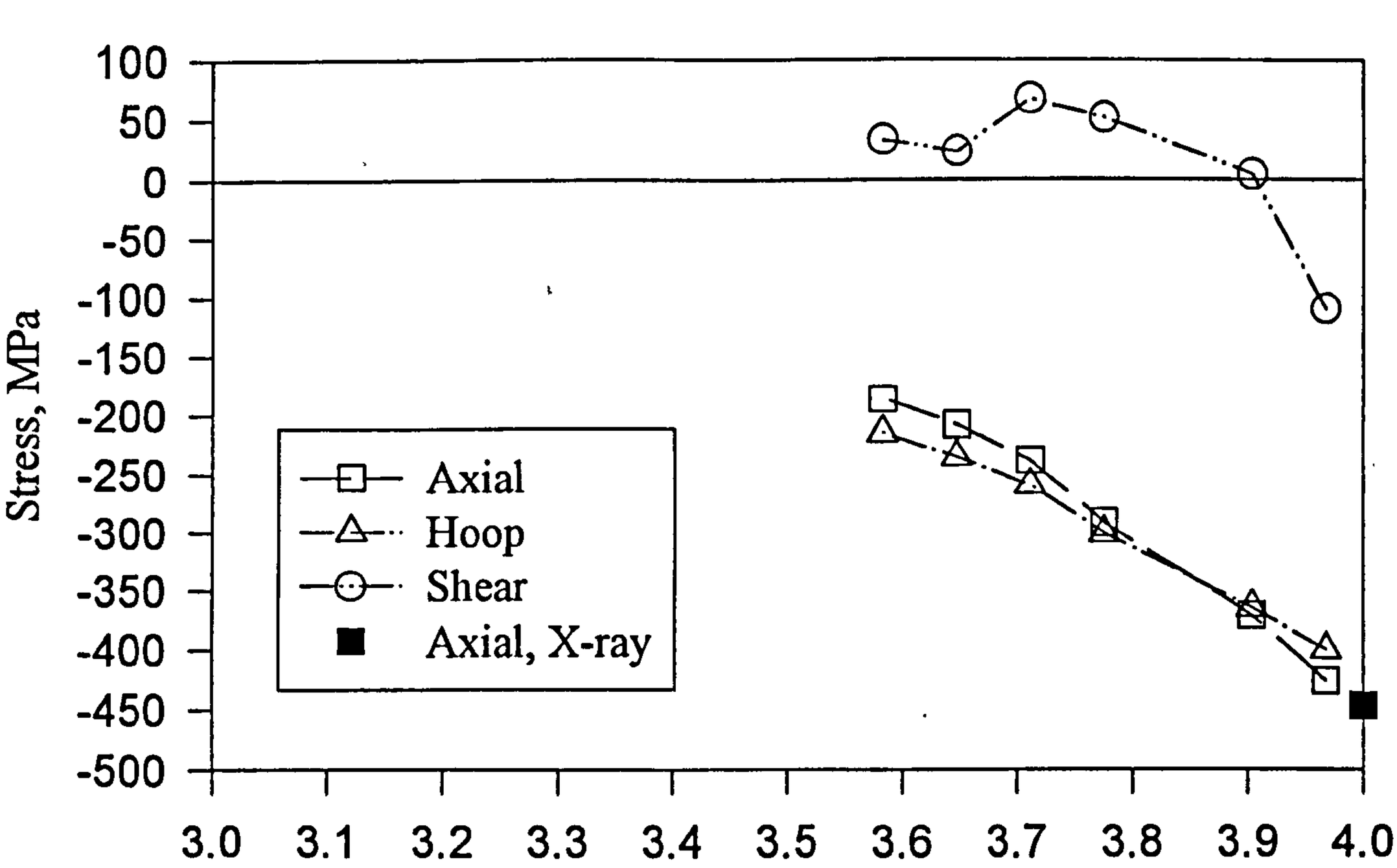

Fig 4.64 Residual stresses of HTS20 on side B by centre hole using average stress method and plastic modification

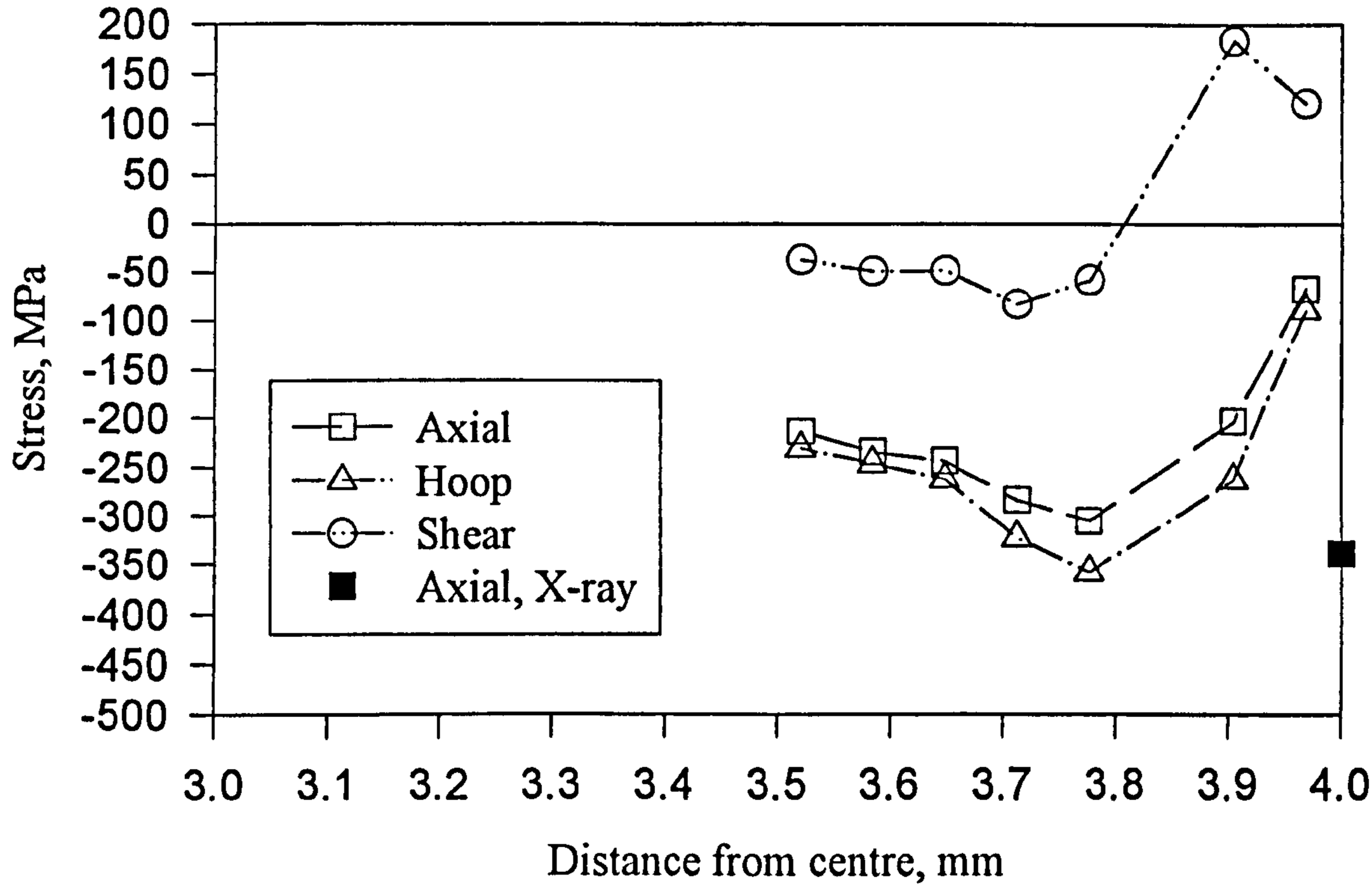

Fig 4.65 Residual stresses of FS16 on side B by centre hole using average stress method and plastic modification

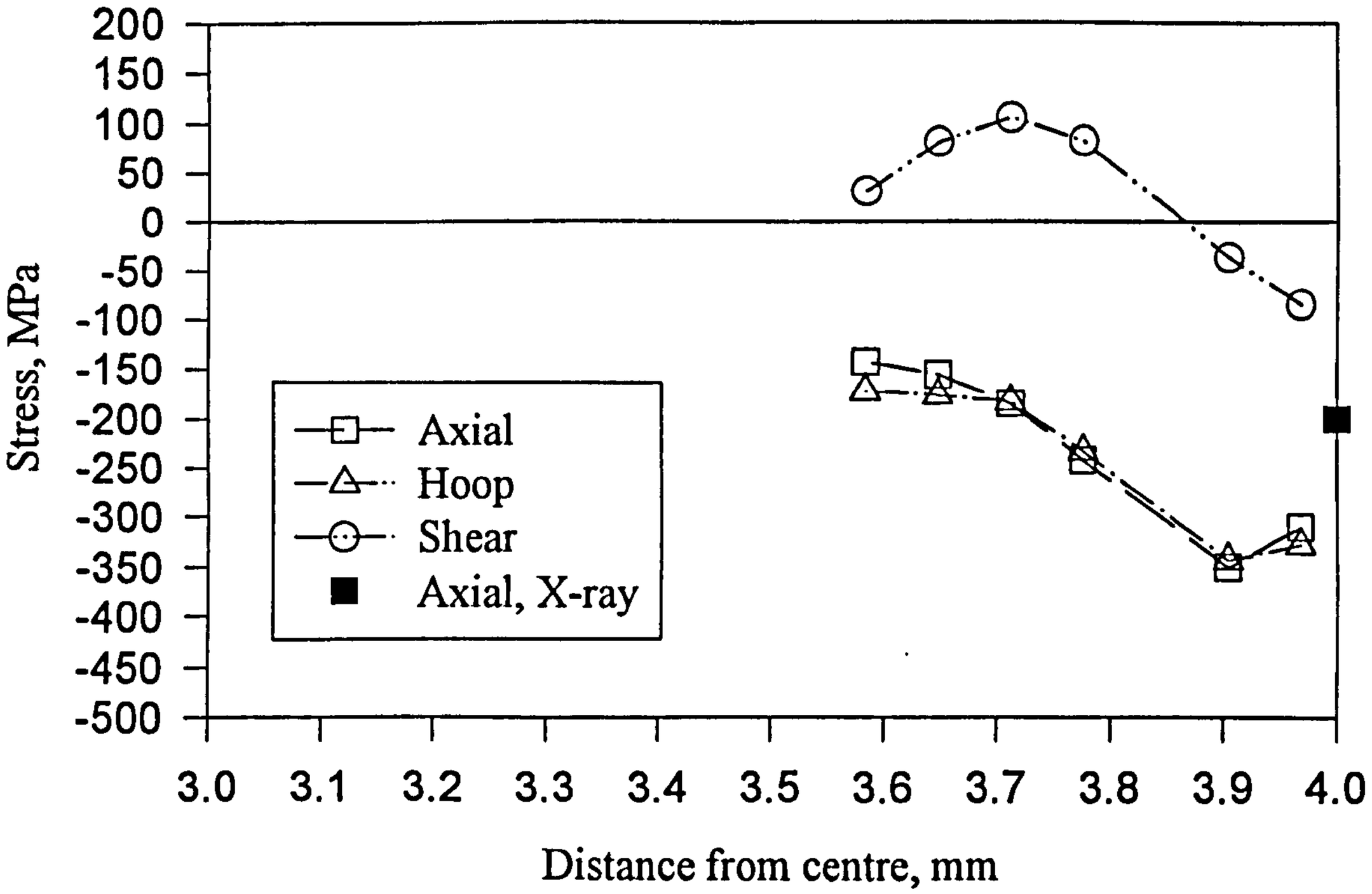

Fig 4.66 Residual stresses of FS18 on side B by centre hole using average stress method and plastic modification

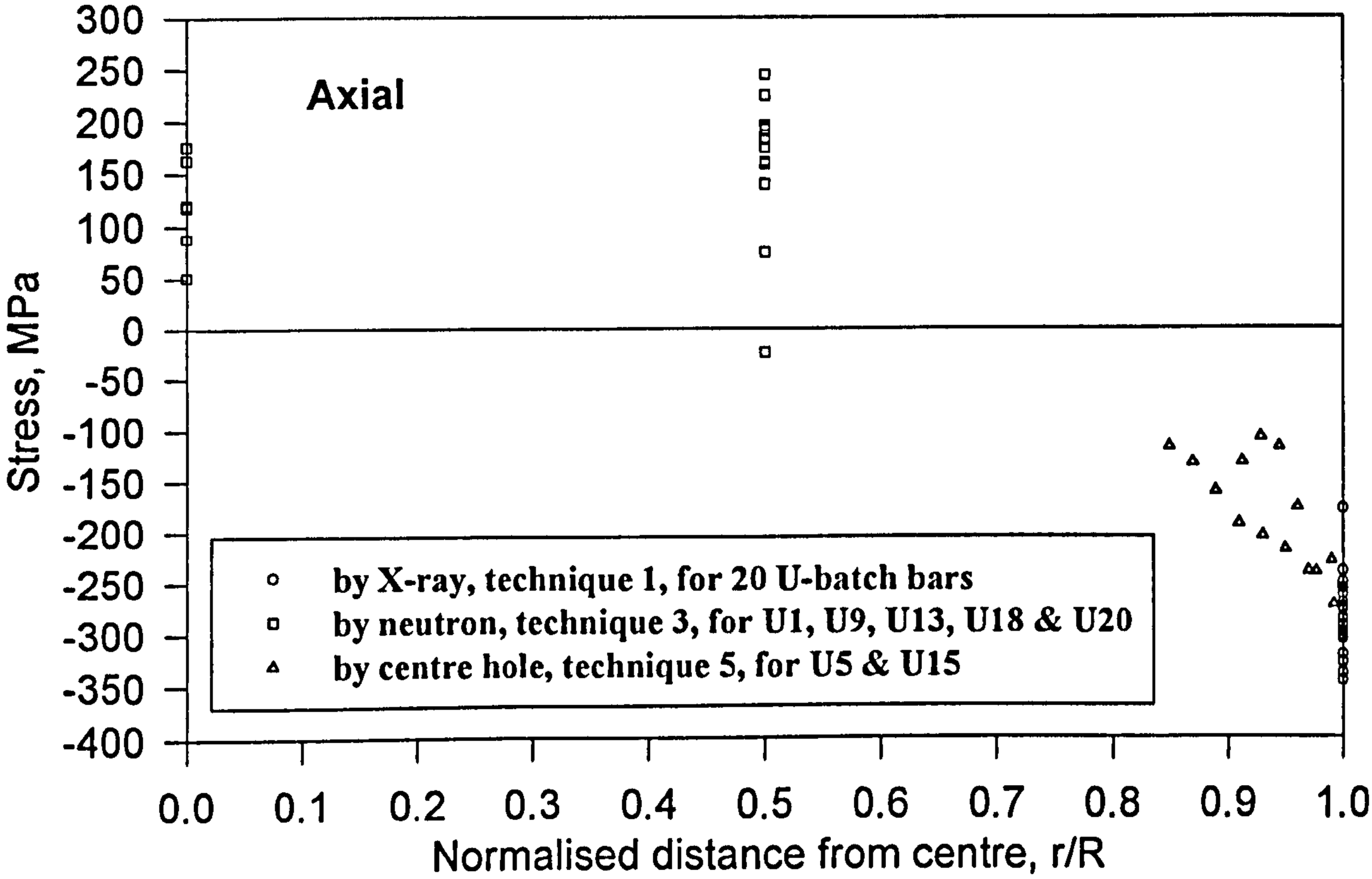

Fig 4.67 Axial residual stresses for specimens from U-batch by using different techniques

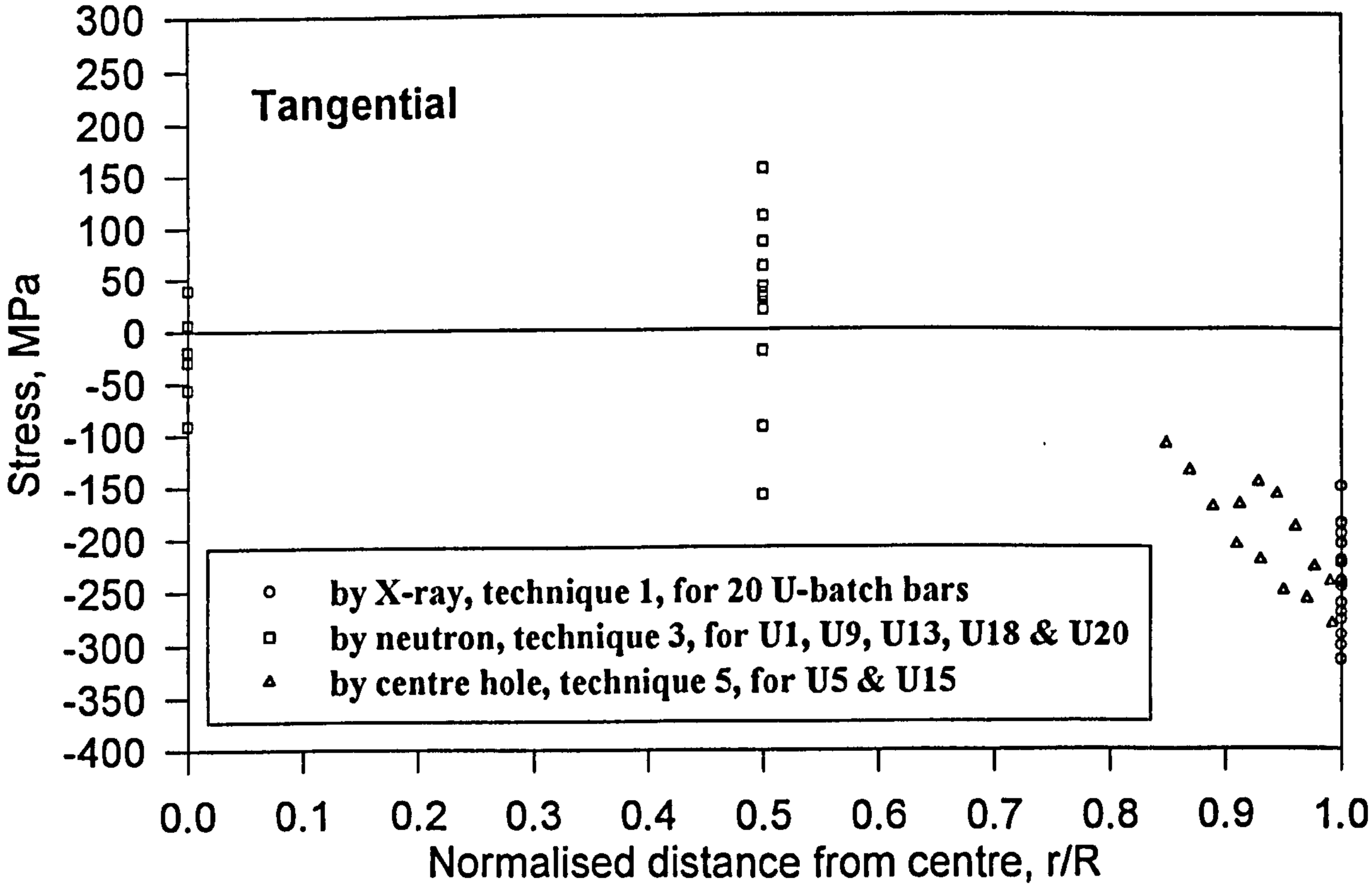

Fig 4.68 Tangential residual stresses for specimens from U-batch by using different techniques

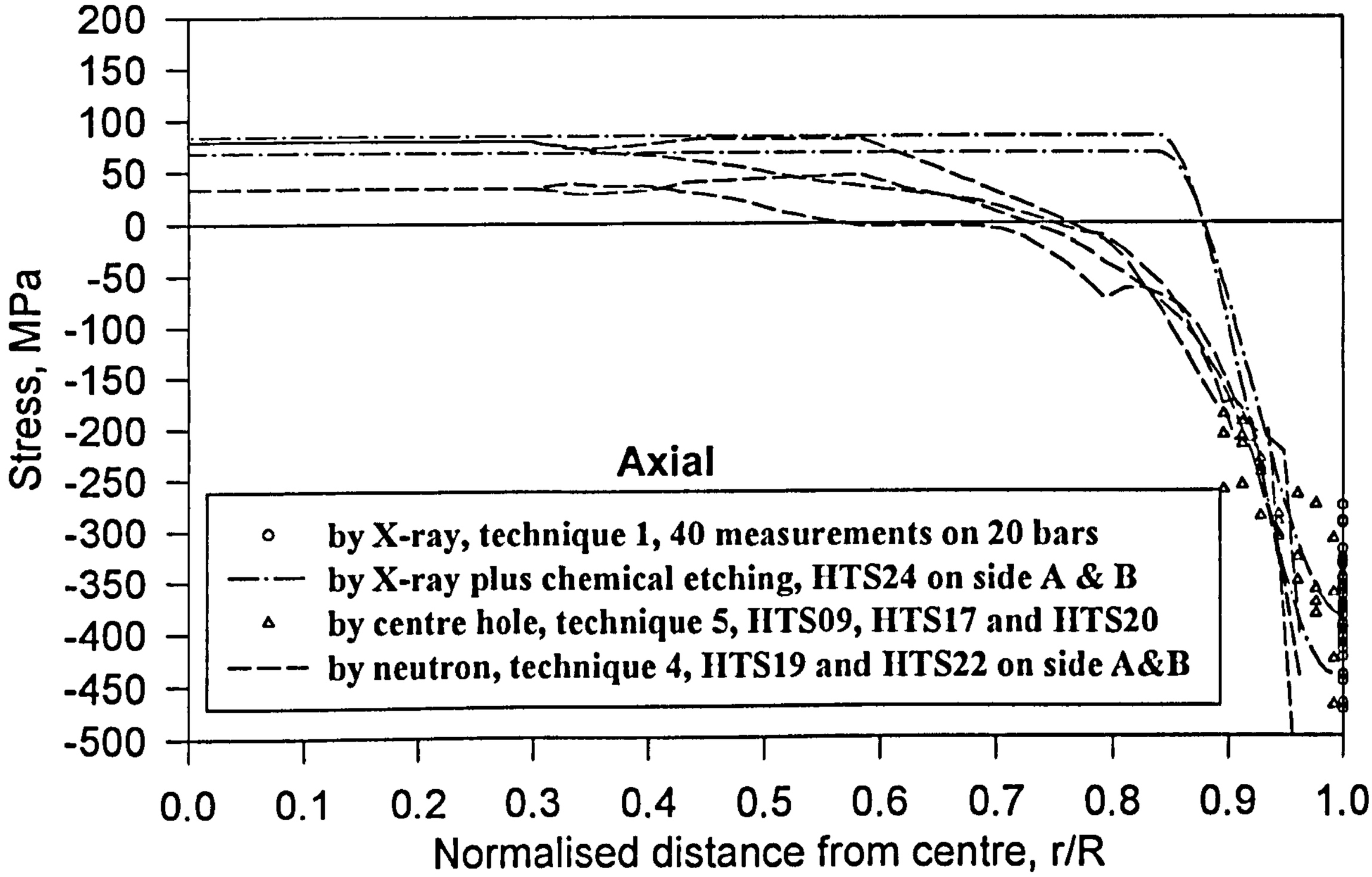

Fig 4.69 Axial residual stresses for specimens from HTS group by using different techniques

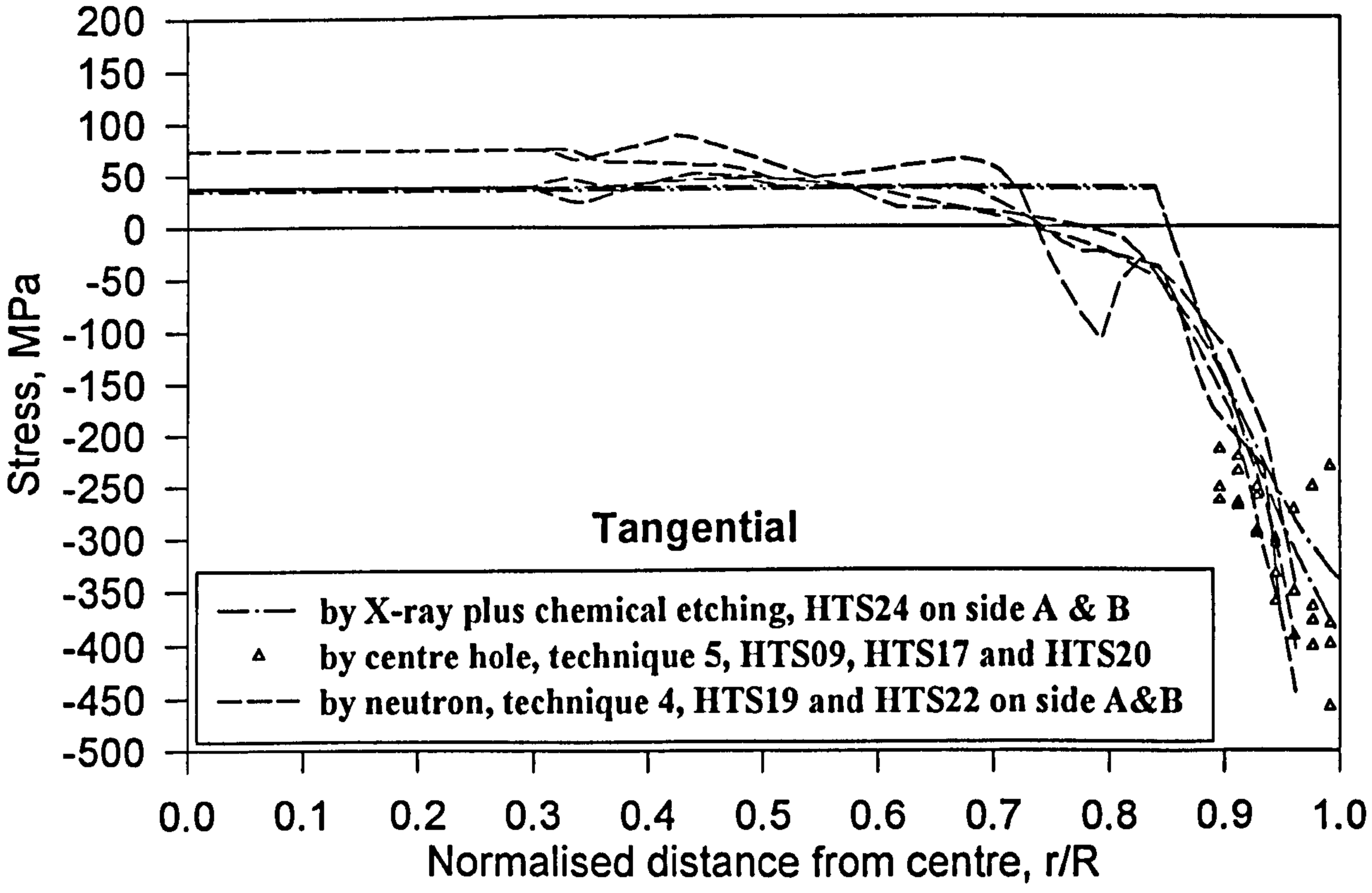

Fig 4.70 Tangential residual stresses for specimens from HTS group by using different techniques

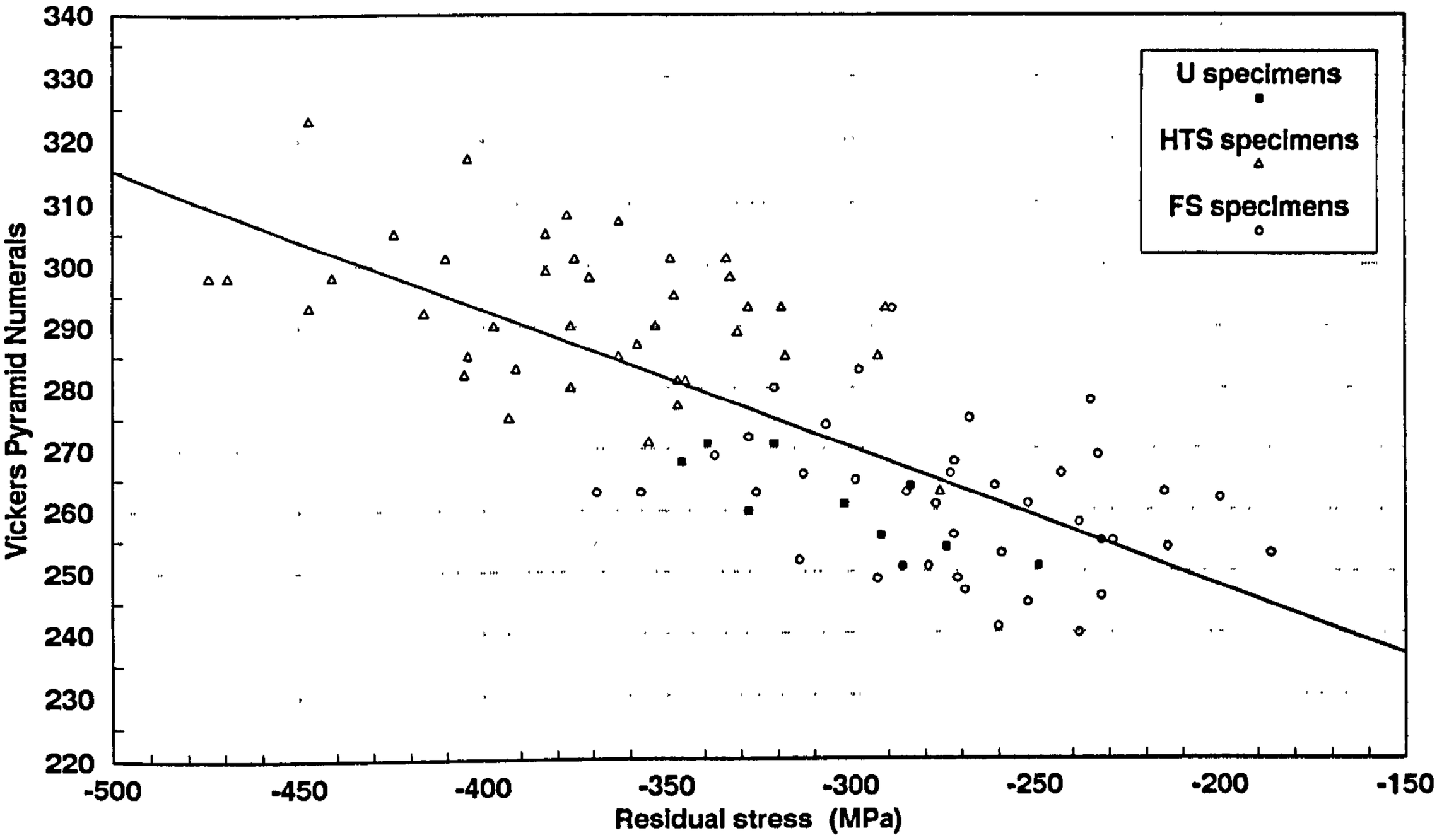

Fig 4.71 Correlation between hardness and residual stresses for shot blasted specimens from HTS, FS and U-batch

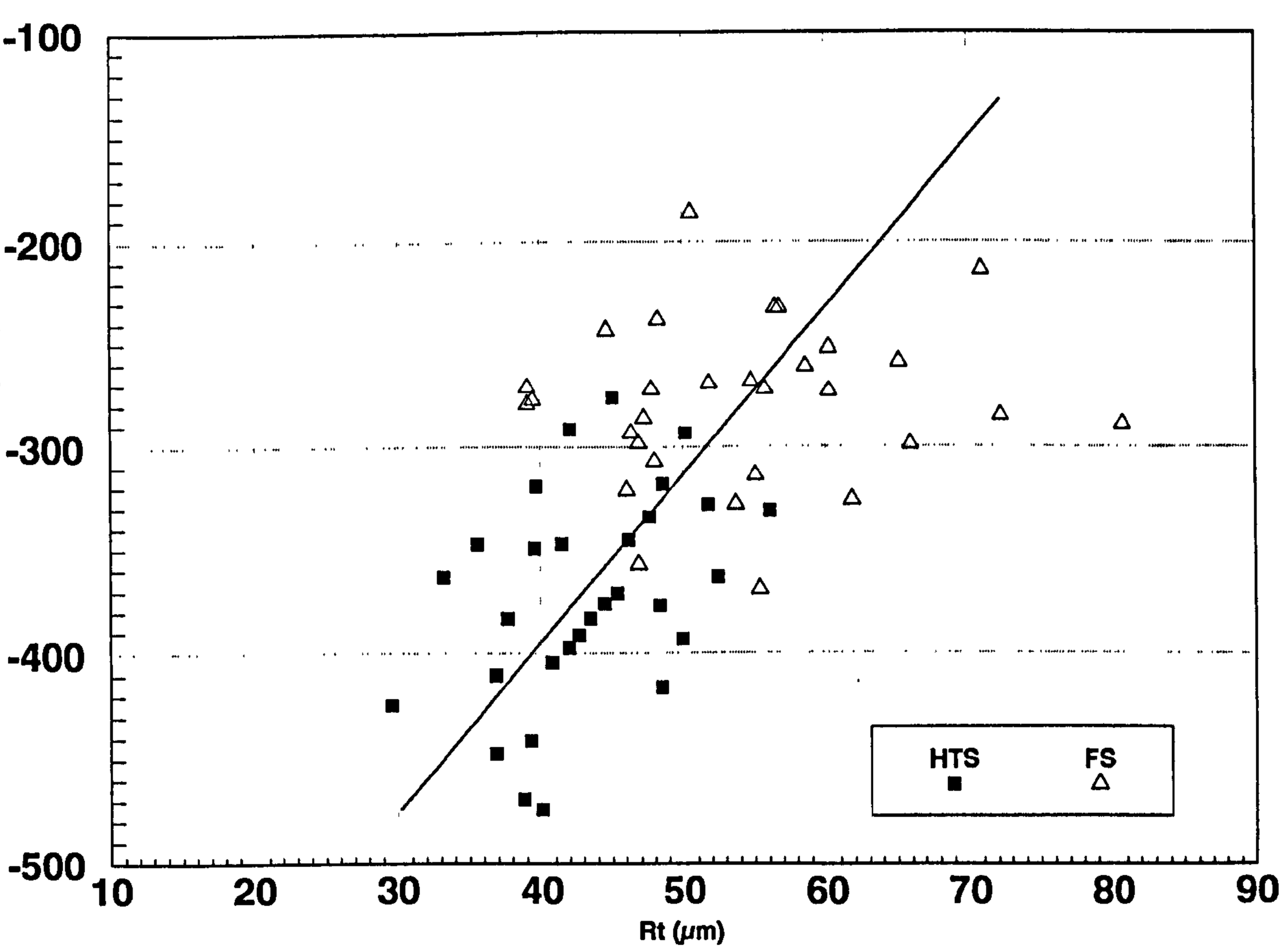

Fig 4.72 Correlation between surface roughness and residual stresses for shot blasted specimens from HTS and FS

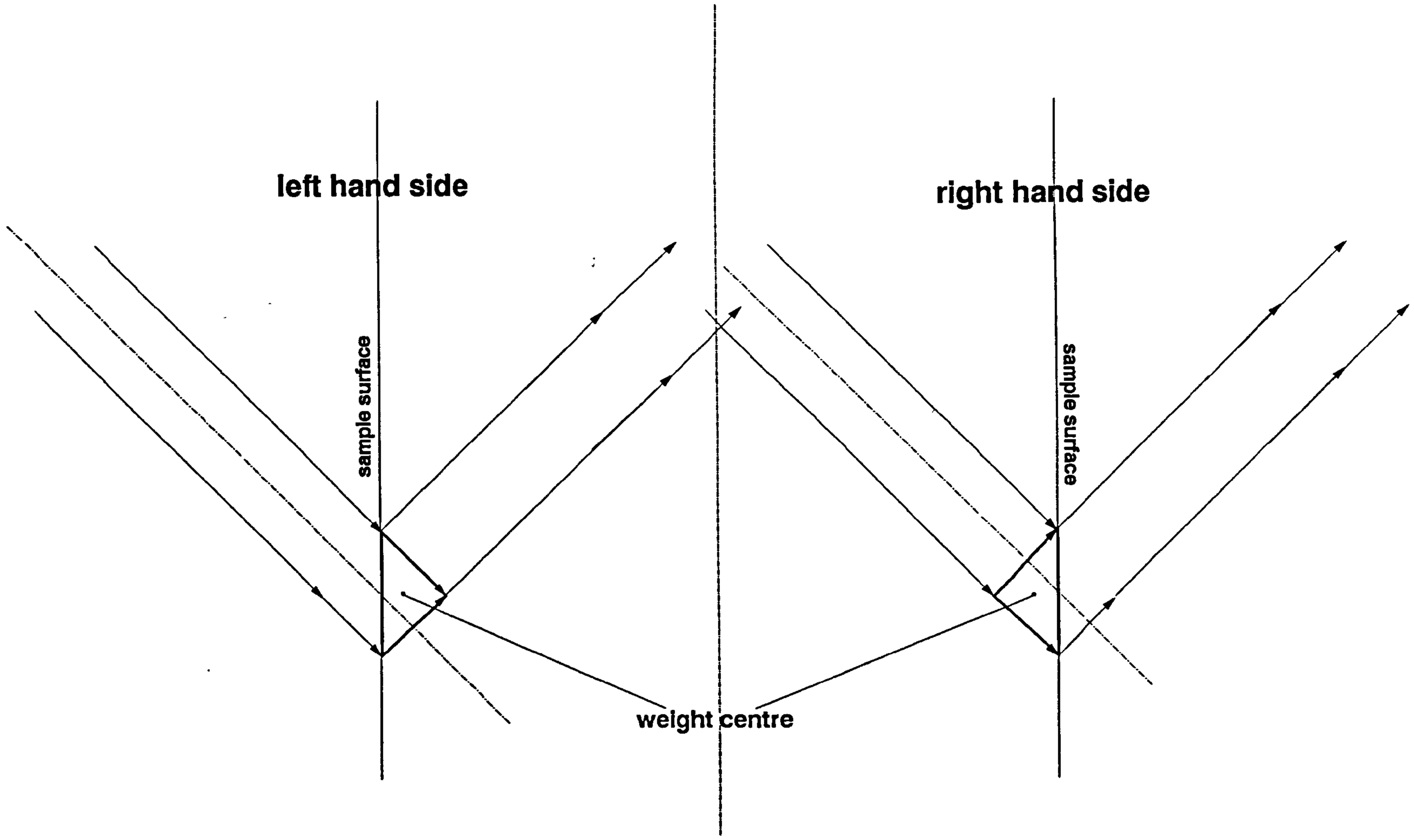

Fig 4.73 Neutron diffraction measurements across section for both axial and tangential strain measurements

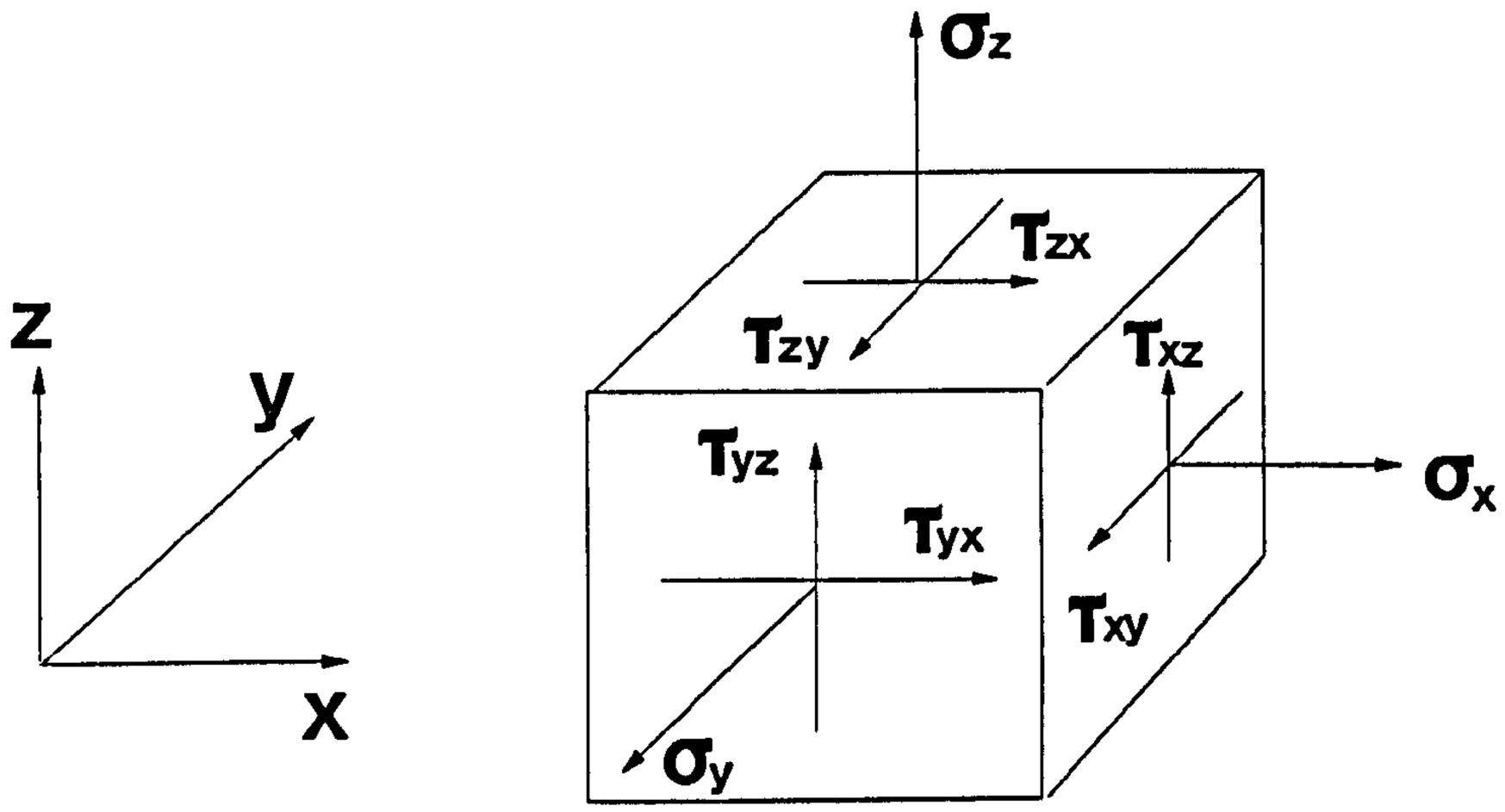

Fig 5.1 Stress element

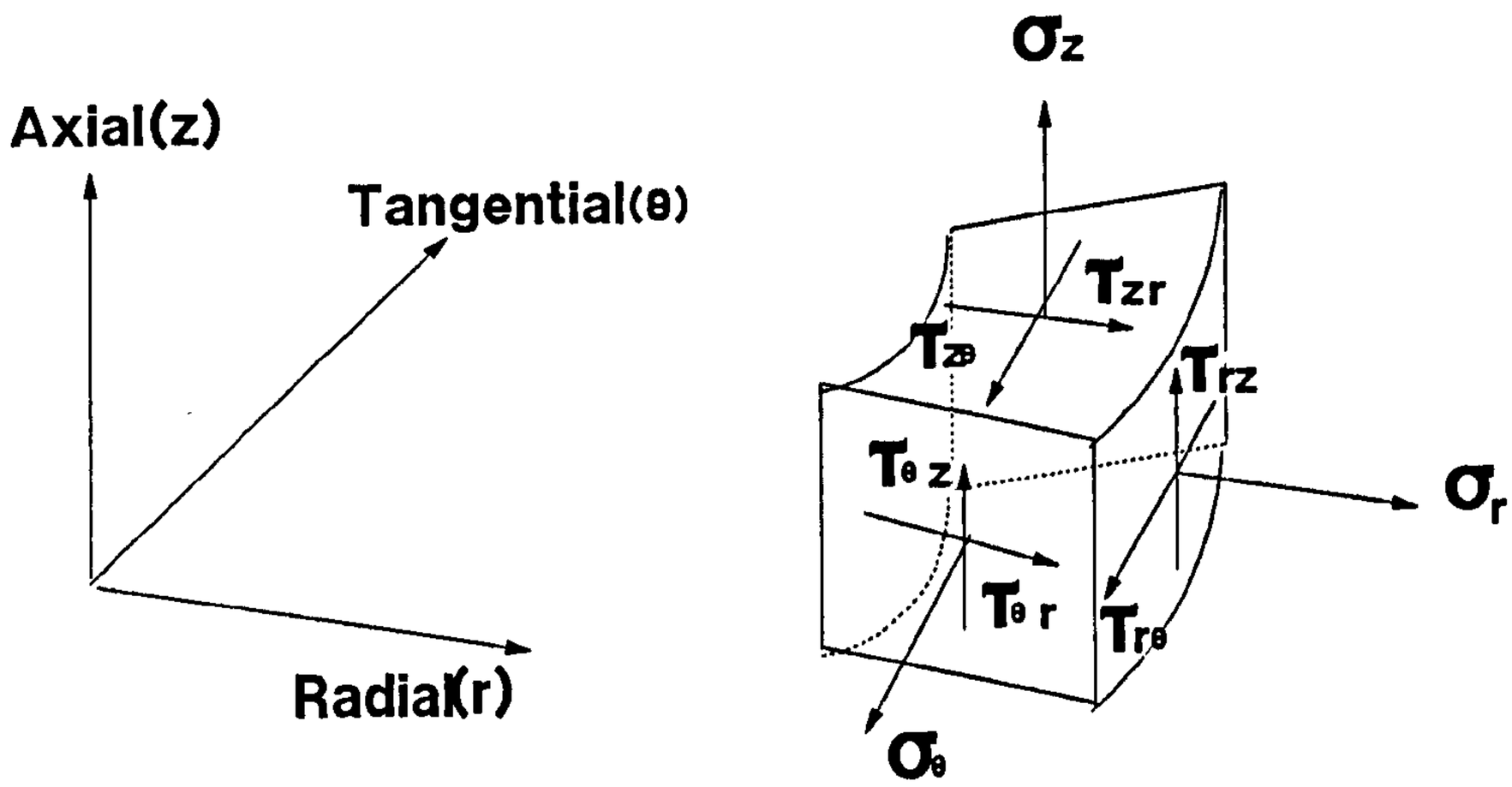

Fig 5.2 Stress element for cylindrical coordinates system

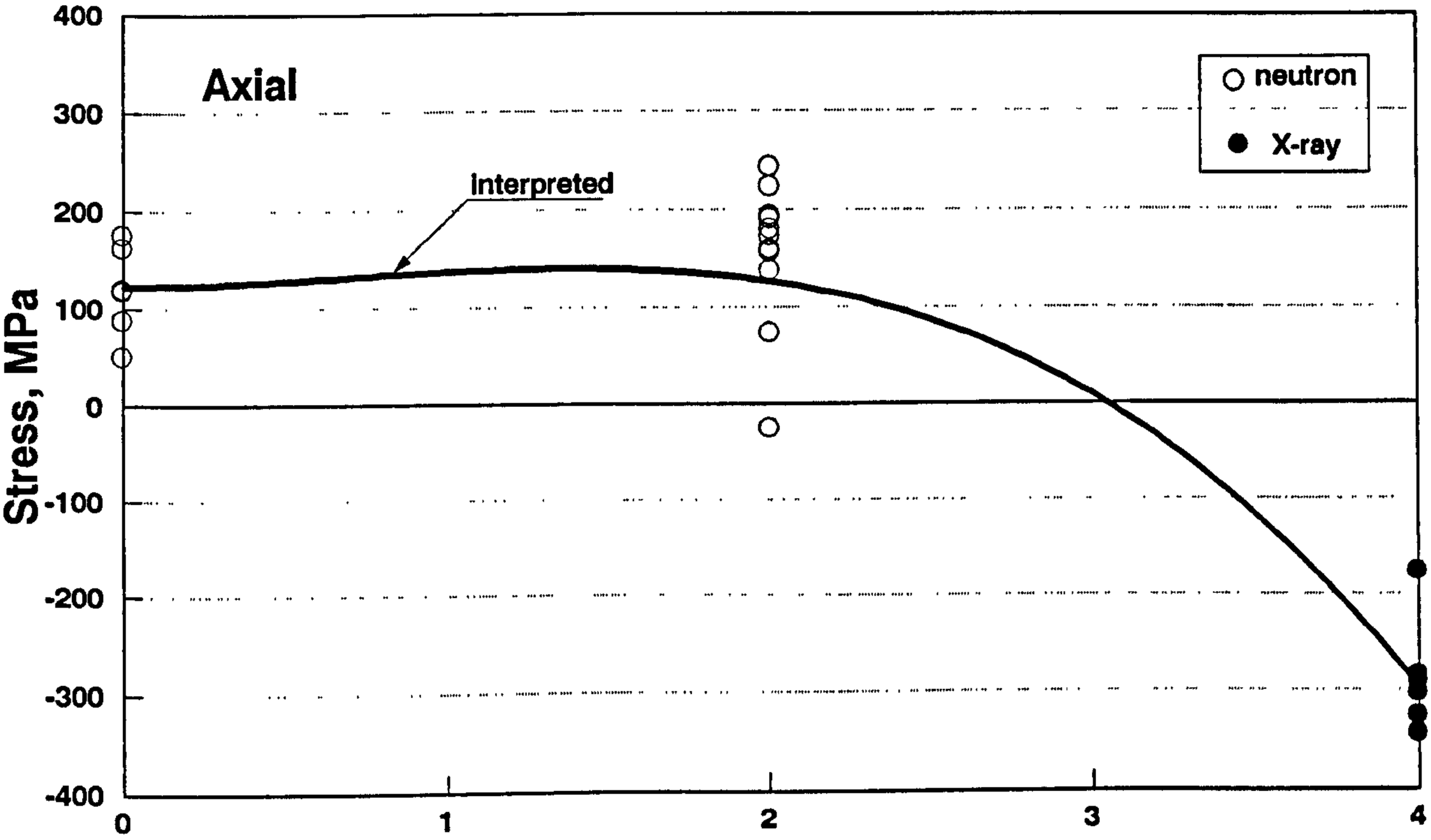

Fig 5.3 Interpreted residual stress distribution (i) axial residual stress

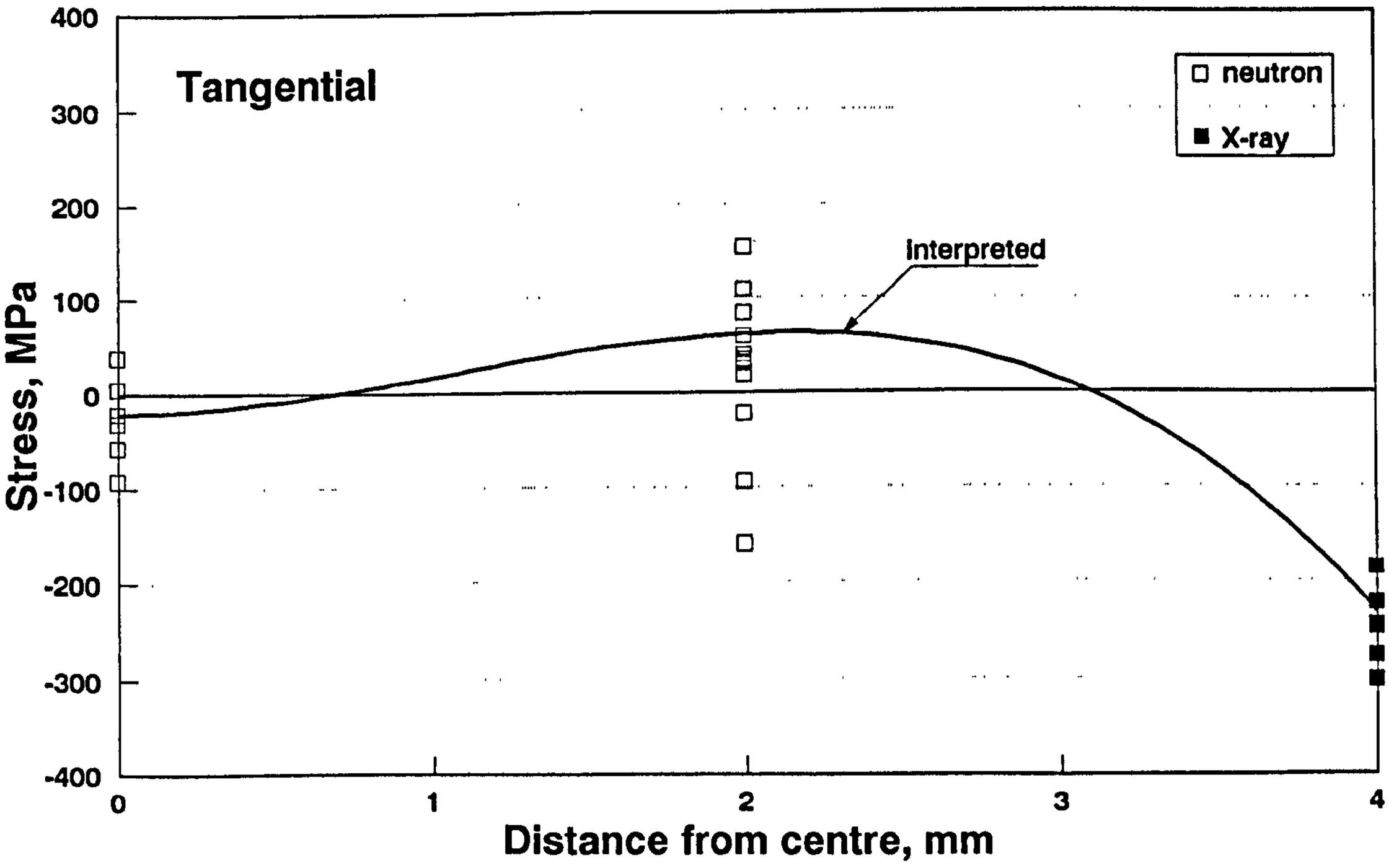

Fig 5.4 Interpreted residual stress distribution (ii) tangential residual stress

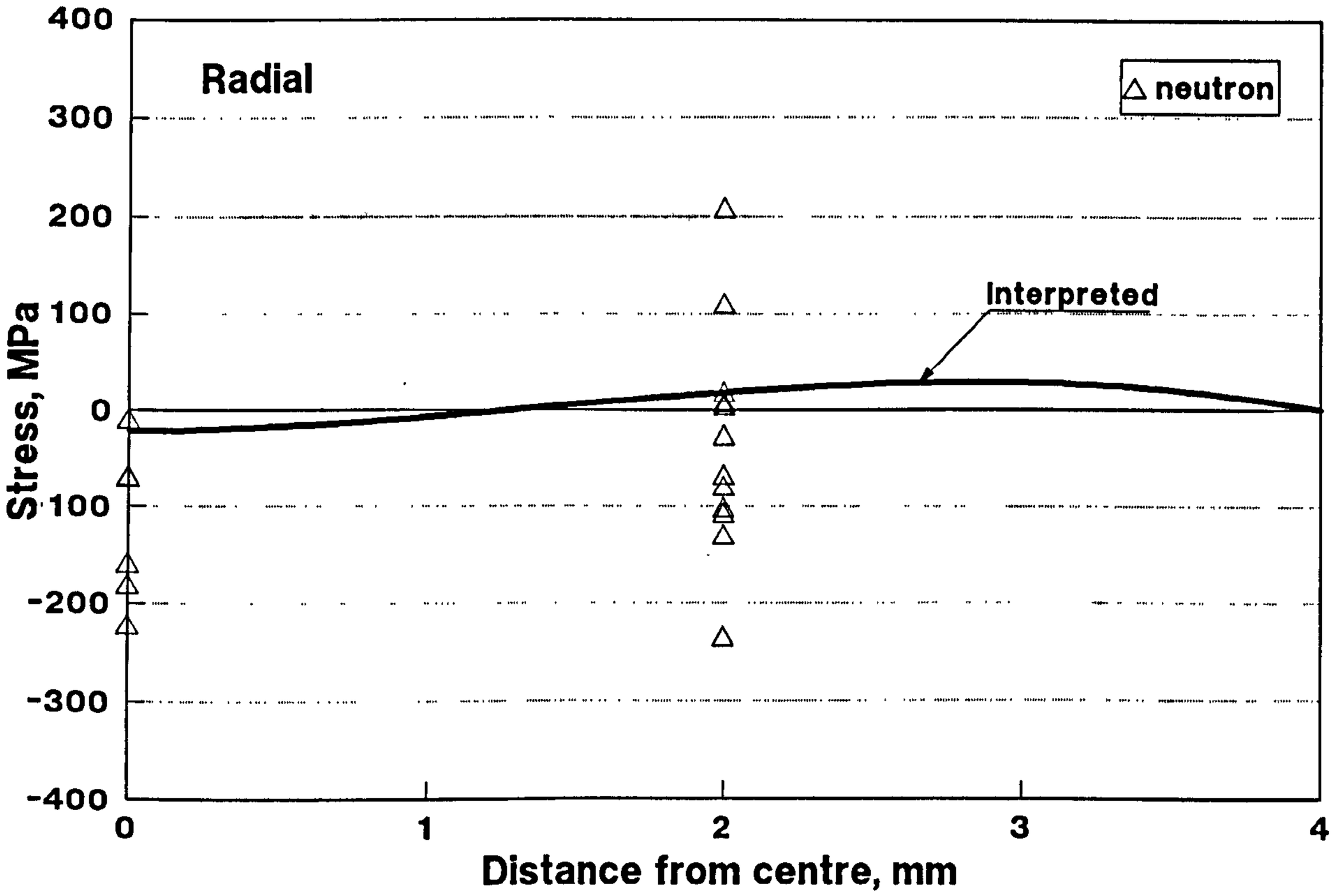

Fig 5.5 Interpreted residual stress distribution (iii) radial residual stress

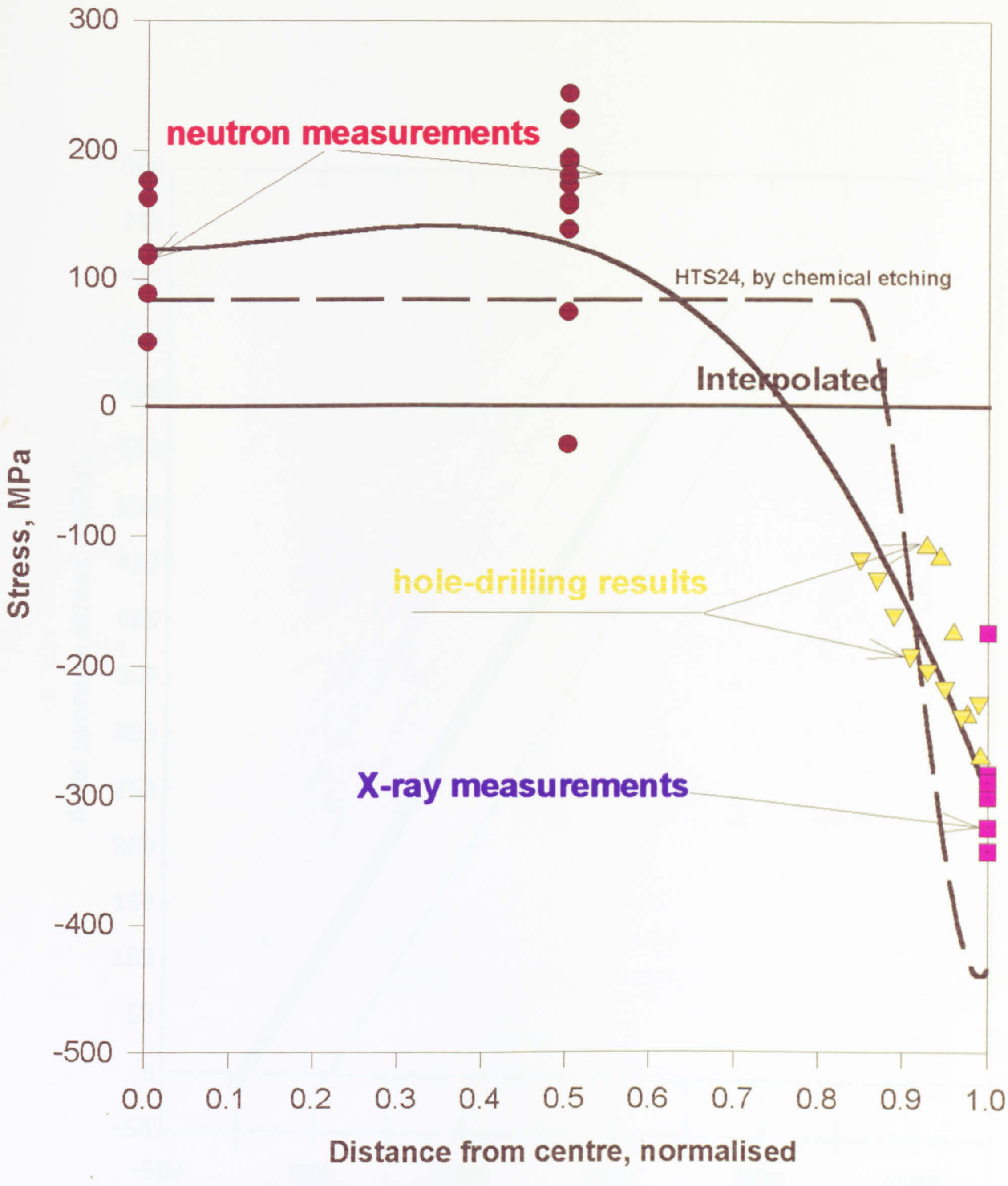

Fig 5.6 Axial residual stresses from measurements by X-ray, neutron and hole-drilling methods

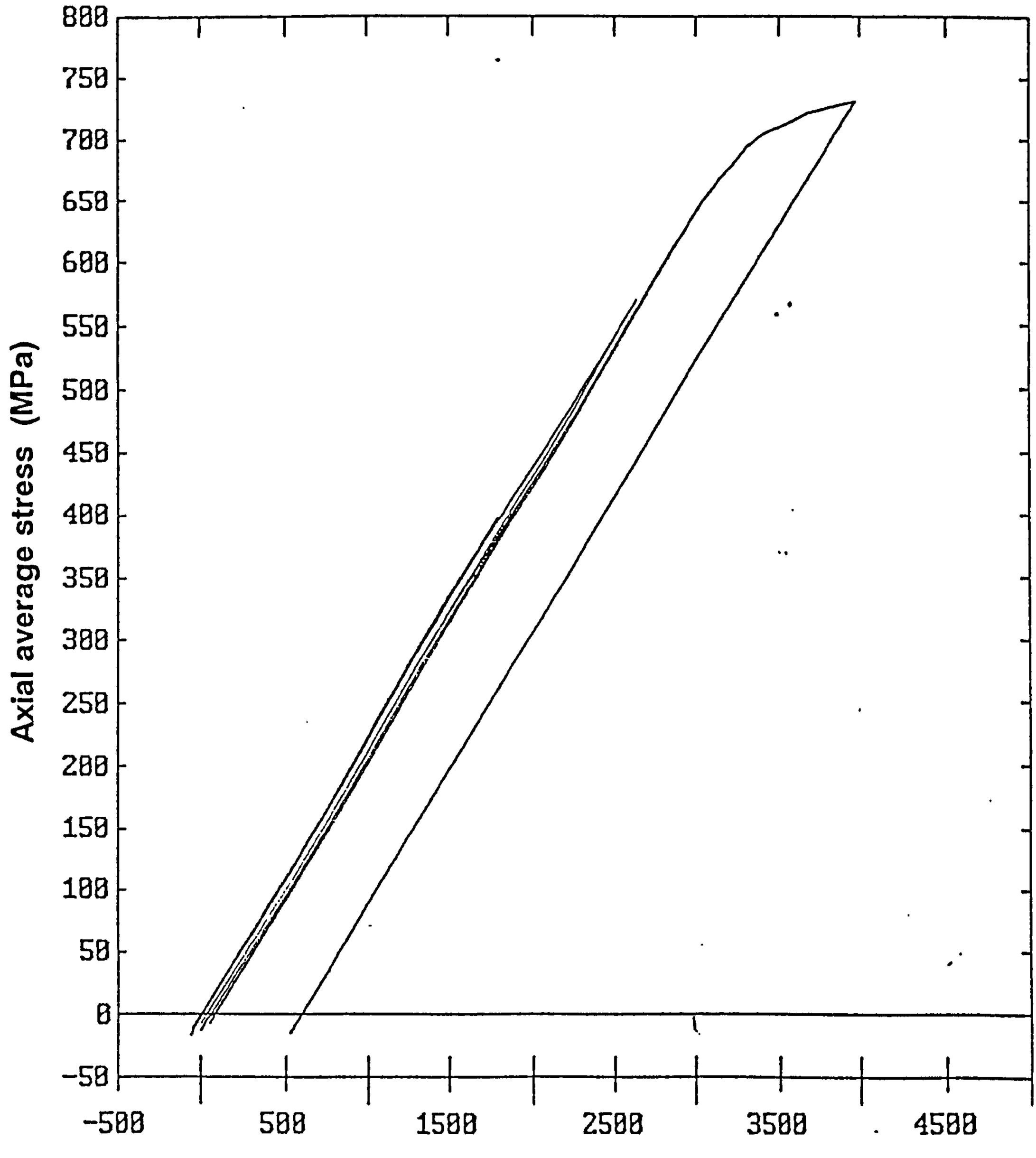

Fig 6.1 Axial loading versus surface axial strain for round bar specimen U19

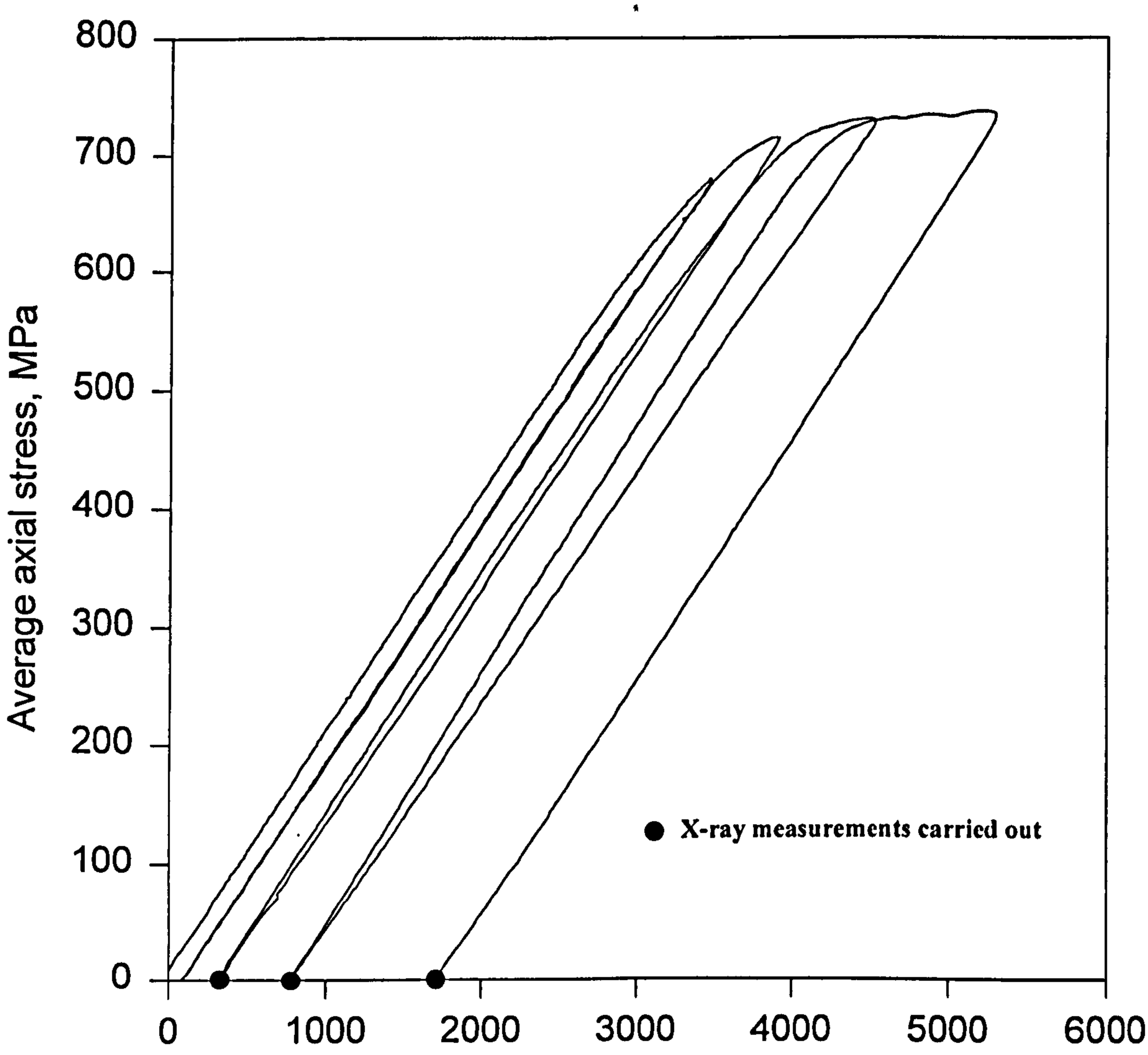

Fig. 6.2 Axial loading versus surface axial strain for round bar specimen U14

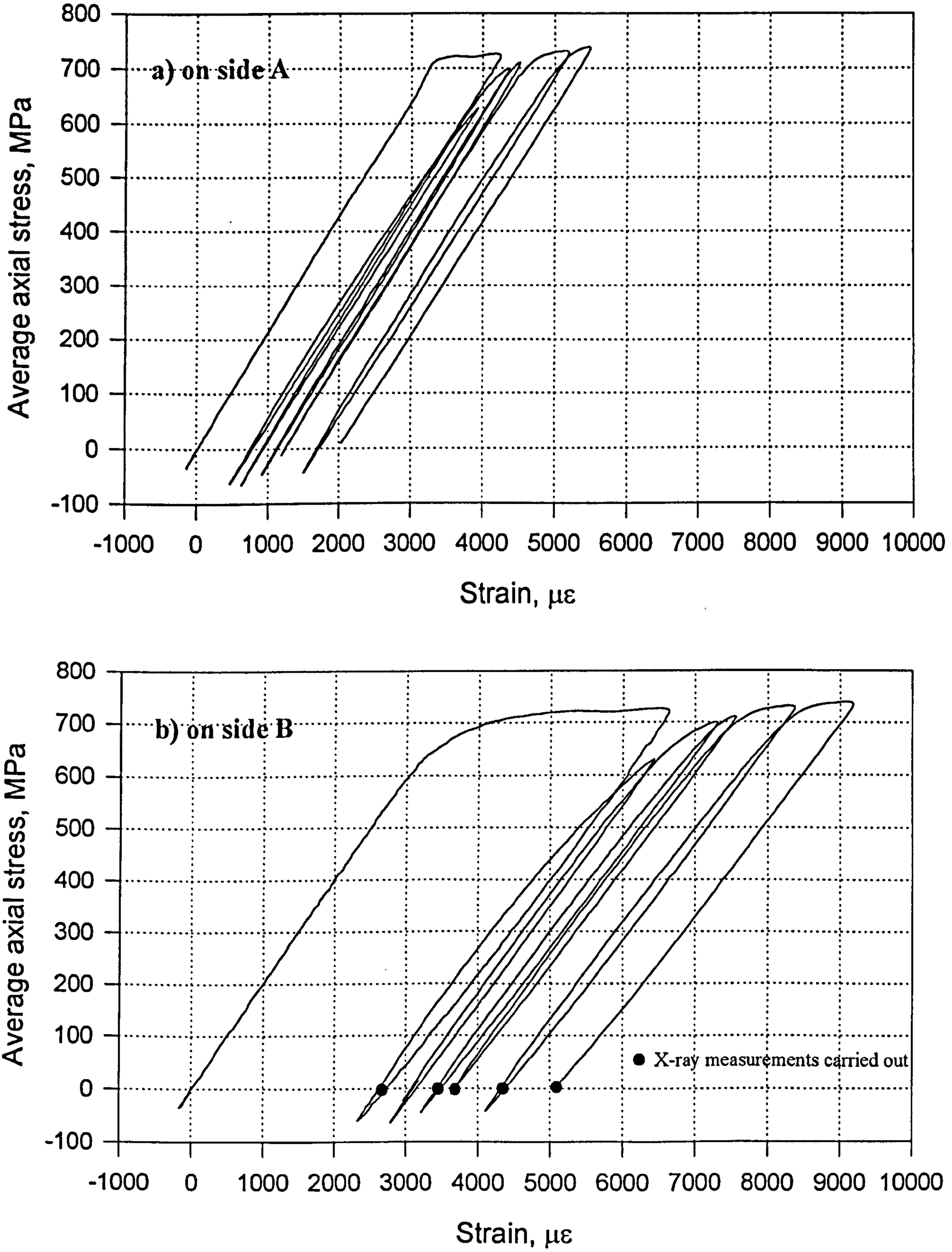

Fig 6.3 Axial average stress against surface axial strain of specimen U10 under tensile cyclic loading

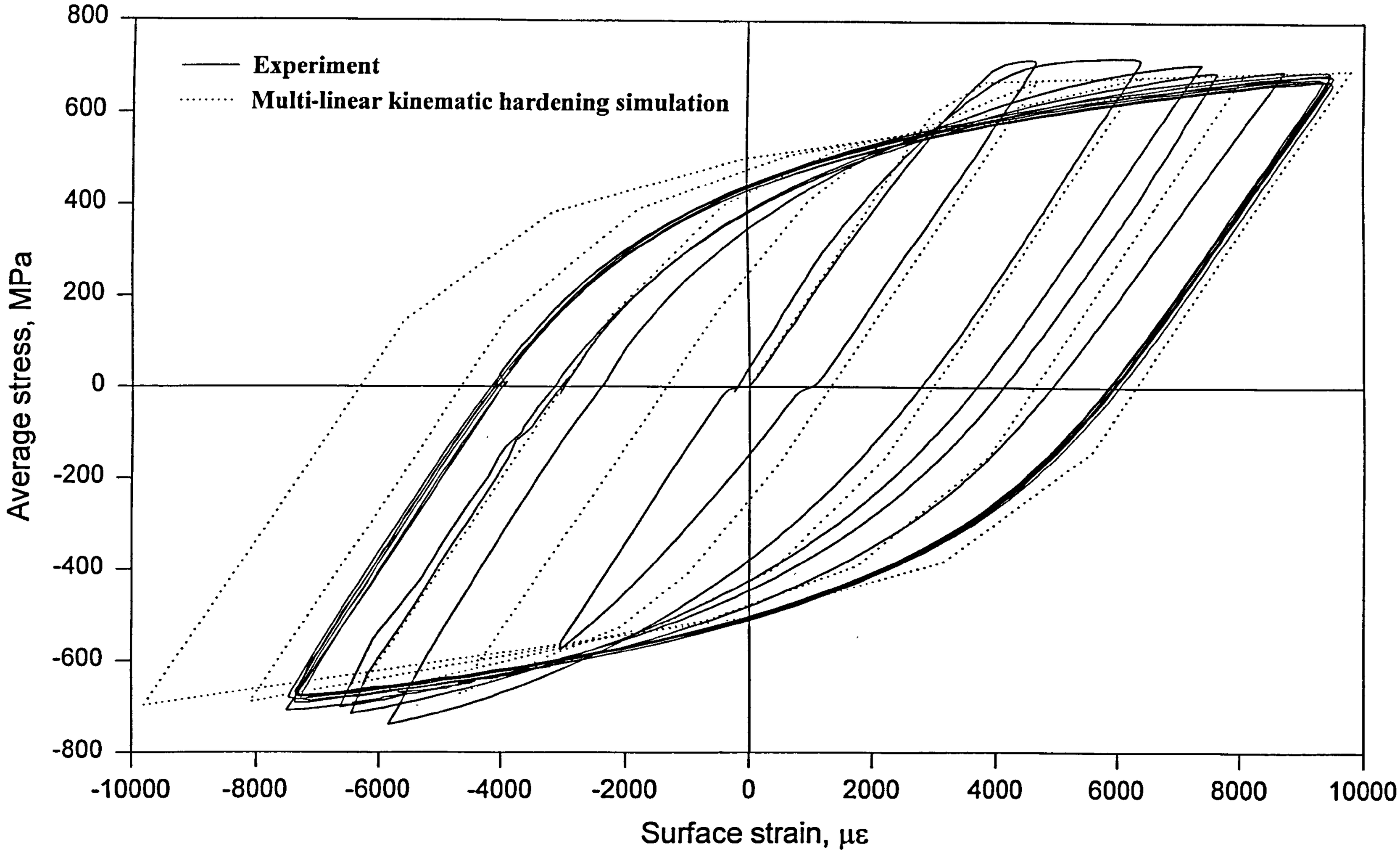

Fig 6.4 Cyclic stress-strain history of U06, 10 cycles

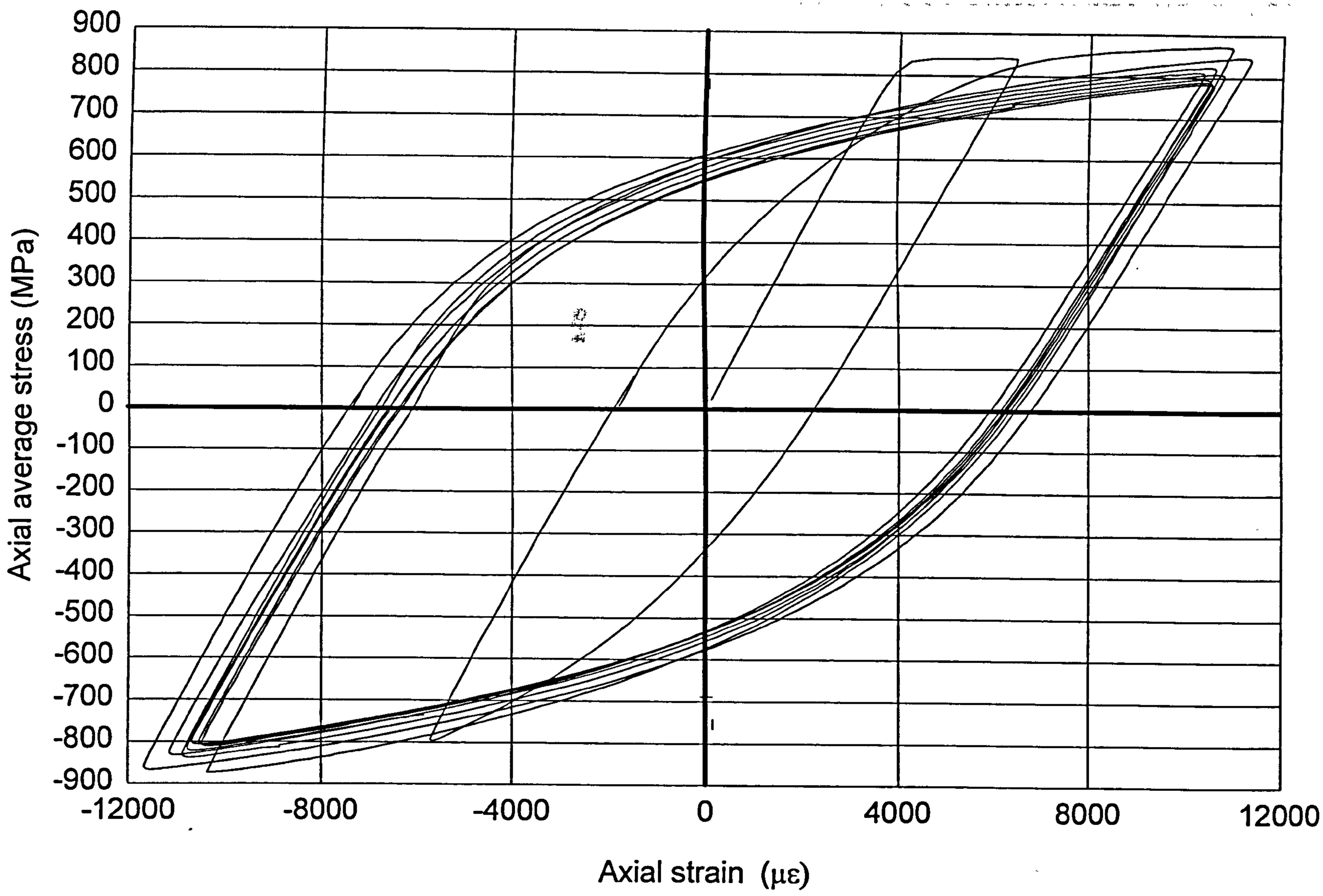

Fig 6.5 Cyclic stress-strain history of HTS18 (9 cycles)

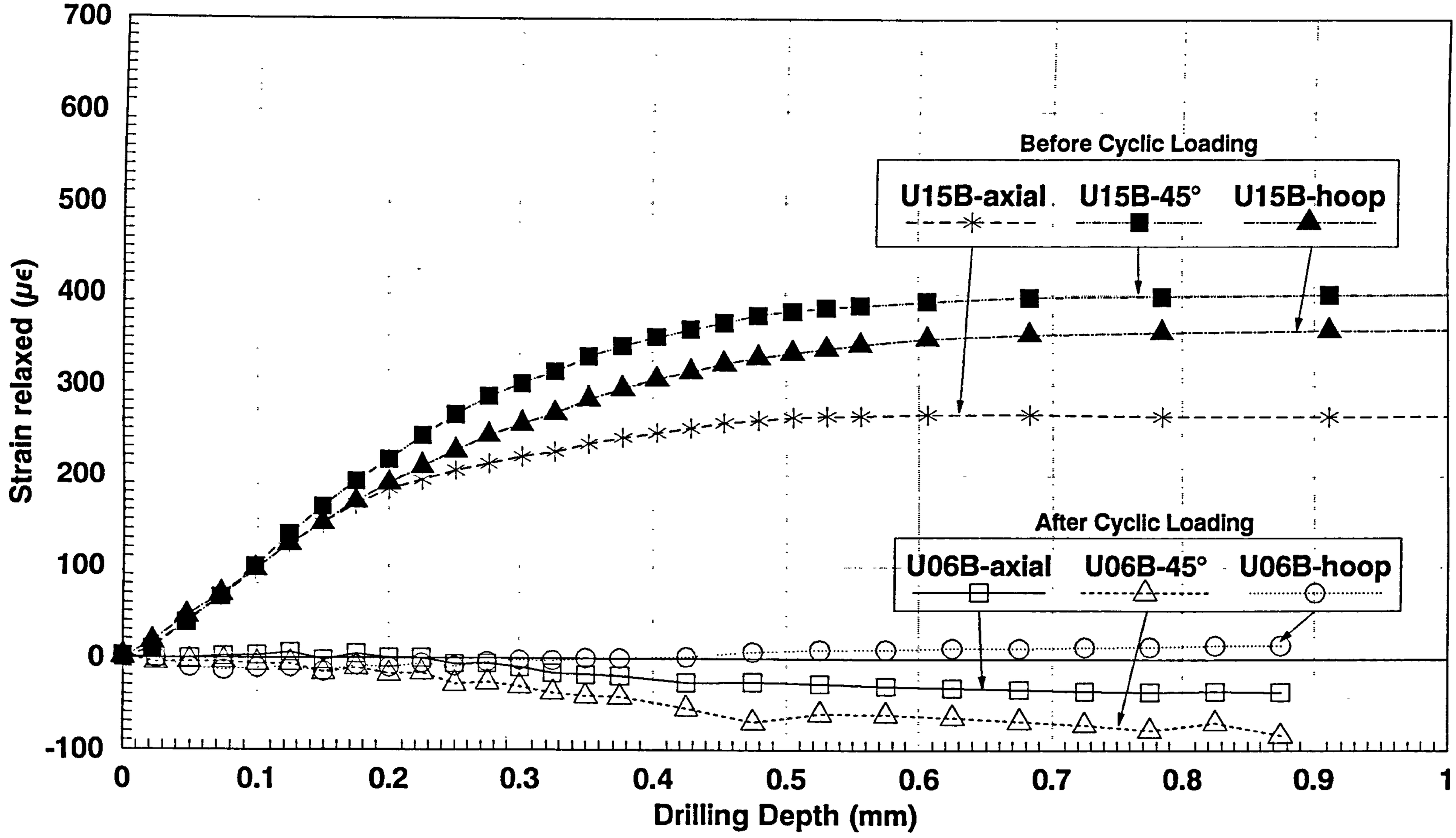

Fig 6.6 Hole drilling strain result of U06 after cyclic loading & comparison with that of U15 before cyclic loading

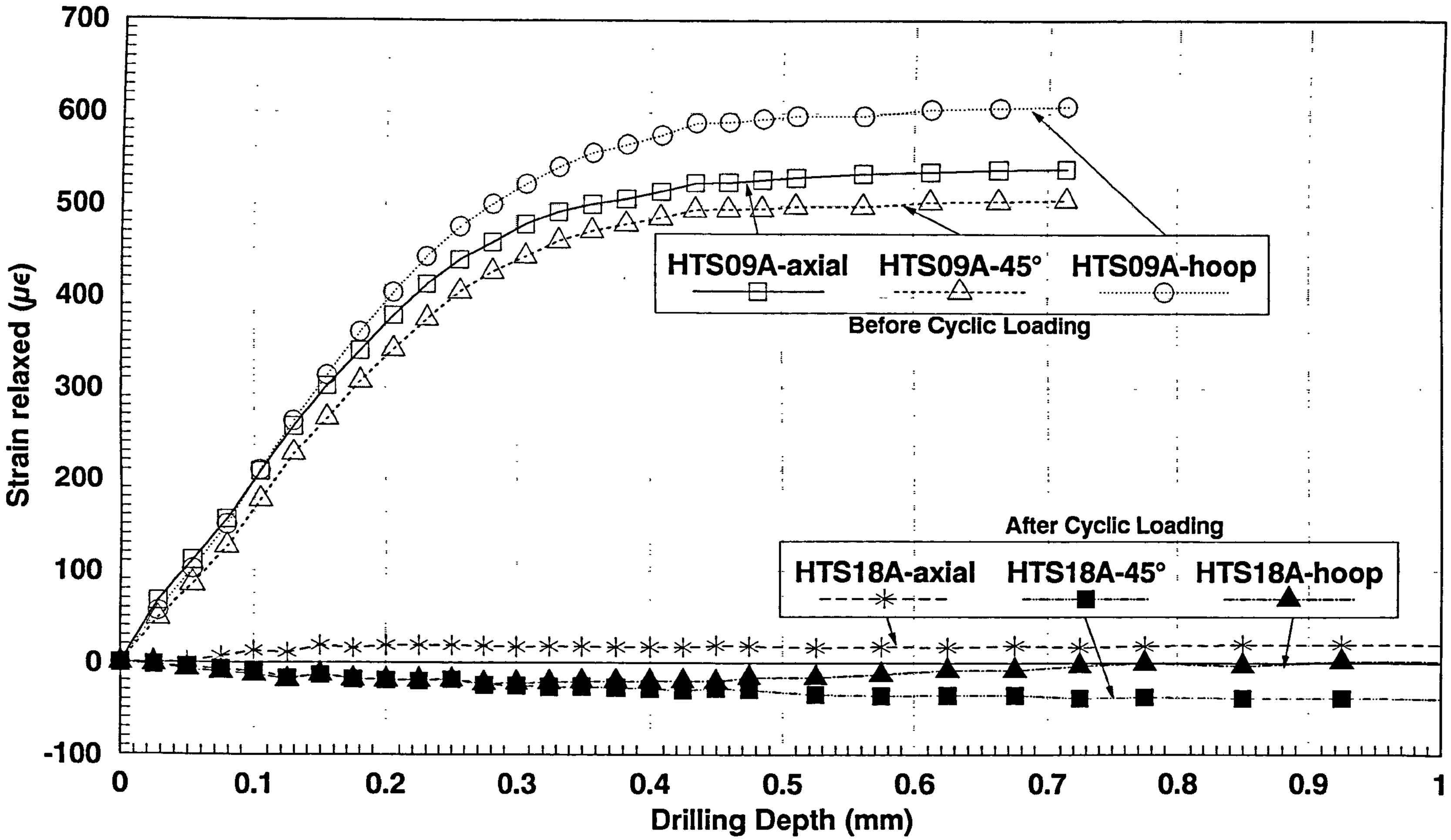

Fig 6.7 Hole drilling strain result of HTS18 after cyclic loading & comparison with that of HTS09 before cyclic loading

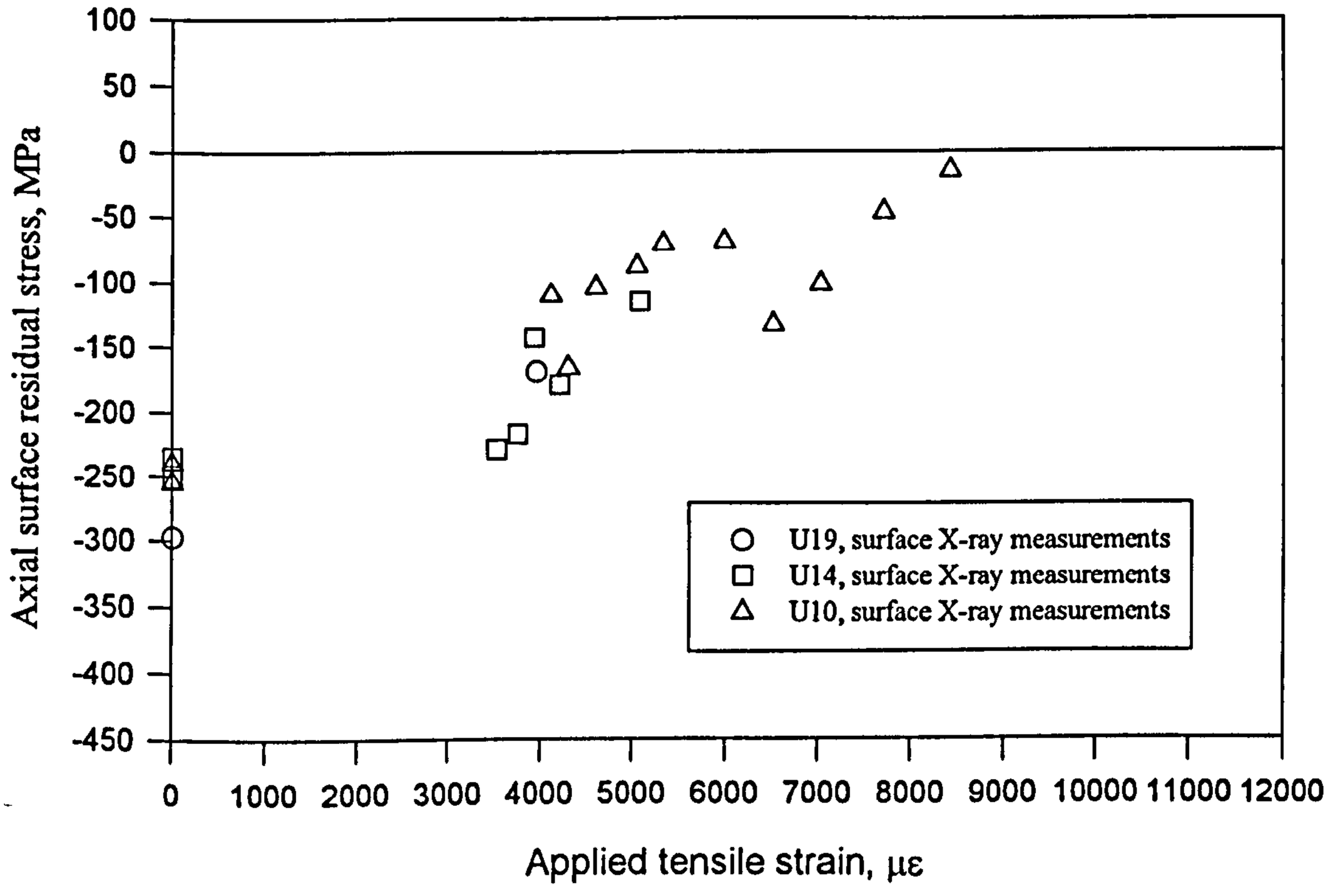

Fig. 6.8 Residual stress relaxation in the round bar specimens after tensile loading

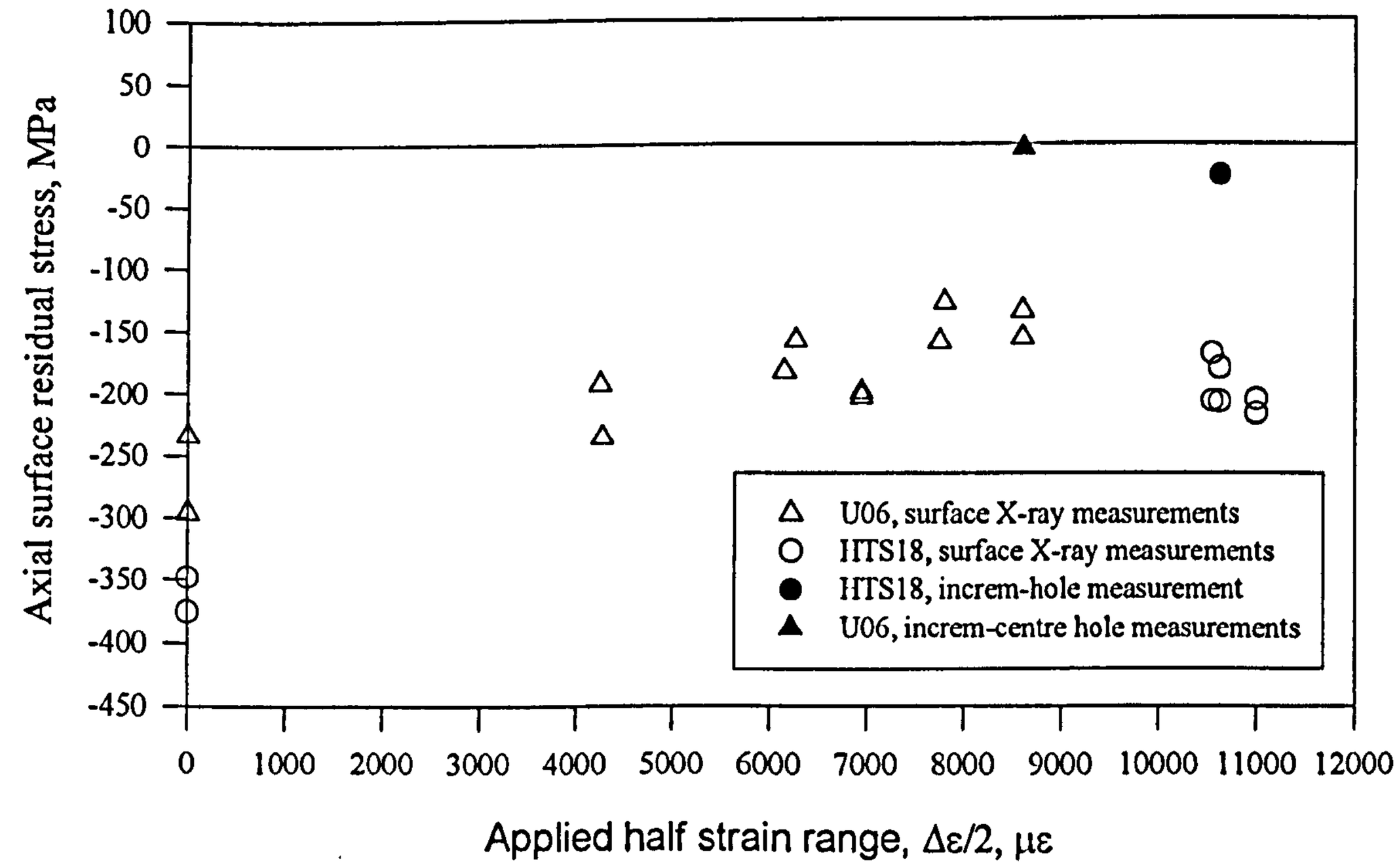

Fig. 6.9 Axial residual stress relaxation after cyclic mechanical loading

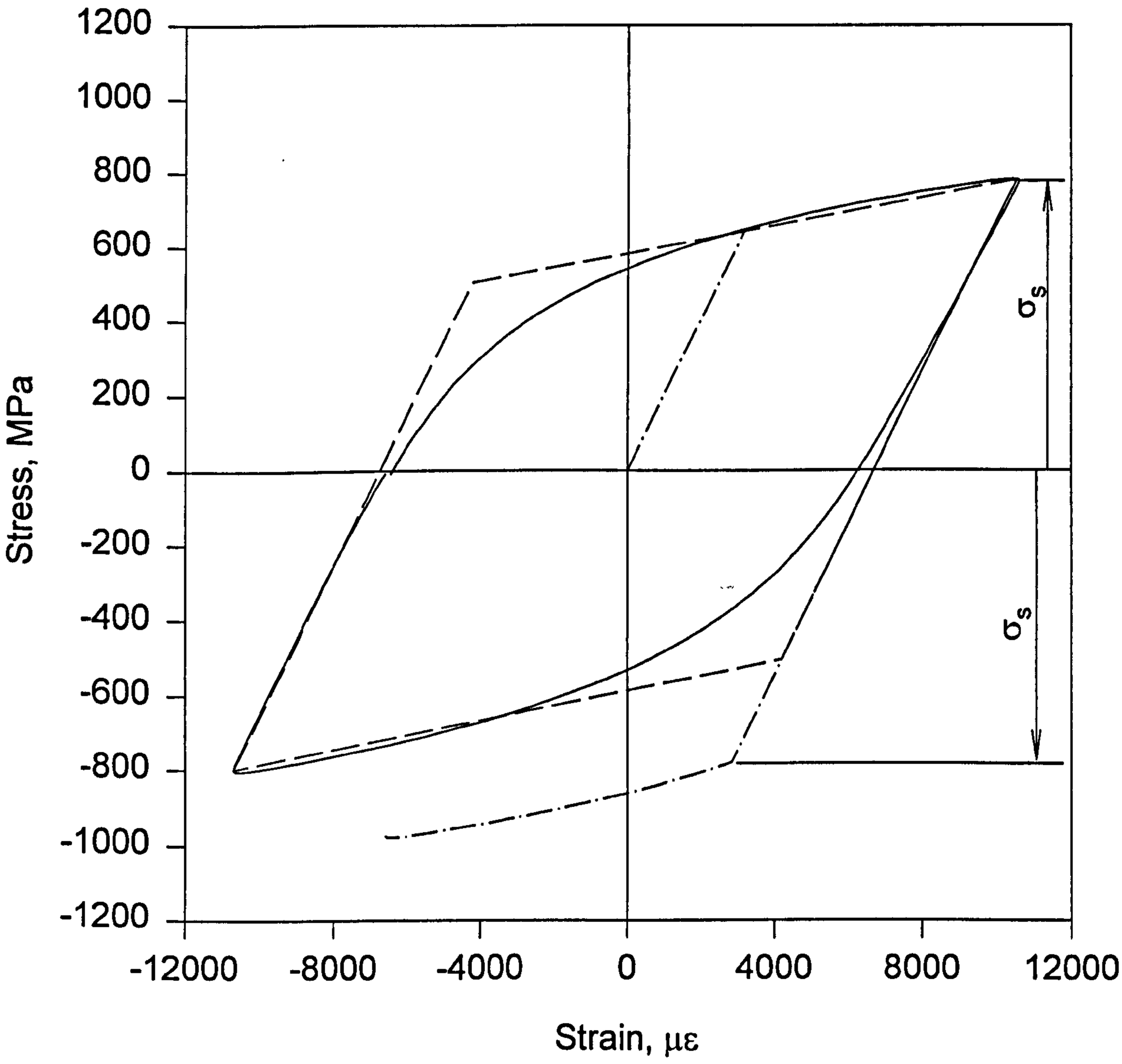

Fig 6.10 Definition of hardening models

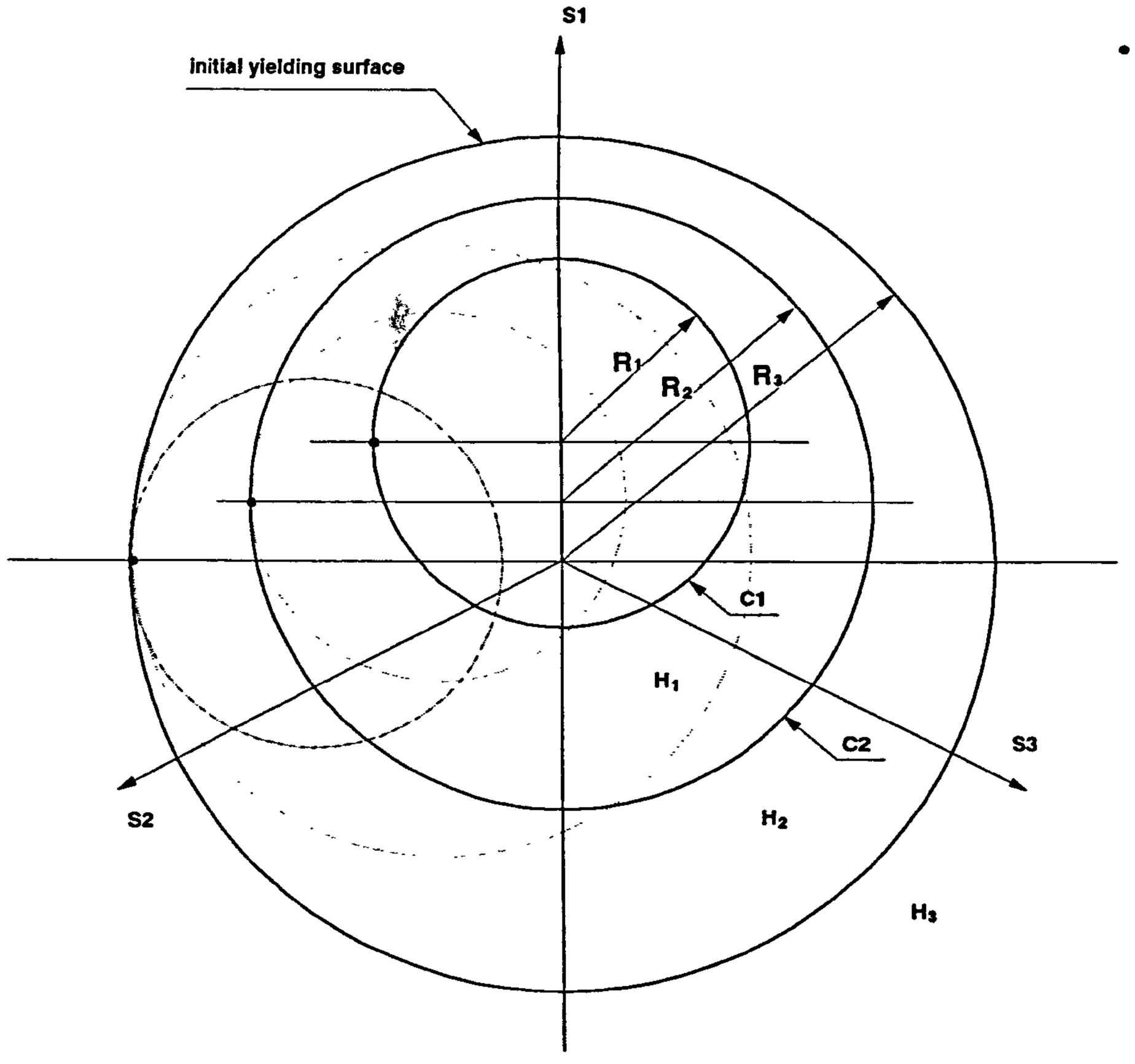

- Loading point

Fig 6.11 Multilayer linear kinematic hardening model with 3 surfaces

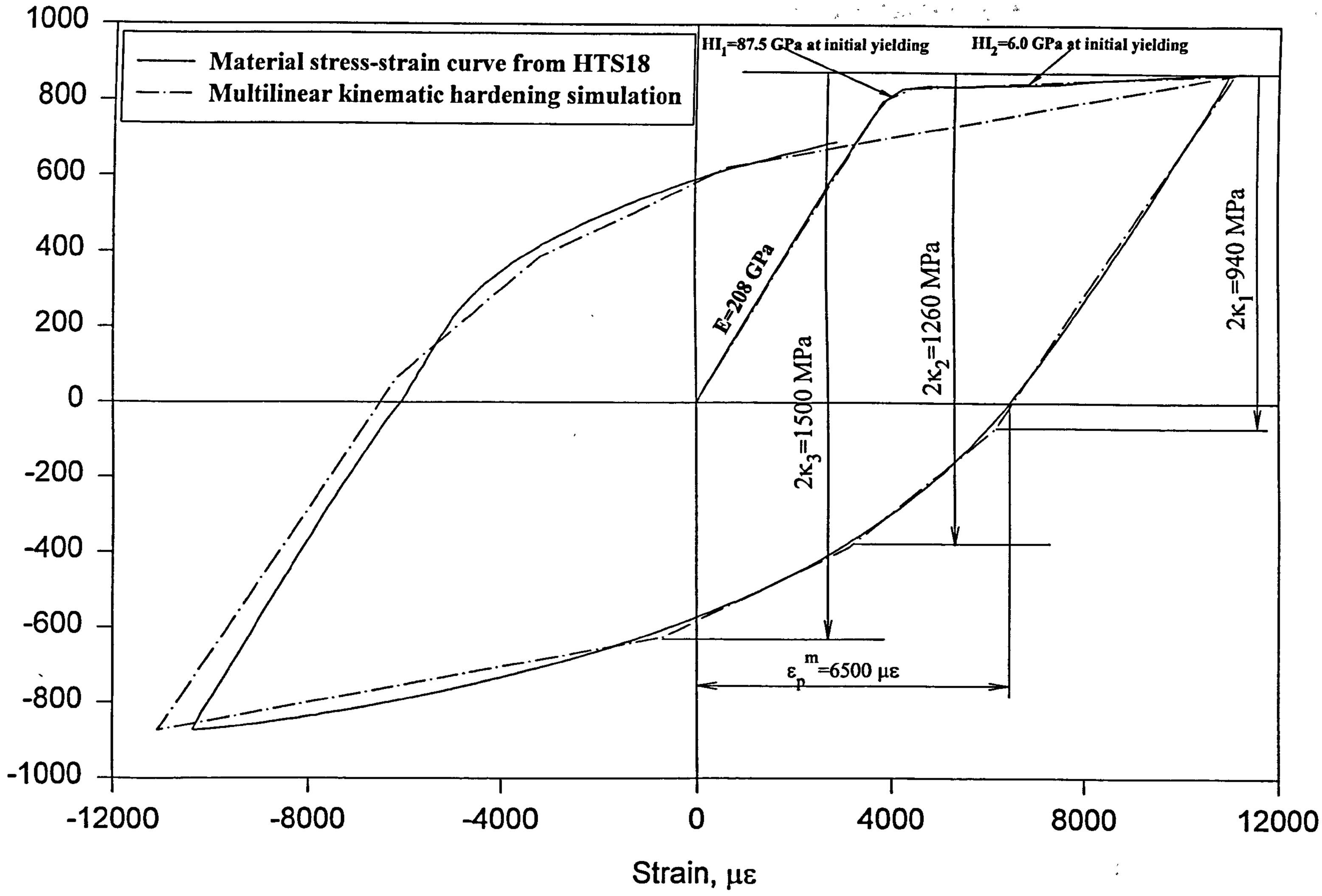

Fig 6.12 Multilinear kinematic hardening simulation of En15R uniaxial stress-strain curve

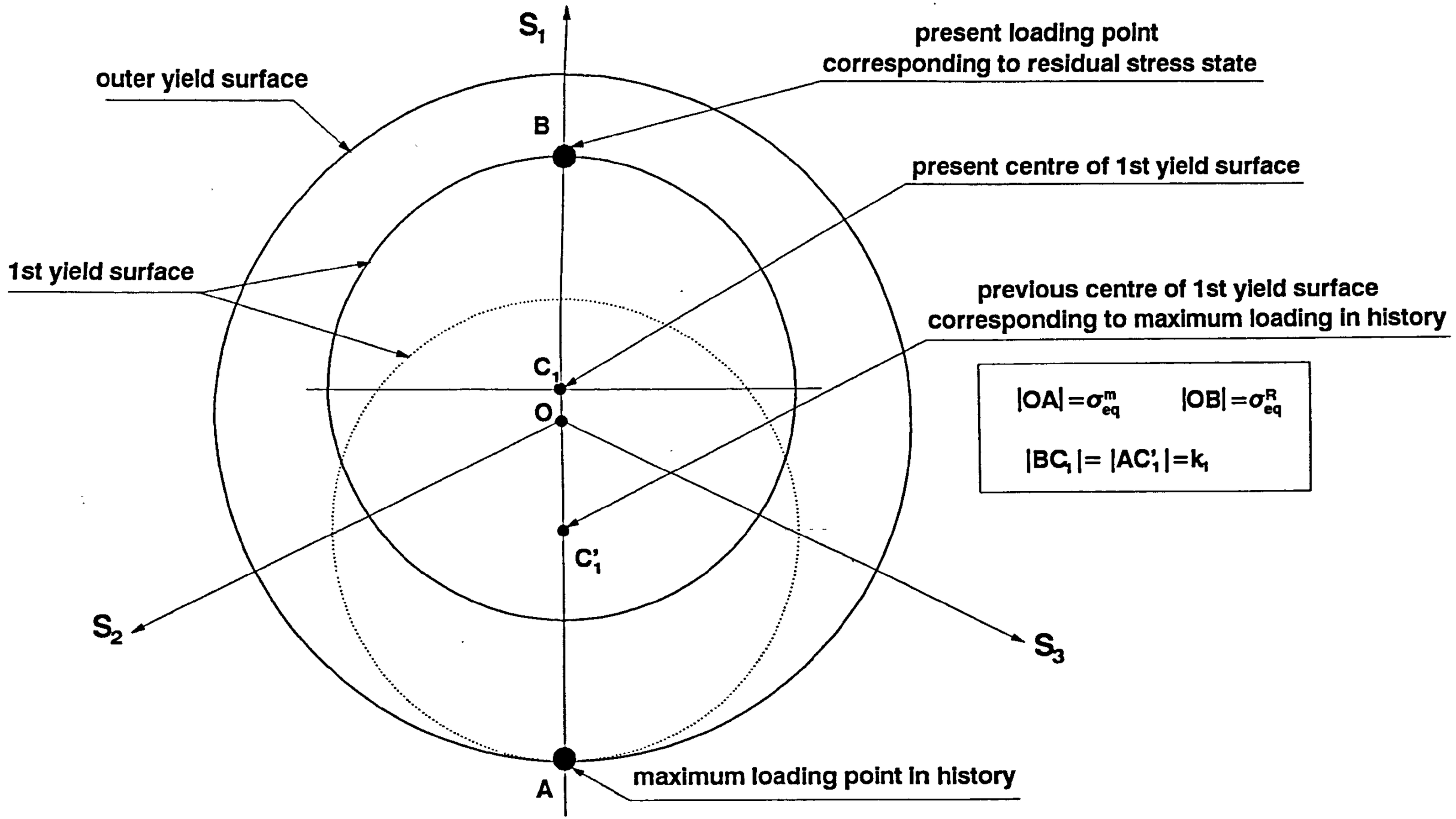

Fig 6.13 Illustration of determining initial positions of yield surfaces for multilinear hardening model

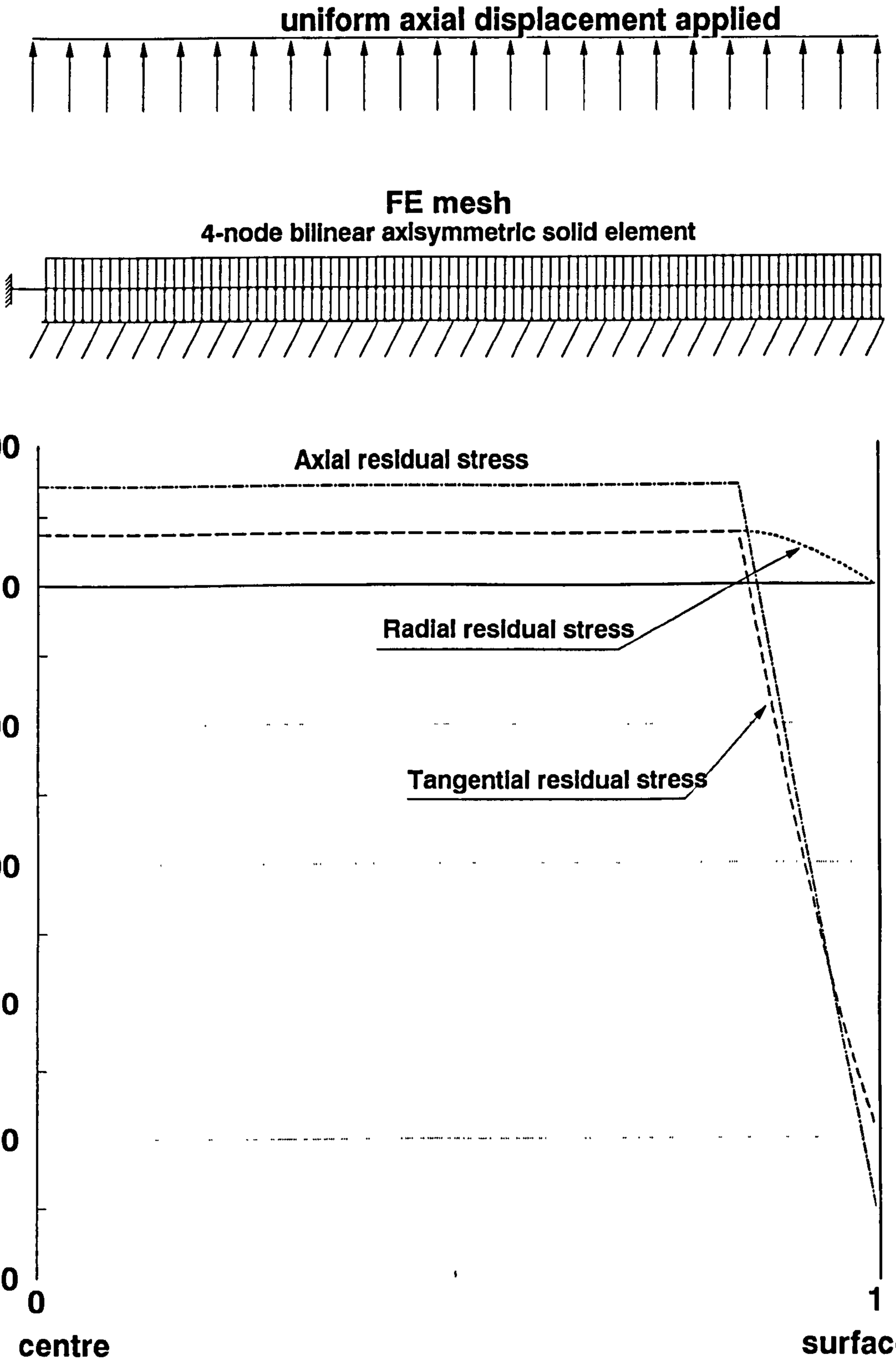

Fig 6.14 FE mesh, load condition and initial residual stress input

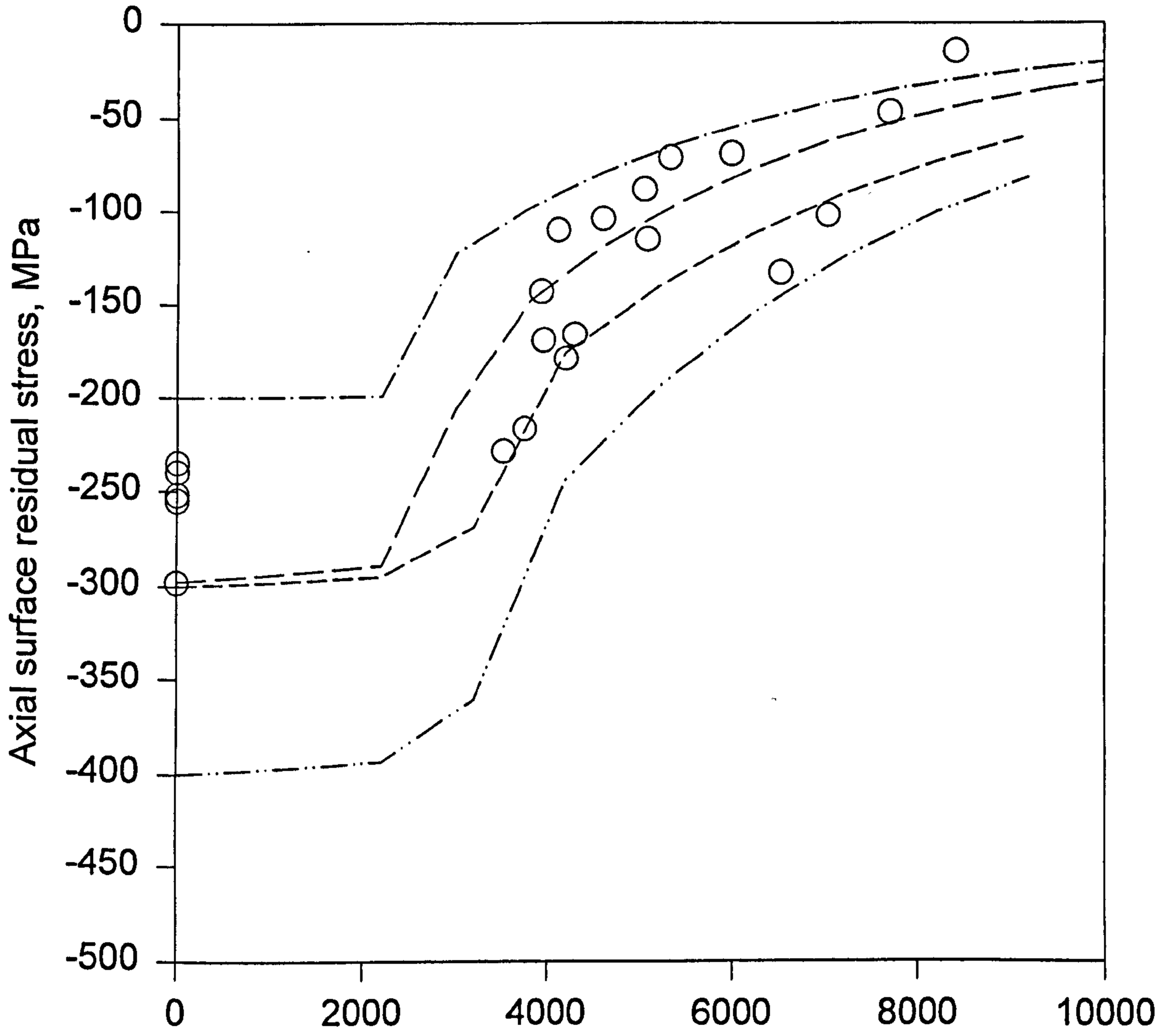

Fig. 6.15 Residual stress relaxation in the round bar specimens after tensile loading

Figure 6.16

Axial residual stress relaxation by FE prediction with different cyclic strain range (half), the initial residual stresses: σ_z=-297.5 MPa, σ_θ=-234.9 MPa

Linear kinematic hardening for U-batch

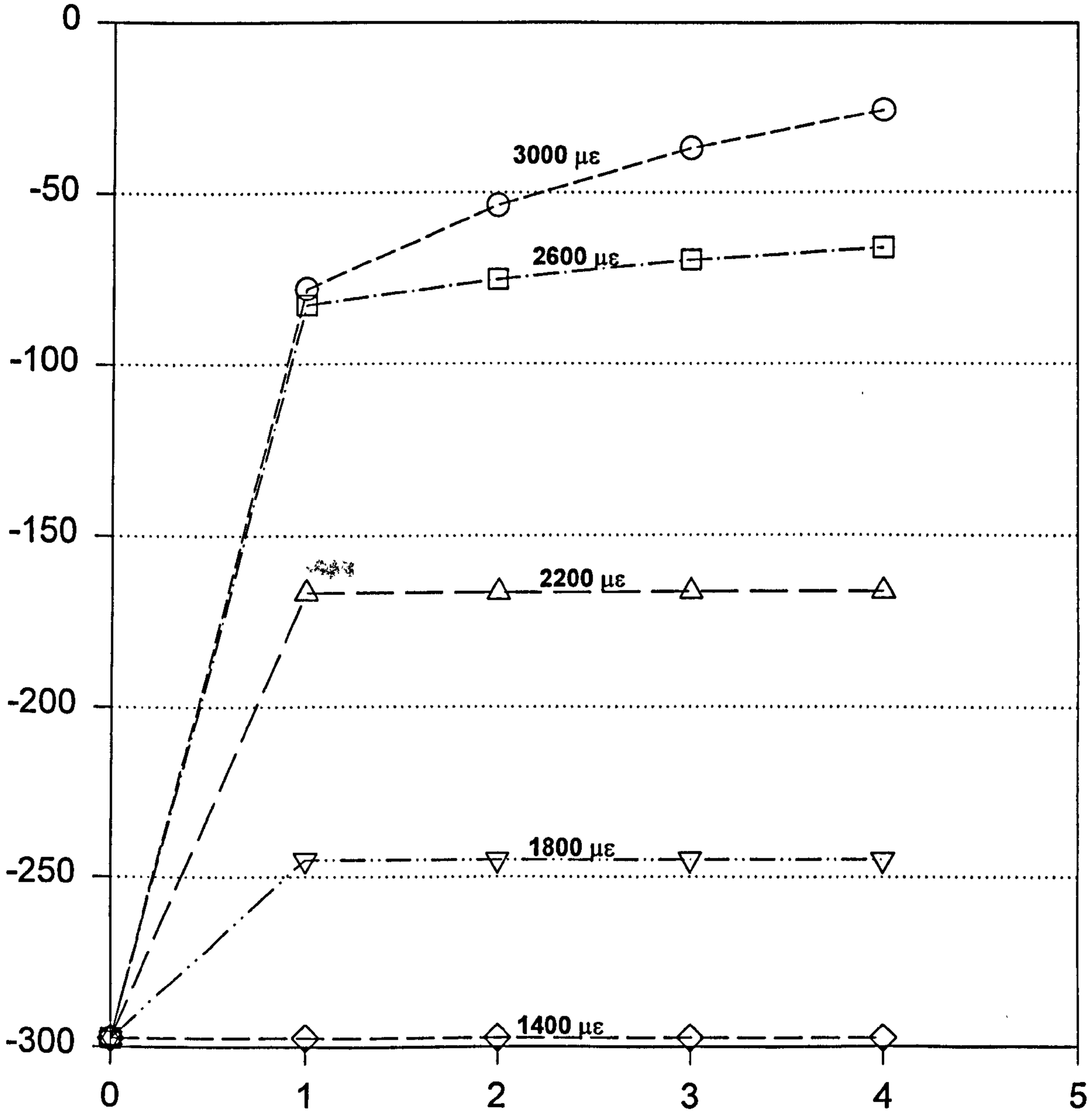

Figure 6.17

Axial residual stress relaxation by FE prediction with different cyclic strain range (half), the initial residual stresses: σ_z=-300 MPa, σ_θ=-280 MPa

Linear kinematic hardening for HTS

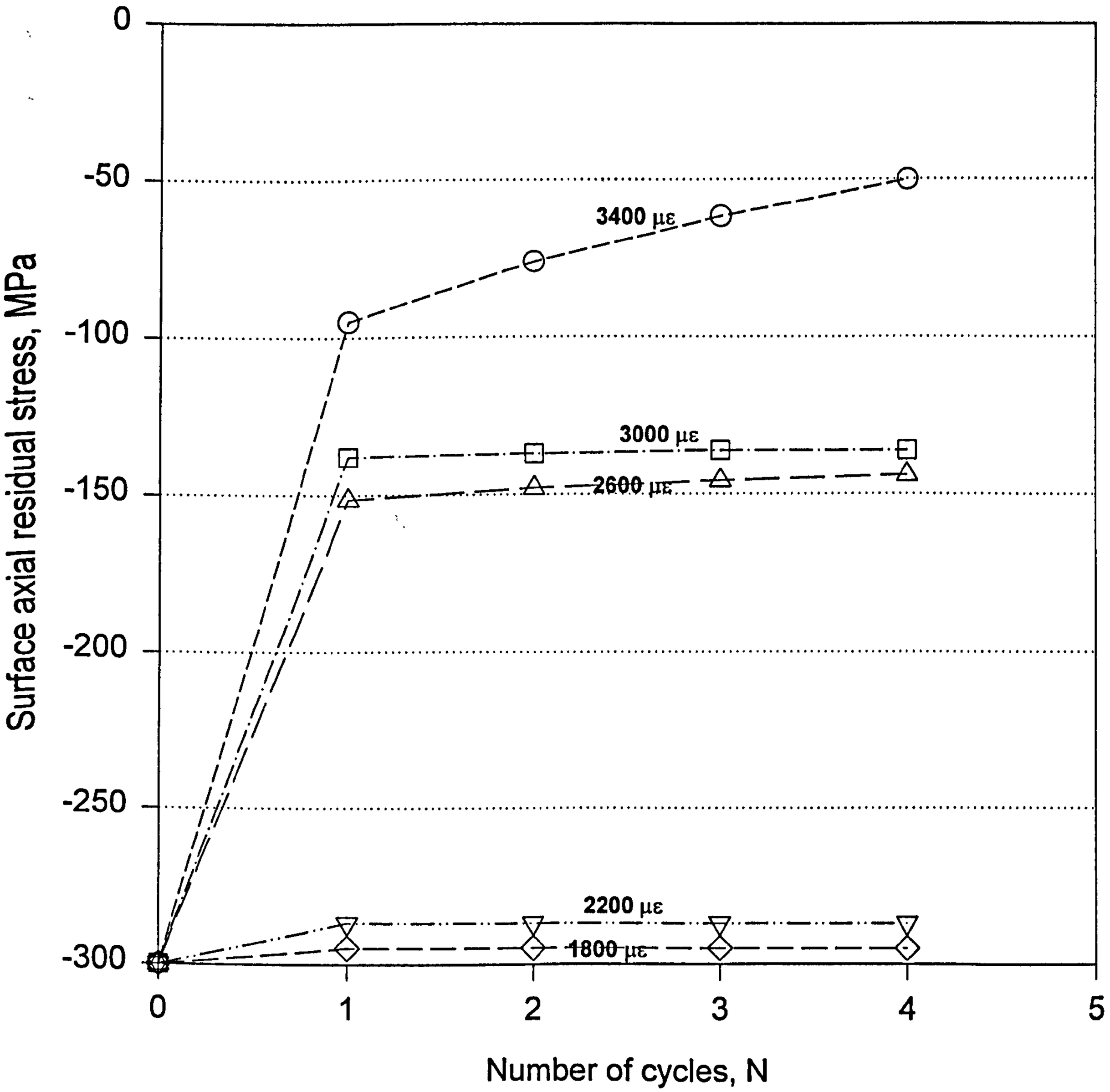

Figure 6.18

Axial residual stress relaxation by FE prediction with different cyclic strain range (half), the initial residual stresses: σ_z=-400 MPa, σ_θ=-350 MPa

Linear kinematic hardening for HTS

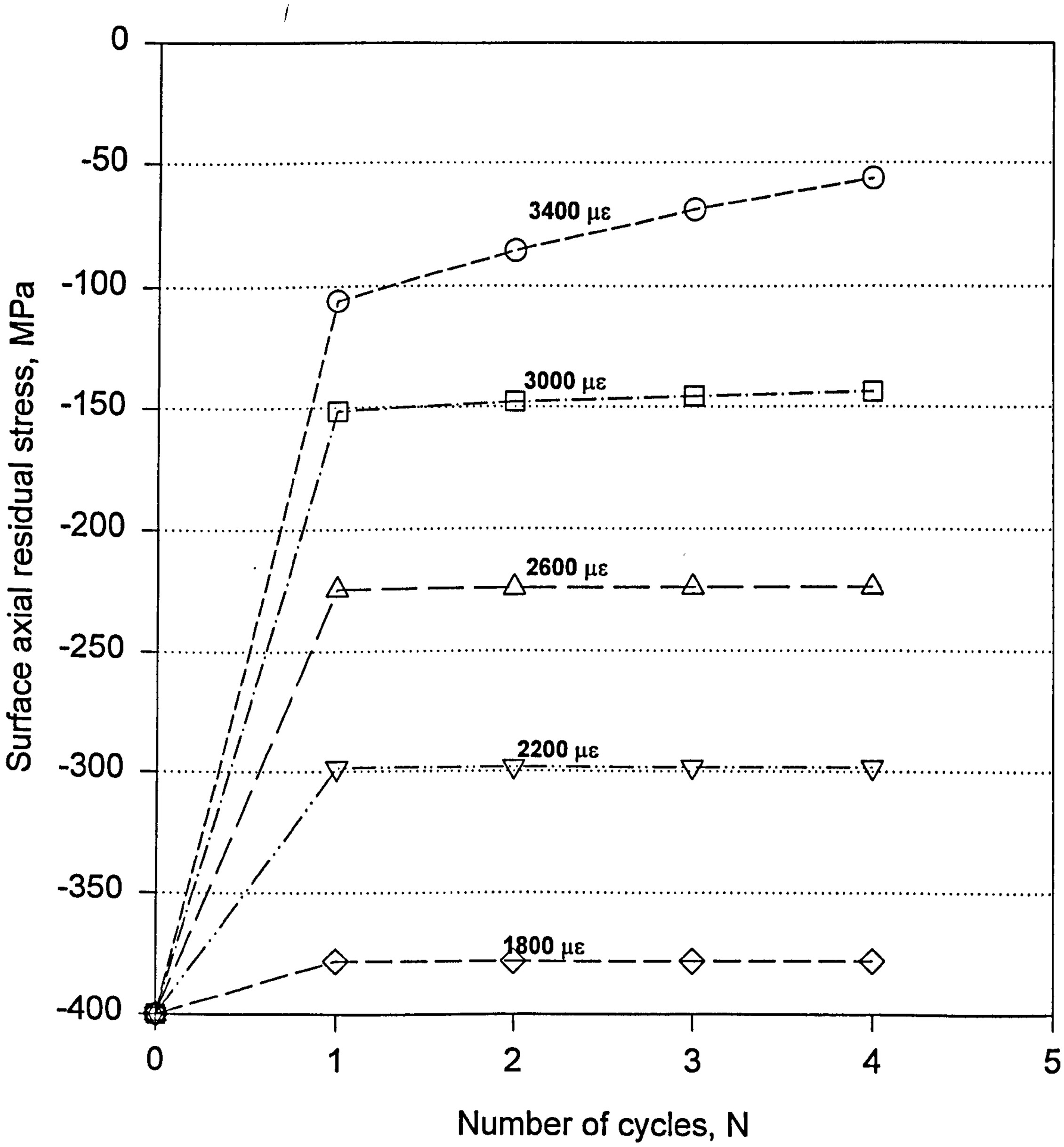

Figure 6.19

Axial residual stress relaxation by FE prediction with different cyclic strain range (half), the initial residual stresses: σ_z=-450 MPa, σ_θ=-400 MPa

Multi-linear kinematic hardening for HTS

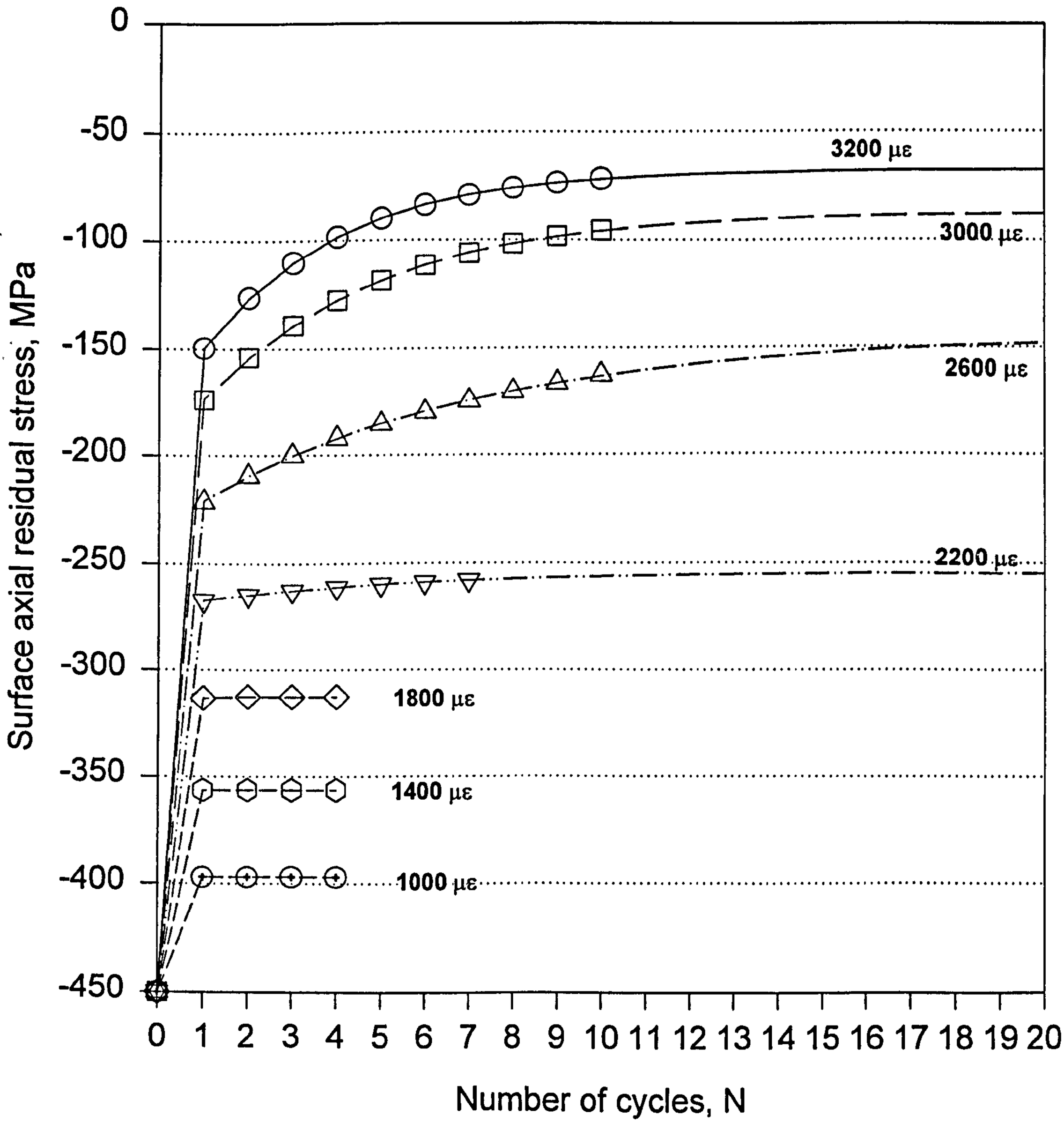

Figure 6.20

Axial residual stress relaxation by FE prediction with different cyclic strain range (half), the initial residual stresses: σ_z=-400 MPa, σ_θ=-350 MPa

Multi-linear kinematic hardening for HTS

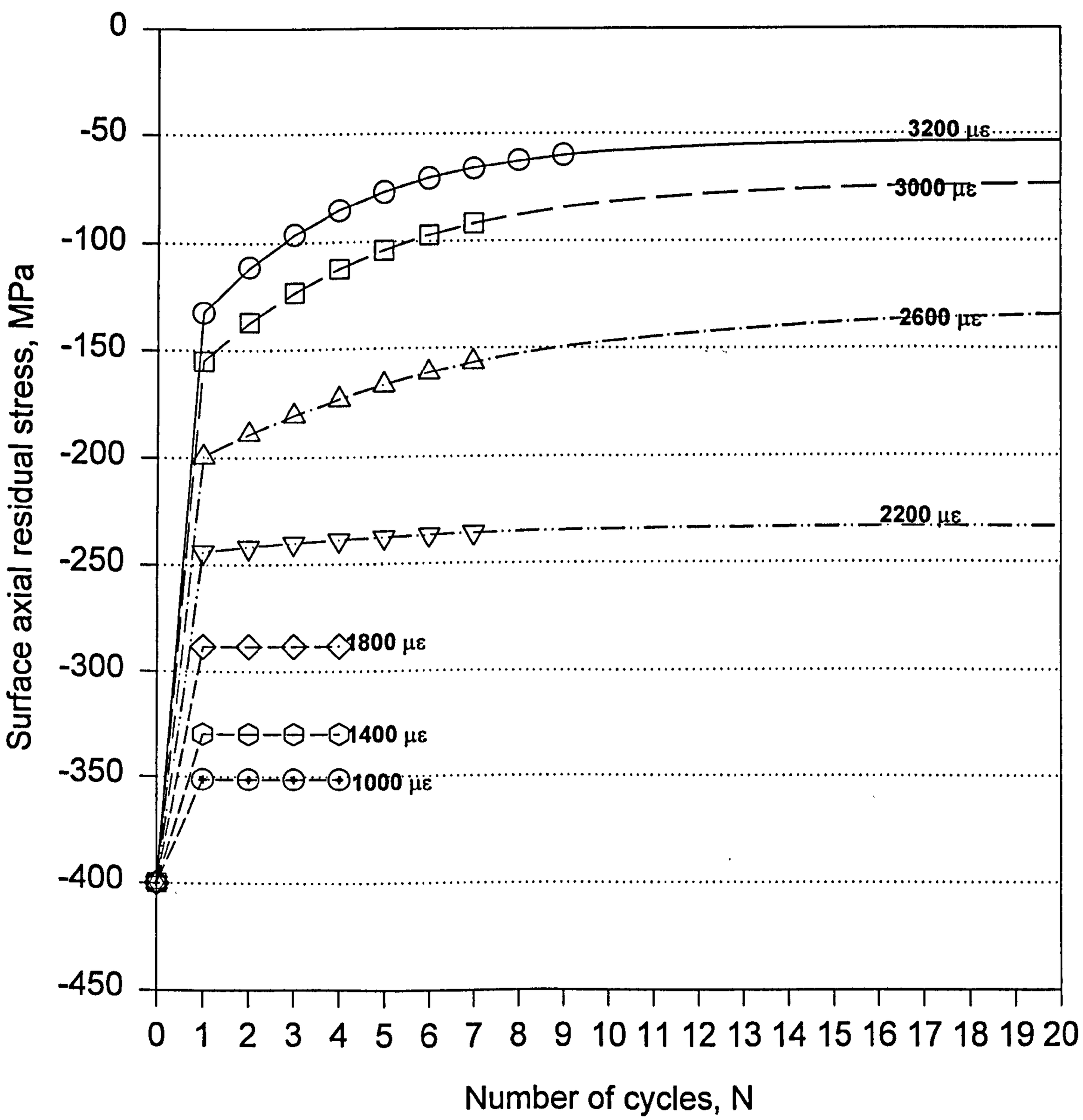

Figure 6.21

Axial residual stress relaxation by FE prediction with different cyclic strain range (half), the initial residual stresses: σ_z=-350 MPa, σ_θ=-310 MPa

Multi-linear kinematic hardening for HTS

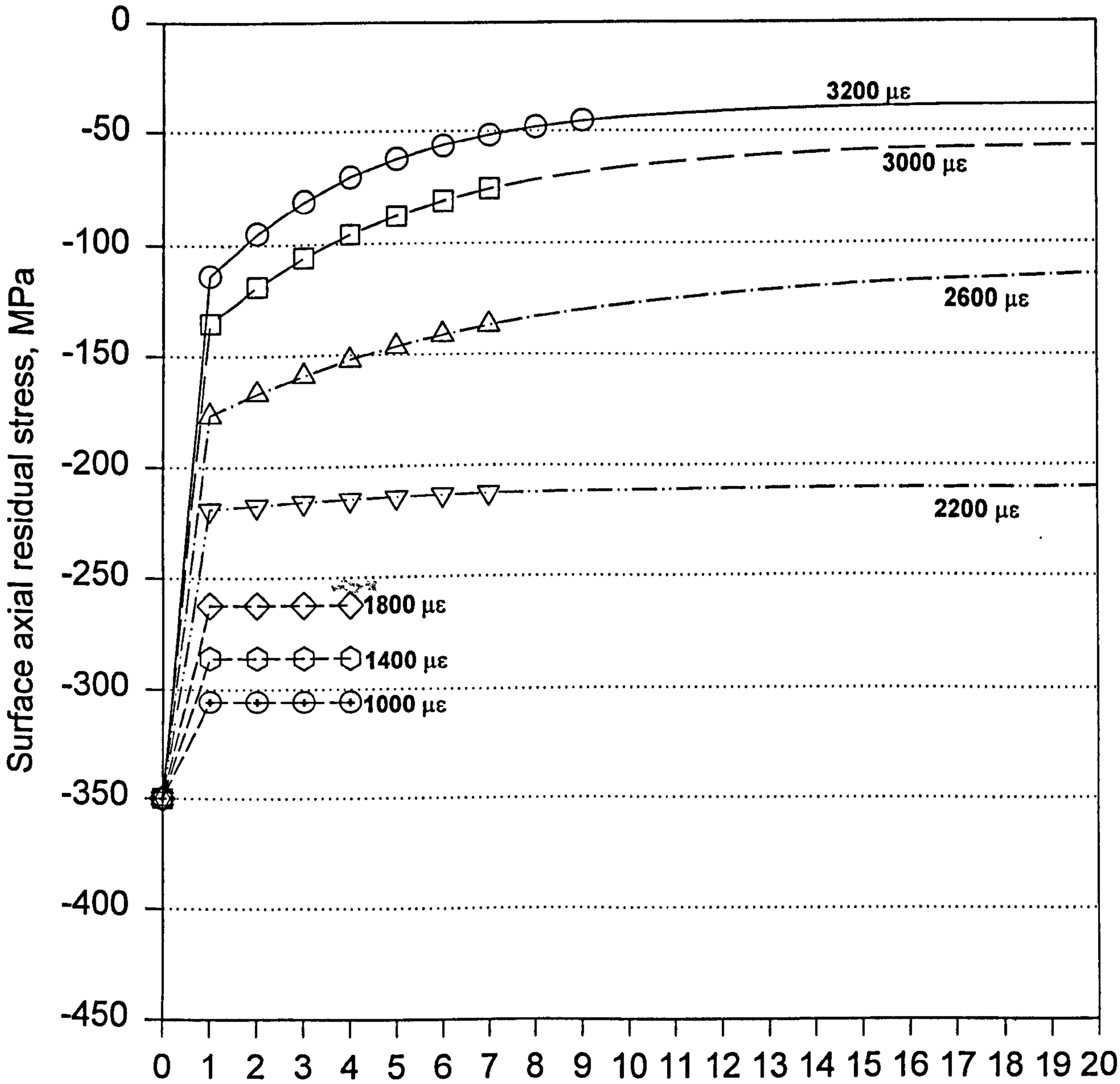

Figure 6.22

Axial residual stress relaxation by FE prediction with different cyclic strain range (half), the initial residual stresses: σ_z=-300 MPa, σ_θ=-280 MPa

Multi-linear kinematic hardening for HTS

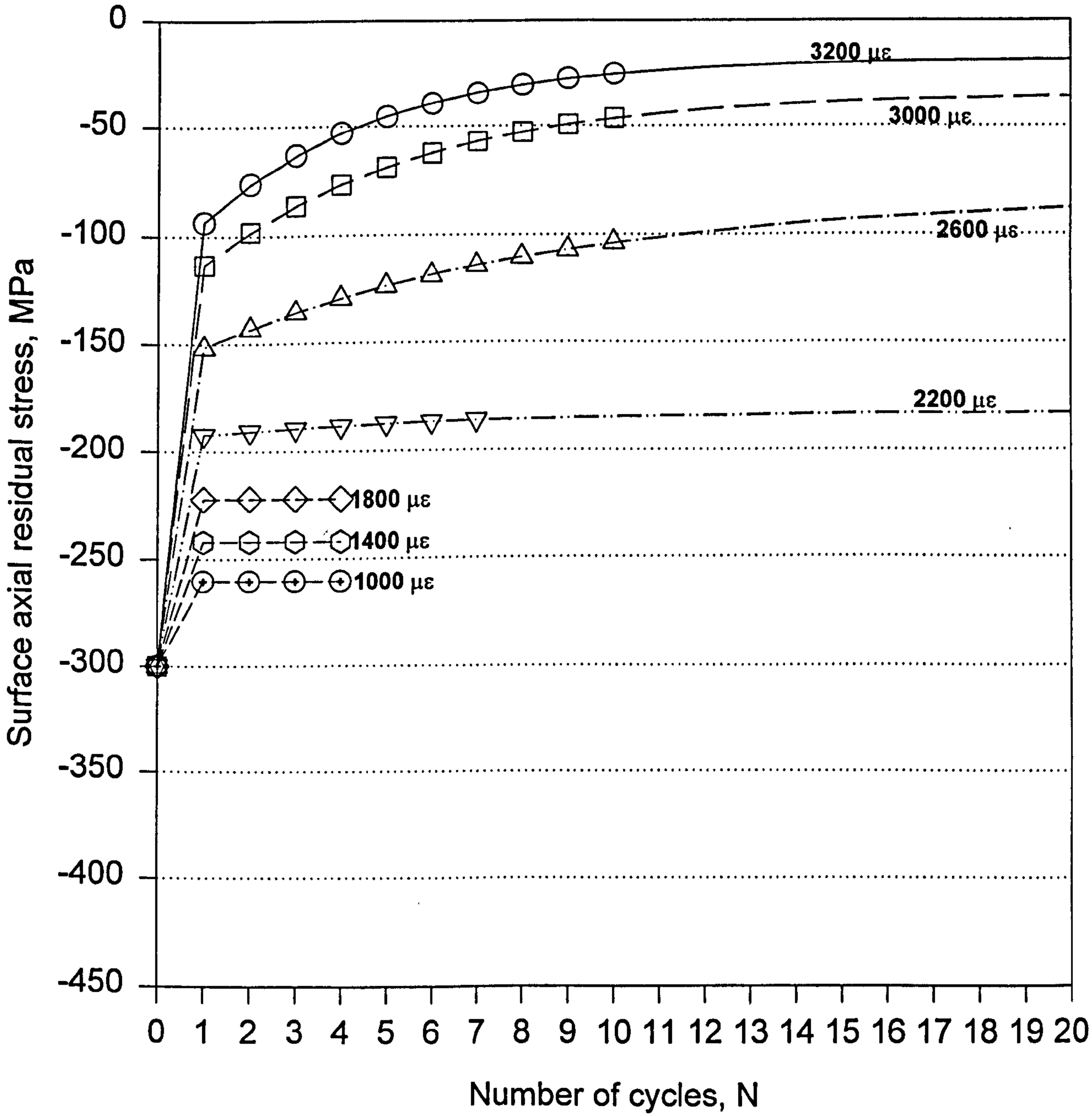

Figure 6.23

Axial residual stress relaxation by FE prediction with different cyclic strain range (half), the initial residual stresses: σ_z=-250 MPa, σ_θ=-250 MPa

Multi-linear kinematic hardening for HTS

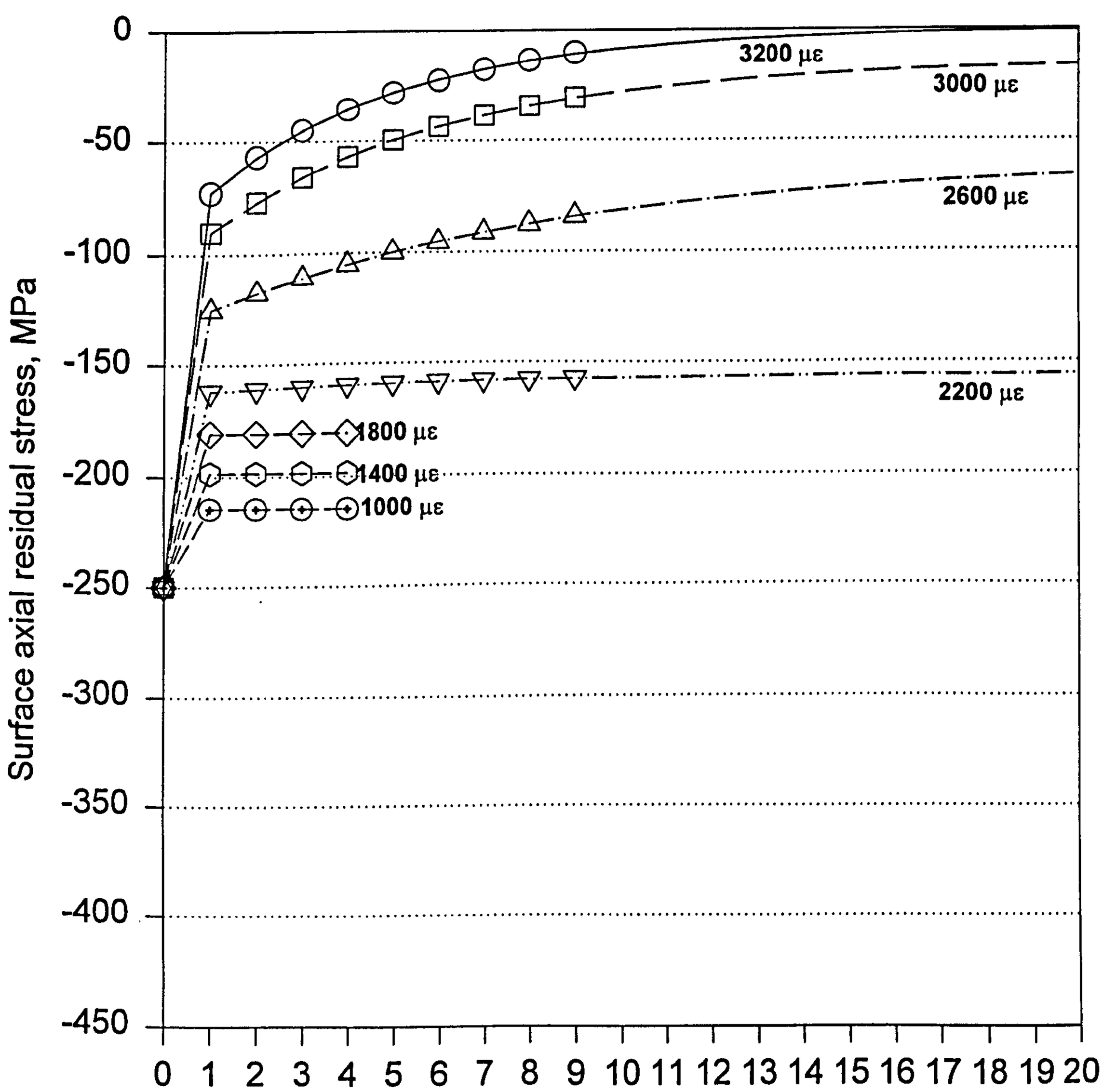

Fig 6.24 Redistribution of axial residual stress in one specimen after first fatigue cycle

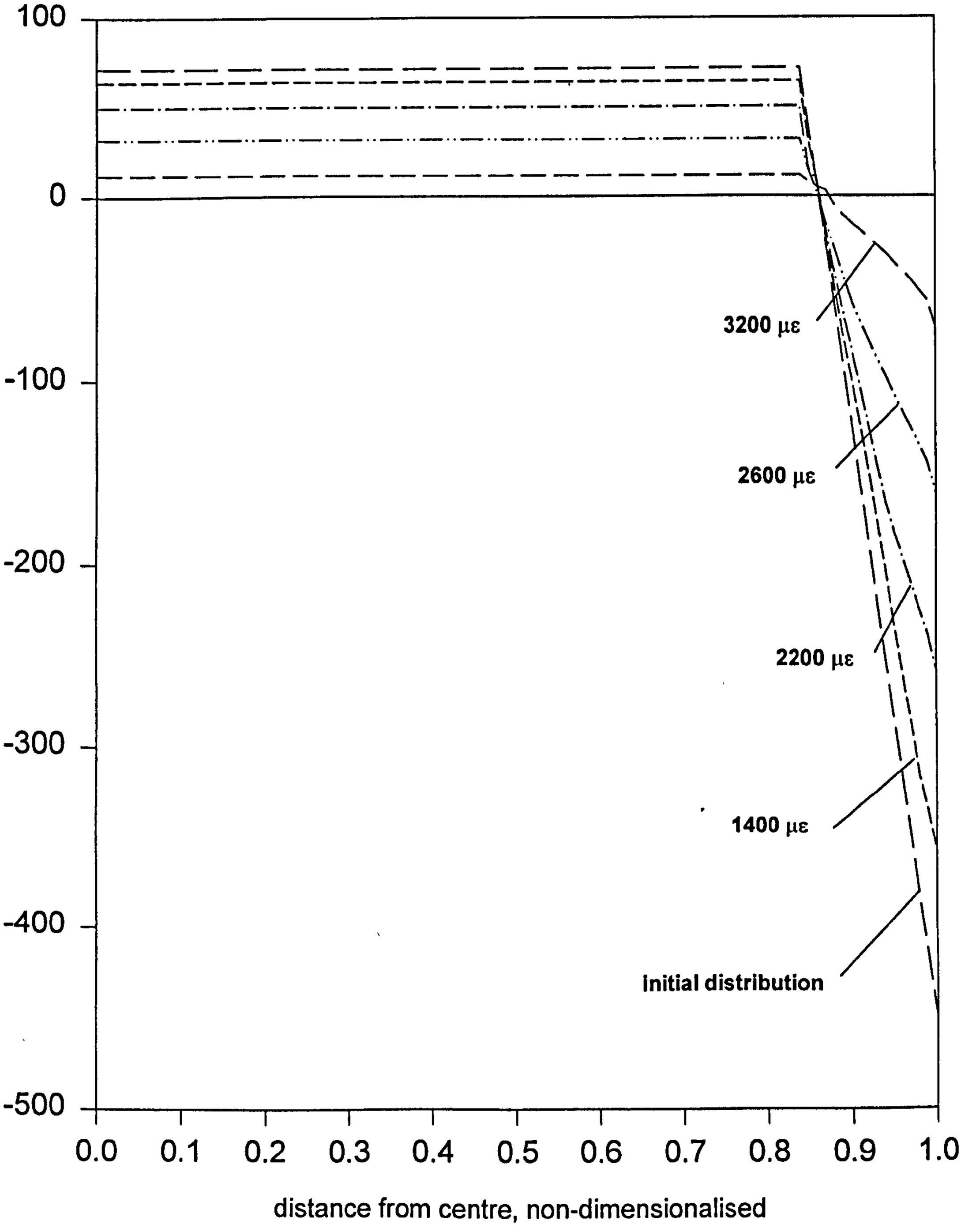

Figure 6.25

Surface axial residual stress relaxation after fatigue cycle for different initial residual stresses

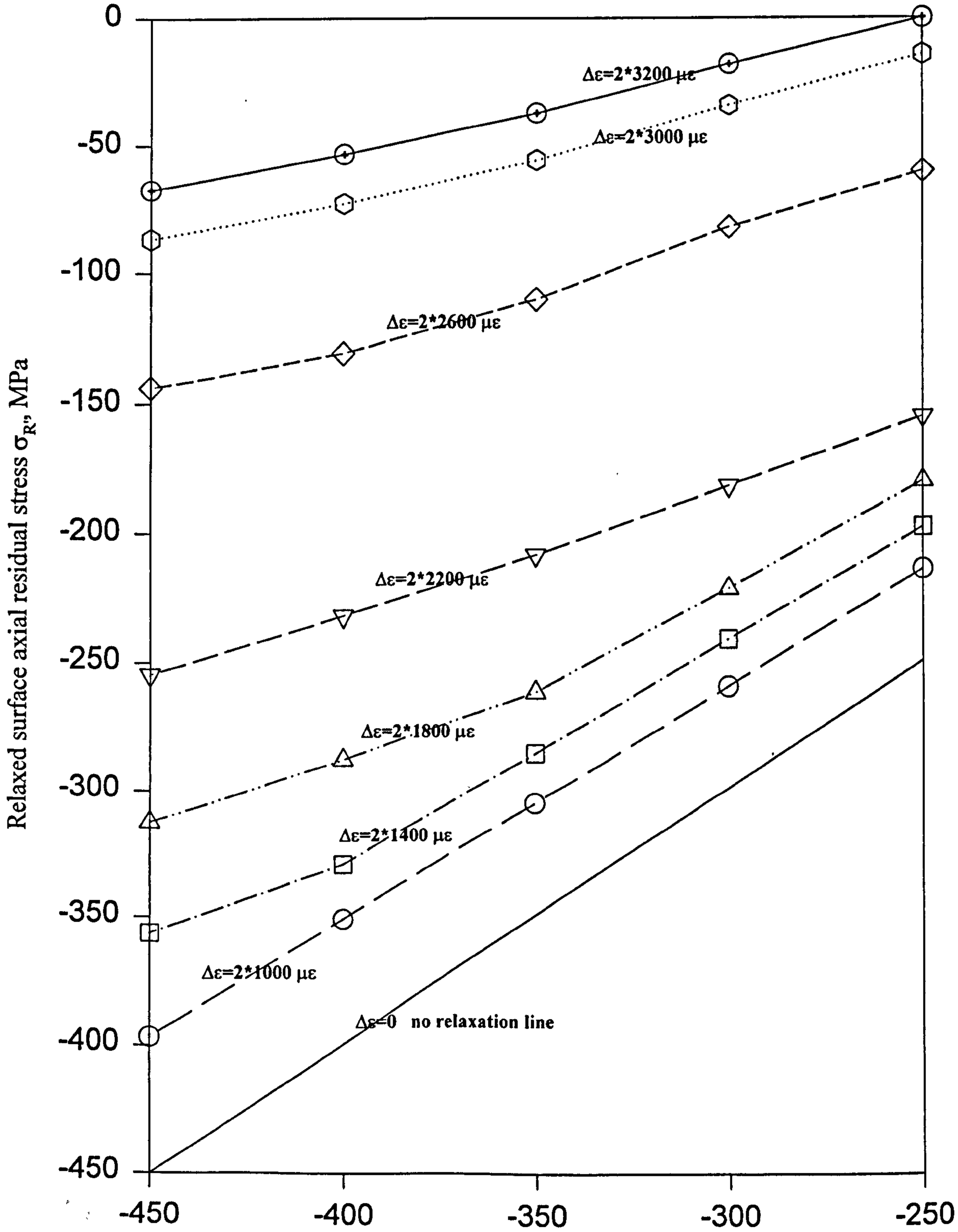

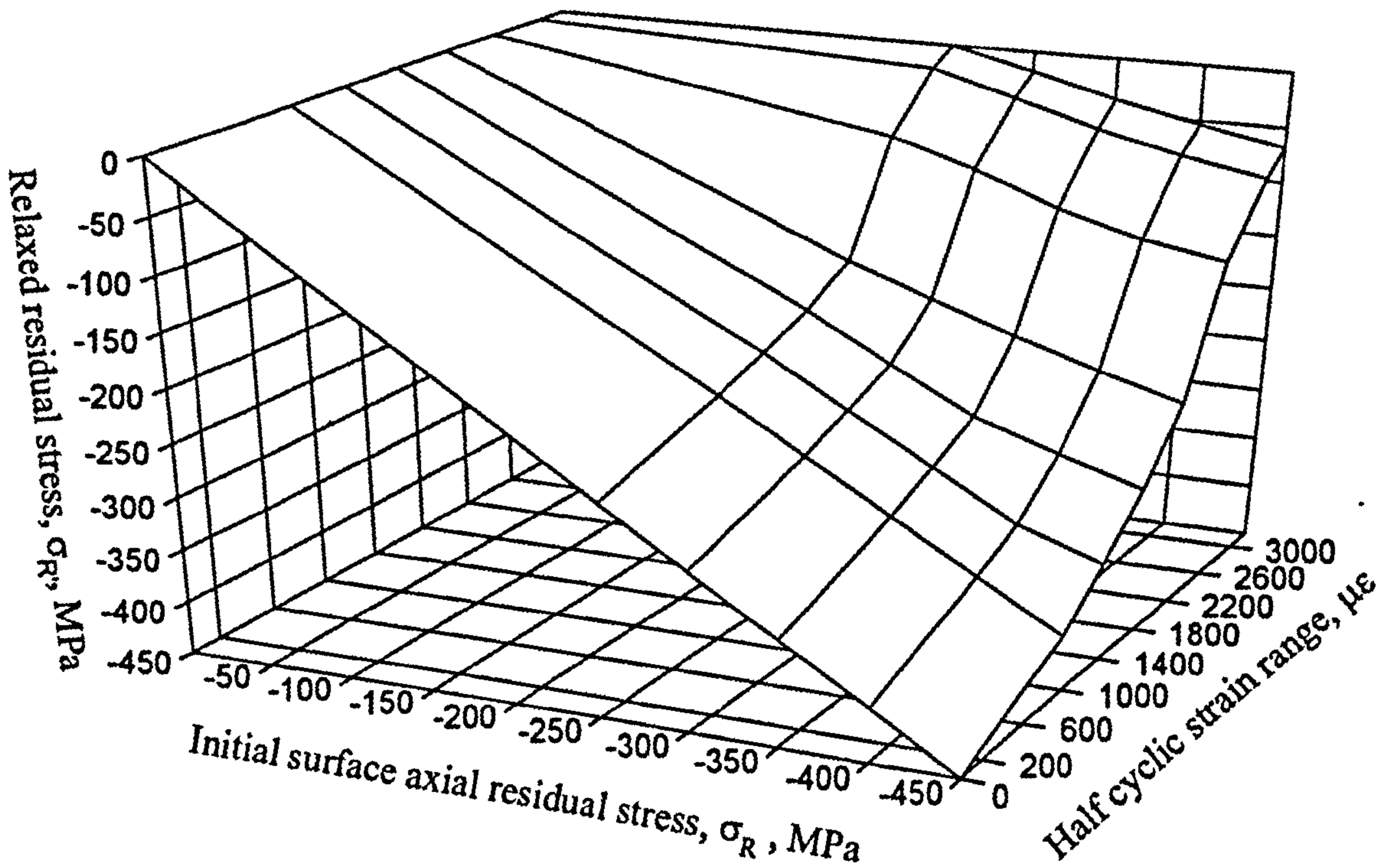

Fig 6.26 Axial residual stress relaxation after fatigue cyclic load by FE calculation

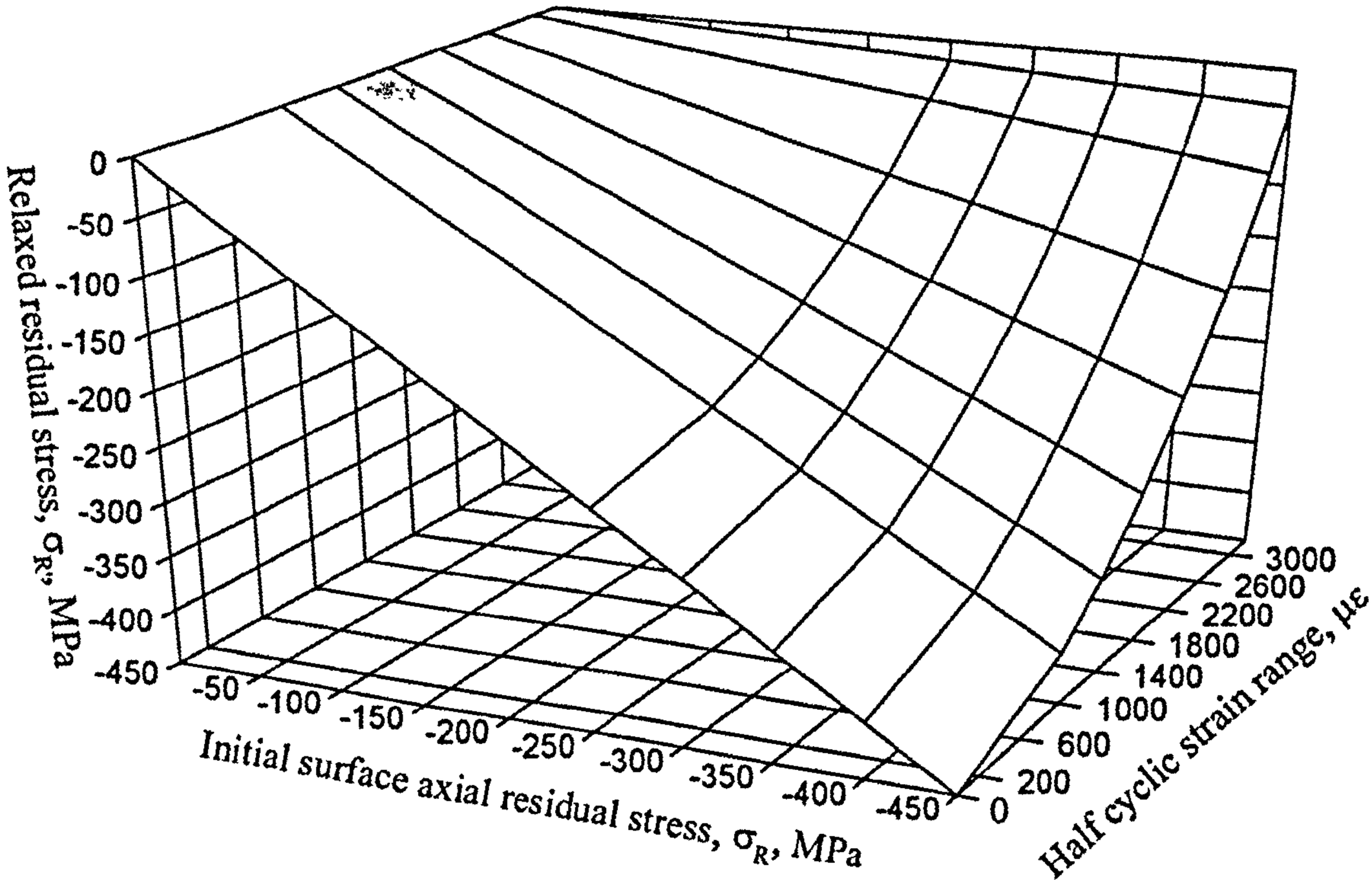

Fig 6.27 Fitted result of axial residual stress relaxatio

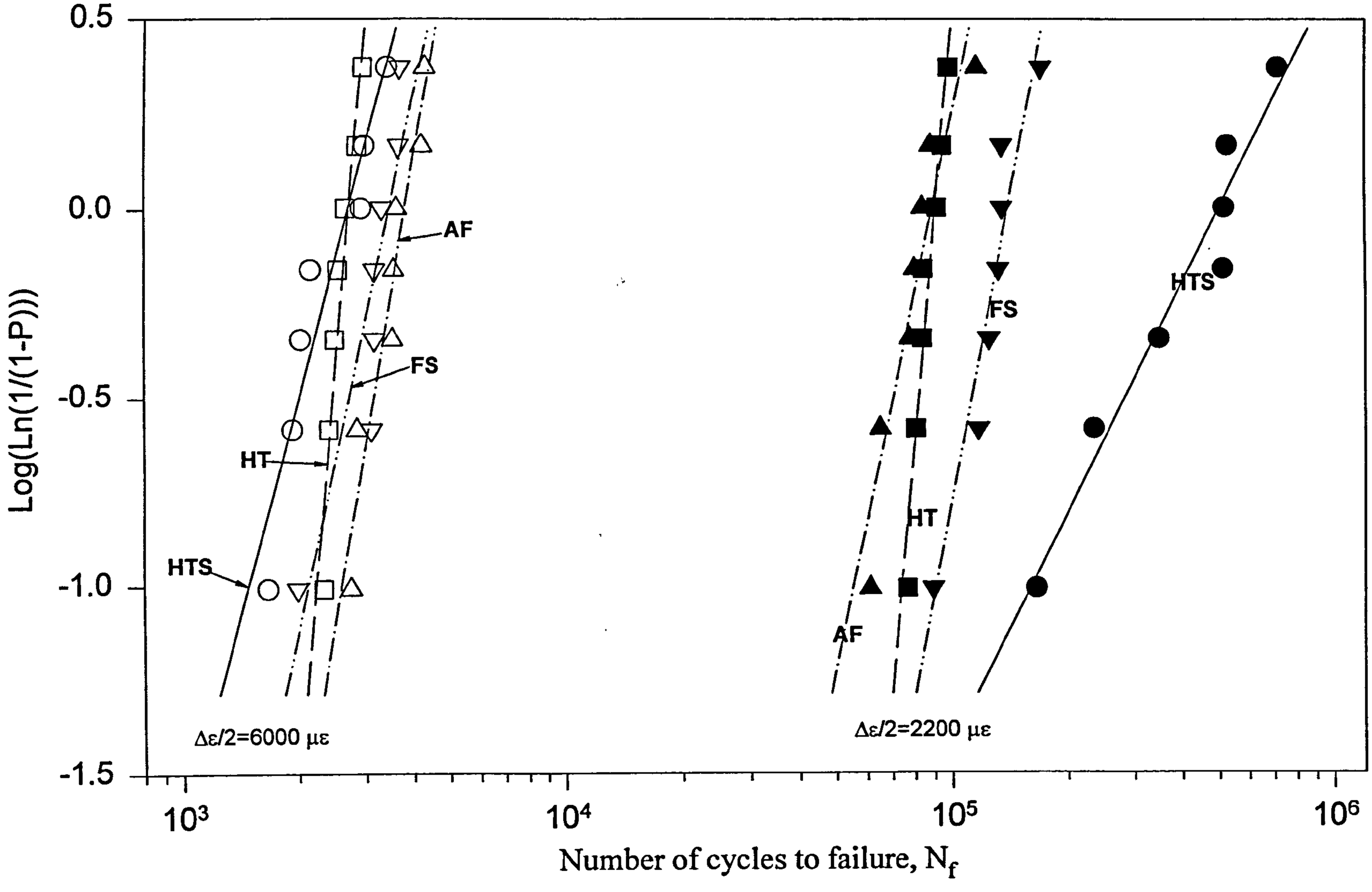

Fig 7.1 Probability of Fatigue Failure for Different Process Conditions

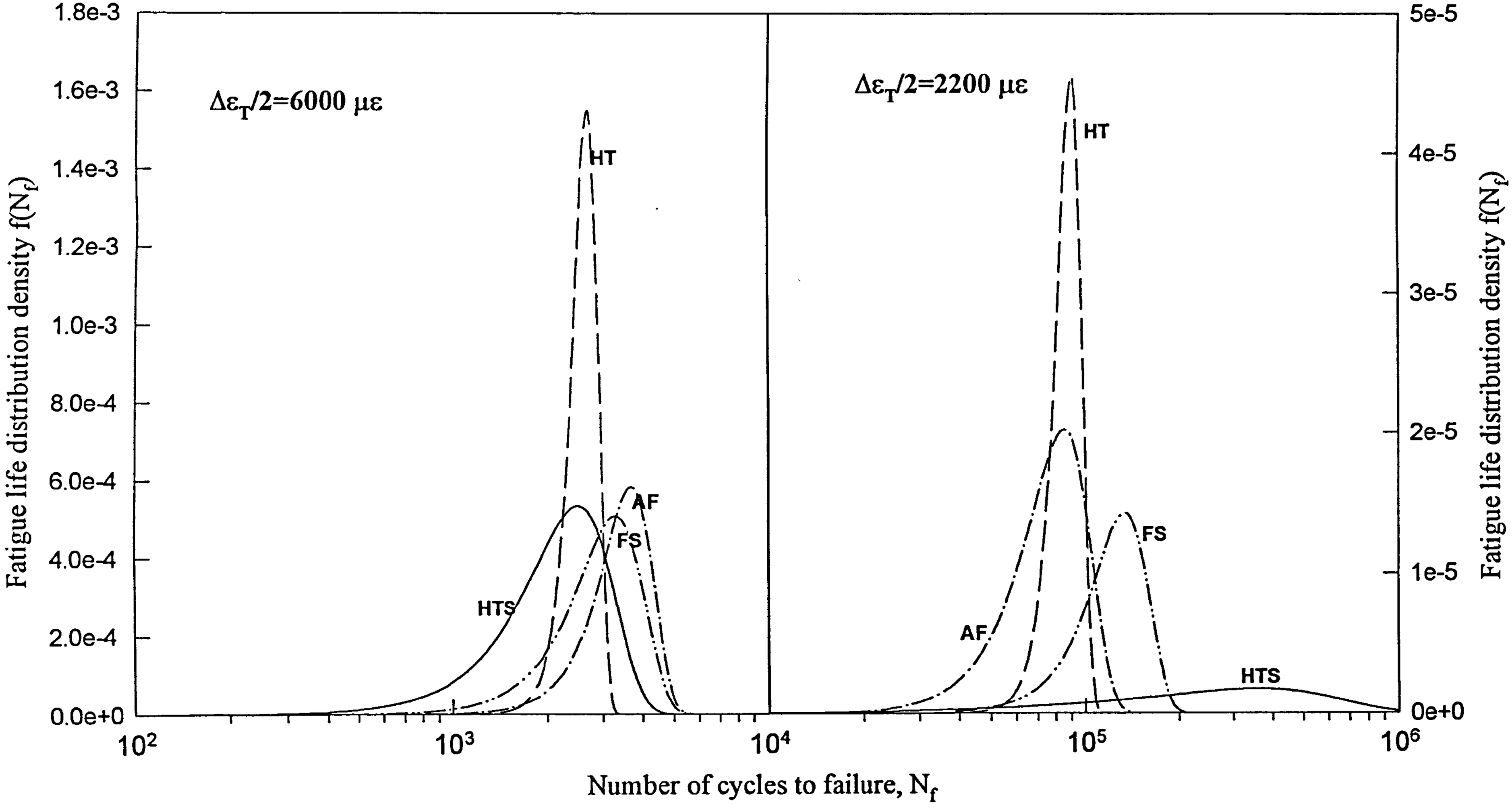

Fig 7.2 Weilbull distribution of fatigue life for different process conditions and two different cyclic strain ranges

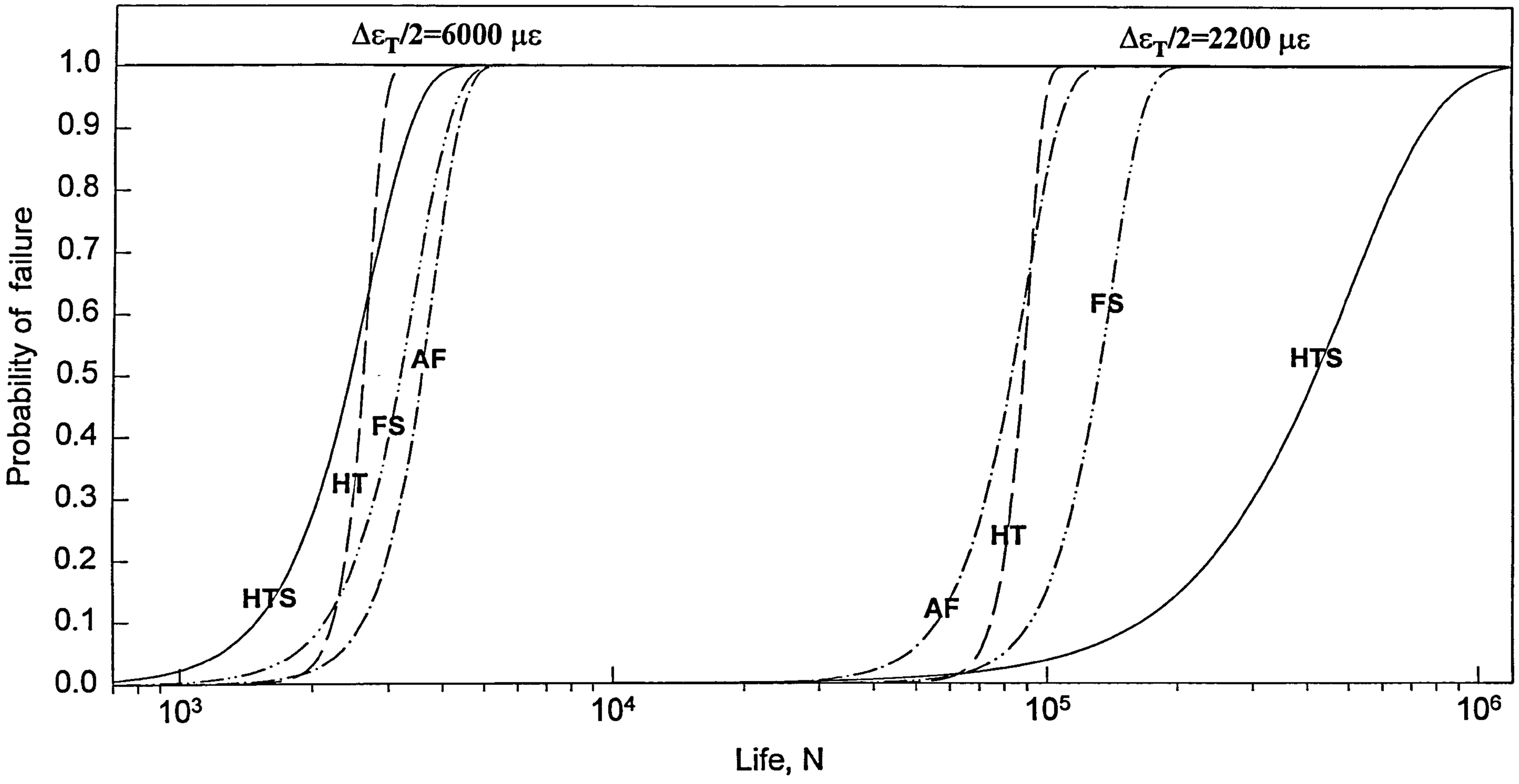

Fig 7.3 Probability of failure of forged round bar specimens

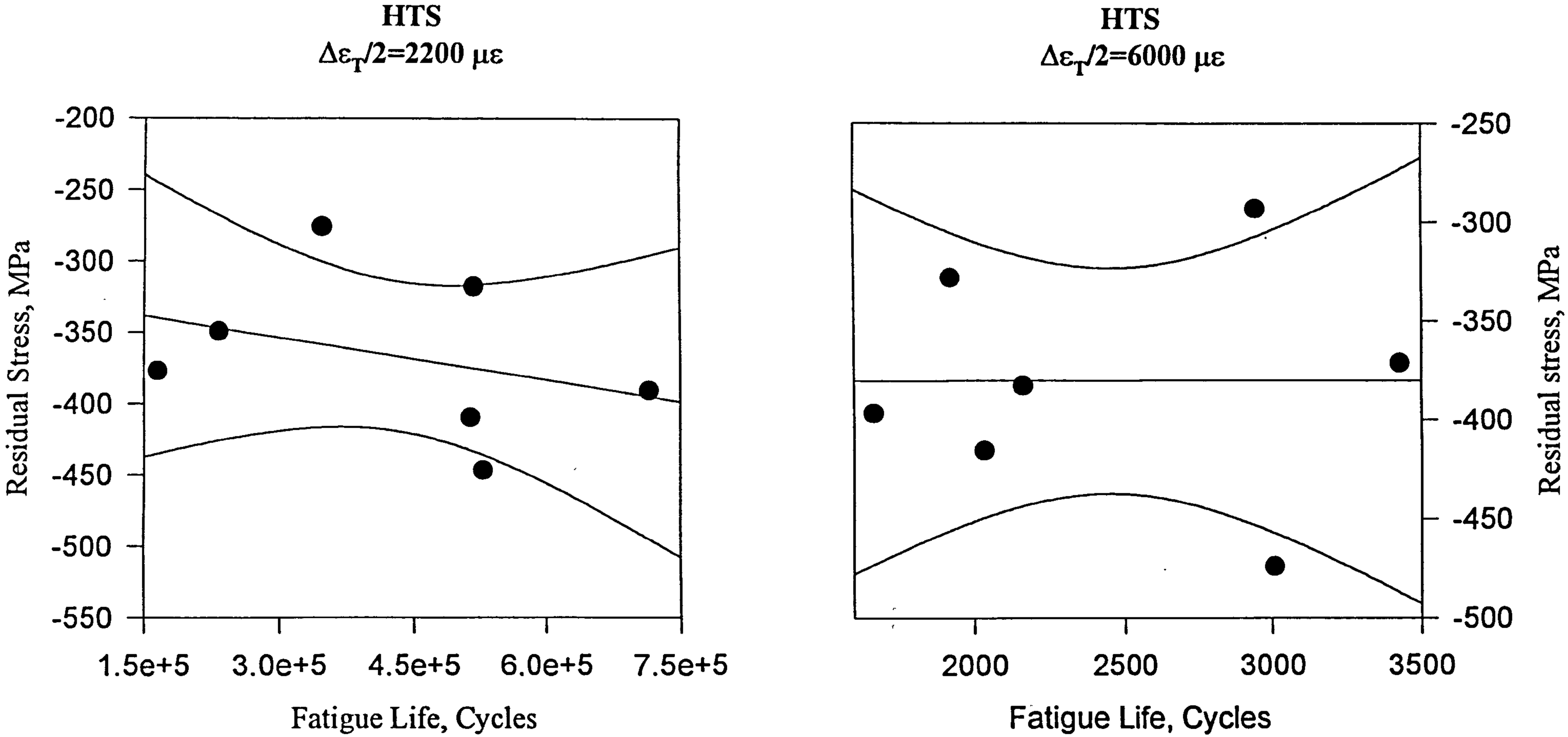

Fig 7.4 Correlation between residual stresses and fatigue lives

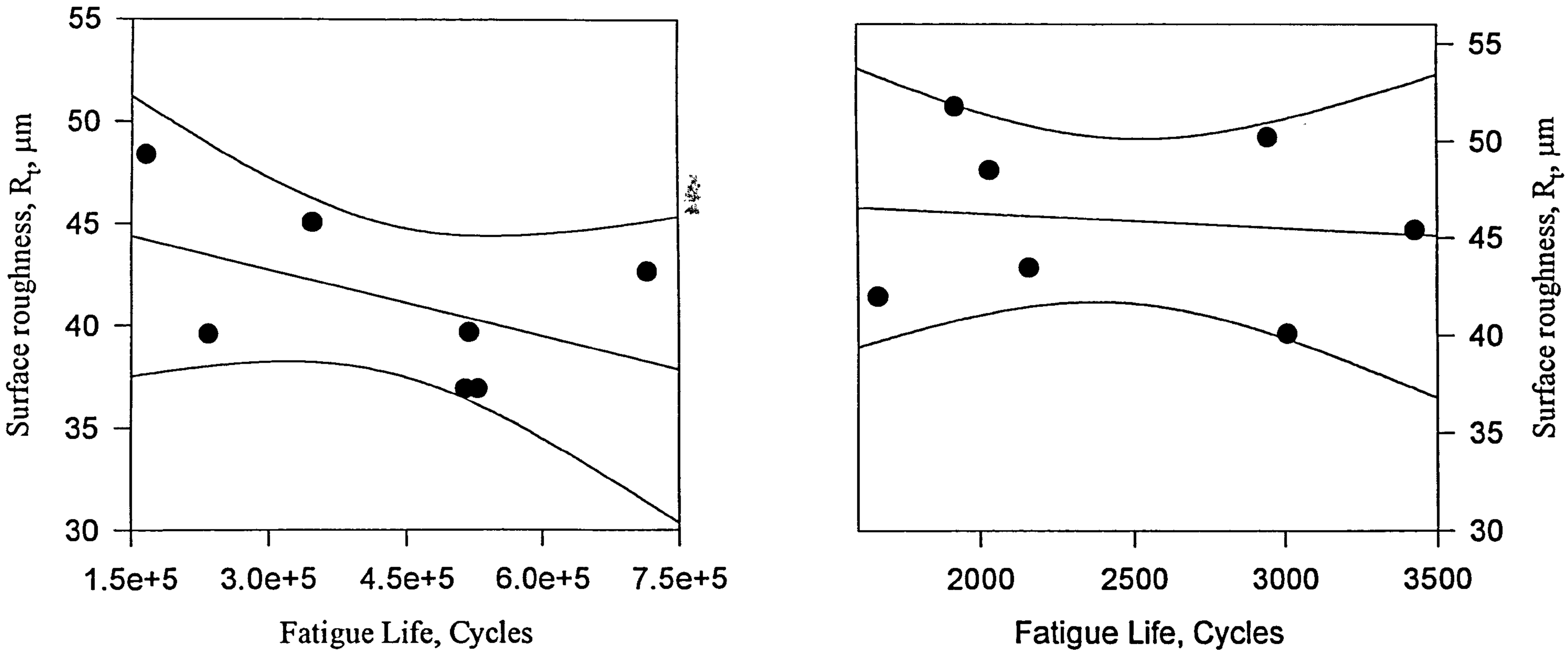

Fig 7.5 Correlation between surface roughness and fatigue lives

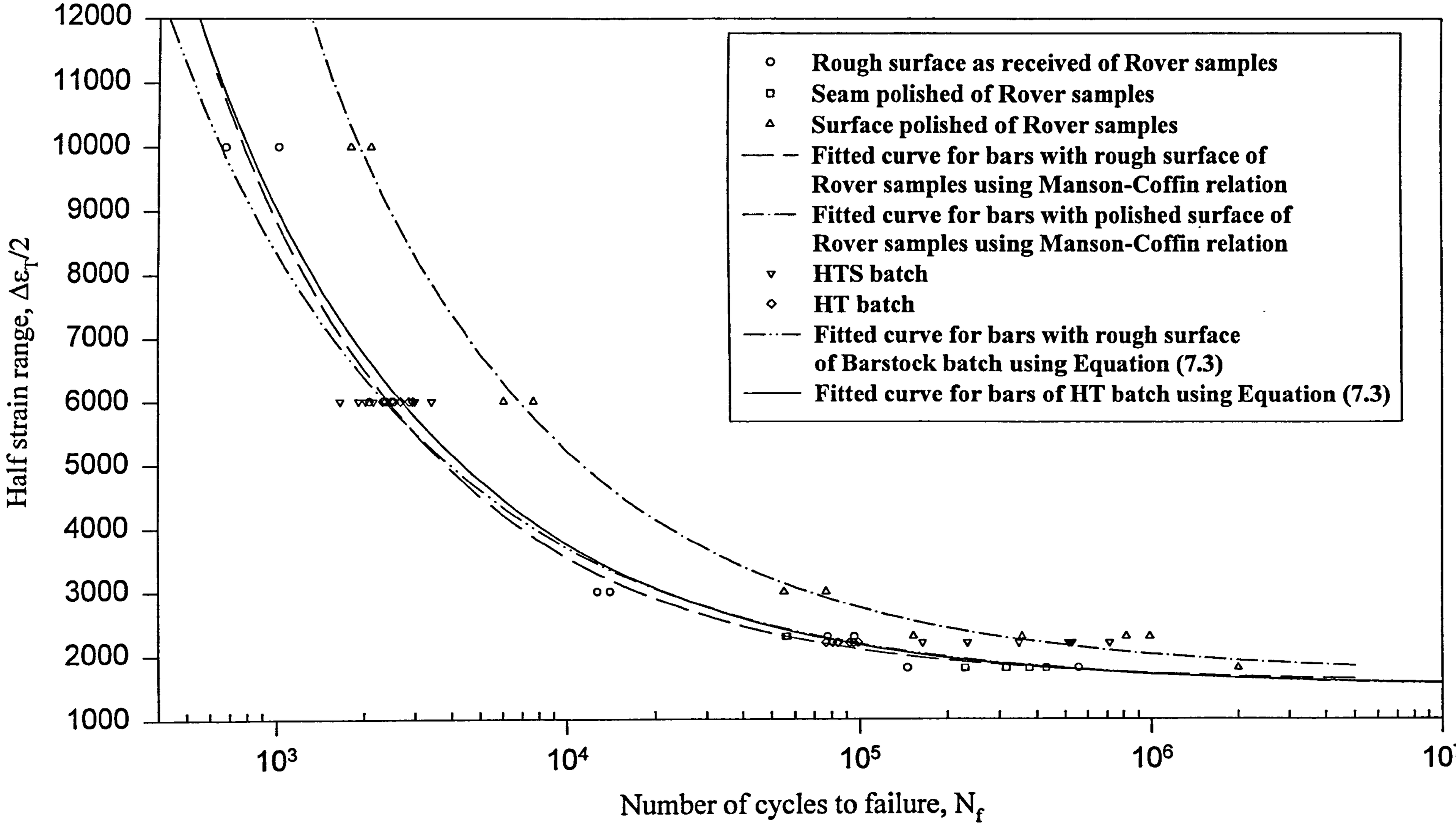

Fig 7.6 Fatigue test data of forged bars from ROVER for different surface finishing and compared with HTS and HT fatigue data

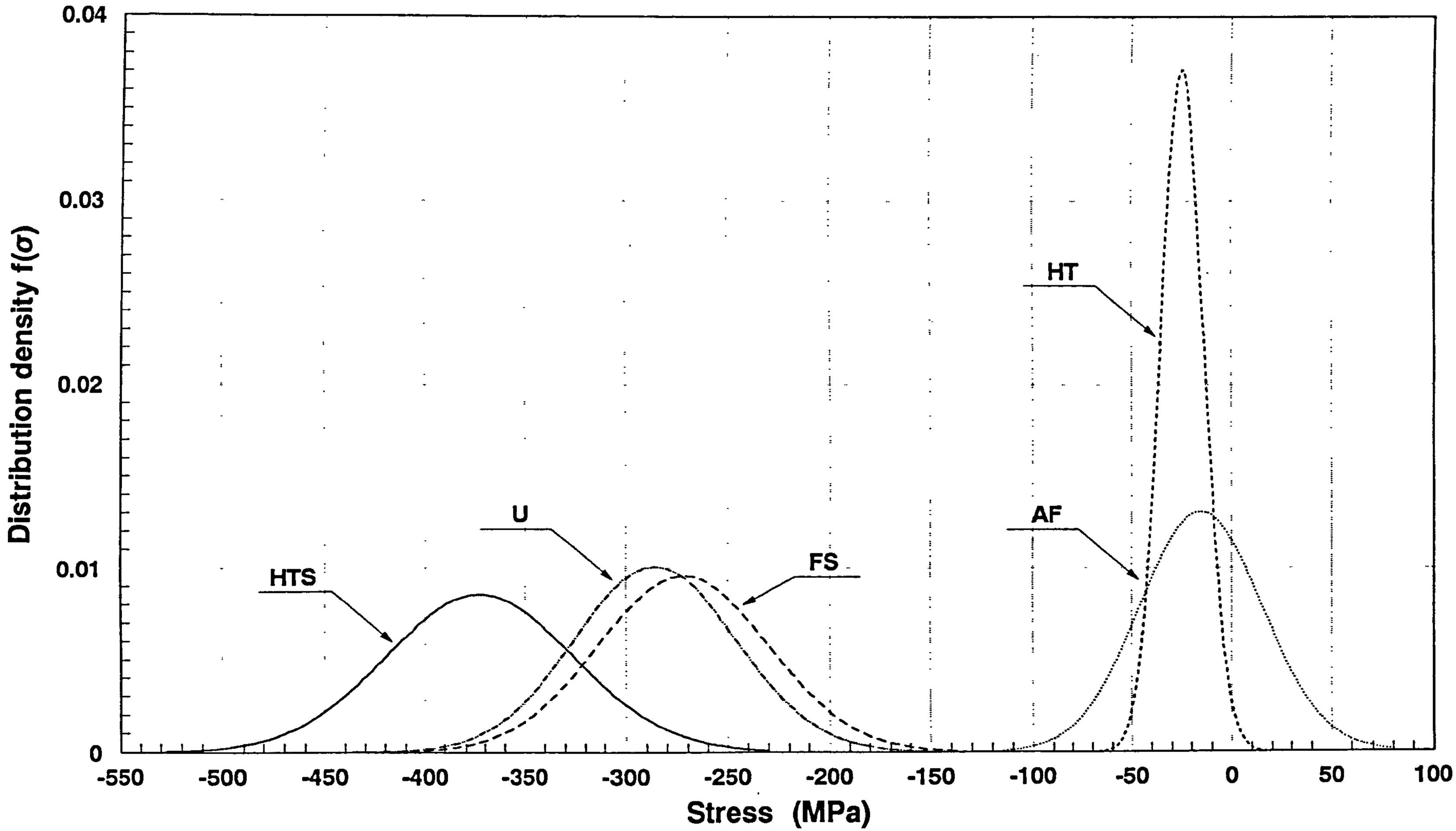

Fig 8.1 Normal distribution of axial residual stress for hot forged specimens measured by X-ray

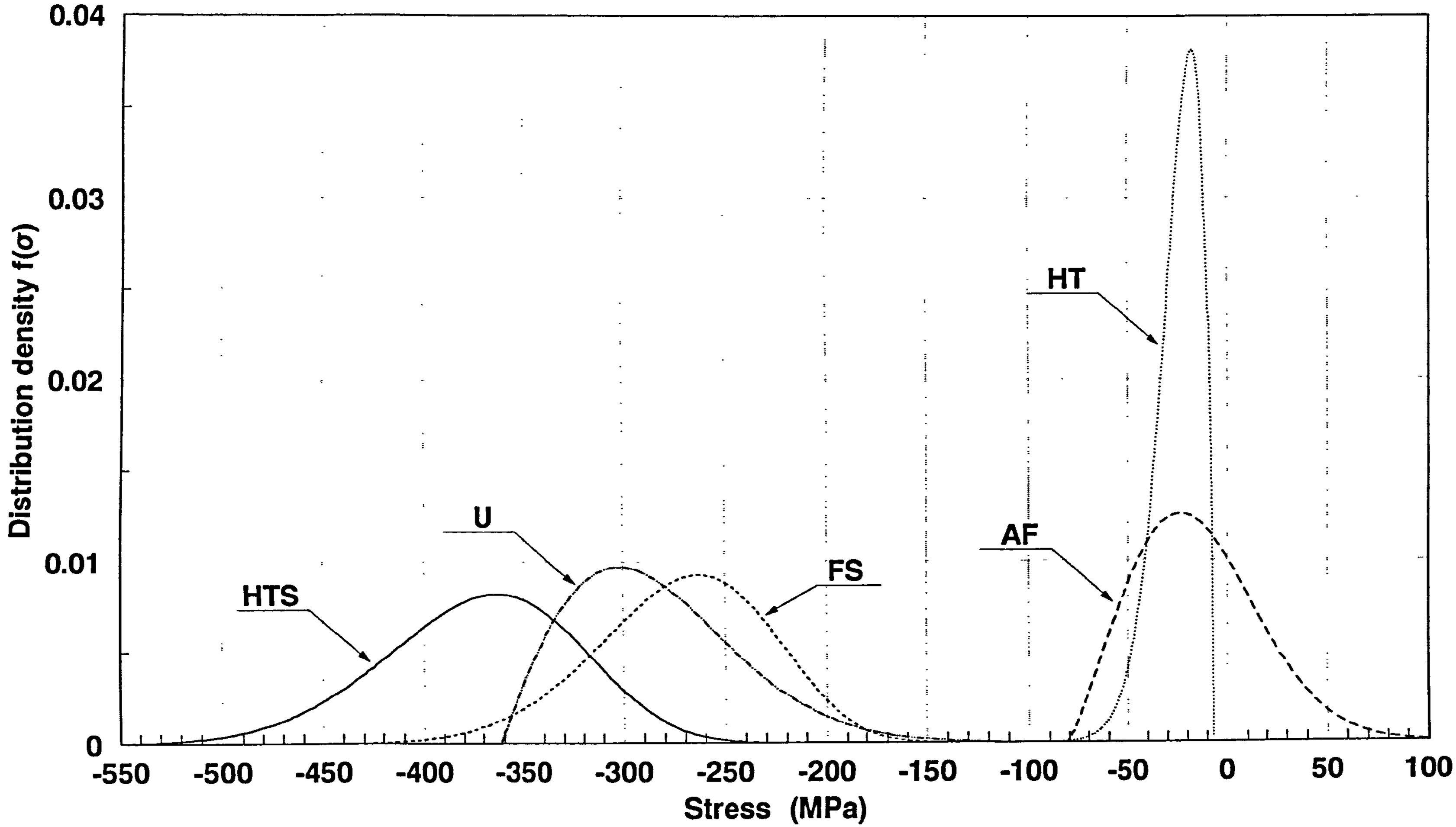

Fig 8.2 Weibull distribution of axial residual stress for hot forged specimens measured by X-ray

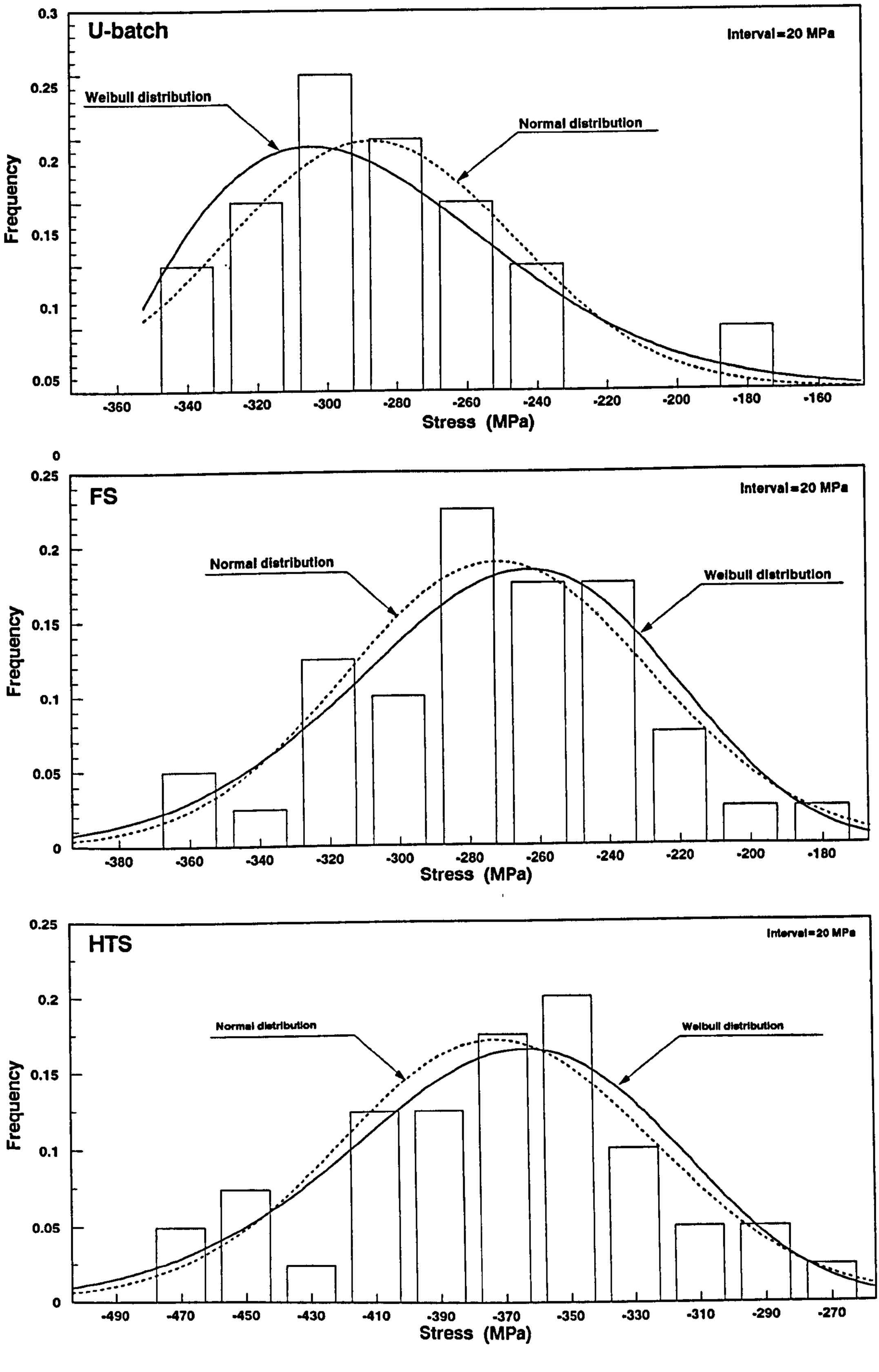

Fig 8.3 Comparison of histograms of axial residual stresses with those of their Normal and Weibull distribution for U-batch, FS and HTS

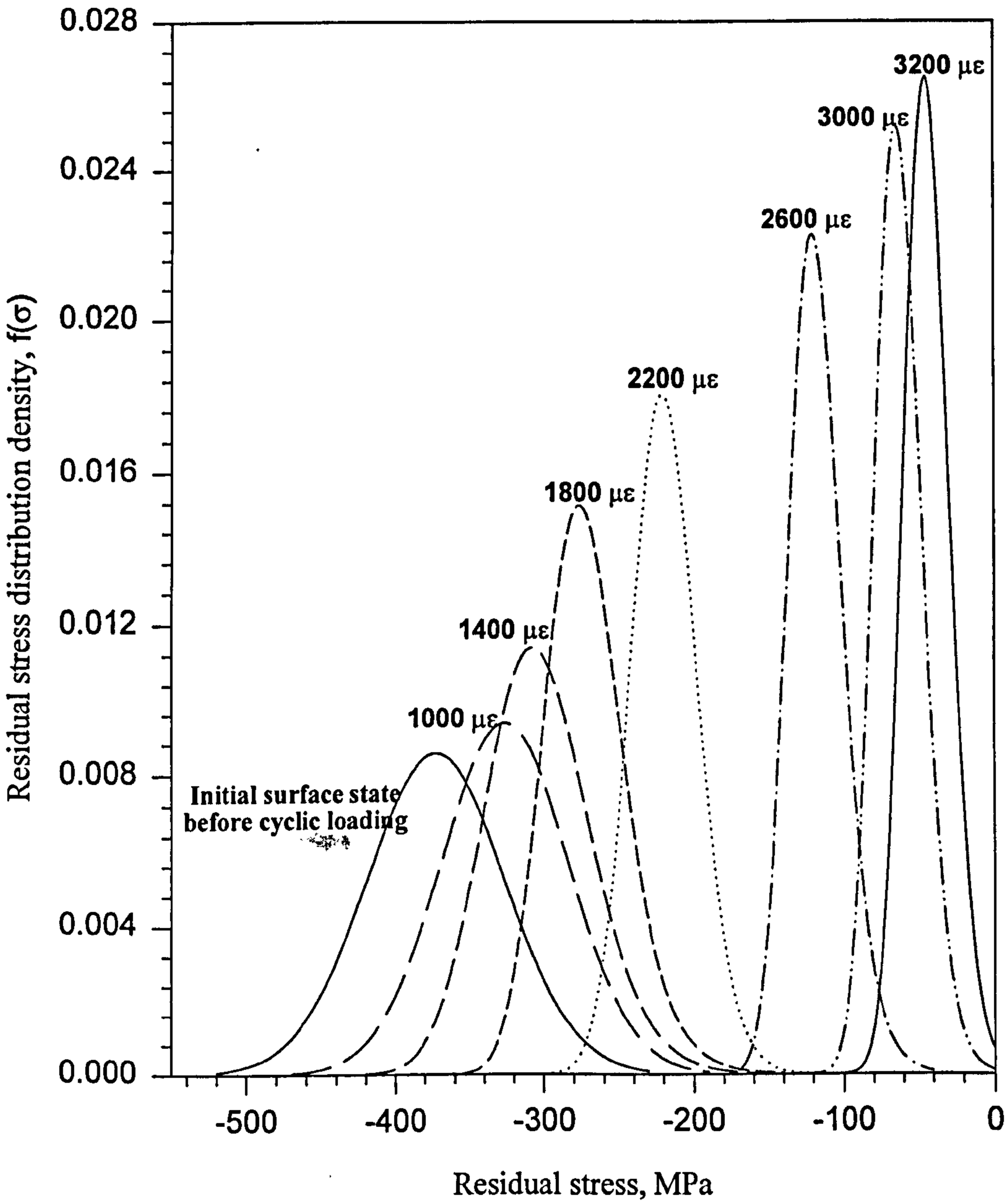

Fig 8.4 Redistribution of surface axial residual stress for HTS group after fatigue cycles

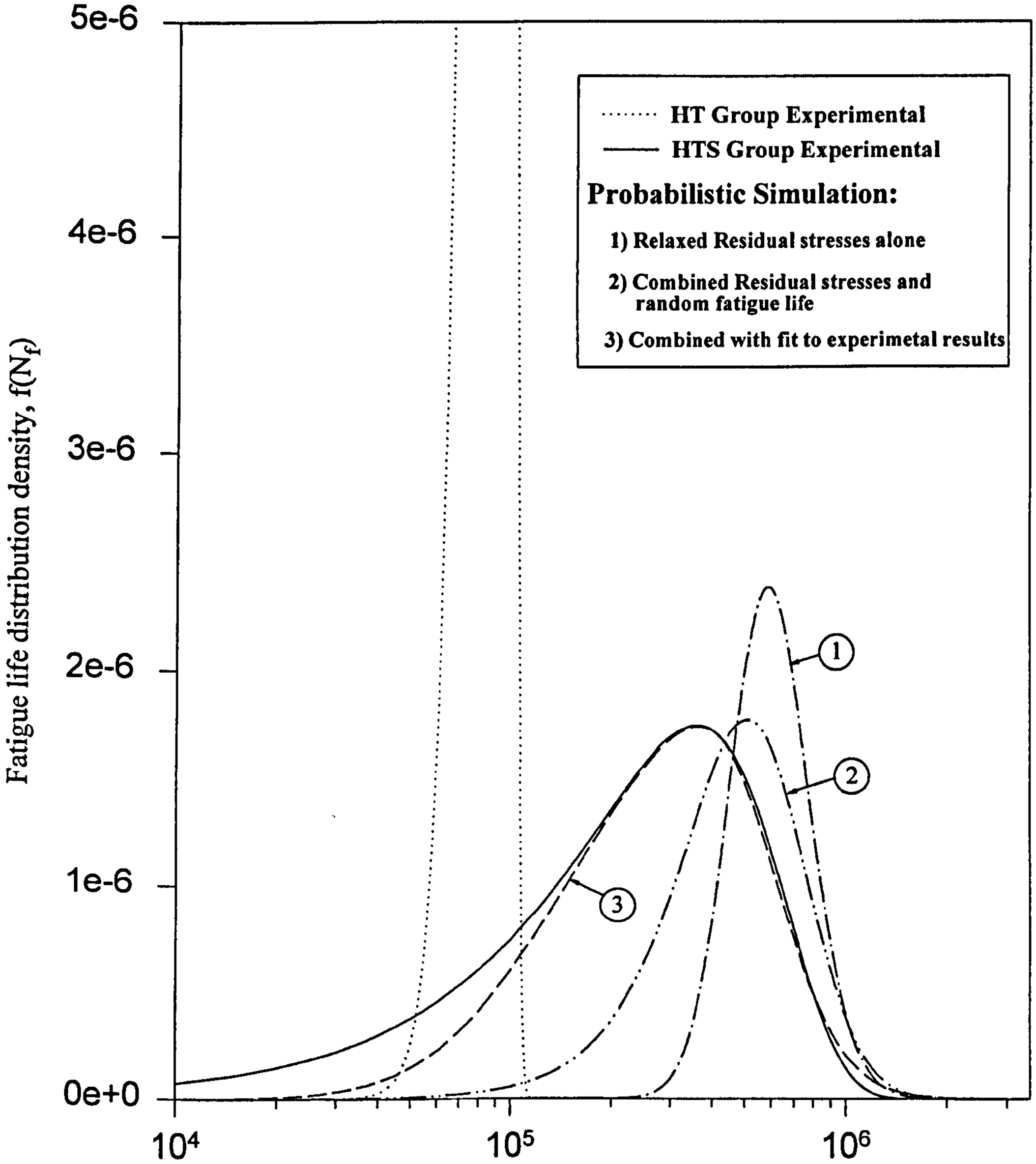

Fig 8.5 Experimental and simulated fatigue life distribution densities

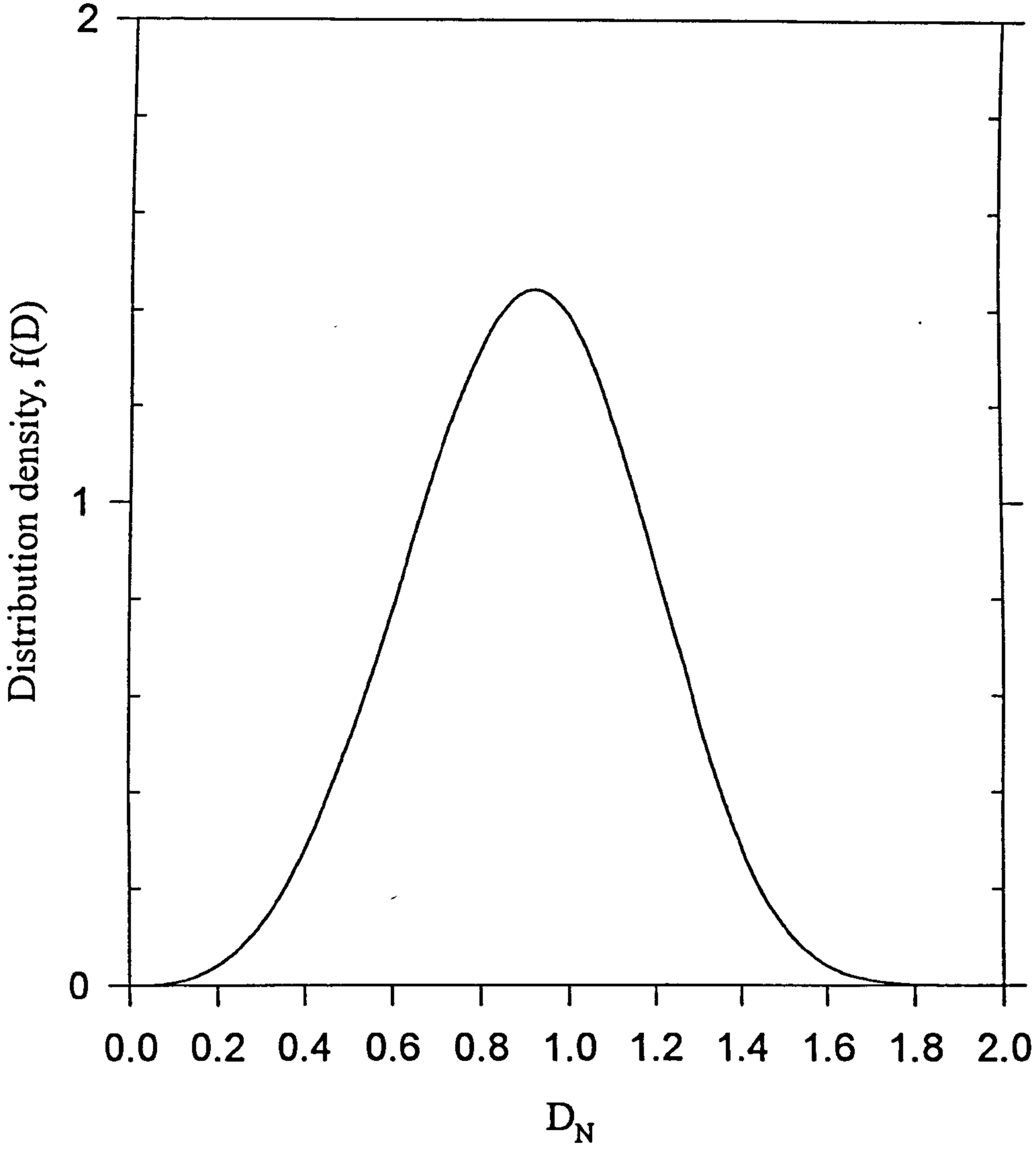

Fig 8.6 The distribution density of random variable D_N for simulation of combined residual stresses and random fatigue life

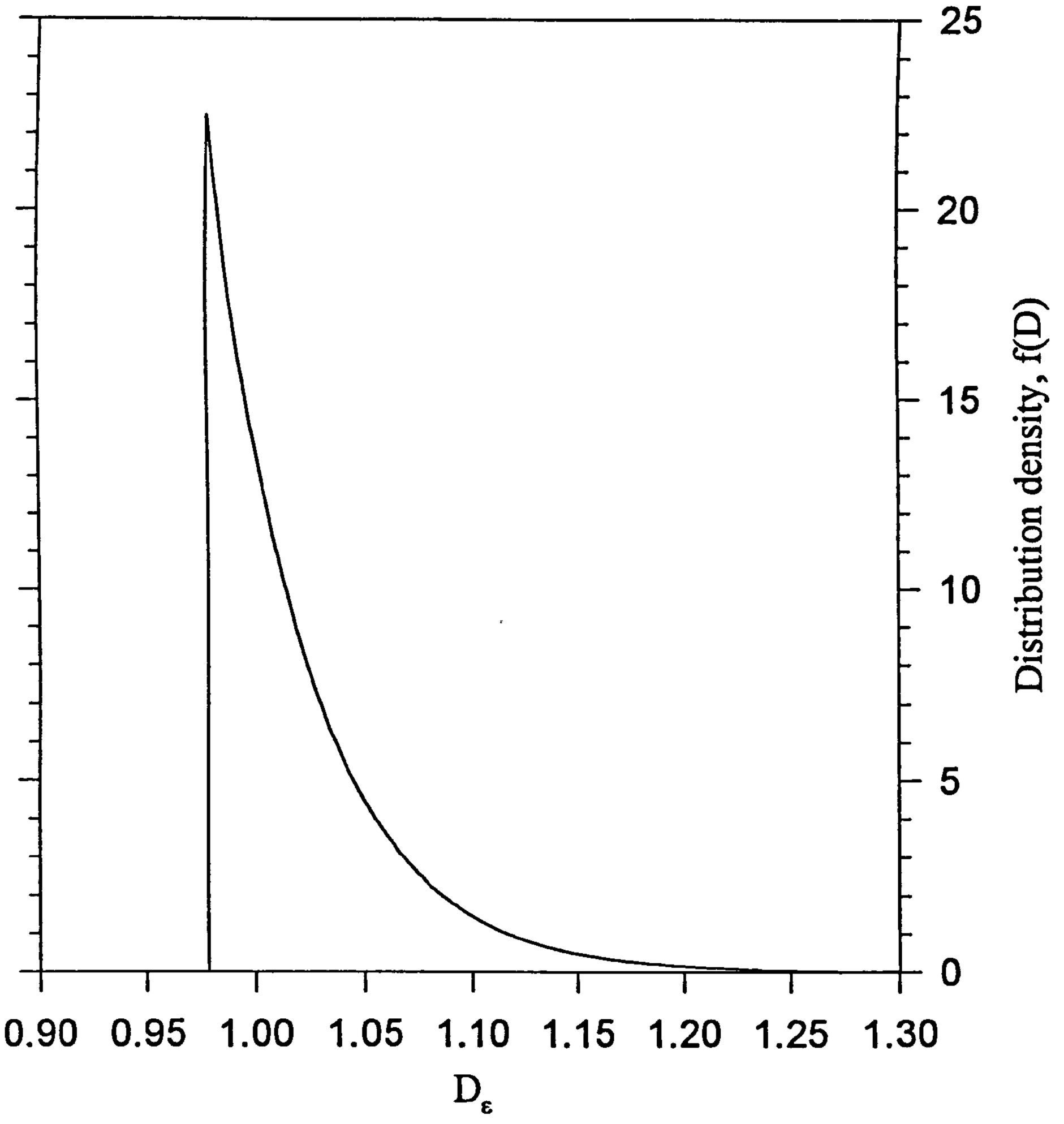

Fig 8.7 The distribution density of random variable D_ε for simulation to fit to experimental results

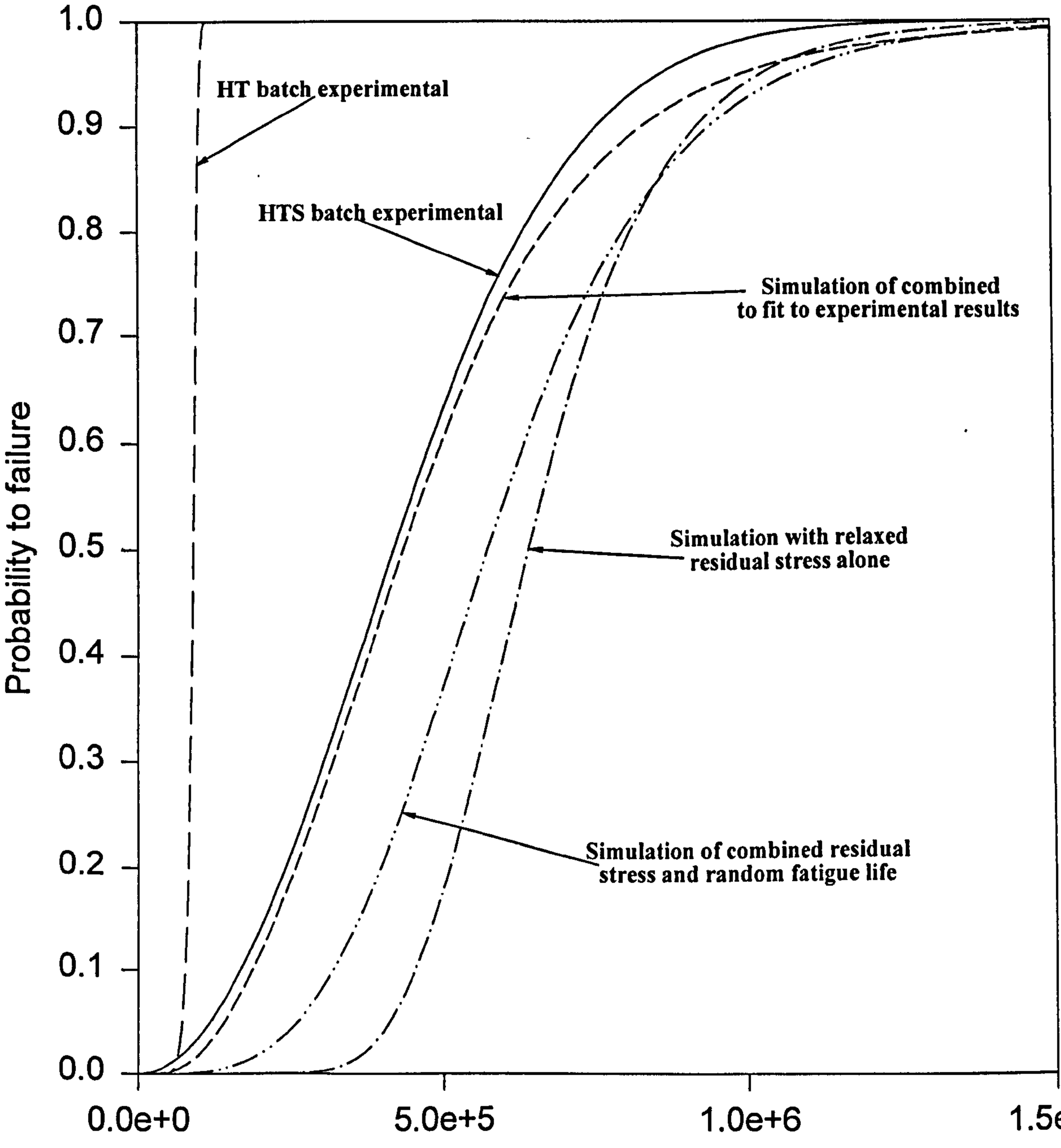

Fig 8.8 Simulations of probability to failure for HTS and comparison with Weibull distribution derived from fatigue test results, $\Delta\varepsilon/2$=2200 $\mu\varepsilon$

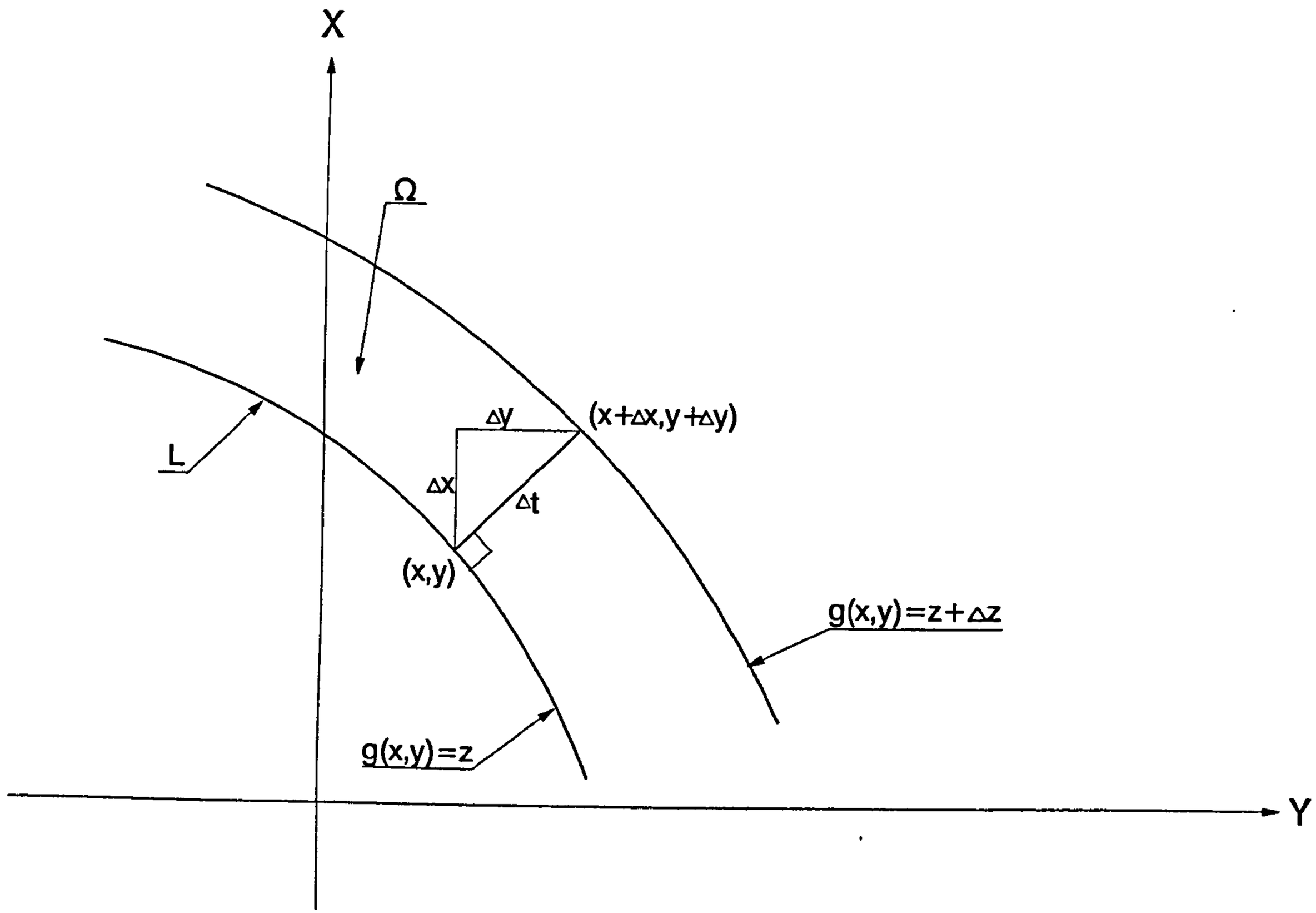

Fig A-1 Illustration of integration area